



U.S. Department of Energy
Idaho Operations Office

HWMA/RCRA Part B Permit Application for the Idaho National Laboratory

Volume 3 General Information for INL Waste Management Units

Book 1 of 1

November 1985

Revision 1 – March 1986

Revision 2 – November 1986

Revision 3 – November 1987

Revision 4 – May 1991

Revision 5 – January 1993

Revision 6 – July 1993

Revision 7 – May 2001

Revision 8 – September 2001

Revision 9 – September 2002

Revision 10 – November 2002

Revision 11 – July 2004

Revision 12 – May 2005

Revision 13 – June 2006

Revision 14 – June 2008

Revision 15 – July 2010

Idaho Cleanup Project

CONTENTS

ACRONYMS.....	vi
INTRODUCTION	1
Organization of Volume 3 of the HWMA/RCRA Permit Application.....	2
PERMIT APPLICATION COMPLETENESS/TECHNICAL EVALUATION CHECKLIST.....	TEC-1
A. PART A PERMIT APPLICATION.....	A-1
B. FACILITY DESCRIPTION.....	B-1
B-1 General Description [IDAPA 58.01.05.012; 40 CFR 270.14(b)(1)]	B-2
B-1(a) Facility Specific Information.....	B-11
B-2 Topographic Maps [IDAPA 58.01.05.012; 40 CFR 270.14(b)(19)]	B-12
B-2(a) Regional Topographic Maps	B-12
B-2(b) Wind Roses	B-14
B-2(c) Wells.....	B-14
B-2(d) Surrounding Land Use	B-19
B-2(e) Access Control.....	B-21
B-2(f) Other Structures	B-21
B-3 Location Information	B-21
B-3(a) Seismic Standard (IDAPA 58.01.05.008 and 58.01.05.012 [40 CFR 264.18(a) and 270.14(b)(11)(i-ii)])	B-21
B-3(b) Floodplain Determination and Prevention of Washout (IDAPA 58.01.05.008 and 58.01.05.012 [40 CFR 264.18(b) and 270.14(b)(11)(iii-iv)])	B-22

B-3(b)(1) Flood Potential from the Big Lost River.....	B-24
B-3(b)(2) Flood Potential from Birch Creek.....	B-25
B-3(b)(3) Flood Diversion Systems at the INL.....	B-25
B-3(b)(4) INTEC 100-Year Storm Water Runoff and 25-Year Runoff Analysis.....	B-26
B-4 Traffic Information [IDAPA 58.01.05.012; 40 CFR 270.14(b)(10)]	B-26
B-4(a) Off-Site Traffic.....	B-26
B-4(b) On-Site Traffic	B-30
B-4(b)(1) INTEC Traffic.....	B-30
B-4(b)(2) RWMC Traffic	B-32
B-4(b)(3) MFC Traffic	B-32
B-5 Literature Cited	B-33
C. WASTE CHARACTERISTICS.....	C-1
D. PROCESS INFORMATION	D-1
E. GROUNDWATER MONITORING.....	E-1
F. PROCEDURES TO PREVENT HAZARDS	F-1
F-1 Security IDAPA 58.01.05.008 and .012 [40 CFR 264.14(b) and(c), and 270.14(b)(4)].....	F-1
G. CONTINGENCY PLAN	G-1
H. PERSONNEL TRAINING	H-1
I. CLOSURE AND POSTCLOSURE REQUIREMENTS	I-1

J. CORRECTIVE ACTION FOR SOLID WASTE MANAGEMENT UNITS
(IDAPA 58.01.05.008 [40 CFR 264.101])J-1

K. OTHER FEDERAL LAWS (IDAPA 58.01.05.012 [40 CFR 270.14(b)(20)
and 40 CFR 270.3])..... K-1

K-1 The Wild and Scenic Rivers Act K-1

K-2 The National Historic Preservation Act of 1966 K-1

K-3 The Endangered Species Act..... K-1

K-4 The Coastal Zone Management Act..... K-5

K-5 The Fish and Wildlife Coordination Act..... K-5

K-6 The Migratory Bird Treaty Act of 1918..... K-5

K-7 Bald Eagle Protection Act..... K-5

K-8 Management of Undesirable Plant on Federal Lands K-5

K-9 Invasive Species Executive Order K-5

K-10 Public Land Orders 318, 545, 637, 1770 K-6

K-11 Clean Water Act..... K-6

L. HWMA/RCRA PERMIT APPLICATION CERTIFICATION [IDAPA 58.01.05.012
40 CFR 270.11(d) and 270.30(k)]

DOE Idaho Operations Office Certification.....L-1

CH2M-WG Idaho.....L-2

APPENDICIES

- Appendix I Topographic Maps
- Appendix II Flood Insurance Rate Maps

- Appendix III Big Lost River Flood Hazard Study, Idaho National Laboratory, Idaho, U.S. Bureau of Reclamation, November 2005

INTEC 100-Year Flood Plain Map (RICOM Flow Model)
- Appendix IV Simulation of Water-Surface Elevations for a Hypothetical 100-Year Peak Flow in Birch Creek at the Idaho National Engineering and Environmental Laboratory, Idaho
- Appendix V 100-Year Storm Water Runoff Floodplain and 25-Year Runoff Analyses for the Idaho Nuclear Technology and Engineering Center at the Idaho National Engineering and Environmental Laboratory (INEEL/EXT-03-001174, Revision 1, January 2004)

EXHIBITS

- B-1. Map of the INL showing facility areas. B-3
- B-2. Location of INL seismic stations and normal faults. B-5
- B-3. Epicenters for historic earthquake events of a magnitude greater than 2.5 occurring from 1872 to 2007..... B-7
- B-4. Generalized geology of the Eastern Snake River Plain showing locations of volcanic rift zones, young lava fields, and basin and range faults..... B-9
- B-5. INTEC, ATR Complex, and TAN/SMC area wind roses..... B-15
- B-6. CITRC, CFA, RWMC, and MFC area wind roses. B-16
- B-7. INL sitewide locations of wells. B-17
- B-8. Enlarged detail of the locations of wells at the ATR Complex, CFA, CITRC, INTEC, LSIT, MFC, NPR, NRF, PERC, RWMC, SMC, STF, TSF, and WRRTF..... B-18
- B-9. Grazing areas at the INL..... B-20
- B-10. USGS miscellaneous investigation map I-2330B-23A & B-23B

B-11. INL roads, highways, and railroads..... B-27

B-12. Access and traffic control at INTEC..... B-31

F-1. Example of an INL boundary no trespassing sign.....F-2

F-2. Example of an INL boundary no grazing sign.....F-3

F-3. Locations of INL warning signs (INL Boundary), grazing boundaries, and current security stations.....F-5

TABLES

B-1. Description of the highway system in the INL vicinity B-28

B-2. Baseline traffic for selected highway segments in the vicinity of INL..... B-29

B-3. Baseline annual vehicle miles traveled for traffic related to the INL B-29

K-1. Listed and proposed endangered species, and candidate species, which may occur at the INL K-2

ACRONYMS

ALARA	as low as reasonably achievable
AMWTF	Advanced Mixed Waste Treatment Facility
AMWTP	Advanced Mixed Waste Treatment Project
ANL-W	Argonne National Laboratory-West
ATR	Advanced Test Reactor
ATR Complex	Advanced Test Reactor Complex (formerly known as RTC)
BOR	Bureau of Reclamation
BORAX	Boiling Water Reactor Experiment
CITRC	Critical Infrastructure Test Range Center (formerly known as WROC)
CFA	Central Facilities Area
CFR	Code of Federal Regulations
CTF	Contained Test Facility
DEQ	Idaho Department of Environmental Quality
DOE	Department of Energy
DOE-ID	Department of Energy Idaho Operations Office
EBR-I	Experimental Breeder Reactor - I
EBR-II	Experimental Breeder Reactor - II
ECF	Expended Core Facility
EDF	engineering design file
EIS	environmental impact statement
EPA	Environmental Protection Agency
ESRP	Eastern Snake River Plain
ETR	Engineering Test Reactor
FEMA	Federal Emergency Management Act
FFA/CO	Federal Facility Agreement and Consent Order
FIA	Federal Insurance Administration
FIRM	flood insurance rate map
HCWHNF	Hazardous Chemical Waste Handling and Neutralization Facility
HEPA	high-efficiency particulate air
HLW	high-level waste
HLLW	high-level liquid waste
HTRE	Heat Transfer Reactor Experiment
HWMA	Hazardous Waste Management Act
ICPP	Idaho Chemical Processing Plant
IDAPA	Idaho Administrative Procedures Act

IET	Initial Engine Test
ILTSF	Intermediate-Level Transuranic Storage Facility
INEEL	Idaho National Engineering and Environmental Laboratory
INL	Idaho National Laboratory (formerly known as INEEL)
INTEC	Idaho Nuclear Technology and Engineering Center
ISFSI	Independent Spent Fuel Storage Installation
LET&D	Liquid Effluent Treatment and Disposal
LLW	low-level waste
MFC	Materials and Fuel Complex (formerly known as ANL-W)
MTR	Materials Test Reactor
MWSF	Mixed Waste Storage Facility
NRC	Nuclear Regulatory Commission
NRF	Naval Reactors Facility
NWCF	New Waste Calcining Facility
OSHA	Occupational Safety and Health Administration
PBF	Power Burst Facility
PCB	polychlorinated biphenyl
PEW	process equipment waste
RCRA	Resource Conservation and Recovery Act
RH	remote-handled
RLWTF	Radioactive Liquid Waste Treatment Facility
RO	radioactive only
RTC	Reactor Test Complex [now known as ATR Complex (formerly known as TRA)]
RTF	Remote Treatment Facility
RWMC	Radioactive Waste Management Complex
SAA	satellite accumulation areas
SBW	sodium-bearing waste
SDA	Subsurface Disposal Area
SHADE	Shielded Hot Air Drum Evaporators
SMC	Specific Manufacturing Capability
SNF	spent nuclear fuel
SPERT	Special Power Excursion Reactor Tests
SWEPP	Stored Waste Examination Pilot Plant
TAN	Test Area North
TFF	Tank Farm Facility
THWS	TAN Hazardous Waste Storage Area

TMI	Three Mile Island
TRA	Test Reactor Area
TREAT	Transient Reactor Test
TRU	transuranic
TSA	Transuranic Storage Area
TSDF	treatment, storage, and/or disposal facility
TSF	Technical Support Facility
USGS	United States Geological Survey
WAC	waste acceptance criteria
WEDF	Waste Engineering Development Facility
WERF	Waste Experimental Reduction Facility
WIPP	Waste Isolation Pilot Plant
WROC	Waste Reduction Operations Complex
WRRTF	Water Reactor Research Test Facility
WWSB	WERF Waste Storage Building

INTRODUCTION

This Hazardous Waste Management Act/Resource Conservation and Recovery Act (HWMA/RCRA) permit application is for waste management units at the U.S. Department of Energy (DOE) Idaho National Laboratory (INL). The DOE uses a variety of contractors to operate the INL's numerous facilities and operations. The Certification, as contained in Section L of this volume, reflects the current contractor with the lead for RCRA. The facility (unit-specific) volumes that follow will similarly reflect responsible operators. The specific waste management units to be permitted under this application are listed in the HWMA/RCRA Work Plan for the INL. This permit application is prepared in conformance with the "A. T. Kearney" format typically used by the Idaho Department of Environmental Quality (DEQ) and the U.S. Environmental Protection Agency (EPA). This format consists of the following sections:

- A. Part A Permit Application
- B. Facility Description
- C. Waste Characteristics
- D. Process Information
- E. Groundwater Monitoring
- F. Procedures to Prevent Hazards
- G. Contingency Plan
- H. Personnel Training
- I. Closure and Postclosure Requirements
- J. Corrective Action for Solid Waste Management Units
- K. Other Federal Laws
- L. Certification.

The INL HWMA/RCRA permit application is, as reflected in the INL HWMA/RCRA Work Plan, a multivolume document organized as follows:

Volume 1 HWMA/RCRA Part A Permit Application for the Idaho National Laboratory – CH2M-WG Idaho, LLC. (CWI)

Volume 1a HWMA/Part A Permit Application for the Idaho National Laboratory – Pads TSA-1/TSA-2 at the Transuranic Storage Area – Advanced Mixed Waste Treatment Project (AMWTP)

- 1 Volume 3 General Information
- 2 • Section B, Facility Description
- 3 • Section J, Corrective Action for Solid Waste Management Units
- 4 • Section K, Other Federal Laws
- 5 • Section L, Certification.

6 Additional volumes are waste management unit-specific and numbered sequentially. Each waste
7 management unit-specific volume provides detailed information for Sections C through I listed above;
8 includes a permit application certification statement in Section L; and contains supplemental information
9 (design drawings, maps, etc.) to support Sections B through I.

10 **Organization of Volume 3 of the HWMA/RCRA Permit Application**

11 This volume (Volume 3) of the HWMA/RCRA permit application for the INL presents general
12 information pertinent to the INL. Volume 3 contains the text of the permit application for Sections B, J,
13 K, L (Certification), and supporting Appendices I through V. Also, as directed by the State of Idaho,
14 information is provided in Sections F and H that supplements the subsequent waste management unit-
15 specific volumes.

16 Following this introduction is a Permit Application Completeness Evaluation Checklist that lists
17 the HWMA/RCRA information requirements for Sections A through L and the corresponding location in
18 the multivolume permit application where the information requirement is addressed. This checklist is
19 provided to assist in the review of this permit application for completeness and technical content.

Permit Application Completeness/Technical Evaluation Checklist

Information Requirement	Complete (Y/N)	Technically Adequate (Y/N)	See Attached Comment	Location of Information
A. PART A APPLICATION	_____	_____	_____	INL HWMA/RCRA Permit Application, Volumes 1 and 1a and in the Unit Specific Volumes
B. FACILITY DESCRIPTION	_____	_____	_____	INL HWMA/RCRA Permit Application, Volume 3, Sections B-1 through B-4
B-1 General description	_____	_____	_____	INL HWMA/RCRA Permit Application, Volume 3, Section §B-1
B-2 Topographic map	_____	_____	_____	INL HWMA/RCRA Permit Application, Volume 3, §B-2
B-2a General requirements	_____	_____	_____	INL HWMA/RCRA Permit Application, Volume 3, §B-2
B-2b Additional requirements for land disposal facilities	_____	_____	_____	Not Applicable (NA)
B-3a Seismic standard	_____	_____	_____	INL HWMA/RCRA Permit Application, Volume 3, §B-3
B-3b Floodplain standard	_____	_____	_____	INL HWMA/RCRA Permit Application, Volume 3, §B-3 and HWMA/RCRA Facility/Unit Specific Volumes (Unit Specific Volumes)
B-3b(1) Demonstration of compliance	_____	_____	_____	INL HWMA/RCRA Permit Application, Volume 3, §B-3 And Unit Specific Volumes
B-3b(1)(a) Flood proofing and flood protection measures; <u>or</u>	_____	_____	_____	INL HWMA/RCRA Permit Application, Volume 3, §B-3 And Unit Specific Volumes
B-3b(1)(b) Floodplain	_____	_____	_____	INL HWMA/RCRA Permit Application, Volume 3, §B-3 And Unit Specific Volumes
B-3b(2) Plan for future compliance with floodplain standard	_____	_____	_____	See Unit Specific Volumes
B-3b(3) Waiver for land storage and disposal facilities	_____	_____	_____	NA
B-4 Traffic information	_____	_____	_____	INL HWMA/RCRA Permit Application, Volume 3, §B-4 And Unit Specific Volumes

Permit Application Completeness/Technical Evaluation Checklist

Information Requirement	Complete (Y/N)	Technically Adequate (Y/N)	See Attached Comment	Location of Information
C. WASTE CHARACTERISTICS	_____	_____	_____	See Unit Specific Volumes
D. PROCESS INFORMATION	_____	_____	_____	See Unit Specific Volumes
E. GROUNDWATER MONITORING	_____	_____	_____	See Unit Specific Volumes
F. PROCEDURES TO PREVENT HAZARDS	_____	_____	_____	Volume 3, §F addresses the INL Site-wide security information
F-1 Security	_____	_____	_____	Volume 3, §F
F-1a Security procedures and equipment	_____	_____	_____	Volume 3, §F
F-1a(1) 24-hour surveillance system	_____	_____	_____	Volume 3, §F
F-1a(2) Barrier and means to control entry	_____	_____	_____	Volume 3, §F
F-1a(2)(a) Barrier	_____	_____	_____	Volume 3, §F
F-1a(2)(b) Means to control entry	_____	_____	_____	Volume 3, §F
F-1a(3) Warning signs	_____	_____	_____	Volume 3, §F
F-1b Waiver	_____	_____	_____	NA
F-2 Inspection schedule	_____	_____	_____	See Unit Specific Volumes
F-3 Waiver or documentation of preparedness and prevention requirements	_____	_____	_____	See Unit Specific Volumes
F-4 Preventive procedures, structures, and equipment	_____	_____	_____	See Unit Specific Volumes

Permit Application Completeness/Technical Evaluation Checklist

Information Requirement	Complete (Y/N)	Technically Adequate (Y/N)	See Attached Comment	Location of Information
F-5 Prevention of reaction of ignitable, reactive, and incompatible wastes	_____	_____	_____	See Unit Specific Volumes
G. CONTINGENCY PLAN	_____	_____	_____	See HWMA/RCRA Facility/Unit Specific Volumes
H. PERSONNEL TRAINING	_____	_____	_____	Volume 3, §H contains the core training program outline
H-1 Outline of the training program	_____	_____	_____	Volume 3, §H
H-1a Job title/job description	_____	_____	_____	See Unit Specific Volumes
H-1b Training content, frequency, and techniques	_____	_____	_____	See Unit Specific Volumes
H-1c Training director	_____	_____	_____	See Unit Specific Volumes
H-1d Relevance of training to job position	_____	_____	_____	See Unit Specific Volumes
H-1e Training for emergency response	_____	_____	_____	See Unit Specific Volumes
H-2 Implementation of training program	_____	_____	_____	See Unit Specific Volumes
H-3 Training records	_____	_____	_____	See Volume 3, §H and Unit Specific Volumes
I. CLOSURE AND POST CLOSURE REQUIREMENTS	_____	_____	_____	See Unit Specific Volumes
J. CORRECTIVE ACTION FOR SOLID WASTE MANAGEMENT UNITS	_____	_____	_____	Volume 3, §J contains the references to the sections of the Unit Specific Volume of each HWMA Partial-Permit that addresses/satisfies the HWMA/RCRA Corrective Action Requirements

Facility/Unit INL General Information
 ID No. ID4890008952
 Review Date July 2010
 Reviewer _____

Permit Application Completeness/Technical Evaluation Checklist

Information Requirement	Complete (Y/N)	Technically Adequate (Y/N)	See Attached Comment	Location of Information
K. OTHER FEDERAL LAWS	_____	_____	_____	Volume 3, §K
L. PART B CERTIFICATION	_____	_____	_____	Volume 3, §L and Unit Specific Volumes

1

A. PART A PERMIT APPLICATION

2

The information for this section is contained in Volumes 1 and 1a of the HWMA/RCRA Part A

3

Permit Application for the INL and in the waste management unit specific volumes of this permit

4

application/permit.

This space was intentionally left blank.

B. FACILITY DESCRIPTION

This section provides a general description of the U.S. Department of Energy (DOE) Idaho National Laboratory (INL), as required by the Idaho Administrative Procedures Act (IDAPA), 58.01.05.012 [Title 40, Code of Federal Regulations (CFR) Part 270.14(b)]. This permit application addresses hazardous waste and mixed waste management activities at the INL. For the purposes of this permit application, “mixed waste” means a waste that contains both Resource Conservation and Recovery Act (RCRA) hazardous waste (40 CFR 261.3) and source, special nuclear, or byproduct material subject to the Atomic Energy Act (40 CFR 266.210).

The INL is a large site (2,305 km² [890 mi²]) with several major facilities and contractors responsible for programs administered by various DOE operations offices.

The HWMA/RCRA Work Plan for the INL identifies the specific waste management units to be permitted, the waste management units that have received a permit from the Idaho Department of Environmental Quality (DEQ), and those waste management units that have interim status (see Volumes 1 and 1a – HWMA/RCRA Part A Permit Applications for the INL) that are to be closed under interim status. This document is available on the Internet at

<https://idahocleanupproject.com/Stakeholders/tabid/122/Default.aspx>

The corrective action requirements for INL facilities (as applicable) are addressed under the following HWMA/RCRA Final Partial Permits (as applicable): the Materials and Fuel Complex (MFC) Storage and Treatment Units HWMA/RCRA Final Permit (PER-116) – Module VI; the HWMA/RCRA Storage and Treatment Permit for the Idaho Nuclear Technology and Engineering Center (Volume 18) - Module VII; and the Advanced Mixed Waste Treatment Project (AMWTP) HWMA/RCRA Permit, Module VI.

Section B is organized as follows:

Subsection B-1 provides a general description of the INL and identifies the location of the waste management units on the INL. The text in Subsection B-1 is supplemented by maps and organized according to the major facility areas at the INL.

Subsection B-2 contains topographic maps and wind rose data for the INL, along with supporting discussion. Subsection B-3 contains location information addressing seismic and floodplain standards. Subsection B-4 contains information on traffic volume and controls at the INL, including both on-Site and off-Site traffic.

1 **B-1 General Description [IDAPA 58.01.05.012; 40 CFR 270.14(b)(1)]**

2 The INL is owned by the United States Government and is operated by DOE. Management and
3 operation of the INL is the responsibility of DOE-designated private contractors working under the
4 direction of DOE Idaho Operations Office (DOE-ID) and the Idaho branch of the Pittsburgh Naval
5 Reactors Office. Exhibit B-1 is a map of the INL that identifies the locations of the facility areas.

6 The INL was established in 1949, by the Atomic Energy Commission, as an area where various
7 types of nuclear reactors, support plants, and associated equipment could be built, tested, and operated
8 with maximum safety. To date, 52 reactors have been built at the INL, including reactors for aircraft
9 propulsion, naval propulsion, fast-breeder reactor development, light-water safety tests, organic
10 moderator and coolant development, materials testing, development of portable power reactors for use in
11 space, and miscellaneous research. One of these reactors is still operable, the Advanced Test Reactor
12 (ATR). A decontamination and decommissioning program is underway to ensure the safe closure of
13 retired facilities and equipment.

14 INL's original emphasis on nuclear physics has been broadened to encompass the entire spectrum
15 of the basic sciences. Presently, the INL is a science-based, applied engineering national laboratory
16 dedicated to supporting the U.S. Department of Energy's missions in nuclear and energy research,
17 science, and national defense. Additionally, paralleling and contributing to this growth in scientific and
18 technical capabilities is the increased emphasis on and dedication of resources to solving the problems of
19 environmental restoration and waste management.

20 The primary facility areas located at the INL are: Materials and Fuel Complex (MFC) [formerly
21 known as the Argonne National Laboratory-West (ANL-W)], Central Facilities Area (CFA), Idaho
22 Nuclear Technology and Engineering Center (INTEC), Naval Reactors Facility (NRF), Critical
23 Infrastructure Test Range Center (CITRC) [formerly known as the Waste Reduction Operations Complex
24 (WROC)/Power Burst Facility (PBF)], Radioactive Waste Management Complex (RWMC), Test Area
25 North (TAN), and Advanced Test Reactor (ATR) Complex [formerly known as the Reactor Technology
26 Complex (RTC) or the Test Reactor Area (TRA)].

27 The INL is located near the northwest margin of the Eastern Snake River Plain (ESRP), a
28 prominent low-elevation arcuate feature of southeastern Idaho. Geographically, this region of the ESRP
29 extends over five counties. The INL lies predominately in Butte county, although it extends into
30 Bingham, Bonneville, Jefferson, and Clark counties. All waste management units are located in Butte
31 county with the exception of MFC units, which are located in Bingham county.

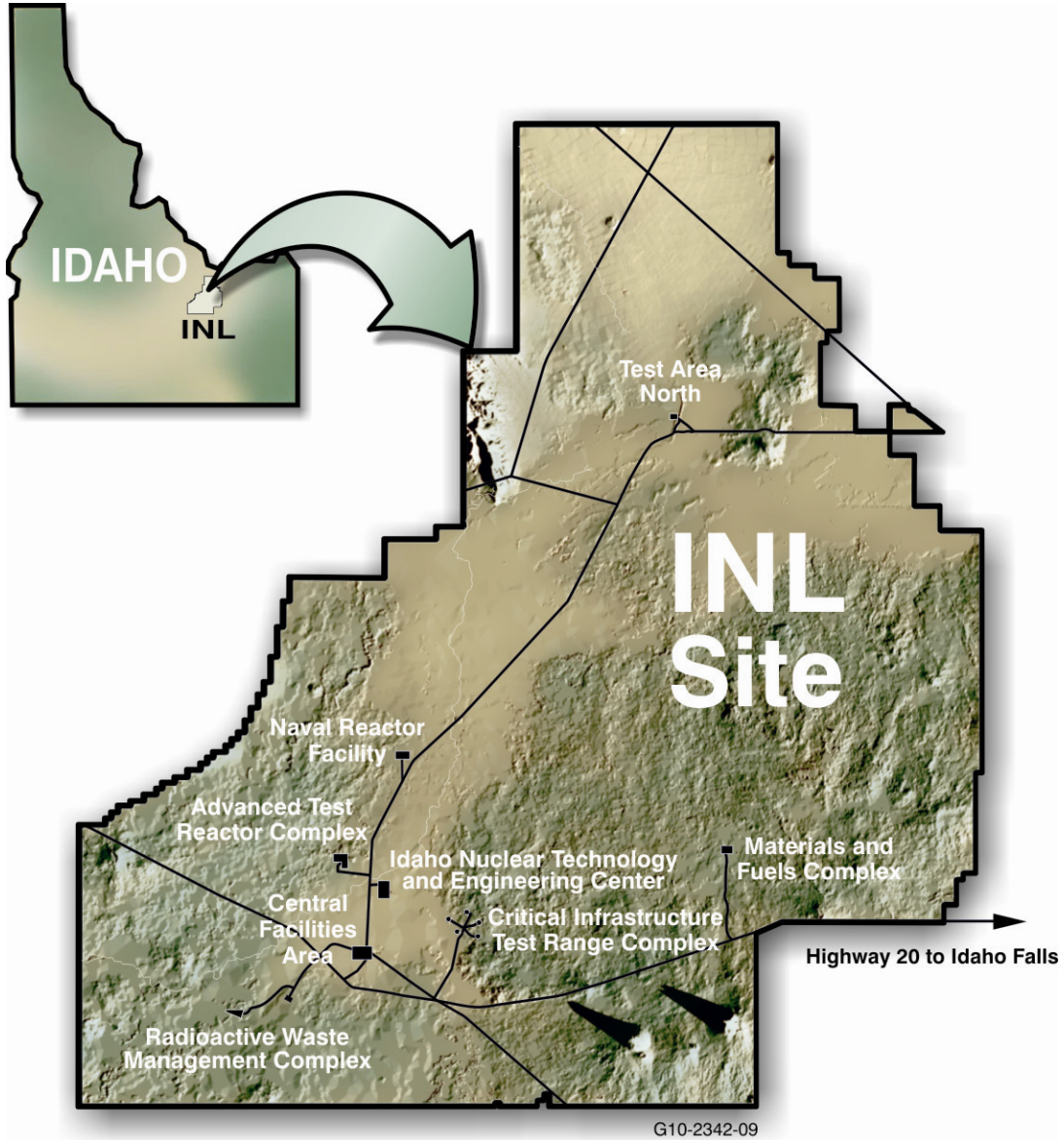


Exhibit B-1. Map of the INL showing facility areas.

1 The ESRP is relatively flat with an average elevation of 1,500 m (4,920 ft) above the mean sea level.
2 Within the INL site, elevations generally range from 1,450 to 1,585 m (4,760 to 5,200 ft). A broad
3 topographic ridge extends to the northeast along the central axis of the ESRP. This ridge effectively separates
4 the drainage of the mountain ranges north and west of the INL site from the Snake River.

5 The ESRP is a northeast-trending zone of late Tertiary and Quaternary volcanism that transects the
6 northwest-trending, normal-faulted mountain ranges of the surrounding Basin and Range Province. The
7 mountain ranges bordering the ESRP, (e.g., Lost River, Lemhi, and Beaverhead) consist of Paleozoic- and
8 Mesozoic-age rocks folded, intruded, and uplifted along normal faults during basin and range tectonism. The
9 mountain ranges and their associated basin and range faults terminate along both sides of the low-lying
10 basalt- and sediment-filled ESRP.

11 Volcanic rocks within the ESRP consist of late Tertiary rhyolitic rocks covered by the latest Tertiary
12 to Holocene basaltic lava flows. At least 1 km (3,281 ft) of basaltic lava flows and intercalated sediments has
13 accumulated over the past 4 million years in the ESRP following the rhyolitic volcanism related to passage of
14 the Yellowstone mantle plume. Most basalt eruptions were effusive, similar to the style of basalt volcanism
15 occurring at Kilauea, Hawaii, today. Throughout the ESRP, the basaltic vents typically formed linear arrays of
16 fissure flows, small shields and pyroclastic cones, pit craters, and open fissures that collectively define
17 northwest-trending volcanic rift zones. The most well known and recently active (2,000 years) is the Great
18 Rift where eight eruptive episodes occurred at Craters of the Moon during the past 15,000 years. Basalt lava-
19 flows within the boundaries of the INL range in age from 12,000 years to greater than 730,000 years old.

20 INL site surficial deposits are quite variable and include eolian (loess and sand dunes), alluvial
21 (gravel, sand, and silt), and lacustrine (clay, silt, and sand) deposits. The surface soils vary widely in thickness
22 and water-holding capacity. Sedimentary interbeds within the subsurface basalt stratigraphy exhibit the same
23 characteristics as the surficial sediments.

24 The INL operates 27 seismic stations and 31 strong-motion accelerographs to monitor earthquake
25 activity occurring in the region. The seismic stations are located on the INL site, on the adjacent ESRP, and
26 throughout the surrounding mountainous region (Exhibit B-2). Accelerographs are located in moderate and
27 high-hazard facilities, at ground surface within facility areas, and at seismic stations. The INL monitors and
28 records earthquake activity within a 161-km (100-mi) radius of the INL, to develop a historical database of
29 times, dates, locations, and magnitudes of earthquakes. This information is used in ground motion analyses to
30 estimate levels of ground shaking (ground motion) from future earthquakes. The seismic monitoring activity
31 provides a way to validate current ground motion models and levels in the event of a large earthquake in the
32 future. The INL seismic network also serves as an early warning detection system for future volcanism.
33 Characteristic low-magnitude earthquake swarms accompany upward movement of magma through the crust
34 of the earth and provide the means to monitor renewed volcanic activity.

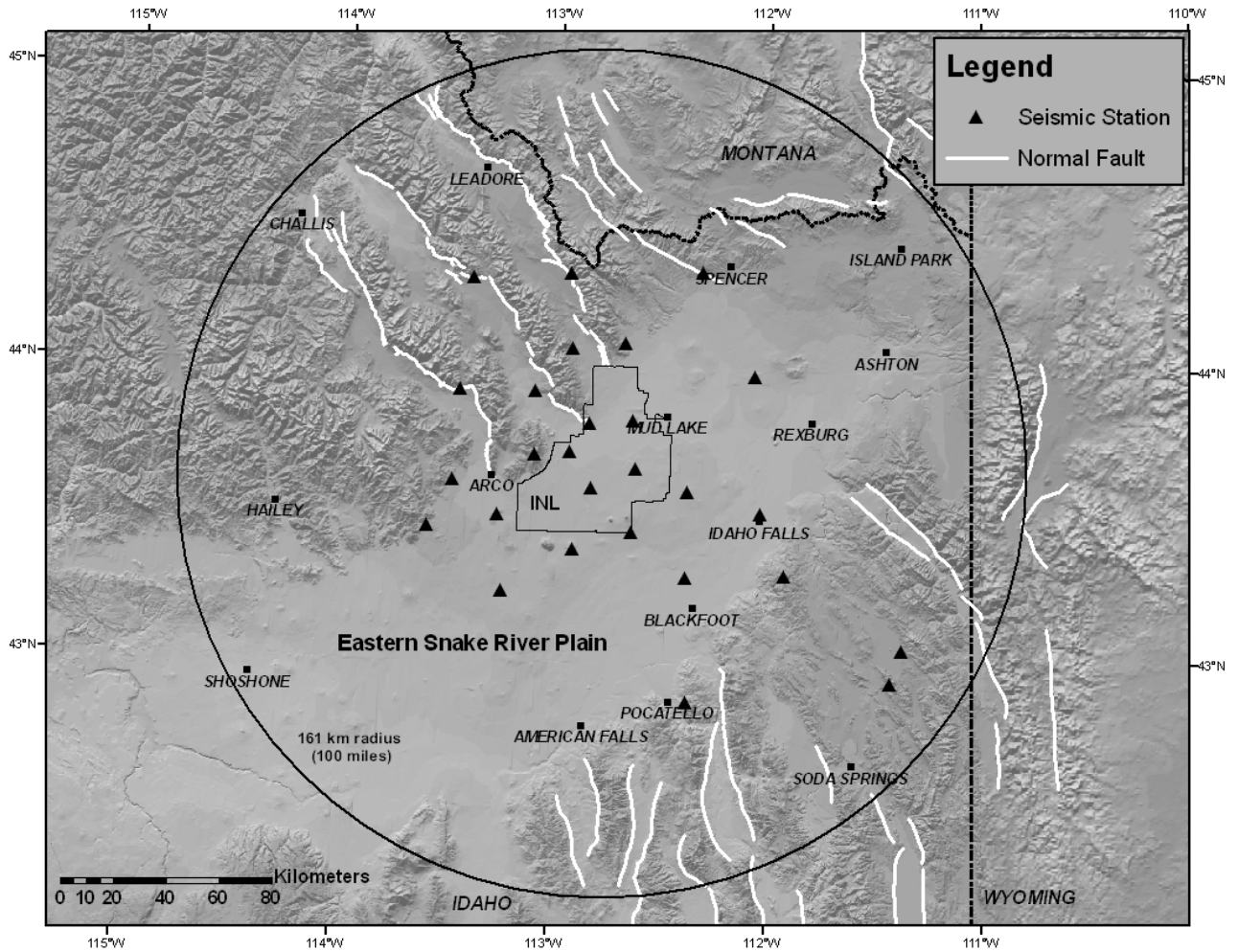


Exhibit B-2. Locations of INL seismic stations (solid triangles) and normal faults (white lines).

1 INL earthquake data have been combined with earthquake data from nearby seismic networks to
2 produce a historical earthquake record. The historical record from 1850 to 2007 for magnitude 2.5 and
3 greater earthquakes shows that the ESRP is seismically quiet relative to the surrounding active Basin and
4 Range Province. Detailed monitoring by the INL seismic network from 1972 to 2007 indicates only 40
5 small magnitude microearthquakes (less than 1.5), have occurred in the ESRP near the INL. In contrast,
6 thousands of earthquakes have occurred in the Basin and Range Province surrounding the ESRP. Two
7 large historic events, the 1983 Borah Peak earthquake (magnitude 7.3) and the 1959 Hebgen Lake
8 earthquake (magnitude 7.5), were felt at the INL but caused no damage because of their great distance
9 from the Site (Exhibit B-3).

10 During the past 15 years, the INL has spent a considerable amount of effort estimating the levels
11 of ground shaking that can be expected at INL facilities from all earthquake sources in the region. The
12 effort included investigating the faults closest to the INL (Exhibit B-2). The Lost River and Lemhi faults
13 were studied in detail to estimate their maximum earthquake magnitudes, distances to INL facilities, ages
14 of earthquakes, and recurrence intervals. The results of these investigations indicate that the closest fault
15 segments are capable of generating magnitude 7 or greater earthquakes and that the most recent
16 earthquakes occurred more than 15,000 years ago on these fault segments.

17 A probabilistic ground motion study was completed for all INL facilities in 1996 and recomputed
18 in 2000. The method incorporated the range of possible seismologic and tectonic interpretations,
19 including earthquake source characteristics (e.g., type of faulting, earthquake magnitude, and fault
20 geometry), attenuation models (the manner in which seismic waves dissipate as they travel through the
21 earth), and subsurface geologic conditions (the manner in which seismic waves are affected by the near-
22 surface sediment and basalt layers). As part of this effort, modeling and earthquake monitoring were
23 conducted to understand how seismic waves are affected by the alternating sequence of basalt lava flows
24 and sedimentary interbeds that composes the ESRP subsurface. As seismic waves pass through layers of
25 alternating competent (hard) basalt and loosely consolidated (soft) sediments scattering and dampening of
26 seismic energy occurs which results in earthquake ground motion levels 15 to 25% less than would be
27 exhibited in uniform rock. Sensitivity analyses were also performed to determine the important
28 contributors to the seismic hazard and to assess the uncertainties in the hazard. The estimates are in the
29 form of the levels of ground shaking that will not be exceeded in specified time periods (such as 500;
30 1,000; 2,500; and 10,000 years).

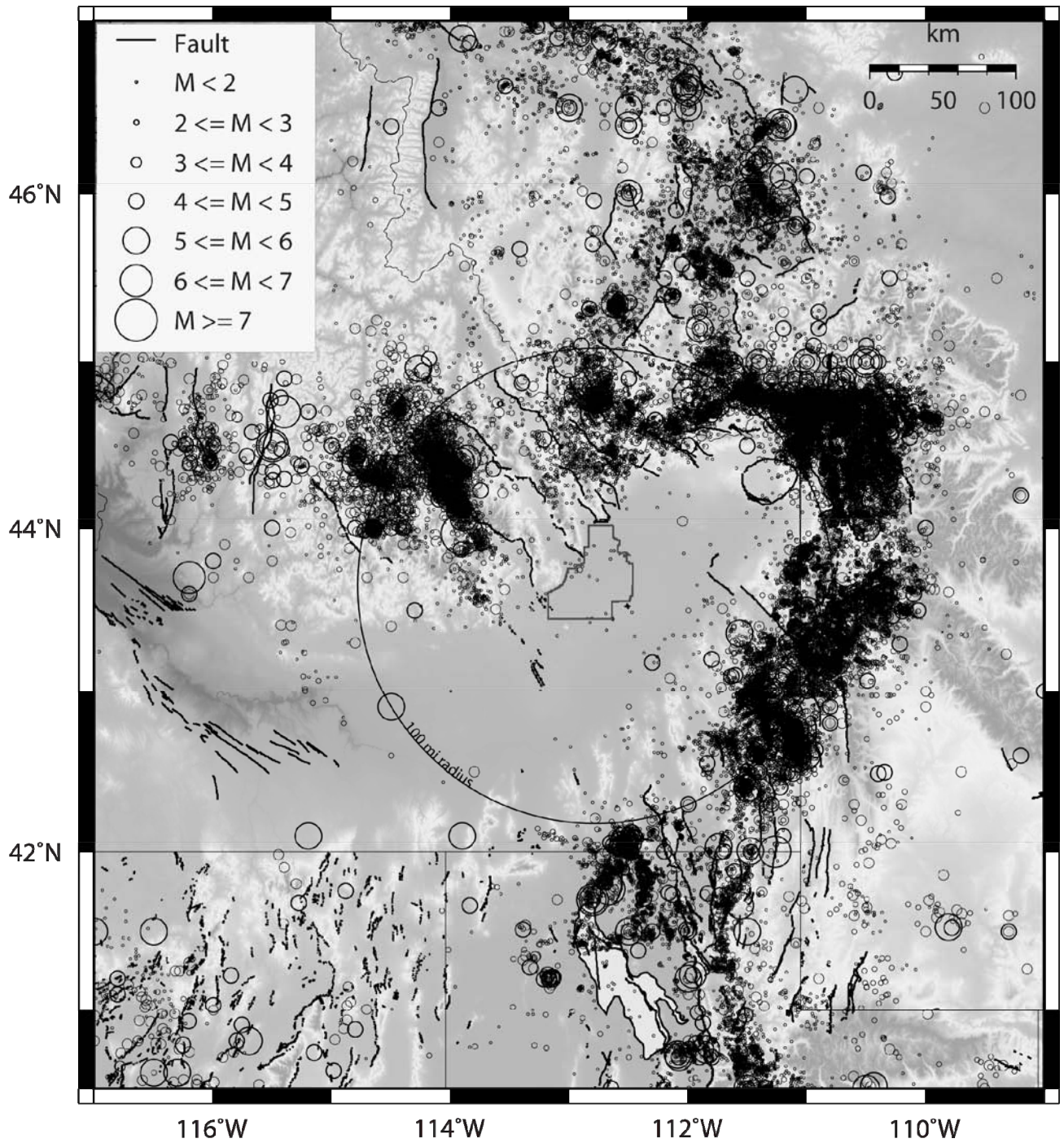


Exhibit B-3. Epicenters for historic earthquakes of magnitude greater than 2.5 occurring from 1872 to 2007 [Carpenter, N.S. (2010)].

1 These results were used to develop design basis earthquake parameters for rock conditions, which
2 were documented in *Development of Probabilistic Design Earthquake Parameters for Moderate and*
3 *High Hazard Facilities at INEEL* (Payne et al. 2002). The expected levels of earthquake ground motions
4 (determined by the recent INL seismic hazards assessment) provide seismic design criteria for new
5 facilities and indicate that past criteria are conservative. The revised seismic criteria are being used in
6 assessments of existing facilities to ensure safety to the public, workers, and environment. INL seismic
7 design criteria have been developed consistent with the requirements of DOE standards, American
8 Society of Civil Engineering standards, Nuclear Regulatory Commission (NRC) requirements, and
9 nuclear quality assurance requirements.

10 Volcanic hazards assessments have been conducted for INL facilities since the ESRP is a
11 volcanic province with recent eruptions of basalt lava flows, relative to geologic time, in association with
12 volcanic rift zones (Exhibit B-4). Volcanism investigations (determination of ages of lava flows,
13 mapping of volcano distribution and volcanic rift zone structures, and analysis of borehole data) have
14 contributed greatly to improved understanding of the volcanic processes affecting the ESRP. This
15 understanding has enabled completion of a rigorous probabilistic volcanic hazards assessment to support
16 an NRC license that was recently granted for a new spent nuclear fuel (SNF) storage facility at the
17 INTEC. Methodologies have been developed to assess the site-specific volcanic hazard for each facility.
18 The shortest recurrence intervals (greatest annual probabilities of eruption) for INL volcanic rift zones are
19 about 16,000 years (or 6.2×10^{-5} per year) for the axial volcanic zone and Arco volcanic rift zone.

20 Surface water at the INL consists of streams draining through intermountain valleys to the west
21 and north, localized snowmelt, and rain. Streams entering the INL include the Big Lost River, Little Lost
22 River, and Birch Creek. Flow from the Little Lost River and Birch Creek is generally diverted for
23 irrigation purposes, before it reaches the INL. However, water from the Big Lost River and Birch Creek
24 enters the INL during years without drought. During drought periods, flow does not reach the INL.
25 These three drainage systems either terminate in one of four playas in the north-central part of the INL or
26 terminate prior to reaching the playas. The INL is not crossed by any perennial streams. All surface
27 outflows are a result of localized slope run-off.

28 Recharge waters from the Big Lost River to the Snake River Plain Aquifer have been significant
29 during wet years. Except for evaporation losses, all water flowing in the Big Lost River through the
30 ESRP is recharged to the ground.

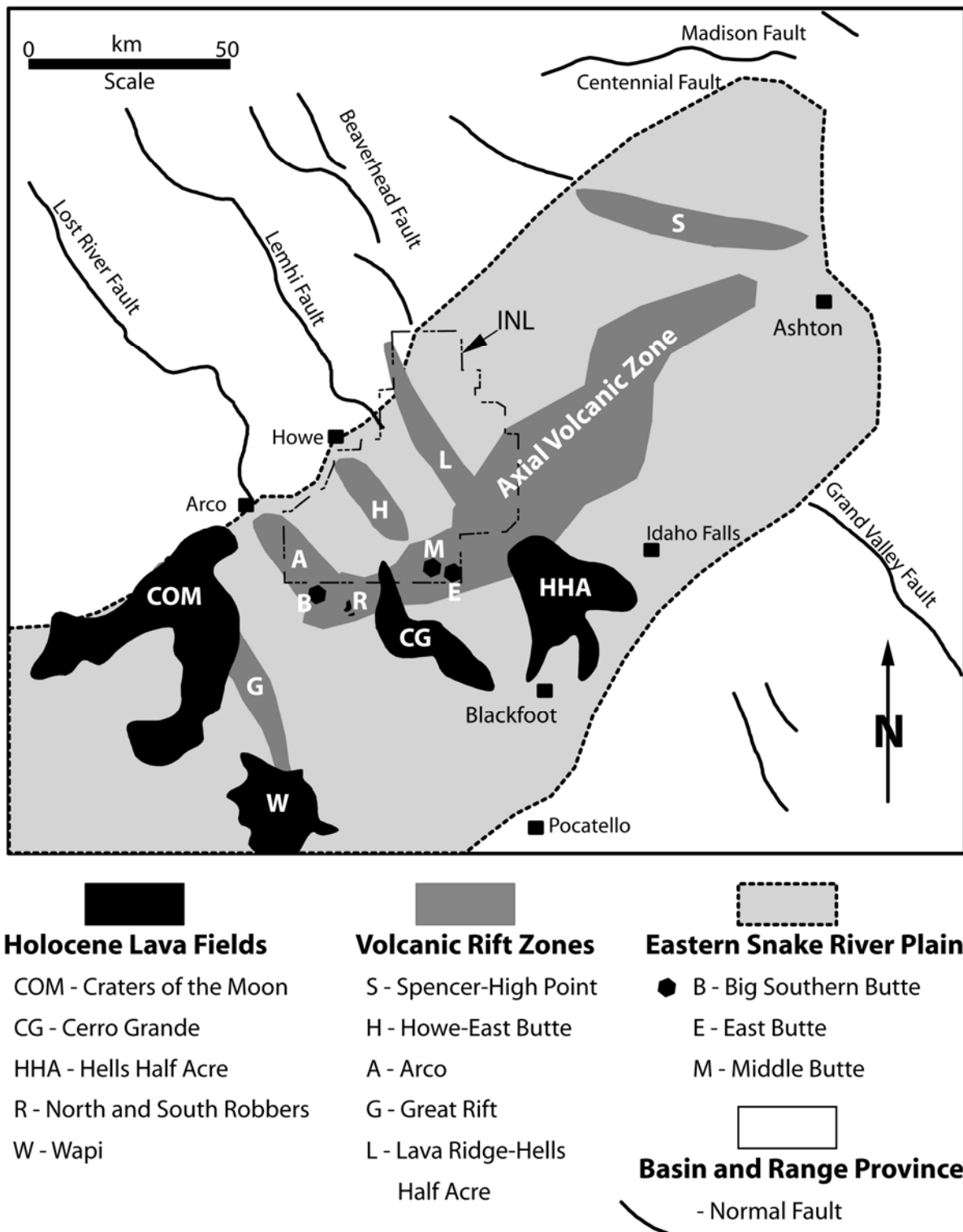


Exhibit B-4. Generalized geology of the Eastern Snake River Plain showing locations of volcanic rift zones, young lava fields, and basin and range faults.

1 The Snake River Plain Aquifer is a continuous body of groundwater that underlies nearly all of
2 the ESRP. The section of the aquifer underlying the ESRP is approximately 320 km (198 mi) long and 48
3 to 97 km (30 to 60 mi) wide. This section of thin basalt flows interbedded with layers of sediments
4 comprises an area of approximately 24,900 km² (15,440 mi²). Most of the permeable zones in the aquifer
5 occur along the upper and lower edges of the basaltic flows, which have large irregular fractures, cavities,
6 and voids. This structure leads to a great degree of heterogeneity and anisotropy in the hydraulic
7 properties of the aquifer. The thickness of the aquifer has not been established, but several holes at the
8 INL indicate that the thickness of the most permeable part is between 100 and 400 m (328 to 1,312 ft).
9 The depth to the aquifer under the INL varies from 60 m (197 ft) in the northeast corner to 275 m (902 ft)
10 in the southwest corner.

11 Groundwater flows southwestward from the north and northeastern recharge areas. Tracer studies
12 at the INL indicate groundwater velocities of 1.5 to 6.1 m (4.9 to 20 ft) per day. The aquifer contains
13 1,230 to 2,460 km³ (300 to 600 mi³) of water, of which 616 km³ (150 mi³) is recoverable. About 8 km³ (2
14 mi³) of groundwater is discharged annually through springs in the Hagerman, Idaho, area, and through
15 irrigation-well withdrawals in the region west of Twin Falls, Idaho. The discharges from the springs
16 make a significant contribution to the flow of the Snake River downstream from Hagerman. Besides
17 providing water for INL operations, the aquifer supplies other industries. Water from springs emerging in
18 the Twin Falls–Hagerman area is used commercially in the aquaculture industry. The spring water flow
19 of 47 m³/sec (1,659 ft³/sec) constitutes 76% of the water used for the commercial production of fish in
20 Idaho. Most of these fish farms discharge water directly into the Snake River.

21 The United States Geological Survey (USGS) maintains an office at the INL and conducts
22 independent environmental monitoring. INL operations produce various types of radioactive effluents.
23 The processes by which the radioactive wastes are produced and controlled at all of the INL facilities are
24 generally similar. The major radioactive contaminants include short-lived nuclides (such as tritium,
25 chromium-51, strontium-90, and cobalt-60) and long-lived nuclides (such as iodine-129, technetium-99,
26 and carbon-14).

27 INL facilities routinely generate a variety of nonradioactive industrial and sanitary waste streams.
28 These waste streams are primarily aqueous and may contain minor quantities of chemicals. Wastes
29 include laboratory wastes, cooling water, effluent from boilers used in space and process steam heating,
30 water treatment waste, and sanitary waste and sewage. Nonhazardous liquid wastes are generally routed
31 to unlined impoundments. In the past, disposal wells have been used at the INL for such wastewater.
32 Some of these wells have now been closed (filled with concrete and capped) or converted to monitoring
33 wells. Several surface water run-off wells are also still in operation throughout the INL. Sanitary wastes
34 and sewage are treated and then discharged to impoundments, evaporation lagoons, or shallow subsurface
35 drainage fields. The ponds and wells described above are not addressed in this

1 permit application, as they are not currently receiving hazardous waste. These disposal areas are
2 addressed under the Federal Facility Agreement and Consent Order (FFA/CO) involving DOE Idaho
3 Operations Office, the State of Idaho, and EPA Region 10 (1991).

4 Hazardous wastes, mixed wastes, polychlorinated biphenyls (PCB), and PCB-contaminated
5 materials are also generated at the INL. The hazardous wastes typically come from support operations
6 and laboratory activities conducted at the INL and include ignitable liquids, acids, bases, solvents,
7 oxidizers, toxics, and reactives. Additional types of waste include laboratory wastes, photographic
8 wastes, spill residues, excess solutions, cleanup solutions, paint-stripping residues, and wastes generated
9 by decontamination and demolition activities. The hazardous wastes may be accumulated on-Site in
10 satellite accumulation areas (SAAs) and in “less than 90-day” storage areas (a.k.a. 90-day storage areas)
11 in accordance with IDAPA 58.01.05.006 (40 CFR 262); stored and treated on-Site under a generator
12 treatment plan or in a RCRA unit; or transported off-Site to a RCRA treatment, storage, and disposal
13 facility (TSDF). PCB liquids, PCB-contaminated transformers, and other PCB-contaminated materials
14 are sent off-Site for disposal, but may be stored on-Site pending shipment.

15 Mixed wastes that are generated include, but are not limited to, contaminated metals, solvents,
16 wastewater, laboratory wastes, and chemical-contaminated rags and other materials used in
17 decontamination. These wastes are generated through a variety of processes and activities such as
18 laboratory operations, equipment cleanup, paint stripping, decontamination operations, demolition
19 activities, and other operations where contact with radioactive materials may occur. Some of these wastes
20 are treated on-Site; others are stored, pending development of treatment or disposal capabilities on-Site or
21 off-Site. Effluents at INTEC from waste evaporation and other operations may be discharged to the CPP-
22 604 Tank Farm Facility or other tank storage units. Additionally, INL accepts mixed waste generated at
23 other DOE facilities for treatment and certification for shipment to the Waste Isolation Pilot Plant
24 (WIPP), in New Mexico.

25 **B-1(a) Facility Specific Information**

26 Facility specific information for INL facilities that have HWMA/RCRA units regulated under 40
27 CFR 265 and 40 CFR 264 (IDAPA 58.01.05.009 and 58.01.05.008) may be found in the following Final
28 Partial HWMA/RCRA Permits and HWMA/RCRA Permit Applications:

- 29 • Volume 1 – HWMA/RCRA Part A Permit Application for the Idaho National Laboratory –
30 CH2M-WG Idaho, LLC. (CWI)
- 31 • Volume 1a – HWMA/RCRA Part A Permit Application for the Idaho National Laboratory –
32 Pads TSA-1/TSA-2 at the Transuranic Storage Area – Advanced Mixed Waste Treatment
33 Project (AMWTP)

- 1 • HWMA/RCRA Storage and Treatment Permit for the Materials and Fuels Complex
2 (PER-116)

- 3 • HWMA/RCRA Storage and Treatment Permit for the Experimental Breeder Reactor-II
4 located at the Materials and Fuels Complex on the Idaho National Laboratory (PER-120)

- 5 • HWMA/RCRA Storage and Treatment Permit for the Liquid Waste Management System at
6 the Idaho Nuclear Technology and Engineering Center on the Idaho National Laboratory
7 (Volume 14 or PER-111)

- 8 • HWMA/RCRA Storage and Treatment Permit for the Idaho Nuclear Technology and
9 Engineering Center on the Idaho National Laboratory (Volume 18 or PER-109)

- 10 • HWMA/RCRA Post-Closure Permit for the Waste Calcine Facility on the Idaho National
11 Laboratory (Volume 21 or PER-112)

- 12 • HWMA/RCRA Storage Permit for the Calcined Solids Storage Facility at the Idaho Nuclear
13 Technology and Engineering Center on the Idaho National Laboratory (Volume 22 or
14 PER-114)

- 15 • Advanced Mixed Waste Treatment Project (AMWTP) HWMA/RCRA Permit

16 **B-2 Topographic Maps [IDAPA 58.01.05.012; 40 CFR 270.14(b)(19)]**

17 This subsection presents topographic map information and supporting information on prevailing
18 winds, wells, surrounding land use, access controls, and other structures present at the INL. This
19 information satisfies the topographic map requirements.

20 **B-2(a) Regional Topographic Maps**

21 The topographic maps for the INL, provided in Appendix I, were confirmed by the Denver Office
22 of the USGS to be the latest available maps. Map #4 previously identified by the USGS as Circular Butte
23 3 NW is now identified by the USGS as East of Howe Peak. Map #5 previously identified by the USGS
24 as Circular Butte 3 NE is now identified by the USGS as North of Rye Grass Flat. Map #6 previously
25 identified by the USGS as Circular Butte 3 SW is now identified by the USGS as North of Scoville. Map
26 #7 previously identified by the USGS as Circular Butte 2 SE is now identified by the USGS as Rye Grass
27 Flat. Additionally, it was verified by use of the USGS web site that the survey date/information on these
28 maps has not been revised/updated therefore the maps are not being updated. The information below

1 cross-references the maps to the waste management unit locations and other required information. Refer
2 to the HWMA/RCRA Work Plan for specific units within the major facility areas.

3 Map No. 1 - Dubois 1:250,000 (1 in. = 20,833 ft) – Shows the INL legal boundary (northern-most
4 portion of facility) and more than 305 m (1,000 ft) around the INL legal boundary. Map No. 1 should be
5 used in conjunction with Map #2. Map No. 1 has 200-ft contours; shows surface waters, land usage,
6 highways, and property boundaries.

7 Map No. 2 - Idaho Falls 1:250,000 (1 in. = 20,833 ft) – Shows the INL legal boundary (southern
8 portion of facility) and more than 305 m (1,000 ft) around the INL legal boundary. Map No. 2 should be
9 used in conjunction with Map No. 1. Map. No. 2 has 200-ft contours; shows surface waters, land usage,
10 highways, and property boundaries.

11 Map No. 3 - Circular Butte 1:24,000 (1 in. = 2,000 ft) – Shows TAN and SMC.

12 Map No. 4 - Circular Butte 3 NW (East of Howe Peak) 1:24,000 (1 in. = 2,000 ft) – Shows NRF.

13 Map No. 5 - Circular Butte 3 NE (North of Rye Grass Flat) 1:24,000 (1 in. = 2,000 ft) – There are
14 no major facility areas on Map No. 5.

15 Map No. 6 - Circular Butte 3 SW (North of Scoville) 1:24,000 (1 in. = 2,000 ft) – Shows RTC,
16 INTEC and CFA.

17 Map No. 7 - Circular Butte 3 SE (Rye Grass Flat) 1:24,000 (1 in. = 2,000 ft) – Shows CITRC and
18 the Auxiliary Reactor Area (ARA).

19 Map No. 8 - Little Butte SW 1:24,000 (1 in. = 2,000 ft) – Shows MFC.

20 Map No. 9 - Arco Hills SE 1:24,000 (1 in. = 2,000 ft) – Shows the area north of RWMC. Map
21 No. 9 should be used in conjunction with Map No. 10. Map No. 9 shows gauging stations on the Big
22 Lost River and the diversion system.

23 Map No. 10 - Big Southern Butte 1:24,000 (1 in. = 2,000 ft) – Shows diversion areas for the Big
24 Lost River diversion system. Map No. 10 should be used in conjunction with Map No. 9.

1 The INL encompasses 2,305 km² (890 mi²) of raised desert plain, with an average topographic
2 elevation of approximately 1,500 m (4,920 ft) above mean sea level. The majority of the INL lies within
3 Butte County, Idaho, although portions extend into Bingham, Bonneville, Jefferson, and Clark counties.
4 All site activities and facilities are situated well within the INL boundaries, which extend for
5 approximately 63 km (39 mi) north to south and 58 km (36 mi) east to west at their longest points.
6 Exhibits B-1 and B-7 provide general facility location maps of the INL.

7 Appendix I provides regional topographic maps (Maps 1 and 2) of the INL complex, at a scale of
8 1.0 in. = 20,833 ft. Additional topographic maps at a scale of 1 in. = 2,000 ft and contour intervals of 5,
9 10, or 20 ft are also provided in Appendix I, as Maps 3 through 10, that are sufficient for this flat area as
10 allowed under the regulation. Topographic maps with a smaller scale and smaller contour intervals are
11 provided in the waste management unit-specific volumes of this permit application. The topographic
12 maps in Appendix I show the topography, surface waters and intermittent streams, surrounding land
13 usage, access roads, and well locations.

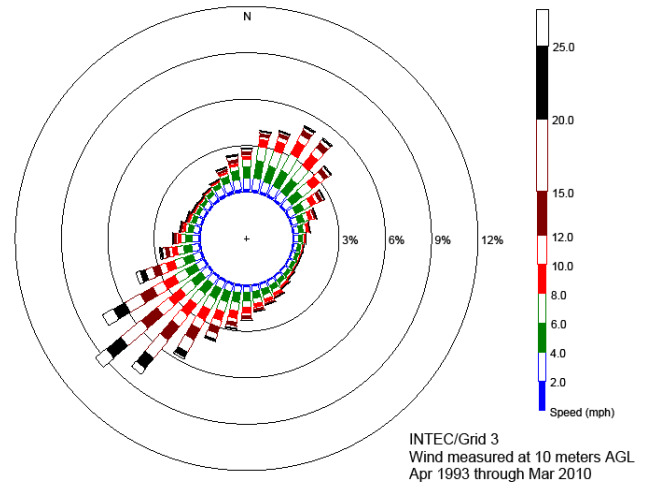
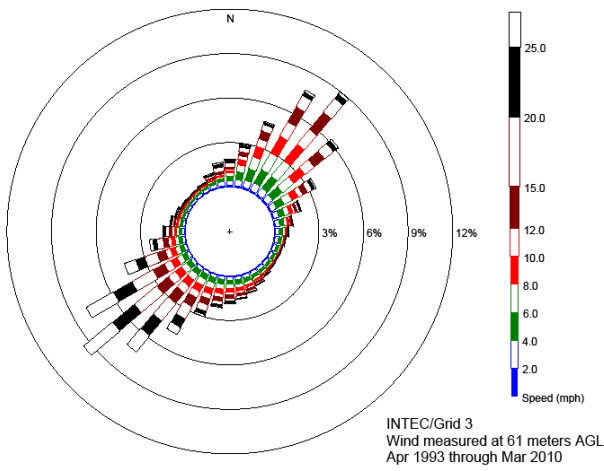
14 USGS topographic maps, which comply with the scale requirement of 1.0 in. = 200 ft under
15 IDAPA 58.01.05.012 [40 CFR 270.14(b)(19)], are not available for the INL. From USGS maps provided,
16 it is evident that the INL is located on an extremely flat desert plain.

17 **B-2(b) Wind Roses**

18 Wind rose data for INTEC and ATR, TAN/SMC, CITRC, CFA, NRF, RWMC, and MFC
19 facilities and their surrounding areas are provided in Exhibits B-5 and B-6. These diagrams indicate a
20 general northeast-southwest wind direction.

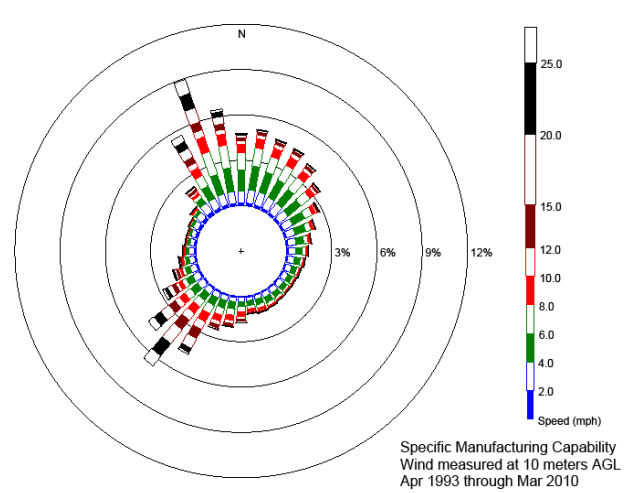
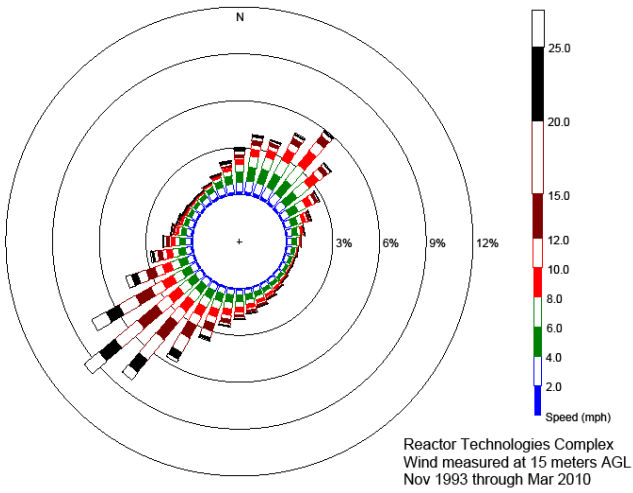
21 **B-2(c) Wells**

22 Updated maps showing the locations of all injection, withdrawal, and monitoring wells at and
23 around the INL are included as Exhibits B-7 and B-8. Additionally, the State of Idaho has been provided
24 with the Idaho National Engineering and Environmental Laboratory Environmental Monitoring Plan
25 (DOE/ID-11088), which provides additional information on wells located at the INL.



INTEC 61M

INTEC 10M



ATR Complex

TAN/SMC

EXHIBIT B-5. INTEC, ATR Complex, and TAN/SMC area wind roses.

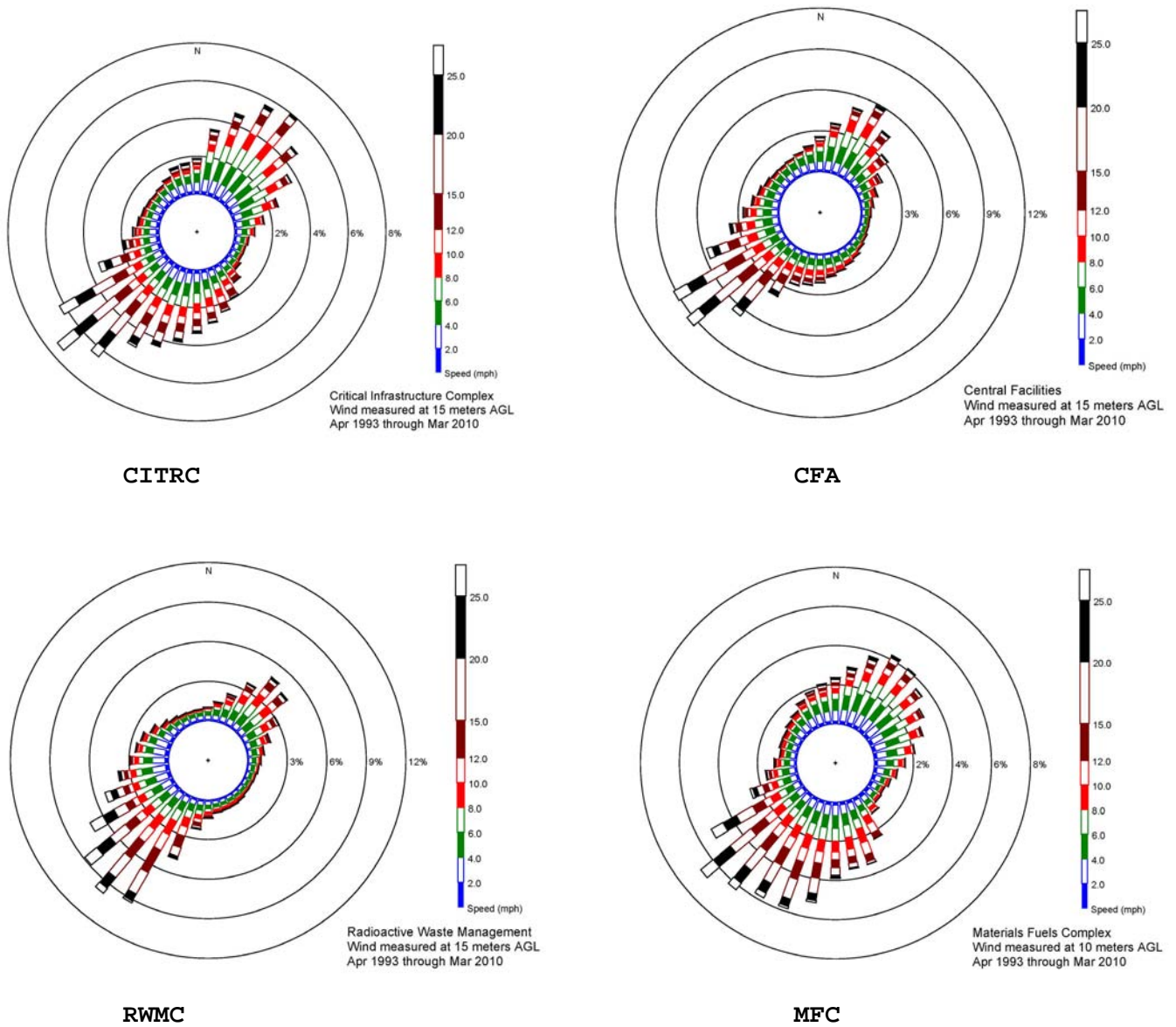


Exhibit B-6. CITRC, CFA, RWMC, and MFC area wind roses.

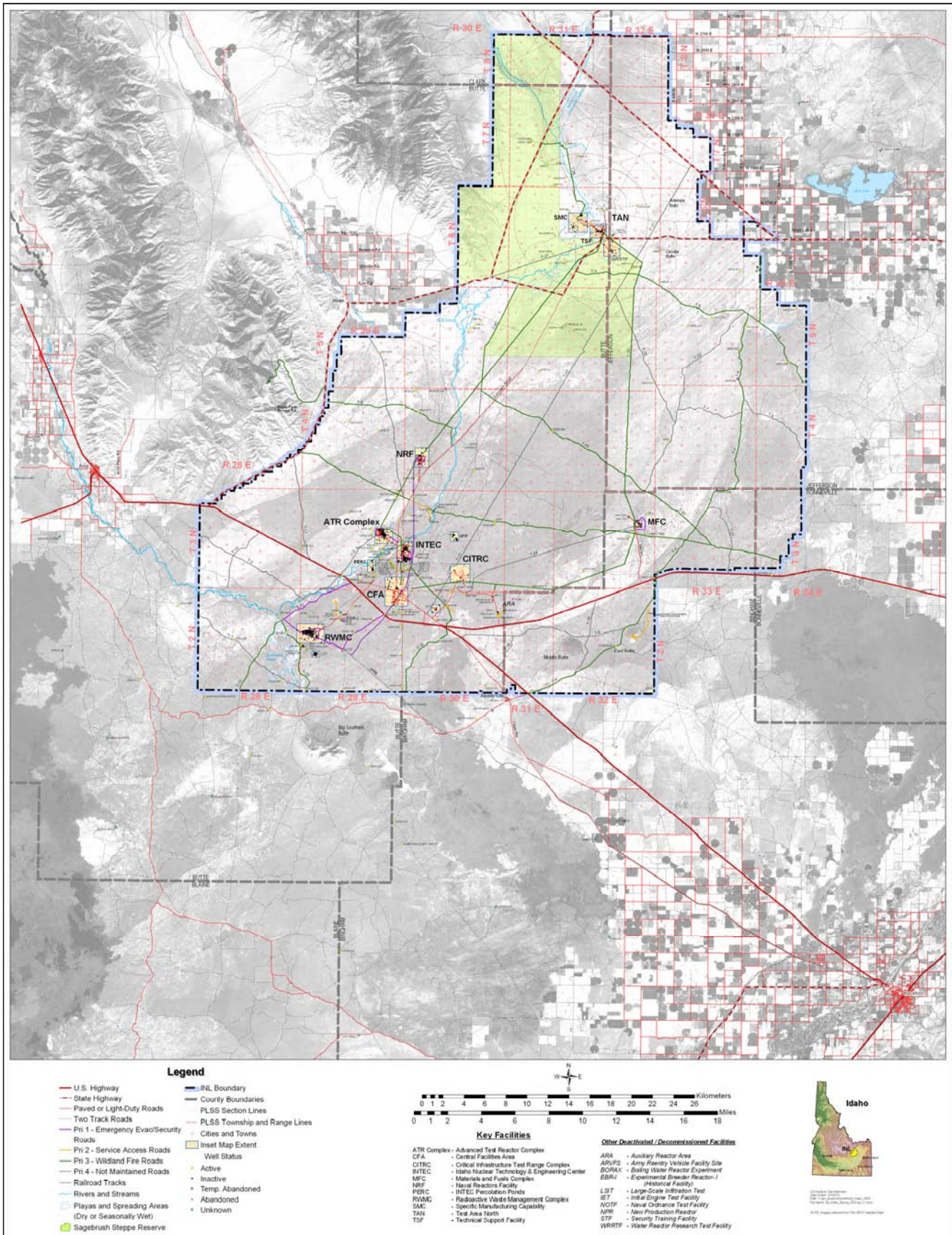


Exhibit B-7. INL sitewide locations of wells



Exhibit B-8. Enlarged Detail of the Locations of Wells at the ATR Complex, CFA, CITRC, INTEC, LSIT, MFC, NPR, NRF, PERC, RWMC, SMC, STF, TSF, and WRRTF

1 **B-2(d) Surrounding Land Use**

2 The federal government, the State of Idaho, and private parties own lands immediately
3 surrounding the INL site. Land uses on federally owned land adjacent to the INL consist of grazing,
4 wildlife management, mineral and energy production, and recreation. State-owned lands are used for
5 grazing, wildlife management, and recreation. Private lands near the INL are used primarily for grazing
6 and farming; irrigated farmlands make up approximately 25% of the land bordering the INL. Several
7 small rural communities are scattered around the borders of the INL: Howe, Mud Lake, Terretton, Atomic
8 City, Butte City, and Arco. The larger communities of Rexburg, Idaho Falls, Blackfoot, and Pocatello are
9 located to the east and southeast of the INL site. The Fort Hall Indian Reservation is located southeast of
10 the INL site.

11 Land immediately outside INL boundaries is used mainly for free-range livestock grazing.
12 Within INL boundaries, approximately 60% of INL land area is open to cattle or sheep grazing by permit;
13 Exhibit B-9 identifies these areas. Some irrigation farming occurs in areas near INL boundaries. Large
14 areas of land are irrigated near the Snake River, approximately 32 km (20 mi) southeast of INL, and in the
15 vicinity of Mud Lake.

16 The INL site and adjacent areas are not likely to experience large-scale residential and
17 commercial development because the INL is remotely located from most developed areas. However,
18 recreation and agricultural uses are expected to increase in the surrounding area in response to greater
19 demand for these types of land uses.

20 Other uses of the land are severely limited because of the climate, lava flows, and general desert
21 soil characteristics. The only INL land suitable for farming is near the terminations of the Big Lost River
22 and Little Lost River, near the town of Howe, and to a distance of 13 km (8 mi) southeast from Howe.

23 Arable land with a moderate irrigation limitation (gravity irrigation) is present on both sides of
24 the Big Lost River and in the remains of the lake bed of prehistoric Lake Terretton (between Mud Lake
25 and Howe). The remainder of the INL, approximately 65% of the surface area, has a low subsurface
26 water-holding capacity, is rocky or covered with basalt, or is classified as having moderate-to-severe
27 limitations for agricultural irrigation.

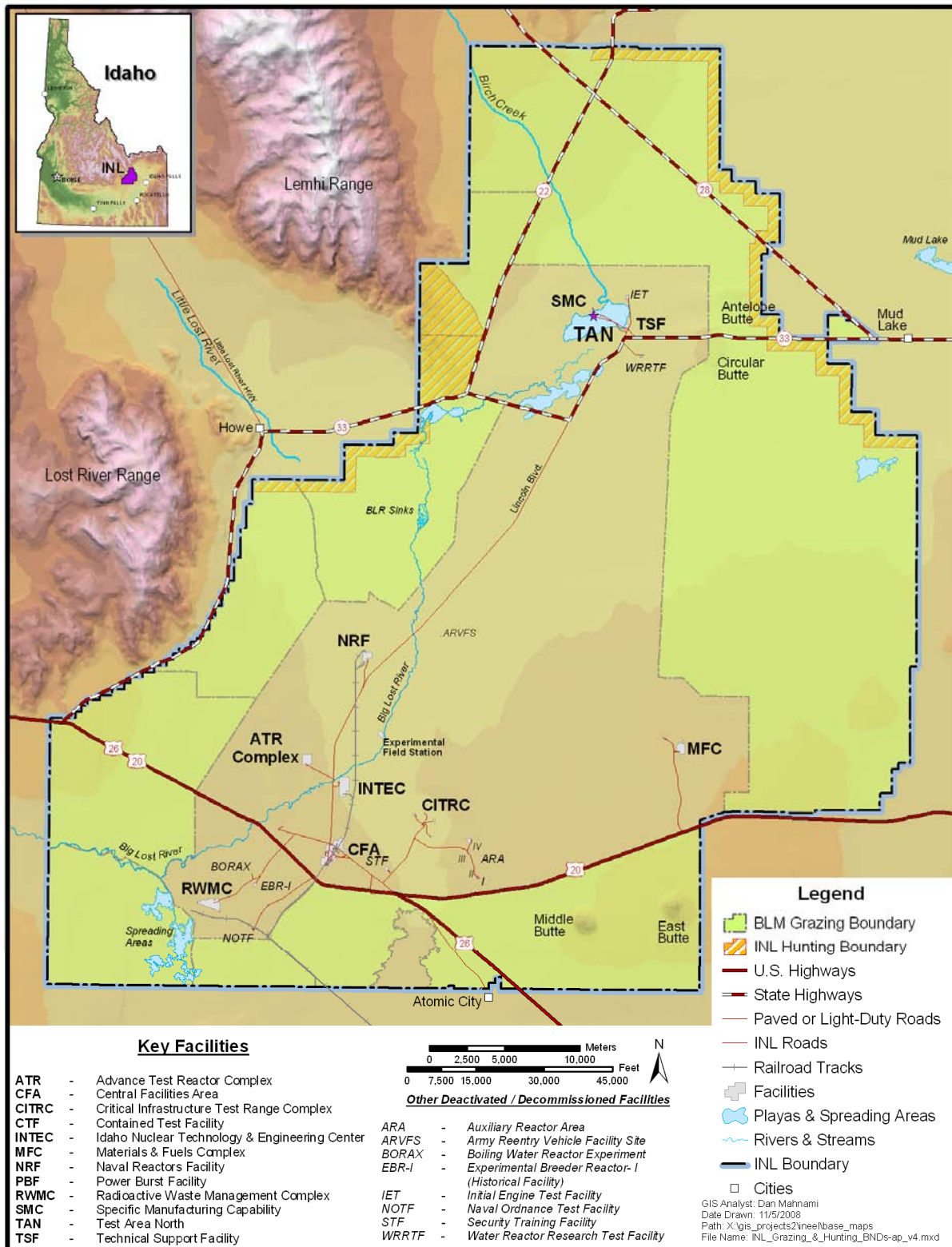


Exhibit B-9. Grazing areas at the INL.

1 **B-2(e) Access Control**

2 The INL is a restricted area patrolled by armed security personnel. No unauthorized access is
3 permitted. Access control to the INL is maintained by security personnel stationed in gatehouses on East
4 Portland Avenue, just off U.S. Route 20; on Van Buren Boulevard, just off U.S. Route 20/26; on Lincoln
5 Boulevard near TAN; at the MFC, and the RWMC. Access badges are required to proceed beyond these
6 points. Additional access controls exist via gatehouses within the INL at ATR, INTEC, and NRF.
7 Access controls in the vicinity of waste management units are described further in Subsection B-4 of this
8 permit application. Details on access controls and specific security features, such as fencing, are
9 discussed in subsequent volumes of this permit application as pertinent to specific waste management
10 units.

11 **B-2(f) Other Structures**

12 The term "other structures" refers to storm, sanitary, and process sewerage systems; loading and
13 unloading areas; fire control facilities; and intake/discharge structures. These systems and facilities are
14 described in subsequent volumes of this permit application as pertinent to specific waste management
15 units. The INL has no intakes or discharges.

16 **B-3 Location Information**

17 The INL is located along the western edge of the ESRP in southeastern Idaho, approximately
18 between latitudes N 43°28' to N 44°02' and longitudes E 112°26' to E 113°15'. The following subsections
19 describe how the INL complies with the seismic and floodplain standards under IDAPA 58.01.05.008 and
20 .012 [40 CFR 264.18 and 40 CFR 270.14(b)(11)].

21 **B-3(a) Seismic Standard (IDAPA 58.01.05.008 and 58.01.05.012 [40 CFR 264.18(a)**
22 **and 270.14(b)(11)(i-ii)])**

23 INL hazardous and mixed waste management units are located in either Butte or Bingham
24 County. Only Bingham County is listed in IDAPA 58.01.05.008 (Appendix VI to 40 CFR 264) as
25 requiring demonstration of compliance with the seismic standard. The MFC facility operates hazardous
26 waste management units that are located in Bingham County, and thus, subject to the seismic standard
27 compliance requirement which is addressed, as applicable, in the MFC HWMA/RCRA Final Partial Part
28 B Permits.

29 USGS data, as detailed in USGS Miscellaneous Investigation Map I-2330, *Geologic Map of the Idaho*
30 *National Engineering Laboratory and Adjoining Areas, Eastern Idaho, 1994*, indicates there are not any

1 faults or other known evidence of Holocene horizon motion within 914 m (3,000 ft) of the RTF. A copy
2 of this map is included as Exhibit B-10.

3 **B-3(b) Floodplain Determination and Prevention of Washout (IDAPA 58.01.05.008**
4 **and 58.01.05.012 [40 CFR 264.18(b) and 270.14(b)(11)(iii-iv)])**

5 As noted above, the INL hazardous and mixed waste management units are located in Butte and
6 Bingham Counties. The Federal Emergency Management Agency (FEMA) Flood Insurance Rate Maps
7 (FIRM) for Butte and Bingham Counties are provided in Appendix II.

8 Four flood zones are identified on the FIRMs: Zone A indicates areas subject to 100-yr floods;
9 Zone B indicates areas between the limits of 100- and 500-yr floods; Zone C indicates areas of minimal
10 flooding; and Zone D indicates areas of undetermined, but possible flood hazards.

11 Federal Insurance Administration (FIA) floodplain maps are normally used to delineate 100-yr
12 floodplains and to determine if a given facility is located within or outside of a 100-yr riverine floodplain.

13 FIRMs exist for the portions of the INL that are within Bingham County. However, for the
14 portions of the INL that are within Butte County, only a FIRM index map is available. The Butte County
15 FIRM Index Map indicates that the map panels that would cover the areas of INL facilities were not
16 published, which means FEMA did not perform hydrologic analyses in these areas. On the index map,
17 these areas are classified as being in “Zone D,” which is defined as “undetermined but possible flood
18 hazards.” For Butte County, all of the panels addressing the area covering the INL are within Zone D, as
19 indicated in the footnote to the map. As shown on the county index map for the INL area, the following
20 individual panels in map series 160033 have not been published: 0400 A, 0425 A, 0550 A, 0575 A, 0600
21 A, 0775 A, 0800 A, 0825 A, 0850 A, 1000 A, 1025 A, 1050 A, 1075 A, 1100 A, 1225 A, 1250 A, 1275
22 A, and 1300A.

23 For Bingham County, MFC facilities are located in the area addressed in Panel
24 160018 0050 B; the footnote to the map indicates that this panel is not published, but the area is
25 designated Zone C. Also, for Bingham County, Map Panel No. 25 of 750, Section 11, includes a small
26 part of the west side of the MFC area designated as Zone C. Facilities located in that area are TREAT
27 area Buildings 720 and 721. None of the hazardous or mixed-waste management units to be permitted are
28 located in those buildings. Map panel no. 25 of 750 is also included in Appendix II.

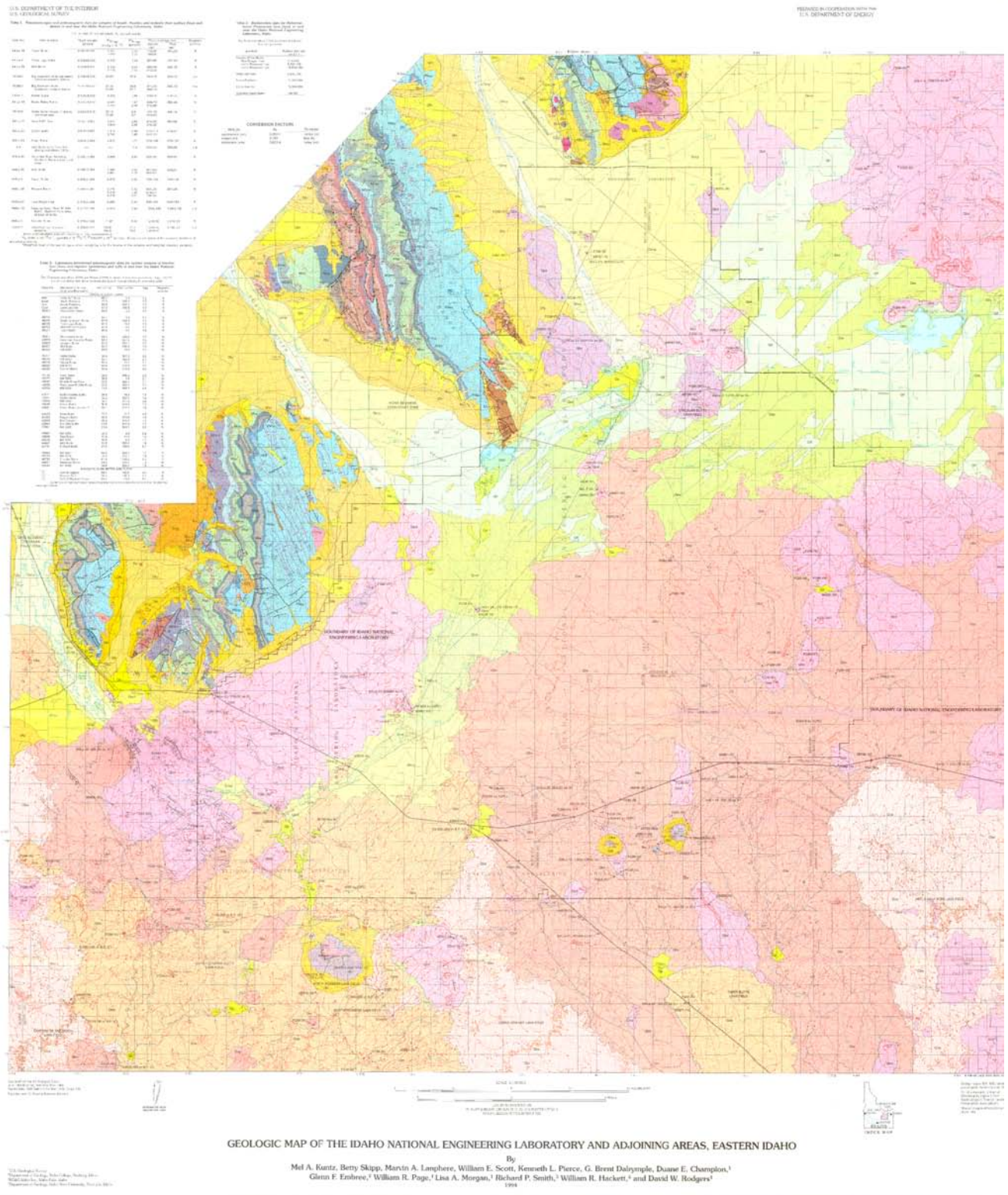


Exhibit B-10. USGS miscellaneous investigation map I-2330 (west portion of map).

NOTE: This information is also available electronically on the CD found in Appendix I

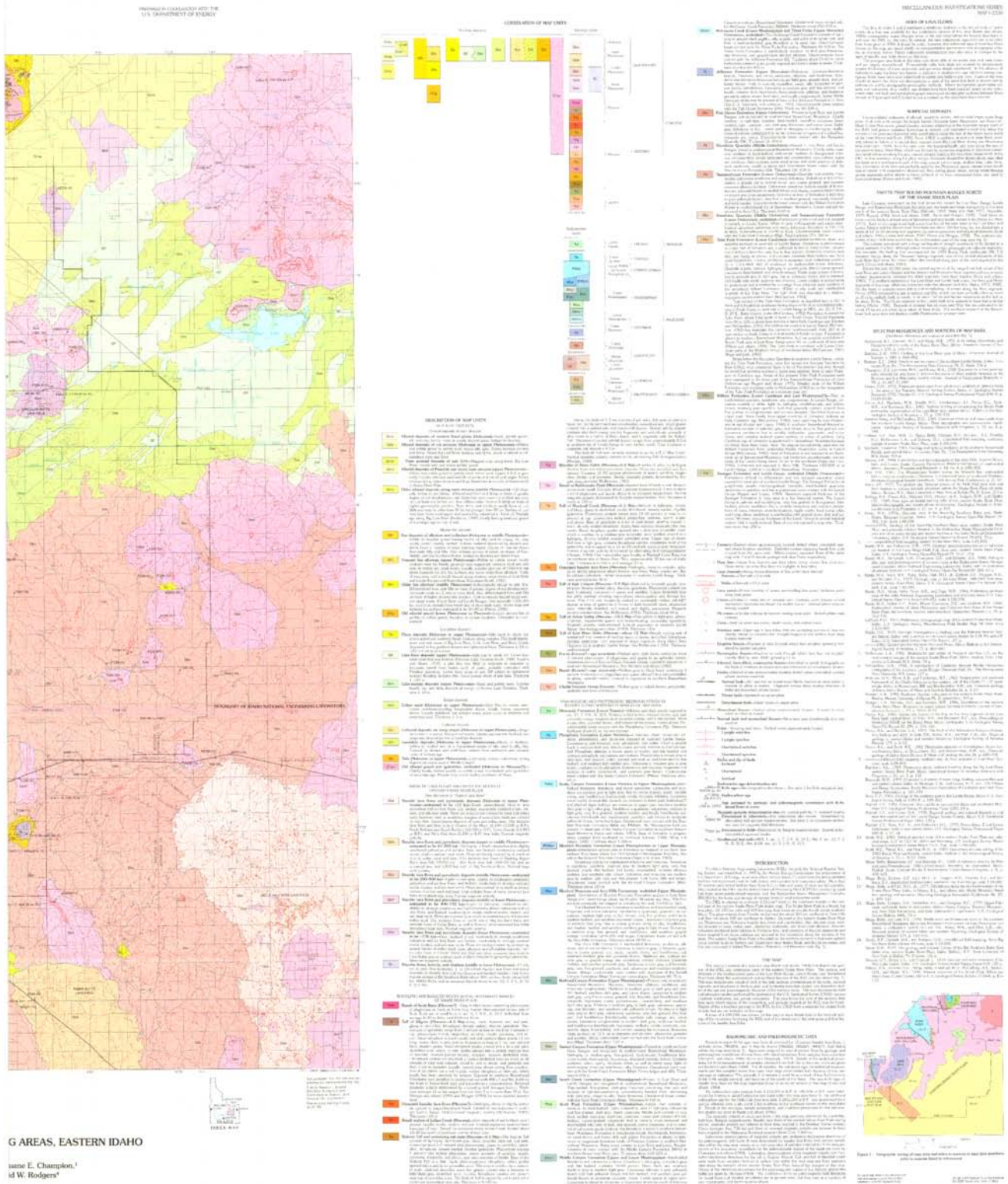


Exhibit B-10. USGS miscellaneous investigation map I-2330 (east portion of map).

NOTE: This information is also available electronically on the CD found in Appendix I

1 Aside from indicating that there may be areas of undetermined but possible flood hazards, the
2 existing FEMA maps do not clearly substantiate whether or not a facility is in the floodplain. As these
3 maps indicate possible but undetermined flood hazards in areas within the INL, FIA equivalent mapping
4 techniques have been employed to determine the elevations of the Big Lost River and Birch Creek floods
5 with respect to INL facilities.

6 The elevation of the 100-yr flood from the Big Lost River with respect to INL facilities is
7 described in Subsection B-3(b)(1) below. The 100-yr flood potential from Birch Creek with respect to
8 INL facilities is described in Subsection B-3(b)(2) below. The existing flood control systems at the INL
9 are described in Subsection B-3(b)(3) below. Flood potential from localized events (such as the 25-yr,
10 24-hr storms, 100-yr precipitation events and rapid snowmelt) for INTEC are described in
11 Section B-3(b)(4) below. The controls for protection against those events are presented in subsequent
12 waste management unit-specific volumes of this permit application.

13 **B-3(b)(1) Flood Potential from the Big Lost River**

14 Floodplain determinations, engineering and structural analyses, in accordance with IDAPA
15 58.01.05.012 [40 CFR § 270.14(b)(11)(iv and v)] are performed for RCRA facilities that are within the
16 100-yr floodplain. The results of engineering analyses are reported in engineering design files (EDFs)
17 generated by INL personnel and presented in the respective waste management unit-specific permits or
18 applications. An EDF will typically provide a description of the RCRA facility's construction
19 parameters, engineering analysis to indicate the various hydrodynamic and hydrostatic forces expected to
20 result at the site as a consequence of a hypothetical 100-yr flood, structural or other engineering studies
21 showing the design of operational units and flood protection devices at the facility and how these will
22 prevent washout. If applicable, and in lieu of the above engineering analyses, a detailed description of
23 procedures to be followed to remove hazardous waste to safety before the facility is flooded may be
24 provided. Such procedures will be presented, if applicable, in subsequent waste management unit-
25 specific volumes of this permit application.

26 In January 2006, the DOE-ID provided the contractors with the "Big Lost River Flood Hazard
27 Study, Idaho National Laboratory, Idaho, U.S. Bureau of Reclamation, 2005" by D. A. Ostenna and D. H.
28 O'Connell, to be used for all Big Lost River flood hazard characterization and delineation efforts on the
29 INL. A copy of this study is provided electronically in Appendix III. This map will be used for
30 determination of whether or not INTEC units are located within the 100-year floodplain of the Big Lost
31 River. Since a previous study provided a more conservative and higher elevation floodplain, buildings
32 previously determined to be within the floodplain have already been evaluated to the more conservative
33 standard. As determinations of floodplain change or new facilities are added, additional EDFs will be

1 prepared as necessary and modification to the unit specific permits will be submitted to the DEQ for
2 approval and incorporation into the permits.

3 **B-3(b)(2) Flood Potential from Birch Creek**

4 Birch Creek flows onto the northern part of the INL and ends in the Birch Creek Playa near TAN.
5 In 1997, the USGS simulated the water surface elevations from the 100-yr peak flows and peak volumes
6 in Birch Creek. Because of the highly braided nature of Birch Creek and several anthropogenic features
7 of the INL, the USGS could only determine the floodprone, not floodplain areas. The methodologies,
8 assumptions, and calculations used by the USGS, and their findings, are summarized in the 1997 report
9 entitled, *Simulation of Water-Surface Elevations for a Hypothetical 100-Year Peak Flow in Birch Creek*
10 *at the Idaho National Engineering and Environmental Laboratory, Idaho*, found in Appendix IV. The
11 100-yr floodprone map of INL from Birch Creek is also shown in the report found in Appendix IV.

12 The Birch Creek study also determined that the potentially affected facilities were protected from
13 the 100-yr flood event by the diking system described in Subsection B-3(b)(3) below.

14 **B-3(b)(3) Flood Diversion Systems at the INL**

15 The Big Lost River intermittently flows through the INL and is the nearest surface body of water
16 with a potential influence to southwestern and central INL facilities. The Big Lost River is controlled by
17 the Mackay Dam, an irrigation storage reservoir, 48 km (30 mi) northwest of Arco. In 1958, a flood
18 diversion system was built along the Big Lost River near the western boundary of the INL, to divert flows
19 on the river that might create flood hazards for INL facilities. This system consists of a small earthen
20 diversion dam and a headgate that diverts water from the main channel, through a connecting channel,
21 and into four spreading areas (A, B, C, and D). Spreading area A is bounded on the southeast by a dike;
22 spreading area B is bounded on the northeast by a dike; and spreading area D is bounded on the southern
23 edge by a dike. Spreading area C has no dike. The present capacity of the diversion system is 58,000
24 acre-ft at an elevation of 5,050 ft (1,540 m) (McKinney 1985). Flow upstream (near Arco) and
25 downstream of the diversion dam, as well as into the diversion channel, is monitored by several USGS
26 gauging stations (Stone et al. 1993).

27 Flood control dikes and drainage systems have been constructed at TAN and include emergency
28 channels on the Birch Creek fan, dikes around the Contained Test Facility, and a dike system around the
29 west end of TAN (Berenbrock and Kjelstrom 1997). These systems were constructed in response to
30 flooding at the Birch Creek playa in 1969. The flood control dikes measure approximately 1.2 m (4 ft)
31 high. This dike system has a capacity of 13,000 acre-ft of water at an elevation 2 feet lower than the top
32 of the dikes (Berenbrock and Kjelstrom 1997).

1 **B-3(b)(4) INTEC 100-Year Storm Water Runoff and 25-Year Runoff Analysis**

2 To ensure that all potential sources of flooding were evaluated for INTEC units, the report “100-
3 Year Storm Water Runoff Floodplain and 25-Year Runoff Analyses for the Idaho Nuclear Technology
4 and Engineering Center at the Idaho National Engineering and Environmental Laboratory” (INEEL/EXT-
5 03-01174, Revision 1, January 2004) was prepared. A copy of this report is provided electronically in
6 Appendix V. This study evaluated the largest 25-year and 100-year storm water flood flows through and
7 in the vicinity of INTEC and determined no flooding impacts to RCRA buildings at INTEC.

8 **B-4 Traffic Information [IDAPA 58.01.05.012; 40 CFR 270.14(b)(10)]**

9 The following subsections describe the traffic pattern, volume of traffic (number, types of
10 vehicles), and INL traffic controls used for off-Site and on-Site traffic.

11 **B-4(a) Off-Site Traffic**

12 The INL is accessible from several highways, shown in Exhibit B-11 and described in Table B-1.
13 Approximately 145 km (90 mi) of highways pass through the southern and northern sections of the INL
14 and are used by the general public. U.S. Highways 20 and 26 are the main access routes through the
15 southern portion of the INL, and Idaho State Routes 22, 28, and 33 pass through the northern portion of
16 INL. Table B-2 shows the baseline (1995) traffic for several of these routes.

17 Four major modes of INL-related transit use the regional highways, community streets, and INL
18 roads to transport people and property: DOE buses and shuttle vans, DOE motor pool vehicles,
19 commercial vehicles, and personal vehicles. Table B-3 summarizes the baseline miles and actual 2004
20 miles for INL-related traffic. Bus traffic is heaviest on nearby highways between 5:00 and 8:00 a.m. and
21 4:00 and 7:00 p.m., Monday through Thursday.

Table B-1. Description of the highway system in the INL vicinity.

Route	Description
I-15	From the Utah/Idaho state line south of Malad northerly through Pocatello, Blackfoot, Idaho Falls, and Dubois to the Idaho/Montana state line at Monida Pass.
I-84	From the Oregon/Idaho state line south of Payette southeasterly through Boise, Mountain Home, Twin Falls and the Burley/Rupert area south to the Idaho/Utah state line.
I-86	From a junction with I-84 east of the Burley/Rupert area, northeasterly to a junction with I-15 in Pocatello.
U.S. 20	From the Idaho/Oregon state line near Nyssa, Oregon, easterly through Boise, Carey, Arco, Idaho Falls, Rigby, and Rexburg to the Idaho/Montana state line near West Yellowstone, Montana.
State Highway 22	From a junction with U.S. 20/26 east of Arco northeasterly through Howe to Dubois; combines with State Highway 33 from its beginning at its junction with U.S. 20/26 to it's junction with State Hwy 33 east of Howe.
U.S. 26	From the Idaho/Oregon state line near Nyssa, Oregon, easterly through Boise, Carey, Arco, Blackfoot, and Idaho Falls to the Idaho/Wyoming state line near Alpine.
State Highway 28	From a junction with I-15 north of Roberts, northwesterly to Terreton, Mud Lake, Leadore, and Lemhi to a junction with U.S. 93 in Salmon.
State Highway 33	From a junction with U.S. 20/26 east of Arco, easterly and northerly to Howe, Mud Lake, Terreton, and Rexburg, and then to the Idaho/Wyoming state line.

Table B-2. Baseline traffic for selected highway segments in the vicinity of INL.

Route	Average daily traffic (number of vehicles)	Peak hourly traffic (number of vehicles)
U.S. Highway 20-Idaho Falls to the Idaho National Engineering and Environmental Laboratory (INL)	2,290	344
U.S. Highway 20/26-INL to Arco	1,500	225
U.S. Highway 26-Blackfoot to INL	1,190	179
State Route 33-west from Mud Lake	530	80
Interstate 15-Blackfoot to Idaho Falls	9,180	1,380

Source: DOE 1995 and DOE 2005.

Table B-3. Baseline annual vehicle miles traveled for traffic related to the INL.

Transit mode	Vehicle miles traveled	Actual mileage traveled in 2004
Department of Energy (DOE) buses	6,068,200	2,639,873
Other DOE vehicles	9,183,100	6,153,406
Personal vehicles on highways to the Idaho National Laboratory	7,500,000	not available
Commercial vehicles	905,900	268,850
TOTAL	23,657,200	

Source: DOE 1995 and DOE 2005.

1 **B-4(b) On-Site Traffic**

2 The INL has an additional 140 km (87 mi) of paved roads within its boundaries, not open to the
3 public; approximately 30 km (18 mi) of the roads are considered service roads. Over 160 km (100 mi) of
4 unpaved roads and trails at the INL are used for emergency, service, and security vehicle access.

5 Union Pacific Railroad lines provide railroad freight service to Idaho Falls from Butte, Montana, to the
6 north, and from Pocatello, Idaho, and Salt Lake City, Utah, to the south. The Union Pacific Railroad's Arco
7 branch runs from Pocatello through Blackfoot to the INL. This branch crosses the southern portion of the Site,
8 providing rail service to the INL. This branch connects at the Scoville Siding with a DOE spur line, which
9 links with developed areas within the INL. The Arco branch also passes approximately 0.8 km (0.5 mi) south
10 of the RWMC. In 1974, a railroad spur to TSA was completed to permit direct shipment of waste to RWMC.
11 Rail shipments to and from the INL usually are limited to bulk commodities, SNF, and radioactive waste.

12 The following subsections present on-Site traffic information for the INTEC, the RWMC, and the
13 MFC, where permitted, interim status, and to be permitted waste management units are located. Traffic
14 information for the AMWTP Facility (which is located within the boundary of the RWMC and has a separate
15 security controlled entrance) may be found in the AMWTP HWMA/RCRA Storage Permit or the AMWTP
16 HWMA/RCRA Treatment Permit.

17 **B-4(b)(1) INTEC Traffic**

18 Access to INTEC is via Lincoln Boulevard to Cleveland Boulevard, which leads to the west side of the
19 facility, the general parking area and primary access portal to the facility. The heaviest traffic on INL roads
20 leading to INTEC occurs between 5:00 and 8:30 a.m. and again from 4:00 to 7:30 p.m., Monday through
21 Thursday. Traffic consists primarily of site transit busses, employee private vehicles, and government
22 contractor vehicles that come from various communities near/surrounding the INL.

23 The INTEC complex is surrounded by perimeter fence. Personnel and vehicle access to and from the
24 INTEC is through entry portals at locations on the east and west sides of the complex. (see Exhibit B-12).
25 Vehicles must pass through a gate arrangement that allows security personnel to conduct thorough inspections.
26 Personnel must pass through the security station to obtain proper dosimetry and verify they have the proper
27 identification and access credentials to gain access to the complex. Personnel who do not have normal access
28 to the INTEC complex are escorted by a person who does.

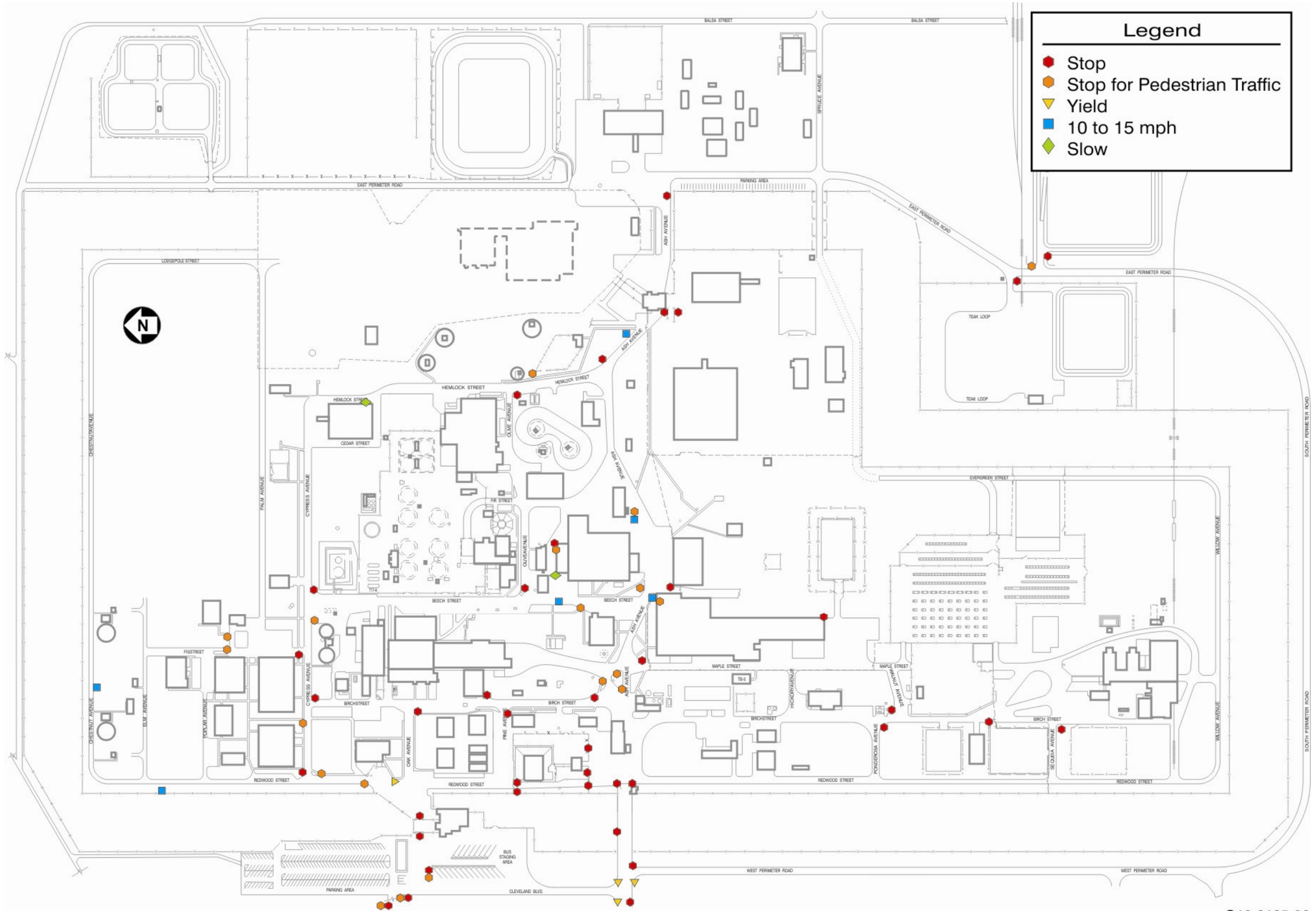


Exhibit B-12. Access and traffic control at INTEC.

G10-2125-06

1 **B-4(b)(2) RWMC Traffic**

2 U.S. Route 20/26 is the general access route for the RWMC. Van Buren Boulevard intersects
3 U.S. 20/26 northeast of the RWMC and is the direct access road leading to EBR-I. Adams Boulevard
4 intersects Van Buren Boulevard just north of EBR-I and is the direct access road leading to the RWMC
5 personnel security and control area. Trucks transporting waste shipments to and from RWMC travel
6 these roads. The heaviest traffic on the roads leading to RWMC occurs between 5:00 and 8:30 a.m. and,
7 again, from 4:00 to 7:30 p.m., Monday through Thursday. Traffic consists primarily of site transit buses,
8 employee-driven private vehicles, and government contractor vehicles that come from various
9 communities near/surrounding the INL. From Memorial Day until Labor Day, private vehicle traffic
10 increases slightly on Van Buren Boulevard, as tourists visit the EBR-I landmark.

11 The RWMC is contained within a security fence. There are two access security stations: one for
12 the RWMC and one for the AMWTP. The following information does not pertain to the AMWTP.
13 Vehicles entering the facility must pass through a one-gate arrangement that allows security personnel to
14 conduct thorough inspections. Personnel must pass through the security station to verify they have proper
15 identification and access credentials. Personnel or visitors without proper credentials are escorted while
16 on the RWMC site. While employees can get to the RWMC through the AMWTP, they are directed to go
17 through the security station located at the RWMC entrance for access to the RWMC.

18 The roads accessing the RWMC are made of asphalt and all have load-bearing capacities of 68
19 metric tons (75 tons). The daily volume of vehicles traveling to the RWMC and the AMWTP currently
20 averages 350 to 400 vehicles, mainly cars or trucks. The average number of vehicles will vary depending
21 upon activities taking place at the RWMC and the AMWTP locations.

22 **B-4(b)(3) MFC Traffic**

23 U.S. Route 20 is the general access route for MFC. Taylor Boulevard intersects U.S. 20 south of
24 MFC and is the direct access road leading to the personnel security and control area. Taylor Boulevard is
25 a 5.6 km paved roadway. A right turn off Taylor Boulevard leads to the MFC entrance. The heaviest
26 traffic on the MFC site roads occurs between 6:00 and 8:30 a.m. and, again, from 4:00 to 6:30 p.m.,
27 Monday through Friday. Traffic consists primarily of site transit buses, employee-driven private vehicles,
28 and government contractor vehicles from various communities near/surrounding the INL.

29 The MFC is located within a security fence. All access is attained through a security station
30 located at the MFC entrance. Vehicles must pass through a two-gate arrangement that allows security
31 personnel to conduct thorough inspections. Personnel must pass through the security station to obtain
32 proper dosimetry and verify they have proper identification and access credentials. Personnel or visitors
33 without proper credentials are escorted while on the MFC site.

1 Access to HWMA units and facilities within MFC is provided by a network of paved and gravel
2 roadways. Any one of these roadways may be used to transport hazardous or mixed waste among MFC
3 facilities. Transport from MCF facilities to other facilities on the INL site is done via U.S. 20. The roads
4 accessing the MFC are constructed of asphalt, with load-bearing capacities of 68 metric tons (75 tons).
5 Roads within the MFC area, used to transport hazardous/mixed waste, have been tested to 45,000 kg
6 (100,000 lb) single-axle loading. Traffic is limited, consisting of a stop sign at one blind intersection, a
7 yield sign at another intersection, and a 15-mph speed limit throughout the site. Traffic is limited to a few
8 government vehicles assigned to the MFC for maintenance and material movement.

9 B-5 Literature Cited

- 10 Carpenter, N.S. (2010) Compilation of Earthquakes from 1850-2007 within 200 miles of the Idaho
11 National Laboratory, Battelle Energy Alliance External report, INL/EXT-10-19120, 65 p.
- 12 EPA/DOE/State of Idaho, 1991, *Federal Facility Agreement and Consent Order and Action Plan*, U.S.
13 Department of Energy, Idaho Operations Office: Idaho Department of Health and Welfare,
14 Division of Environmental Quality: U.S. EPA, Region 10, August 18.
- 15 DOE, Department of the Navy, State of Idaho, 1995, Settlement Agreement to Public Service Co. of
16 Colorado v. Batt, No. CV 91-0035-S-EJL (D. Id.) and United States v. Batt,
17 No. CV-91-0065-S-EJL (D. Id.). October 16.
- 18 Berenbrock, C. and L. C. Kjelstrom, 1997, "Simulation of Water-Surface Elevations for a Hypothetical
19 100-Year Peak Flow in Birch Creek at the Idaho National Engineering and Environmental
20 Laboratory, Idaho," *U.S. Geological Survey Water-Resources Investigations Report 97-4083*,
21 DOE/ID-22138.
- 22 DOE, 1995, *Department of Energy Programmatic Spent Nuclear Fuel Management and Idaho National*
23 *Engineering Laboratory Environmental Restoration and Waste Management Programs Final*
24 *Environmental Impact Statement*, Volumes 1, 2, & 3, EIS-0203F; U.S. Department of Energy,
25 Office of Environmental Management, Idaho Operations, April.
- 26 DOE, 2005, *2005 Supplemental Analysis of the INL Site Portion of the April 1995 Programmatic Spent*
27 *Nuclear Fuel Management and Idaho National Engineering Laboratory Environmental*
28 *Restoration and Waste Management Programs Final Environmental Impact Statement*,
29 DOE/EIS-0203-F-SA-02, United States Department of Energy, Idaho Operations Office, June.
- 30 DOE-ID, 2004, Idaho National Engineering and Environmental Laboratory Environmental Monitoring
31 Plan, DOE/ID-11088, Department of Energy Idaho Operations Office, Idaho Falls, Idaho, April.

- 1 INL, 2008, *Hazardous Waste Management Act/Resource Conservation and Recovery Act (HWMA/RCRA)*
2 *Work Plan for the Idaho National Laboratory (INL)*, EPA No. ID4890008952, Idaho National
3 Laboratory, Idaho Falls, Idaho, April 8, 2008.
- 4 INEEL/EXT-03-01174 100-Year Storm Water Runoff Floodplain and 25-Year Runoff Analyses for the
5 Idaho Nuclear Technology and Engineering Center at the Idaho National Engineering and
6 Environmental Laboratory, Revision 1, January 2004.
- 7 McKinney, J. D., 1985, *Big Lost River 1983-1984 Flood Threat*, PPD-FPB-002, EG&G Idaho Inc., Idaho
8 Falls, ID.
- 9 Ostenaar, D. A. and D. R.H. O’Connell, 2005, *Big Lost River Flood Study Idaho National Laboratory,*
10 *Idaho, Summary Document*, Report 2005-2. Seismotectonics and Geophysics Group, Technical
11 Service Center, Bureau of Reclamation, Denver, CO.
- 12 Payne S.J., Gorman V.W., Jensen S. A., Nitzel M.E., Russell M.J., and Smith R.P., 2002, Development of
13 probabilistic design basis earthquake (DBE) parameters for moderate and high hazard facilities at
14 INEEL, Bechtel BW XT Idaho, LLC, External Report INEEL/EXT-99-000775, Final Report,
15 Rev 2, June, 101 pp.
- 16 Stone, M. A. J., L. J. Mann, and L. C. Kjelstrom, 1993, “Statistical Summaries of Streamflow Data for
17 Selected Gaging Stations on and near the Idaho National Engineering Laboratory, Idaho, Through
18 September 1990,” U. S. Geological Survey Water-Resources Investigations Report 92-4196.

1

C. WASTE CHARACTERISTICS

2

The information for this section is contained in the waste management unit-specific volumes of

3

the INL HWMA/RCRA Part B permits, or permit applications.

1

D. PROCESS INFORMATION

2

The information for this section is contained in the waste management unit-specific

3

volumes of the INL HWMA/RCRA Part B permits, or permit applications.

1

E. GROUNDWATER MONITORING

2

The information for this section is contained in the waste management unit-specific volumes of

3

the INL HWMA/RCRA Part B permits, or permit applications.

1 **F. PROCEDURES TO PREVENT HAZARDS**

2 **F-1 Security IDAPA 58.01.05.008 and .012 [40 CFR 264.14(b) and(c), and 270.14(b)(4)]**

3 Security at the INL is maintained by trained security personnel who monitor site access and
4 provide security presence at the various complexes throughout the INL site. The size of INL (890 mi²),
5 and its location with respect to highways (Idaho State Highways 22, 28, and 33, and U.S. Routes 20 and
6 26), have made construction of a Site boundary security fence impractical. Rather, security at the INL
7 and at the waste management units located therein is maintained by a security system, consisting of
8 property warning signs and surveillance patrolling, security access control points placed at the entrances
9 to the various complexes within the INL, and specific security measures taken at the individual areas,
10 such as fencing, warning signs, and building security.

11 Property warning signs read "No Trespassing - By Order of the United States Department of
12 Energy." Signs with this inscription are located along the INL property boundary and along the five
13 public highways that pass through INL property. Exhibit F-1 is an example of this sign. The waste
14 management unit-specific volumes of the INL HWMA/RCRA Part B permits and permit applications
15 address access processes on a unit specific basis.

16 Areas along the boundary of the INL are open to grazing by livestock, as described in Subsection
17 B-2, Surrounding Land Use. Limits of these grazing areas that lie inside the property boundary are
18 denoted by the second type of sign; this sign has the same message as the first, with the addition of "No
19 Grazing Beyond this Point." Exhibit F-2 is an example of this sign.

20 Both types of signs are legible from a distance of 7.6 m (25 ft) and are spaced at regular intervals.
21 Signs are located closer together in areas where the line of sight is obstructed; in such cases, the warning
22 signs are placed where they can be seen. Exhibit F-3 is a schematic diagram of the INL, identifying
23 locations of warning signs, grazing boundaries, and current security stations.

24 Access control points are located at the entry and egress points to and from the various INL
25 complexes. Only authorized personnel and escorted, authorized visitors holding the appropriate
26 identification passes are cleared for entry and egress. Exhibit F-3 identifies the INL boundary and the
27 current access control points. Visitors or authorized personnel without identification passes must check in
28 at these stations.

DOE PROPERTY BOUNDARY SIGN

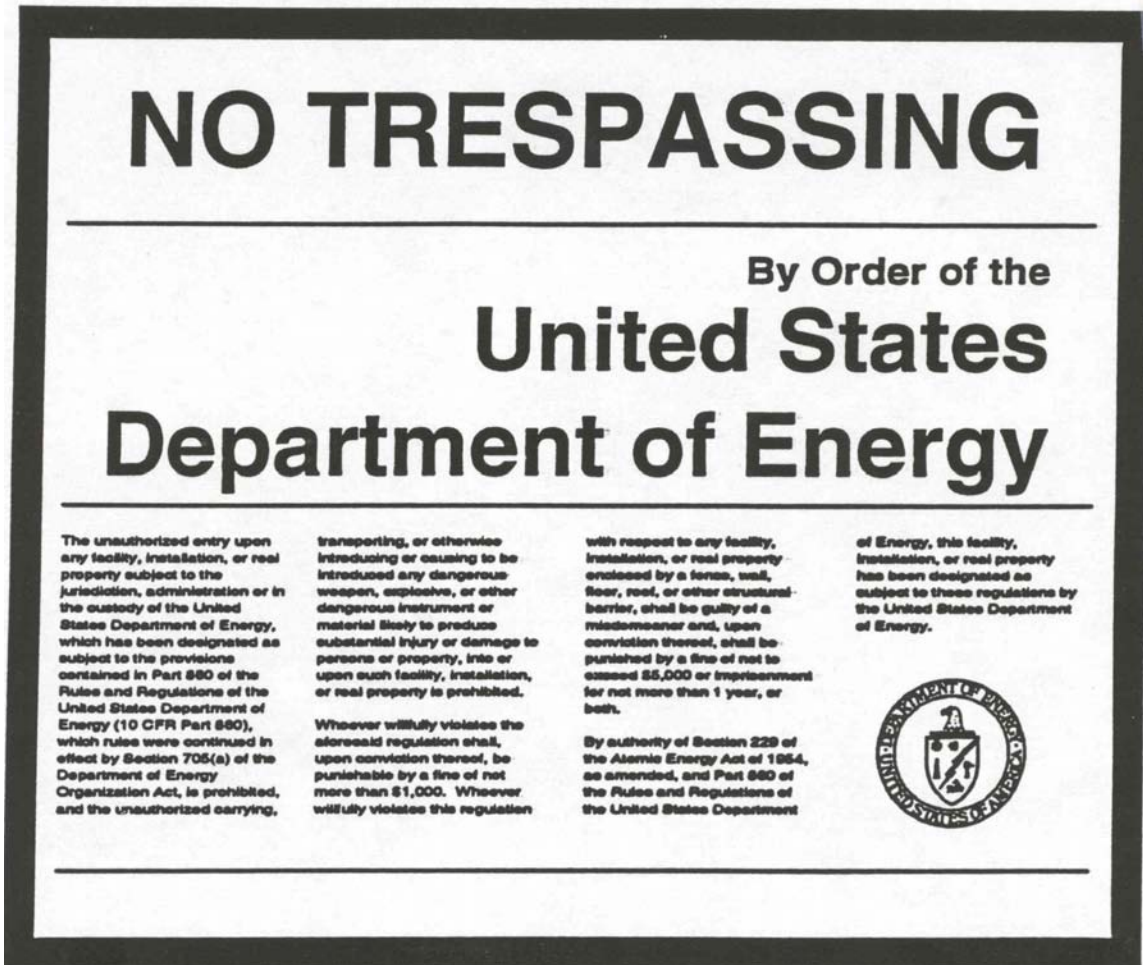


Exhibit F-1. Example of an INL boundary no trespassing sign.

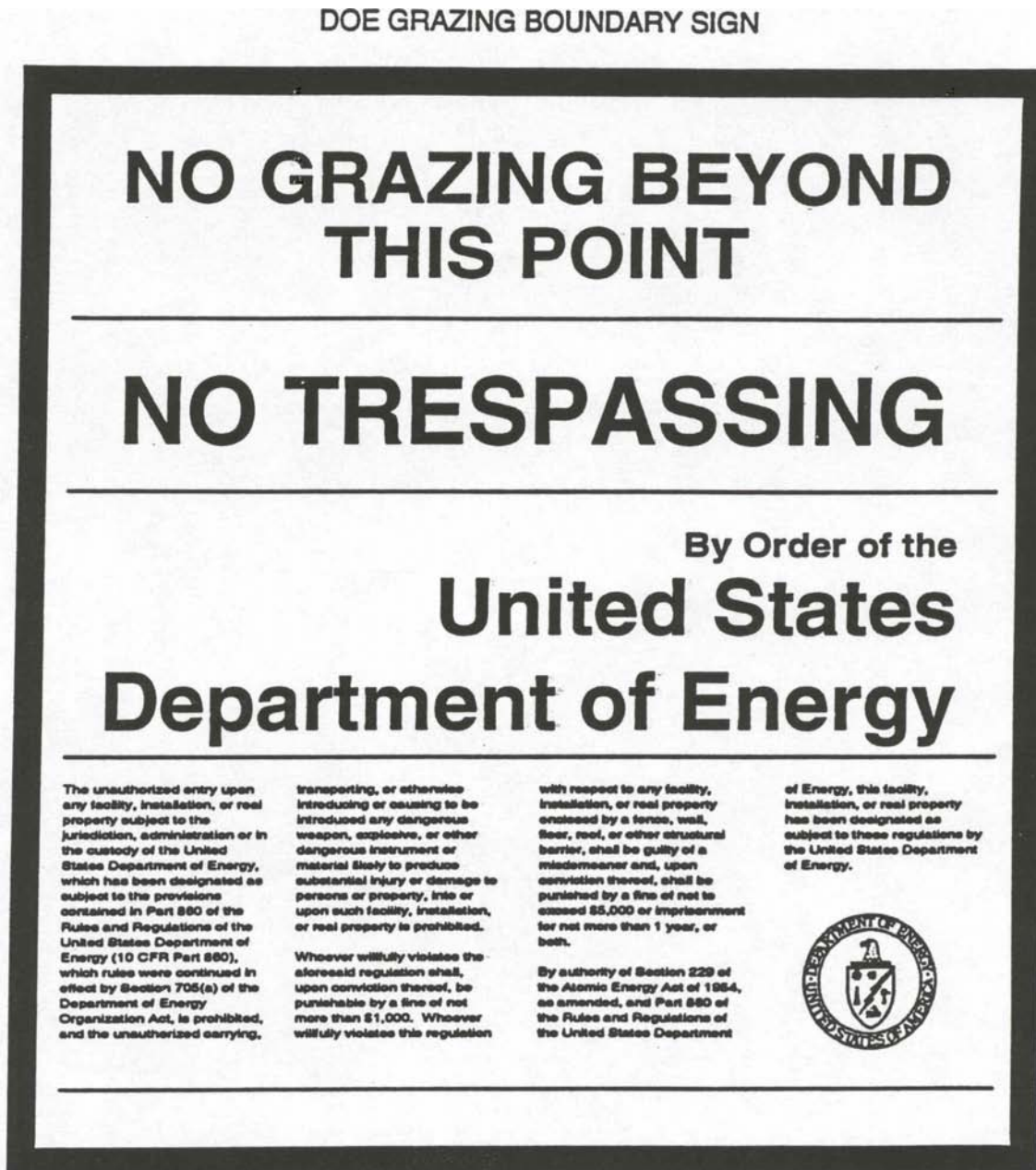


Exhibit F-2. Example of an INL boundary no grazing sign.

1 In addition to the security presence at the manned stations, security personnel randomly patrol
2 INL boundaries, roadways, and facilities in ground patrol vehicles and on foot. All patrol routes are
3 nonrepetitive and random. When a domestic animal or a group of animals has entered an active portion
4 of the INL beyond the designated grazing boundaries, security-surveillance personnel contact security
5 personnel in the area in which the animals have wandered, and if the problem persists, they contact the
6 Bureau of Land Management, who has jurisdiction over wildlife on the INL.

7 Security is specific to each INL area and its component buildings, and involves the use of security
8 fencing, locks on gates, and warning signs placed on the exterior of buildings and within general building
9 areas.

10 Additionally, several other features contribute to the safety and security of the INL, such as,
11 ample lighting throughout the facility areas, security and operations personnel are equipped with two-way
12 communication devices to report upset or trespass conditions, and an internal telephone system that
13 encompasses most of the INL that is used for communication outside INL premises. The waste
14 management unit-specific volumes of the INL HWMA/RCRA Part B permits and permit applications
15 address the requirements associated with security, in more detail, on a unit-specific basis.

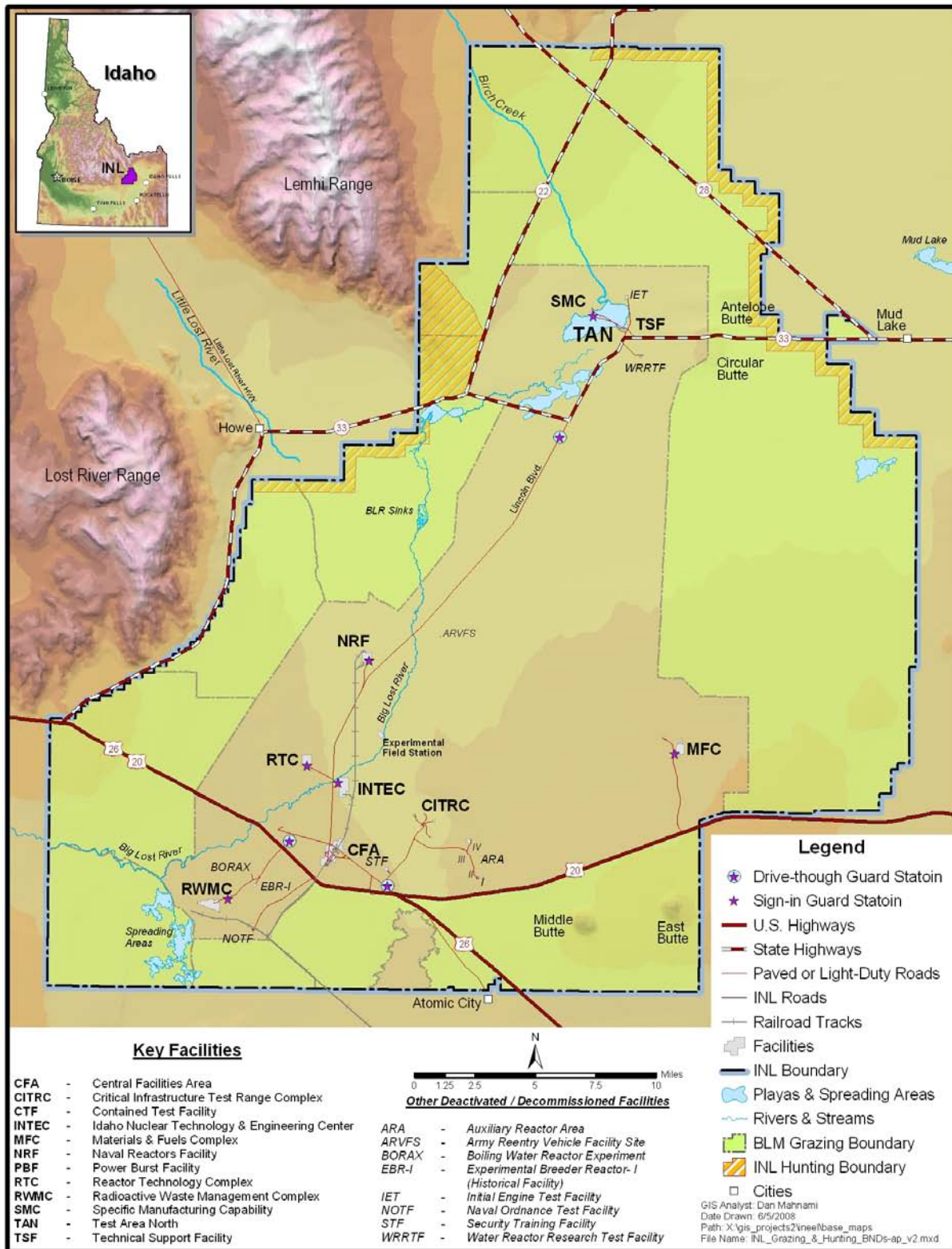


Exhibit F-3. Locations of INL warning signs (INL Boundary), grazing boundaries, and current security stations.

1

G. CONTINGENCY PLAN

2

The information for this section is contained in the waste management unit-specific volumes of

3

the INL HWMA/RCRA Part B permits, or permit applications.

1
2
3
4
5
6
7
8
9
10
11
12
13
14
15
16
17
18
19
20
21

H. PERSONNEL TRAINING

DOE policy requires that all personnel involved with hazardous and mixed-waste handling, management, and unit operations be trained in the proper and safe receipt, handling, storage, and shipment of hazardous/mixed waste. Personnel receive training in the following HWMA areas, as appropriate to their individual job assignments:

- Occupational Safety and Health Administration (OSHA) 1910.120 Hazardous Waste Operations and Emergency Response Training (40- or 24-hour training as appropriate to job position). These courses are designed for all employees engaged in hazardous waste operations and have the potential of being exposed to a variety of hazards associated with such operations.
- Hazardous Materials Transportation Safety Training. This course provides a basic understanding of packaging, marking, labeling, and shipping requirements.
- Respirator Training. Provides information and guidance needed for the proper use, selection, and care of respirators.
- Hazard Communication. Provides awareness of the OSHA Hazard Communication Standard.
- General Employee Radiological Training. Provides basic information related to the “as low as reasonably achievable” (ALARA) principle.

The waste management unit-specific volumes of the INL HWMA/RCRA Part B permits and permit applications will address the requirements of IDAPA 58.01.05.008 and IDAPA 58.01.05.012 [40 CFR 264.16 and 40 CFR 270.14(b)(12)].

1

I. CLOSURE AND POSTCLOSURE REQUIREMENTS

2

The information for this section is contained in the waste management unit-specific volumes of

3

the INL HWMA/RCRA Part B permits, or permit applications.

1
2
3
4
5
6
7
8

**J. CORRECTIVE ACTION FOR SOLID WASTE MANAGEMENT UNITS
(IDAPA 58.01.05.008 [40 CFR 264.101])**

The corrective action requirements for INL facilities (as applicable) are addressed under the following HWMA/RCRA Final Partial Permits (as applicable): the Materials and Fuel Complex (MFC) Storage and Treatment Units HWMA/RCRA Final Permit – Module VI; the HWMA/RCRA Storage and Treatment Permit for the Idaho Nuclear Technology and Engineering Center (Volume 18) – Module VII; and the Advanced Mixed Waste Treatment Project (AMWTP) HWMA/RCRA Permit – Module VI.

1 **K. OTHER FEDERAL LAWS**
2 **(IDAPA 58.01.05.012 [40 CFR 270.14(B)(20) AND 40 CFR 270.3])**

3 **K-1 The Wild and Scenic Rivers Act**

4 The activities under this permit application do not involve the construction of any water resource
5 projects or other actions that will have any effect, adverse or otherwise, on the values for which a national
6 wild and scenic river were established.

7 **K-2 The National Historic Preservation Act of 1966**

8 EBR-I, the first reactor built at the INL, was decommissioned in 1964. In 1966, EBR-I was
9 officially designated a national historic landmark. The activities to be considered under this permit
10 application will have no effect on EBR-I or any other properties currently on the national register or
11 eligible for listing on the National Register of Historic Places.

12 **K-3 The Endangered Species Act (ESA)**

13 There are no known endangered or threatened plants or animal species on the INL Site.
14 Table K-1 contains information on listed species, candidate species, and non-listed species of concern.
15 There are several animal species that are known to, or having the potential to occur on or near the Site
16 that are species of special concern. Among these species is the ferruginous hawk, which nests near the
17 juniper woodlands and elsewhere on INL land. In addition, Townsend's big-eared bats roost in caves on
18 the Site. Burrowing owls use the Site's grassland and sagebrush-steppe habitat, and loggerhead shrikes
19 are found in the sagebrush areas and near facilities over much of the INL site. The relatively undisturbed
20 areas of the INL site provide habitat for threatened, endangered, candidate, and other species. Research
21 has shown that some species of ants once thought to be rare (and potential candidates) are much more
22 abundant than previously believed.

Table K-1. ESA Listed Species, ESA Candidate Species, and species of concern, which may occur at the INL.

Plants or Animals	ESA Listed Species	Conservation Status Rank* and Comments
	None	None
Plants or Animals	ESA Candidate Species	Conservation Status Rank and Comments
Birds	Greater sage-grouse (<i>Centrocercus urophasianus</i>)	On March 23, 2010 the U.S. Fish and Wildlife Service (FWS), announced a 12-month finding on petitions to list three entities of the greater sage-grouse (<i>Centrocercus urophasianus</i>) as threatened or endangered under the Endangered Species Act of 1973, as amended (Act). They found that listing the greater sage-grouse (range wide) is warranted, but precluded by higher priority listing actions. They will develop a proposed rule to list the greater sage-grouse as priorities allow. The Western Watersheds Project filed suit the next day claiming the ruling was “arbitrary and capricious”.
Plants or Animals	Idaho Species of Greatest Conservation Need	Conservation Status Rank and Comments
Mammals	Townsend’s big-eared bat (<i>Corynorhinus townsendii</i>)	G4 and S3
	Pygmy rabbit (<i>Brachylagus idahoensis</i>)	G4 and S2. The U.S. FWS has missed several deadlines to rule on listing this species, however, the Western Watersheds Project filed a lawsuit in February of 2010 to force the U.S. FWS to make a decision.
	Merriam’s shrew (<i>Sorex merriami</i>)	G5 and S2
	Gray Wolf (<i>Canis lupus</i>)	G4 and S3
	Trumpeter Swan (<i>Cygnus buccinator</i>)	G4, S1B, and S2N
	Northern Pintail (<i>Anas acuta</i>)	G5, S5B, and S2N
	Lesser Scaup (<i>Aythya affinis</i>)	G5 and S3
	Greater Sage-Grouse (<i>Centrocercus urophasianus</i>)	G4 and S2S
	Western Grebe (<i>Aechmophorus occidentalis</i>)	G5 and S2B
	Clark’s Grebe (<i>Aechmophorus clarkia</i>)	G5 and S2B
	Great Egret (<i>Ardea alba</i>)	G5 and S1B
	Snowy Egret (<i>Egretta thula</i>)	G5 and S2B
	Cattle Egret (<i>Bubulcus ibis</i>)	G5 and S2B

Table K-1. (Continued)

Plants or Animals	Idaho Species of Greatest Conservation Need	Conservation Status Rank* and Comments
Mammals (continued)	Black-crowned Night-Heron (<i>Nycticorax nycticorax</i>)	G5 and S2B
	White-faced Ibis (<i>Plegadis chihi</i>)	G5 and S2B
	Bald Eagle (<i>Haliaeetus leucocephalus</i>)	G4, S3B, and S4N
	Swainson's Hawk (<i>Buteo swainsoni</i>)	G5 and S3B
	Ferruginous Hawk (<i>Buteo regalis</i>)	G4 and S3B
	Merlin (<i>Falco columbarius</i>)	G5, S2B, and S2N
	Peregrine Falcon (<i>Falco peregrines</i>)	G4T3, S2B, and S
	Sandhill Crane (<i>Grus canadensis</i>)	G5 and S3B
	Black-necked Stilt (<i>Himantopus mexicanus</i>)	G5 and S3B
	American Avocet (<i>Recurvirostra americana</i>)	G5 and S5B
	Long-billed Curlew (<i>Numenius americanus</i>)	G5 and S2B
	Wilson's Phalarope (<i>Phalaropus tricolor</i>)	G5 and S3B
	Franklin's Gull (<i>Larus pipixcan</i>)	G4, G5, and S2B
	California Gull (<i>Larus californicus</i>)	G5 and S2B
	Caspian Tern (<i>Sterna caspia</i>)	G5 and S2B
	Forster's Tern (<i>Sterna forsteri</i>)	G5 and S1B
	Black Tern (<i>Chlidonias niger</i>)	G4 and S1B
	Burrowing Owl (<i>Athene cunicularia</i>)	G4 and S2B
	Short-eared Owl (<i>Asio flammeus</i>)	G5 and S4
	Brewer's Sparrow (<i>Spizella breweri</i>)	G5 and S3B

Table K-1. (Continued)

Plants or Animals	Idaho Species of Greatest Conservation Need	Conservation Status Rank* and Comments
Plants	Idaho Rare Plant List	
	Lemhi milkvetch (<i>Astragalus aquilonius</i>)	GP3
	Meadow milkvetch (<i>Astragalus diversifolius</i>)	GP2
	Wing-seeded evening primrose (<i>Camissonia pterosperma</i>)	S
	Welsh’s buckwheat (<i>Eriogonum capistratum</i> var. <i>welshii</i>)	GP2
	Spreading gilia (<i>Ipomopsis polycladon</i>)	SP2
	Obscure phacelia (<i>Phacelia inconspicua</i>)	GP1
	Blue Mountain catchfly (<i>Silene scaposa</i> var. <i>lobata</i>)	M

* NatureServe Conservation Status Ranking system.

G is the global or range wide rank and S is the statewide range.

G1 or S1 – Critically imperiled.

G2 or S2 – Imperiled.

G3 or S3 – Vulnerable.

G4 or S4 – Apparently Secure.

G5 or S5 – Secure.

B – Breeding Population.

N – Non-breeding population.

T – indicates an infraspecific taxon or the status of a subspecies or variety of the species being discussed

Idaho Native Plant Society Conservation Status Categories.

GP1 – Critically Imperiled Globally.

GP2 – Imperiled Globally.

GP3 – Vulnerable Globally.

SP1 – Taxa in danger of becoming extinct or extirpated from Idaho.

SP2 – Taxa likely to become classified as SP1 within the foreseeable future in Idaho.

S – Sensitive taxa with small localized populations that may be in jeopardy without active management.

M – Taxa common within a limited range in Idaho.

1 The activities under this permit application are relatively small in scale, confined, and consistent with
2 ongoing operations at the INL Site. These activities are not likely to jeopardize the continued existence of any
3 endangered or threatened species or adversely affect their critical habitat.

4 **K-4 The Coastal Zone Management Act**

5 The activities under this permit application will not affect land or water use in any
6 coastal zone.

7 **K-5 The Fish and Wildlife Coordination Act**

8 The activities under this permit application do not involve impoundment, diversion, or other control or
9 modification of any body of water that might impact wildlife.

10 **K-6 The Migratory Bird Treaty Act of 1918**

11 The migratory bird treaty act governs the taking, killing, possession, transportation, and importation of
12 migratory birds, their eggs, parts, and nests. The activities under this permit application are not likely to
13 jeopardize the species protected under this act.

14 **K-7 Bald Eagle Protection Act (16 U.S.C. 668)**

15 This law provides for the protection of the bald eagle (the national emblem) and the golden eagle by
16 prohibiting, except under certain specified conditions, the taking, possession and commerce of such birds. The
17 activities under this permit application are not likely to jeopardize the species protected under this act.

18 **K-8 Management of Undesirable Plants on Federal Lands (7 USC 2814)**

19 This act provides that Federal agencies shall develop and coordinate an undesirable plants
20 management program for control of undesirable plants on Federal lands under the agency's jurisdiction. The
21 activities under this permit application are not likely to interfere with this program.

22 **K-9 Invasive Species Executive Order (EO 13112)**

23 This order established a council whose charter is to prevent the introduction of invasive species and
24 provide for their control and to minimize the economic, ecological, and human health impacts that invasive
25 species cause. The activities under this permit application will not interfere with this program.

1 **K-10 Public Land Orders 318, 545, 637, and 1770**

2 Public Land Orders 318, 545, 637, and 1770 are decrees for the public land withdrawals that provided
3 the land for the INL. The activities under this permit application will not interfere with these orders.

4 **K-11 Clean Water Act (33 U.S.C. 1251 et. seq.)**

5 This act regulates the discharges of pollutants into the waters of the United States. The act also sets
6 requirements for all contaminants in surface waters and makes it unlawful for any person to discharge any
7 pollutant from a point source into navigable waters, unless a permit is its provisions. The activities under this
8 permit application are not likely to interfere with this program.

REGULATORY CERTIFICATION [IDAPA 58.01.05.012; 40 CFR 270.11(d) and 270.30(k)]

**FOR THE HAZARDOUS WASTE MANAGEMENT ACT/RESOURCE CONSERVATION
AND RECOVERY ACT PART B PERMIT APPLICATION FOR
THE IDAHO NATIONAL LABORATORY
VOLUME 3 – GENERAL INFORMATION FOR INL WASTE MANAGEMENT UNITS**

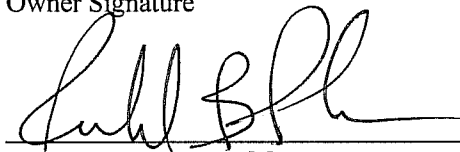
REVISION 15 – JULY 2010

EPA I.D. Number ID4890008952

The undersigned certifies as required per 40 CFR 270.11(d) and 270.30(k) as follows:

I certify under penalty of law that this document and all attachments were prepared under my direction or supervision according to a system designed to assure that qualified personnel properly gather and evaluate the information submitted. Based on my inquiry of the person or persons who manage the system, or those persons directly responsible for gathering the information, the information submitted is, to the best of my knowledge and belief, true, accurate, and complete. I am aware that there are significant penalties for submitting false information, including the possibility of fine and imprisonment for knowing violations.

Owner Signature



Richard B. Provéncher, Manager
Department of Energy Idaho Operations Office

7/27/2010
Date

REGULATORY CERTIFICATION [IDAPA 58.01.05.012; 40 CFR 270.11(d) and 270.30(k)]

**FOR THE HAZARDOUS WASTE MANAGEMENT ACT/RESOURCE CONSERVATION
AND RECOVERY PART B PERMIT APPLICATION FOR
THE IDAHO NATIONAL LABORATORY
VOLUME 3 – GENERAL INFORMATION FOR INL WASTE MANAGEMENT UNITS**

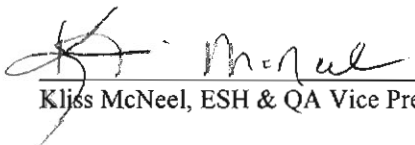
REVISION 15 – JULY 2010

EPA I.D. Number ID4890008952

The undersigned certifies as required per 40 CFR 270.11(d) and 270.30(k) as follows:

I certify under penalty of law that this document and all attachments were prepared under my direction or supervision according to a system designed to assure that qualified personnel properly gather and evaluate the information submitted. Based on my inquiry of the person or persons who manage the system, or those persons directly responsible for gathering the information, the information submitted is, to the best of my knowledge and belief, true, accurate, and complete. I am aware that there are significant penalties for submitting false information, including the possibility of fine and imprisonment for knowing violations.

Operator Signature



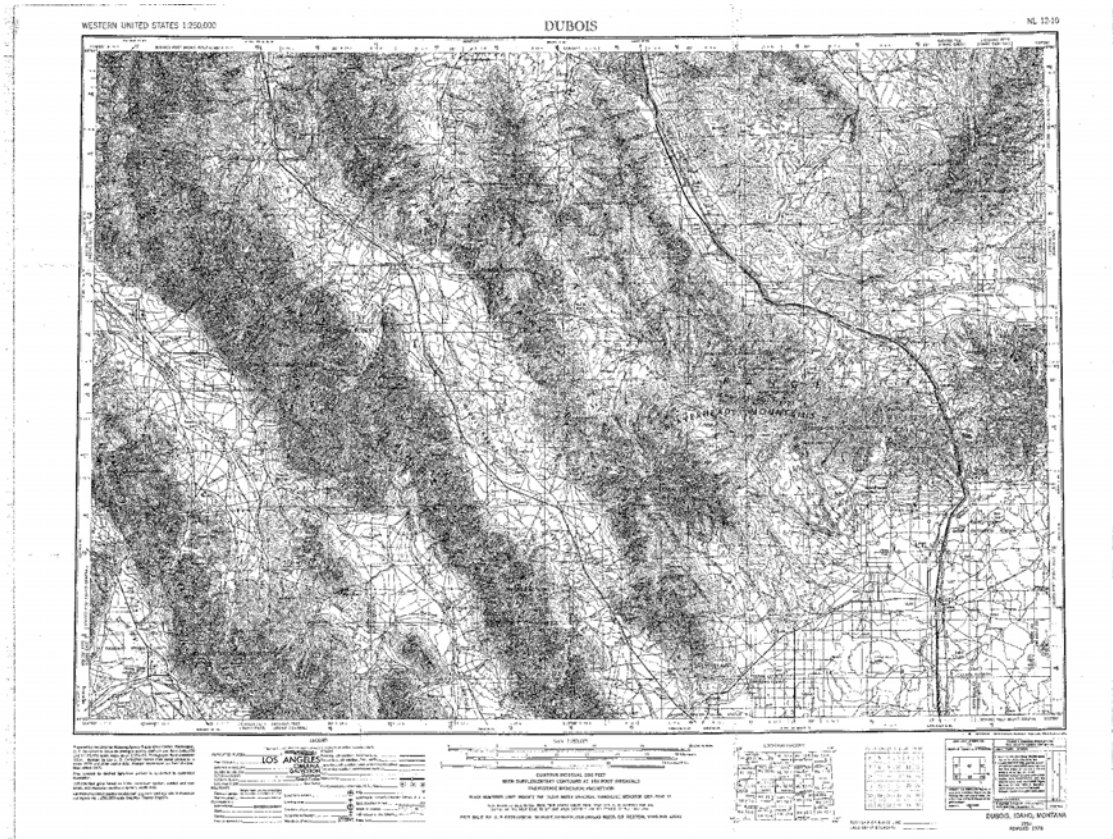
Kljss McNeel, ESH & QA Vice President, CH2M-WG Idaho, LLC.

6/22/10

Date

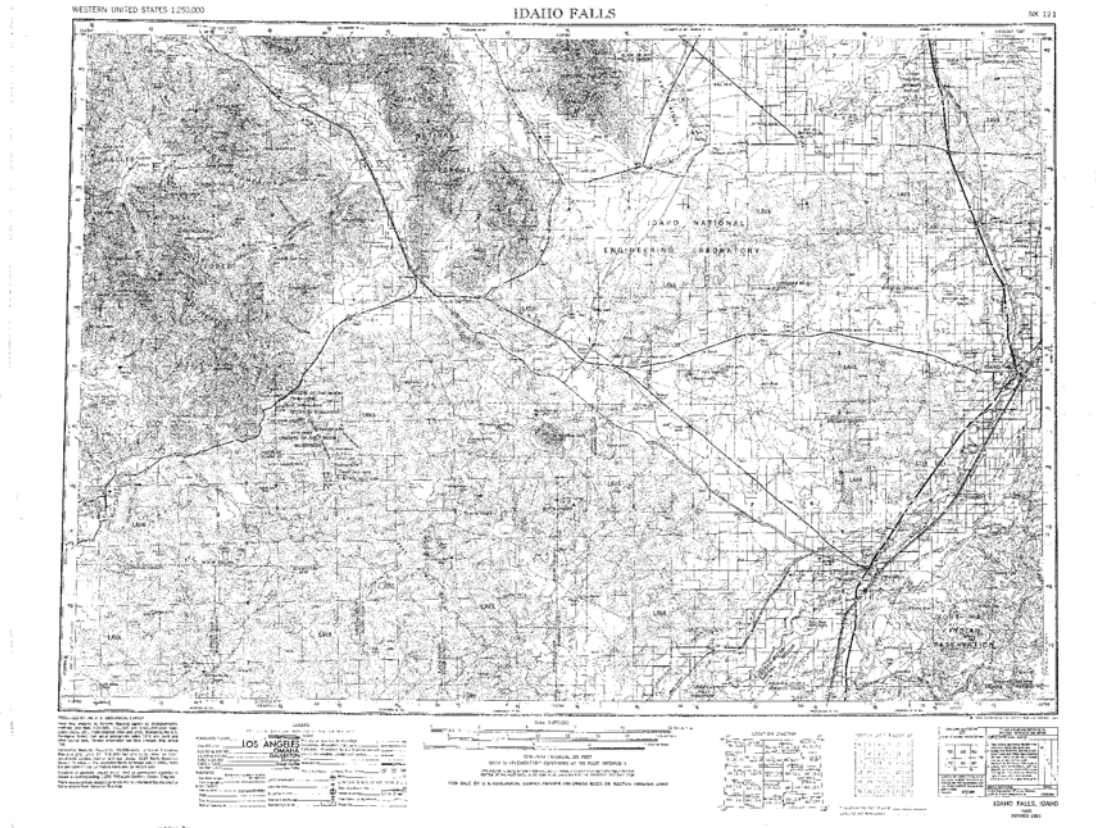
APPENDIX I

TOPOGRAPHIC MAPS



APPENDIX I
MAP #1 – DUBOIS 1:250,000

INL BOUNDARY (northern most portion of facility). Use in conjunction with Map #2



APPENDIX I
MAP #2 – IDAHO FALLS 1:250,000

INL BOUNDARY (southern portion of facility). Use in conjunction with Map #1



SECTIONALIZED TOWNSHIP

6	5	4	3	2
7	8	9	10	11
12	13	14	15	16
17	18	19	20	21
22	23	24	25	26
27	28	29	30	31
32	33	34	35	36

LOCATION DIAGRAM

100° 00' 00" W				
43° 00' 00" N				

CONTOUR INTERVALS AT 100 FOOT INTERVALS

100	200	300	400	500	600	700	800	900	1000
1100	1200	1300	1400	1500	1600	1700	1800	1900	2000
2100	2200	2300	2400	2500	2600	2700	2800	2900	3000
3100	3200	3300	3400	3500	3600	3700	3800	3900	4000
4100	4200	4300	4400	4500	4600	4700	4800	4900	5000
5100	5200	5300	5400	5500	5600	5700	5800	5900	6000
6100	6200	6300	6400	6500	6600	6700	6800	6900	7000
7100	7200	7300	7400	7500	7600	7700	7800	7900	8000
8100	8200	8300	8400	8500	8600	8700	8800	8900	9000
9100	9200	9300	9400	9500	9600	9700	9800	9900	10000

FOR SALE BY U.S. GEOLOGICAL SURVEY, DENVER, COLORADO, 80225 OR RESTON, VIRGINIA, 20192

WITH SUPPLEMENTARY CONTOURS AT 100 FOOT INTERVALS

2000 FOOT CONTOUR INTERVALS FOR THE DENVER METRO AREA TO BE AVAILABLE IN 2002

Scale: 1:250,000

LEGEND

Produced by the U.S. Geological Survey

Scale: 1:250,000

Projection: UTM Zone 12N

Datum: NAD 83

Units: Meters

Color: 256 Colors

Resolution: 300 DPI

File Name: NK12-1

Map Date: 1981

Map Title: IDAHO FALLS

Map Scale: 1:250,000

Map Projection: UTM Zone 12N

Map Datum: NAD 83

Map Units: Meters

Map Color: 256 Colors

Map Resolution: 300 DPI

Map File Name: NK12-1

Map Map Date: 1981

Map Map Title: IDAHO FALLS

Map Map Scale: 1:250,000

Map Map Projection: UTM Zone 12N

Map Map Datum: NAD 83

Map Map Units: Meters

Map Map Color: 256 Colors

Map Map Resolution: 300 DPI

Map Map File Name: NK12-1

Map Map Map Date: 1981

Map Map Map Title: IDAHO FALLS

Map Map Map Scale: 1:250,000

Map Map Map Projection: UTM Zone 12N

Map Map Map Datum: NAD 83

Map Map Map Units: Meters

Map Map Map Color: 256 Colors

Map Map Map Resolution: 300 DPI

Map Map Map File Name: NK12-1

Produced by the U.S. Geological Survey

Scale: 1:250,000

Projection: UTM Zone 12N

Datum: NAD 83

Units: Meters

Color: 256 Colors

Resolution: 300 DPI

File Name: NK12-1

Map Date: 1981

Map Title: IDAHO FALLS

Map Scale: 1:250,000

Map Projection: UTM Zone 12N

Map Datum: NAD 83

Map Units: Meters

Map Color: 256 Colors

Map Resolution: 300 DPI

Map File Name: NK12-1

Map Map Date: 1981

Map Map Title: IDAHO FALLS

Map Map Scale: 1:250,000

Map Map Projection: UTM Zone 12N

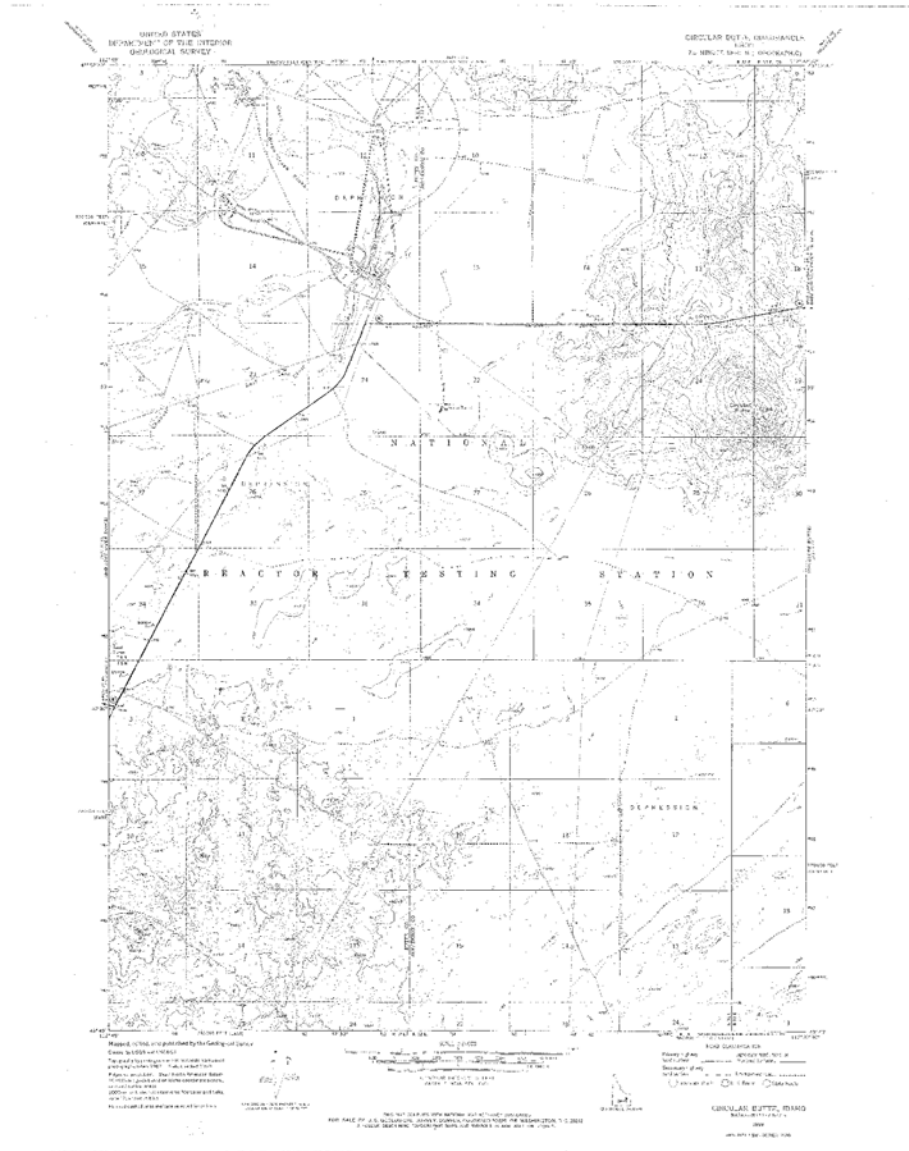
Map Map Datum: NAD 83

Map Map Units: Meters

Map Map Color: 256 Colors

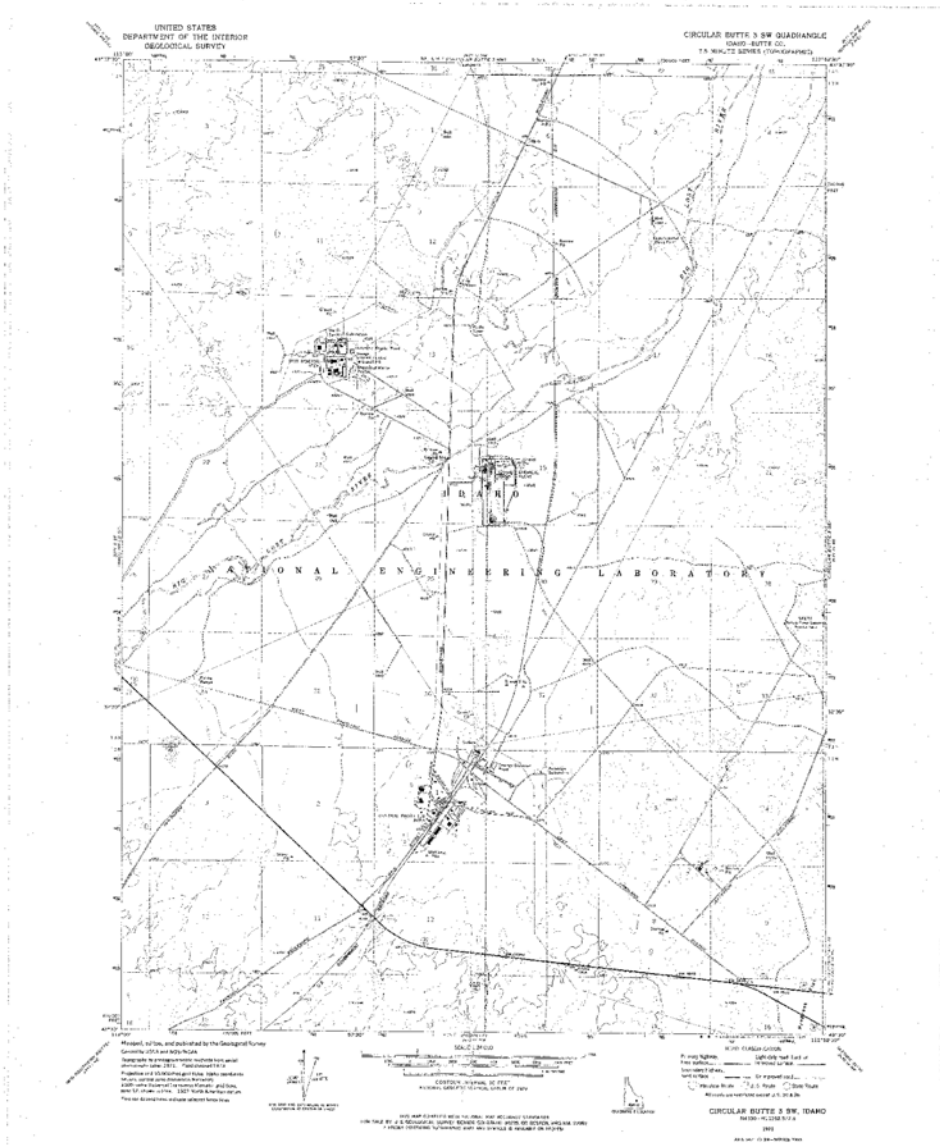
Map Map Resolution: 300 DPI

Map Map File Name: NK12-1



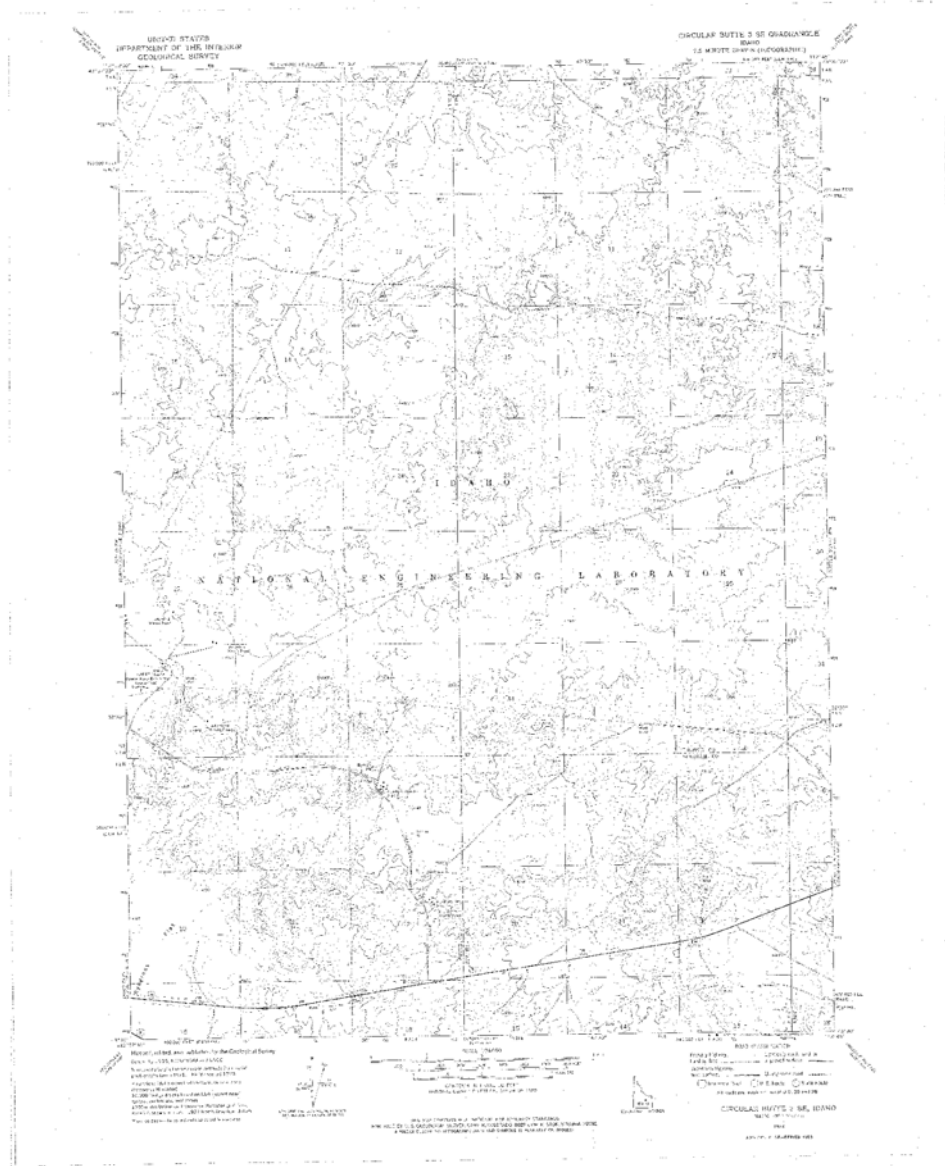
APPENDIX I
MAP #3 – CIRCULAR BUTTE 1:24,000

TAN, WRRTF, SMC



APPENDIX I
MAP #6 – CIRCULAR BUTTE 3 SW (North of Scoville) 1:24,000

TRA (RTC), INTEC, CFA, NODA



APPENDIX I

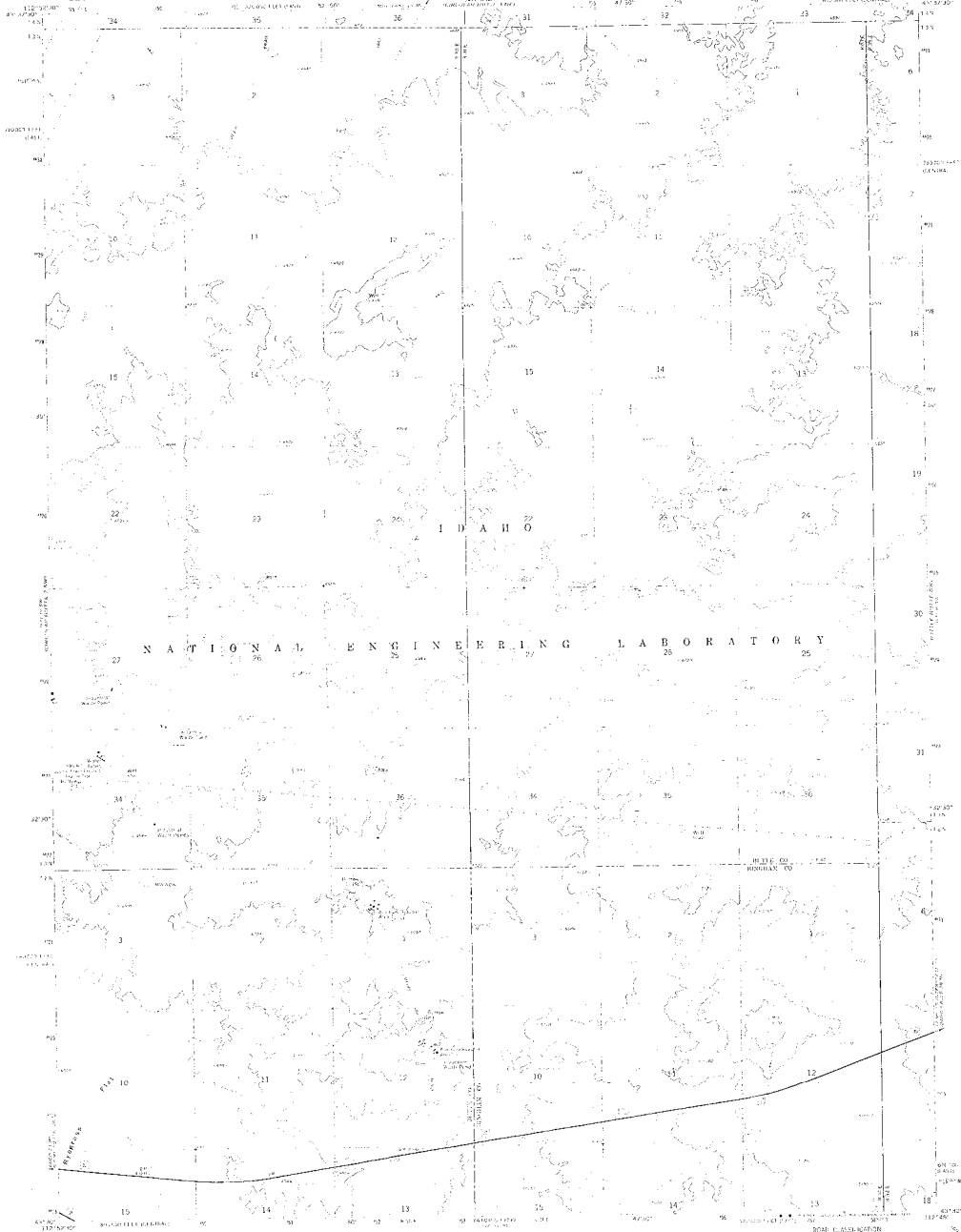
MAP #7 – CIRCULAR BUTTE 3 SE (Rye Grass Flat)

1:24,000

SPERT II, SPERT III, SPERT IV, PBF (CITRC), ARA

UNITED STATES
DEPARTMENT OF THE INTERIOR
GEOLOGICAL SURVEY

CIRCULAR BUTTE 3 SE QUADRANGLE
IDAHO
7.5 MINUTE SURVEY (TOPOGRAPHIC)



NATIONAL ENGINEERING LABORATORY

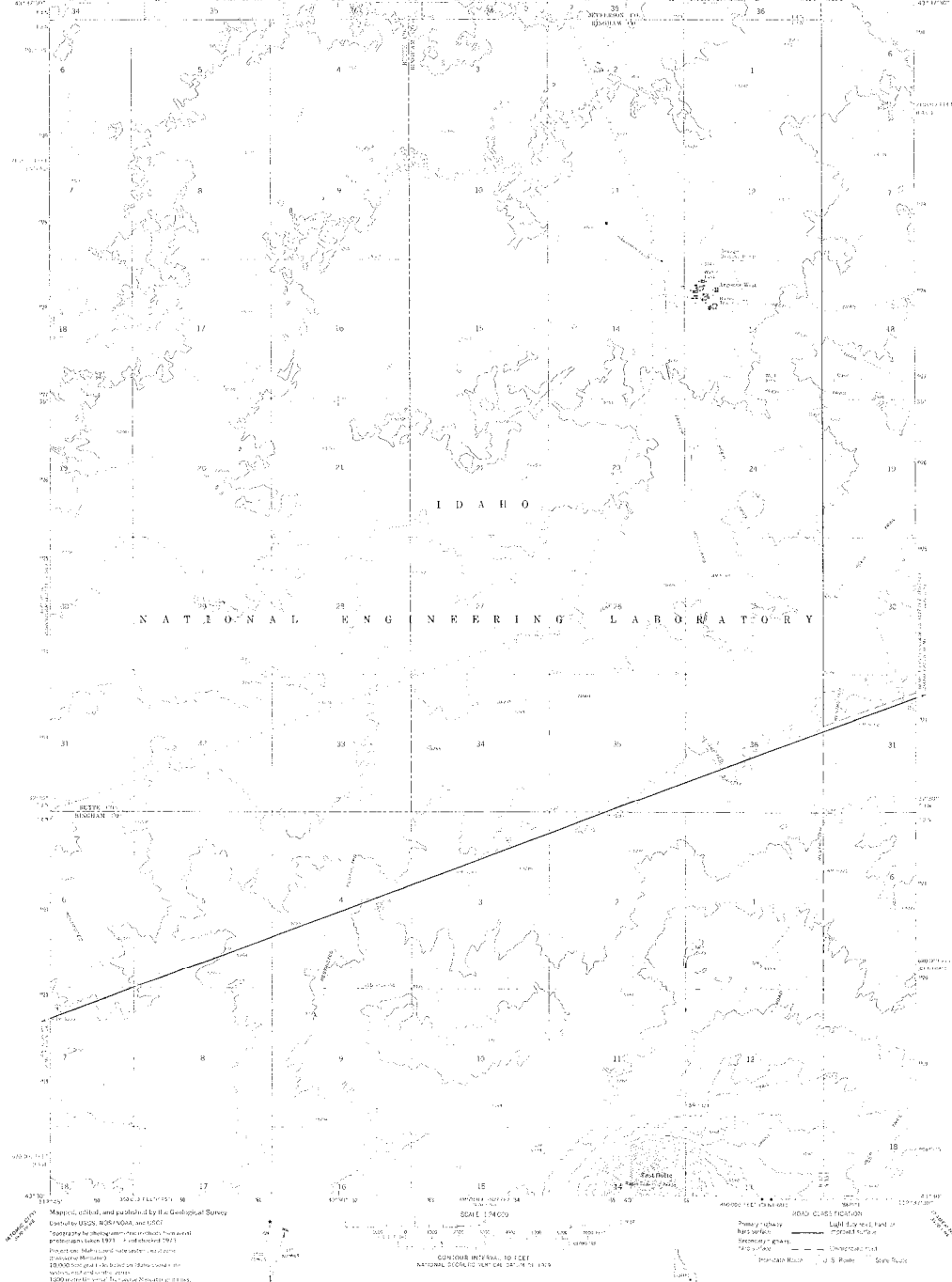
Map is based on data published by the Geological Survey
and other sources. It is not a legal document.
It is intended for use as a guide only.
It is not intended to be used as a basis for
any legal action.
It is not intended to be used as a basis for
any legal action.
It is not intended to be used as a basis for
any legal action.

SCALE 1:25,000
VERTICAL DATUM: MEAN SEA LEVEL
HORIZONTAL DATUM: NAD 83
PROJECTION: UTM
EQUIVALENT RECTANGULAR PROJECTION
SPHEROID: GRS 80
SEMI-MAJOR AXIS: 6378137.0 meters
SEMI-MINOR AXIS: 6356752.3141453 meters
FLATTENING: 1/298254.189
EARTH EQUATORIAL RADIUS: 6378137.0 meters
EARTH MEAN RADIUS: 6371007.178 meters
EARTH FLATTENING: 1/298254.189
EARTH EQUATORIAL RADIUS: 6378137.0 meters
EARTH MEAN RADIUS: 6371007.178 meters
EARTH FLATTENING: 1/298254.189

Primary Profile: 1:25,000
Secondary Profile: 1:25,000
Tertiary Profile: 1:25,000
Quaternary Profile: 1:25,000
Quinary Profile: 1:25,000
Sextenary Profile: 1:25,000
Septenary Profile: 1:25,000
Octonary Profile: 1:25,000
Nonary Profile: 1:25,000
Decenary Profile: 1:25,000
Circular Butte 3 SE, IDAHO
1979
4750 5411 79 10000 7900

UNITED STATES
DEPARTMENT OF THE INTERIOR
GEOLOGICAL SURVEY

LITTLE BUTTE SW QUADRANGLE
IDAHO
7.5 MINUTE SERIES (CONTOUR MAP)



Map made, edited, and published by the Geological Survey
Control to USGS, BOSTON, and WASHINGTON
Copyright by the Geological Survey, Department of the Interior
Reproduction of this map is prohibited without the written permission of the Chief of the Geological Survey
This map is a reproduction of the original map published by the Geological Survey in 1913
The original map is in the possession of the National Engineering Laboratory

SCALE 1:50,000
CONTOUR INTERVAL, 10 FEET
NATIONAL ENGINEERING LABORATORY

ROAD CLASSIFICATION
Double Highway
Single Highway
Railroad
Proposed Road
Proposed Railroad
Light Railway
Proposed Light Railway
Proposed Light Railway
Proposed Light Railway
Proposed Light Railway

THIS MAP IS A REPRODUCTION OF THE ORIGINAL MAP ACCURATELY SCALING
FOR SALE BY THE GEOLOGICAL SURVEY, DEPARTMENT OF THE INTERIOR, WASHINGTON, D.C.
A REPRODUCTION OF THIS MAP IS PROHIBITED WITHOUT THE WRITTEN PERMISSION OF THE GEOLOGICAL SURVEY

LITTLE BUTTE SW, IDAHO
NAD83-111715-775
1913
1:50,000 SW 10000 1913

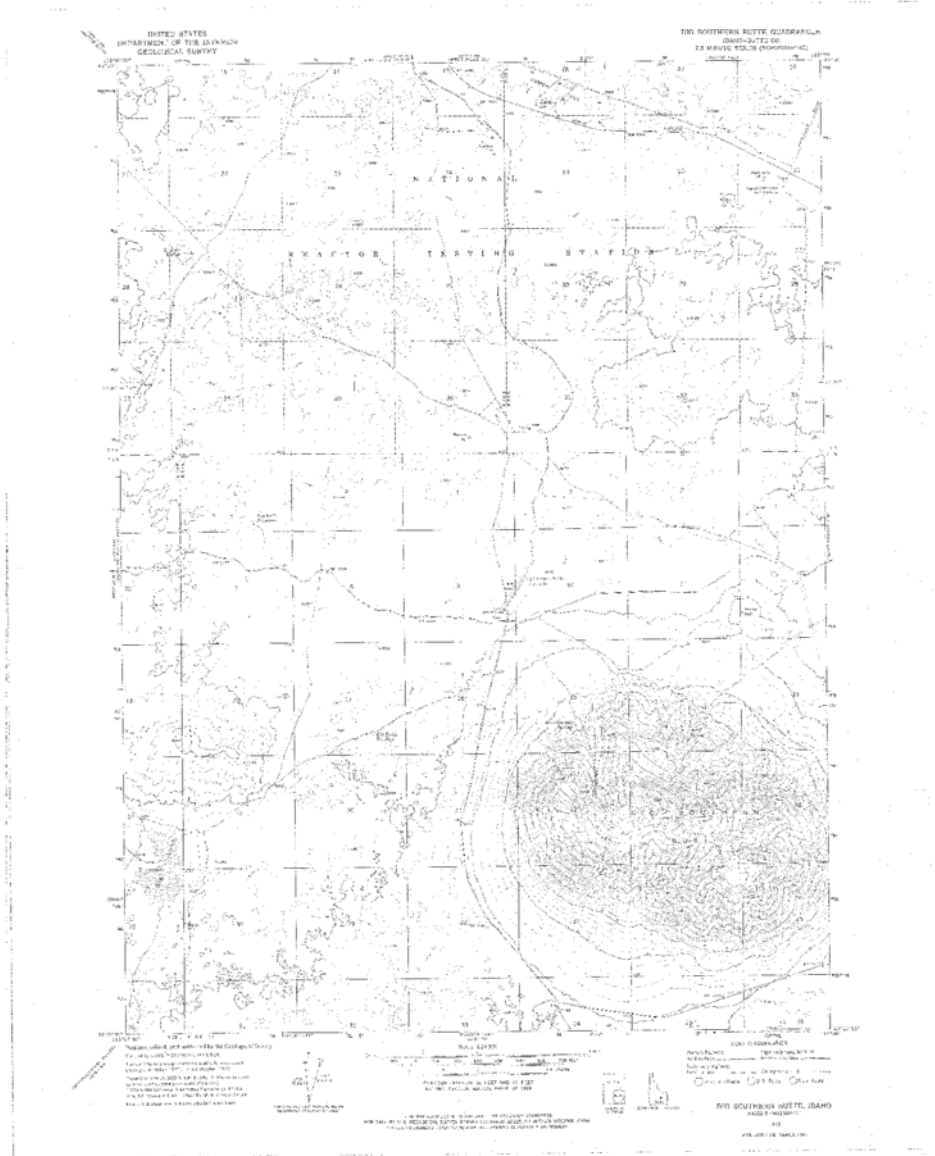


Map, index, and published by the Geological Survey
 Geology, 1925 and 1926
 Topography, 1925 and 1926
 Hydrography, 1925 and 1926
 Soil Survey, 1925 and 1926
 Aerial Photographs, 1925 and 1926

Scale 1:24,000
 Contour Interval 20 Feet
 National Engineering Laboratory

FOR SALE BY THE GEOLOGICAL SURVEY OF THE UNITED STATES DEPARTMENT OF THE INTERIOR
 A FOLDER DESCRIBING SIGNIFICANT MAPS AND MATERIALS IN THIS AREA ON REQUEST

ARCO HILLS SE. IDAHO
 7.5 MINUTE SERIES
 1927



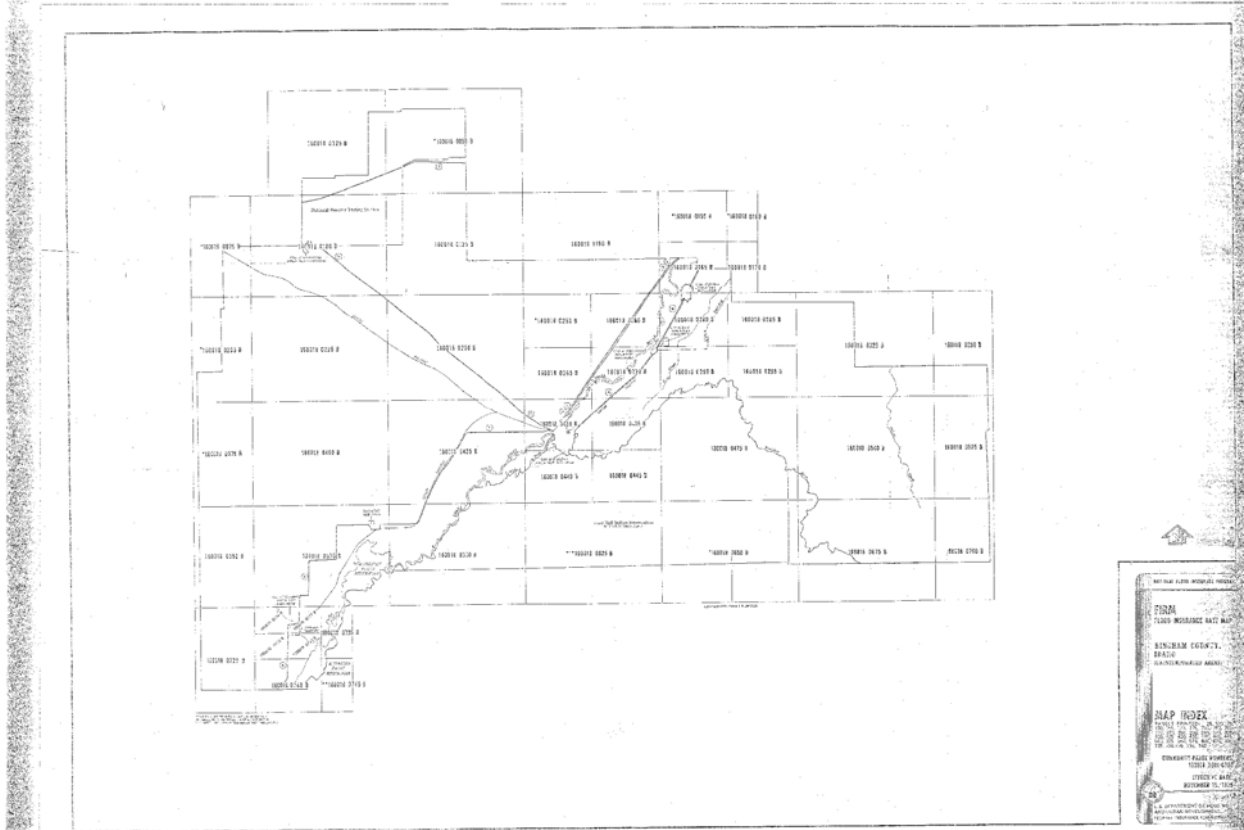
APPENDIX I
MAP #10 – BIG SOUTHERN BUTTE 1:24,000

RWMC, Diversion System

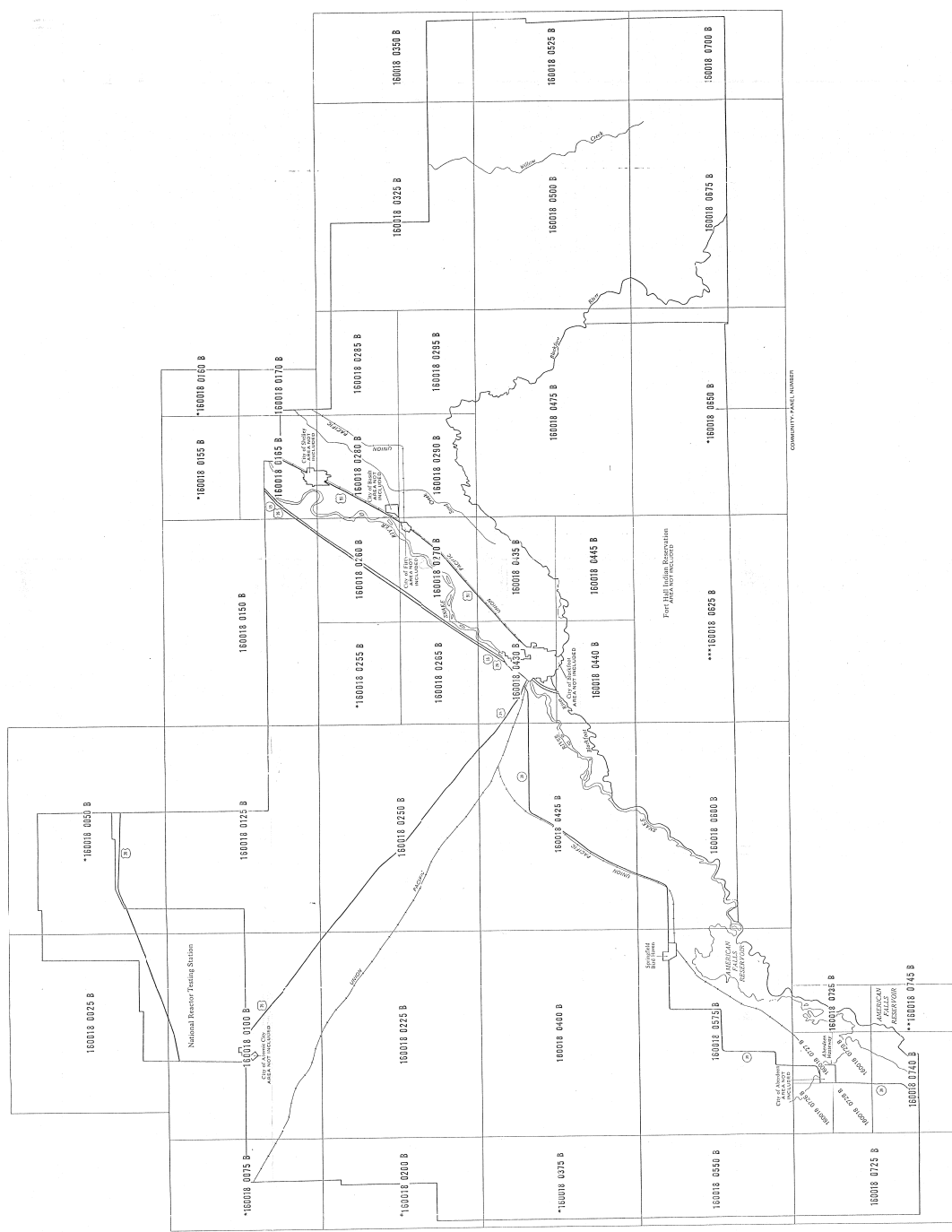
APPENDIX II

FLOOD INSURANCE RATE MAPS

NOTE: ALSO SEE CD LOCATED IN APPENDIX I FOR THIS INFORMATION ELECTRONICALLY



APPENDIX II
MAP #1 – FLOOD INSURANCE MAP
BINGHAM COUNTY, IDAHO



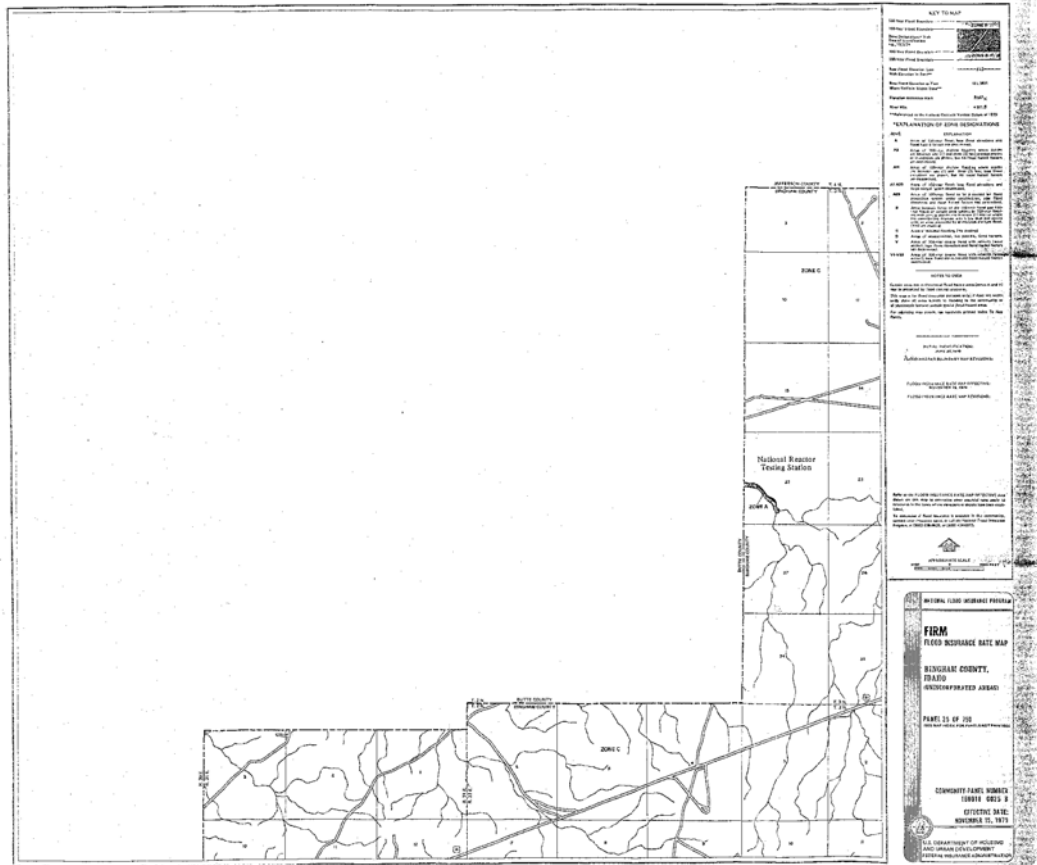
160018 0025 B
 160018 0100 B
 160018 0150 B
 160018 0160 B
 160018 0170 B
 160018 0200 B
 160018 0225 B
 160018 0250 B
 160018 0275 B
 160018 0300 B
 160018 0325 B
 160018 0350 B
 160018 0375 B
 160018 0400 B
 160018 0425 B
 160018 0440 B
 160018 0445 B
 160018 0475 B
 160018 0500 B
 160018 0525 B
 160018 0550 B
 160018 0575 B
 160018 0600 B
 160018 0625 B
 160018 0650 B
 160018 0675 B
 160018 0700 B
 160018 0725 B
 160018 0740 B
 160018 0745 B



COMMUNITY PANEL NUMBERS

From U.S. Public Information
 Office, Washington, D.C.

160018 0025 B
 160018 0100 B
 160018 0150 B
 160018 0160 B
 160018 0170 B
 160018 0200 B
 160018 0225 B
 160018 0250 B
 160018 0275 B
 160018 0300 B
 160018 0325 B
 160018 0350 B
 160018 0375 B
 160018 0400 B
 160018 0425 B
 160018 0440 B
 160018 0445 B
 160018 0475 B
 160018 0500 B
 160018 0525 B
 160018 0550 B
 160018 0575 B
 160018 0600 B
 160018 0625 B
 160018 0650 B
 160018 0675 B
 160018 0700 B
 160018 0725 B
 160018 0740 B
 160018 0745 B



APPENDIX II
MAP #3 - FLOOD INSURANCE MAP

BINGHAM COUNTY, IDAHO

APPENDIX III

BIG LOST RIVER FLOOD HAZARD STUDY,
IDAHO NATIONAL LABORATORY, U.S. BUREAUS OF RELCAMATION, 2005

**APPENDIX IV. Big Lost River Flood Hazard Study, Idaho National Laboratory,
Idaho, U.S. Bureau of Reclamation**

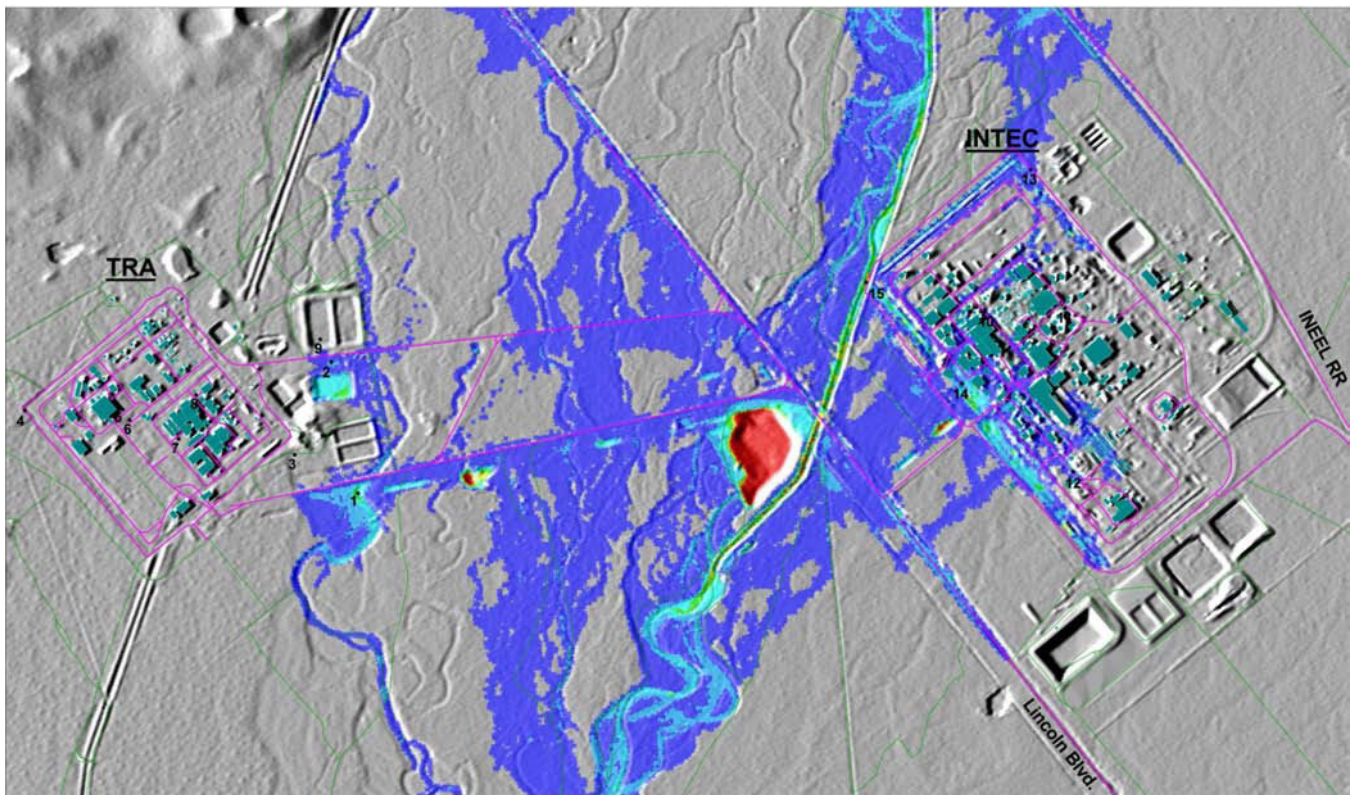
RECLAMATION

Managing Water in the West

Big Lost River Flood Hazard Study

Idaho National Laboratory, Idaho

Summary Document



U.S. Department of the Interior
Bureau of Reclamation
Technical Service Center
Seismotectonics and Geophysics Group
Denver, Colorado

November 2005

Mission Statements

The mission of the Department of the Interior is to protect and provide access to our Nation's natural and cultural heritage and honor our trust responsibilities to Indian Tribes and our commitments to island communities.

The mission of the Bureau of Reclamation is to manage, develop, and protect water and related resources in an environmentally and economically sound manner in the interest of the American public.

Big Lost River Flood Hazard Study Idaho National

Idaho National Laboratory, Idaho

Summary Document

Report 2005-2

Prepared by

**Dean A. Ostenaar
Daniel R.H. O'Connell**



**U.S. Department of the Interior
Bureau of Reclamation
Technical Service Center
Seismotectonics and Geophysics Group
Denver, Colorado**

November 2005

Prepared by:

Dean A. Ostenaar

November 14, 2005
Date

Daniel R.H. O'Connell

November 14, 2005
Date

TSC Peer Review by:

Jon P. Ake

November 14, 2005
Date

OVERVIEW

Introduction and Objectives

Paleoflood studies of the Big Lost River (Ostenaar et al., 1999; 2002) indicated that potential flood hazards for the Big Lost River at the Idaho National Laboratory (INL) (previously Idaho National Environmental and Engineering Laboratory (INEEL)) might be significantly different than portrayed by previous studies (e.g., Kjelstrom and Berenbrock, 1996). Because of the significant discrepancy between the previous studies (**Table SO-1**), additional studies aimed at reducing the uncertainty in flood hazard estimates at INL have been undertaken by both U.S. Geological Survey (USGS) (e.g., Hortness and Rousseau, 2003; Berenbrock and Doyle, 2004; Berenbrock et al., in prep.) and Bureau of Reclamation (BOR). The present document and the associated appendices describe the results from BOR studies of the Big Lost River flood hazard at INL. Differences in the estimate of the 100-year peak flow shown by previous studies (**Table SO-1**) are primarily due to the use of differing data in each of the analyses. Kjelstrom and Berenbrock (1996) and Hortness and Rousseau (2003) used stream-gage data from Big Lost River and surrounding region. Ostenaar et al. (1999, 2002) used stream-gage and paleoflood data from the Big Lost River at INL. Estimates of 100-year peak flow require extrapolation beyond the length of the available stream gage data record, whereas inclusion of geologic paleoflood data lengthens the record of peak flow to many times beyond a hundred-year time period.

The major objectives of the BOR studies are focused on two broad technical arenas; 1) geologic, geomorphic, and hydraulic modeling studies to reduce the uncertainty associated with paleohydrologic estimates used in flood frequency analyses, and 2) developing probabilistic flood stage estimates for specific facility locations at INTEC and TRA.

The paleohydrologic studies have focused on detailed studies of a 5-km (3-mi) reach of the Big Lost River that extends between the INEEL Diversion Dam and the historic Pioneer Diversion. In this reach, 1:4000-scale aerial photography flown in September 2000 was used to develop a 3-ft topographic grid that could be rendered as the base map for detailed geomorphic mapping of the study reach and as topographic input for updated two-dimensional hydraulic modeling. To improve the geologic data for paleoflood and paleohydrologic bound estimates, seven trenches at three detailed study sites were excavated within the study reach. From the geomorphic mapping,

trenching data and updated hydraulic modeling, revised estimates of paleofloods and paleohydrologic bounds for the Big Lost River were developed. These data were used to revise and update the unregulated flood frequency analyses for the Big Lost River.

Table SO-1 Comparison of Revised Flood Frequency for the Big Lost River at the Diversion Dam with Previous Study Results.

AEP (1/yr)	Return period (yr)	Present Study			Previous Studies		
		5% (m ³ /s)	mean m ³ /s (ft ³ /s)	95% (m ³ /s)	Ostenaar et al. (1999)	Kjelstrom and Berenbrock (1996)	Hortness and Rousseau (2003)
					mean m ³ /s (ft ³ /s)	mean m ³ /s (ft ³ /s)	mean m ³ /s (ft ³ /s)
5 x 10 ⁻²	20	63	75 (2649)	83	57 (2023)		
2 x 10 ⁻²	50	75	83 (2931)	91	72 (2545)		
1 x 10 ⁻²	100	78	87 (3072)	97	82 (2910)	206 (7260)	106 (3750)
5 x 10 ⁻³	200	82	96 (3390)	114	92 (3252)		
2 x 10 ⁻³	500	89	110 (3885)	137	104 (3669)		
1 x 10 ⁻³	1000	101	131 (4626)	163	112 (3960)		
5 x 10 ⁻⁴	2000	127	159 (5615)	194	120 (4232)		
2 x 10 ⁻⁴	5000	148	188 (6639)	236	129 (4564)		
1 x 10 ⁻⁴	10,000	185	279 (9853)	412	136 (4796)		
5 x 10 ⁻⁵	20,000*	245	416*(14691)	628*	142 (5012)		

* Values with diminished or little statistical significance.
AEP - Annual Exceedence Probability

Developing probabilistic stage estimates for INTEC and TRA facility sites included three major work activities: 1) reprocessing of the 1993 1:10,000-scale aerial photography along the Big Lost River to generate a 5-ft topographic grid for use in two-dimensional hydraulic modeling, 2) two-dimensional hydraulic modeling of multiple flow scenarios between the INEEL Diversion Dam to downstream of INTEC and TRA, and 3) estimating stage probability curves for facility sites that could include alternate views and uncertainties in flood frequency, infiltration, and culvert flows on the INL site.

Initial hydraulic modeling for the paleohydrologic studies based on the 3-ft grid topographic data for the Diversion Dam reach showed results that differed significantly from the previous studies

of Ostenaar et al. (1999, 2002) which used topographic data derived from the 1993 INEEL 2-ft contour map. Because the same two-dimensional hydraulic model was being used in both studies, the cause of this difference was clearly related to the input topography used in the models. To resolve these discrepancies, extensive GPS field surveys along the Big Lost River were conducted to assess the accuracy of the topographic mapping used in all phases of these studies. The GPS field surveys found that the 1993 INEEL 2-ft contour map did not appear to meet standards for 4-ft contour interval mapping and that in the area of the paleoflood study reach the surface defined by this mapping was apparently warped (**Appendix A**). The lack of resolution and accuracy associated with the 1993 2-ft contour map resulted in systematic overestimation of stages associated with discharge in the Big Lost River in the previous studies. Because similar issues to topographic accuracy would affect model estimates of flood stage probability at INTEC and TRA, data from the 1993 aerial photography was reprocessed to provide an updated topographic dataset for the hydraulic modeling. GPS field surveys of selected areas along the Big Lost River corridor demonstrate that the topographic data from the 2000 photography in the paleoflood study reach and reprocessed data from the 1993 photography both meet accuracy standards needed for the high-resolution flood modeling (**Appendix A**).

Outline of the Final Report

The overall scope of the present study is large and has included extensive data acquisition, field investigations, and computational efforts. Documentation of the study is contained in three elements: 1) this Overview, 2) Summary Document, and 3) Appendices. This Overview provides the major results of these efforts and key conclusions for flood hazard studies of the Big Lost River at INL. Within the Summary Document, **Section 1** provides introduction and background. **Section 2** and **Section 3** describe the geologic, geomorphic and hydraulic modeling investigations to further evaluate the paleohydrologic data used for flood frequency estimates of the Big Lost River. **Section 4** provides an updated flood frequency analyses based on these data. **Section 5** describes the hydraulic modeling and conceptual framework for evaluating stage-probability estimates for selected sites at INTEC and TRA. Topographic and geomorphic maps for the Diversion Dam study reach are shown on **Plate 1** and **Plate 2**. Additional supporting documentation is contained in several appendices that accompany this report as follows:

Appendix A - Quality Assurance of Topographic Data**Appendix B - Geologic Data**

Soil Profile Descriptions

Soil Particle Size Analysis Results from Colorado State University

Examination of Bulk Soil for Radiocarbon Datable Material from Along the Big Lost River on the Idaho National Engineering and Environmental Laboratory (INEEL) site by K. Puseman, Paleo Research Institute.

Radiocarbon Dating Results and Calibration Data from Beta Analytic

Summary Report on Detrital Zircon Ages of Samples from Big Lost River Trenches by P.K. Link, Idaho State Univ., and C.M. Fanning, Australian National University

Explanation, Plots, and Procedures for Point and Pebble Counts and Sieve Data by V. Sheedy, Idaho State Univ.

Gamma Ray Spectrometry Results from J. Budahn, U.S. Geological Survey

Trench Sample Listings

Appendix B - Electronic Supplement - Trench Logs**Appendix C - Hydraulic Modeling Methodology and Quality Assurance**

Part A - Methodology, mesh generation, and models

Part B - Quality Assurance

Appendix D - Hydraulic Modeling Results for Paleoflood Analyses

Evaluating Paleohydrologic Data with Stream Power and Shear Stress Results from Hydraulic Models

Appendix D - Electronic Supplement - Plots of Modeled Depth, Stream Power and Shear Stress for the Big Lost River, INEEL Diversion Dam Reach**Appendix E - Hydraulic Modeling to Estimate Big Lost River Flood Inundation at INEEL Facility Sites**

Estimating Channel Infiltration Parameters from Historical Flow Data at INEEL

Infiltration Rates to Support High-Resolution Hydraulic Modeling at Idaho National Engineering and Environmental Laboratory by F.R. Fiedler, University of Idaho

Culvert Survey Summary by C.O. Kingsford, Bechtel BWXT

Stage-Discharge Relations for Selected Culverts and Bridges in the Big Lost River Flood Plain at the Idaho National Engineering and Environmental Laboratory, Idaho by C. Berenbrock and J.D. Doyle, U.S. Geological Survey

Appendix E - Electronic Supplement - Plots of Modeled Flood Inundation for the Big Lost River Downstream of the INEEL Diversion Dam**Appendix F - Stage Probability Plots for Selected Locations at INEEL Facility Sites**

Geomorphic and Paleoflood Investigations

The paleohydrologic studies of the Diversion Dam study reach are a continuation and expansion of the studies described in previous reports (Ostenaar et al., 1999, 2002). The objective of further studies is to further identify and reduce the uncertainty associated with previous estimates. Field-scale investigations included four major tasks: 1) acquisition and processing of new detailed aerial photography to serve as a base map for geomorphic mapping and hydraulic modeling, 2) compilation of a detailed geomorphic map of the study reach, 3) trenching and detailed geologic descriptions and analyses in three areas of the study reach to confirm geologic/geomorphic relationships, and 4) additional two-dimensional hydraulic modeling using the new topographic data. The results of these investigations were expected to provide refined estimates, with improved understanding of the uncertainties, of the paleohydrologic parameters used in the prior flood frequency analyses. The present study results largely confirm and add additional details to the geologic components of the paleohydrologic parameters derived from the previous studies. However, because of the deficiencies associated with the topographic data (**Appendix A**) used in the earlier studies, hydraulic modeling for the present study results in substantially different estimates of discharge for the paleohydrologic parameters.

In evaluating discharge estimates for paleohydrologic bounds, the focus is on developing an estimate of the flood discharge required to modify or erode a geomorphic surface for which stability can be demonstrated for some prior length of time (e.g. Levish, 2002). Many geomorphologists have used stream power as a measure of the potential for channel and landscape modification with a focus on channel power or average cross section power (e.g., Baker and Costa, 1987; Magiligan, 1992). For engineering applications of erosion, channel stability, and sediment transport studies, many empirical and semi-theoretical relationships have been developed for hydraulic parameters such as depth, velocity, shear stress and stream power (e.g., see Carson and Griffiths, 1987 for a summary). However, in neither body of literature are there many examples of sites which might be considered long existing paleohydrologic bounds which have been overtopped by historical floods, and associated model estimates of the flow parameters associated with this overtopping developed. As noted by Jarrett and England (2002), documentation for the relationships between HWM (high water marks) and the estimated stage

required to modify a geomorphic surface and thus define a paleohydrologic bound is lacking in the general literature.

In the present study, we develop a more formal framework for the application of shear stress and stream power to the problem of specification of discharge estimates for paleohydrologic bounds. The difficulties associated with developing conclusions within this framework are similar to those faced in seismic hazard assessment (e.g., SSHAC, 1995), in that uncertainty of the estimates is derived from several sources including limited data, imperfect knowledge and models of salient physical processes, and legitimate differences of scientific opinion.

Three major types of information are used to estimate the discharge range associated with a paleohydrologic bound: 1) geomorphic/geologic map and unit descriptions, 2) hydraulic modeling results of depth, unit stream power, and bed shear stress for differing input parameters, and 3) a criterion for erosion/modification of geomorphic surfaces based on empirical data compilations of unit stream power and shear stress.

Geomorphic map units define the spatial extent of areas with similar geologic/geomorphic processes and history. Individual map units are characterized by similarity in relative and absolute age, geomorphic processes and history over broad areas. Differences in age, process, and history between different areas define different geomorphic units. Thus, based on detailed mapping along the Diversion Dam study reach of the Big Lost River (**Section 2, Plate 2, and Appendix B**), four major geomorphic map groups, H1-2, H3-4, P2, and P3, are of primary importance to the issues of specifying paleohydrologic bounds. The similarities and differences within these broad map units are highlighted and defined through "point" investigations with trenches or soil description sites where stratigraphic details are described in detail. These detailed site descriptions provide the basis for areal extrapolation represented by the areal extent of the geomorphic map units. Individual geomorphic map unit areas naturally define the spatial limits of areas within which the variability of hydraulic parameters such as unit stream power and bed shear stress can be evaluated when that geomorphic unit is inundated by a modeled flow.

Two-dimensional hydraulic modeling (**Section 2 and Appendix C**) based on small grid cells relative to channel width is used to develop detailed information on the extent and spatial

variability of flow for each modeled discharge. From the model results, shear stress and stream power are calculated for each grid cell providing a detailed depiction of the magnitude and spatial variability of these parameters over the inundated areas. This information can then be compared to the spatial extent and characteristics of differing geologic/geomorphic units. Results from the two-dimensional modeling of each discharge that are used to evaluate paleohydrologic information are 1) depth and spatial extent of inundation over a particular stratigraphic site or geomorphic surface, 2) magnitude and spatial extent of bed shear stress and/or unit stream power over a site or geomorphic surface, and 3) magnitude and spatial extent of bed shear stress and unit stream power in channel reaches. Evaluation based on depth and extent of inundation primarily considers whether or not a particular site or surface area is inundated by a given flow. For many sites, as a greater percentage of a given site or geomorphic surface is inundated, to progressively greater depths, the probability of surface modification and development of a preservable geologic record increases. Likewise, as the extent and depth of inundation increase, the magnitude and distribution of unit stream power and bed shear stress change across the geomorphic surface as well. The hydraulic conditions associated with flow across a geomorphic surface are varied and non-uniform due to topography, small- and large-scale roughness, turbulence, and mixing. Thus, actual and calculated values of stream power and shear stress vary spatially in magnitude across a given cross section and throughout the area of flow. The results or conclusions drawn from application of any criteria for surface modification is therefore dependent on the location chosen for evaluation. One advantage of the use of high-resolution, two-dimensional hydraulic models is that these models provide outputs that show the spatial variability of flow characteristics. Ideally, the spatial variability shown by hydraulic modeling can be evaluated separately for each geomorphic surface of interest.

The third major type of information used to estimate discharge associated with a paleohydrologic bound are empirical criteria and observational data on the magnitudes of stream power and shear stress that are likely associated with modification or erosion of differing geomorphic surfaces (**Appendix D**). From these data, limiting values for the estimated erosion or modification of differing surfaces can be subjectively estimated for the specific surface conditions and physical properties (e.g., vegetation, soil, and grain size) of each site or geomorphic surface. Because estimates of paleohydrologic bounds will ultimately have a probabilistic description for use in the

flood frequency analyses, these criteria are formulated as probability density functions (PDF) that relate the relative probability of surface modification to particular values of shear stress or stream power. In general, the PDF's that describe the probability of surface modification are triangular distributions based on three estimated values. A lower value of shear stress or stream power represents a limit for which there is judged to be a reasonable possibility based on the existing empirical data that significant erosion or surface modification will occur. A central or preferred value represents a large body of data with high confidence. For some PDF's, the central values include a range of equal relative likelihood. An upper value limit defines a boundary beyond which there is virtual certainty of significant erosion or modification based on the available data. For application to the Diversion Dam reach of the Big Lost River, three separate criteria have been developed for unit stream power and bed shear stress, respectively (**Appendix D**). Two of the criteria are for application to the differing site, soil, and geologic conditions associated the geomorphic surfaces along the Big Lost River. The third criteria describes the more general conditions under which significant geomorphic modification of portions of the Big Lost River channel might result from various discharge levels.

Soils and geologic data from the Big Lost River lead to two general categories for erosion and surface modification, termed soil erosion and terrace erosion, based on the contrasting physical and vegetative characteristics of the soils and terrace deposits. Most of alluvial soils have an upper horizon(s), usually less than 30 cm thick, composed of silt and sand which is generally loose and unconsolidated. These horizons, usually designated as A, AB, and sometimes Bw in soil descriptions (**Section 2** and **Appendix B**), lack carbonate cementation, are often bioturbated, and may include in their upper portions some component of recently active eolian sand. Some small grasses and plants have shallow roots in these horizons. In contrast, at most stream terrace sites, below a depth of more than 20-30 cm in most profiles, there is either carbonate cementation or gravel. In deposits that are mostly fine-grained, i.e., silty and sandy, soils with carbonate accumulation are stage I to II. In the gravel deposits maximum clast sizes are generally less than 200 mm, and carbonate stages range from Stage I to III. Larger plants, such as sage, have widely scattered roots that extend into the gravel horizons. Based on the carbonate cementation and generally larger clast size associated with the terrace deposits, larger values of stream power and shear stress are required to initiate erosion.

The criteria developed for channel stability is mainly derived from geomorphic study observations of major channel widening or change following floods (**Appendix D**). This criteria is only applicable to channels where banks are cut in alluvium. Most channel banks along the Big Lost River Diversion Dam study reach are composed of fine-grained alluvium with weakly to moderately developed carbonate soils similar to sections exposed in trenches T4, T5, T6, and description sites BLR2, BLR6, BLR7 and BLR8. Gravel, in Holocene fluvial deposits, is not present more than about 1 m above the present channel floor at these exposures. Based on geomorphic mapping (**Plate 2**), only very scattered sections of the channel banks are cut directly in the gravelly Pleistocene alluvium without an inset fine-grained fill terrace. More commonly, scattered basalt outcrops confine one or both channel banks. Within this varied channel setting, the hydraulic modeling results indicate large longitudinal variation in channel stream power and shear stress throughout the Diversion Dam study reach for a subset of modeled flows.

Table S0-2 summarizes the conclusions and evidence for paleofloods and paleohydrologic bounds that resulted from the current study of the Diversion Dam reach, primarily based on the geologic observations gleaned from several trenches (**Section 2** and **Appendix B - Electronic Supplement**). As shown by previous studies (Ostenaar et al., 1999, 2002), there is clear evidence of late Holocene floods along the Big Lost River that are substantially larger than the largest historic floods. The present study confirms the approximate 400-yr age of one of these floods and suggests the possibility of infrequent, earlier floods of similar size as well as the existence of a more recent and slightly smaller paleoflood (**Section 2** and **Appendix B**). The geologic and geomorphic basis for paleohydrologic bounds based on these data are consistent with previous studies but discharge estimates for both paleofloods and paleohydrologic bounds are substantially revised based on the updated hydraulic modeling (**Section 2**, **Section 3** and **Appendix D**). Changes in these discharge estimates compared to previous studies are directly attributable to stage differences resulting from the use of new, more accurate topographic data in the current study (**Appendix A**). Results of the flow modeling are depicted on color-contoured plots of depth, unit stream power and bed shear stress overlain on shaded relief images of the high-resolution topography and the geomorphic map units from **Plate 2** in **Appendix D - Electronic Supplement**.

Table S0-2 Big Lost River Paleofloods and Paleohydrologic Bounds

Event name	Age or time span (Cal yrs or Cal yr B.P.) ¹	Discharge (m ³ /s) and type of distribution	Summary of Evidence
Paleofloods			
"white flood"	>100yr (pre-gaging) but less than 400-600yr	90 (80-100) uniform	Based on thin deposit in T4. Not recognized in T5 or T6 (slightly higher sites). Possible correlative in T9(?). Age - most likely 100 to 150 years based on absence of soil development. Discharge - Upper limit based on rapid increase in power/shear stress at T4 and lack of deposit in T5/T6.
"400-yr" flood	400 to 600 years	150 (130-175) triangular	Apparently correlative deposits in T4, T5, T6 (also BLR2, BLR7 & BLR8) with similar soils, stratigraphic setting, and radiocarbon ages. Soil has stage I- Bk horizon. Stripping of A- and AB/Bw horizons at T8c, partial stripping at T8b; lack of erosion at T8a. May represent more than one flood.
"older flood"	1000 to 2000 years	150 (130-175) triangular	Deposits with Stage I to I+ Bk horizon that underlie "400-yr flood" deposits in T4, T5, T6 and T9. Appears to indicate long period of stability with little or no deposition at these sites before deposition of deposits associated with "400-yr" flood. Similar stratigraphy at BLR2 and BLR8. Likely represents multiple floods of similar or smaller maximum discharge. Minimum discharge must inundate FP1-FP4, FP6-8, most of FP7, FP11-13, FP17-18, and FP19-21, which are areas with H1-2 geomorphic surfaces that appear to indicate Holocene flooding.
Paleohydrologic Bounds			
400-yr #1	400-600	130 (110-150) triangular	Preservation of recognizable stratigraphy at T4 and T6. No stripping of A-horizons from the youngest deposits at T4 and T6. Apparently correlative H1-2 geomorphic surfaces at FP1, FP3-4, FP7, FP11-13, FP17, and FP19-20.
early Holocene (H1 surfaces)	6000 to 8000	225 (175-250) triangular	Preservation of stratigraphy in T6, T4, and T8a,b,c. Banks at BLR6 and continuity of H1-2 geomorphic surfaces along BLR.
Pleistocene	>10000	250 (225-400) triangular	Preservation of Pleistocene gravel surfaces throughout the study reach. Actual age of the underlying deposits is older than 12-15 ka (minimum age of deglaciation) and some may be older than 20-25 ka (Last glacial maximum). Length of time span for paleohydrologic bound is limited by post-glacial, warmer climate more similar to present.
Notes: ¹ All age distributions have uniform probability over the indicated time span uncertainty.			

Revised Big Lost River Flood Frequency Analyses

The approach taken for this study is to incorporate paleoflood estimates and paleohydrologic bounds (Levish, 2002; Levish et al., 1994, 1996, 1997; Ostenaar and Levish, 1996) into nonparametric Bayesian flood frequency analysis that uses likelihood functions that incorporate both parameter and data (discharge and geologic age) measurement uncertainties (O’Connell et al., 1996, 1998; O’Connell, 2005).

A paleohydrologic bound is the time interval during which a given discharge has not been exceeded. Paleohydrologic bounds are not actual floods, but instead are limits on paleostage over a measured time interval. These bounds represent stages and discharges that have not been exceeded since a geomorphic surface stabilized. Through hydraulic modeling, discharge for a paleohydrologic bound can be derived from stage, just as a discharge is derived from the paleostage indicators of past floods. Used appropriately, paleohydrologic bounds are powerful constraints in flood frequency analyses, even if the number, timing, and magnitude of individual paleofloods are uncertain (Stedinger and Cohn, 1986).

It is necessary to revise flood frequency estimates from previous studies for two reasons. First, peak discharge values have been modified for several data points, including the paleohydrologic non-exceedence bounds. Second, the distribution of observed peak discharges and paleohydrologic information is sufficiently complex that parametric flood frequency functions are ill-suited to determine statistical quantities, such as credible or “confidence” limits for flood frequency estimates. Consequently, a newly-published nonparametric Bayesian flood frequency estimation approach (O’Connell, 2005) is used to obtain probabilistic minimum-bias estimates of flood frequency. This method accommodates complex flood behaviors such as event clustering (repeated instances of similar magnitude floods) and can use varied data, such as gage and historical peak discharges, and paleohydrologic upper and lower bounds on peak discharge, while rigorously accounting for a wide variety of measurement uncertainties. In contrast to nonparametric kernel estimation approaches, the stochastic assumption is used to generate flood frequency models that span the data and provide about twice the number of degrees of freedom of the data. Each generated flood frequency model is scored using likelihoods that account for data measurement uncertainties. A parametric estimation approach ensures high precision because

posterior sampling is known. However, parametric approaches can produce substantial biases because the classes of allowed flood frequency models are restricted. These biases are completely undetectable within a parametric paradigm. To minimize these types of biases, the nonparametric approach used here surrenders some precision, but produces greater overall accuracy and assurance; it reveals the annual probabilities where discharge becomes unconstrained by the data, thereby eliminating unsubstantiated extrapolation. Parametric flood frequency estimation introduces strong extrapolation priors that make it difficult, if not impossible, to determine when flood frequency is not longer constrained by the data. These problems are apparent in the parametric method of O'Connell et al. (2002) used in the previous INL flood-frequency analyses (Ostenaar et al., 1999, 2002).

Present results show limits of extrapolation on AEP to be inversely proportional to about twice the length of record, corresponding to a minimum AEP of $\sim 1/20,000$ for which discharge estimation is credible. The data provide no constraints on how infrequent discharges larger than $300 \text{ m}^3/\text{s}$ may be, but place strong constraints on the maximum AEPs that can be associated with any discharge.

The present analysis only assumes that for extreme floods, upstream regulatory structures and diversions do not increase flood magnitudes downstream compared to the unregulated natural flows, except for cases where upstream regulating structures might fail. Flood probabilities for such scenarios should be evaluated separately, and account for the overall failure probability of the structure under all conditions. The impacts of regulation and variations in smaller flows, such as those of historical experience, on frequency estimates of extreme floods were addressed through sensitivity analyses in previous analyses (Ostenaar et al., 1999).

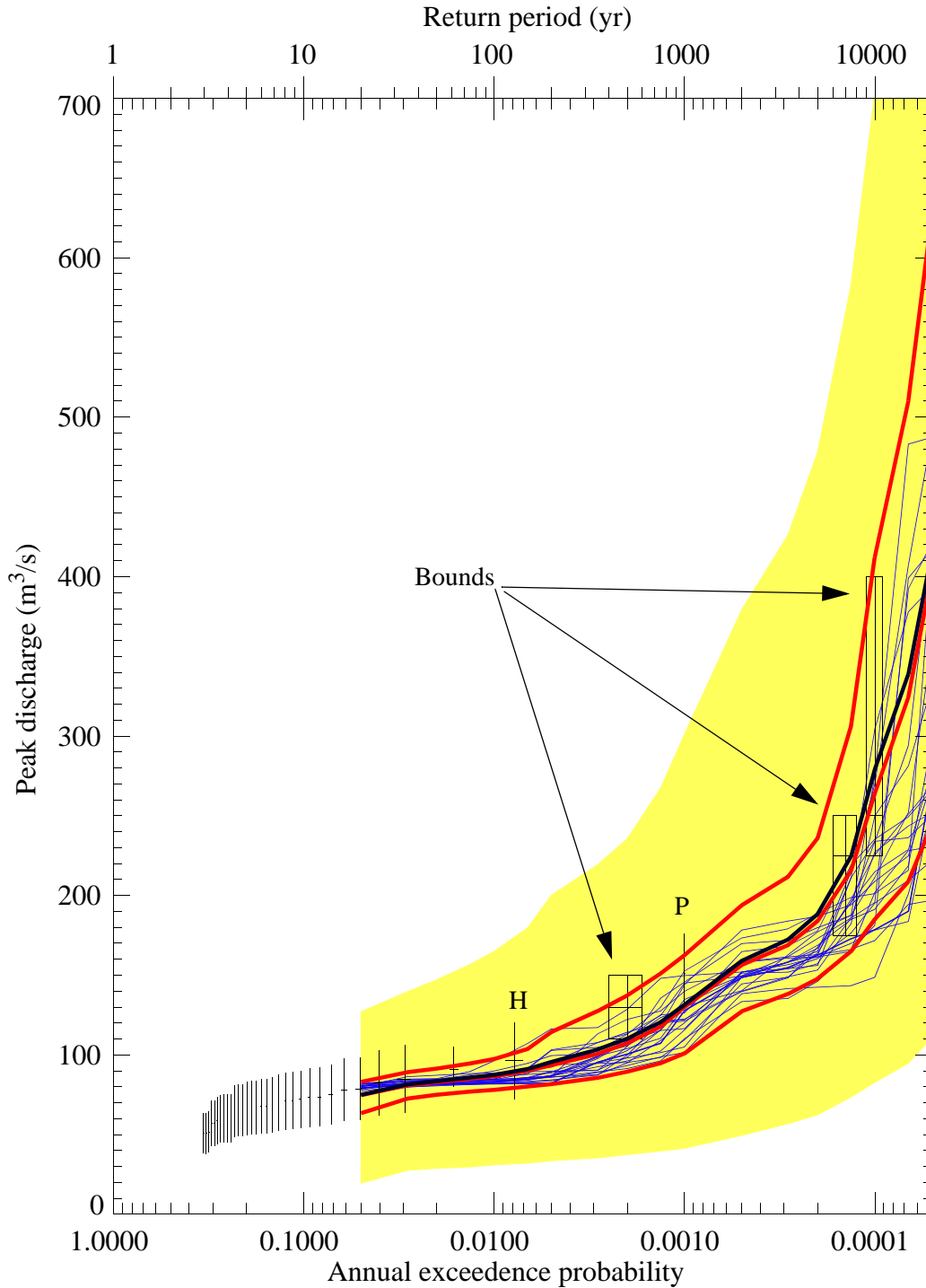


Figure SO-1 Revised flood frequency for Big Lost River at the INEEL Diversion Dam. Gaged flows (vertical black lines, with short horizontal lines indicating preferred discharge and plotting position uncertainty) are from Big Lost River at Howell Ranch (94 years) attenuated to the INEEL Diversion Dam based on methods of Hortness and Rousseau (2002). Geologic data includes two paleofloods (largest discharges labeled H and P) and three paleohydrologic bounds (black boxes - vertical lines indicate discharge range, horizontal lines indicate duration range). Lower and upper red curves are 5% and 95% credible limits (middle red is median, and middle black is mean). Blue curves are models with relative likelihoods > 0.25 of the maximum likelihood. Yellow region indicates the limits of sampling.

Table SO-3 Nonparametric Flood Frequency for the Big Lost River at the Diversion Dam.

AEP (1/yr)	Return period (yr)	5% (m ³ /s)	mean (m ³ /s)	95% (m ³ /s)
5×10^{-2}	20	63	75	83
2.86×10^{-2}	35	73	81	89
2×10^{-2}	50	75	83	91
1.33×10^{-2}	75	77	86	95
10^{-2}	100	78	87	97
6.67×10^{-3}	150	80	91	104
5×10^{-3}	200	82	96	114
2.86×10^{-3}	350	86	103	127
2×10^{-3}	500	89	110	137
1.33×10^{-3}	750	95	121	151
10^{-3}	1000	101	131	163
5×10^{-4}	2000	127	159	194
2.86×10^{-4}	3500	138	172	212
2×10^{-4}	5000	148	188	236
1.33×10^{-4}	7500	165	224	306
10^{-4}	10,000	185	279	412
6.67×10^{-5}	15,000	209	339*	510*
5×10^{-5}	20,000	245	416*	628*
* Values with diminished or little statistical significance.				

Probabilistic Flood Stage at INTEC and TRA

The two-dimensional (depth-averaged) flow models TrimR2D and RiCOM (**Appendix C**) were used to calculate inundation and flow velocities for paleoflood and site inundation investigations at INL. TrimR2D uses a fixed-spacing staggered finite-difference approach that was used for hydraulic modeling of steady-state discharges in the paleoflood reach and with a larger grid spacing for the site inundation studies. RiCOM uses a staggered finite-element approach that provided an opportunity to employ high-resolution topography in a variable-sized element mesh constructed for the INL site inundation investigations. Both TrimR2D and RiCOM were used to investigate site inundation scenarios to assess the importance of parameters including topographic grid resolution, infiltration, and culvert performance, on estimated inundation corresponding to long-duration (~20 hour-steady-state) discharges. Results from both models were post-processed for estimates of unit stream power and bed shear stress.

Monte Carlo nonparametric flood frequency estimation was used to incorporate measurement uncertainties in gaged, historical, and paleoflood discharges and nonexceedence bounds and to produce fully probabilistic flood frequency estimates for annual exceedence probabilities of specific discharges of interest. These annual exceedence probabilities were combined with stage estimates from TrimR2D and RiCOM discharge, infiltration, culvert, and topographic resolution scenarios to produce scenario probabilistic stage hazard curves for 15 sites located in the TRA/INTEC facilities (**Appendix F**). Annual exceedence probabilities and associated credible limits are provided for map-scale inundation plots to provide scenario probabilistic inundation maps (**Appendix E**). These products provide a basis to develop weights for logic tree branches associated with infiltration and culvert performance scenarios to produce probabilistic inundation maps.

Two-dimensional hydraulic modeling using a broad range of discharges conducted for the reach of the Big Lost River downstream of the INEEL Diversion Dam to approximately the INEEL railroad grade downstream of INTEC and TRA provide one element needed for probabilistic flood stage estimates at these facilities. A conceptual framework for evaluating the model results and flood frequency information was developed in the early stages of this study to guide the evaluations. Uncertainties in probabilistic flood stage estimates are discussed in the context of

that framework. Based on this framework, results and uncertainties for stage - probability curves for fifteen specific sites within INTEC and TRA are discussed.

Appendix E - Electronic Supplement presents maps depicting the results of two-dimensional hydraulic modeling conducted to estimate probabilistic flood stage at INTEC and TRA. These maps show results for both the entire reach downstream of the INEEL Diversion Dam as well as enlarged views in the immediate vicinity of the facilities. For TrimR2D, the output flow quantities included water surface elevations and vector flow velocities interpolated to the water surface elevation positions at cell-centered positions in the staggered grid. Using the input topography, derived quantities such as depth, bed shear stress, and unit stream power were obtained. For RiCOM, the output flow quantities included water surface elevations and vector flow velocities interpolated to the element vertices using the finite-element basis functions. The inverse transformation operators were then applied to produce flow quantities in the INL state-plane coordinate system. For most modeled discharges, results are presented for modeled flow depth, unit stream power, and bed shear stress based on the TrimR2D results. RiCOM results are presented mostly as plots showing the difference in water-surface elevation from TrimR2D results for the same input discharge. A full set of RiCOM results (depth, unit stream power, bed shear stress) are presented only for four quantile results of the 100- and 500- yr discharges from the flood frequency analyses. Additional depth difference plots from TrimR2D models depict end member differences for infiltration and culvert scenarios.

Each of the inundation maps for a specific discharge could be associated with mean and credible limits on AEP associated with that discharge. However, such AEP's would not represent complete probabilistic inundation maps (PIM) for INL. There are additional probabilities (or weights) that must be assigned to aleatory (random-by-nature) parameters, such as infiltration and culvert conveyance. A conceptual framework for evaluating these uncertainties that was developed in the early stages of this study to guide the investigations. Epistemic uncertainties include factors such as flow model variability and appropriate scenario terrain models used in the simulations. Elicitation and assignments of weights to all aleatory and epistemic factors are required to produce comprehensive PIM's. Each of the major elements will be briefly described below.

Aleatory uncertainties include estimated flood frequency, hydrograph shape, infiltration, and culvert discharge characteristics. Several different infiltration and culvert performance scenarios were used to incorporate aleatory uncertainties associated with these parameters. A wide range of discharges were used to quantify the impacts of flood frequency aleatory uncertainty on probabilistic stage estimates. A long-duration steady-state flow assumption was used. Consequently, the impacts of varying hydrograph shape were not investigated. Generally, infiltration and culvert uncertainties had only small impacts relative to epistemic topography uncertainties, as discussed below.

Epistemic uncertainties include topography and computational flow models. Potential epistemic uncertainties associated with the two flow models are discussed in **Appendix C, Part B, Section 1**. These tests and output comparisons (difference plots in **Appendix E - Electronic Supplement**) show that negligible differences in water-surface elevation at most sites can be attributed to the choice of flow model. Much larger epistemic uncertainty is associated with the ability to accurately resolve subtle topographic features in the model inputs. Epistemic uncertainty associated with the input topography for the hydraulic models is not quantified in a statistical sense, but is shown by the differences in stage hazard plots for TrimR2D compared to RiCOM. These effects are often largest for flows less than about 200 m³/s where the differences in the ability of the input grids to resolve subtle features of the input topography leads to areas inundated to higher or lower levels between the flow models (See TrimR2D minus RiCOM difference plots in **Appendix E - Electronic Supplement**). A full appreciation of the impact of these factors on inundation characteristics is best provided by the large-scale inundation maps. The stage - AEP curves for the fifteen TRA/INTEC sites suggest these effects are mostly less than ~ 0.5 ft (**Appendix F**), but it is the maps (**Appendix E - Electronic Supplement**) that provide the best illustrations of the strong sensitivity of portions of the inundation to topographic resolution and relatively subtle topographic features such as roads and old diversion structures.

Inundation Discussion

Stage hazard curves are provided in Appendix F for fifteen specific sites near TRA or INTEC as listed in **Table SO-4** and **Table SO-5**. For each site there are four plots of flow simulation results: 1) TrimR2D, 2) RiCOM, 3) TrimR2D - RiCOM comparisons, and 4) RiCOM Lincoln Ave

blockage scenarios. Comparisons within and between these four sets of plots isolate or compare specific factors that could influence estimated stages. The TrimR2D simulations are the primary suite of results for final estimate of stage hazard curves and isolate the effects of variations in infiltration and secondary culvert blockage. Generally, the secondary culverts have virtually no impact on inundation at most sites, with only minor impacts on inundation at sites outside TRA along Monroe Avenue. Infiltration has only a modest impact on inundation and generally does not change the hazard curves much. The RiCOM simulations and TrimR2D -RiCOM simulations illustrate the impacts of topographic resolution and persistent topographic features such as roads, old diversions, etc. These factors have the strongest impacts on inundation over the entire site. The RiCOM simulations with blockage of the Big Lost River channel at Lincoln Avenue has the strongest impact on inundation for portions of INTEC, particularly for the simulations of discharges less than about $250 \text{ m}^3/\text{s}$.

The inundation maps in **Appendix E - Electronic Supplement** provide an essential tool to understand the stage hazard curves in **Appendix F**. It is clear that small-scale (possibly transient) changes to topography can significantly impact inundation at TRA and INTEC. This is a consequence of the relatively flat terrain in the vicinity of the Big Lost River and these INL facilities. However, the maps also provide a tool to determine small-scale changes to topography that could substantially reduce inundation hazards at TRA and INTEC. For instance, flow along the northern side of the old diversion channel west of TRA could be blocked by rather small-scale topographic modifications about 3.2 km west of TRA near the western end of the old diversion channel. The inundation impacts of topographic modification scenarios could be easily investigated by running new flows with modifications to the detailed topographic RiCOM mesh. Clearly, the performance of the Big Lost River culverts at Lincoln Avenue have a profound influence on stage hazards for several sites at INTEC, especially for the lower end of the discharges simulated. Similarly, although an explicit culvert blocking scenario was not constructed for the railroad embankment bridge downstream of INTEC, blockage of conveyance through the railroad embankment may also significantly influence stage hazards for portions of INTEC.

The stage hazard curves contained in Appendix F have the same limitations for extrapolation to small AEP (AEP < 0.0001) as do the flood frequency results presented in **Section 4**. Because the flood frequency results are largely unconstrained for small AEP, no meaningful estimate of 95% limits is contained in the revised flood frequency analyses to promulgate into the stage probability estimate. Given the nearly unlimited upper bounds of extrapolation that might be possible for small AEP from the present flood frequency analyses, development of stage hazard curves for smaller AEP would also require additional hydraulic modeling for discharges much larger than 700 m³/s, which is the largest discharge considered in the present study.

Table SO-4 Probabilistic Stage Estimates for INTEC and TRA Sites (100- and 500-year floods).

Map Ref #	Site Description	AEP = 10 ⁻² Return period = 100 yr			AEP = 2 x 10 ⁻³ Return period = 500 yr		
		5%	mean	95%	5%	mean	95%
TRA Sites							
1	TRA - Monroe Ave	4924.49-4924.56	4924.55-4924.60	4924.61-4924.65	4924.58-4924.63	4924.67-4924.70	4924.72-4924.75
2	TRA-715 (evap. pond)	4918.36-4918.56	4918.50-4918.64	4918.63-4918.71	4918.57-4918.67	4918.73-4918.81	4918.81-4918.91
3	TRA southeast corner	dry	dry	dry	dry	dry	dry
4	TRA northwest corner	dry	dry	dry	dry	dry	dry
5	TRA-670 (ATR)	dry	dry	dry	dry	dry	dry
6	TRA-670 (ATR)	dry	dry	dry	dry	dry	dry
7	TRA-632	dry	dry	dry	dry	dry	dry
8	TRA-621	dry	dry	dry	dry	dry	dry
9	TRA-715 (evap. pond)	dry	dry	dry	dry	dry	dry
INTEC Sites							
10	INTEC Tank Farm	4912.57-4913.12	4912.92-4913.29	4913.26-4913.45	4913.09-4913.37	4913.50-4913.65	4913.72-4913.85
11	NWCF (Bldg 659)	dry	dry	dry	dry	dry	dry
12	CPP-749	4916.30-4916.40	4916.42-4916.51	4916.54-4916.60	4916.48-4916.55	4916.63-4916.69	4916.71-4916.78
13	INTEC - NE corner	4907.04-4907.17	4907.18-4907.27	4907.31-4907.35	4907.25-4907.31	4907.42-4907.47	4907.53-4907.59
14	INTEC -nr west gate	4916.30-4916.40	4916.42-4916.51	4916.54-4916.60	4916.48-4916.55	4916.63-4916.69	4916.71-4916.78
15	BLR - NW corner of INTEC	4913.03-4913.10	4913.13-4913.18	4913.22-4913.26	4913.18-4913.22	4913.34-4913.38	4913.46-4913.50

Table SO-5 Probabilistic Stage Estimates for INTEC and TRA Sites (2000- and 10,000-year floods).

Map Ref #	Site Description	AEP = 5 x 10 ⁻⁴ Return period = 2000 yr			AEP = 1 x 10 ⁻⁴ Return period = 10000 yr		
		5%	mean	95%	5%	mean	95%
TRA Sites							
1	TRA - Monroe Ave	4924.68-4924.71	4924.77-4924.80	4924.86-4924.90	4924.83-4924.86	4925.04-4925.09	4925.36-4925.43
2	TRA-715 (evap. pond)	4918.74-4918.82	4918.91-4918.99	4919.06-4919.13	4919.01-4919.07	4919.36-4919.45	4919.89-4919.99
3	TRA southeast corner	dry	dry-4922.21	4922.36-4922.45	4922.20-4922.37	4922.81-4922.96	4923.76-4924.02
4	TRA northwest corner	dry	dry	dry	dry	4923.38-4923.52	4924.14-4924.20
5	TRA-670 (ATR)	dry	dry	dry	dry	dry	dry
6	TRA-670 (ATR)	dry	dry	dry	dry	dry	4923.29-4923.32
7	TRA-632	dry	dry	dry	dry	dry	dry
8	TRA-621	dry	dry	dry	dry	dry	dry
9	TRA-715 (evap. pond)	dry	dry	dry	dry	dry	dry
INTEC Sites							
10	INTEC Tank Farm	4913.54-4913.68	4913.87-4913.98	4914.08-4914.18	4914.01-4914.11	4914.49-4914.57	4914.86-4914.89
11	NWCF (Bldg 659)	dry	dry-4911.35	4911.77-4911.81	4911.22-4911.77	4911.93-4911.96	4912.03-4912.06
12	CPP-749	4916.64-4916.71	4916.79-4916.85	4916.93-4916.96	4916.88-4916.92	4917.15-4917.24	4917.45-4917.48
13	INTEC - NE corner	4907.44-4907.49	4907.58-4907.64	4907.71-4907.77	4907.66-4907.72	4907.91-4907.95	4908.09-4908.13
14	INTEC -nr west gate	4916.64-4916.71	4916.79-4916.85	4916.93-4916.96	4916.88-4916.92	4917.15-4917.22	4917.41-4917.45
15	BLR - NW corner of INTEC	4913.36-4913.40	4913.52-4913.62	4913.71-4913.75	4913.64-4913.71	4913.90-4913.93	4914.07-4914.13

TABLE OF CONTENTS

<u>Section</u>	<u>Title</u>	<u>Page</u>
	OVERVIEW.....	III
1.0	INTRODUCTION	1
1.1	Present Study Objectives.....	1
1.2	Acknowledgments	3
	Figures for Section 1.0	7
	Tables for Section 1.0	10
2.0	GEOLOGIC AND GEOMORPHIC STUDIES OF THE DIVERSION DAM STUDY REACH	12
2.1	Geologic and Geomorphic Setting of the Diversion Dam Study Reach	12
2.1.1	Big Lost River historical stream flow.....	13
2.1.2	Big Lost River – Diversion Dam study reach.....	14
2.2	Geomorphic Mapping of the Diversion Dam Study Reach.....	17
2.2.1	Quaternary Basalts - Rb, Rbe, Rd and Rde	17
2.2.2	Pleistocene Units - P1 to P3	19
2.2.2.1	Age Constraints from Regional Glaciation.....	20
2.2.2.2	Earth Mounds.....	21
2.2.2.3	Geomorphic Evidence for Holocene Modification of the Pleistocene Units.....	23
2.2.3	Holocene Units - H1 to H4	24
2.2.4	Channel Deposits.....	26
2.3	Trenching Studies.....	27
2.3.1	Trenches T1, T2, and T3 - Big Loop Study Area.....	28
2.3.1.1	Trench T1.....	28
2.3.1.2	Trench T2.....	29
2.3.1.3	Trench T3.....	30
2.3.2	Trenches T4, T5, T6, and T7 - Saddle Constriction Study Area.....	31
2.3.2.1	Trench T4.....	31
2.3.2.2	Trench T5.....	33
2.3.2.3	Trench T6.....	35
2.3.2.4	Trench T7.....	37
2.3.3	Trenches T8 and T9 - BLR8 Study Area.....	38
2.3.3.1	Trench T8.....	39
2.3.3.2	Trench T9.....	43
2.4	Summary of Geomorphic and Geologic Data for Paleofloods and Paleohydrologic Bounds.....	45
2.4.1	Paleofloods	45
2.4.1.1	"White Flood"	46
2.4.2	"400-yr Flood"	46
2.4.3	"Older Flood".....	47
2.4.4	Paleohydrologic Bounds.....	48
2.4.4.1	400-yr Flood Bound.....	48
2.4.4.2	Early Holocene (H1 surfaces) Bound	49
2.4.4.3	Pleistocene Bound.....	49
2.5	Hydraulic Modeling of the Diversion Dam Study Reach	50

TABLE OF CONTENTS

<u>Section</u>	<u>Title</u>	<u>Page</u>
2.5.1	Results	52
2.5.1.1	Effects of Varied Manning's n.....	53
2.5.1.2	Effects of Input Topography.....	53
2.5.1.3	Comparisons to Previous Studies	54
2.5.1.4	Results from Specific Study Areas	55
	Figures for Section 2.0	60
	Tables for Section 2.0	117
3.0	PALEOFLOODS AND PALEOHYDROLOGIC BOUNDS FOR THE BIG LOST RIVER.....	121
3.1	Background to the Use of Paleohydrologic Bounds.....	121
3.1.1	Geologic and geomorphic evidence of flooding.....	121
3.2	Criteria and Approach for Evaluating Paleohydrologic Information.....	122
3.2.1	Evaluating Spatial Extent and Variability	127
3.2.1.1	Uncertainty in Discharge Estimates of Modification for each Subarea.....	129
3.2.1.2	Combining Estimates from Multiple Subareas.....	130
3.3	Age and Discharge Estimates for Paleofloods	131
3.3.1	"White Flood"	132
3.3.2	"400-yr Flood"	133
3.3.3	"Older Flood".....	134
3.4	Age and Discharge Estimates for Paleohydrologic Bounds.....	135
3.4.1	400-yr Flood Bound.....	135
3.4.2	Early Holocene (H1 surfaces) Bound.....	137
3.4.3	Pleistocene Bound	138
3.4.3.1	Catastrophic Channel Change.....	139
	Figures for Section 3.0	141
	Tables for Section 3.0	151
4.0	REVISED FLOOD FREQUENCY FOR THE BIG LOST RIVER AT THE IN- EEL DIVERSION DAM.....	161
4.1	Nonparametric Flood Frequency for the Big Lost River at INL.....	161
	Figures for Section 4.0	166
	Tables for Section 4.0	180
5.0	PROBABILISTIC FLOOD STAGE AT INTEC AND TRA	183
5.1	Topographic Input to Two-Dimensional Models.....	183
5.2	Two Dimensional Hydraulic Modeling.....	183
5.2.1	Infiltration Implementation and Scenarios	184
5.2.2	Culvert Implementation and Scenarios.....	184
5.2.3	Flow Initialization.....	184
5.2.4	Flow Parameters	185
5.2.5	Flow Completion	185
5.2.6	Flow Output.....	186
5.3	Conceptual Framework for Development of Probabilistic Inundation Maps and Flood Stage Estimates for Facility Sites at INL	186
5.3.1	Aleatory Uncertainties	187

TABLE OF CONTENTS

<u>Section</u>	<u>Title</u>	<u>Page</u>
5.3.1.1	Flood Frequency Analyses.....	187
5.3.1.2	Hydrograph Shape	188
5.3.1.3	Infiltration	188
5.3.1.4	Culverts.....	188
5.3.2	Epistemic Uncertainties.....	189
5.3.2.1	Topography and Flow Model Uncertainty.....	189
5.3.3	Scope of Results	189
5.4	Evaluation of Results.....	190
5.4.1	Flood Stage - Probability at TRA	191
5.4.2	Flood Stage - Probability at INTEC	191
5.5	Inundation Discussion	192
	Figures for Section 5.0	194
	Tables for Section 5.0	201
6.0	REFERENCES	207

LIST OF FIGURES

<u>Figure No.</u>	<u>Title</u>	<u>Page</u>
Figure SO-1	Revised flood frequency for Big Lost River at the INEEL Diversion Dam.	xv
Figure 1-1	Location map of INL (INEEL) and study area.	8
Figure 1-2	INL study area, Big Lost River and significant facility locations.	9
Figure 2-1	Annual peak discharge estimates for upstream (light shaded bars) and downstream gaging stations (dark shaded bars) on the Big Lost River.	61
Figure 2-2	Area around Trenches T1, T2, and T3.	62
Figure 2-3	Area around "Saddle" and Trenches T4 and T5 downstream of saddle constriction	63
Figure 2-4	Detail of area around Trenches T4, T5 and T6 downstream of saddle constriction	64
Figure 2-5	Area around BLR8 and Trenches T8 and T9.	65
Figure 2-6	Modeled water surface elevation near trenches T4 and T5.	66
Figure 2-7	Modeled water surface elevation near trench T9.	67
Figure 2-8	Summary plot of age constraints for late Holocene paleofloods.	68
Figure 2-9	Channel power for the Diversion Dam study reach subareas.	69
Figure 2-10	Model results for 100 and 150 m ³ /s from Ostenaar et al. (1999, 2002) near the Saddle.	70
Figure 2-11	Figure 5 from Ostenaar et al. (2002) with revised stage estimates at BLR study sites	71
Figure 2-12	6-ft flow model results for 130 m ³ /s in the Big Loop study area.	72
Figure 2-13	6-ft flow model results for 150 m ³ /s in the Big Loop study area.	73
Figure 2-14	6-ft flow model results for 175 m ³ /s in the Big Loop study area.	74
Figure 2-15	6-ft flow model results for 200 m ³ /s in the Big Loop study area.	75
Figure 2-16	6-ft flow model results for 225 m ³ /s in the Big Loop study area.	76
Figure 2-17	6-ft flow model results for 250 m ³ /s in the Big Loop study area.	77
Figure 2-18	5-ft flow model results for 200 m ³ /s in the Big Loop study area.	78
Figure 2-19	5-ft flow model results for 250 m ³ /s in the Big Loop study area.	79
Figure 2-20	5-ft flow model results for 300 m ³ /s in the Big Loop study area.	80
Figure 2-21	5-ft flow model results for 350 m ³ /s in the Big Loop study area.	81
Figure 2-22	5-ft flow model results for 400 m ³ /s in the Big Loop study area.	82
Figure 2-23	6-ft flow model results for 150 m ³ /s in the Saddle constriction study area.	83
Figure 2-24	6-ft flow model results for 200 m ³ /s in the Saddle constriction study area.	84
Figure 2-25	6-ft flow model results for 250 m ³ /s in the Saddle constriction study area.	85
Figure 2-26	5-ft flow model results for 200 m ³ /s in the Saddle constriction study area.	86
Figure 2-27	5-ft flow model results for 250 m ³ /s in the Saddle constriction study area.	87
Figure 2-28	5-ft flow model results for 300 m ³ /s in the Saddle constriction study area.	88
Figure 2-29	5-ft flow model results for 350 m ³ /s in the Saddle constriction study area.	89
Figure 2-30	5-ft flow model results for 400 m ³ /s in the Saddle constriction study area.	90
Figure 2-31	6-ft flow model results for 70 m ³ /s in the T4/T5/T6 study area.	91
Figure 2-32	6-ft flow model results for 100 m ³ /s in the T4/T5/T6 study area.	92
Figure 2-33	6-ft flow model results for 130 m ³ /s in the T4/T5/T6 study area.	93
Figure 2-34	6-ft flow model results for 150 m ³ /s in the T4/T5/T6 study area.	94
Figure 2-35	6-ft flow model results for 175 m ³ /s in the T4/T5/T6 study area.	95

LIST OF FIGURES

<u>Figure No.</u>	<u>Title</u>	<u>Page</u>
Figure 2-36	6-ft flow model results for 200 m ³ /s in the T4/T5/T6 study area.	96
Figure 2-37	6-ft flow model results for 225 m ³ /s in the T4/T5/T6 study area.	97
Figure 2-38	6-ft flow model results for 250 m ³ /s in the T4/T5/T6 study area.	98
Figure 2-39	5-ft flow model results for 200 m ³ /s in the T4/T5/T6 constriction study area. ..	99
Figure 2-40	5-ft flow model results for 250 m ³ /s in the T4/T5/T6 constriction study area.	100
Figure 2-41	5-ft flow model results for 300 m ³ /s in the T4/T5/T6 constriction study area.	101
Figure 2-42	5-ft flow model results for 350 m ³ /s in the T4/T5/T6 constriction study area.	102
Figure 2-43	5-ft flow model results for 400 m ³ /s in the T4/T5/T6 constriction study area.	103
Figure 2-44	6-ft flow model results for 70 m ³ /s in the BLR8 study area.	104
Figure 2-45	6-ft flow model results for 100 m ³ /s in the BLR8 study area.	105
Figure 2-46	6-ft flow model results for 130 m ³ /s in the BLR8 study area.	106
Figure 2-47	6-ft flow model results for 150 m ³ /s in the BLR8 study area.	107
Figure 2-48	6-ft flow model results for 175 m ³ /s in the BLR8 study area.	108
Figure 2-49	6-ft flow model results for 200 m ³ /s in the BLR8 study area.	109
Figure 2-50	6-ft flow model results for 225 m ³ /s in the BLR8 study area.	110
Figure 2-51	6-ft flow model results for 250 m ³ /s in the BLR8 study area.	111
Figure 2-52	5-ft flow model results for 200 m ³ /s in the BLR8 constriction study area.	112
Figure 2-53	5-ft flow model results for 250 m ³ /s in the BLR8 constriction study area.	113
Figure 2-54	5-ft flow model results for 300 m ³ /s in the BLR8 constriction study area.	114
Figure 2-55	5-ft flow model results for 350 m ³ /s in the BLR8 constriction study area.	115
Figure 2-56	5-ft flow model results for 400 m ³ /s in the BLR8 constriction study area.	116
Figure 3-1	Schematic representation of different types of geomorphic and stratigraphic evidence for paleofloods and paleohydrologic bounds.	142
Figure 3-2	Probability density functions for erosion based on shear stress and stream power for Big Lost River applications.	143
Figure 3-3	Probability distributions for major channel modifications based on channel averaged stream power and shear stress values.	144
Figure 3-4	Stream power and shear stress sample areas along Big Lost River Diversion Dam study reach.	145
Figure 3-5	Example of stream power and shear stress results for subarea FP11.	146
Figure 3-6	Combined discharge limits for late Holocene paleofloods and paleohydrologic bounds.	147
Figure 3-7	Combined discharge limits for early Holocene paleohydrologic bound.	148
Figure 3-8	Combined discharge limits for Pleistocene paleohydrologic bound.	149
Figure 3-9	Combined discharge limits for catastrophic channel change.	150
Figure 4-1	Measurement uncertainties for gage, bound, and paleoflood discharges on the Big Lost River at the INEEL Diversion Dam.	167
Figure 4-2	Revised flood frequency for Big Lost River at the INEEL Diversion Dam.	168
Figure 4-3	Peak discharges distributions for AEP's 0.01 and 0.00667 on the Big Lost River at the INEEL Diversion Dam.	169
Figure 4-4	Peak discharges distributions for AEP's 0.005 and 0.00286 on the Big Lost River at the INEEL Diversion Dam.	170
Figure 4-5	Peak discharges distributions for AEP's 0.002 and 0.00133 on the Big Lost River	

LIST OF FIGURES

<u>Figure No.</u>	<u>Title</u>	<u>Page</u>
	at the INEEL Diversion Dam.....	171
Figure 4-6	Peak discharges distributions for AEP's 0.001 and 0.0005 on the Big Lost River at the INEEL Diversion Dam.	172
Figure 4-7	Peak discharges distributions for AEP's 0.000286 and 0.00002 on the Big Lost River at the INEEL Diversion Dam.....	173
Figure 4-8	Peak discharges distributions for AEP's 0.000133 and 0.00001 on the Big Lost River at the INEEL Diversion Dam.....	174
Figure 4-9	Peak discharges distributions for AEP's 0.0000667 and 0.000005 on the Big Lost River at the INEEL Diversion Dam.....	175
Figure 4-10	AEP distributions for 250 m ³ /s and 300 m ³ /s on the Big Lost River at the INEEL Diversion Dam.	176
Figure 4-11	AEP distributions for 400 m ³ /s and 700 m ³ /s on the Big Lost River at the INEEL Diversion Dam.	177
Figure 4-12	AEP distributions for 106 m ³ /s and 150 m ³ /s on the Big Lost River at the INEEL Diversion Dam.	178
Figure 4-13	AEP distributions for 176 m ³ /s and 200 m ³ /s on the Big Lost River at the INEEL Diversion Dam.	179
Figure 5-1	Map of monitoring site locations (numbered black squares within blue boxes) for inundation at TRA and INTEC	195
Figure 5-2	Conceptual logic tree for probabilistic INL inundation modeling.....	196
Figure 5-3	Stage hazard curves for site TRA map ref #1.	197
Figure 5-4	Stage hazard curves for TRA-632 map ref #7.	198
Figure 5-5	Stage hazard curves for INTEC map ref #13.....	199
Figure 5-6	Stage hazard curves for the INTEC tank farm map ref #10.	200

LIST OF TABLES

<u>Table No.</u>	<u>Title</u>	<u>Page</u>
Table SO-1	Comparison of Revised Flood Frequency for the Big Lost River at the Diversion Dam with Previous Study Results.	iv
Table SO-2	Big Lost River Paleofloods and Paleohydrologic Bounds.....	xii
Table SO-3	Nonparametric Flood Frequency for the Big Lost River at the Diversion Dam.....	xvi
Table SO-4	Probabilistic Stage Estimates for INTEC and TRA Sites (100- and 500-year floods)	xxii
Table SO-5	Probabilistic Stage Estimates for INTEC and TRA Sites (2000- and 10,000-year floods)	xxiii
Table 1-1	Summary of some results from previous flood hazard studies at INL	11
Table 1-2	Comparison of Measured and Required Accuracy Values for Areas Downstream of INEEL Diversion Dam (Appendix A)	11
Table 2-3	Geologic and Geomorphic Summary for Big Lost River Paleofloods and Paleohydrologic Bounds	117
Table 2-1	Discharge and modeling scenarios for the INEEL Diversion Dam study reach.....	118
Table 2-2	Soils and Radiocarbon Summary	119
Table 2-3	Geologic and Geomorphic Summary for Big Lost River Paleofloods and Paleohydrologic Bounds	120
Table 3-1	Hydraulic modeling sample area characteristics - floodplain subareas	152
Table 3-2	Hydraulic modeling sample area characteristics - channel subareas	155
Table 3-3	Summary of limiting discharge values from hydraulic modeling sample areas.....	157
Table 3-4	Applicability of hydraulic modeling sample areas to paleofloods and paleohydrologic bounds estimates	158
Table 3-5	Big Lost River Paleofloods and Paleohydrologic Bounds.....	159
Table 4-1	Least frequent peak discharge generation nodes.	181
Table 4-2	Nonparametric Flood Frequency for the Big Lost River at the Diversion Dam.....	182
Table 5-1	Discharge and modeling scenarios used to construct the stage - probability estimates.....	202
Table 5-2	Discharge-AEP Results from the FFA.....	203
Table 5-3	Stage - Probability Sites.....	204
Table 5-4	Probabilistic Stage Estimates for INTEC and TRA Sites (100 and 500 floods).....	205
Table 5-5	Probabilistic Stage Estimates for INTEC and TRA Sites (2000 and 10000 year floods)	206

List of Plates

(Folded sheets in pocket and PDF files on CD)

<u>Plate</u>	<u>Title</u>
1	Shaded Relief, Contour, and Orthophoto Maps of the INEEL Diversion Dam Study Reach - Big Lost River, Idaho
2	Geomorphic Maps of the INEEL Diversion Dam Study Reach - Big Lost River, Idaho

Appendices

(Separate documents or on CD's)

<u>Appendix</u>	<u>Title</u>
-----------------	--------------

A	<i>Topographic Data for Flood Hazard Modeling at INEEL</i>
----------	---

Quality Assurance of Topographic Data for the Big Lost River Flood Hazard Study, Idaho
National Engineering and Environmental Laboratory, Idaho

Shaded Relief, Contour, and Orthophoto Maps of the INEEL Diversion Dam Study
Reach - Big Lost River, Idaho

Shaded Relief, Contour, and Orthophoto Maps of the INEEL Reach - Big Lost River,
Idaho

Coordinate and Photogrammetric Data Appendices

B	<i>Geologic Data</i>
----------	-----------------------------

Soil Profile Descriptions

Soil Particle Size Results from Colorado State University

Examination of Bulk Soil for Radiocarbon Datable Material from Along the Big Lost River
on the Idaho National Engineering and Environmental (INEEL) Site, Southern Idaho, by
Kathryn Puseman, Paleo Research Institute.

Radiocarbon Dating Results and Calibration Data from Beta Analytic

Summary Report on Detrital Zircon Ages of Samples from Big Lost River Trenches, P.K
Link, Idaho State University and C.M Fanning, Australian National University

Explanation, Plots, and Procedures for Point Count and Pebble Counts and Sieve Data, by V.
Sheedy, Idaho State University

Gamma-Ray Spectrometry Results from J. Budahn, U.S. Geological Survey

Trench Sample Listings

Appendix B - Electronic Supplement - Trench Logs

C	<i>Hydraulic Modeling Methodology and Quality Assurance</i>
----------	--

Part A - Methodology, Mesh Generation, and Models

Part B - Numerical Model Validation and Verification/Peer Review Comments

D *Hydraulic Modeling Results for Paleoflood Analyses*

Evaluating Paleohydrologic Data with Stream Power and Shear Stress Results from Hydraulic Models

Appendix D - Electronic Supplement - Plots of modeled depth, stream power and shear stress for the Big Lost River, INEEL Diversion Dam Study Reach

E *Hydraulic Modeling to Estimate Big Lost River Flood Inundation at INEEL Facility Sites*

Estimating Channel Infiltration Parameters from Historical Flow Data at INEEL

Infiltration Rates to Support High-Resolution Hydraulic Modeling at Idaho National Engineering and Environmental Laboratory by F.R. Fiedler, University of Idaho

Culvert Survey Summary by C.O. Kingsford, Bechtel BWXT

Stage-Discharge Relations for Selected Culverts and Bridges in the Big Lost River Flood Plain at the Idaho National Engineering and Environmental Laboratory, Idaho by C. Berenbrock and J.D. Doyle, 2003, DOE/ID-22184, WRIR 03-4066, U.S. Geological Survey

Appendix E - Electronic Supplement - Plots of modeled flood inundation for the Big Lost River downstream of the INEEL Diversion Dam

F *Stage Probability Plots for Selected Locations at INEEL Facility Sites*

1.0 INTRODUCTION

Paleoflood studies of the Big Lost River (Ostenaar and others, 1999; 2002) indicated that potential flood hazards for the Big Lost River at the Idaho National Laboratory (INL) (**Figure 1-1**) might be significantly different than portrayed by previous studies (e.g., Kjelstrom and Berenbrock, 1996). Because of the significant discrepancy between the previous studies (**Table 1-1**), several further studies aimed at reducing the uncertainty in flood hazard estimates at INL have been undertaken by both USGS and BOR. The present document and the associated appendices describe the results from BOR studies of the Big Lost River flood hazard at INL.

In previous studies of flood hazard for the Big Lost River, Kjelstrom and Berenbrock (1996) and Hortness and Rousseau (2003) used stream-gage data from Big Lost River and surrounding region. Ostenaar et al. (1999, 2002) used stream-gage and geologic paleoflood data from the Big Lost River at INL. The differences in the resulting estimate of the 100-year peak flow shown by previous studies (**Table 1-1**) are primarily due to the use of differing data in each of the analyses. The lower peak flow estimate by Hortness and Rousseau (2003) can be attributed to their evaluation of flow attenuation within the Big Lost River system downstream of stream gages used to estimate flood frequency. The paleoflood study sites of Ostenaar et al. (1999, 2002) are downstream of the gages and should therefore include this attenuation. All estimates of 100-year peak flow require extrapolation beyond the length of the available stream gage data record. The geologic paleoflood data lengthens the available record of peak flow and constrain estimates of the 100-year peak flow to be within the data record of geologic observation.

1.1 Present Study Objectives

The major objectives of the BOR studies are focused on two broad technical arenas; 1) geologic, geomorphic, and hydraulic modeling studies to reduce the uncertainty associated with paleohydrologic estimates used in flood frequency analyses, and 2) developing probabilistic flood stage estimates for specified facility locations at INTEC and TRA.

The paleohydrologic studies have focused on detailed studies of a 5-km (3-mi) reach of the Big Lost River that extends between the INEEL Diversion Dam and the historic Pioneer Diversion (**Figure 1-2**) In this reach, 1:4000-scale aerial photography flown in September 2000 was used to

develop a 3-ft topographic grid that could be rendered as the base map for detailed geomorphic mapping of the study reach and as topographic input for updated two-dimensional hydraulic modeling (**Plate 1**). To improve the geologic data for paleoflood and paleohydrologic bound estimates, seven trenches at three detailed study sites were excavated within the study reach. From the geomorphic mapping, trenching data and updated hydraulic modeling, revised estimates of paleofloods and paleohydrologic bounds for the Big Lost River were developed. These data were used to revise and update the flood frequency analyses.

Developing probabilistic stage estimates for INTEC and TRA facility sites included three major work activities: 1) reprocessing of the 1993 1:10,000-scale aerial photography along the Big Lost River to generate a 5-ft topographic grid, 2) two-dimensional hydraulic modeling of multiple flow scenarios between the INEEL Diversion Dam to downstream of INTEC and TRA, and 3) estimating stage probability curves for facility sites that could include alternate views and uncertainties in flood frequency, infiltration, and culvert flows on the INL site.

Initial hydraulic modeling based on the 3-ft grid topographic data for the Diversion Dam reach showed results that differed significantly from the previous studies of Ostenaar and others (1999) which used topographic data derived from the 1993 INEEL 2-ft contour map. Because the same two-dimensional hydraulic model was being used in both studies, the cause of this difference was clearly related to the input topography used in the models. To resolve these discrepancies, extensive GPS field surveys along the Big Lost River were conducted to assess the accuracy of the topographic mapping used in all phases of these studies. The GPS field surveys found that the 1993 INEEL 2-ft contour map did not appear to meet standards for 4-ft contour interval mapping (**Table 1-2**) and that in the area of the paleoflood study reach the surface defined by this mapping was apparently warped (**Appendix A**). The lack of resolution and accuracy associated with the 1993 2-ft contour map resulted in systematic overestimation of stages associated with discharge in the Big Lost River in the previous studies. GPS field surveys of selected areas along the Big Lost River corridor demonstrate that the topographic data from the 2000 photography in the paleoflood study reach and reprocessed data from the 1993 photography both meet accuracy standards needed for the high-resolution flood modeling (**Table 1-2**) (**Appendix A**).

The two-dimensional (depth-averaged) flow models TrimR2D and RiCOM (**Appendix C**) were used to calculate inundation and flow velocities for paleoflood and site inundation investigations at INL. TrimR2D uses a fixed-spacing staggered finite-difference approach that was used for hydraulic modeling of steady-state discharges in the paleoflood reach and with a larger grid spacing for the site inundation studies. RiCOM uses a staggered finite-element approach that provided an opportunity to employ high-resolution topography in a variable-sized element mesh constructed for the INL site inundation investigations. Both TrimR2D and RiCOM were used to investigate site inundation scenarios to assess the importance of parameters including topographic grid resolution, infiltration, and culvert performance, on estimated inundation corresponding to long-duration (~20 hour-steady-state) discharges. Results from both models were post-processed for estimates of stream power and shear stress.

Monte Carlo nonparametric flood frequency estimation was used to incorporate measurement uncertainties in gaged, historical, and paleoflood discharges and nonexceedence bounds and to produce fully probabilistic flood frequency estimates for annual exceedence probabilities of specific discharges of interest. These annual exceedence probabilities were combined with stage estimates from TrimR2D and RiCOM discharge, infiltration, culvert, and topographic resolution scenarios to produce scenario probabilistic stage hazard curves for 15 sites located in the TRA/INTEC facilities (**Appendix F**). Annual exceedence probabilities and associated credible limits are provided for map-scale inundation plots to provide scenario probabilistic inundation maps (**Appendix E**). These products provide a basis to develop weights for logic tree branches associated with infiltration and culvert performance scenarios to produce probabilistic inundation maps.

1.2 Acknowledgments

This project has been funded through an Interagency Agreement (DE-AI07-00ID13972) between the Department of Energy (DOE) Idaho Operations Office and the Bureau of Reclamation (BOR) Technical Service Center in Denver. Robert Creed is the DOE Program Manager, who has enabled the extensive assistance and coordination required for the assembly of data and field activities on the INL site. Chris Martin (S.M. Stoller Corp.) developed initial QA documents and provided assistance with review activities.

The overall framework of this study as developed by R. Creed was intended to be a collaborative and inclusive effort that included contributions, inputs, and viewpoints from other individuals and institutions. While BOR was the primary lead on the paleohydrologic and hydraulic modeling components, assistance from a participatory review group following development of the initial scope of work consisting of N. Katapodes (University of Michigan), P.K. House (Nevada Bureau Mines and Geology), and K. Coppersmith (Coppersmith Consulting, Inc.) was highly beneficial. Other collaborators in the study including many INL staff, and study collaborators from USGS, University of Idaho, Idaho State University (ISU) also provided significant input.

J. Ake (BOR) worked with us and the participatory review group to develop the original and revised scope of work for this project. He also provided final review comments on the summary document.

Matt Jones (BOR) is a co-principal investigator responsible for production of many products that are integral to this project. Matt conducted the GPS surveys for the photogrammetry and topographic analyses, generated all of the photogrammetric products and topographic grid data used as input for the hydraulic modeling, and generated all of the visualizations used to display the results of the geomorphic mapping and hydraulic modeling.

Roger Denlinger of the USGS provided the 2D explicit finite-volume flow code and performed flow calculations on the Verde and Stanislaus rivers that provide a unique opportunity to provide an independent check of the TrimR2D and RiCOM flow codes (**Appendix C**). Roy Walters developed the TrimR2D and RiCOM flow codes and performed many tests of these codes to replicate and supplement testing performed by the authors of the report (**Appendix C**).

Collection and analyses of topographic data from the INL site could not have been completed without the extensive help of K. Beard (INL). Ken assisted with GPS surveys upstream of the INEEL Diversion Dam and graciously provided extensive assistance and consultations regarding the topographic and survey issues at the INL site. We also thank R. Smith (INL) for extensive help locating data needed for reanalyses of the 1993 aerial photography data. The INL GIS Laboratory provided several pieces of GIS data used to construct base maps for the inundation modeling.

Matt Norake (VECTORS, Inc.) assisted with reduction of much of GPS data used for control on the 2000 photography and with field surveys to evaluate the 1993 topographic results.

The insight and assistance of R. Smith (INL) with basalt stratigraphy and overall geologic processes at the INL was indispensable to this project. The initial phase of geomorphic mapping, conducted prior to the trenching, also benefited greatly from the insights and review comments of R. Klinger (BOR).

Logging and description of the trenches required extended field efforts and assistance from several individuals. Val Sheedy (ISU) provided extended assistance with logging and descriptions of the trenches and with sedimentological analyses. David Simpson (URS Consultants) assisted with soil descriptions for trenches T1 to T7. Lucy Piety (BOR) provided additional expertise in interpretations of the soils, and with extending the soil descriptions and mapping throughout the trenches. Piety and L. Anderson (BOR) also assisted in logging of trenches T8/T9. K. Duran and W. Gonzales (BOR) provided field assistance in the initial phases of trench gridding and surveying and extensive support in assembling the photomosaics used as base maps for trench logging (**Appendix B-electronic supplement**).

Many helpful and insightful comments were received along the way from G. Thackery and P. Link of ISU through several field visits and discussions during the mapping and trench logging. In addition, they provided oversight to V. Sheedy and the sedimentological analyses. P. Link conducted detrital zircon analyses of several samples.

Kathy Puseman at PaleoResearch Laboratories provided macrofloral identifications of samples from the trenches. Radiocarbon dating was conducted through Beta Analytic. Mel Kuntz (USGS) provided assistance with attempts to identify potential tephras in samples from the trenches. Jim Budahn (USGS) conducted gamma-ray spectrometry on a set of test samples to evaluate isotopic activity.

In February 2005, after most maps and supporting documentation for this report had been finalized, the Idaho National Laboratory (INL) became the new official name of the former Idaho National Environmental and Engineering Laboratory (INEEL). The new name has been adopted

in the text of this summary report for most references to the site and staff. Exceptions include figures where the boundaries and features are labeled with the INEEL name on underlying images and references to stream-gaging stations and data, all references to the INEEL Diversion Dam. The previous name was retained for consistency in this report because all of the supporting maps and images were completed with the old name. Most site references within appendices to this report were completed prior to the name change and thus retain the old name.

Figures for Section 1.0

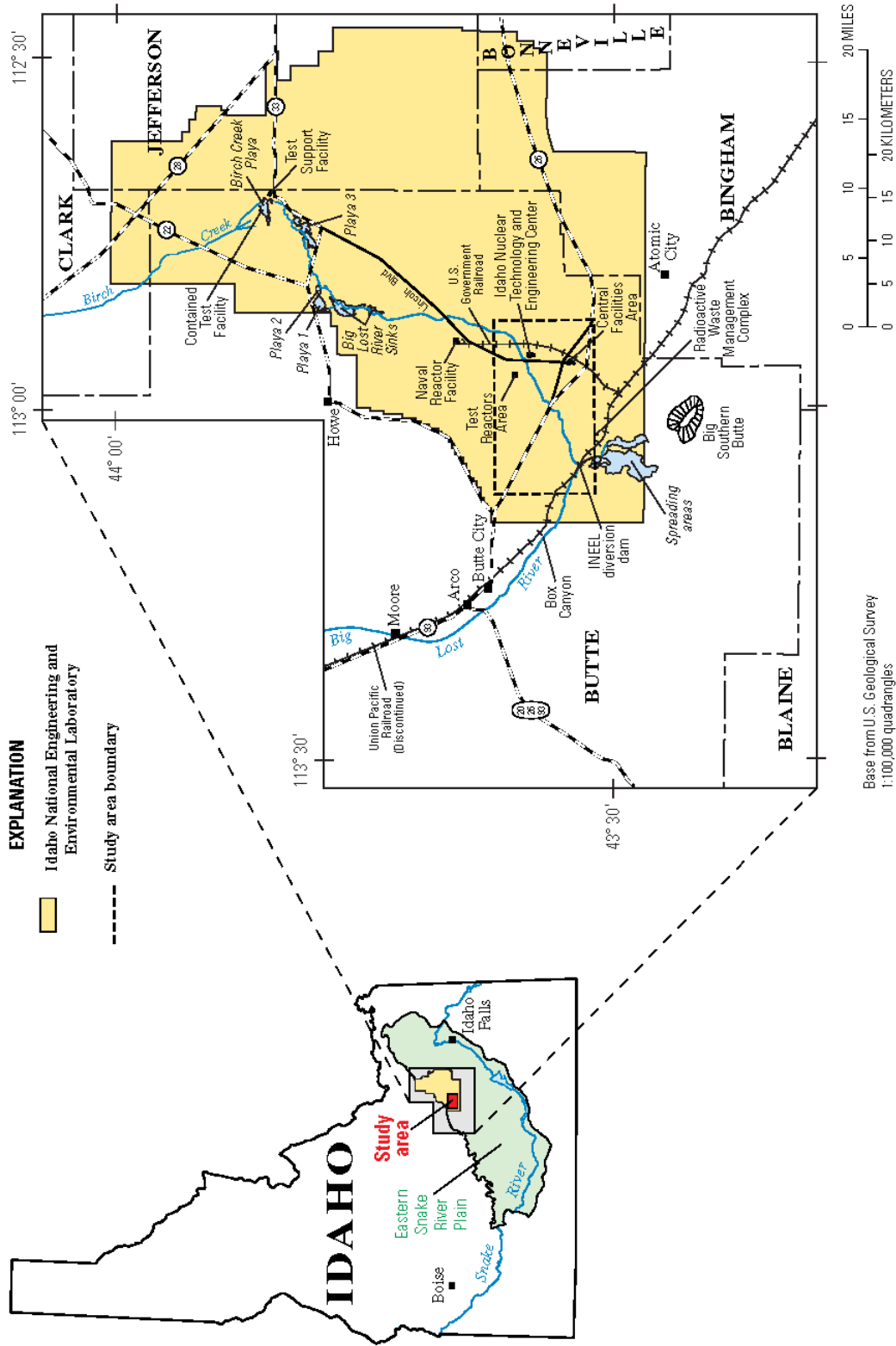


Figure 1-1 Location map of INL (INEEL) and study area. Diversion Dam study reach is located along the Big Lost River between the Union Pacific Railroad and Highway 26. Figure from Berenbrock and Doyle (2002).

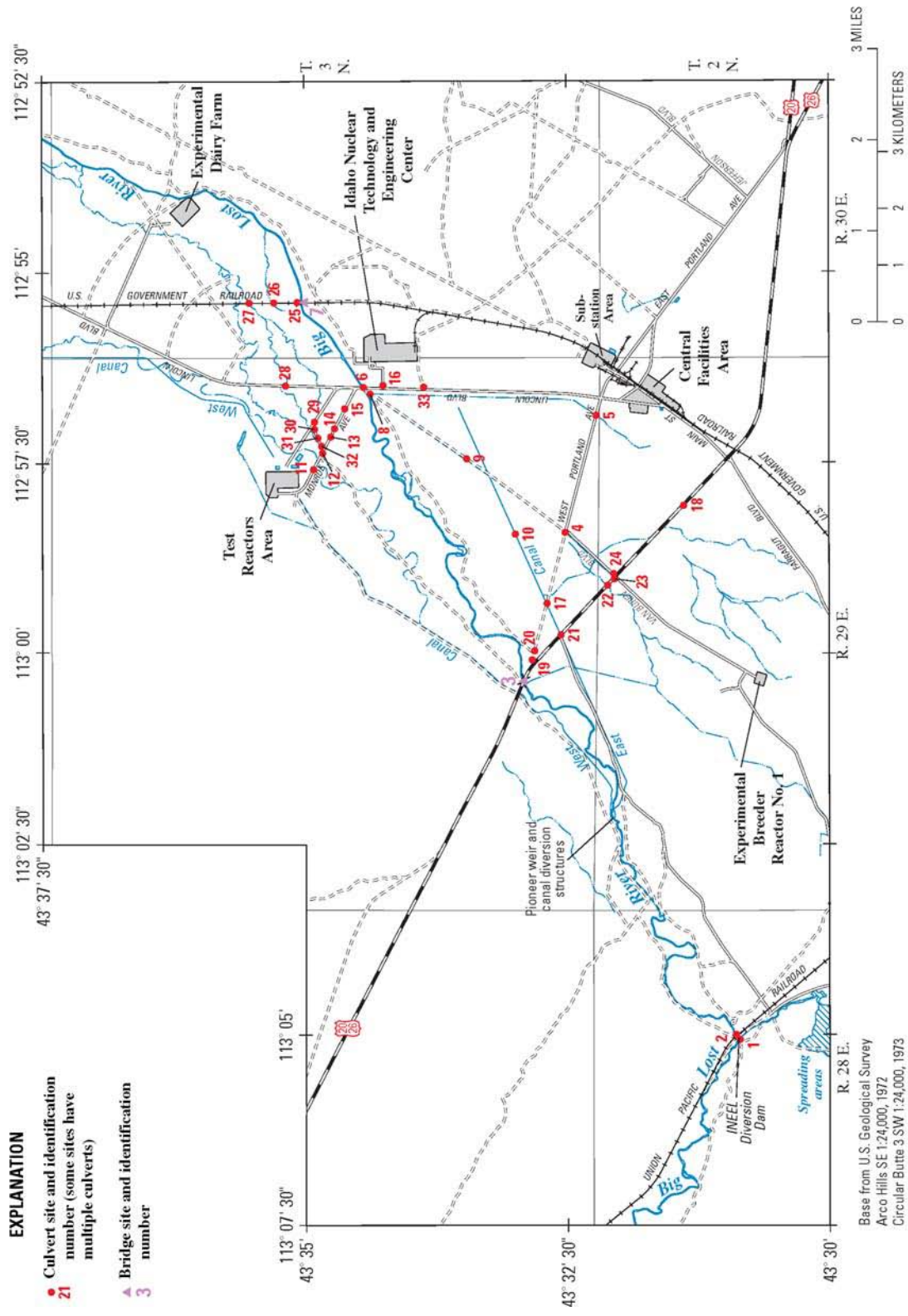


Figure 1-2 INL study area, Big Lost River and significant facility locations. Paleohydrologic studies were conducted for the reach between the INEEL Diversion Dam and the Pioneer diversion structures. Stage probability estimates are required for sites at the Test Reactor Area (TRA) and Idaho Nuclear Technology and Engineering Center (INTEC). Figure from Berenbrock and Doyle (Appendix E).

Tables for Section 1.0

Table 1-1 Summary of some results from previous flood hazard studies at INL

Estimates of 100-year peak flow for the Big Lost River near INEEL Diversion Dam m ³ /s (ft ³ /s)		
Kjelstrom and Berenbrock (1996)	Ostenaar et al. (1999, 2002)	Hortness and Rousseau (2003)
206 (7260)	82 (2910)	106 (3750)

Table 1-2 Comparison of Measured and Required Accuracy Values for Areas Downstream of INEEL Diversion Dam (Appendix A)

Map/Data Source	Measured Values			Required Values			
	NSSDA			NMAS (Accuracy)		ASPRS class 1 (RMSE _z)	
	n=	Accuracy	RMSE _z	2-ft CI	4-ft CI	2-ft CI	4-ft CI
1993 AG 2-ft Contours (Paleoflood Study Reach)				1.192	2.383	0.677	1.333
Aug. 2000 panel points	61	2.246	1.146				
July 2002 check survey	827	3.038	1.550				
(Downstream Hwy 20/26)							
Oct. 2002 check survey	519	2.446	1.248				
2003 BOR 5-ft Grid (Paleoflood Study Reach)							
Aug. 2000 panel points	61	1.752	0.894				
July 2002 check survey	827	1.746	0.891				
(Downstream Hwy 20/26)							
Oct. 2002 check survey	519	1.586	0.809				
Shaded values do not meet NMAS standards or ASPRS class 1 standards for 4-ft contour mapping							

2.0 GEOLOGIC AND GEOMORPHIC STUDIES OF THE DIVERSION DAM STUDY REACH

The paleohydrologic studies of the Diversion Dam study reach are a continuation and expansion of the studies described in previous reports (Ostenaar et al., 1999, 2002). The objective of further studies is to identify and reduce the uncertainty of the previous estimates. Field-scale investigations included four major tasks: 1) acquisition and processing of new detailed aerial photography to serve as a base map for geomorphic mapping and hydraulic modeling, 2) compilation of a detailed geomorphic map of the study reach, 3) trenching and detailed geologic descriptions and analyses in three areas of the study reach to confirm geologic/geomorphic relationships, and 4) additional two-dimensional hydraulic modeling using the new topographic data. In the following sections, the setting of study reach is reviewed (**Section 2.1**), followed by discussions of the geomorphic mapping (**Section 2.2**), and trenching investigations (**Section 2.3**). **Section 2.4** summarizes the combined results of the geomorphic and trenching investigations. The scope and updated results from new two-dimensional modeling of the Diversion Dam study reach are in **Section 2.5**. **Section 3.0** describes the framework for evaluating the geomorphic and hydraulic modeling data to support conclusions regarding paleofloods and paleohydrologic bounds for the Big Lost River. These conclusions are outlined in **Section 3.3** and **Section 3.4** and used in the updated flood frequency analyses presented in **Section 4.0**.

2.1 Geologic and Geomorphic Setting of the Diversion Dam Study Reach

Ostenaar et al. (1999, 2002) summarize the setting and extent of the Diversion Dam study reach, and the application of paleohydrologic bounds to the issues of estimating flood frequency for the Big Lost River.

The INL site is located on the eastern Snake River Plain of Idaho (**Figure 1-1**), a large area of Quaternary basaltic lava flows that are mantled with extensive, thin, wind-blown deposits and lesser areas of alluvium and lacustrine deposits (Kuntz et al., 1994). Mid- to late Cenozoic extension in the Basin and Range Province mountains that lie to the north and south is overprinted by the volcanic activity on the eastern Snake River Plain, presumably in response to passage of the Yellowstone Hot Spot (e.g., Pierce and Morgan, 1992).

The headwaters of the Big Lost River are in the glaciated mountains of the Idaho Basin and Range Province north of the Snake River Plain. The upper basin includes peaks that exceed elevation 3500 m in the northeast-facing basins of the Pioneer Mountains and the southeastern portion of the steep southwest-facing front of the Lost River Range. The river flows southeast for a distance of about 80-km through the Big Lost River Valley, a late Cenozoic structural basin filled with alluvium. Mackay Reservoir, about 30-km upstream of Arco, stores irrigation water for users in the downstream Big Lost River Valley. At the northern edge of the Snake River Plain near Arco, the drainage basin includes an area of about 3650 km² that lies above an elevation of 1550 m. About 10-km downstream of Arco, the river flows onto the INL site where it turns northeast and flows another 35 km to its natural terminus in the Big Lost River Sinks and several playas at the northern edge of the INL site. The last portion of the river course parallels the axis of the Big Lost Trough, a late Cenozoic depositional center on the north side of the eastern Snake River Plain (Geslin et al., 2002). Subsidence along the Big Lost Trough has been more or less matched by the rate of volcanic and sedimentary infill (Geslin et al., 2002). Thus, on the Snake River Plain and the INL site, a sequence of late Pleistocene terraces along the Big Lost River records only a few meters of net incision in the last 95 ka (Ostenaar et al., 1999; Simpson et al., 1999).

2.1.1 Big Lost River historical stream flow. Average annual precipitation in the Big Lost River basin ranges from about 1250 mm/yr in the mountainous upper basin areas to about 200 mm/yr across much of the INL site on the Snake River Plain. This precipitation occurs mostly in the winter months and is largely derived from moisture from the northern Pacific Ocean (Kjelstrom, 1991). During the late spring and summer snowmelt period, the air flow from the Pacific generally consists of relatively dry, subtropical air that produces only sporadic thunderstorms across Idaho. Southeastern Idaho can be affected as well by summer monsoon flow from the south and southwest, which can cause increased precipitation (Kjelstrom, 1991). Meteorological conditions favorable for long-duration winter rainfall are uncommon (Kjelstrom, 1991), especially for large drainage basins.

Annual stream flow, and the largest annual peak discharge, in the Big Lost River are dominated by the spring and early summer snowmelt and runoff from the mountains in the upper drainage basin. Stream flow records are available from the upper basin since 1904 and from the Arco area

since 1947 (Ostenaar et al., 1999, 2002) (**Figure 2-1**). The timing of the snowmelt is regular, usually beginning in late May or early June of each year, with significant flows extending into July. The magnitude of the annual peak discharge typically decreases in a downstream direction with increasing drainage area. Significant downstream decreases in peak discharge, even in the wettest years, indicate that the decrease is at least in part due to large amounts of natural channel infiltration and storage in the Big Lost River Valley (Stearns et al., 1938). Additional decreases in peak discharge result from storage in Mackay Reservoir, about 65 km upstream of the INL site, and irrigation diversions upstream of Arco and the INL site. Hortness and Rousseau (2003) evaluated the changes in peak discharge at gaging stations along the Big Lost River and documented a systematic attenuation in peak discharge from the upstream gaging stations to the INL area. This attenuation appears to exist even for the largest historical streamflows and is not solely due to regulation effects.

2.1.2 Big Lost River – Diversion Dam study reach. South of Arco, the Big Lost River leaves the alluvium-filled Big Lost River valley (**Figure 1-1**) and flows across middle to late Quaternary basalt on the Snake River Plain that is locally mantled with alluvium of varied thickness (Kuntz et al., 1994). Near Box Canyon (**Figure 1-1**), the river is incised from 5- to 30-m into the basalt, and only small areas of alluvium are preserved in the canyon. Downstream of Box Canyon, on the southwestern portion of the INL site, Kuntz et al. (1994) mapped extensive areas of alluvium along the Big Lost River. However, even in this reach, basalt exposures are common in the bed and banks of the river and as isolated outcrops on the alluvial surfaces near the channel, indicating that the alluvium overlying the basalt is relatively thin in this area (**Plate 2**).

The geologic and geomorphic descriptions, and hydraulic modeling analyses, focus on a 6-km-long study reach just downstream of the INEEL Diversion Dam (**Plates 1 and 2**). Throughout the Diversion Dam reach, the Big Lost River is incised about 2- to 4-m into the relatively flat alluvial surfaces on either side. Areas of relief are associated with Pleistocene basalt outcrops that stick out above the alluvium. Previous mapping depicts most of this alluvium as Pleistocene in age based on the degree of soil development and alluvial surface morphology (e.g., Rathburn, 1991; Kuntz et al., 1994). The Pleistocene alluvium is gravelly with a 0.5- to 1-m-thick cover of loess, mostly deposited before about 10 ka (Forman et al., 1993). Exposures in nearby gravel pits,

stream banks, and trenches excavated for this study show a moderate- to well-developed soil with stage II or greater calcium carbonate accumulation in the gravel and loess.

Soils at sites BLR3 and BOR25 contain stage II or greater calcium carbonate accumulation (Ostenaar et al., 1999, 2002) as do soils exposed in the trench intervals excavated into the Pleistocene alluvium (e.g., T1, T2, T3, T6, T7, T8 and T9; see **Plate 2** for locations). Soils in the gravelly alluvium and overlying loess have well developed calcic horizons, (stage II to III), generally considered indicative of a late Pleistocene age (e.g., Scott, 1982; Birkeland, 1999).

Topographic maps and images of the Pleistocene surfaces show a distinct pattern of relic channels with a subdued morphology (**Plate 2**). The pattern of these channels is consistent with the development of these surfaces as Pleistocene glacial outwash plains, as is the sedimentology of the gravels exposed in the trenches. The youngest fluvial-related features on these gravel surfaces are 1- to 1.5-m deep braid channels infilled with fine sand and silt in which a Stage II carbonate soil is developed, consistent with a Pleistocene age. The surfaces also have a well-developed pattern of earth mounds, which often follow and overprint the channels (Tullis, 1995).

The overall channel configuration of the Big Lost River in this study reach (**Plate 2**) is controlled by several locations where the river crosses outcrops of basalt. The sharp bend at the INEEL Diversion Dam results from the impingement of the Big Lost River on a flow tongue of Quaking Aspen Basalt. Downstream of this bend, through the study reach extent shown on **Plates 1 and 2**, the overall sinuosity is about 1.5. However, upstream of BLR2 (see **Plate 1** for locations), sinuosity is about 1.2. The central section from BLR2 to the Saddle Constriction area has sinuosity of 2.4, while downstream sections have an overall sinuosity of about 1.2. The most sinuous sections of the channel are formed in reaches with mostly alluvial banks upstream of where the Big Lost River impinges on partially buried basalt outcrops, such as at the Saddle Constriction study area (**Plate 2** and **Figure 2-3**). Reaches with relatively lower sinuosity tend to have more areas of outcropping basalt in the channel bed and banks, suggesting that the stream course and form is primarily controlled by interactions with rock outcrops. The basalt outcrops in the study reach form constrictions that locally create hydraulic controls on flow and indicate that the overall configuration of the channel has been stable since the river incised below the level of the Pleistocene surfaces. Well-developed soils on some of the inset fine-grained terraces, such as

at BLR6 and in Trench T6 and T8, and radiocarbon ages from these deposits (**Table 2-2**), indicate that this incision has an age of at least 10 ka and more likely 13 ka.

In the central portion of the Diversion Dam study reach, the Big Lost River flows through a narrow basalt constriction (**Saddle Constriction study area - Plate 2**). This constriction is formed by a ridge of basalt that extends across the Big Lost River and protrudes above the level of the Pleistocene alluvial surface south of the river. Upstream of this constriction lies a meandering reach of the river that is flanked by an extensive area of Holocene alluvium inset below the level of the Pleistocene alluvial surfaces on either side (**Plate 2**). On the north side of the river, a low ridge apparently underlain by basalt forms the contact between the Holocene and Pleistocene alluvium (**Figure 2-3**). The surface of the ridge is capped with gravel and eolian deposits. The low point along this ridge, informally known as the Saddle, is a location where high flows could spill over onto the Pleistocene surface downstream of the ridge due to elevated stage caused by hydraulic ponding at the basalt constriction.

Throughout the Diversion Dam study reach are Holocene surfaces with distinctly different morphology that are inset within, and below the level of the Pleistocene surfaces. An extensive area of Holocene alluvium lies just upstream of the Saddle (**Plate 2**), but elsewhere in the reach these deposits are of limited extent. Downstream of the Saddle, Holocene surfaces are limited to narrow terraces that mostly parallel the main channel, but which are somewhat wider at locations where high flows have cut across bends, such as near site BLR8 (**Figure 2-5**). On the higher Holocene surfaces, approximately 2- to 3-m above the low-flow channel, the surface morphology is generally smooth, with only small, subdued channels evident. In contrast to the Pleistocene surfaces, earth mounds are absent. A 0.5- to 1-m-high terrace riser is often present at the back edge of these surfaces defining the contact with the Pleistocene surfaces. On the geomorphic maps these surfaces are mapped as the H1-2 units (**Appendix B** and **Plate 2**). Surfaces that are less than 2-m above the low-flow channel are distinctly channeled (H3-4 units on **Plate 2**). Floated historical debris indicates that these lower surfaces and deposits have been flooded by recent flows.

Descriptions in trenches T4, T5, T6, T8 and T9, (**Section 2.3**) and at sites BLR2, BLR7, and BLR8, (Ostenaar et al., 1999, 2002) in the Diversion Dam reach show that the Holocene terrace

deposits of the Big Lost River are generally fine-grained, consisting of sand and silt. Gravel is generally present only as small bars in the channel, or underlying the fine-grained deposits in these terraces. Rathburn (1991) also noted that the Holocene deposits of the Big Lost River on the INL site are more fine-grained than the Pleistocene alluvium.

2.2 Geomorphic Mapping of the Diversion Dam Study Reach

Mapping of the Diversion Dam study reach was done using stereo photography and digital terrain models using Intergraph ZI Imagestation Software. Imagery and terrain models were obtained from the 2000 aerial photography flown for this study (**Appendix A**). Most final contacts were not field checked in detail, but the mapping was heavily supplemented with field notes compiled on 1993 and 2000 aerial photography and their associated topographic map products, as well as data from previous mapping. One major mapping objective was to characterize the spatial extent of the significant geomorphic units within the study reach for comparison and analyses with the results of the two-dimensional flow modeling. A second objective was identify and characterize sites for subsurface investigations of stratigraphy and soils. Characteristics of the major units depicted on **Plate 2** are discussed in the following subsections, followed by summaries of the setting of the sites identified for further investigations.

2.2.1 Quaternary Basalts - Rb, Rbe, Rd and Rde. Previous geologic mapping of the INL site area (Kuntz et al., 1994) depicts two Quaternary basalt units in the area of the Diversion Dam study reach. An older unit, previously mapped as Qbd, includes basalt flows with estimated ages of 400 to 730 ka, mostly derived from sources north of the present Big Lost River. For the present study (**Plate 2**), flows of this group are mapped as Rd, and Rde for outcrop areas discontinuously and thinly covered by eolian sand and loess. A younger unit, previously mapped as Qbb, includes flows dated between 15 to 200 ka. Qbb flows in the Diversion Dam study reach have sources near Quaking Aspen Butte, several km to the southwest. Dating studies near the RWMC, just south of the Diversion Dam study reach, indicate that the flow at that site is about 95 ka (Forman et al., 1993; Kuntz et al., 1994). For the present study, the Quaking Aspen flows are mapped as Rb, and Rbe for outcrop areas discontinuously and thinly covered by eolian sand and loess.

Both of the basalt map units are locally covered by a variable thickness of loess and eolian cover. Locally, many areas have a well-developed stone pavement consisting of angular basalt pebbles and carbonate detritus. Earth mounds are present in some areas where loess accumulation is apparently thicker. The flow tops are highly irregular, with local surface relief that exceeds 5 m.

At least two flows from the Quaking Aspen Butte lava field (Rb) intercepted the course of the Big Lost River in the map area (**Plate 2**). One flow tongue extends northeast from the INEEL Diversion Dam for about 2 km and appears to have deflected the late Pleistocene course of the Big Lost River to the northeast. A second flow extends across the course of the Big Lost River from the Saddle area to the Old Pioneer Diversion Dam area. This flow tongue extends southeast to the RWMC area where it has an estimated age of 95 ka (Forman et al., 1993; Kuntz et al., 1994). Pleistocene gravel sheets, mapped here as P1-2, bury the margins of the flow tongues, and have breached the low areas of both flow tongues as shown by radial, fan-shaped surfaces downstream of the Rb flows. In addition, the Pleistocene gravel surface extends around the northwest side of the Rb flow about 2 km north of the Old Pioneer Diversion Dam. Rb outcrops are present in bed and banks of the Big Lost River channel at the INEEL Diversion Dam, and from the Saddle area to the Old Pioneer Diversion Dam area. Outcrops that protrude above the Pleistocene surfaces by more than about 1 m generally retain primary cooling features including vesicular plates on flow tops. Limited areas of loess accumulation are present on larger outcrops, which often have well-developed pavements of basalt fragments. Fissures along the crests of pressure ridges are only partially infilled with eolian deposits. In hand specimens, the Rb flows are distinguished by very fine-grained groundmass with common olivine phenocrysts.

The Rd units are part of a large area of basalt, mapped as Qbd by Kuntz et al. (1994) that lies north and northwest of Big Lost River downstream of the INEEL Diversion Dam. The margins of these flows are buried by Pleistocene alluvium. Extensive outcrops are present in the river channel bed and banks downstream of the INEEL Diversion Dam near BOR20, and scattered outcrops are present along the river downstream from BLR7 to BLR2 and the meander bend upstream of BLR3. The Rd units generally have a thicker cover of eolian deposits and more subdued morphology than Quaking Aspen (Rb) flows. In hand specimen, these basalts are

distinguished by fine-grained groundmass, common plagioclase phenocrysts, and rare olivine phenocrysts.

2.2.2 Pleistocene Units - P1 to P3. Initial mapping of the study reach defined three relative-age subdivisions, termed P1-2, P2, and P3, of the Pleistocene surfaces within the Diversion Dam study reach. The oldest surfaces, P1-2, are composed of broad, low-relief, fan-shaped surfaces that radiate from low saddles in the basalt ridges. Relic channels are subdued or not apparent, and large earth mounds up to 0.5-m-high are common and appear evenly spaced or random across the surface (**Plate 2**). The P1-2 surfaces are generally most distant from the present Big Lost River channel and are about 4.0 to 4.5 m above the channel.

The P2 surfaces are the most extensive Pleistocene surface within the Diversion Dam study reach and are generally 3.5 to 4.0 m above the channel. These surfaces have prominent relic cutoff and braid channels that are clear on aerial photography, and typically have 0.5-m relief as shown by contour maps. Because these surfaces are slightly inset relative to the P1-2 surface, the radial pattern from saddles in the basalt ridges is slightly subdued, but is still present. Large earth mounds up to 0.5-m-high are also common on the P2 surfaces. In some areas, the mounds often appear to follow relic channels, but are also present on interfluves. Over some large areas of P2 surfaces the mound pattern is subdued, but other morphology is unchanged. The mapped extent of P2 includes some slightly higher areas that are gradational to P1-2 and not mapped separately.

The gravel deposits that underlie the P1-2 and P2 surfaces are distal, glacial outwash from late Pleistocene glaciation in the upper Big Lost River drainage (Kuntz et al., 1994). The surface morphology on these units indicates deposition as an extensive gravel braid-plain, that predates the incision and establishment of the present Big Lost River channel. Thus, surface slopes and patterns on the P1-2 and P2 surfaces are generally unrelated to the present Big Lost River channel system. Rathburn (1991) also noted this, but viewed the gravels as having been deposited by the waning stages of a late Pleistocene glacial outburst flood, about 20 ka (Cerling et al., 1994). Subsequent work has suggested that any exceptionally large glacial outburst flood on the Big Lost River is likely older than about 50 ka (Ostenaar et al., 1999; Knudsen et al., 2002).

The gravel deposits that underlie the P1-2 and P2 surfaces are typically overlain by 25-150 cm of loess, with stage II-III carbonate developed in the loess and underlying gravel (Ostenaar et al., 1999, 2002; and **Section 2.3** following).

The P3 surfaces, 3.0 to 3.5 m above the Big Lost River channel are of limited extent compared to older P1-2 and P2 surfaces (**Plate 2**). In contrast to the older Pleistocene surfaces, the average surface gradient of the P3 surfaces is generally consistent with the Holocene channel and the inset H1-2 surfaces, although some P3 surfaces have a gentle slope towards the channel. A pattern of earth mounds are apparent on aerial photography and digital imagery (**Plates 1 and 2**), but larger mounds with topographic relief are present only on the rear, higher portions of these surfaces. Mounds with topographic relief are absent along lower portions. A distinct plant mound pattern is apparent on all surfaces; more developed than on H1 surfaces. The P3 surfaces are underlain by gravels, capped by a layer of loess which is generally thinner than on the P1-2 or P2 surfaces. Soils generally have Stage II carbonate in the gravels (**Section 2.3** following).

2.2.2.1 Age Constraints from Regional Glaciation.

Regional approaches have linked loess deposition to glaciation because the landscapes associated with regional glaciation such as aggraded river valleys, active alluvial fans, and fluctuating pluvial lake margins, provide the most viable sources for the loess (Forman et al., 1993). Based on luminescence ages from loess samples at INL, Forman et al. (1993) concluded that the latest period of loess deposition commenced about 35,000 to 40,000 years ago and ceased approximately 10,000 years ago. The youngest luminescence ages for loess on the eastern Snake River Plain near INL are 20-30 ka, and the age for cessation of loess deposition was based on age estimates for deglaciation in the Eastern Snake River Plain region.

Limiting ages for glaciation in the region surrounding the Snake River Plain are available from three areas, 1) Yellowstone, Wyoming to the east, 2) Wallowa Mountains Oregon to the northwest, and 3) Sawtooth Mountains, Idaho, to the north.

Radiocarbon ages on materials recovered from drill holes at Jackson Lake, Wyoming indicate that the southern outlet glaciers of the Yellowstone Plateau ice cap had retreated from maximum

positions in the Jackson Lake area by about 15,000 ^{14}C yr B.P., an age roughly equivalent to 17,000 to 18,000 calendar years (Pierce and Good, 1992; Good and Pierce, 1997; Connor, 1998). Northern outlet glaciers may have reached maximum positions somewhat later, about $16,200 \pm 300$ ^{10}Be yr B.P. ($16,500 \pm 400$ ^3He yr B.P.) possibly reflecting differences in ice accumulation source area characteristics (Licciardi et al., 2001). Earlier work in the area had suggested somewhat older ages for glacial maximums in northern Yellowstone (e.g., Sturchio et al., 1994), but all agree that deglaciation of the area was well underway, or even nearly complete, no later than about 14,000 cal. yr B.P. (e.g., Licciardi et al., 2001; Whitlock, 1993; Richmond, 1986; Pierce, 1979). In the Wallowa Mountains, Oregon, Licciardi et al., 2004 infer significant glacial advances at about $17,000 \pm 300$ ^{10}Be yr B.P. based on ages from moraines located only a short distance upvalley of the LGM moraines dated to $21,100 \pm 400$ ^{10}Be yr B.P. In the Sawtooth Mountains of Idaho, just to the west of the headwaters of the Big Lost River, Thackery et al. (2004) showed that the maximum glacial advances occurred shortly before about $\sim 14,000$ ^{14}C yr B.P. ($16,900$ cal. yr B.P.), roughly 4000 years later than the regional LGM. These ice positions were either maintained until or reoccupied as late as about 11,900 ^{14}C yr B.P. ($13,950$ cal. yr B.P.), followed shortly by major deglaciation.

2.2.2.2 Earth Mounds. A ubiquitous feature of the Pleistocene surfaces, particularly the P1 and P2 surfaces, are large circular features termed earth mounds by Tullis (1995) in a previous study of these features on the INL. Tullis reviewed the extensive literature on the similar features which exist throughout the world, with several potential origins, including biological (primarily burrowing animals) and cryogenic (related to past glacial climates). Although unable to fully characterize all aspects of the origin of the earth mounds, Tullis (1995) concluded that a cryogenic origin was most likely for the INL mounds, although biological activity was a clear factor in the present mound characteristics. Soil development within and between the mounds indicated that the mounds developed during the late Pleistocene (Tullis, 1995) and many areas between the mounds have a weak to moderate gravel pavement (e.g., McFadden et al., 1998). Recent literature provides additional mechanisms for the initial origin of the mounds that would be consistent with a cryogenic origin (e.g., Kessler and Werner, 2003), as well as concepts for the biological exploitation of such sites (Johnson and Johnson, 2003).

Trench exposures (**Appendix B - Electronic Supplement** and **Section 2.3** following) through eleven mounds for this study confirm the relative antiquity and longevity of the mounds. The mounds formed in a variety of stratigraphic settings, clearly post-date gravel deposition, but also include strongly developed soils that indicate long-term spatial persistence. The trench exposures did not reveal evidence for eroded or abandoned mound sites. Only limited evidence of mound-related cryogenic features were observed in the trenches for this study. As noted by Tullis (1995), the mounds are preferred locations for Holocene biological activity based on abundant active and inactive burrows and disrupted soils of various development and ages.

Soil development within the mounds that indicates long-term spatial persistence, probably since the late Pleistocene, together with the occasional observations of associated cryogenic features noted in the trenches and by Tullis (1995), seems to support the hypothesis that the initiating condition for the mounds at INL was likely cryogenic. Mechanisms such as those discussed by Kessler and Werner (2003) would have led to formation of shallow depressions that would initially provide thicker sites of finer sediments on the gravel braid plain. Most likely these would then become colonizing sites for biological activity (e.g., Johnson and Johnson, 2003) and the process of building the topographic relief that distinguishes the present mounds. This framework of origin and mound growth implies a cryogenic process for initial subsurface relief and expression of the mounds, which are then strongly modified by the biological activity that is primarily responsible for building the surface relief and expression of the mounds. It further implies a strong likelihood that the topographic expression of the mounds on the Pleistocene surfaces has been gradually increasing, primarily due to biological processes, since they were initiated.

The surficial expression of the mounds consist largely of loess (Tullis, 1995) and would be highly erodible, as would the loess cover on the Pleistocene alluvium, if there was significant surface flow around or over the mounds. As shown on **Plate 2**, there are significant variations in the expressions of the earth mounds throughout the study reach. On the older Pleistocene surfaces, P1-2 and P2, these variations are not clearly related to obvious any patterns of flow that develop based on modeling of extreme flood discharges through the study reach. A likely cause of some of the observed variations is mound deflation due to wind following the August 2000 wildfire which

burned over most of Diversion Dam study reach a few weeks prior to the flight for aerial photography used for the base map images of **Plates 1 and 2**. In other areas, mounds have been modified by cultural activities at INL, especially early agriculture and grazing.

In contrast to the older Pleistocene surfaces, the geomorphic expression of the mounds on the P3 surfaces does appear to be modified by flow related to the present Big Lost River system. Earth mounds are only prominent on the higher, more distal portions of the P3 surfaces. The absence of mounds on the inset Holocene surfaces is more complex. Similar mounds may not have formed due to differences in the materials underlying the Holocene surfaces, or if the initial origin of the mounds required a much colder climate, the Holocene surfaces may post-date periods of climate favorable for mound initiation. Alternately, the expression of mounds on the Holocene surfaces may have been modified by younger floods.

2.2.2.3 Geomorphic Evidence for Holocene Modification of the Pleistocene

Units. The pattern of relic braid channels on the P1-2 and P2 surfaces shows no evident relation to potential patterns of large flows associated with the present Big Lost River channel. Rather, these channels are directly related to the overall radial fan shape of the P1-2 and P2 surfaces that is controlled by breaches through low saddles in the basalt ridges that flank and cross the Big Lost River (**Plate 2**). The braid channels have overall similar morphology, and do not display geomorphic evidence of having conveyed any significant, recent flow. One site that could appear as a possible exception to this is located about 250 m northeast of trench T1 (**Figure 2-2** and **Plate 1**) where a sharp cut is present in the terrace riser onto the P2 surface. Field inspection of this feature suggests that it was excavated for vehicle access and was not an erosional feature and there are numerous other old wheel tracks and ruts in this area. About 150 m north of that site, the upstream continuation of the same terrace riser intersects a channel at the back edge of the highest P3 surface in this area, and at this location there appears to be a small fan built from the mouth of this channel onto the H1-2 surface. Trench T3 crosses this channel about 80 m to the west (upchannel) from this site. Exposures in trench T3 are permissive of small flows and limited amounts of sediment transport (**Section 2.3.1.3** following).

The morphology of several areas of the P3 surface contrasts sharply with the P1-2 and P2 surfaces. The large area mapped as P3 on the northwest edge of the Big Loop study area (**Plate 2**)

lacks earth mound morphology and there is subtle evidence of small fans built off the downstream edge of this surface. Just downstream, on the north side of the Big Lost River between the large meanders, another large area of P3 has smoother morphology, and small erosional features on its downstream edge. On the higher portions of the surface, more distant from flow, earth mounds are present. This area also appears to have been plowed or farmed, as evidenced by the surface morphology and by diversion canals built across it and on the upstream edge. It is not clear how much of the morphology results from anthropomorphic activities versus geomorphic modifications due to floods. On the next meander bend, on the south side of the river, the P3 surface also shows two distinct morphologies. To the northwest, on the lower portions of the surface closest to the river bend, the surface is smooth, and downstream edges of terrace risers appear to be channelled and eroded. To the southeast, the surface is slightly higher, and the surface is rougher, with obvious earth mounds. These morphology differences on the P3 surfaces appear to bracket the limits of significant flow modification by floods that are much younger than the surfaces. Two other areas of P3 surfaces, one upstream across from BLR7, and a section downstream of the Saddle Constriction study area near trenches T6 and T7, are both slightly higher and do not display geomorphic evidence of recent flooding.

2.2.3 Holocene Units - H1 to H4. Previous mapping has recognized the presence of a generally fine-grained fill inset within the Pleistocene gravels along the Big Lost River (Rathburn, 1991; Kuntz et al., 1994). The oldest portions of this fill likely relate to the latest Pleistocene deglaciation and changes in flow regime at the end of the Pleistocene (Rathburn, 1991). Subsequently, the fill has been partially reworked and a series of surfaces, cut onto the original fill and younger deposits.

In the present mapping, four groups of surfaces, H1 to H4 were defined according to their geomorphic characteristics. The oldest surface, H1, is preserved only as small, often narrow, remnants along the outer, higher, margins of the Holocene fill deposits. These surfaces appear to be underlain by an intact early Holocene soil characterized by >0.5-m-thick Bk-horizons with Stage II carbonate accumulation. The slope of these surfaces generally follows the present channel slope and these surfaces are typically ~ 2.5 to 3.0 m above the channel.

Inset H2 surfaces record erosion and deposition by at least one late Holocene flood (s), most recently about 400-600 years ago (Ostenaar et al., 1999, 2002). Locally, the boundary of H1-2 surfaces is expressed by a subtle break in slope with < 0.5-m relief, but in other areas, there is only a gradual slope or rise towards the back edge of the Holocene surfaces. The H2 surfaces are typically ~1.8 to 2.2 m above the present channel. Areas of the H2 surfaces that are more than a few meters from the bank of the Big Lost River appear to be mostly underlain by early Holocene fine-grained fill deposits with variably stripped remnants of a soil similar to that developed on the H1 surfaces as shown by exposures in trenches T6 and T8 (**Section 2.3.2.3** and **Section 2.3.3.1** following). The outer margins of the H2 surfaces, and streambank exposures along the edge of the H2 surfaces typically expose a ~1-m-thick section of fine-grained fill in which the upper-most deposits have weakly developed soils and a Bk horizon with Stage I- carbonate accumulation. Radiocarbon ages from the upper-most deposits indicate an age of 400-600 years, for the units with Stage I- carbonate in the Bk horizon (Ostenaar et al., 1999, 2002). Some of these soils may be partly cumulic, and the subsequent addition of thin deposits (1-5 cm) of fine sand and silt to the uppermost soil horizons probably cannot be ruled out.

In some of the lowest exposures along the edges of the H2 surfaces, for example trench T4 (**Section 2.3.2.1** following), these younger additions to the soil profile are readily recognizable and appear to indicate a subsequent, and smaller discharge paleoflood. In most other exposures, it appears that the deposits of the 400-600 year flood extend to the present ground surface with only a few cm of eolian sand mixed into the upper most A-horizon. Deposits of the 400-600 year flood are typically 20-50 cm thick in the streambank exposures, e.g., BLR2, 7, and 8 (Ostenaar et al., 1999, 2002). In trench exposures T4, T5, and T6, deposits of 400-600 year old late Holocene flood thicken toward the streambanks, to a maximum of 0.5 m, but all of the trench exposures begin about 1-2 m from present bank margin. In most bank exposures, and in channel-ward ends of the trench exposures, ~1 m of stratified silt and sand underlie the deposits of the 400-600 flood. Locally, these deposits retain a variably developed, and sometimes eroded carbonate horizon, indicating that a wide range in ages for the underlying deposits. Where there is sufficient depth of exposure, gravels often underlie the fine-grained section, but generally only to elevations about 1 m above the current streambed. Exposures at T8b and T8c (**Section 2.3.3.1** following) are an

exception to this, where channel-facies, fine gravels are higher in the section of the early Holocene deposits just upstream of a bedrock constriction.

Deposits that underlie the H3 and H4 surfaces are not exposed in any of the trenches, and were not described as soil description sites in this or previous studies (e.g., Ostenaar et al, 1999, 2002). Field reconnaissance of many bank exposures along the margins of the H3 and H4 surfaces shows that deposits that underlie these surfaces are well stratified, with very weakly developed soils. Recognizable soil horizons are limited to thin A- and AB- horizons, consistent with the inferred historical ages of these surfaces. With the exception of the meandering reach of the Big Lost River that lies upstream of the Saddle constriction and downstream of BLR7, H3 surfaces are generally limited to very narrow, <1 m wide, terrace treads that are inset below the edges of the more extensive H2 surfaces. Within the meandering reach upstream of the Saddle constriction, H3 surfaces are more extensive and the underlying deposits are more heterogeneous. In that subreach, deposits underlying H3 surfaces likely include stripped and eroded remnants of the early Holocene fine-grained fill deposits that underlie H1 surfaces, abandoned channel and associated overbank deposits of early- to late-Holocene ages, and late Holocene to historic fine-grained deposits capping older units. The upper limit of the H3 surfaces is typically about 1.8 m above the present channel and is often expressed as a subtle scallop on gently sloping surfaces. At a few locations, near BLR2 and the Saddle Constriction area, this limit appeared to coincide the floated, milled timber, suggesting that this may have been associated with an earlier, historic flood. However, much this evidence was burned in the August 2000 wildfire.

Throughout the Diversion Dam study reach, the H4 surfaces are characterized by narrow, paired, terrace treads, typically <1- to 5- m wide, that are about 1 m above the low-flow channel. These surfaces are often capped by thin sand deposits from the 1997 flows, which resulted in shallow overtopping of the H3 surfaces, and these surfaces support a thicker cover of grass and vegetation than any other surfaces. The underlying deposits consist of well stratified silt, sand, and gravel. Soil profiles consist of very thin A-horizons, although silty and fine sand units are significantly bioturbated and there are extensive roots which penetrate throughout exposures in these deposits.

2.2.4 Channel Deposits. Sand and gravel within the low-flow channel are the most recent deposits of the Big Lost River. These deposits occur in small bedforms, generally less than

0.5 to 1 m in height. Over much of the study reach the bed is armored with small cobbles. Near constrictions, the armor is absent and bedforms composed of finer gravel are present. Many of these bedforms appear fresh and likely were reactivated during flows in 1995-1999, when there was peak flow in the range of 10-13 m³/s on multiple occasions downstream of the INEEL Diversion Dam (**Appendix E**). Downstream of bedrock constrictions, there are often small pendant and lateral bars composed of larger, more angular blocks of basalt that appear to be locally derived from the outcrop constriction immediately upstream. Maximum clasts in these bars are typically less than about 0.5 m, and bar heights are similar.

Berenbrock et al. (2003) characterized the bed armor and channel deposits in the central part of the study area from near BLR8 to upstream of the Saddle Constriction study area (**Plate 1**). They found that d_{50} of the armor layer ranged from 6-49 mm and was typically 15-35 mm at sites away from constrictions. The underlying channel deposits were slightly finer, with d_{50} ranging from 0.17-35 mm. Trench exposures showed that these deposits ranged from massive to stratified. Maximum clast sizes in the underlying gravels were typically less than about 50 mm.

2.3 Trenching Studies

Within the Diversion Dam study reach, three areas were selected based on the initial geomorphic mapping as sites for subsurface investigations and more detailed study: 1) Big Loop, 2) Saddle Constriction, and 3) BLR8 (**Plate 2**). The overall objectives of additional detailed investigations were to improve the characterization of the Big Lost River paleofloods and paleohydrologic bounds portrayed in Ostenaar et al. (1999, 2002). Each of the areas identified had the potential to provide differing types of data towards those goals based on their individual geomorphic and hydraulic setting. Improved characterization of the paleoflood record required excavation at sites where deposits of paleofloods might be preserved and at sites where erosion from these floods might be evident. It was also hoped that these sites would yield additional datable samples that could improve the knowledge of the age(s) of Big Lost River paleoflood(s). Improved characterization of the paleohydrologic bounds required extension of the trenching to additional sites where no geomorphic evidence of recent floods was apparent. At these sites, exposures of soils and stratigraphy would permit better assessment of the time spans over which the geomorphic conclusions could be extended.

In 2002, nine shallow trenches with a total length of 635 m were excavated at the three study sites. Trench configurations and procedures were generally similar at all three study areas and are described in **Appendix B - Electronic Supplement**. The trench logs were mapped in the field on a photographic base and are presented in that format here. The final logs (**Appendix B - Electronic Supplement**) are compiled at a scale of ~1:45 when printed on 11x17-inch paper. This permits assembly of pairs of 15-m long sections of the trenches on a single sheet and facilitates visualization of the lateral continuity of the deposits. In the digital version, high resolution is maintained and the logs can be printed on larger sheets or in sections at a larger scale. Two sets of logs are presented in **Appendix B - Electronic Supplement**, one set with interpretations, and a second set of unmarked photographs. On the interpretive logs, stratigraphic contacts and units are labeled with lithofacies codes adapted from Miall (1996); soil horizons use nomenclature adapted from Birkeland (1999). Soil profile descriptions are contained in **Appendix B**. Sample locations are labeled and numbered on the logs. Data from sample analyses and disposition of samples are compiled in **Appendix B**.

2.3.1 Trenches T1, T2, and T3 - Big Loop Study Area. The Big Loop study area encompasses three trenches, T1, T2, and T3, sited on the large expanse of Pleistocene surfaces south of the Big Lost River about 0.5- to 1.5-km downstream of the INEEL Diversion Dam (**Plate 1**). Much of this area is mapped as P2, but the study area includes the transition area between P2 and P3 (**Section 2.2.2**). Braid channels and large earth mounds are prominent throughout the area and the three trenches were sited to intersect both types of features (**Figure 2-2**). The objectives of trenching in this area include: 1) to evaluate whether differences in the morphology of the P3 units compared to P2 might have resulted from Holocene paleoflood inundation of those surfaces; 2) to evaluate further the characteristics of the earth mounds, particularly in areas where they appeared somewhat subdued or muted; and 3) to confirm, with soils and stratigraphic observations, the geomorphic conclusion that the braid channels on the P2 surfaces were relic features, and were not features produced by post-Pleistocene modification of the P2 surface.

2.3.1.1 Trench T1. Trench T1, about 73-m long, was sited across an area that is transitional between P2 surfaces and P3 surfaces (**Figure 2-2**). The southern end of the trench begins with a short section on the P2 surface, then drops down a small terrace riser into a channel

bounding an slightly lower area mapped as P3. The trench alignment exposed two earth mounds, centered at stations 25 and 53.

Trench logs for trench T1 are contained on three sheets (**Appendix B- Electronic Supplement**). No age dates were obtained from samples in this trench. No sedimentological analyses were conducted on samples from this trench. Soil profiles were described at Stations 3, 15, 20, and 61; particle size data is available for all four profiles. (**Appendix B**).

The basal units in trench T1 are a sequence of lateral accretion gravels composed of beds ~20 - 100-cm thick. The uppermost bed in this sequence is coincident with the surface channel at approximately stations 15 to 35. The channel fill, massive-to-poorly-stratified, pebbly-to-silty sand, is best expressed near stations 8 - 14. Loess, 30-50 cm thick, extends the entire length of the trench although it is difficult to distinguish from the channel fill in many areas. The sequence of loess over gravel and soil development in these deposits illustrated in soil descriptions at stations 3, 15, 20, and 61 appears typical of that repeated on the Pleistocene deposits throughout the study reach.

Soil horizons mapped in the gravels, vary laterally, but continue through the channel sequence suggesting the channel is similar in age to the gravels. Within the channel, there is no deposit or erosional feature that disrupts stratigraphy or soil horizons implying significant Holocene flow through this channel. Conversely, carbonate morphology through the channel section of trench T1 is somewhat weaker compared to channels in trenches T2, T3, T6, and T7. Thus, if Holocene flow has been present in the channel at T1, it was limited to amounts that did not result in any significant soil erosion at the site.

2.3.1.2 Trench T2. Trench T2, about 44-m long, crosses a prominent braid channel on the interior of the P2 surface (**Figure 2-2**). The braid channel follows a terrace riser that separates slightly lower areas of the P2 surface to the north from slightly higher areas to the south. In addition to crossing the channel and flanking surfaces, the trench alignment crossed and exposed two earth mounds, centered on stations 19 and 36.

Trench logs for trench T2 are contained on three sheets (**Appendix B- Electronic Supplement**). No age dates were obtained from samples in this trench. No sedimentological analyses were conducted on samples from this trench. Soil profiles were described at Stations 1, 20, and 28. Particle size data is available for profiles at stations 1 and 28. (**Appendix B**).

The basal units in trench T2 are a sequence of lateral accretion gravels composed of beds ~20 - 100 cm thick. These gravels are overlain throughout the trench by 30-50 cm of sandy to pebbly silt, of which loess is a major component. Frequency of pebbles decreases upward from the gravel contact and where the finer deposits thicken; Bk horizons are formed in the finer units.

Earth mounds in trench T2 are large and well-developed. Carbonate accumulation beneath the mounds is enhanced, suggesting long-term spatial stability. Deposits and soils within the mounds are highly variable and disrupted, indicating continued bioturbation within the mounds.

2.3.1.3 Trench T3. Trench T3, about 57-m long, crosses a prominent braid channel on the back side of the P2 surface (**Figure 2-2**). The braid channel follows a terrace riser that separates the slightly higher P1-2 areas to the south from the main extent of P2 surfaces to the north. At the T3 site, the riser is very subdued, and the trench did not extend far enough south to expose a soil that might be fully representative of soils associated with the P1-2 surfaces. The south end of trench T3 begins on this subdued riser, drops into the channel and extends onto the main P2 surface to the north. Two earth mounds are crossed by the alignment, centered at stations 15 and 53.

The log of trench T3 is contained on three sheets (**Appendix B- Electronic Supplement**). No age dates were obtained from samples in this trench. Pebble and point counts were done on a sample from station 5 and sieve analyses of a sample from station 20 (**Appendix B**). Soil profiles were described at stations 2, 15, and 28. Particle size data is available for profiles at stations 2 and 28 (**Appendix B**).

The basal units in trench T3 are a sequence of lateral accretion gravels composed of beds ~30 - 50 cm thick. The uppermost bed in this sequence is gently undulatory along the length of the trench and appears to have a low point that would be approximately coincident with the surface channel

at stations 13 to 17, where a large earth mound is located and no channel fill deposits are recognized. Stage III carbonate is extensive beneath this mound, as well as the mound at station 54, and there is high variability of soils within both mounds. Between the two mound crossed by trench T1, loess that overlies the gravel is ~25-cm thick. The base of the loess in this area is highly irregular, suggesting disruption by frost wedges and bioturbation.

2.3.2 Trenches T4, T5, T6, and T7 - Saddle Constriction Study Area. The Saddle Constriction study area encompasses four trenches, T4, T5, T6, and T7, that include two very distinct settings (**Plate 1** and **Figure 2-3**). Trenches T4, T5, and the southern portion of T6 are sited on narrow areas of H1-2 surfaces that flank the river downstream of a bedrock constriction (**Figure 2-4**). These sites were chosen because they appeared likely to preserve a record of vertical accretion deposits from Holocene floods and/or a record of erosion resulting from floods that may have overtopped them. The lower portions of trenches T4, T5, and T6, were located on portions of the H1-2 surface that appeared to include deposits of the "400-yr" paleoflood identified in the previous study (Ostenaar et al., 1999, 2002). The northward extension of trenches T6 and T7 extend across higher P3 and P2 units, and lie downstream of the feature known as the Saddle, from previous studies (Ostenaar et al., 1999, 2002) (**Section 2.1.2**). The objectives of these trenches are to evaluate, through soils and geomorphic observations, whether or not there was evidence on these surfaces of flow having overtopped the saddle during the Holocene. Geomorphic evidence, shown by faint channels on the P3 surface at trench T6 and the southern end of T7 suggests that the youngest flow on these surfaces was associated with the inset of the P3 surface into the P2 surface and that flow was through the bedrock constriction at the present channel location (**Figure 2-3**). Flow through the saddle would be in a direction orthogonal to these channels. Similar to the objective for trenching in the Big Loop area, the northern continuation of trench T7 would allow evaluation of whether differences in the morphologies of P3 and P2 surfaces might be related to younger flooding, and to confirm geomorphic conclusions related to the origins and ages of the braid channels on the P2 surfaces and issues related to the earth mounds.

2.3.2.1 Trench T4. Trench T4, about 21-m-long, is located on a small H1-2 terrace about 100 m downstream of the Saddle bedrock constriction (**Figure 2-3**). The terrace is inset on the downstream side of a basalt outcrop that deflects the channel slightly to the north. The south

end of the trench was limited by a small road and lies on the edge of the slope off the P2 surface south of the river. That portion of the trench encountered a small area of gravels overlain by a pebbly silt that is probably related to a poorly expressed earth mound whose expression was muted by activity along the road and position coincident with the terrace riser on the north. Excavation depth of the trench was limited by outcrops of basalt through much of the central and sloping section of the trench which crosses the terrace riser. Loess, colluvium, and deposits related to the earth mound are intermixed in the central portion of the trench, then grade laterally and downslope to stratified sequence of fine-grained flood deposits that underlie the flattest portion of the H1-2 surface.

Trench logs for T4 are contained on a single sheet (**Appendix B- Electronic Supplement**). Five radiocarbon ages were obtained from samples in this trench (**Table 2-2**). Gamma-ray spectrograph data is available for three samples from station 20 and one sample from the H4 terrace deposit immediately below the trench (**Appendix B**). No sedimentological analyses were conducted on samples from this trench. One soil profile was described at station 20 (**Appendix B**).

The sequence of flood units exposed in the lower portion of trench T4, stations 17-21, provides evidence of at least three late Holocene paleofloods. The basal unit in this section of trench T4 is a ~1-m-thick silty fine sand with a stage II carbonate morphology in the upper portion. A radiocarbon age of 7320-7200 cal yr B.P. from this soil horizon provides a minimum age for this deposit (**Table 2-2** and **Appendix B**). Similar ages, sedimentology, and soil development are observed in other sections that underlie the higher portions of H1-2 surfaces along the Big Lost River (**Section 2.2.3**). The top of this unit is eroded, and three separate overlying silty-fine sand units are recognized primarily through soil properties. The lower and thickest unit is wedge-shaped and increases in thickness from about 40 cm at station 18 to nearly 1 m at station 21. In the upper portion of the unit, an ~20-cm thick Ab1 horizon with no visible carbonate morphology overlies a thicker Bk1b horizon with stage I- carbonate morphology. Radiocarbon ages from this unit at stations 19 and 20 range between 1000 to 2000 cal yr B.P. (**Table 2-2** and **Appendix B**). This age range may represent a minimum time range for deposition and subsequent soil formation. Alternatively, it could indicate that the deposit includes multiple stratigraphic units

whose boundaries have been overprinted by soil development. This deposit is considered part of the evidence for the "older paleoflood" discussed in later sections.

The second sand unit is less than 20-30 cm thick, and extends from about stations 18.5-21. The soil in the underlying unit does not suggest significant erosion associated with this deposit, but the basal contact is inset into the underlying soil upslope. This unit is mostly at the surface and includes the A1/A2 horizons of the soil on the present H1-2 surface at this site. A single radiocarbon age in the lower part of this unit from station 20 indicates an age of 630-510 cal yr B.P. (**Table 2-2** and **Appendix B**). This is the age range associated with other similar flood deposits on the lower portions of the H1-2 surfaces. These sites collectively are evidence for the "400-yr" paleoflood.

The third, and youngest flood deposit in trench T4 consists of a thin, 5-10 cm layer of highly calcareous silty fine sand, slightly lighter in color than is present only about station 20-21 and is referred to as the "white flood". This unit is at the surface and has minimal soil development. It must be considerably younger than the underlying soil because the underlying A-horizon is relatively depleted in carbonate and much less effervescent. No datable material was recovered from samples of this unit. Cesium and lead activity from a sample at station 20 was similar to that in the underlying deposits, but substantially lower than a sample from an H4 terrace in the bank just below the trench (**Appendix B**). The H4 terrace is overtopped by post-INEEL Diversion Dam flows and is therefore likely younger than the mid-1950's. The lower activity in the samples from this unit appears to indicate that it pre-dates that time period.

2.3.2.2 Trench T5. Trench T5, about 10-m long, is located on a H1-2 surface about 100-m downstream of the Saddle bedrock constriction and directly across from trench T4 (**Figure 2-3**). The T5 site is at the very upstream end of a long, narrow H1-2 terrace that extends several hundred meters downstream on the north side of the river. The H1-2 surface at T5 is slightly higher than at trench T4 (**Figure 2-6**).

The south or lower end of T5, beneath the flattest portion of the H1-2 surface, exposed a sequence of fine-grained flood deposits that are generally similar to those in trench T4. These flood deposits are cut into well-bedded gravels that dip moderately to the north and which underlie the back

portion of the H1-2 surface and lower portion of the terrace riser at the back edge of the surface. Trench excavation was rapidly limited by basalt outcrops which were overlain by loess and colluvium.

The log for Trench T5 is contained on a single sheet (**Appendix B- Electronic Supplement**). Two radiocarbon ages were obtained from samples in this trench (**Table 2-2**). No sedimentological analyses were conducted on samples from this trench. One soil profile was described at station 2 (**Appendix B**).

The gravels that underlie the terrace slope between stations 4-10 dip moderately to the north and other than orientation they appear similar to P2/P3 gravels in all other trenches. Stratification and bedding in the gravels is disrupted in a steeply dipping zone between stations 6-7 and suggests that these gravels are possibly involved in a small bank failure that rotated and displaced them slightly. The fill of colluvium and loess near the upper end of the trench straddles the contact between basalt outcrops and the gravels. Significant carbonate accumulation in this fill suggests that the block has been stable for at least a few thousand years.

A sequence of flood deposits are cut into the gravels between stations 0-5. A basal colluvium is overlain by a stratified sequence of sand to sandy silt that probably represents one or more paleofloods. This sequence is capped by a Bk1b soil horizon at a depth of about 20-25 between stations 0-2. Overlying this contact and soil horizon boundary between stations is a thin deposit of silty fine sand that appears to be inset into an A1/A2 horizon in silty eolian deposits south of station 2. A radiocarbon age of 760-660 cal yr B.P. at station 0, from the top of the Bk1b indicates the minimum age of burial of this unit by the upper silty fine sand. The underlying deposit has an interval of stronger carbonate development at a depth of 56-74 cm, is also more silty than units above and below. This interval may represent an older, eroded soil buried by two flood deposits, or has more carbonate because of the finer texture. The contact and horizon boundary is not obviously erosional, based on sharpness and irregularity. Deposits below this interval are distinctly more pebbly and incorporate clasts derived from the underlying colluvium. A radiocarbon age near the base of the lower unit gave an age of 1900-1720 cal yr B.P. (**Table 2-2** and **Appendix B**).

Based on the radiocarbon ages and soils from this site, the upper silty fine sand south of station 2 is correlated to the "400-yr flood" and the underlying deposits are considered correlative with the "older flood".

2.3.2.3 Trench T6. Trench T6, about 121 m long, is located about 100 m downstream of trench T5 (**Figure 2-3**). The south end of T6 begins on the same H1-2 surface as trench T5, extends north across that surface, then up the terrace riser onto the adjacent P3 surface. The southernmost section of the trench, stations 1-5, exposes late Holocene flood deposits similar to those in trenches T4 and T5. Stations 5 to 25 expose mid- to early-Holocene soils and fine-grained channel fill. The sequence of deposits beneath the terrace riser, stations 25-45, includes a sequence of gravels that records the lateral migration and incision of the Big Lost River below the level of the P3 surface. Overlying slope colluvium and soils on the riser grade into equivalent units that underlie the H1-2 surface to the south. The remainder of the trench, stations 45-121, exposes mostly plane-stratified gravels, similar to those in trenches T1, T2, and T3. The gravels are overlain in most areas by ~20 cm of finer gravels which grade laterally into a pair of channels between stations 66 to 96. The finer gravels and channels appear to represent the last phase of fluvial erosion and deposition on the P3 surface. Loess, typically ~20 cm thick, overlies the entire sequence from stations 45-121 and forms the upper horizons of the carbonate soil developed through all the deposits. The low point in the same ridge to the west, termed the Saddle, lies about 50-70 west of the section of trench T6 near stations 75-100. Near station 95, an earth mound deposit overprints the edge of the channel sequence.

Trench logs for Trench T6 are compiled on four sheets (**Appendix B- Electronic Supplement**). Six radiocarbon ages were obtained from samples in this trench (**Table 2-2**). Detrital zircons were analyzed from samples at stations 12 and 66 (**Appendix B**). Pebble and point counts were done on samples from stations 23 and 99 (**Appendix B**). Gamma-ray spectrograph data is available for two samples each from stations 0 and 4 (**Appendix B**). Seven soil profiles were described at stations 1, 7, 17, 43, 57, 72, and 118. Particle size data are available for profiles at stations 43 and 57 (**Appendix B**).

The physical stratigraphy and soils at the southern end of T6, stations 1-5, appear very similar to the sequences in trenches T4 and T5. A stratified wedge of silty-fine sand, with relatively weakly

developed soils, truncates sand silt and sand units with much stronger carbonate soils. At station 1-2, this wedge appears to consist of a single unit of silty fine sand which contains an increasing percentage to the north of carbonate-cemented cicada clasts that appear to be derived from Bk soil units similar to those between stations 4-20. The basal part of the wedge is contains about 10 per cent pieces of older soil. At station 4, two radiocarbon ages from a bulk sample of this unit barely overlap in the range of 790-540 cal yr B.P. Based on these ages and the associated soil development, it appears most likely that this deposit is correlative to the "400-yr" flood. Deposits correlative to an "older flood" may be represented by the lower-most units at the very end of the trench.

Trench T6 extends across the entire H1-2 terrace at this location and the trench exposure demonstrates the lateral continuity of stratigraphy and soils beneath the surface. From the south end of the trench to near station 23, a thick basal sand unit, locally stratified, is overlain by a similarly thick silty fine sand in which a strong Bk horizon is developed with abundant cicada burrows. From the south to north in this interval, the surface horizons that overlie this Bk horizon become thicker and more complex. Beyond about station 14, to station 25, the horizons are consistent and thick. This change, near station 14, appears to mark the northern limit of erosion associated with the younger flood deposit that contains clasts of Bk material near stations 1-4.

Three radiocarbon ages potentially limit the age of Bk soil and associated deposits in the southern end of trench T6. At station 4, a radiocarbon age on a mixture of very small charcoal fragments recovered from a large bulk soil sample has an age of 3480-3360 cal yr B.P. (**Table 2-2** and **Appendix B**). The sample site is surrounded by prominent burrows, and has an anomalously young age compared to samples from other sites with similar soil development. A similarly anomalous age was obtained at station 20, again on a mixture of very small charcoal fragments recovered from a bulk sample of the basal sand unit. This sample had an age of 2870-2760 cal yr B.P. (**Table 2-2** and **Appendix B**). An apparently more reliable age is from a snail shell recovered from a bulk sample of the basal sand at station 6. This sample had an age of 12,800 - 11,940 cal yr B.P. (**Table 2-2** and **Appendix B**). This age implies a very late Pleistocene age for incision of the Big Lost River that is consistent with the regional glacial chronology (**Section 2.2.2.1**) and with

ages from similar soils at trench T4 (**Section 2.3.2.1**) and BLR6 (Ostenaar et al., 1999, 2002) located just downstream of trench T6 (**Plate 1**).

The ages, soil development, and continuity of the stratigraphy and soils beneath the H1-2 terrace indicate that this surface has been largely unmodified by floods through much of the Holocene. Stabilization of the surface, and formation of the Bk soil horizon in the silty fine sand unit, likely post-dates deposition of the basal sand at 12 ka, but is still most likely early Holocene, based on comparisons to ages at other sites. Since that time, there has been only limited modification of the surface, as recorded by the sequence of deposits at stations 1-4 which are cut into the Bk horizon, and which stripped the upper horizons to approximately station 14.

The objectives of extending trench T6 north across the P3 surface downstream of the Saddle were to determine if there was evidence of erosion due to flows through the Saddle during the Holocene. From station 45-121, the trench exposes stratified gravels, which in many areas are capped with a finer, sandy gravel that appears to laterally grade into fine-grained channel fills. A thin loess, in turn capped by a very thin layer of eolian sand, overlies both the gravels and the channel fills. Basal units in the channels are typically sandy to pebbly and fine upwards to silty fine sands that are texturally similar to loess. A carbonate soil with highly variable, but common stage II morphology, appears to be continuous across the entire sequence. Variability in the soil is apparently related to small variations in texture of the uppermost gravels. A single radiocarbon age was obtained from near the top of the Bk in the channel fill at station 68. The age of 660-540 cal yr B.P. (**Table 2-2** and **Appendix B**) is a very minimum age that reflects the continuing input of young material into the soil profile.

There is no apparent stratigraphic evidence of erosion removing significant thicknesses of loess, or of erosion affecting the top of the gravels. The channel fills coincide with faint geomorphic suggestions of flow parallel to the ridge that forms the Saddle, suggesting that they are related to flow from south to north on the P3 surface, not west to east indicated by flow through the Saddle (**Figure 2-3**).

2.3.2.4 Trench T7. Trench T7, about 256 m long, overlaps and continues north from the north end of trench T6 (**Figure 2-3**). The southern portion of T7, stations 1-25, exposes gravels

with channel fill, loess thickness, and soils that are similar to those in the central and northern portions of trench T6. This section of trench T7 coincide with the mapped extent of the P3 surface (**Plate 1**) and a ~0.4-m-step in the ground surface between stations 25-30. From about station 25 to 50, excavation depth was limited by basalt beneath the gravels. Thin exposures of gravels are overlain by another group of channel deposits and loess that underlie a slightly higher surface than the area near stations 1-25. Beyond station 50, the surface steps up another 0.3-0.4 m to the level of the main P2 surface downstream of the northern continuation of the ridge near the saddle. North from station 50, channel fill deposits that overlie the main gravel units thin, and laterally grade to thin sandy gravel and gravelly sand units. These are in turn typically overlain by 20-30 cm of loess, and a variable thickness of eolian sand, including locally mappable accumulations of post-2000 sand. These are identified where they overlie the 2000 burn horizon. Beyond station 130, to the north end of the trench at station 256, the upper sandy units are not present, and variably stratified gravels are overlain by 20-40 cm of loess. Earth mound deposits interrupt the stratigraphic continuity along the trench near stations 60, 116, 166, and 258.

Trench logs for T7 are compiled on nine sheets (**Appendix B- Electronic Supplement**). No radiocarbon ages were obtained from samples in this trench. Detrital zircons were analyzed from samples at stations 107 and 109 (**Appendix B**). Pebble and point counts were done on a sample from station 231 and sieve analyses of a sample from station 136 (**Appendix B**). Seven soil profiles were described at stations 36, 44, 95, 108, 158, 167, and 237 (**Appendix B**).

Similar to trench T6, there is no apparent stratigraphic evidence of erosion removing significant thicknesses of loess or of erosion affecting the top of the gravels throughout the length of trench T7. The channel fills coincide with faint geomorphic suggestions of flow parallel to the ridge that forms the Saddle, suggesting that they are related to flow from south to north on the P3 surface, not west to east, as indicated by flow through the Saddle (**Figure 2-3**).

2.3.3 Trenches T8 and T9 - BLR8 Study Area. The BLR8 study area includes two trenches, T8 and T9, on the south side of a sharp bend located upstream of a bedrock constriction (**Figure 2-5**). The BLR8 site of Ostenaar (1999, 2002) is on the opposite bank. Trench T8 is located mostly on an H1-2 surface, the lower part of which appears correlative to the position of BLR8. The site is downwind and adjacent to extensive areas of basalt outcrops and associated eolian

sand deposits (**Plate 1**). Thus, all units in this area have relatively thicker eolian surface units than most other sites. Trench T8 was originally proposed as a continuous excavation that extended from the H3-4 units through the H1-2 and into units mapped as P3. However, pre-trenching archaeological investigations showed this to be a potentially significant cultural site. A scaled-back trench layout was adopted consisting of three short trenches, each about 6 to 7 m long, designated T8a, T8b, and T8c. Prior to excavation of these smaller trenches, an extensive archaeological mitigation investigation was carried out which included excavating several test units along the trench alignments (Peterson and Harding, 2002). The final trenches partly incorporated and retained the archeology units so that stratigraphy in those units could be related to the trenches. Trench T9 was excavated on the upstream side of the bedrock constriction where the channel impinged on the edge of the P3 surface. Because the sites were located upstream of a bedrock constriction, and based on the exposures at BLR8, there appeared to be potential for both trenches to expose a datable record of paleofloods. This would be most likely in the northern end of the trenches. The southern end of both trenches extended onto higher and older surfaces, thus providing the potential to define the limits of erosion associated with past floods.

2.3.3.1 Trench T8. The final excavation for Trench T8 consisted of three trench segments (**Figure 2-5**), labeled from south to north, T8a, T8b, and T8c. The locations of two archaeology units not incorporated in the final trenches, designated Locality A, 101N/100E and 105N/100E (Peterson and Harding, 2002) lie between T8b and T8c. Correlation of units described by Peterson and Harding with those mapped in the trenches follows discussion of the three trenches.

Trench logs for T8 are compiled on one sheet (**Appendix B - Electronic Supplement**). No radiocarbon ages were obtained from samples in this trench. Artifacts recovered by the archaeology investigations provide some evidence for the age of these sites. Pebble and point counts were done on a sample from T8a, station 3 (**Appendix B**). No soil profiles were described separately; horizons are mapped on the logs.

Trench T8a. Trench T8a, the southernmost of the three trenches was about 7 m long and sited on the edge of a small P3 surface surrounded by basalt (**Plate 1**). Gravels, with overlying loess and eolian sand at the southern end of this trench are similar to and have similar soils to the

Pleistocene gravels in trenches at the Big Loop (**Section 2.3.1**) and Saddle Constriction study areas (**Section 2.3.2**). These gravels interfinger with a channel fill, also with stage II carbonate morphology, and again are very similar to the channel fills and soils exposed in T6 and T7 at the Saddle Constriction study area. The stratigraphic relationships of the gravels and channel fill in T8a, and the soil developed across these boundaries demonstrate the late Pleistocene age of these channel fills on the P3 and P2 surfaces. Pebble stringers, found near the middle of the channel fill at stations 4-5, show that much of the fill is fluvial. The upper portion of the fill grades upwards and laterally with loess that overlies the gravels. The complete soil profile, and upper eolian units are truncated or removed from the northern portion of the trench and reflected in the surface topography by a 20-30 cm high, gentle scarp. Removal of these upper units is old enough that the top of the Bk in the channel fill section and parallels the ground surface and maintains a constant depth.

Trench T8b. Trench 8b is the middle trench at site and is about 6 m long. Locality A, 96N/100E and 95N/100E units of Peterson and Harding (2002) are partially retained in the north end of the trench. The basal units exposed in T8b are fluvial as shown by beds of sand and fine sandy silt. The section fines upward, becoming more silty and similar in texture to loess. Extensive cicada burrows and soil carbonate have overprinted any bedding or stratification. The section in T8b is slightly coarser than the channel fill in T8a and is likely the lateral extension of the same channel fill unit. Stratification of the upper part of the fill in T8b is based primarily on the relatively abrupt increase in soil carbonate (2Bk1/2Bk2 horizon boundary). The same horizon boundary in T8a is gradational. This difference may be due to subtle texture differences in the original stratified fill, or to erosion and redeposition of the upper unit in T8b. Carbonate morphology of the Bk1 horizons in both trenches is similar. Surficial soils in T8b and the north end of T8a are similar, suggestive of removal or stripping of surface horizons in the past few hundreds of years.

Trench T8c. Trench T8c is the northernmost trench at the site, about 6 m long, and closest to the Big Lost River channel (**Figure 2-5**). The basal units exposed in T8c are fine pebbly sands and sandy gravels which may or may not be a lateral facies of the channel fill sands exposed in T8b and T8a. The lower units in T8c are capped by the eroded remnants of a well-developed

carbonate soil, similar to that present in the other trenches. The uppermost unit in T8c is mostly a massive sand that contains abundant carbonate-cemented cicada burrow clasts. These appear to be derived from a Bk horizon of channel fill or a fine-grained fluvial deposit similar to those exposed in the southern portion of T6 (**Section 2.3.2.3**). Soil development in this upper unit is very weak, limited to scattered occurrences of stage I carbonate morphology on occasional pebbles and filaments on the edges of the cicada clasts.

Correlation to Archaeological Stratum. Peterson and Harding (2002) designated the area around trench T8 as Locality A, and defined twelve stratigraphic units (stratum) based on bedding, grain size, and soil development. The oldest, basal stratum is designated I, and the youngest stratum at the surface is XII. They divided the recovered cultural remains into two components based on the diagnostic projectile points and natural stratigraphy. Diagnostic materials for the younger component were recovered on the surface, but were associated with stratums X, XI, and XII based on soil development. Diagnostic points from the older component were identified in stratum IX and at the top of stratum VIII at depths of 30-40 cm in Locality A, 95N/100E and 105N/101E.

The location of 95N/100E at Locality A corresponds to stations 4-6 in trench T8b. In trench T8b, stratum XII and XI of Peterson and Harding (2002) appear to correspond to eolian sand and the AB soil horizon, about 10-15 cm thick across the trench. A 2Bk1 soil horizon formed in the upper fluvial sand corresponds to stratum IX and X of Peterson and Harding. A 2Bk2 soil horizon formed in a lower fluvial sand corresponds to stratum VIII. The depth range of 30-40 is coincident with the contact between two the fluvial units.

105N/101E at Locality A is located 10 m north of T8b, and 5 south of T8c (**Figure 2-5**). We did not remap this exposure, but from field inspection, it appears that the eolian sand is thinner and that more likely, stratum XI corresponds to an A-horizon formed in fluvial silty sand. Stratum IX includes a Bk horizon forming in silty sand that appears to include re-worked cicada burrow clasts similar to the uppermost fluvial unit and Bk horizon in trench T8c. Correlation of this unit to the upper fluvial unit in T8b is less clear, because reworked and broken cicada clasts are not so obvious in T8b, and the upper fluvial unit in T8b is slightly finer. The irregular contact at the base of stratum IX in 105N/101E suggests it is erosional, as does the significant increase in carbonate

morphology observed in stratum VIII beneath this contact. Because of the irregularity of the basal contact, the recovered artifacts may have been originally part of either unit. Stratum VIII to I in 105N/101E resemble lateral equivalents of the lower fluvial units in trench T8c. The lower fluvial units in T8c are finer, and the lower units in 105N/101E and T8c may either be equivalent lateral facies to T8b or a younger inset.

Peterson and Harding (2002) Locality A site 111N/1000E and 112N/100E correspond to stations 0-2 of trench T8c. In T8c, units mapped as eolian sand correspond to stratum XI and XII. The upper most fluvial unit in T8c includes all of Peterson and Harding stratum IX and X, as well as portions of stratum VIII. This fluvial unit contains extensive broken and reoriented cicada burrow clasts and has an irregular, erosional basal contact. Below this contact are eroded remnants of a Bk horizon with stage II+ carbonate formed in a bedded sequence of silt, sand, and gravel beds and lenses. Peterson and Harding designated individual beds within this fluvial sequence as stratum II through VIII. From the larger exposure of trench T8c, it appears that most of their stratum VIII corresponded to the eroded remnant of a well-developed Bk horizon formed in a silty sand capping a well-bedded fluvial sequence. Variability in carbonate accumulation within the sequence is the result of variations of carbonate accumulation in the lower portions of soil profile in beds of differing initial texture.

Peterson and Harding (2002) and Harding (2002) identified two Northern Side-notched projectile points from their Component I, which are considered to range in age from 7500 to 4400 years ago. Recovery of these points at depths of 30-40 cm suggests that they were most likely entrained in the upper fluvial unit exposed in T8c, and possibly T8b as well. These units appear to contain reworked clasts of cicada burrows derived from the underlying soils. It seems less likely that these points had been worked into the underlying Bk horizon of the lower fluvial unit in the trenches, because artifact recovery decreased dramatically below 30-40 cm depths. Artifacts recovered at the surface have a potential age range of ~100 to 1700 years. This age range brackets the possible age range of late Holocene paleofloods along the Big Lost River and is thus not diagnostic here.

T8 Combined Interpretations. The lack of continuous exposure across the T8 site somewhat limits interpretations, but the physical stratigraphy and soils have enough similarities that some conclusions can be reached. Soils and stratigraphy in the southern portion of T8a,

stations 1-3, are very similar to those found on the Pleistocene surface elsewhere in trenches T1, T2, T3, T6, and T7. This appears to be typical of the soil profile and stratigraphy developed on unmodified Pleistocene surfaces throughout the site, with the addition of eolian sand on top of the loess. Long-term stability of the site is shown by the development of stage II Bk-horizons across the boundary of gravel, fine-grained channel fill, and loess units. Soil horizons and stratigraphy are truncated at the northern end of T8a, indicating a lateral limit to erosion in this trench at about stations 3-4. Erosion of the profile in the underlying loess/channel fill sequence is minimal in the northern section of the trench. Depth-to-top of Bk horizon is ~20 cm, suggesting this erosion is at least a few hundred years in age. The upper portion of trench T8b is somewhat more stratified than T8a, but is generally similar to the channel fill/loess sequence in T8a. The presence of two Bk horizons may result from burial of an older soil by the upper-most fluvial unit or increased carbonate accumulation due to subtle difference in texture of the original deposits. Horizons at the surface are similar in both trenches.

The stratigraphy of the upper unit in trench T8c is distinctly different. The uppermost fluvial unit in T8c is a fine sand that contains clasts of broken and reoriented carbonate-cemented cicada burrows. Coarser sand and pebbly lenses along the base are cut into a Bk horizon with stage II morphology developed in an underlying fluvial sequence. The Bk in the upper fluvial unit has stage I- morphology, suggesting an age of no more than a few hundred years. The cicada burrow clasts consist of carbonate-cemented silty, fine sand that could be derived older channel fill units or H1 age units. Incorporation of Middle Prehistoric artifacts (7500 - 4500 years old) would be consistent with the apparent age of soils incorporated as clasts in this much younger deposit. These ages may indirectly indicate a minimum age for the underlying deposits in T8c as well.

2.3.3.2 Trench T9. Trench T9 is approximately 35-m long and extends on the south from the relatively flat, sand covered P3 surface down a ~2-m-high terrace riser onto a small H3-4 terrace (**Figure 2-5**). The site is located just upstream of a bedrock constriction, which results in backwater effects even for moderate flows (see plots in **Appendix D - Electronic Supplement**). In this setting the H3-4 terrace was inferred as likely site of fine-grained deposition during floods, and the presence of several subtle steps and inflections in the terrace riser (see log profile at stations 30 and 32) suggested a possibility of an extended record of paleofloods at this site. The

trench was extended back onto the P3 surface to expose the continuity of stratigraphy through the riser and because preliminary hand-auger borings suggested a thick, fine-grained sequence was present. Pre-trenching archaeological investigations (Peterson and Harding, 2002) along this trench alignment found only a few artifacts. The final trench incorporates a portion of archaeological excavations between stations 11-14. No diagnostic artifacts were recovered at this site.

Trench logs for T9 are compiled on one sheet (**Appendix B - Electronic Supplement**). Three radiocarbon ages were obtained from samples in this trench (**Table 2-2**). Pebble and point counts were done on a sample from station 18 and on a sample from a mid-channel bar just below the end of the trench (**Appendix B**). No soil profiles were described separately; horizons are mapped on the logs.

At the south end of trench T9, the basal gravels exposed from stations 1-30, resemble the Pleistocene gravels that underlie P2 and P3 surfaces in other trenches. These gravels are interrupted between stations 23-28 by a channel fill with steeply inclined stratification along one side. In the southern portion of the trench, the gravels are overlain by about 1 m of fine sand. A well-developed Bk horizon in this sand has stage II and locally stage III carbonate morphology and to the north, as the sand thins, the strong Bk horizon extends from the sand into the gravel. A radiocarbon age of about 2750 cal yr B.P on a small piece of charcoal (**Table 2-2** and **Appendix B**) found in the lower part of the sand at station 2 is anomalously young based on soil development in the sand. Extensive burrowing in the sand is likely responsible for downward transport of young charcoal to this depth. The burrowing has also disrupted the soil to a significant extent. The upper horizons of the soil in the southern part of the trench show that there is significant input of younger sand across this surface at this site. Soil profile development in the sands, channel fill, into the gravels are similar to profiles developed in Trench 8a, as well as other trenches on the Pleistocene P2 and P3 surfaces at the Big Loop (**Section 2.3.1**) and Saddle Constriction study areas (**Section 2.3.2**). A similar age is inferred at trench T9 for the gravels, channel fill and overlying sand with strong Bk development. The uppermost sands above the Bk are possibly younger, reflecting new eolian input from sand dunes on the basalt to southwest (upwind) of this site. North of station 14, the slope steepens, and near the edge of the terrace riser

these upper loose, sandy horizons thin and terminate northward. Similar to soil evidence at T8a and T8b, some stripping of the uppermost portion of the Pleistocene profile between stations 14 to 28.

Colluvium on the terrace riser slope grades downslope to a sequence of fine-to-medium sand beds. Between stations 32-33, these are separated by A/Bw horizons, with abundant organic material. Radiocarbon ages from this section calibrate to ages less than 300 cal yr B.P. and include historic ages (**Table 2-2** and **Appendix B**). The high limit of these deposits on the terrace riser slope corresponds to a discharge of about 70 m³/s (**Figure 2-7** and **Section 2.5.1.4** following), roughly the upper limit of historic flood discharge in the Big Lost River (**Section 2.1.1**). Some of these deposits could potentially correlate to the youngest flood deposit in trench T4 (**Section 2.3.2.1**), but this correlation is only speculative. The radiocarbon ages, and discharge range that inundates this site, suggest that these deposits are most likely associated with floods that pre-date the INEEL Diversion Dam and had discharges near or only slightly larger than the largest historical floods.

The lowest deposits in trench T9 are a sequence of sand beds that underlie the flat portion of the H3-4 terrace at station 34-35. This inset sequence is inundated by discharges of less than 50 m³/s (**Figure 2-7**) and likely accumulated from historic floods. Minimally developed soils in these deposits are consistent with a young age.

2.4 Summary of Geomorphic and Geologic Data for Paleofloods and Paleohydrologic Bounds

The geologic studies described in the preceding sections found evidence of at least three late Holocene paleofloods, and are the basis for describing three paleohydrologic bounds that can be used with these data in the flood frequency analyses (**Section 4.0**).

2.4.1 Paleofloods. From the geomorphic mapping and trenching investigations, evidence of three paleofloods have been identified within the Diversion Dam study reach of the Big Lost River (**Table 2-3**). This evidence is briefly reviewed below. Studies to date have not located any site along the study reach that dependably preserves a long or detailed full record of large floods. Rather, over time, there is a progressive self-censoring (House et al., 2002) such that

only successively smaller floods can be recognized for shorter periods of time. For the sites observed, any large flood essentially obliterates the record of smaller floods that preceded it. Likewise, only limited remnants of larger, but older floods might remain. The primary focus for selecting sites for this study has been of evaluating evidence for floods that potentially much larger than the largest historical floods. All but a small portion of 1 of the trenches used for this study are located outside the inundation limits of historic floods.

2.4.1.1 "White Flood". Stratigraphic evidence for this flood is recognized at a single site, Trench T4 (**Section 2.3.2.1**). A thin, ~ 7 cm, deposit of silty sand caps the sequence of flood deposits exposed beneath the lowest surface at the end of trench T4, stations 19-21, and appears to bury the soil formed on deposits of the "400-yr" flood. Soil descriptions (**Appendix B**) designate this unit as the A1-horizon of the present soil and soil development is weak in comparison to other sites. The deposit is not associated with historic floods because no historic floods would have been large enough to inundate the site (**Section 2.1.1** and **Figure 2-6**). No similar deposit is present or recognized in trenches T5 or T6, both of which are only slightly higher relative to the discharge at which they are inundated (e.g. **Figure 2-6**) and it does not appear that soils in deposits of the "400-yr" flood were eroded more recently at these sites (**Section 2.3.2.2** and **Section 2.3.2.3**). A radiocarbon age from the underlying A2 horizon at T4 has a calibrated age range between 630-510 cal yr B.P. (**Table 2-2** and **Appendix B**). Deposits in lowest portions of trench T9 have young radiocarbon ages (**Section 2.3.3.2** and **Table 2-2**), but are also inundated by discharges that might have occurred prior to construction of the INEEL Diversion Dam (**Figure 2-7**). Thus, the age of a paleoflood associated with this deposit is constrained to be prior to the beginning of stream-gaging records (A.D.1903) by the minimum discharge required to reach the site. The deposit is younger than the 630-510 cal yr B.P. age from the underlying soil, and is most likely about 100-150 years based on the relative soil development.

2.4.2 "400-yr Flood". Stratigraphic evidence for this paleoflood was recognized in the earlier paleoflood study by Ostenaar et al. (1999, 2002) at four sites in the Diversion Dam study reach (**Figure 2-11**). Deposits with similar soils and stratigraphy that are apparently correlative are present in trenches T4, T5 and T6 (**Table 2-3** and **Section 2.3.2**). These deposits appear to be associated with the prominent geomorphic expression of the H2 surface that can be mapped

throughout the study reach (**Plate 2** and **Section 2.2.3**). Soil development in these deposits, and radiocarbon ages from these deposits and from underlying deposits constrain the age to about 600 - 400 cal yr B.P. (**Figure 2-8**).

Because the flood deposits recognized by Ostenaar (1999, 2002) and in the trenches for this study appear to be associated with H2 geomorphic surface (**Plate 2**), one constraint for evaluating the discharge of this paleoflood is that the discharge be large enough to inundate the full extent of this surface throughout the study reach.

2.4.3 "Older Flood". Trench and bank exposures along the H1-2 surface all demonstrate that the deposits of the "400-yr" paleoflood overlie eroded soils developed in slightly older, similar flood deposits (Ostenaar et al., 1999, 2002; and **Section 2.3**). The soils in these deposits are generally similar, or slightly more developed than soils developed in the past 400-600 years. This implies a similar length of time over which no flood either eroded or resulted in significant deposition over these deposits. Likewise, the limited extent of the deposits of the "400-yr" flood relative to the H1-2 surface indicate that overall the surface must be a composite of deposits with similar origins, but differing ages. The significant scatter in radiocarbon ages from site to site, and the variability in soils that underlie the "400-yr" flood deposits appear to support this concept. As shown on **Figure 2-8**, there is much less correlation of the potential time brackets for a single older flood than for the "400-yr" paleoflood and some possibility that multiple floods may have occurred in the time interval since about 3000 cal yr B.P. However, both the stratigraphic and the chronologic resolution to define multiple floods in this time period are lacking in the present exposures. The existing age constraints appear to indicate that a conservative age range for this flood would lie in the range of 2000 to 1000 Cal yr B.P.

The stratigraphy in trenches T4 and T5, where evidence of this flood is best expressed, could also be interpreted as evidence for more than one flood. Interpretations of multiple floods in these sections is most supported by breaking out beds in the lower portions of these stratigraphic sections. If that is done, the upper stage limit to associate with these floods is no longer associated with the H1-2 surface, but is down in the section at an elevation below the stage level that would be associated with the largest historic floods, $\sim 70 \text{ m}^3/\text{s}$ (**Figure 2-6**). The addition of temporally sparse data in that discharge range does not improve the assessment of the flood frequency. This

type of information would be more useful if it could be independently reasoned that these floods must have been much larger than historical floods, either near or exceeding the discharge of the "400-yr" flood.

Because deposits that are associated with the "older flood" underlie the H1-2 surfaces, inundation of the full spatial extent of those surfaces provides a constraint for evaluating the discharge associated with this paleoflood.

2.4.4 Paleohydrologic Bounds. For use in the flood frequency analyses, geomorphic and stratigraphic data are used to define three paleohydrologic bounds that span differing time intervals over the past 10,000 years (**Table 2-3**). The geologic basis for each of these bounds is summarized below.

The geologic data show that over different time intervals and areas along the Big Lost River, there is evidence of relative geomorphic stability. Thus, the preservation of paleoflood deposits as the surface units on portions of the H1-2 geomorphic surfaces shows that no floods large enough to modify or remove these deposits have occurred since the time of those paleofloods. As summarized in, there is stratigraphic and geologic data along the Big Lost River that allows for defining three paleohydrologic bounds. Geomorphic mapping delineates the characteristics and extent of surfaces of similar age that are potentially useful as paleohydrologic bounds (**Section 2.1.2**). Stratigraphic data from trenches and exposures defines the characteristics of the surfaces and the evidence for relative surface stability over time.

2.4.4.1 400-yr Flood Bound. In trenches at the Saddle Constriction study area, deposits of a paleoflood with an age of 400- to 600- years are the parent materials of the surface soils (**Section 2.3.2**). Weakly developed soils developed in the flood deposits at these sites indicate that no significant erosion or deposition by other floods or other geomorphic processes have disrupted these surfaces in that time span. Similar relationships, preserved at multiple sites, demonstrate stability of these surfaces since the time of the "400-yr" flood, approximately 400- to 600-years ago (**Section 2.4.2**). Even at trench T4, where the "400-yr" deposits are buried by thin deposit of a younger paleoflood, the soil profile in the underlying deposits is intact, indicating that this site was not significantly eroded by that flood (**Section 2.4.1.1**), and hence has been stable

since deposition 400-600 years ago. Throughout the reach, the H1-2 surfaces which include these deposits are unmodified by younger erosion (**Section 2.2.3** and **Plate 2**).

The H1-2 surfaces and deposits of the "400-yr" flood are preserved in many differing hydraulic settings throughout the Diversion Dam study reach. Thus, for use as a paleohydrologic bound, some of these sites are much more strongly limiting than others (**Section 3.2.1.2** following). In particular, at Trench T4, unit stream power and bed shear stress increase very rapidly with increasing discharge and thus that site is very important to discharge limits for "400-yr" bound.

2.4.4.2 Early Holocene (H1 surfaces) Bound. The stratigraphic evidence to support this paleohydrologic bound is the preservation of extensive areas of generally fine-grained fluvial sediments with well-developed carbonate soils that underlie the H1-2 surfaces. The most extensive exposures of these sediments and soils are in trench T6, stations 1 to ~30, and in the disconnected sequence of trenches at BLR8 study area, T8a,b,c (**Section 2.3.2.3**, and **Section 2.3.3.1**). Smaller remnants are present at T4, stations 16 to 20 (**Section 2.3.2.1**), and at BLR6 (Ostenaar et al., 1999, 2002). These deposits and soils apparently are part of an aggradational fill of latest Pleistocene to early Holocene age (**Section 2.2.3**). Stage II carbonate soil horizons in these deposits are generally 50- to 100 cm thick, indicative of an early Holocene age for stabilization of the surface, and radiocarbon ages from these deposits ranging from about 12,800-7200 cal yr B.P support this age (**Section 2.2.3** and **Section Table 2-2**). Based on these data, a conservative time interval of 6000 to 8000 years has been chosen for use as a paleohydrologic bound. Most of radiocarbon ages from these sites are older than this range, but the shorter time interval reflects the possibility interpretation that aggradation of the sequence continued and the surfaces did not stabilize and begin forming soils until somewhat later.

2.4.4.3 Pleistocene Bound. The extensive areas of unmodified Pleistocene surfaces that flank the Big Lost River are the stratigraphic and geomorphic basis for this paleohydrologic bound (**Table 2-3**). The Pleistocene P2 surfaces have a braid-channel morphology that is inherited from Pleistocene gravel deposition and unrelated to present flows in the Big Lost River (**Section 2.2.2**). The more limited areas of Pleistocene P3 surfaces generally follow the present river channel and are also underlain by gravels, and likely represent the last episode of Pleistocene deglaciation (**Section 2.2.2**). Trench exposures in T6, T7, T8 and T9 indicate that the last phase of

deposition on these surfaces was aggradation of fines in small channels on the P3 surfaces (**Section 2.2.2**, **Section 2.3.2**, and **Section 2.3.3**). Subsequent deposition, shown by the inset deposits that underlie the Holocene surfaces has been dominated by fines. Soils on the Pleistocene surfaces are characterized by an upper loess cap, generally less than 0.5-m-thick in the Diversion Dam study reach and well-developed carbonate morphology (**Section 2.2.2**). The Pleistocene age of both the P2 and P3 surfaces is established regionally by depositional links to regional glaciation, and in a local context by radiocarbon ages of ~10,000 to 12,800 cal yr B.P. obtained from the inset fine-grained deposits (**Section 2.2.2** and **Table 2-2**).

2.5 Hydraulic Modeling of the Diversion Dam Study Reach

TrimR2D (**Appendix C, Part A**; Ostenaar et al., 1999) was used with the topographic data for the Diversion Dam reach (**Appendix A**) to calculate steady-state 2D inundation and flow velocities using a 6-ft cell flow grid for the discharges listed in **Table 2-1**. A 3 ft-spacing uniform grid was produced after a clockwise rotation of 31.4° of a subset of the high-resolution topographic grid (2000 photography, **Appendix A**) for the Diversion Dam study reach, which was subsampled by TrimR2D to produce a 6-ft staggered finite-difference grid. To accommodate the larger inundated areas associated with discharges larger than 200 cms, a larger region of topography containing the Diversion Dam study reach was extracted from the 5-ft spacing topographic mesh from the reprocessed 1993 aerial photography at INL (**Appendix A**) after a 36.9° clockwise rotation of the topographic mesh and interpolated to produce a 2.5-ft-spacing topographic input grid for TrimR2D. TrimR2D then subsampled the 2.5-ft-spacing topographic grid to produce a 5-ft-spacing staggered finite-difference grid. To ensure that flow was entrained within the grid to the downstream edges of the grids, high elevation walls were added to the western, northern, and southern edges of the grids. The impact of these walls in the 6-ft grid is most clearly apparent for the larger discharges (generally discharges of 200 cms or larger, see **Table 2-1** and plots in **Appendix D**) and motivated the development of the 5-ft grid that encompassed a larger area south of the channel to allow more realistic routing of discharges of 200 cms or larger.

In both grids the minimum elevation in the grid was removed from all points in the grid to maximize numerical precision in quantities involving elevations. Coordinate transformation

equations were constructed for both the 5-ft and 6-ft TrimR2D flow grids to convert the TrimR2D local grid coordinates to their original INL state-plane coordinates and elevations.

The grids were initially wetted using springs distributed along the channel and that were activated for several minutes of flow to partially fill the channels. To produce steady-state flows for specific discharges, springs were activated immediately downstream of the diversion dam in the active channel with a total flux equal to the specific discharge. For the smaller flows on the 6-ft grid, 22 springs were used to minimize stages in the vicinity of the springs and 28 springs were used with the larger discharges on the 5-ft grid. Flows for all discharges were calculated using a sequential approach, where the first flow calculation started with the smallest discharges. The results of the preceding smaller discharge were used as the initial wetting condition to start flow calculations for the next larger discharge. This minimized the impact of transient flow features like bores on the wetted area. Outlet flow water surface elevations were set to ensure subcritical outflow conditions.

Time steps were established at 5 s for the 6-ft grid and the smaller discharges to ensure Courant numbers of larger than 4 given main channel flow velocities of 1-2 m/s for discharges of 10 cms to ~200 cms. Main channel flow velocities for discharges of 200 cms and larger were generally > 2 m/s. Consequently, a time step of 3 s for the 5-ft grid to ensure Courant number larger than 4. As indicated in **Table 2-1**, two bed roughness scenarios using Manning's n of 0.030 and 0.038 were implemented in the 6-ft-grid flow calculations.

A total of 15 hydrograph monitoring positions were established throughout the channel sections of the study reaches. These hydrographs were monitored to determine when the flows had reached steady state. Typically, flow times of about four hours were required to achieve steady-state conditions throughout both study reaches. Steady-state conditions were defined as attaining an essentially static water surface elevation at all the hydrograph monitoring positions (natural high-frequency water surface elevation oscillations, typically of several centimeters, were ignored).

The flow quantities output included water surface elevations and vector flow velocities interpolated to the water surface elevation positions at cell-centered positions in the staggered grid. Using the known topography, derived quantities such as depth, shear stress, and power were

obtained. The inverse transformation operators were then applied to produce flow quantities in the INL state-plane coordinate system.

2.5.1 Results. Complete results of the flow modeling are depicted on maps contained in **Appendix D - Electronic Supplement**. Color-contoured plots of depth, stream power and shear stress are overlain on shaded relief images of the high-resolution topography and the geomorphic map units shown on **Plate 2**. Plots showing differences in flow depth for simulations with varied inputs of Manning's n or the input topographic grid are also included in **Appendix D - Electronic Supplement**. Plots in **Appendix F (Figures D3-6 through D3-37)** depict the effects of these same variations on unit stream power and bed shear stress in each of the sampling subareas. The plots in **Appendix F** can be used to directly assess the affects of the varied inputs on the estimated discharges associated with paleofloods and paleohydrologic bounds (see **Section 3.2**).

The model results show that depth, stream power, and shear stress vary significant throughout the study reach based on the local conditions of flow. For example, along the length of the channel, unit stream power increases and decreases significantly for areas with more or less constricted flow (**Figure 2-9**). Unit stream power increases with discharge in reaches which are less constricted; but locally decreases significantly upstream of some constrictions as flow stagnates with increasing discharge. The smallest flows simulated, 10, 12, and 15 m³/s, correspond to the range of the largest gaged flows downstream of the INEEL Diversion Dam, including a series of flows from 1995-1999 (**Appendix E**). In channel values of unit stream power and bed shear stress from this range of discharge that generally remain within the ranges of values associated with soil erosion (**Appendix D and Figure 3-2**) appear to be qualitatively consistent with field observations of a mostly intact, armored gravel bed through many areas of the central part of the study reach (**Section 2.2.4**). Areas at channel constrictions have somewhat higher values unit stream power and bed shear stress, and appear to be areas where sediment was mobilized by these flows.

For simulations up to about 70 m³/s, most flow remains confined to the main channel system with progressively greater inundation of flanking H3-4 and locally, limited areas of some H1-2 surfaces. Flows up to this level generally do not reach the geomorphic surfaces of interest for this study. The complex network of abandoned and cutoff channels in the Big Loop area and upstream

of the Saddle constriction gradual inundates with relatively low velocity and stagnated flow that is independent of the pattern of channel cutoffs, but instead controlled by changing patterns of flow constrictions through and downstream of the Big Loop area. Simulations for discharges of 100 and 130 m³/s show that essentially all areas of H1-2 surfaces along the Big Lost River become inundated by shallow flow, and simulations for 150 m³/s and larger discharges show progressive encroachment of this flow into the lowest areas of Pleistocene deposits and surfaces along the river. Discharges greater than 200 m³/s show progressive expansion of flows through the networks of braid channels on the Pleistocene surfaces.

2.5.1.1 Effects of Varied Manning's n . Difference plots of TrimR2D flow depth with varied Manning's n of 0.038 and 0.030, for discharges of 100, 200, and 250 m³/s, show that effects on the flow depth from variations in this parameter vary spatially throughout the study reach (**Appendix D - Electronic Supplement**). The largest differences are present in subreaches where flow accelerates, and flow depths for the lower n -value are reduced by 0.5 - 1-ft (0.1 - 0.3 m). In subreaches where flow stagnates, which includes large areas of the study reach, this parameter has little effect on flow depth. Thus, simulations based on a Manning's n of 0.030 indicate slightly reduced depths as flow is initiated through braid channels leading to trench T3, and in the straight reach between trenches T4/T5 and T6. However, initiation of flow over the Saddle and across the large area of Pleistocene (P2) surfaces north of the Big Lost River between the Saddle and the BLR8 site is unaffected by variations of Manning's n because flow depth in those areas is controlled by backwater effects at bedrock constrictions in the channel.

Effects on estimates of unit stream power and bed shear stress also vary spatially throughout the reach. On the plots in **Appendix F (Figures D3-6 through D3-37)**, dotted lines depicting the results for simulations using a Manning's n of 0.030 are close to, or shifted slightly to the right of lines for simulations using a Manning's n of 0.038. This implies a potential increase in the discharge associated with a threshold criteria of about 0 - 25 per cent, depending on the characteristics of flow through any specific subarea.

2.5.1.2 Effects of Input Topography. Most flow simulations for the study reach were used a 6-ft computational grid derived from the 2000 topographic data. However, as modeling commenced, it became clear that the extent model reach needed to expanded to simulate

the larger discharges. Thus, a 5-ft topographic grid of larger extent was derived from the reprocessed 1993 topographic data. As shown in **Appendix A**, the 1993 data has somewhat reduced accuracy compared to the 2000 data resulting in a lower resolution topographic input model, particularly in channelled or confined areas. These effects were shown on difference plots of flow depth for two discharges, 200 and 250 m³/s, common to both sets of simulations (**Appendix D - Electronic Supplement**). In general, simulations based on the 1993 topographic data resulted in flow depths that were 0.5 - 1 ft (0.1 - 0.3 m) larger throughout most of the study reach. Effects on estimates of unit stream power and bed shear stress are complex and controlled by local flow conditions (See plots in **Appendix D, Figures D3-6 through D3-37**). In some areas, unit stream power and bed shear stress increase due to the higher stage and flow velocity represented in the 5-ft grid model. In other areas, higher stage results in increased backwater and flow stagnation, leading to a reduction in unit stream power and bed shear stress.

2.5.1.3 Comparisons to Previous Studies. Initial inspections of model results derived from the 6-ft grid showed significant differences compared to the flow results developed for previous studies (Ostenaar et al., 1999, 2002) using the same flow model. These differences are illustrated by results from the Saddle area depicted in Ostenaar et al. (1999, 2002) (**Figure 2-10**). Increasing discharge from 100 m³/s to 150 m³/s resulted in a new path for flow named the Saddle, and development of high values of unit stream power on the geomorphic surfaces just downstream of the Saddle. In contrast, results from the 6-ft grid for this study showed that for a discharge of 150 m³/s (**Figure 2-23**), flow through the Saddle did not commence until modeled discharge reached of 250 m³/s (**Figure 2-24** and **Figure 2-25**). The smallest discharge modeled with the 5-ft grid was 200 m³/s (**Figure 2-26**) and these results showed significant flow through the Saddle as well as at a similar location slightly upstream. Because the initiation of through the Saddle is controlled by the backwater effects at the bedrock constriction (Ostenaar et al., 1999, 2002, and **Figure 2-10**) it appears that much of this difference is attributable to the lack of resolution in the original 2-ft contour data used in the earlier modeling. This resulted in higher stages upstream of the constriction for relatively lower discharges compared to the topographic models used as inputs for the present study.

Initial comparisons of modeling results for other areas of the study reach did not show a consistent difference (**Section Figure 2-11**). At BLR7, the most upstream site in the Diversion Dam study reach, modeled stage increased by about 0.5 m compared to the previous results. At BLR2, BLR6, and BLR8, modeled stage decreased by about 0.1-0.2 m compared to the previous results. When evaluation of the topographic data (**Appendix A**) revealed discrepancies in the accuracy of the 2-ft contour data used as input for the modeling by Ostenaar et al. (1999, 2002), the previous modeling results were eliminated from further consideration.

2.5.1.4 Results from Specific Study Areas. As a supplement to the reach-scale plots of the flow simulation results contained in **Appendix D - Electronic Supplement**, large-scale plots near the detailed geologic study areas were prepared that show unit stream power and bed shear stress. The plots in this section illustrate results for TrimR2D simulations using a Manning's n of 0.038, and results are shown for both 6-ft and 5-ft topographic grids. Only the larger flow simulations, those which are pertinent to the evaluations of paleofloods and paleohydrologic bounds for each of the study reaches are included. The full set of flow simulations is included in **Appendix D - Electronic Supplement** and used to define specific discharge limits as discussed in **Appendix D, Figures D3-6 through D3-37**, and following this section in **Section 3.2**.

Big Loop Study Area, Trenches T1, T2 and T3. Trenches T1, T2, and T3 were all located across braid channels on the extensive Pleistocene (P2) surface (**Plates 1, 2, and Section 2.3.1**). Trench T1 is lowest of these sites, and flow through the channel at T1 and on the P3 surface surrounding the trench is seen in simulations for discharges of 130 m³/s and larger (**Figure 2-12**). For modeled flows of 150 and 175 m³/s (**Figure 2-13** and **Figure 2-14**), inundation extent extends across most of the P3 surface and low values of unit stream power (<2 W/m²) and bed shear stress (1-5 N/m²) are present in limited areas of channels where flow is concentrated. For larger discharges, 200, 225, and 250 m³/s (**Figure 2-15** through **Figure 2-17**), the magnitude and extend of unit stream power exceeding 2 W/m² and bed shear stress exceeding 1-5 N/m² increases with discharge, particularly as flow concentrates in the braid channels and is diverted around small area of higher topography. For this discharge range, some flow is beginning in upstream braid channels on the P2 surface, but no flow has reached trenches T2 or T3.

Flow simulations using the 5-ft topographic grid for discharges of 200 and 250 m³/s (**Figure 2-18** and **Figure 2-19**) show increased flow depth and extent compared to the simulations using the 6-ft topographic grid (discussed above in **Section 2.5.1.2**). Thus, flow extent, and the magnitude and extent of values of unit stream power and bed shear stress for 200 m³/s on the 5-ft grid is only slightly less than values shown for 250 m³/s on the 6-ft grid (compare **Figure 2-18** and **Figure 2-17**). Flow simulations for 300, 350, and 400 m³/s (**Figure 2-20** through **Figure 2-22**) show increased flow across the P2 surface in the Big Loop study area, first concentrated in former braid channels, but gradually expanding across much of the surface. For this range of discharges, unit stream power and bed shear stress commonly reach values of 10-30 W/m² and 10-25 N/m², respectively, in the braid channels on the P2 surface where flow first concentrates. In the braid channels crossed by trenches T2 and T3, unit stream power and bed shear stress reach values of 5-10 W/m² and 5-10 N/m², respectively.

Saddle Constriction and T4/T5/T6 Study Areas. The initiation of flow through the Saddle area and onto the extensive Pleistocene (mostly P2) surfaces downstream of the Saddle was an important piece of evidence used by Ostenaar et al. (1999, 2002) to define the basis for a paleohydrologic bound over the past 10,000 years (**Section 2.3.2**). As noted above, (**Section 2.5.1.3**), flow simulations for this study, using the 6-ft grid derived from the 2000 topography, showed that flow was not initiated across the Saddle except for discharges of 250 m³/s and larger (**Figure 2-23** through **Figure 2-25**). Trenches T6 and T7 were sited to determine if there was geologic evidence downstream of the Saddle area of such flows. Flow simulations using the 5-ft topographic grid from the 1993 topography again show higher stages compared to simulations based on the 6-ft topographic grid (**Section 2.5.1.2**). For the smallest discharge simulated using the 5-ft grid, 200 m³/s, significant flow is present through the saddle, as well as at a second location about 200 m to the northwest (**Figure 2-26**). For the northernmost portion of trench T6 and a small area at the south end of trench T7, unit stream power and bed shear stress exceed 5-10 W/m² and 5-10 N/m², respectively, due to flow through the Saddle. Simulations based on either the 6-ft or 5-ft topographic grid (**Figure 2-25** and **Figure 2-26**) indicate that the initial flow onto the P3 surface from the Saddle would cross the geomorphic patterns on the P3 surface downstream of the Saddle. Flows that would follow channel patterns on the P3 surface at trench T6 and the southern end of trench T7 must reach that surface due to high stages in the Big Lost River downstream of

the Saddle constriction. Flow simulations based on the 5-ft grid indicate that this does not happen except for discharges of $250 \text{ m}^3/\text{s}$ and larger (**Figure 2-27** through **Figure 2-30**). These simulations show that as flow across the topographic barrier associated with the Saddle increases, unit stream power and bed shear stress commonly reach values of $10\text{-}30 \text{ W/m}^2$ and $10\text{-}25 \text{ N/m}^2$, respectively, in the braid channels on the P2 surface downstream as flow re-concentrates in these channels.

The T4/T5/T6 study area is located along the main Big Lost River channel downstream of the Saddle constriction (**Plate 1**). For flow simulations as large as about $70 \text{ m}^3/\text{s}$ (**Figure 2-31**), flow remains confined to the relatively straight channel flanked by H1-2 and P2 surfaces. Flow simulations of $100 \text{ m}^3/\text{s}$ (**Figure 2-32**) show inundation of the lowest portions of H1-2 surfaces, such as near T4, and for a discharge of $130 \text{ m}^3/\text{s}$ (**Figure 2-33**), the entire H1-2 surface near T4/T5/T6 is inundated. In some areas, such as the north end of trench T4, unit stream power and bed shear stress increase rapidly with increased discharge and begin to exceed 30 W/m^2 and 25 N/m^2 , at a discharge of $100 \text{ m}^3/\text{s}$. In other areas, such as along the main H1-2 surface on the north side of the river between T5 and T6, the increase is slower and patchy, with unit stream power and bed shear stress generally $<5 \text{ W/m}^2$ and 5 N/m^2 for a discharge of $130 \text{ m}^3/\text{s}$. Increasing discharge results in progressive increases in the extent of larger values of unit stream power and bed shear stress on the H1-2 surfaces. For a discharge of $150 \text{ m}^3/\text{s}$ (**Figure 2-34**), large areas of unit stream power and bed shear stress in the range of $10\text{-}30 \text{ W/m}^2$ and $10\text{-}25 \text{ N/m}^2$, respectively, are shown on the H1-2 surface, and these expand over most of that surface in simulations for $175 \text{ m}^3/\text{s}$ (**Figure 2-35**). These values continue to increase in simulations for 200, 225, and $250 \text{ m}^3/\text{s}$ (**Figure 2-36** through **Figure 2-38**). Simulations for $225 \text{ m}^3/\text{s}$ show unit stream power and bed shear stress in the range of $30\text{-}50 \text{ W/m}^2$ and $25\text{-}50 \text{ N/m}^2$, respectively, over most of H1-2 surface between T5 and T6, and unit stream power exceeding 50 W/m^2 in many areas for a discharge of 250 W/m^2 .

Simulation results for the T4/T5/T6 study area based on the 5-ft topographic grid again show greater flow depth than do equivalent discharge simulations based on the 6-ft topographic grid (**Section 2.5.1.2**). However, for discharges of $200 \text{ m}^3/\text{s}$, unit stream power and bed shear stress magnitude and extent on the H1-2 surfaces are generally similar, near 30 W/m^2 and 25 N/m^2 , respectively, for simulations using either the 5-ft or 6-ft topographic grid (compare **Figure 2-36**

and **Figure 2-39**). Because of the higher stage present in the 5-ft grid model, flow overtops edge of the P3 surface north of the river, resulting in slightly reduced unit stream power and bed shear on the flanking H1-2 surface. For larger discharges simulated using the 5-ft topographic grid (**Figure 2-40** through **Figure 2-43**), the high values unit stream power and unit stream power are present across the entire extent of the H1-2 surface near trenches T5 and T6.

In both sets of flow simulations, for discharges larger than $150 \text{ m}^3/\text{s}$, unit stream power exceeds 100 W/m^2 bed shear stress approaches 100 N/m^2 over most of the channel area through this subreach.

BLR8 Study Area, Trenches T8 and T9. For discharges up to $70 \text{ m}^3/\text{s}$ (**Figure 2-44**), flow simulations indicate that the main path of flow follows the Big Lost River channel around the sharp bends that define this subreach. For the larger discharges in this range, there is a decrease in channel power and shear stress in the downstream portion of the reach, and an increase in area near the Rb outcrops flanking the downstream bedrock constriction. Near trench T8a,b,c, the inundation extent for a discharge of $70 \text{ m}^3/\text{s}$ is roughly coincident with the transition between H1-2 and H3-4 surfaces (**Figure 2-44**). Deposits at the north end of trench T9 are inundated by discharges of less than $50 \text{ m}^3/\text{s}$, and unit stream power and bed shear stress remains low at this site through the full range of simulated discharges flow depth increases. Discharges of 100 and $130 \text{ m}^3/\text{s}$ (**Figure 2-45** and **Figure 2-46**) both inundate the full extent of H1-2 surfaces to the vicinity of trench T8b. Unit stream power and bed shear values increase significantly near trench T8c with each increase in the modeled discharge, but remain low at the edge of the flow near trench T8b. Discharge of $150 \text{ m}^3/\text{s}$ (**Figure 2-47**) results in inundation to the southern end of trench T8a and is roughly coincident with the lower edge of the P3 surface near trench T9. At this discharge and larger, unit stream power and bed shear stress near trench T8c, the northernmost trench, remain generally above values of 50 W/m^2 and 25 N/m^2 . For discharges of 175 , 200 , 225 , and $250 \text{ m}^3/\text{s}$ (**Figure 2-48** through **Figure 2-51**) flow depth progressively increases in the areas of T8a and T8b, increasing the range unit stream power and bed shear stress to $5\text{-}25 \text{ W/m}^2$ and $5\text{-}30 \text{ N/m}^2$, respectively. Near T8c, values of unit stream power and bed shear stress increase somewhat but remain above 50 W/m^2 and 25 N/m^2 . Near trench T9, increasing discharge above $150 \text{ m}^3/\text{s}$,

results in gradual southward extension of the inundation extent with low unit stream power and bed shear stress values.

Simulations of the larger discharges using the 5-ft grid topography have higher stages and greater flow depths (**Section 2.5.1.2**), but the most significant difference from the 6-ft grid results is a small shift to the south in the band of highest intensity unit stream power and bed shear stress across the H1-2 surface near T8b and T8c. The results based on the 5-ft topographic grid for 200 and 250 m³/s (**Figure 2-52** and **Figure 2-53**) show a distinctly different pattern of high values of unit stream power and bed shear stress compared to results based on the 6-ft topographic grid (**Figure 2-49** and **Figure 2-51**). For the larger discharges modeled, 300, 350 and 400 m³/s (**Figure 2-54** through **Figure 2-56**) the full extent of the P3 surface near the trenches becomes inundated. In the largest flows, unit stream power and bed shear stress begin to decrease across the site due to backwater effects from the bedrock outcrops at the downstream edge of the study area.

Figures for Section 2.0

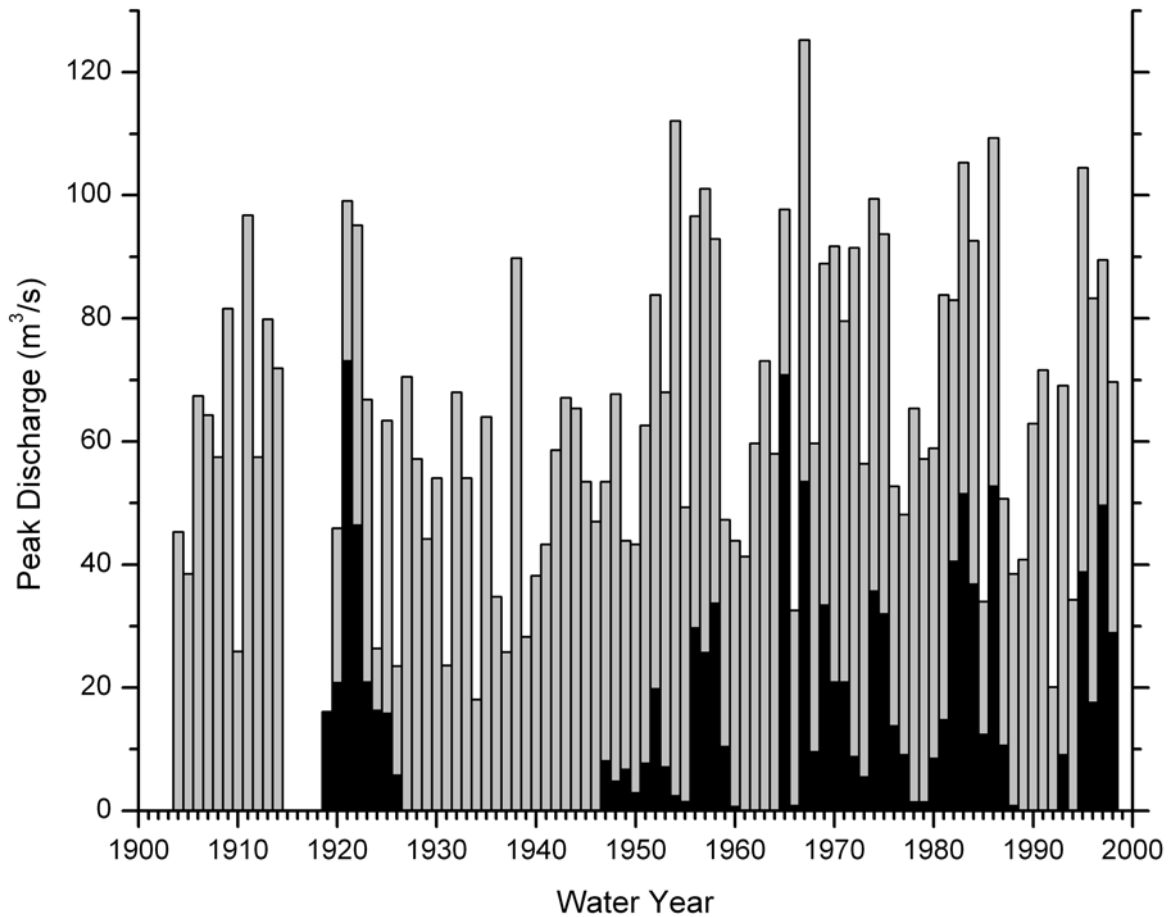


Figure 2-1 Annual peak discharge estimates for upstream (light shaded bars) and downstream gaging stations (dark shaded bars) on the Big Lost River. Upstream estimates are from Big Lost River at Howell Ranch from 1904 to 1998. Downstream estimates are from Big Lost River near Arco from 1947 to 1998 except for period 1919 to 1926 which are peak discharge estimates from stations at Leslie and near Moore, early gages located a short distance upstream of Arco. No peak discharge estimates are available from sites near Arco for the periods 1905 to 1918, 1927 to 1945, and 1962 to 1964. Figure from Ostenaar et al., 2002.

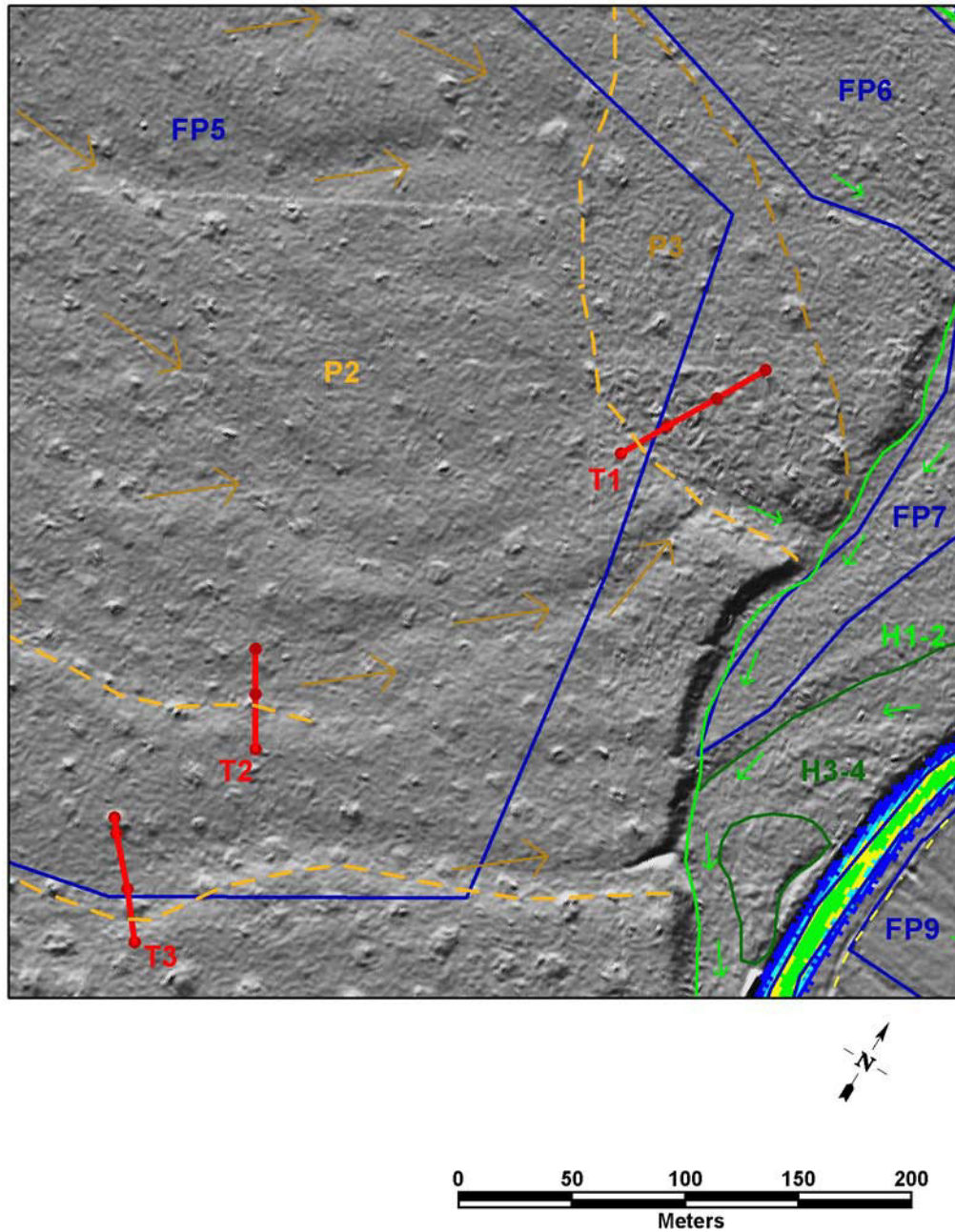


Figure 2-2 Area around Trenches T1, T2, and T3. Shaded relief image and geology from **Plate 2**. Blue boxes are stream power and shear stress sample areas (**Section 3.2**). Red lines are trench locations; red dots along the lines show end stations and 25-m stationing intervals beginning at south end. See **Plate 2** for explanation of geologic symbols and labels. Flow direction in Big Lost River is from upper left to lower right.

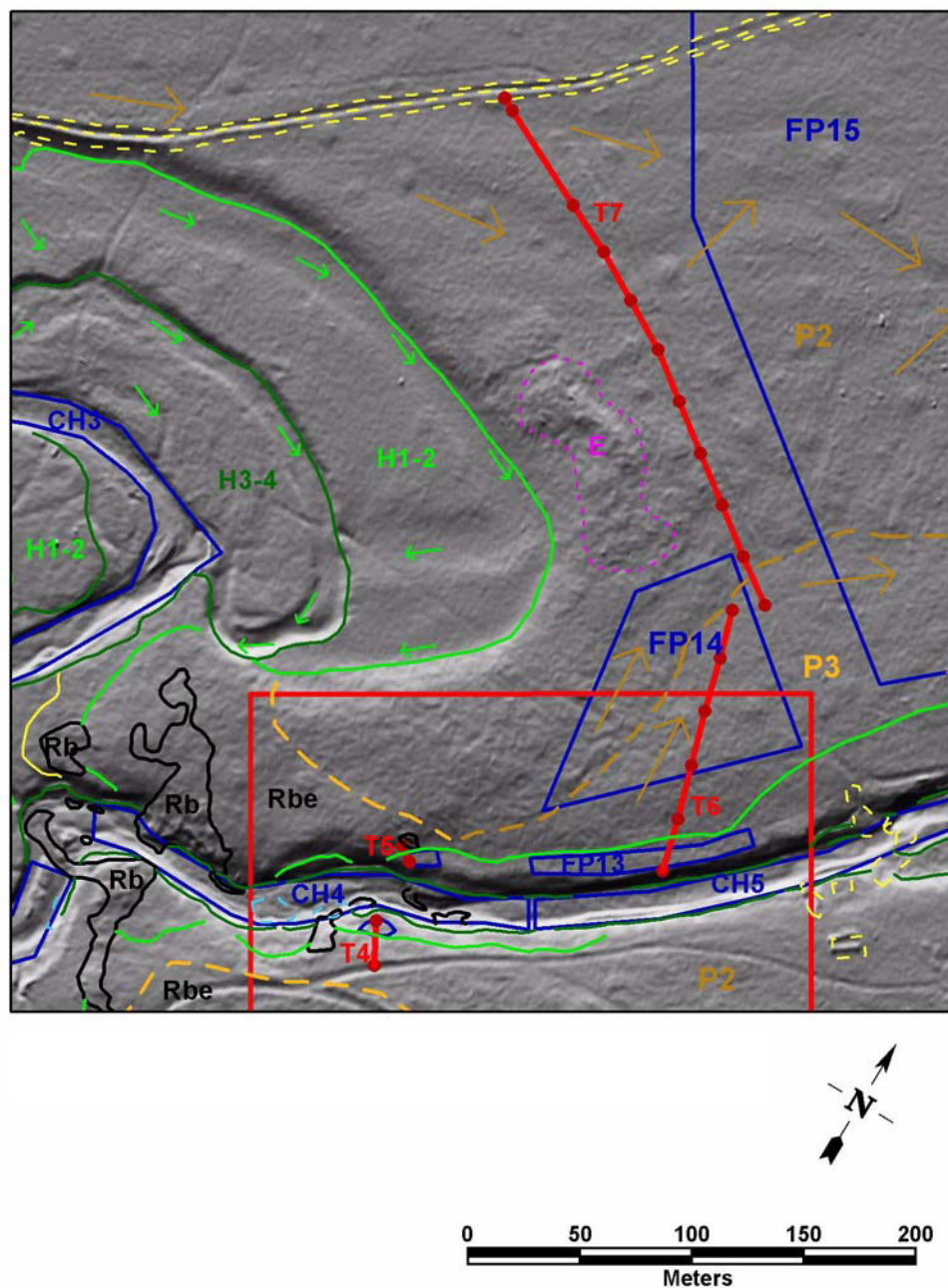


Figure 2-3 Area around "Saddle" and Trenches T4 and T5 downstream of saddle constriction.

Shaded relief image and geology from **Plate 2**. Blue boxes are stream power and shear stress sample areas (**Section 3.2**). Red lines with dots and labels show trench locations; red dots along the lines show end stations and 25-m stationing intervals beginning at south end. Red box in lower part of figure shows partial extent of inset area shown in **Figure 2-4**. See **Plate 2** for explanation of geologic symbols and labels. River flow direction is from left to right.

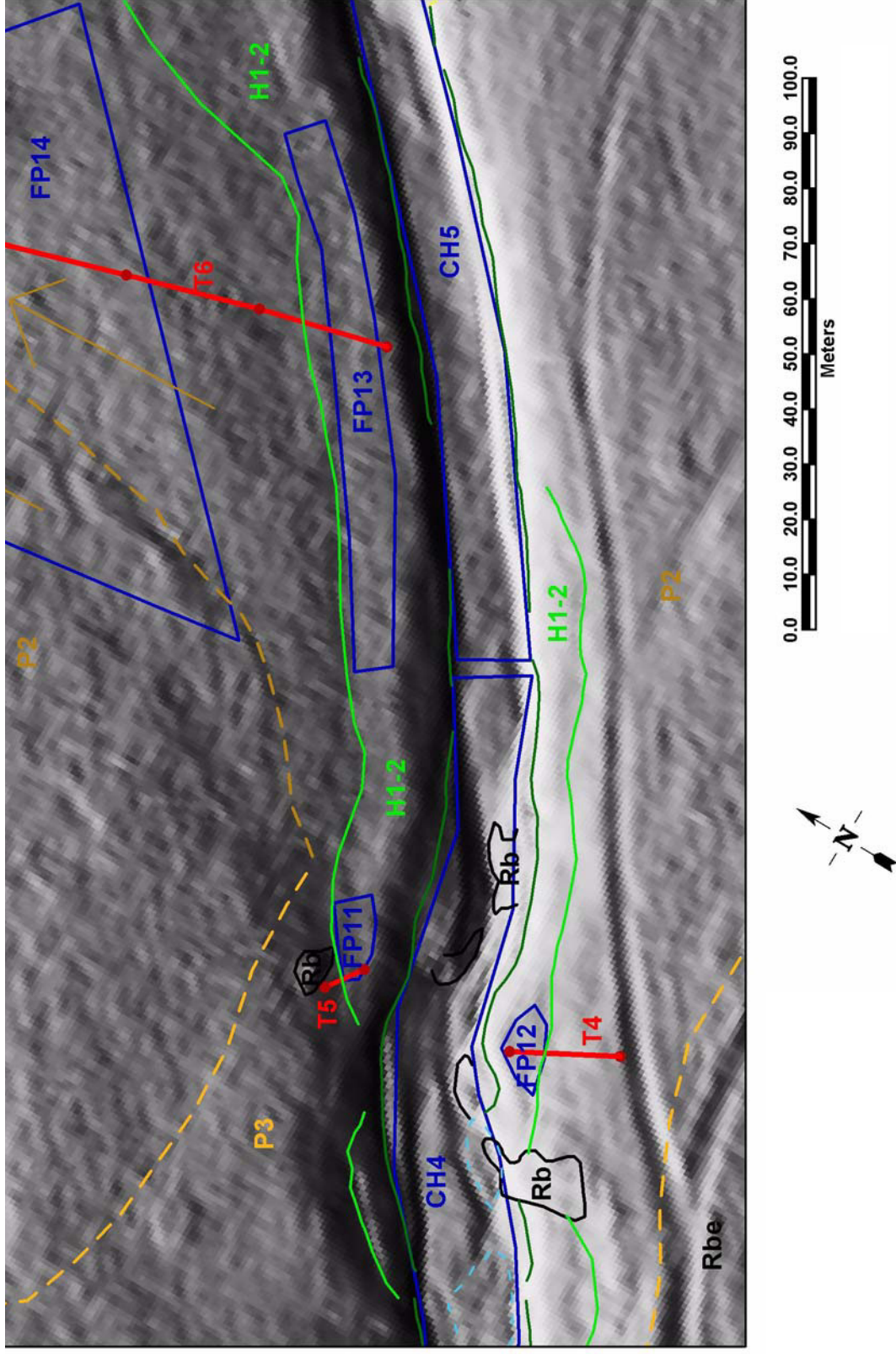


Figure 2-4 Detail of area around Trenches T4, T5 and T6 downstream of saddle constriction. Shaded relief image and geology from **Plate 2**. Blue boxes are stream power and shear stress sample areas (**Section 3.2**). Red lines with dots and labels show trench locations; red dots along the lines show end stations and 25-m stationing intervals beginning at south end. See **Plate 2** for explanation of geologic symbols and labels.

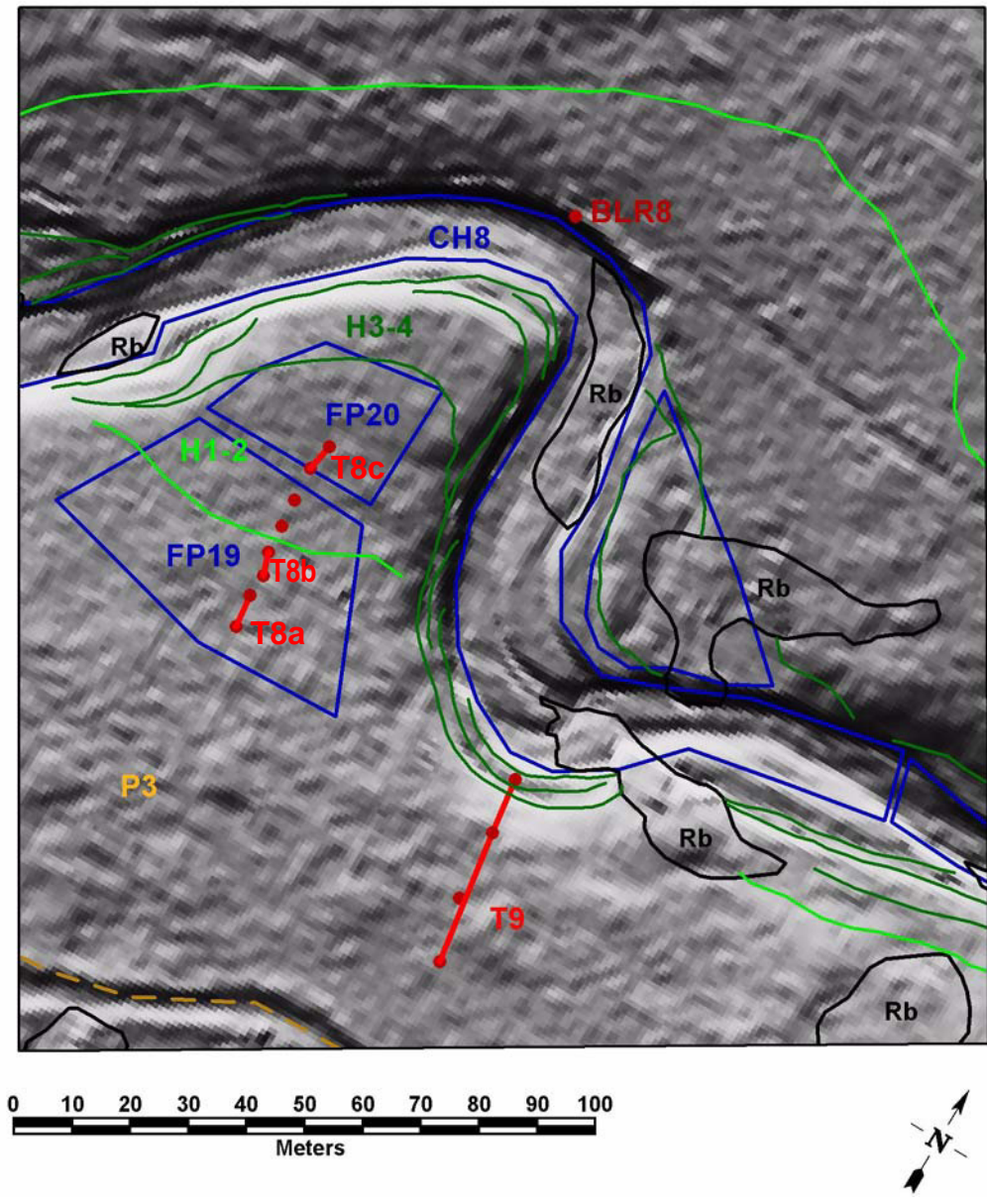


Figure 2-5 Area around BLR8 and Trenches T8 and T9. Shaded relief image and geology from **Plate 2**. Blue boxes are stream power and shear stress sample areas (**Section 3.2**). Red lines with dots and labels show trench locations; red dots along the lines show end stations and 25-m stationing intervals beginning at south end. See **Plate 2** for explanation of geologic symbols and labels. River flow is from left to right.

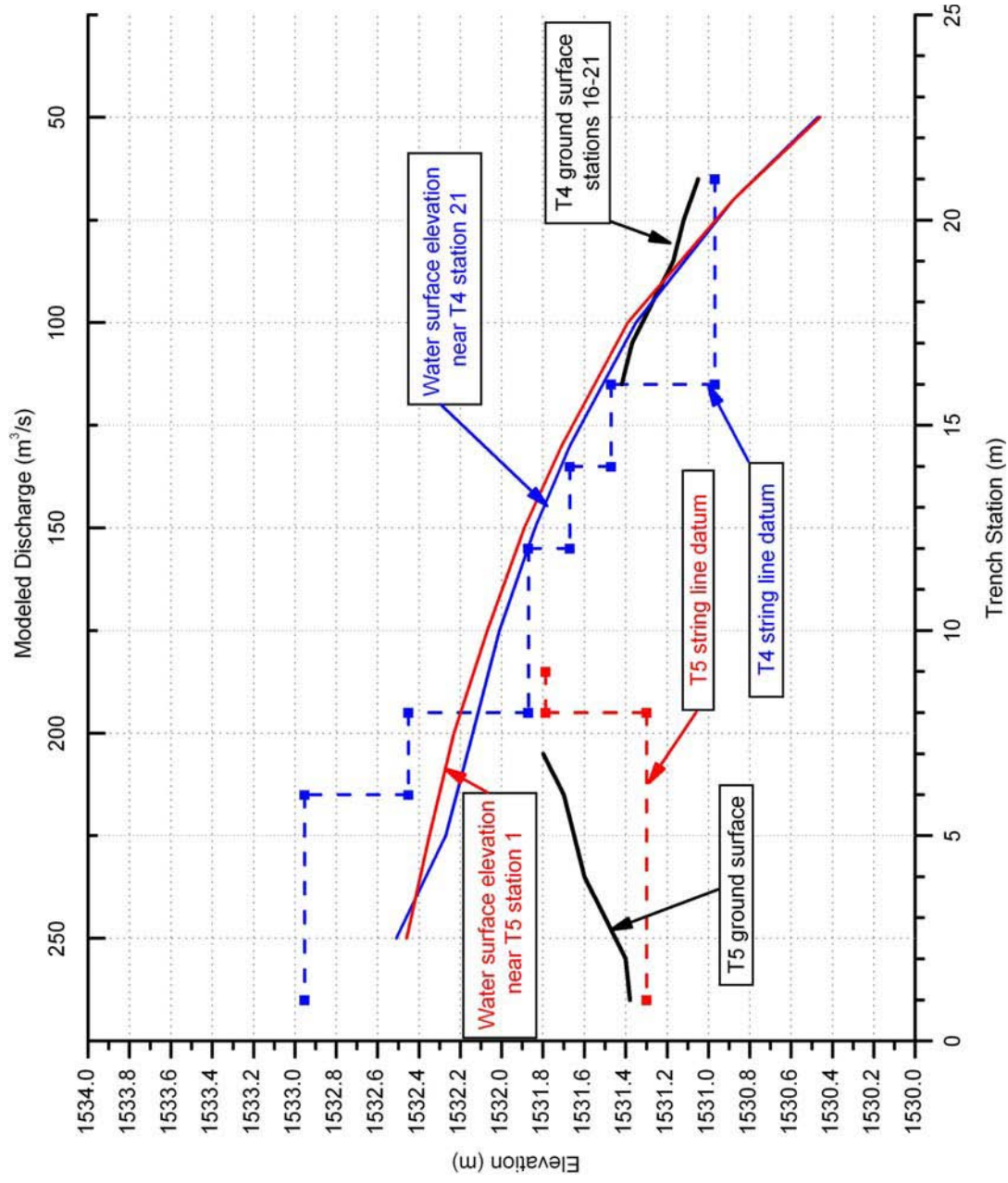


Figure 2-6 Modeled water surface elevation near trenches T4 and T5. Results for n=0.038 from TrimR2D models on 6-ft topographic grid. S

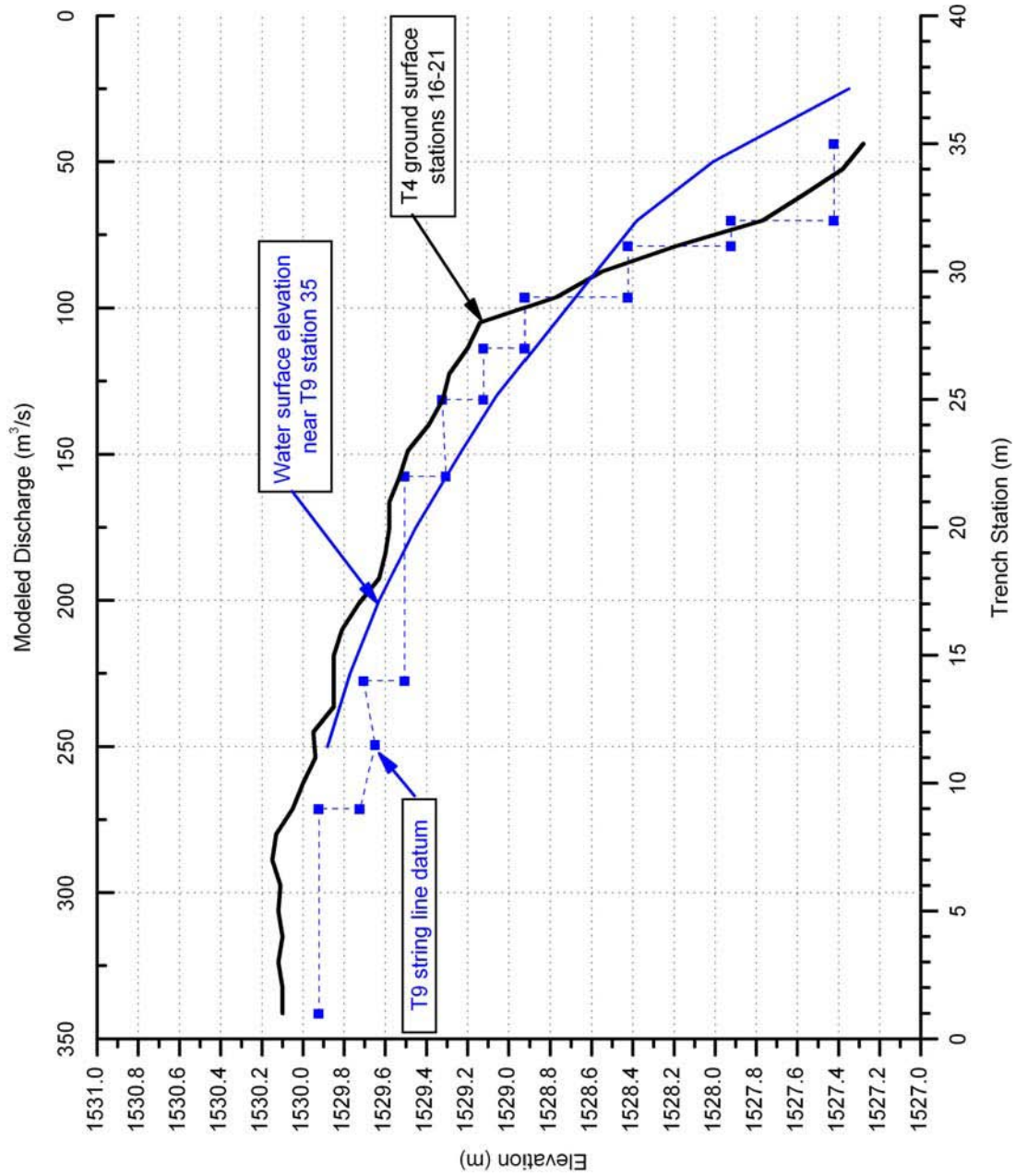


Figure 2-7 Modeled water surface elevation near trench T9. Results for n=0.038 from TrimR2D models on 6-ft topographic grid. S

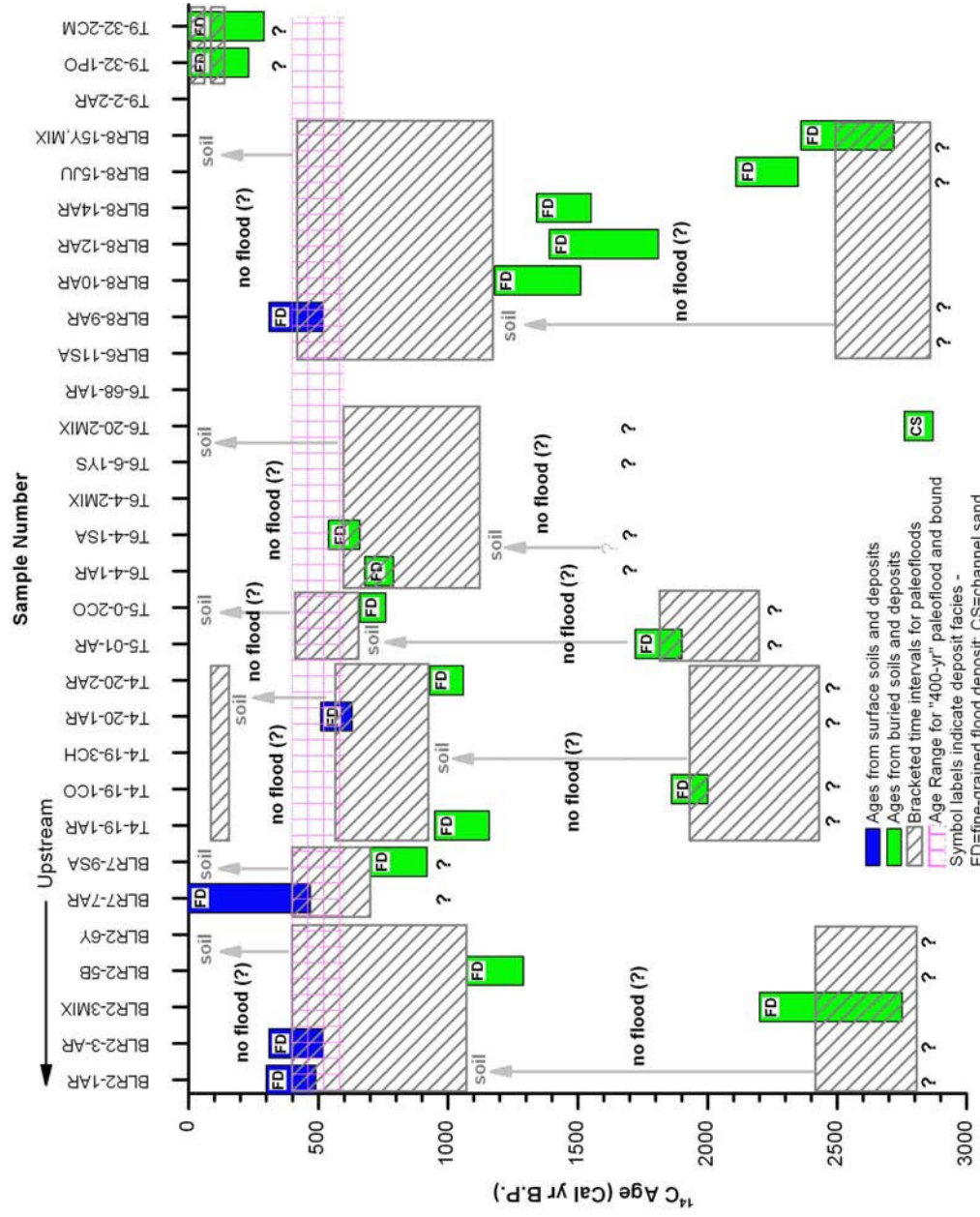


Figure 2-8 Summary plot of age constraints for late Holocene paleofloods. Cross-hatched boxes correspond to bracketed time intervals for paleoflood deposits at each site and are wider for sites with more age control. Green and blue boxes are calibrated radiocarbon age ranges (Table 2-2). BLR* samples are from Ostenaar et al. (1999, 2002); T* samples are from this study. Samples from within a paleoflood deposit either date the flood directly or are minimum soil ages that overlap the bracketed range. Samples that are buried by the paleoflood deposit are shown abutting the bracketed time intervals and are presumed to be maximum ages for the paleoflood. Vertical arrows show relative intervals of soil development on bracketed deposits at each site. ? ? show maximum age which for which paleofloods at each site can be constrained.

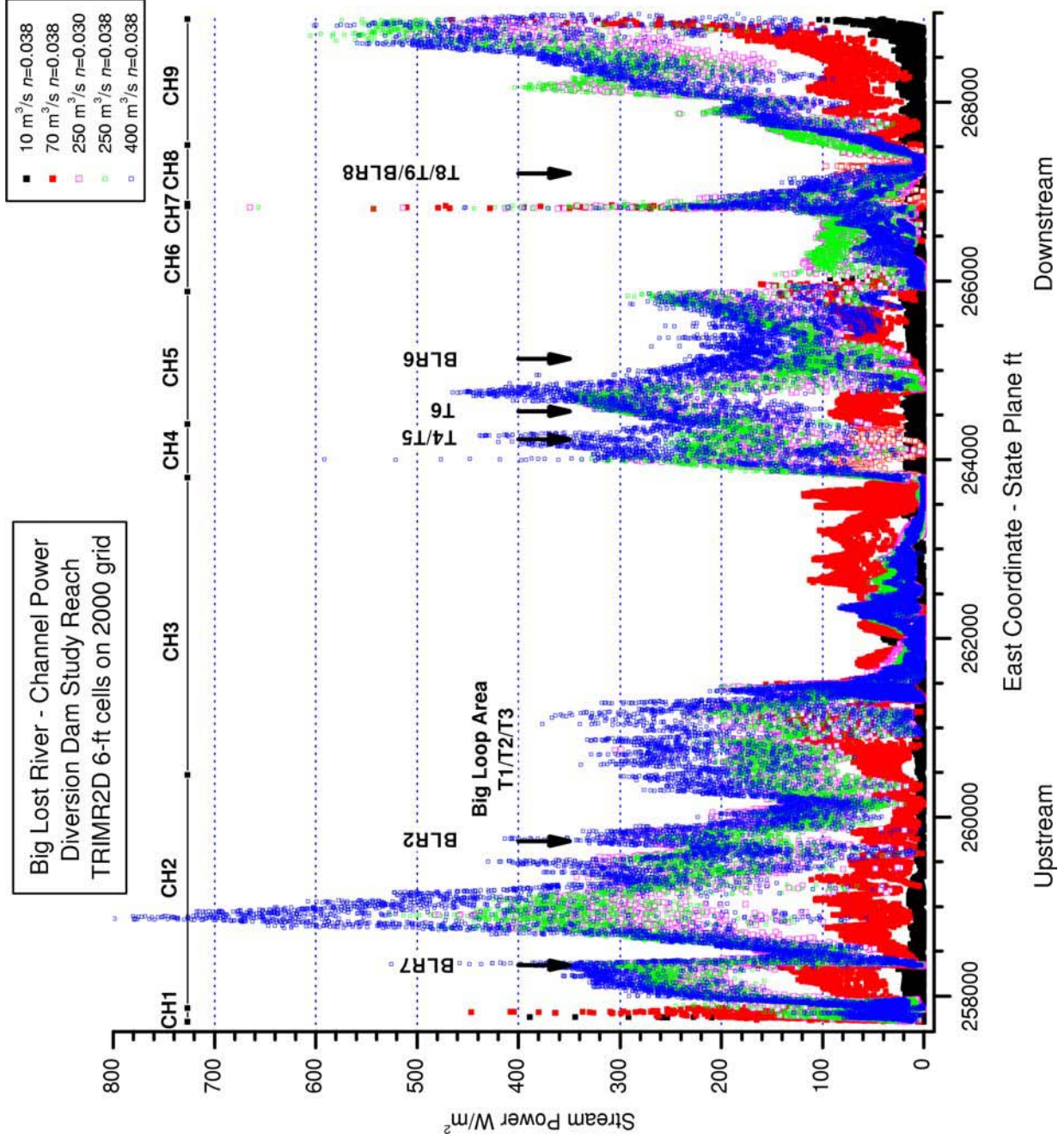


Figure 2-9 Channel power for the Diversion Dam study reach subareas. Longitudinal extent of channel reach subareas is shown by bars along top of plot. Subarea extent and sampling is described in **Appendix D.**

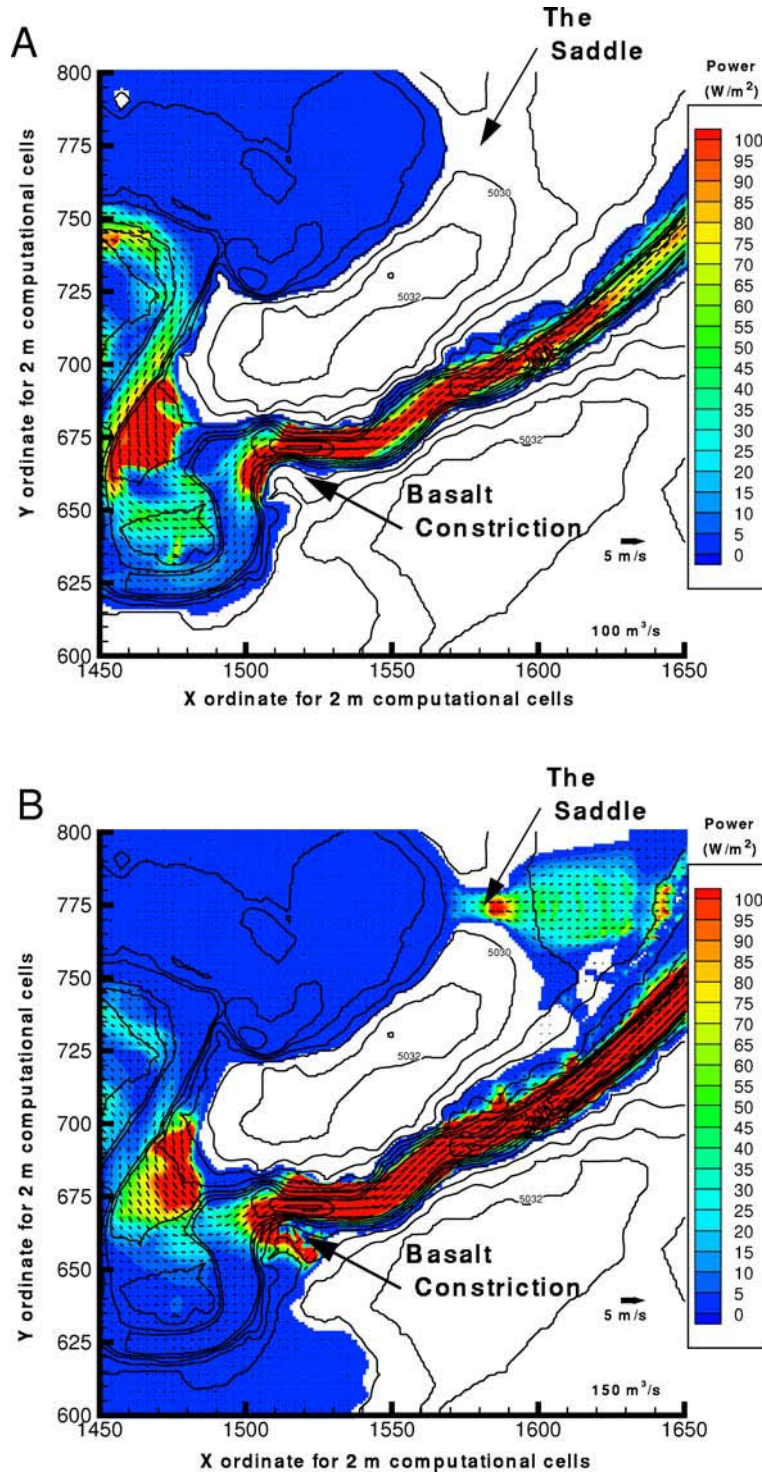


Figure 2-10 Model results for 100 and 150 m³/s from Ostenaar et al. (1999, 2002) near the Saddle.
 A) Inundation and unit stream power for 100 m³/s; B) Inundation and unit stream power for 150 m³/s. Flow is from left to right in both plots.

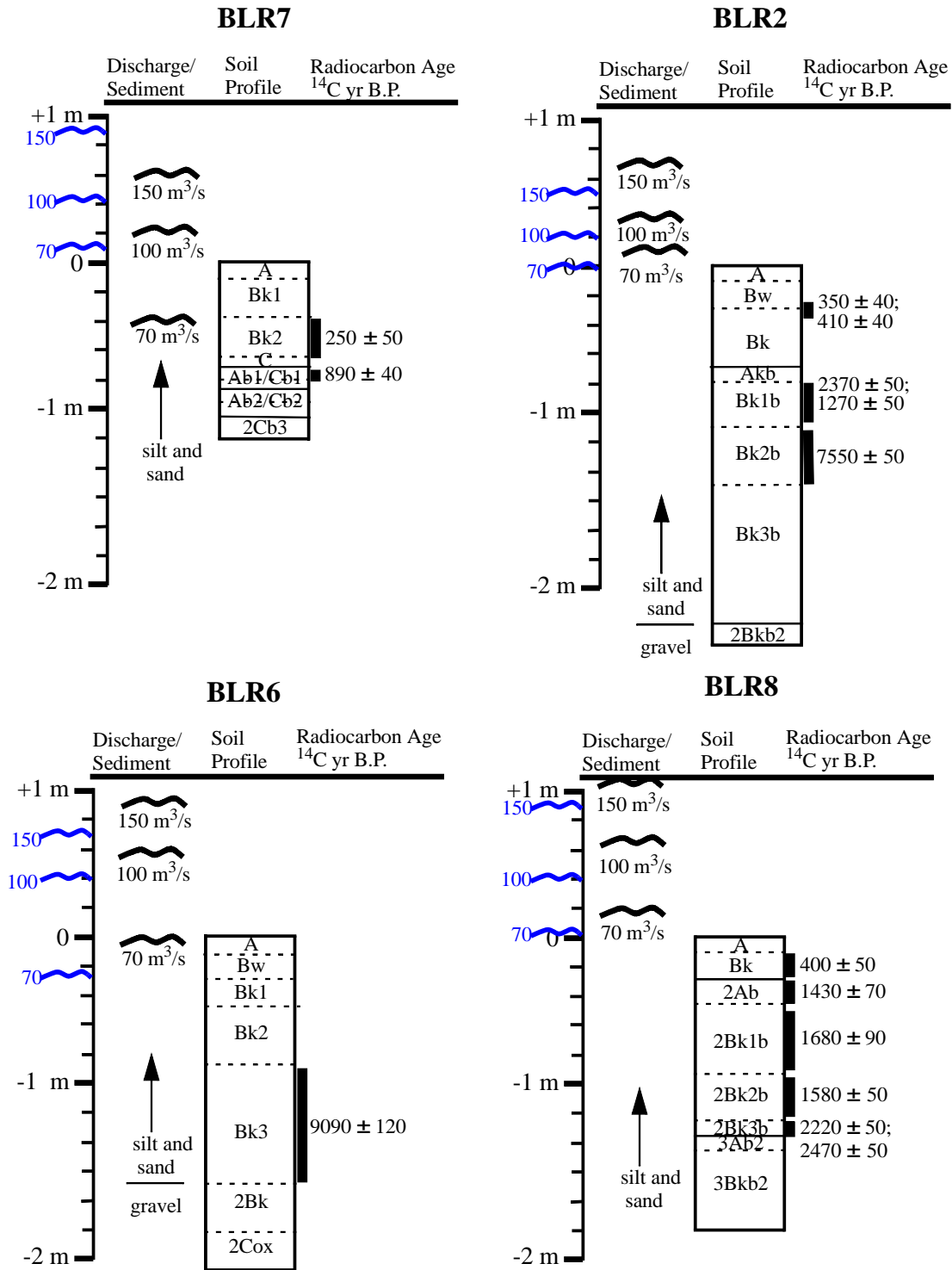


Figure 2-11 Figure 5 from Ostenaar et al. (2002) with revised stage estimates at BLR study sites. Wavy blue lines along axis show current study model results from 6-ft grid for $n=0.038$. All other data from Ostenaar et al. (2002). Study site locations are shown on **Plates 1** and **2**.

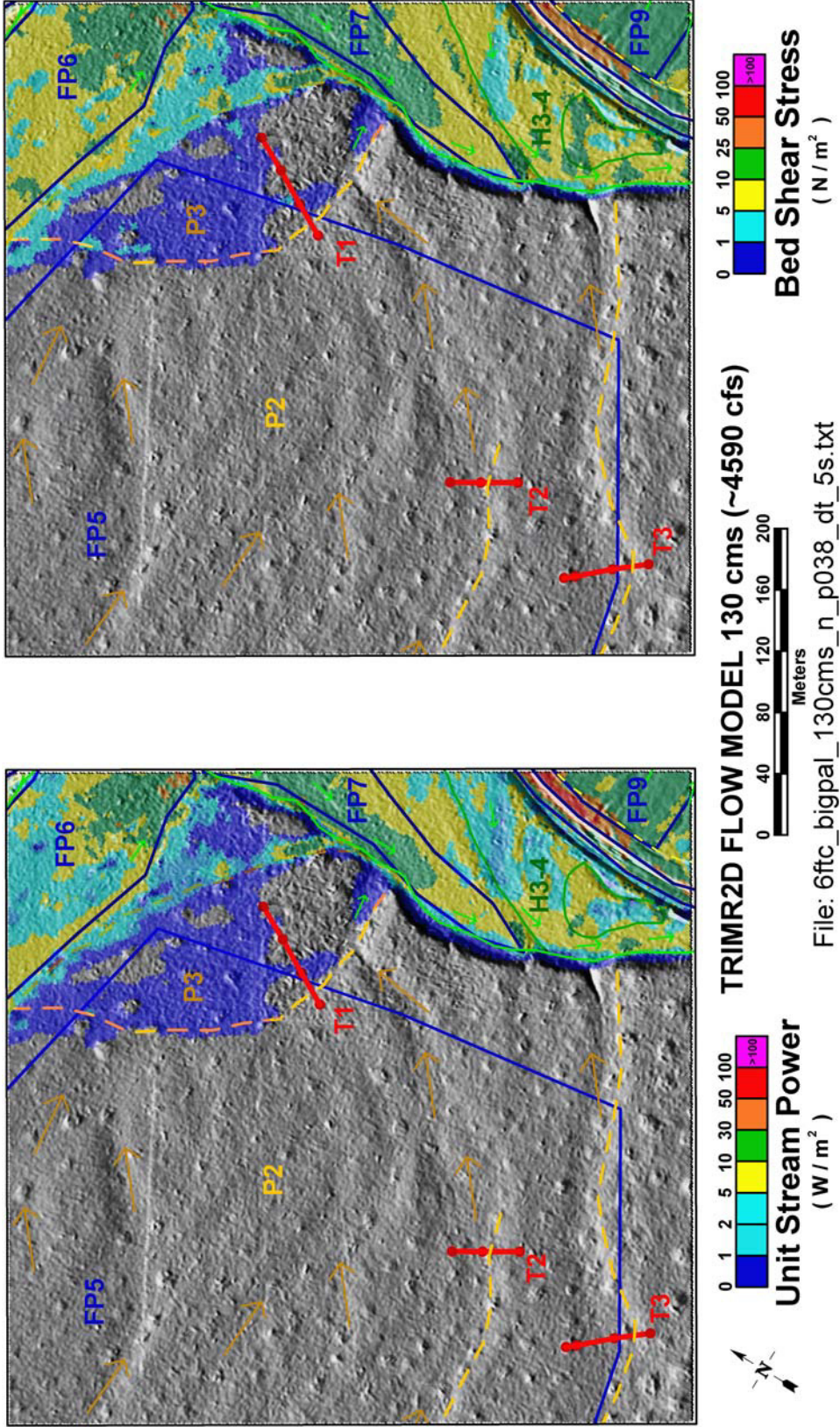


Figure 2-12 6-ft flow model results for $130 \text{ m}^3/\text{s}$ in the Big Loop study area. Base map symbology is from Figure 2-3 and Plate 2.

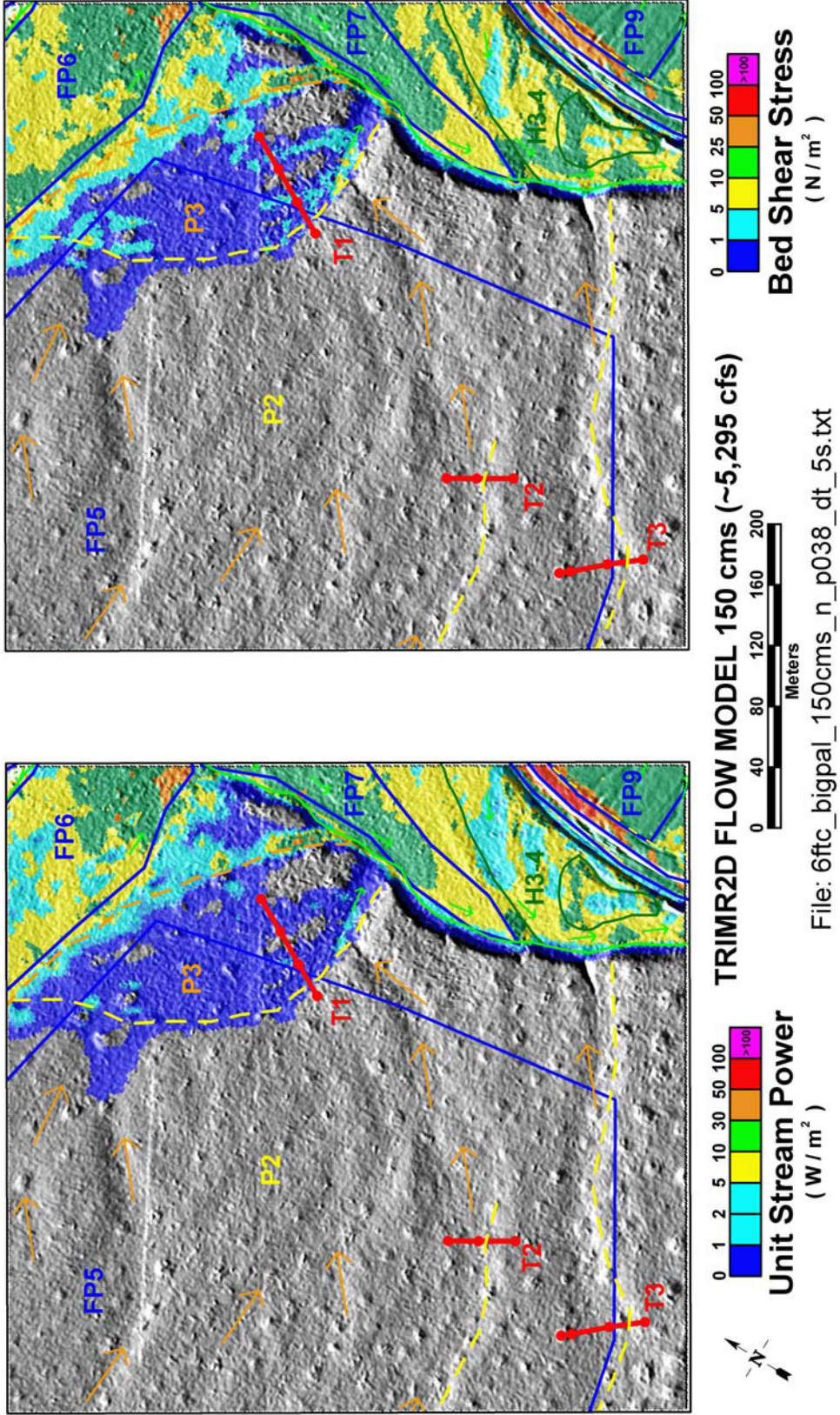


Figure 2-13 6-ft flow model results for $150\text{ m}^3/\text{s}$ in the Big Loop study area. Base map symbology is from Figure 2-3 and Plate 2.

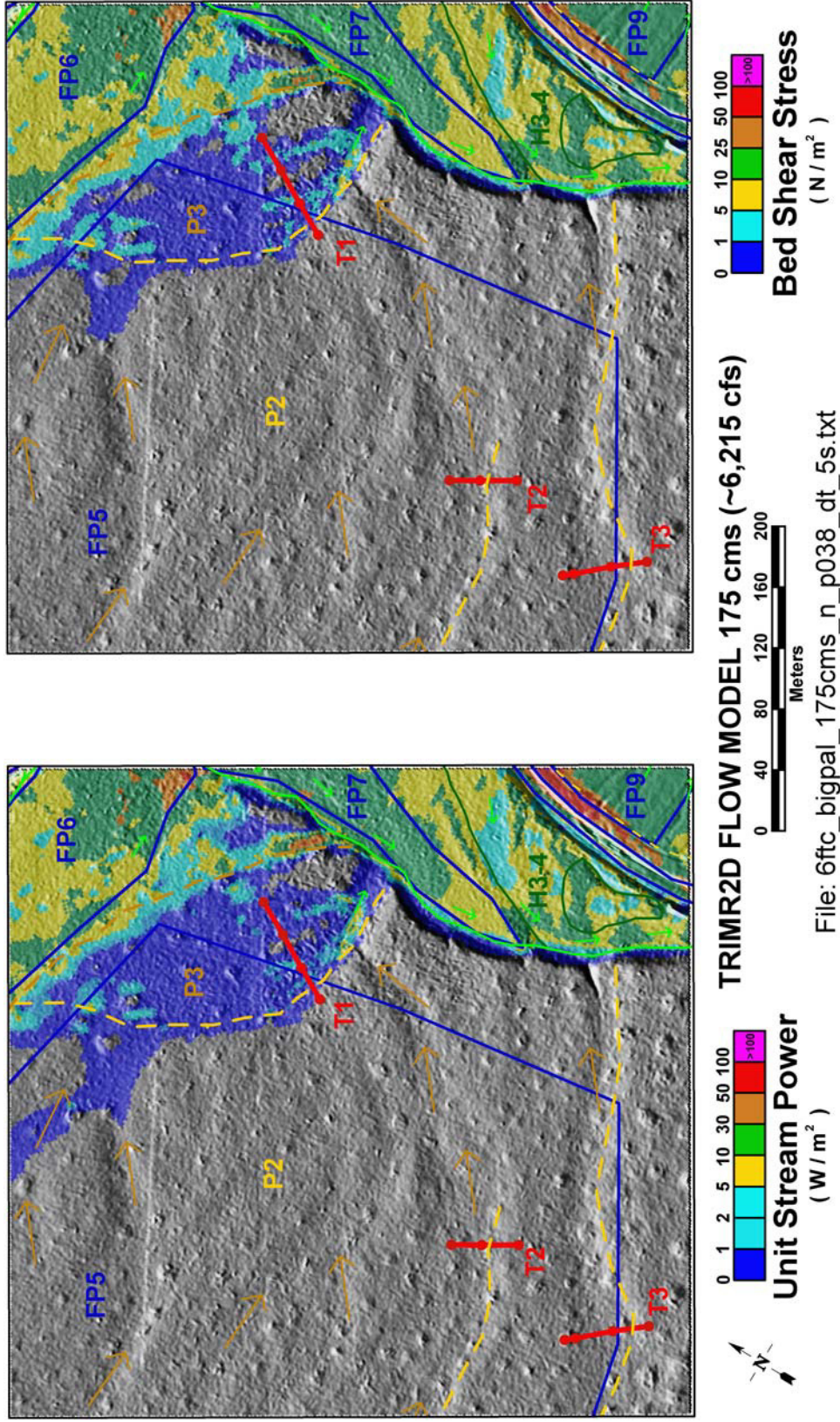


Figure 2-14 6-ft flow model results for 175 m³/s in the Big Loop study area. Base map symbology is from Figure 2-3 and Plate 2.

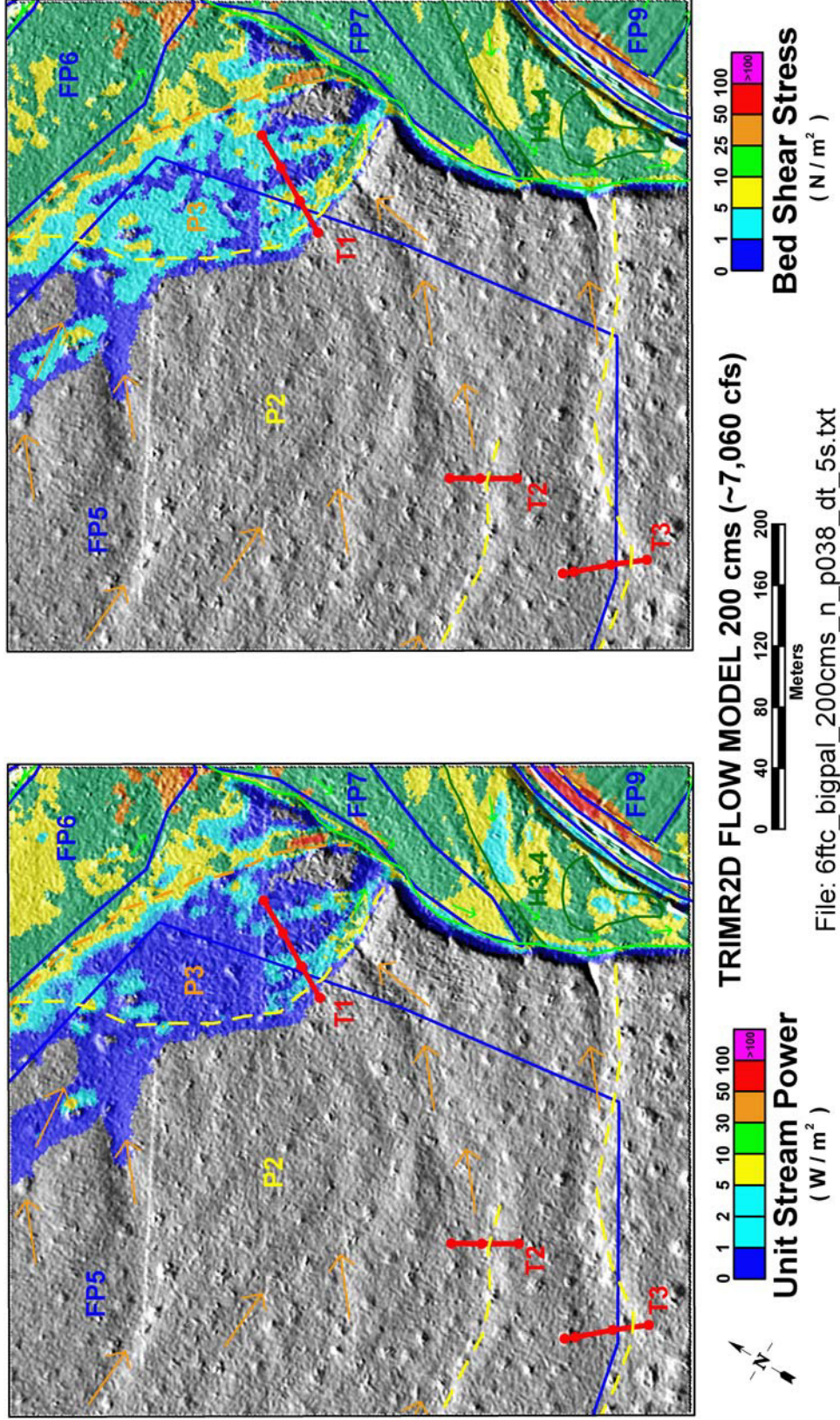


Figure 2-15 6-ft flow model results for $200 \text{ m}^3/\text{s}$ in the Big Loop study area. Base map symbology is from Figure 2-3 and Plate 2.

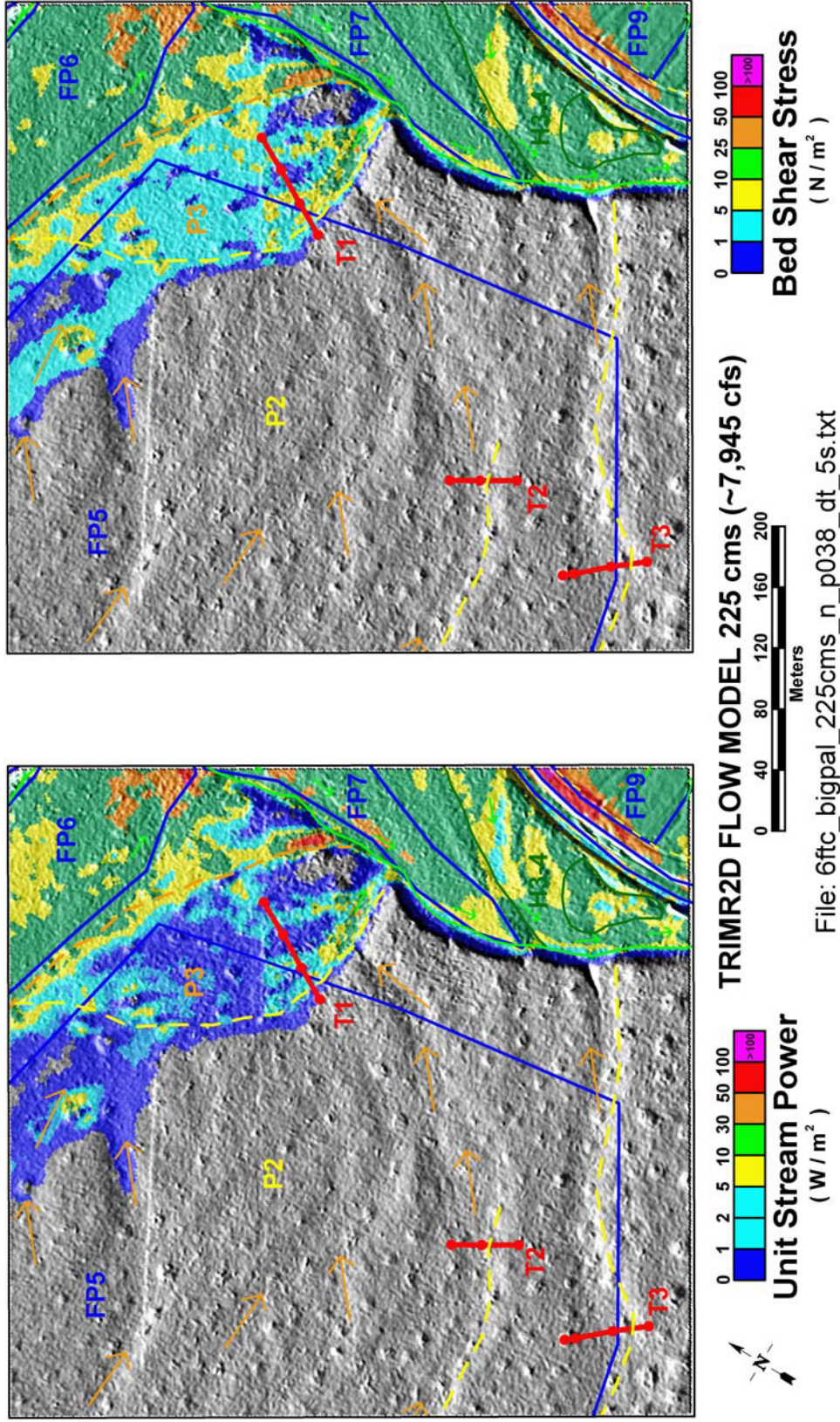


Figure 2-16 6-ft flow model results for 225 m³/s in the Big Loop study area. Base map symbology is from Figure 2-3 and Plate 2.

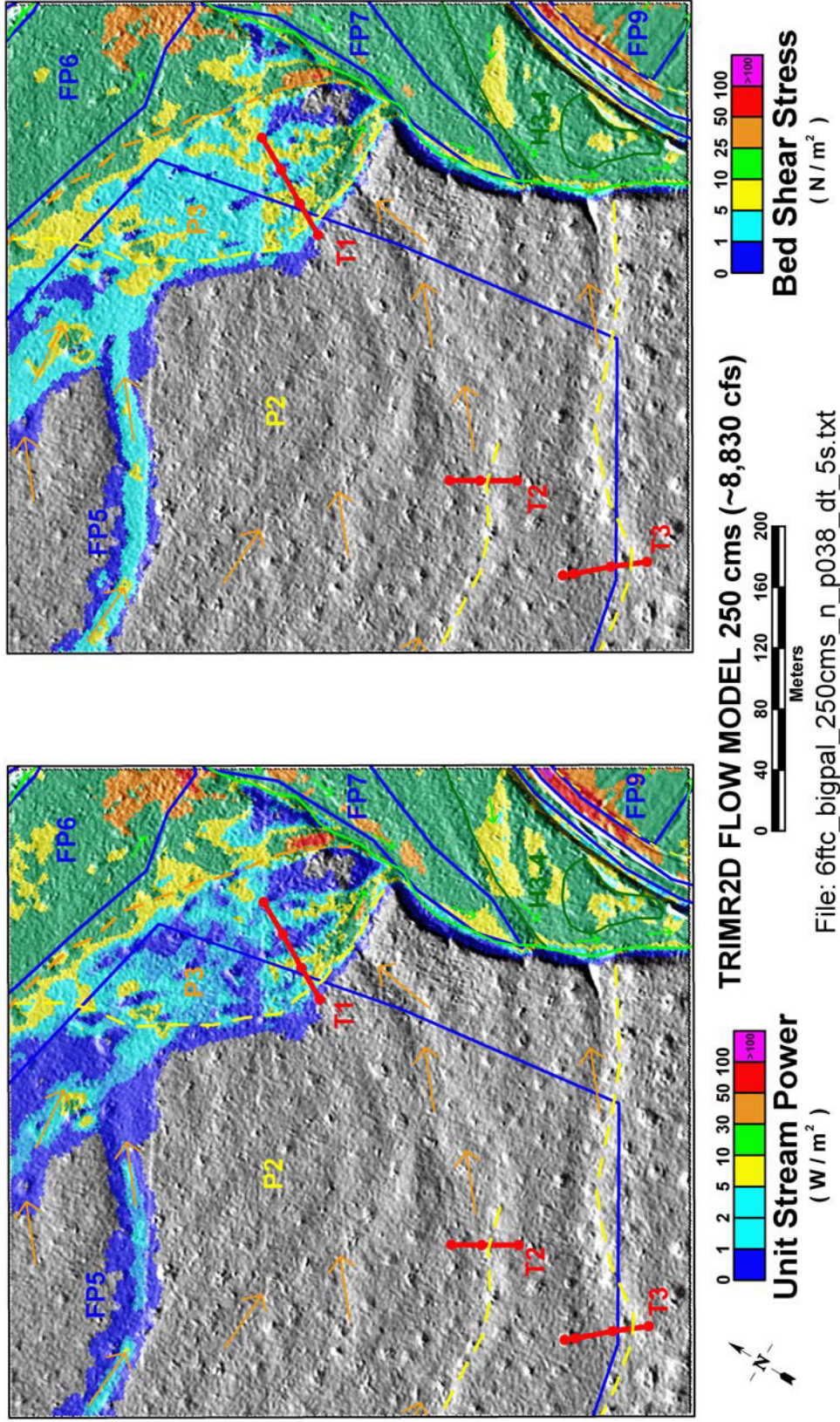


Figure 2-17 6-ft flow model results for 250 m³/s in the Big Loop study area. Base map symbology is from Figure 2-3 and Plate 2.

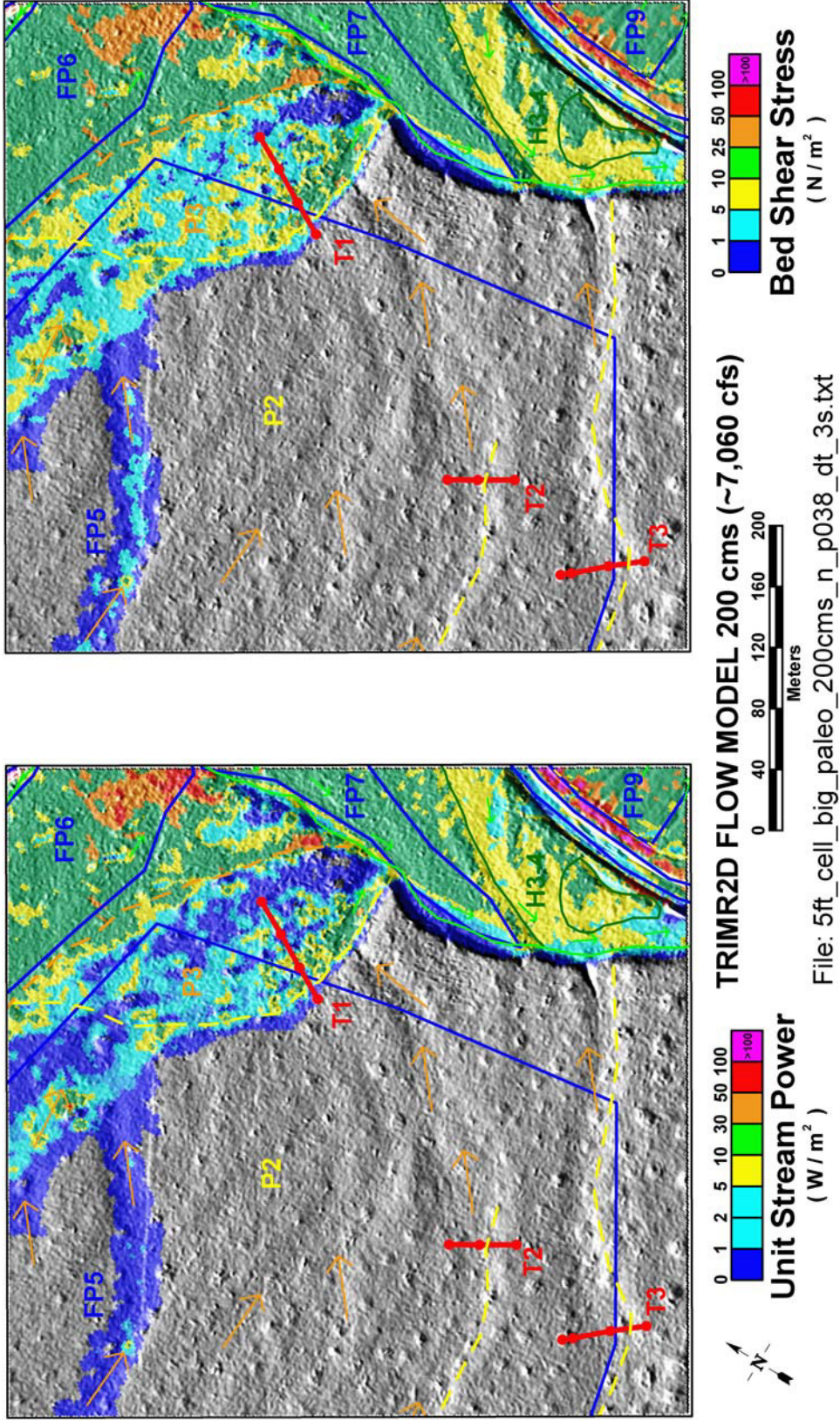


Figure 2-18 5-ft flow model results for 200 m³/s in the Big Loop study area. Base map symbology is from Figure 2-3 and Plate 2.

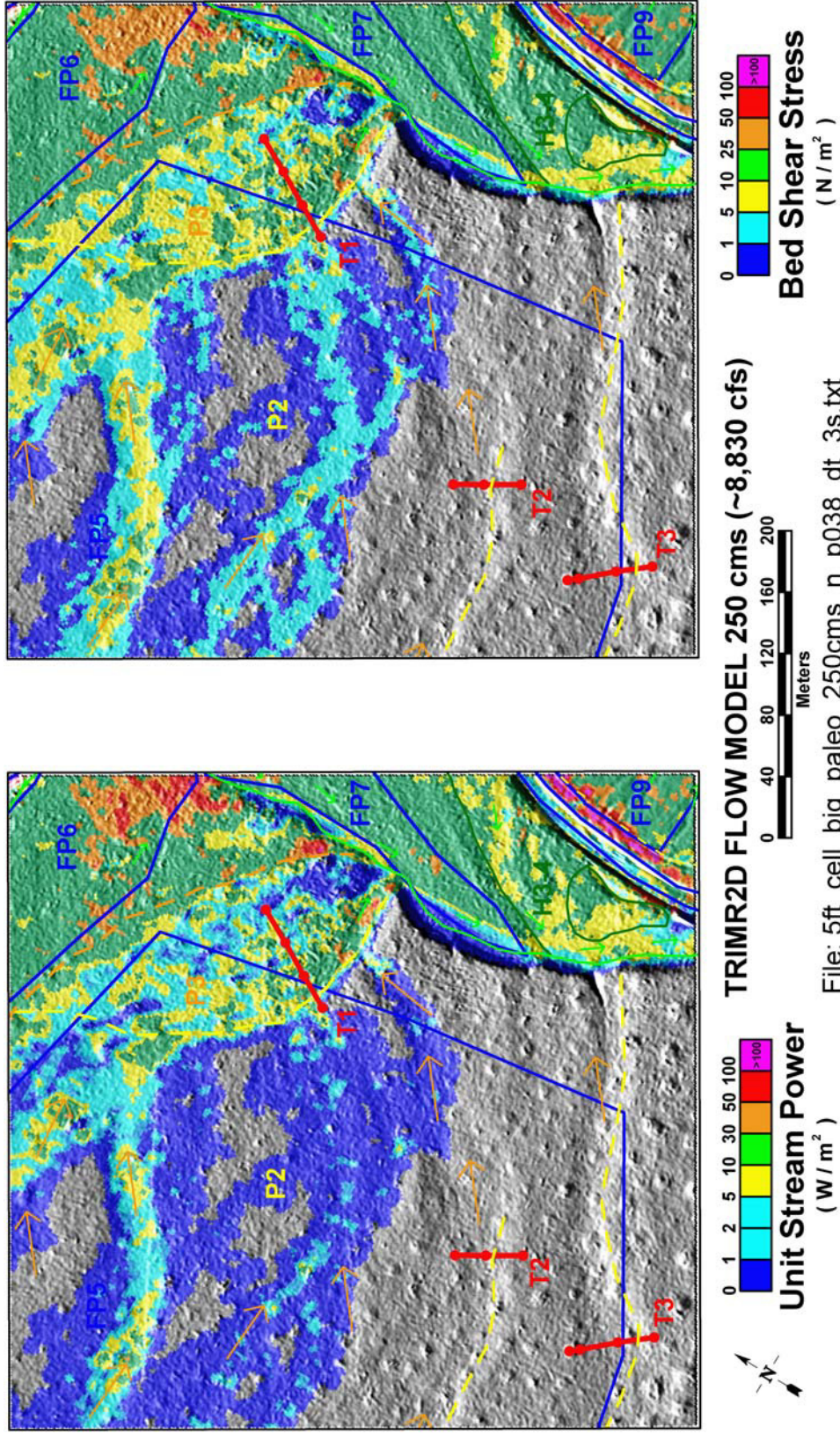


Figure 2-19 5-ft flow model results for $250\text{ m}^3/\text{s}$ in the Big Loop study area. Base map symbology is from Figure 2-3 and Plate 2.

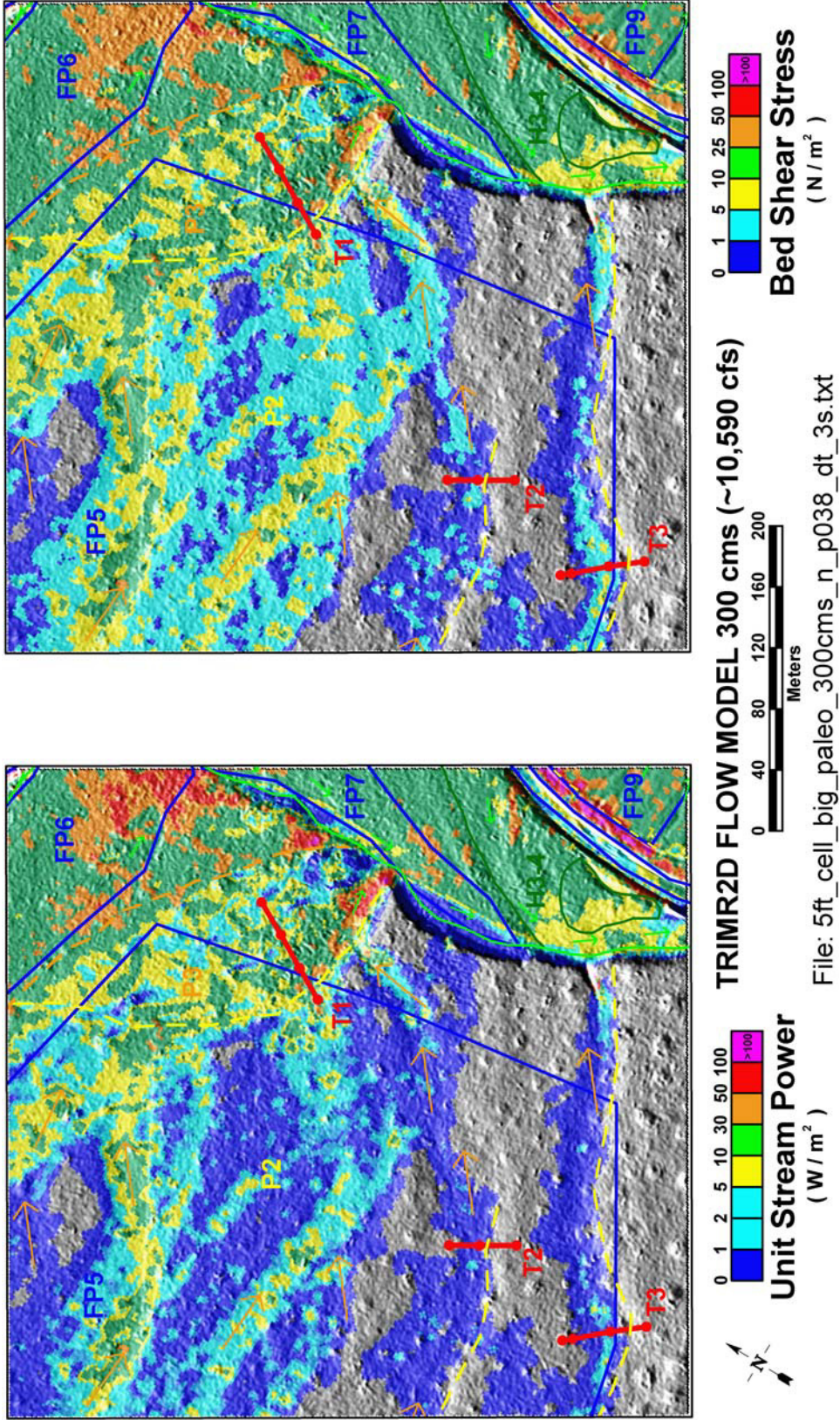


Figure 2-20 5-ft flow model results for 300 m³/s in the Big Loop study area. Base map symbology is from Figure 2-3 and Plate 2.

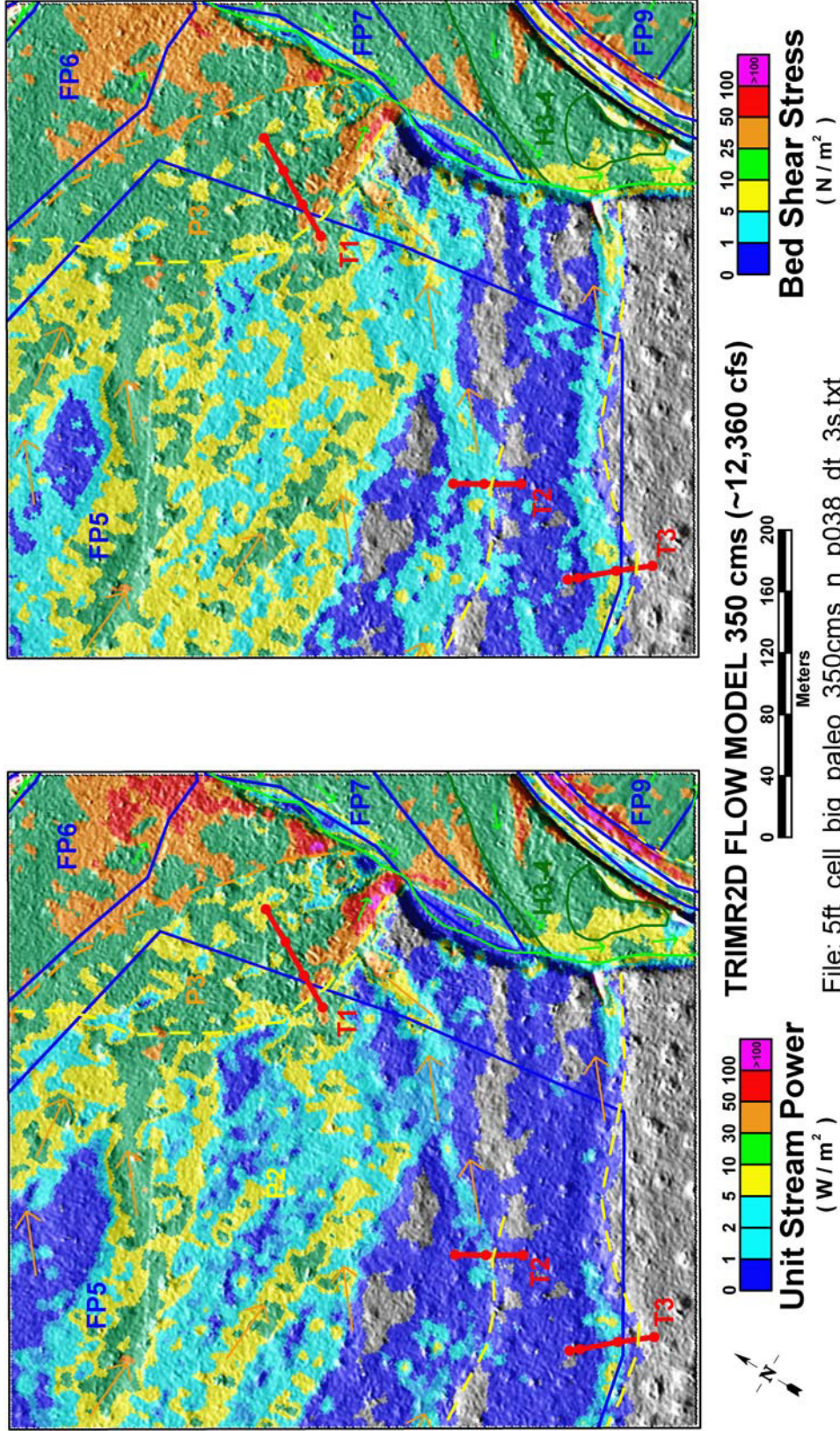


Figure 2-21 5-ft flow model results for 350 m³/s in the Big Loop study area. Base map symbology is from Figure 2-3 and Plate 2.

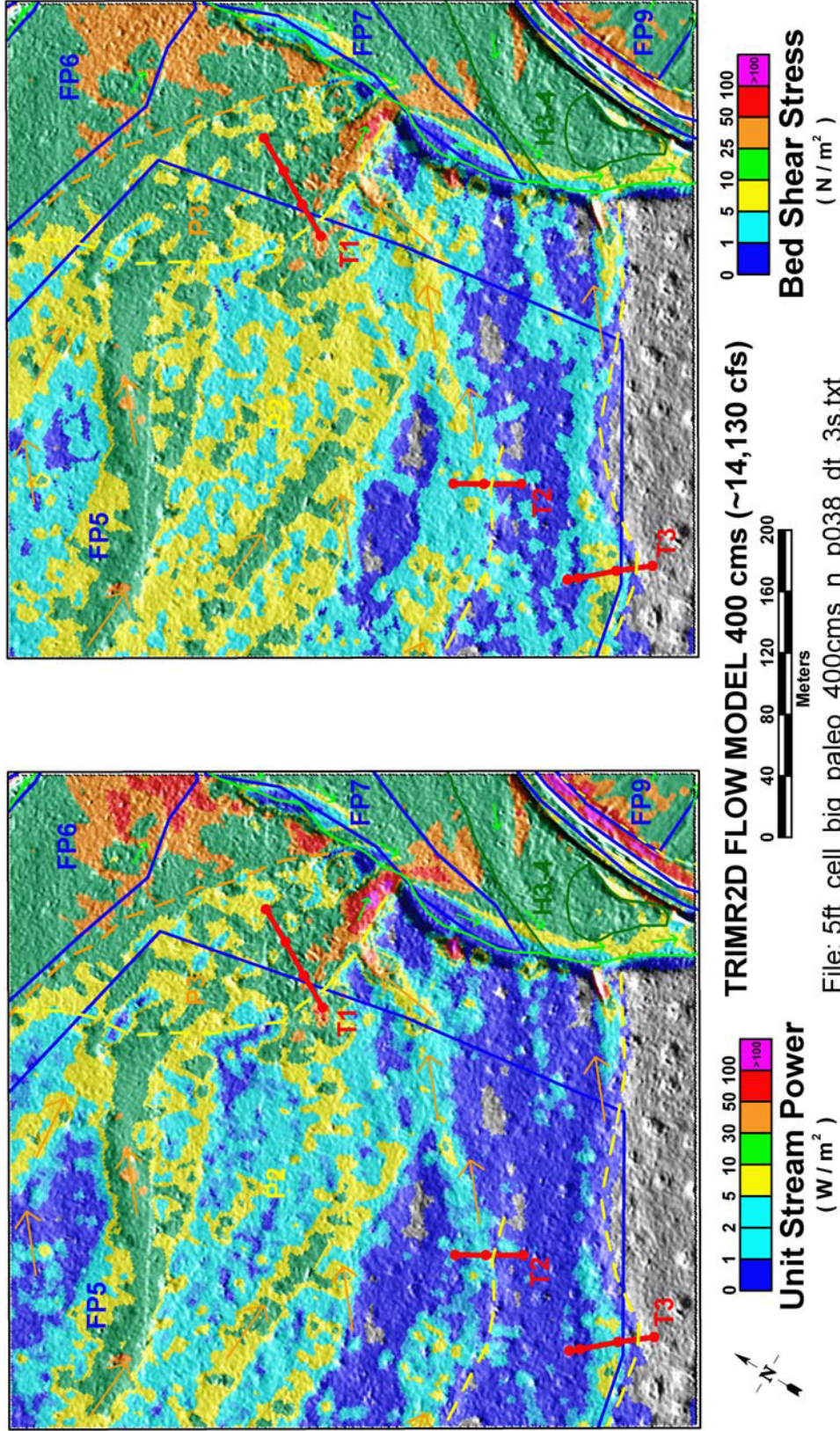


Figure 2-22 5-ft flow model results for 400 m³/s in the Big Loop study area. Base map symbology is from Figure 2-3 and Plate 2.

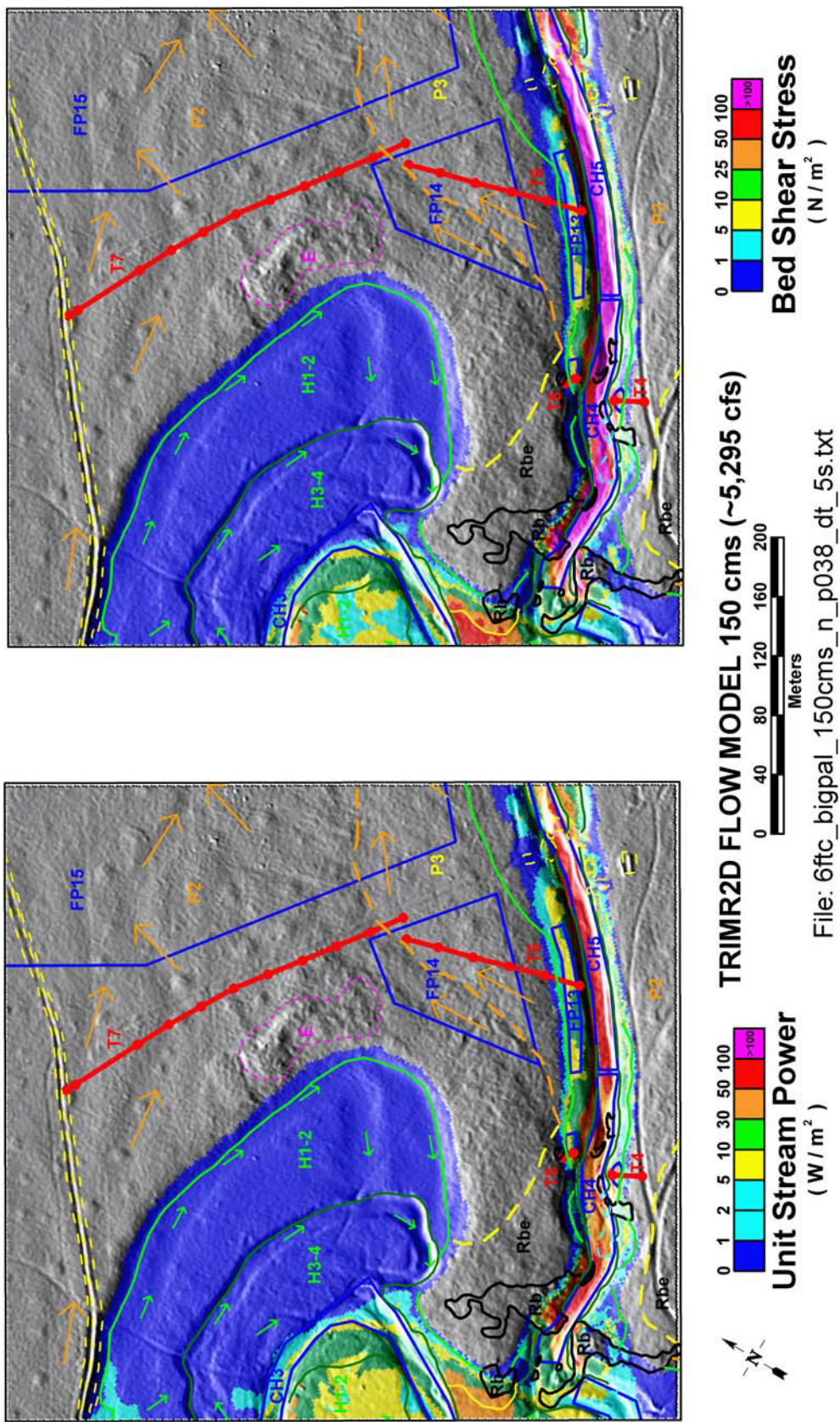


Figure 2-23 6-ft flow model results for 150 m³/s in the Saddle constriction study area. Base map symbology is from Figure 2-3 and Plate 2.

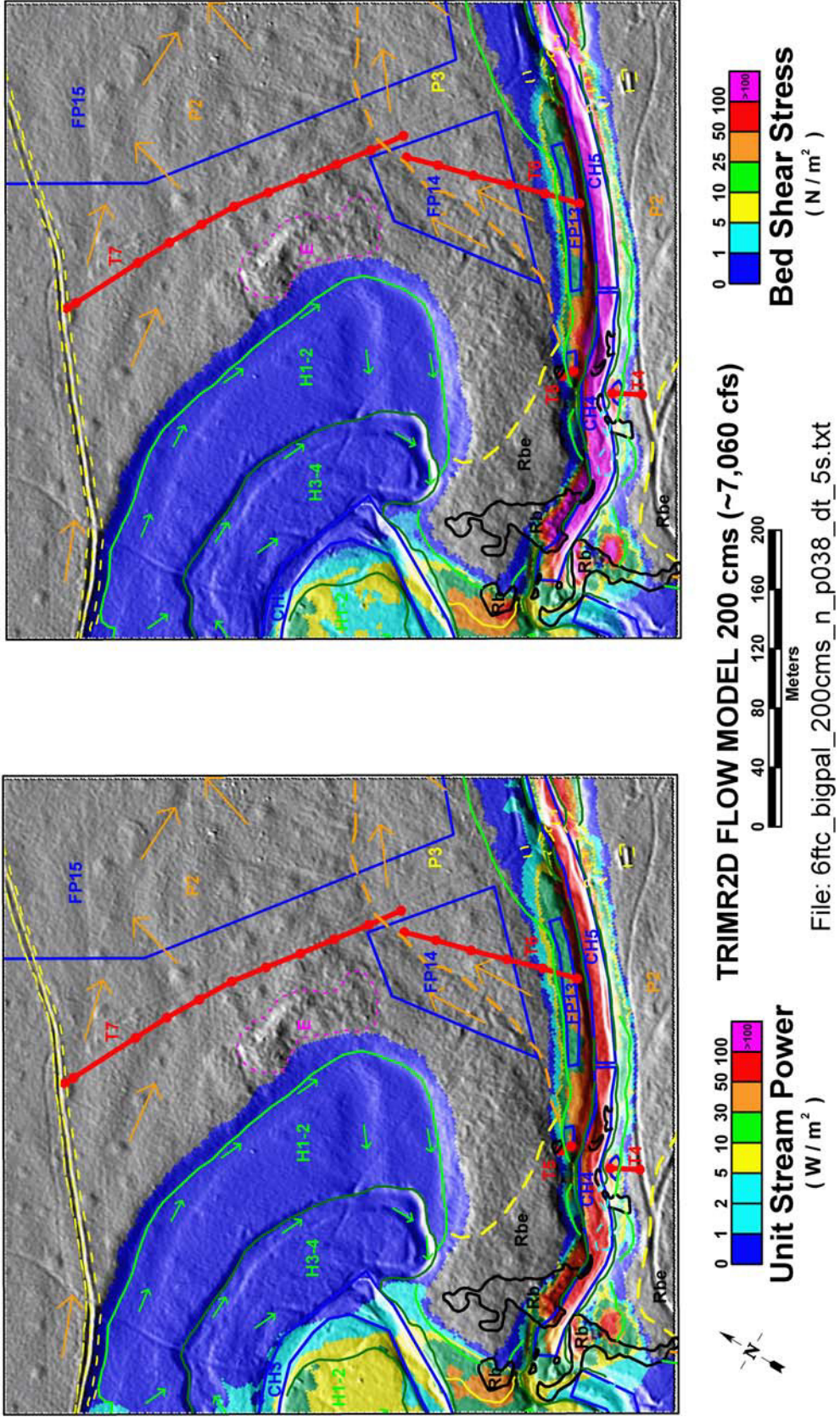


Figure 2-24 6-ft flow model results for 200 m³/s in the Saddle constriction study area. Base map symbology is from Figure 2-3 and Plate 2.

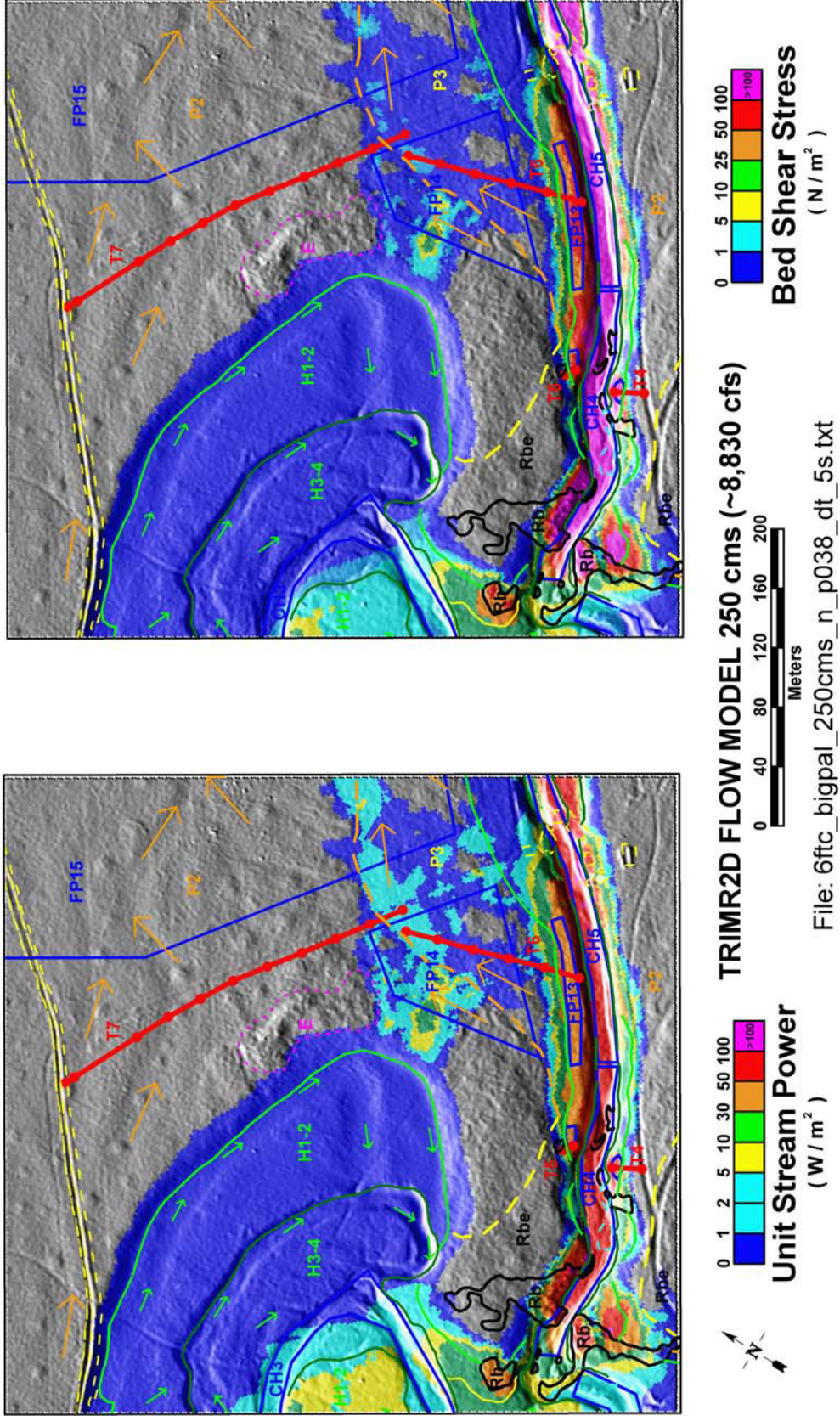


Figure 2-25 6-ft flow model results for 250 m³/s in the Saddle constriction study area. Base map symbology is from Figure 2-3 and Plate 2.

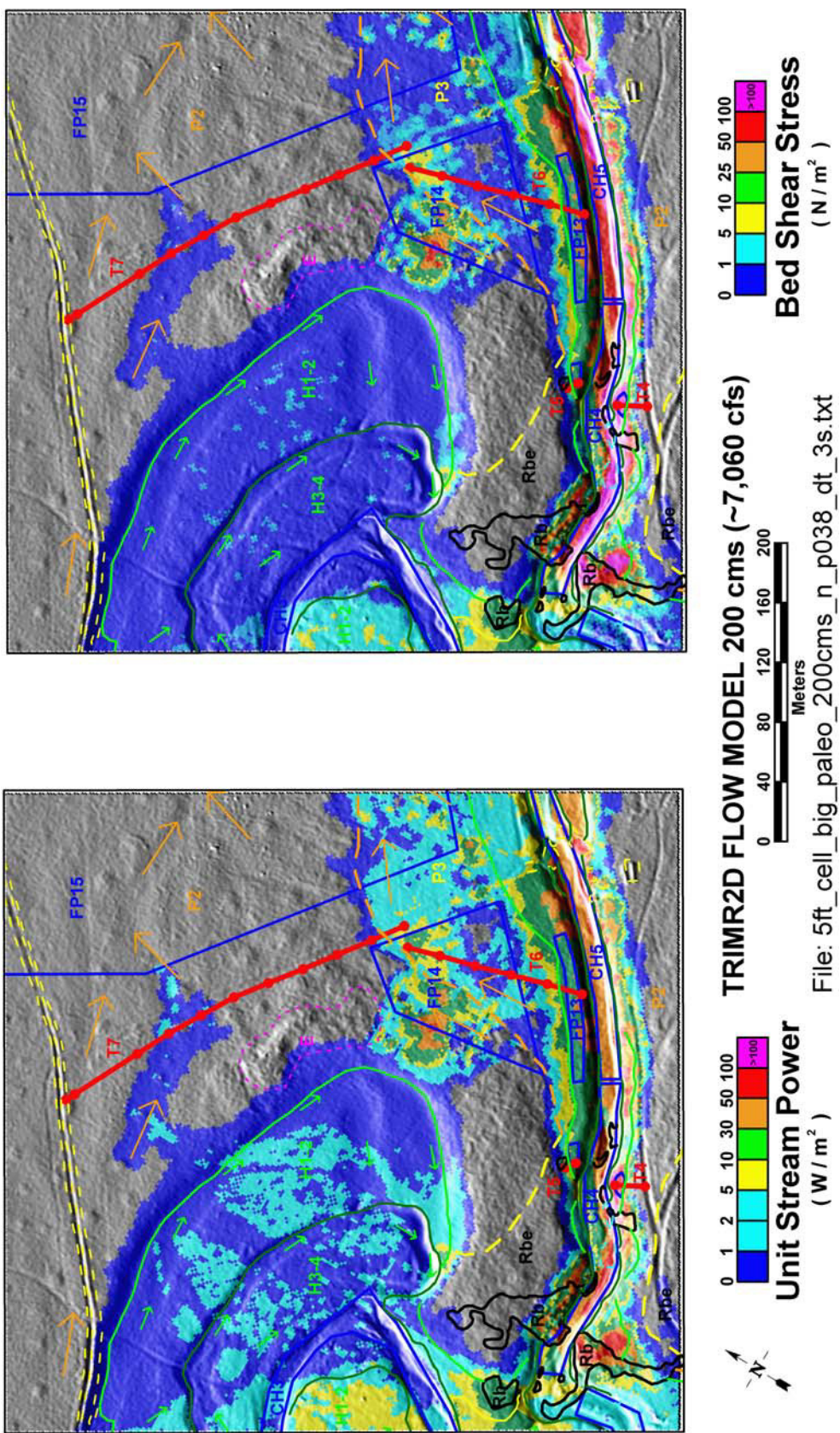


Figure 2-26 5-ft flow model results for 200 m³/s in the Saddle constriction study area. Base map symbology is from Figure 2-3 and Plate 2.

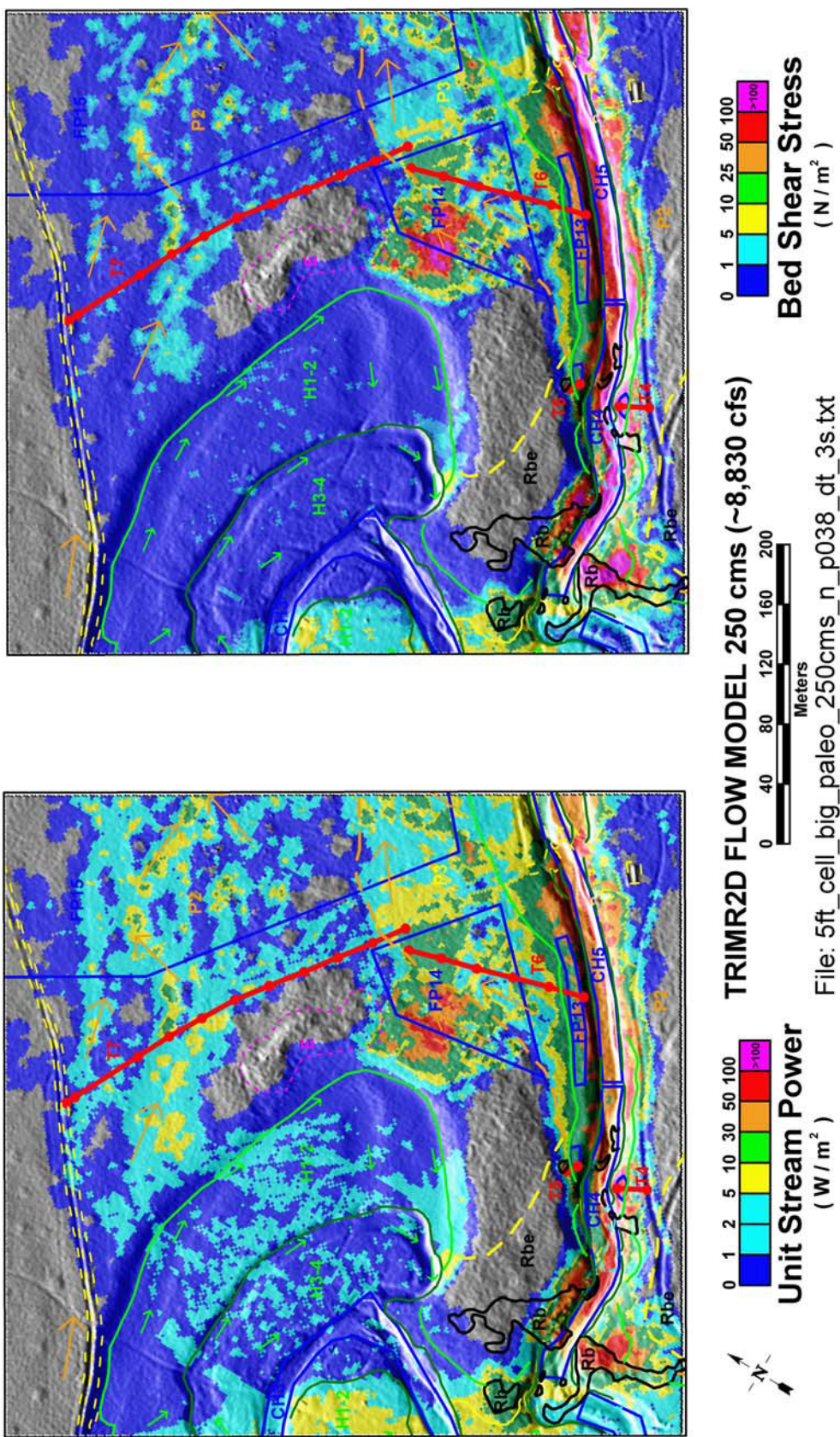


Figure 2-27 5-ft flow model results for 250 m³/s in the Saddle constriction study area. Base map symbology is from Figure 2-3 and Plate 2.

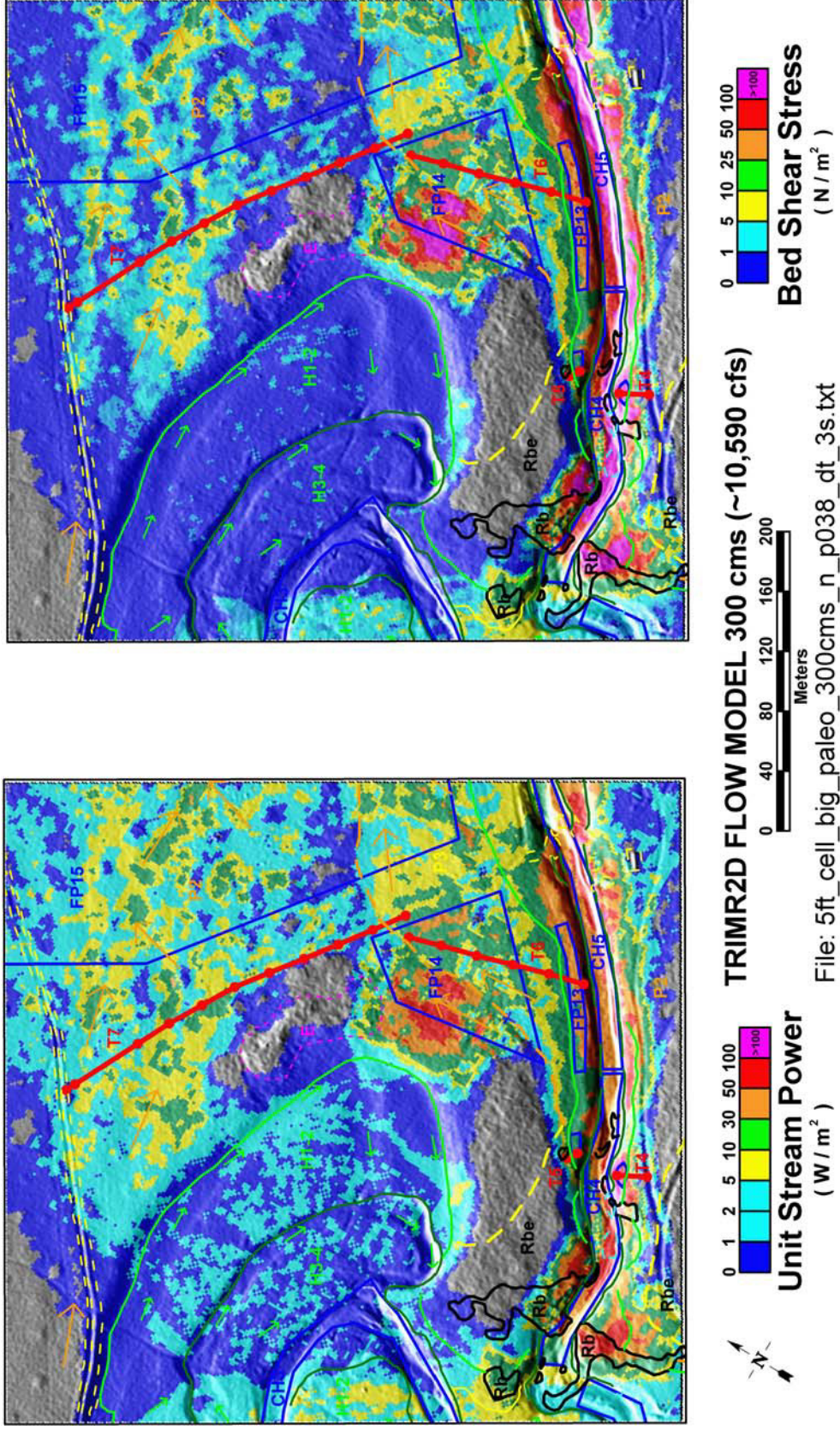


Figure 2-28 5-ft flow model results for 300 m³/s in the Saddle constriction study area. Base map symbology is from Figure 2-3 and Plate 2.

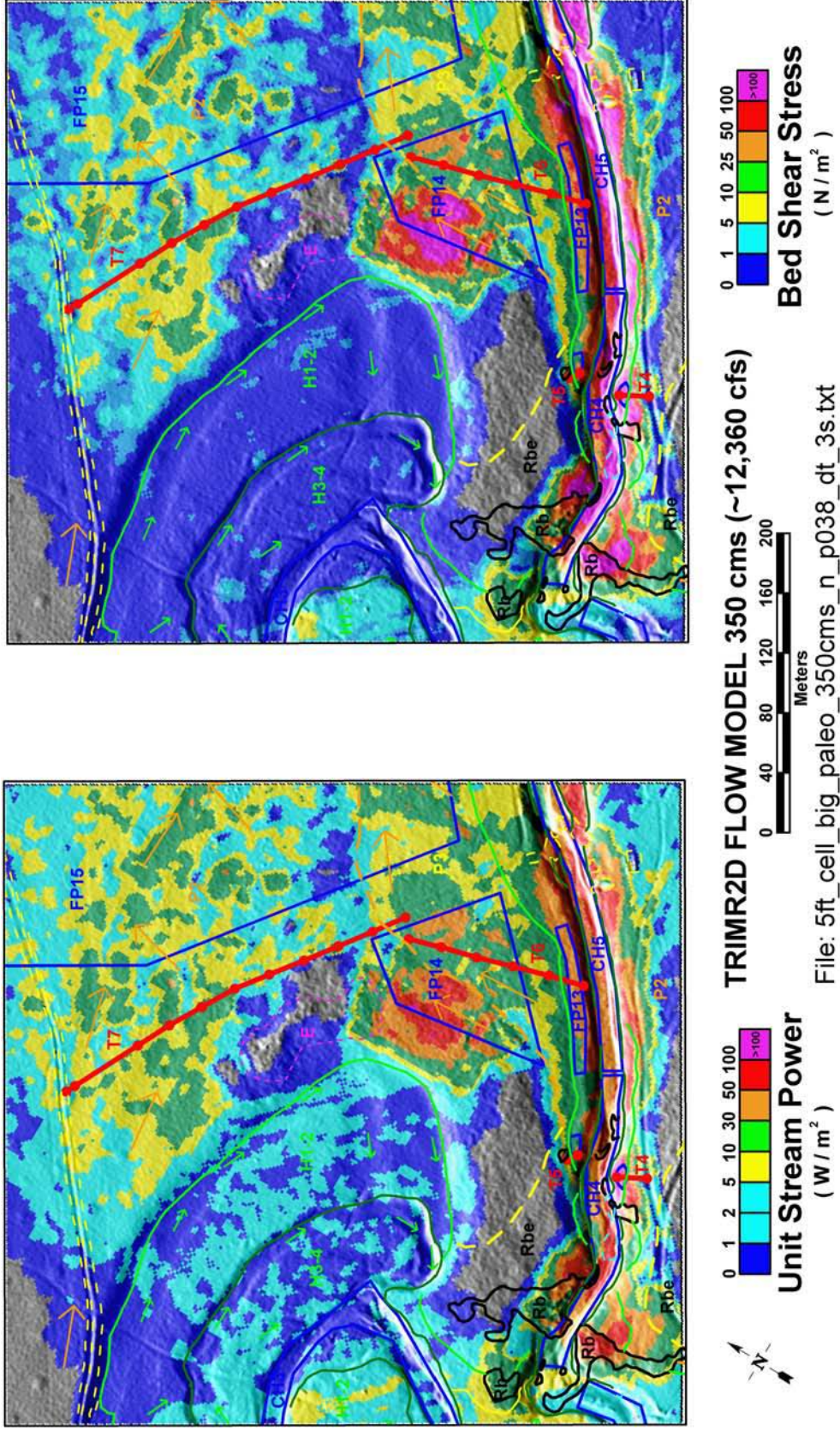


Figure 2-29 5-ft flow model results for $350\text{ m}^3/\text{s}$ in the Saddle constriction study area. Base map symbology is from Figure 2-3 and Plate 2.

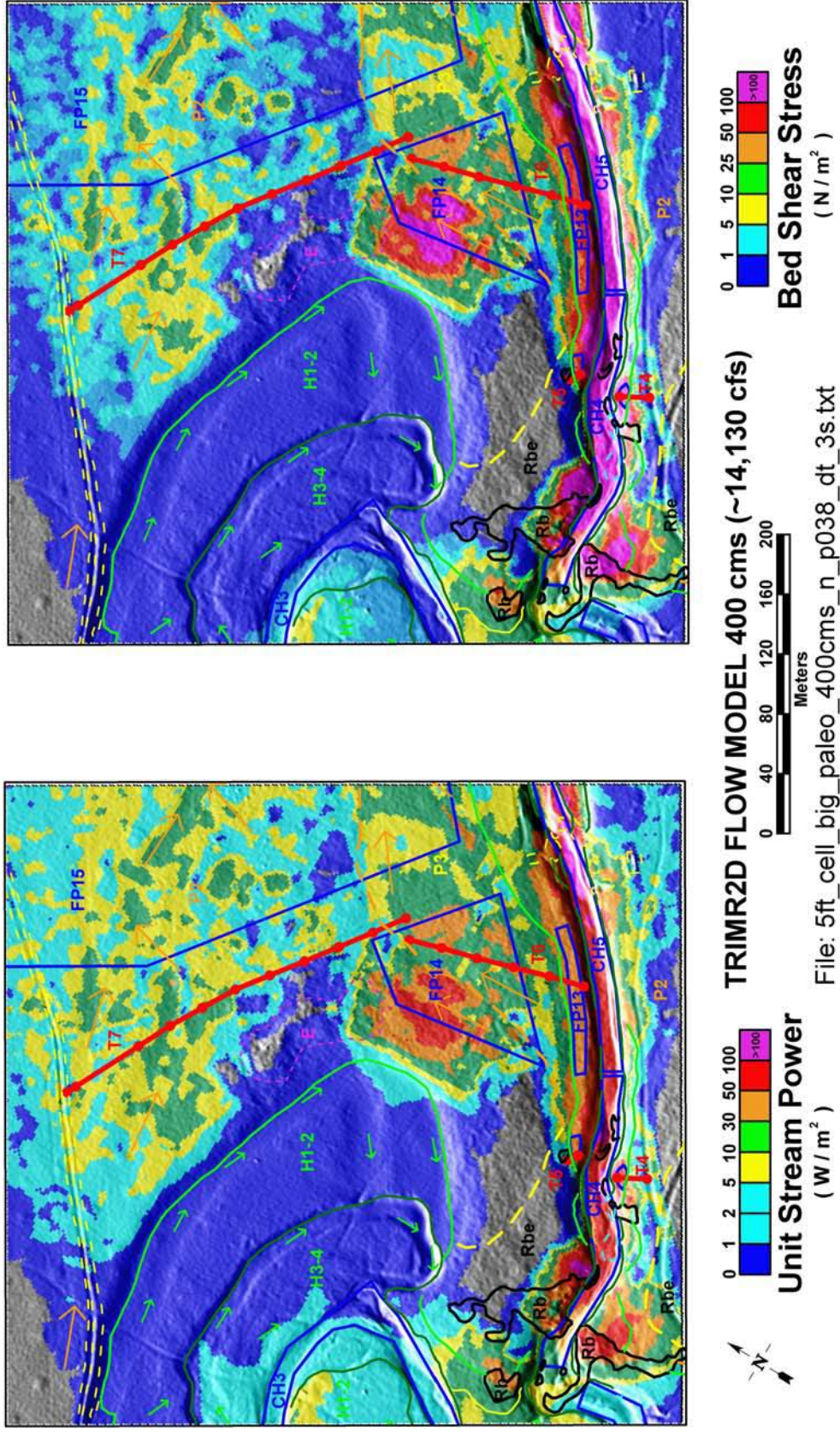


Figure 2-30 5-ft flow model results for 400 m³/s in the Saddle constriction study area. Base map symbology is from Figure 2-3 and Plate 2.

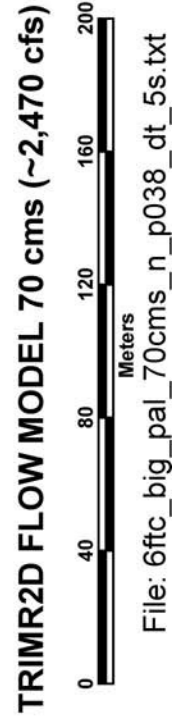
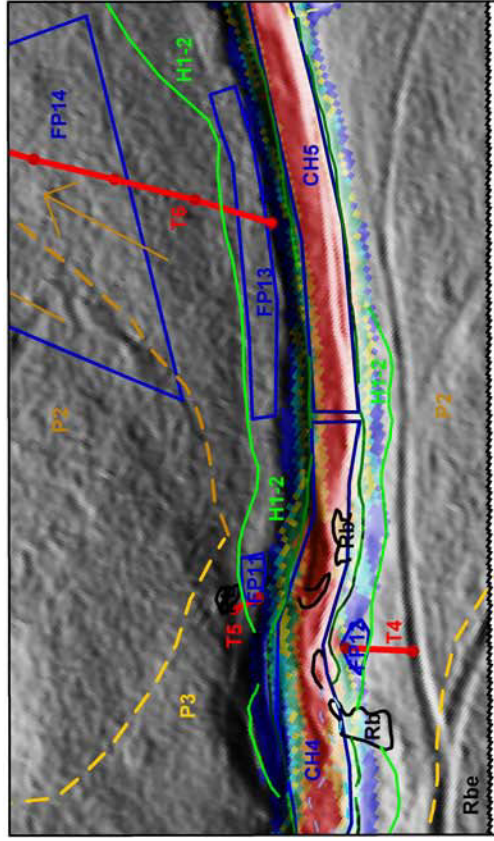
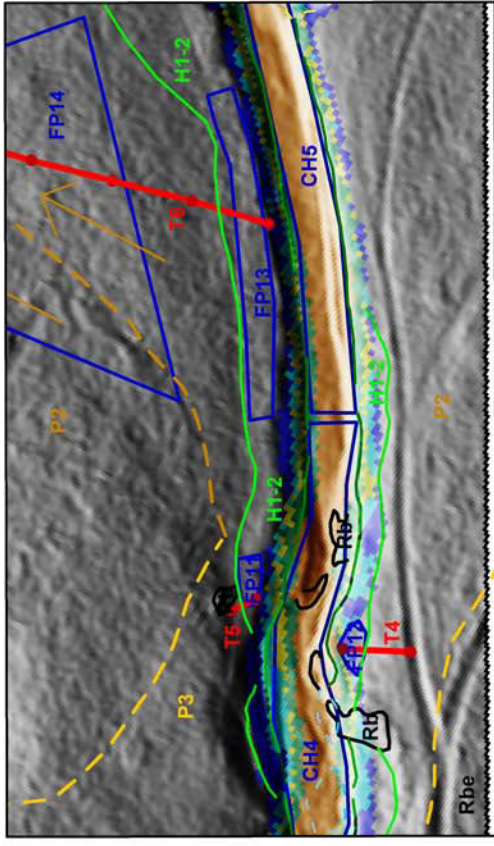


Figure 2-31 6-ft flow model results for $70 \text{ m}^3/\text{s}$ in the T4/T5/T6 study area. Base map symbology is from Figure 2-3 and Plate 2.

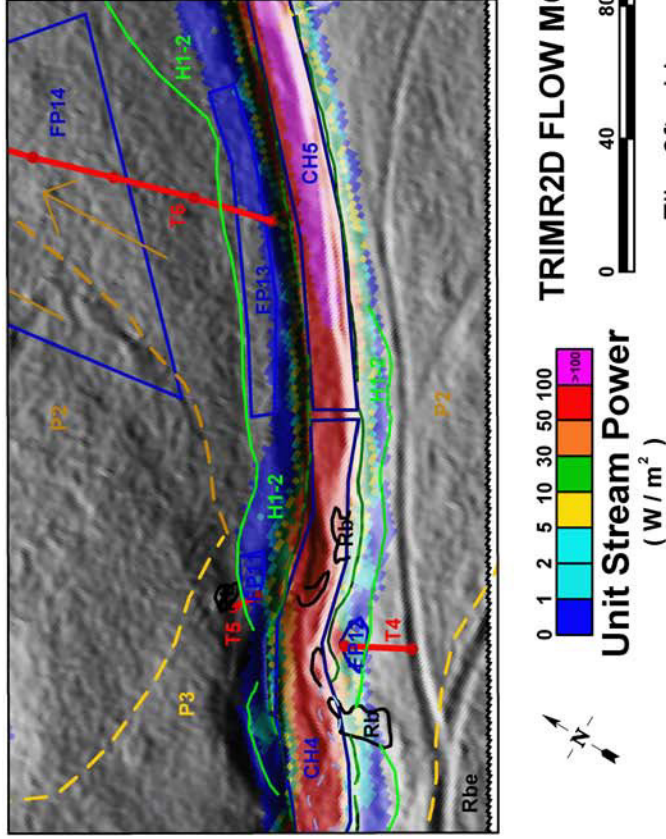
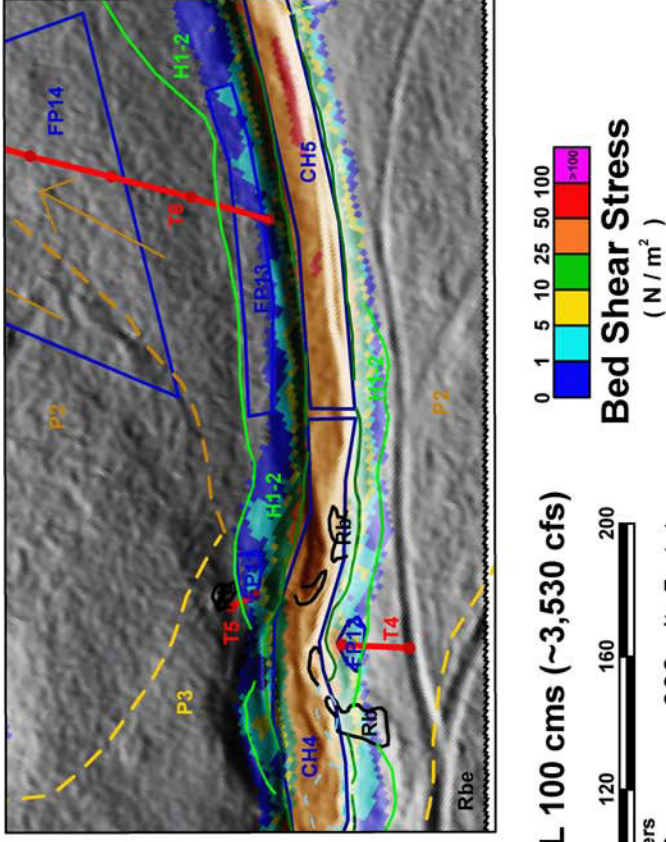


Figure 2-32 6-ft flow model results for 100 m³/s in the T4/T5/T6 study area. Base map symbology is from Figure 2-3 and Plate 2.

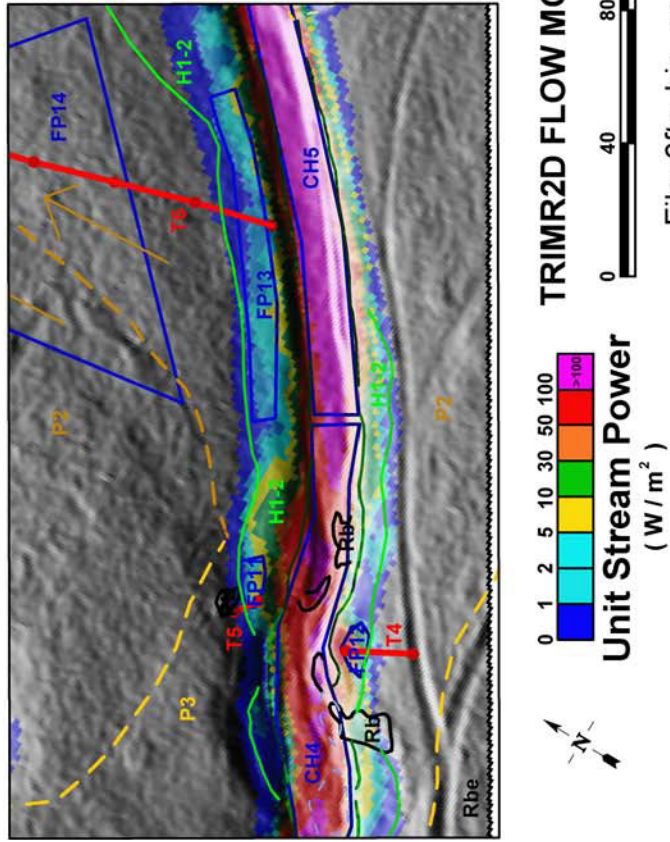
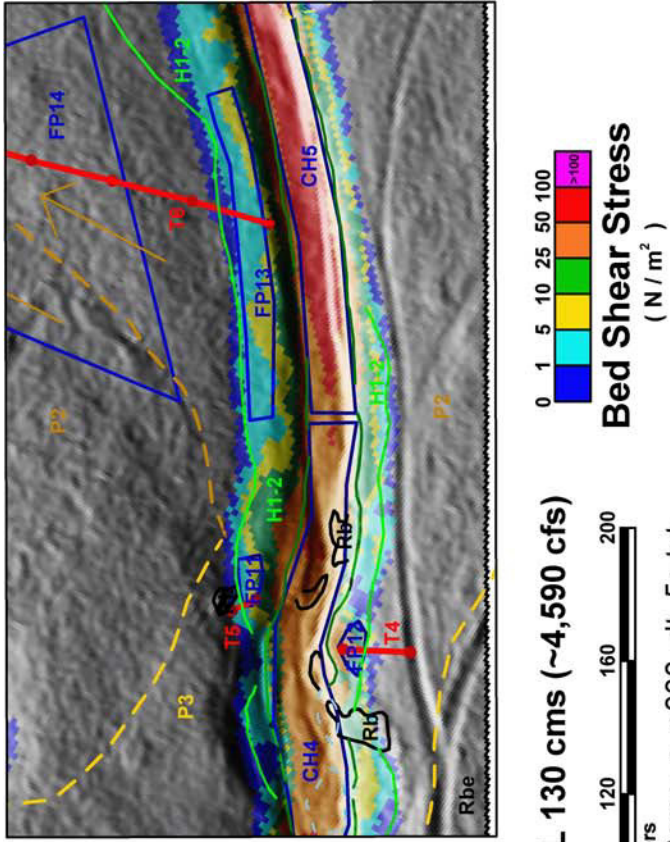
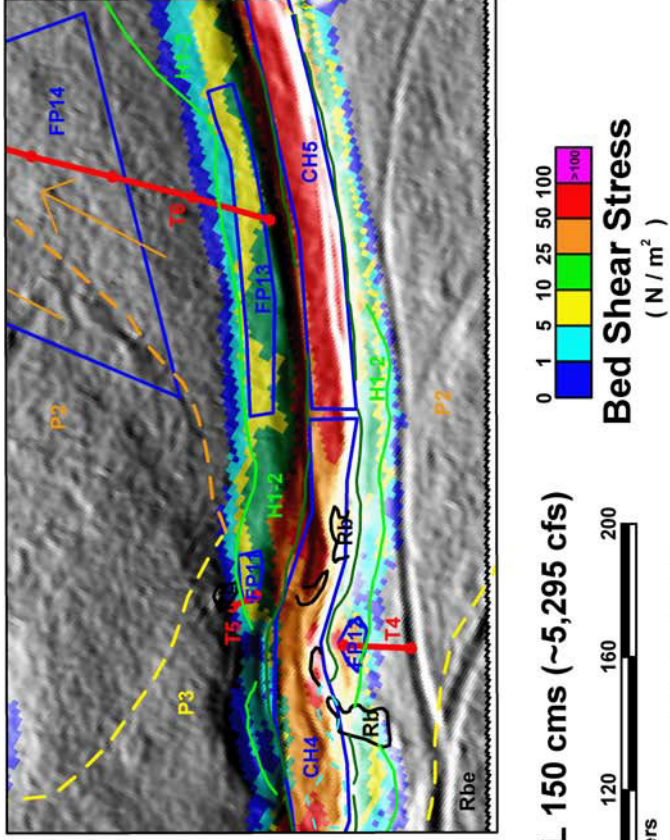


Figure 2-33 6-ft flow model results for $130 \text{ m}^3/\text{s}$ in the T4/T5/T6 study area. Base map symbology is from Figure 2-3 and Plate 2.



TRIMR2D FLOW MODEL 150 cms (~5,295 cfs)

Figure 2-34 6-ft flow model results for $150 \text{ m}^3/\text{s}$ in the T4/T5/T6 study area. Base map symbology is from Figure 2-3 and Plate 2.

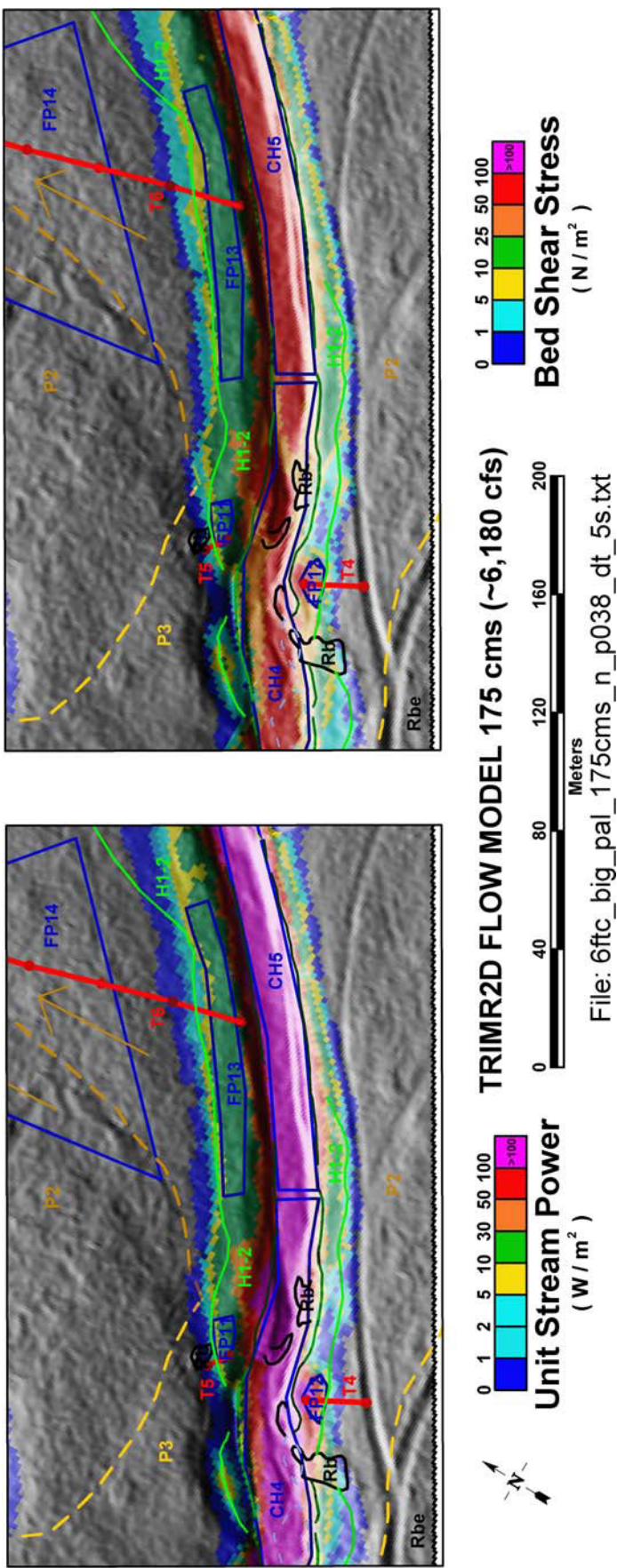
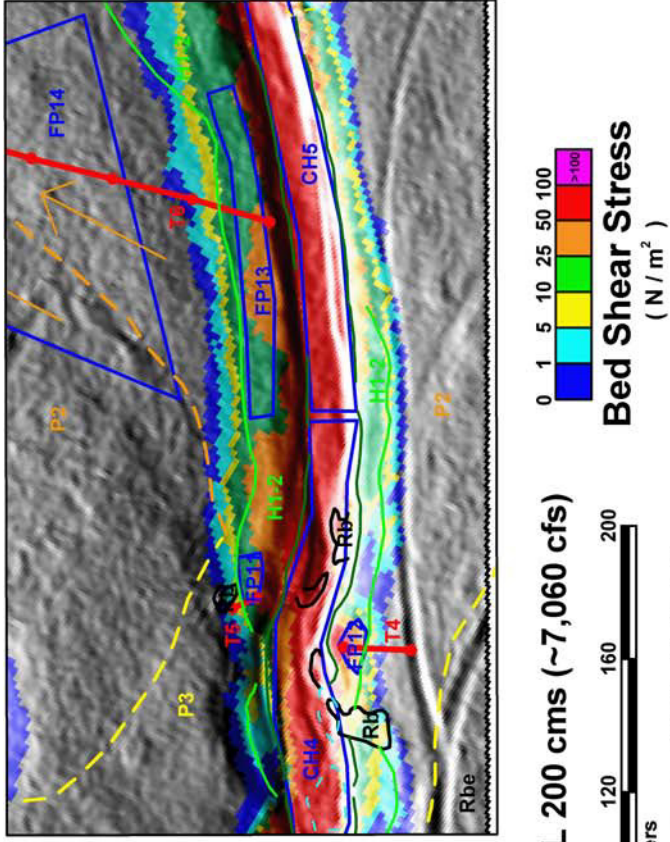
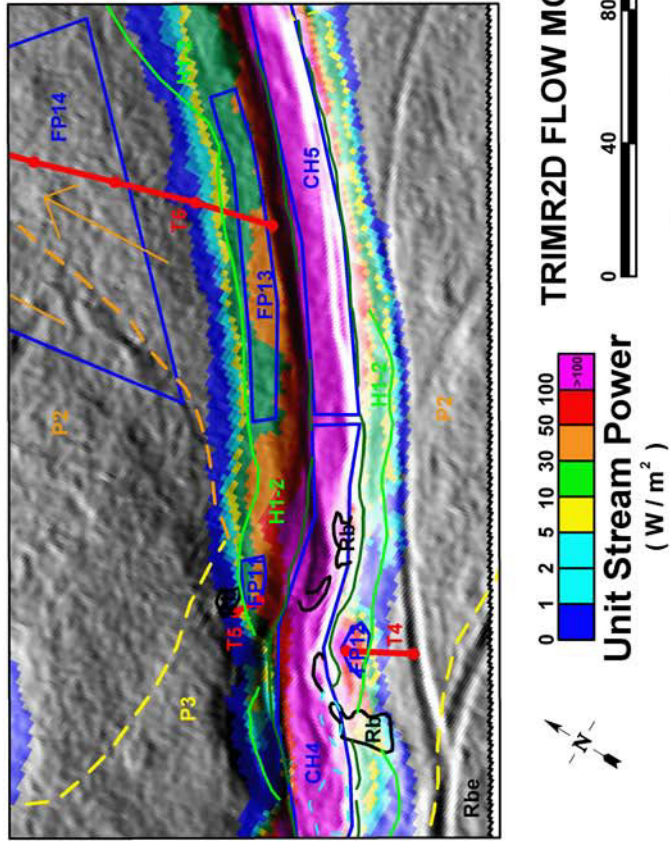


Figure 2-35 6-ft flow model results for $175 \text{ m}^3/\text{s}$ in the T4/T5/T6 study area. Base map symbology is from Figure 2-3 and Plate 2.



Unit Stream Power
(W / m^2)



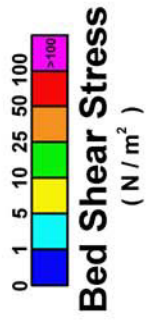
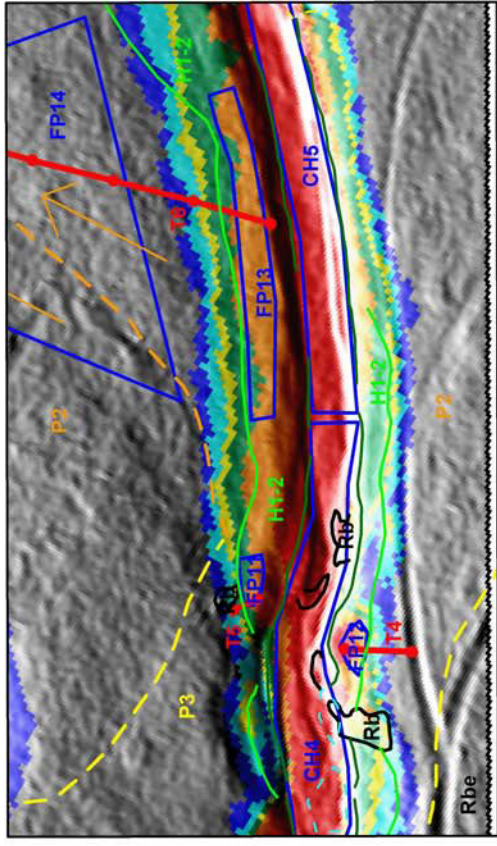
Bed Shear Stress
(N / m^2)

TRIMR2D FLOW MODEL 200 cms (~7,060 cfs)



File: 6ftc_bigpal_200cms_n_p038_dt_5s.txt

Figure 2-36 6-ft flow model results for $200 \text{ m}^3/\text{s}$ in the T4/T5/T6 study area. Base map symbology is from Figure 2-3 and Plate 2.



TRIMR2D FLOW MODEL 225 cms (~7,945 cfs)



File: 6ftc_bigpal_225cms_n_p038_dt_5s.txt

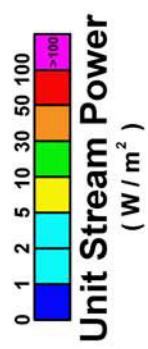
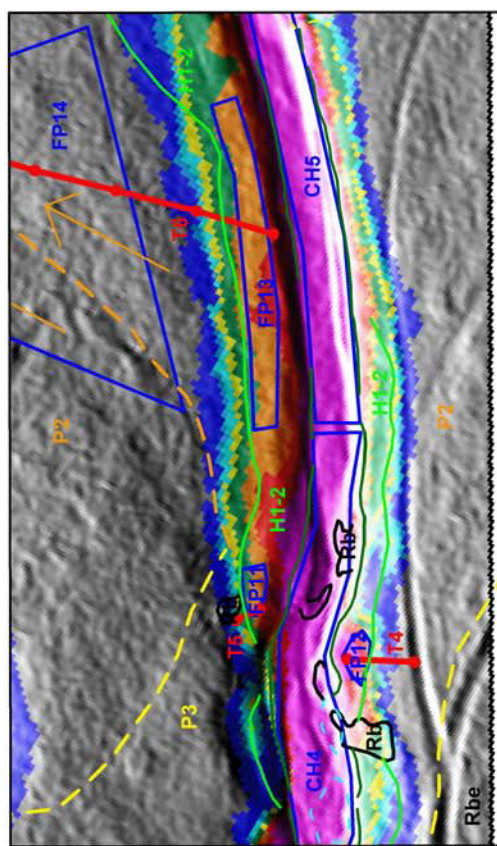
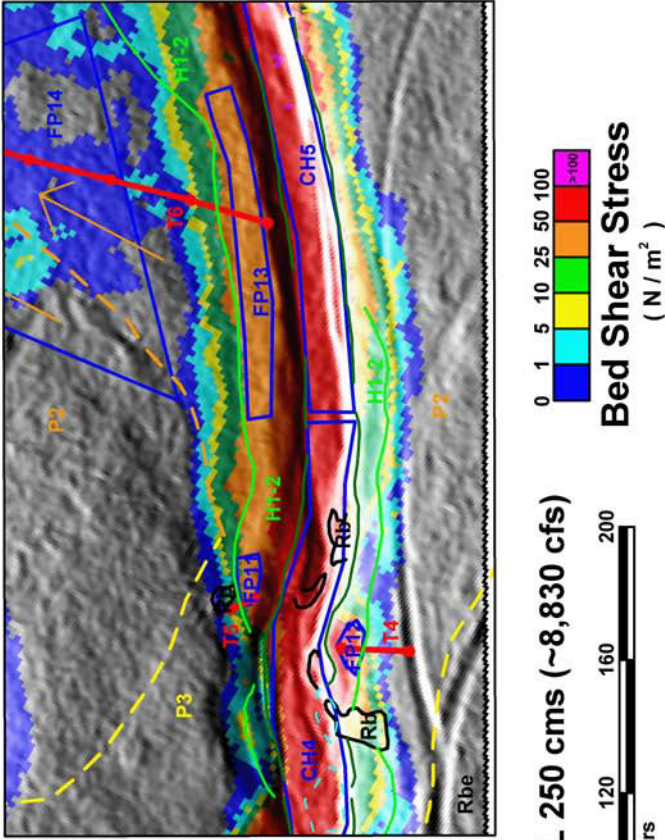


Figure 2-37 6-ft flow model results for 225 m³/s in the T4/T5/T6 study area. Base map symbology is from Figure 2-3 and Plate 2.



TRIMR2D FLOW MODEL 250 cms (~8,830 cfs)

Figure 2-38 6-ft flow model results for $250 \text{ m}^3/\text{s}$ in the T4/T5/T6 study area. Base map symbology is from Figure 2-3 and Plate 2.

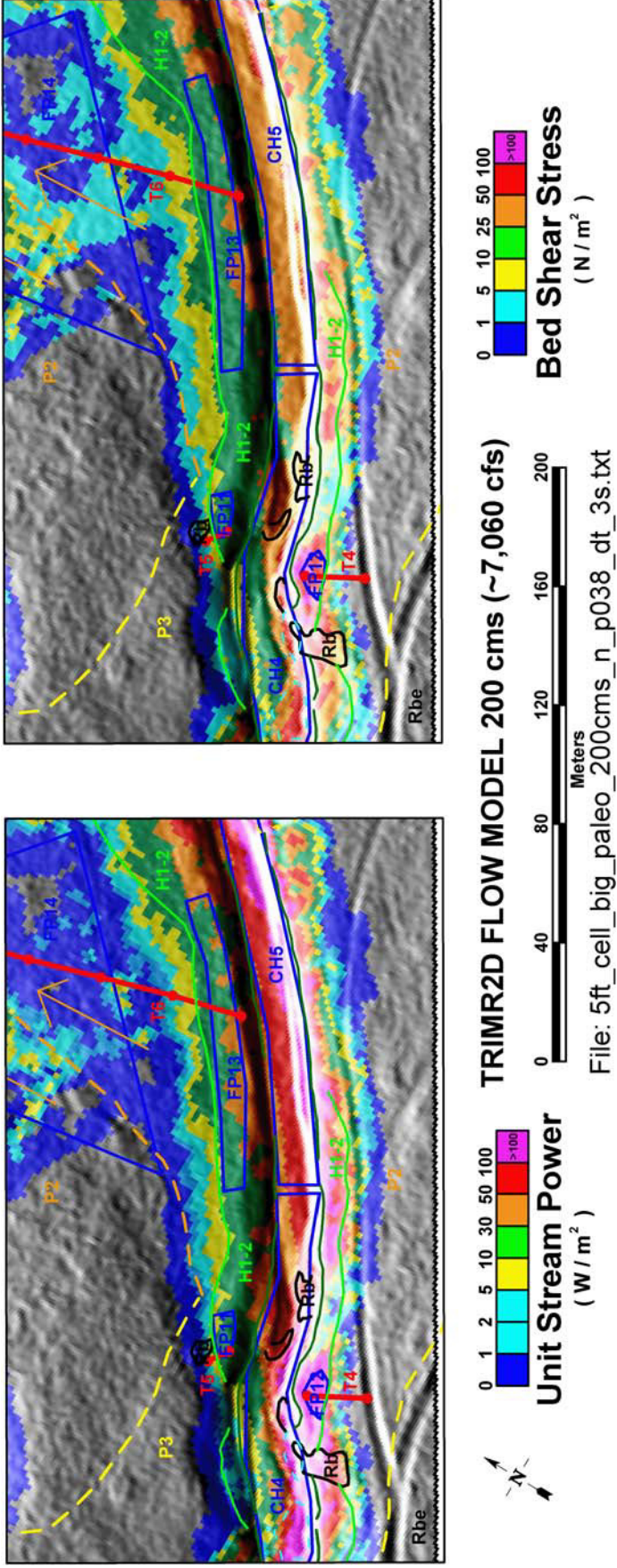


Figure 2-39 5-ft flow model results for $200 \text{ m}^3/\text{s}$ in the T4/T5/T6 constriction study area. Base map symbology is from Figure 2-3 and Plate 2.

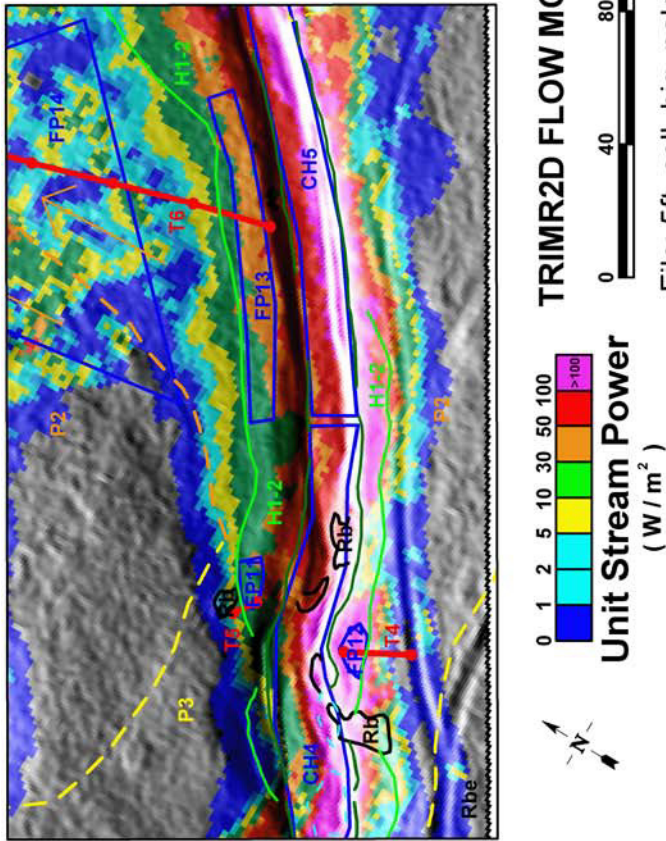
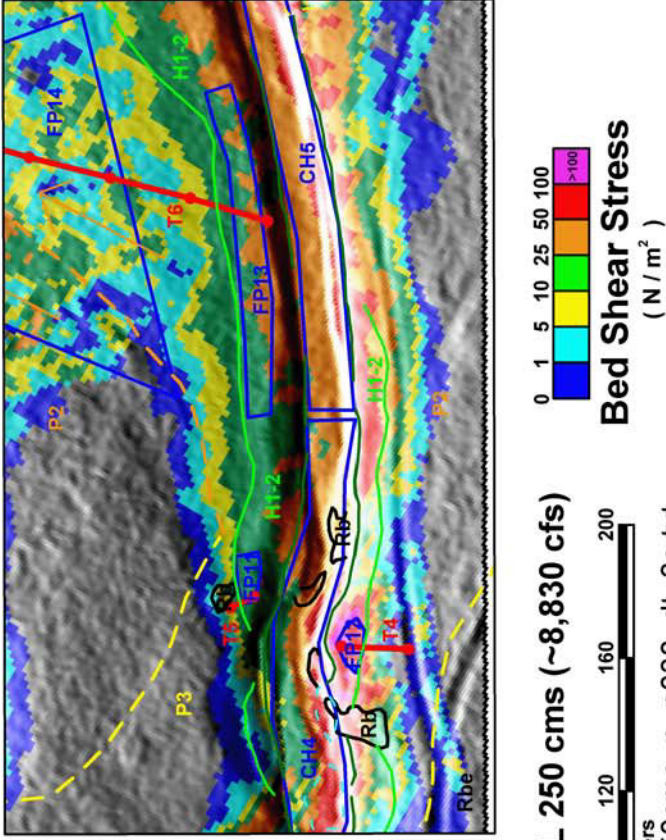


Figure 2-40 5-ft flow model results for $250 m^3/s$ in the T4/T5/T6 constriction study area. Base map symbology is from Figure 2-3 and Plate 2.

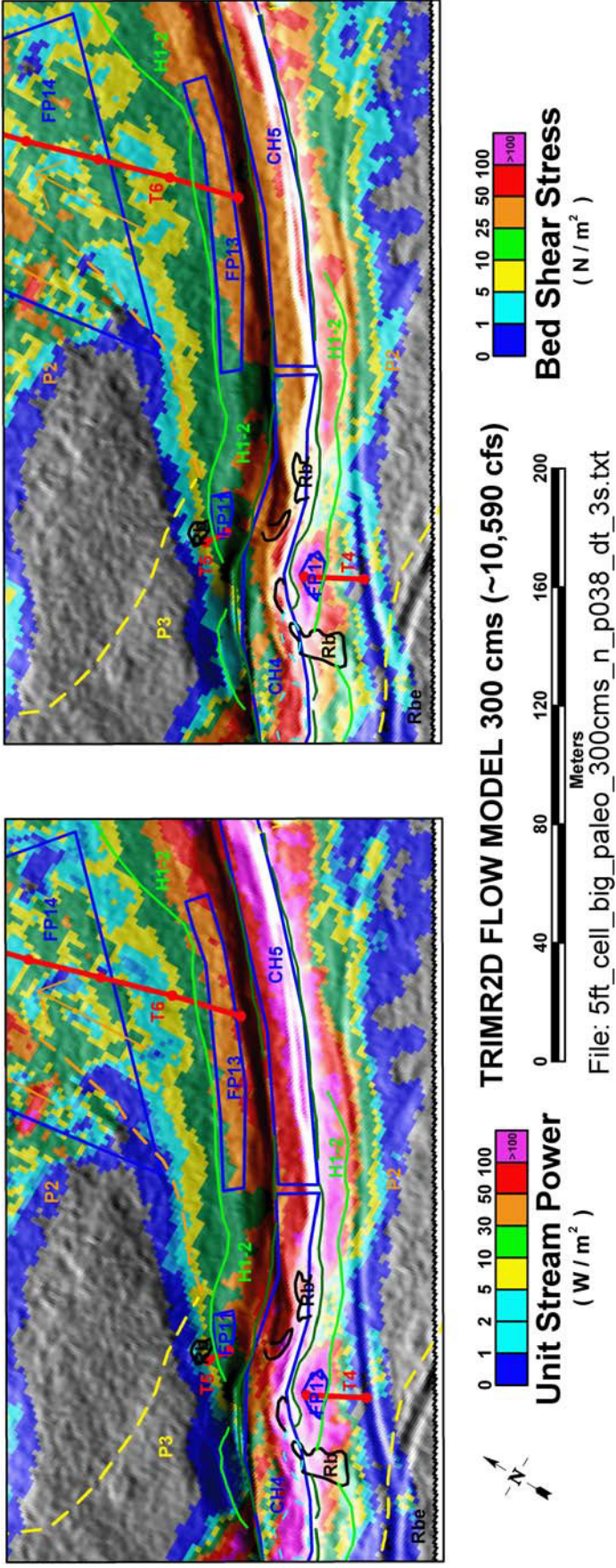


Figure 2-41 5-ft flow model results for $300\text{ m}^3/\text{s}$ in the T4/T5/T6 constriction study area. Base map symbology is from Figure 2-3 and Plate 2.

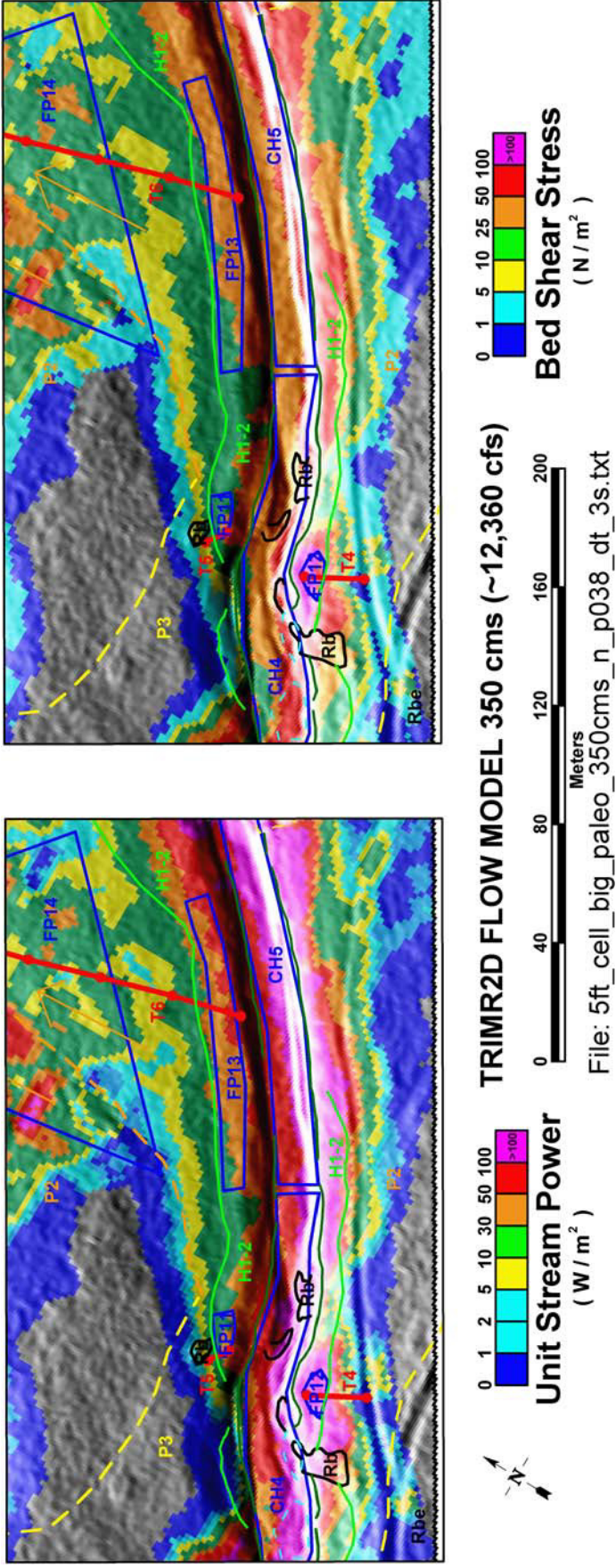


Figure 2-42 5-ft flow model results for $350\text{ m}^3/\text{s}$ in the T4/T5/T6 constriction study area. Base map symbology is from Figure 2-3 and Plate 2.

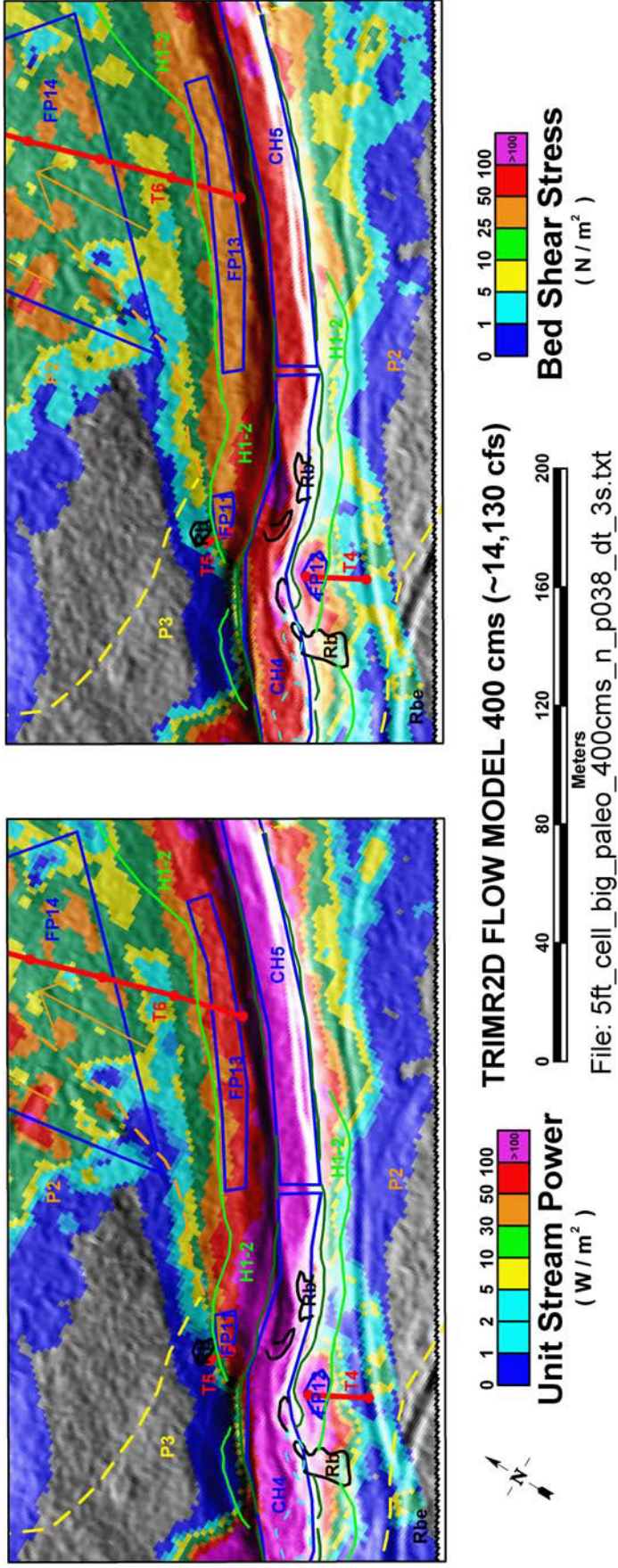


Figure 2-43 5-ft flow model results for $400\text{ m}^3/\text{s}$ in the T4/T5/T6 constriction study area. Base map symbology is from Figure 2-3 and Plate 2.

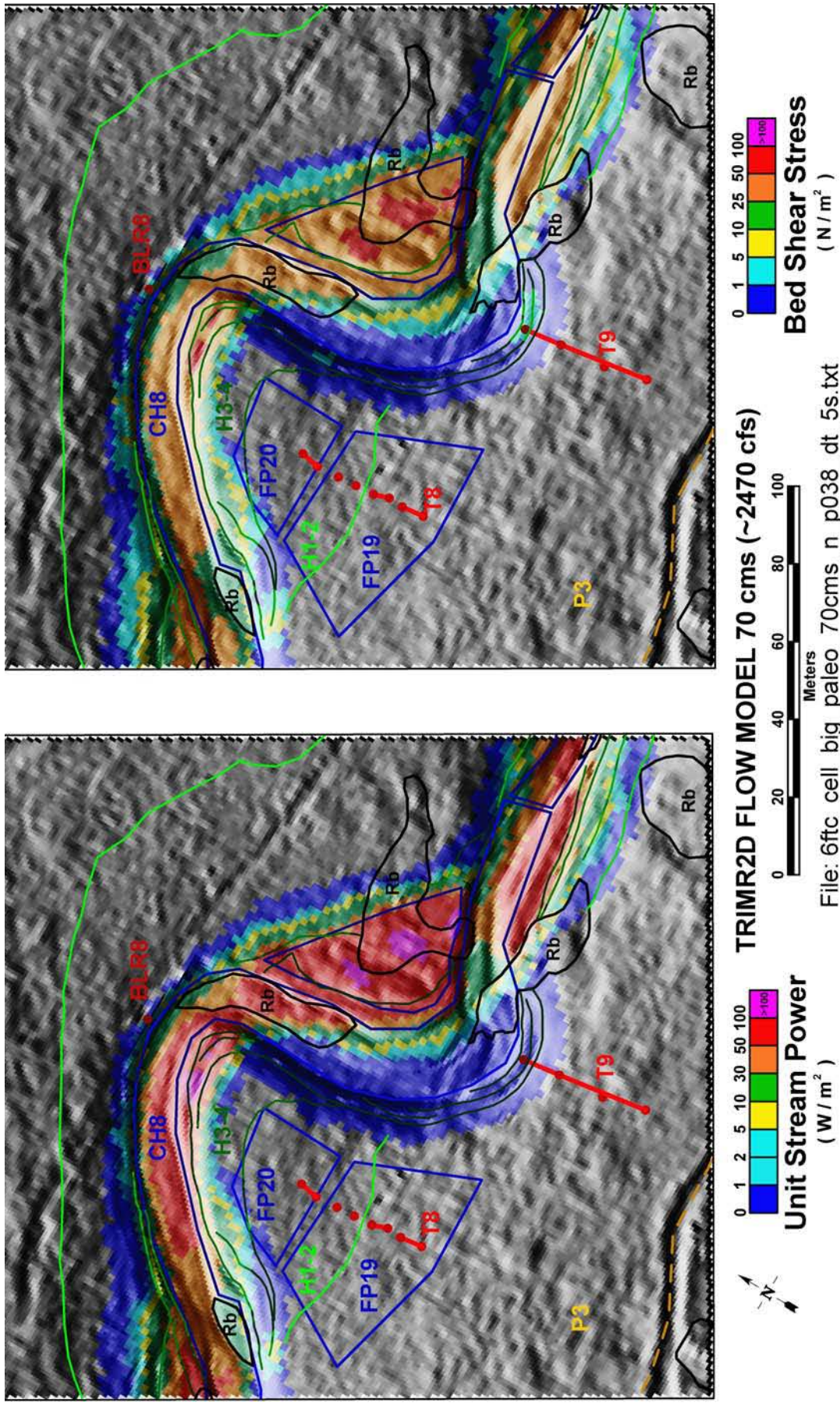


Figure 2-44 6-ft flow model results for 70 m³/s in the BLR8 study area. Base map symbology is from Figure 2-3 and Plate 2.

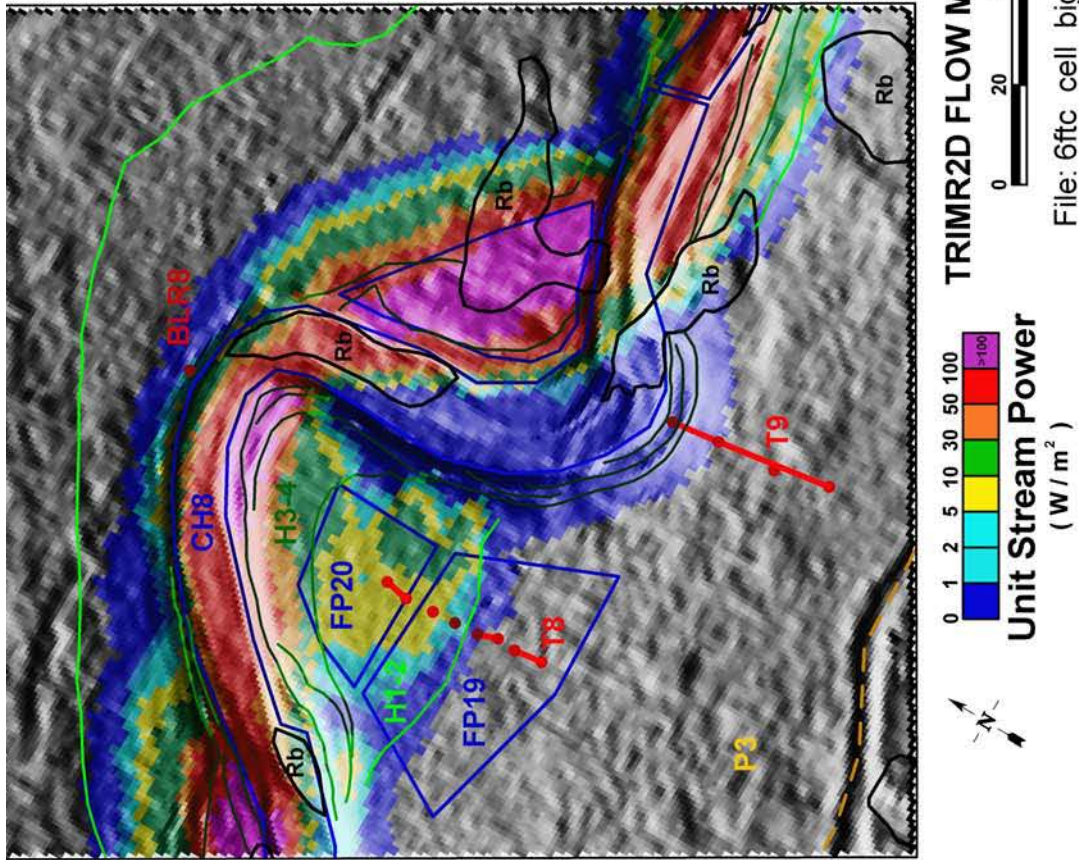
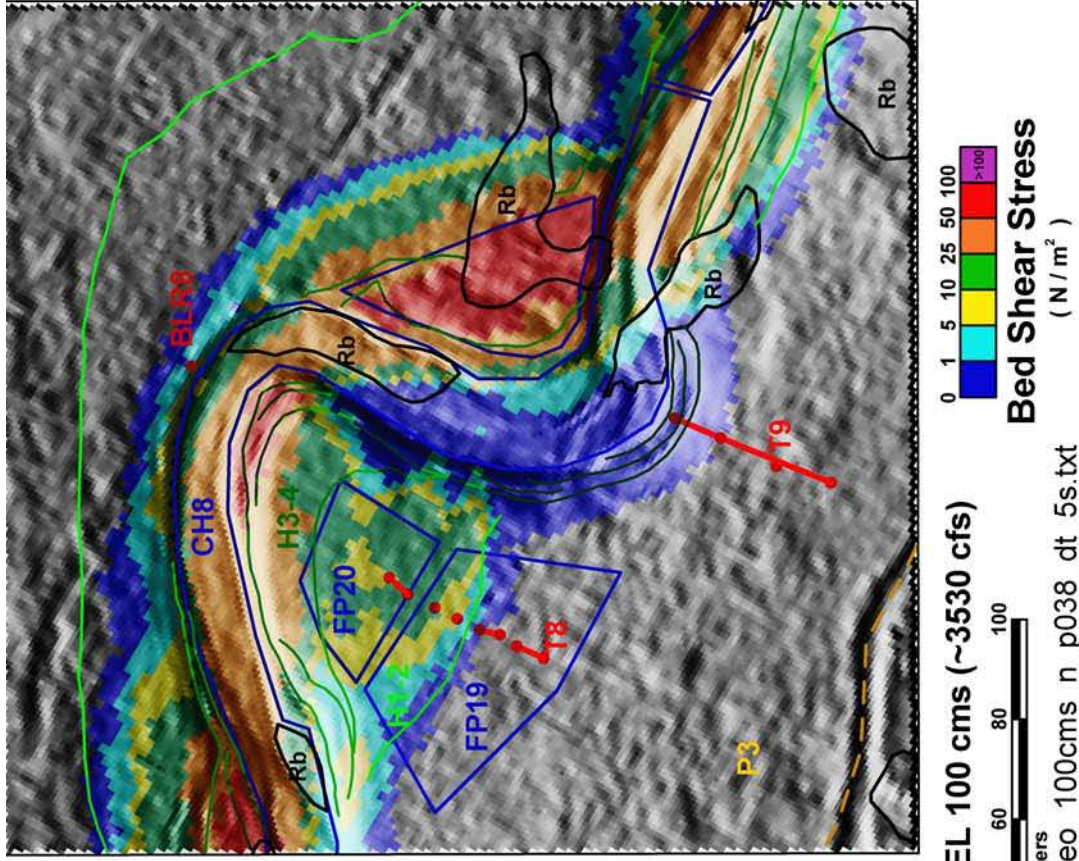


Figure 2-45 6-ft flow model results for $100\text{ m}^3/\text{s}$ in the BLR8 study area. Base map symbology is from Figure 2-3 and Plate 2.

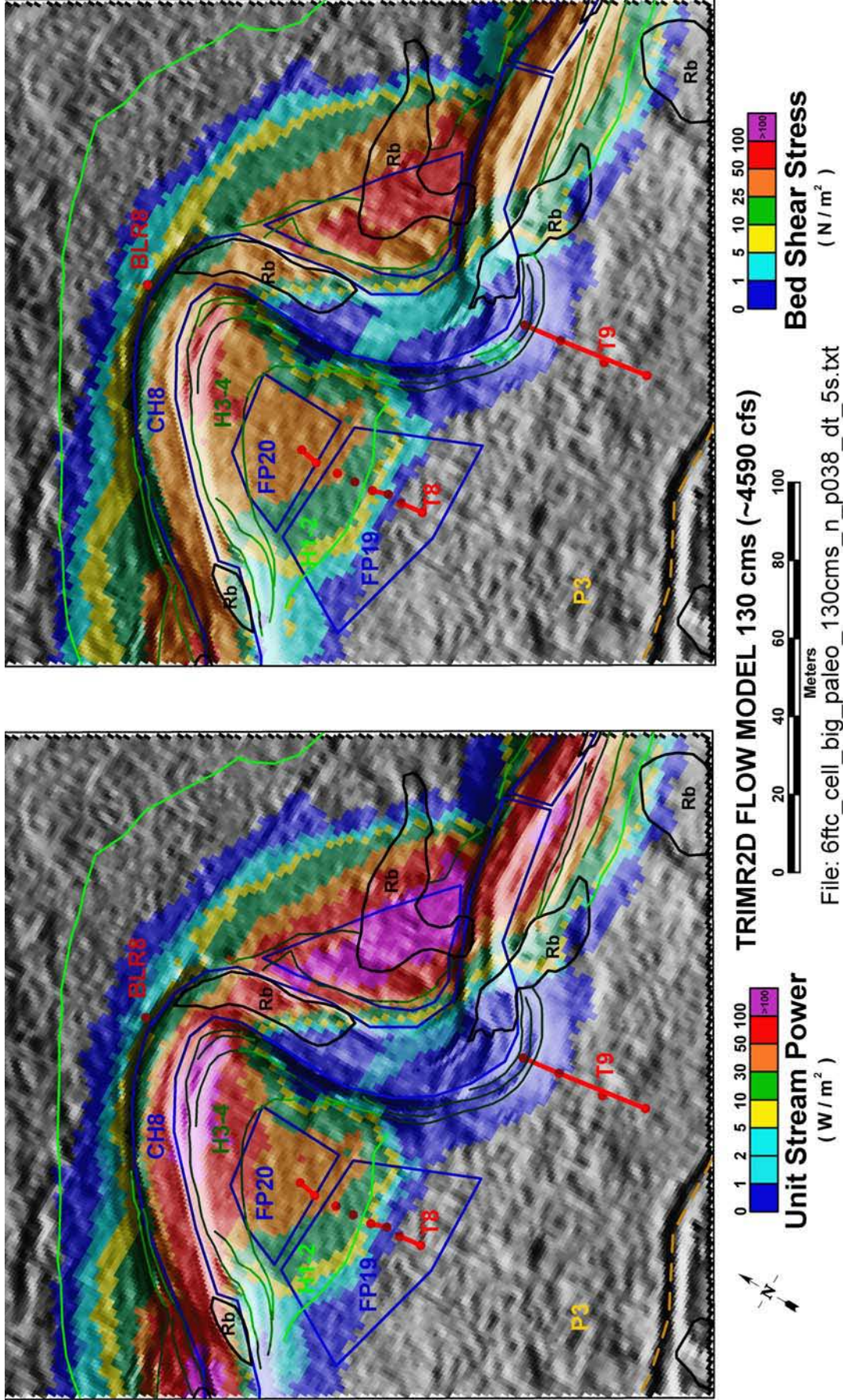


Figure 2-46 6-ft flow model results for 130 m³/s in the BLR8 study area. Base map symbology is from Figure 2-3 and Plate 2.

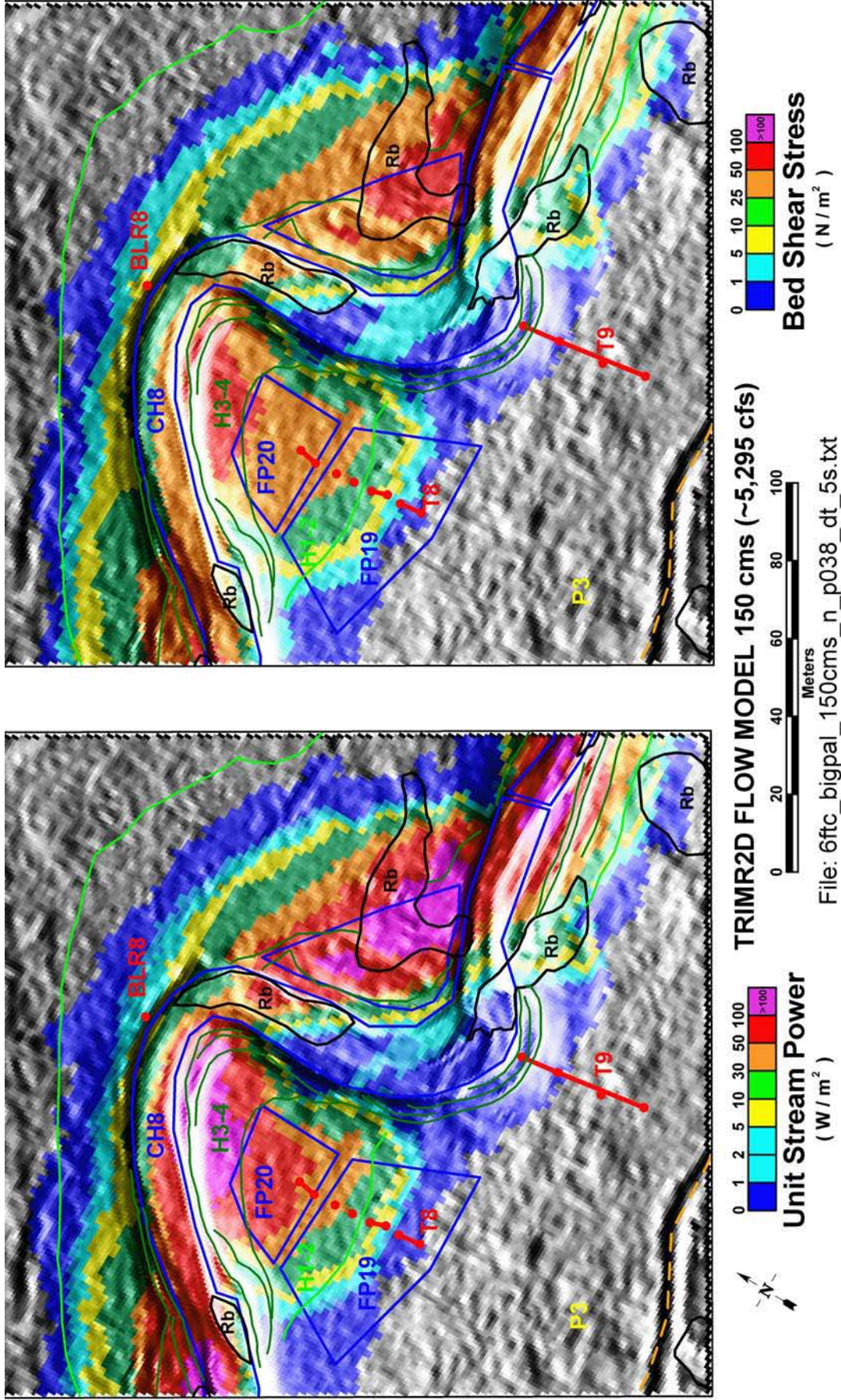


Figure 2-47 6-ft flow model results for 150 m³/s in the BLR8 study area. Base map symbology is from Figure 2-3 and Plate 2.

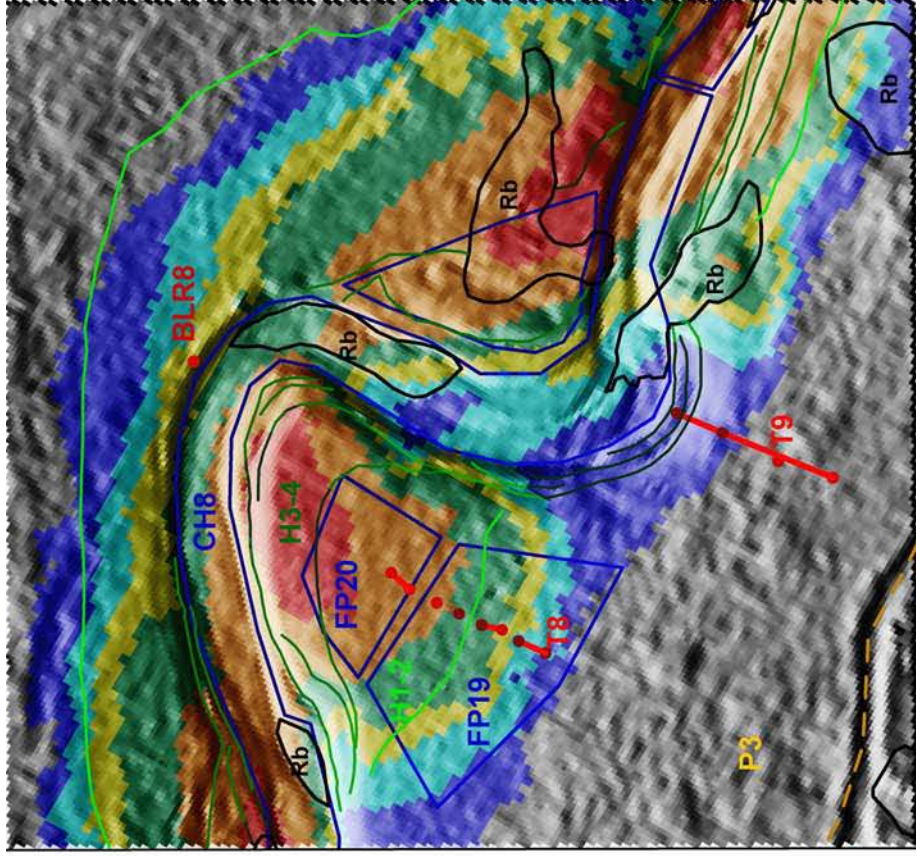
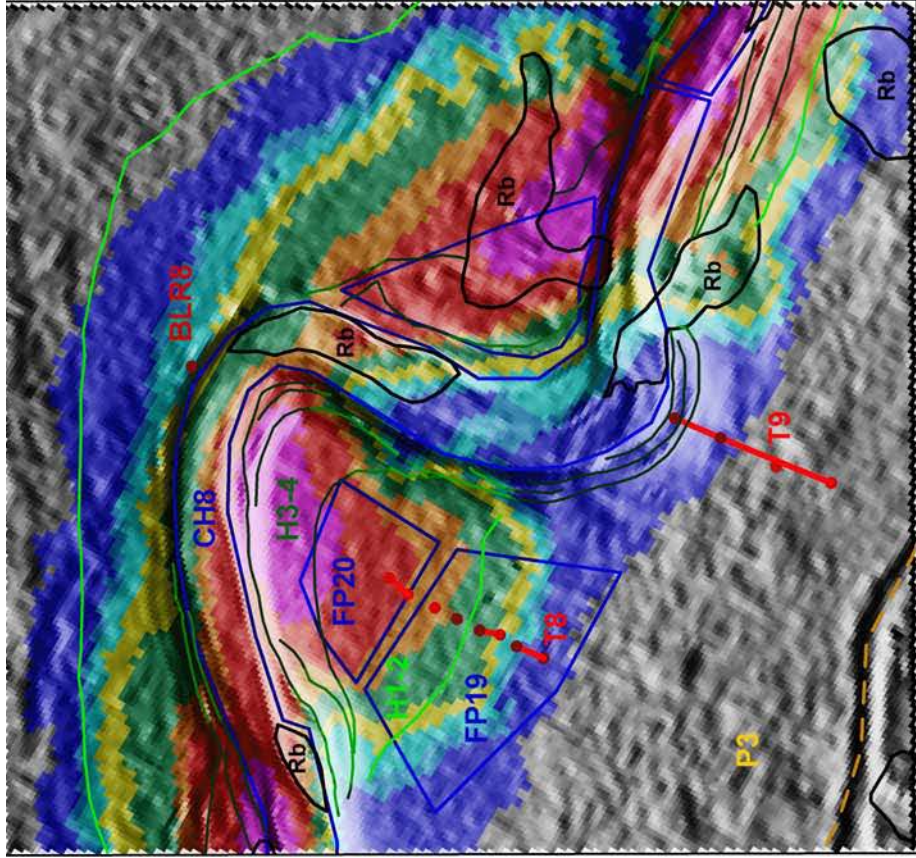


Figure 2-48 6-ft flow model results for 175 m³/s in the BLR8 study area. Base map symbology is from Figure 2-3 and Plate 2.

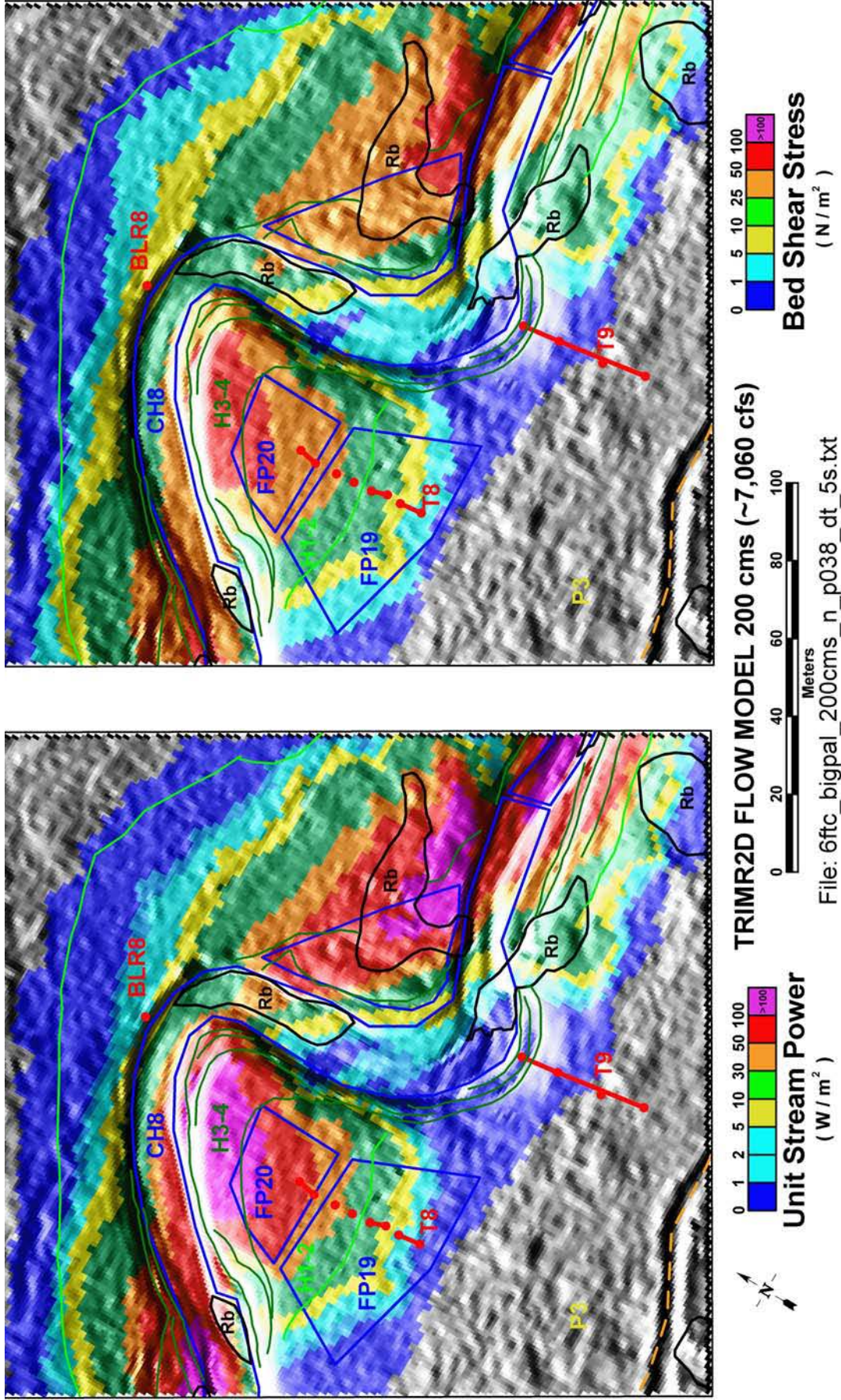


Figure 2-49 6-ft flow model results for 200 m³/s in the BLR8 study area. Base map symbology is from Figure 2-3 and Plate 2.

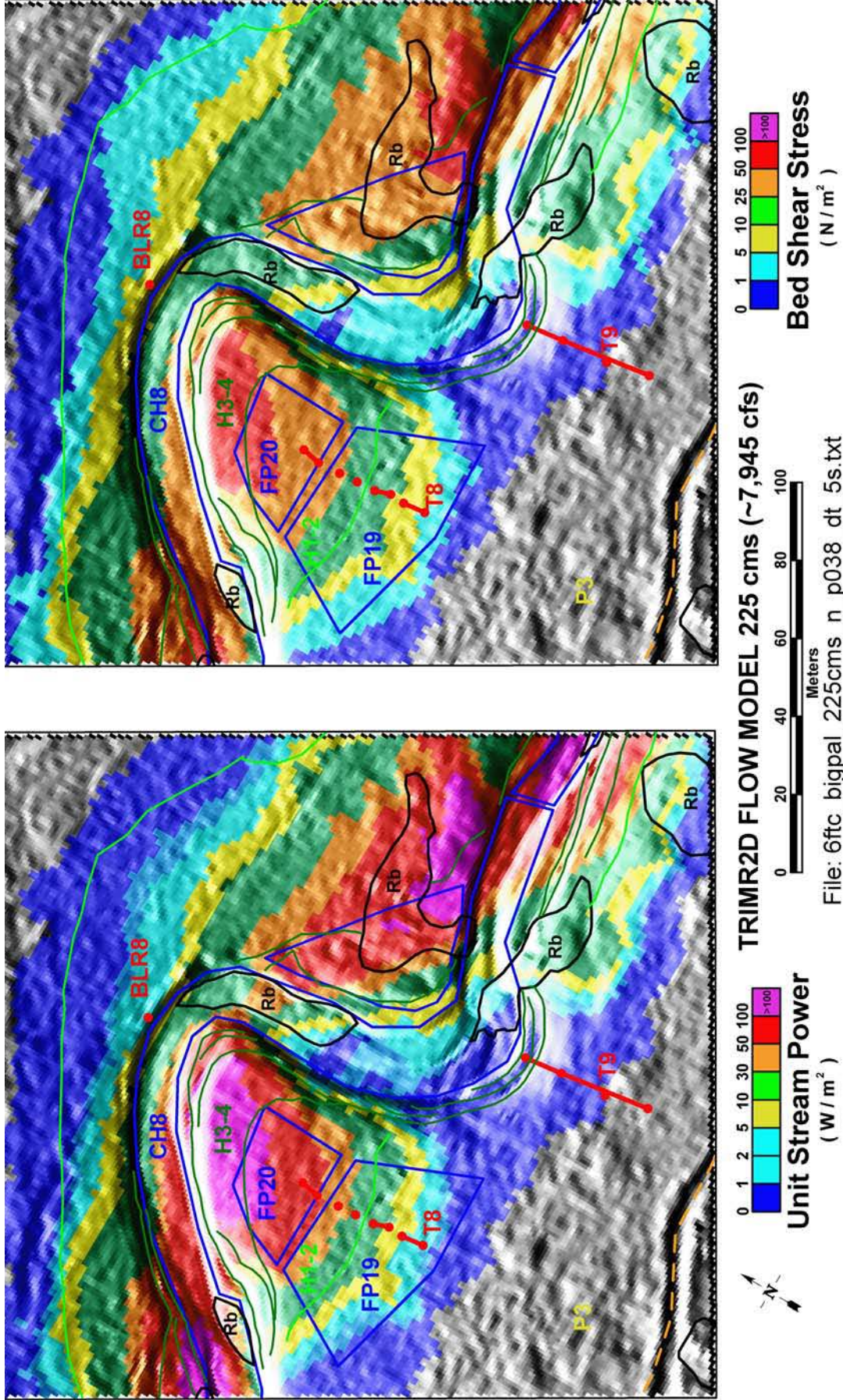


Figure 2-50 6-ft flow model results for 225 m³/s in the BLR8 study area. Base map symbology is from Figure 2-3 and Plate 2.

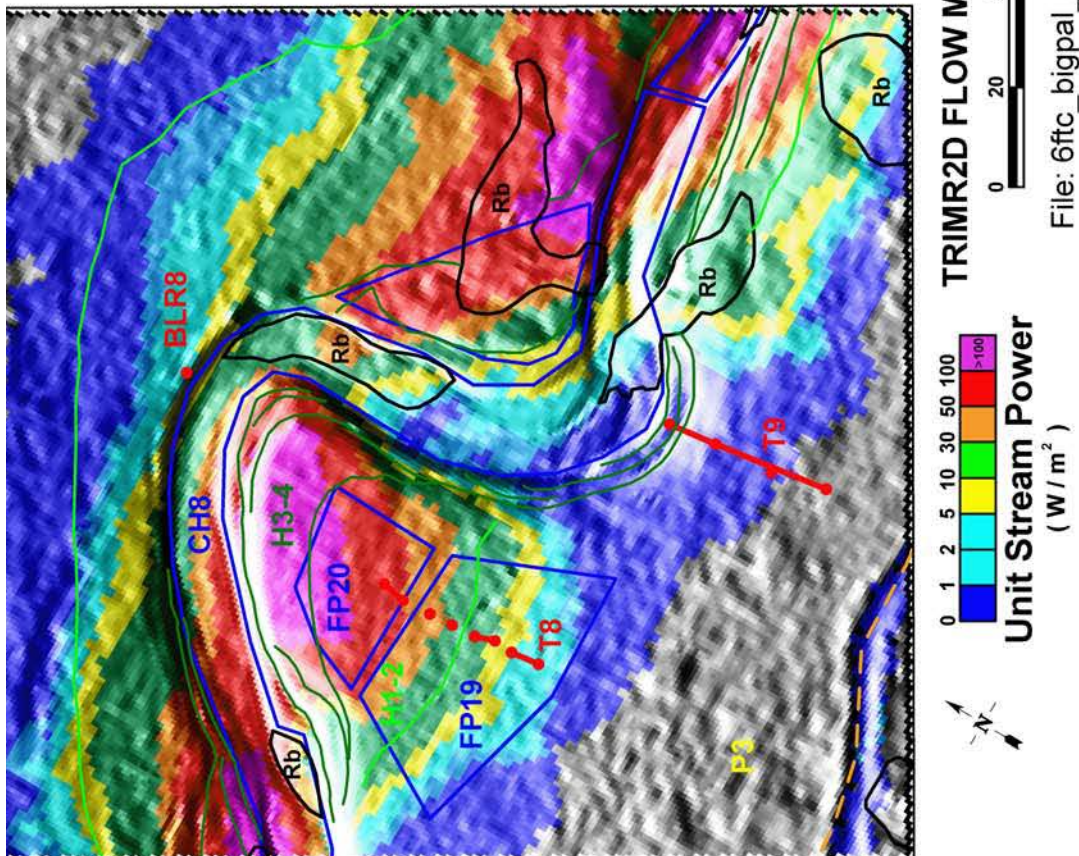
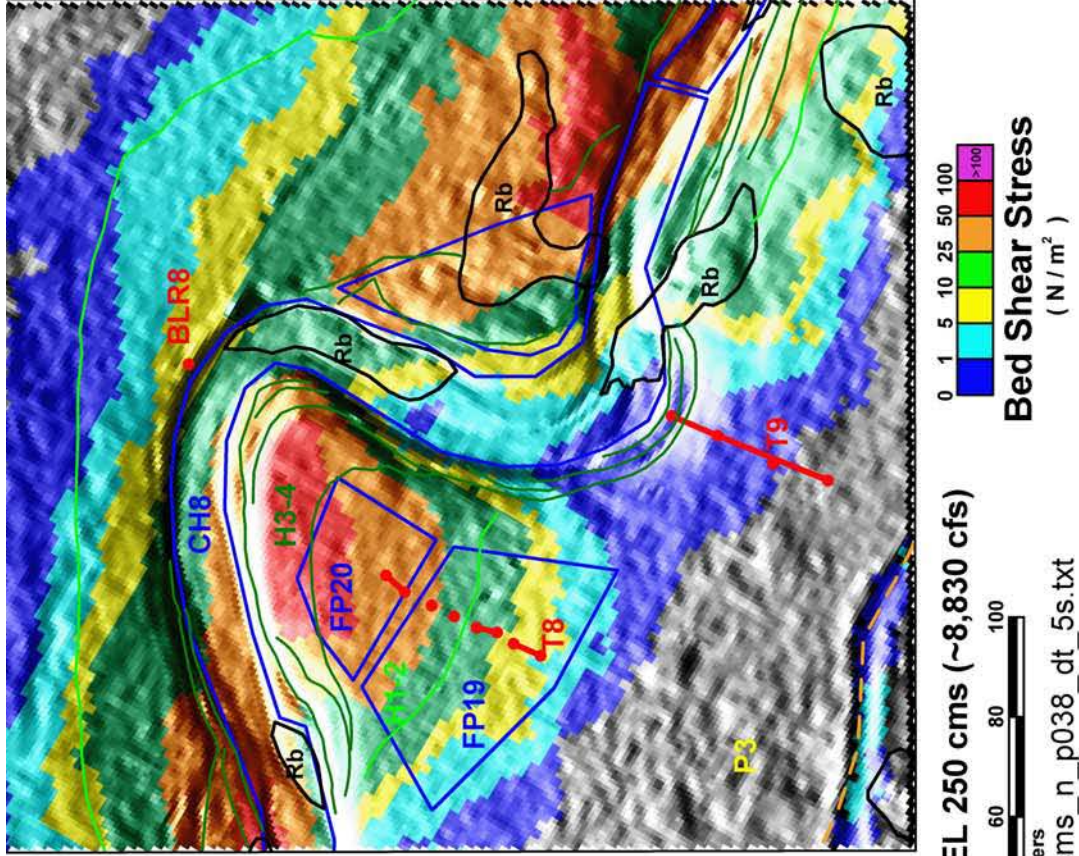


Figure 2-51 6-ft flow model results for 250 m³/s in the BLR8 study area. Base map symbology is from Figure 2-3 and Plate 2.

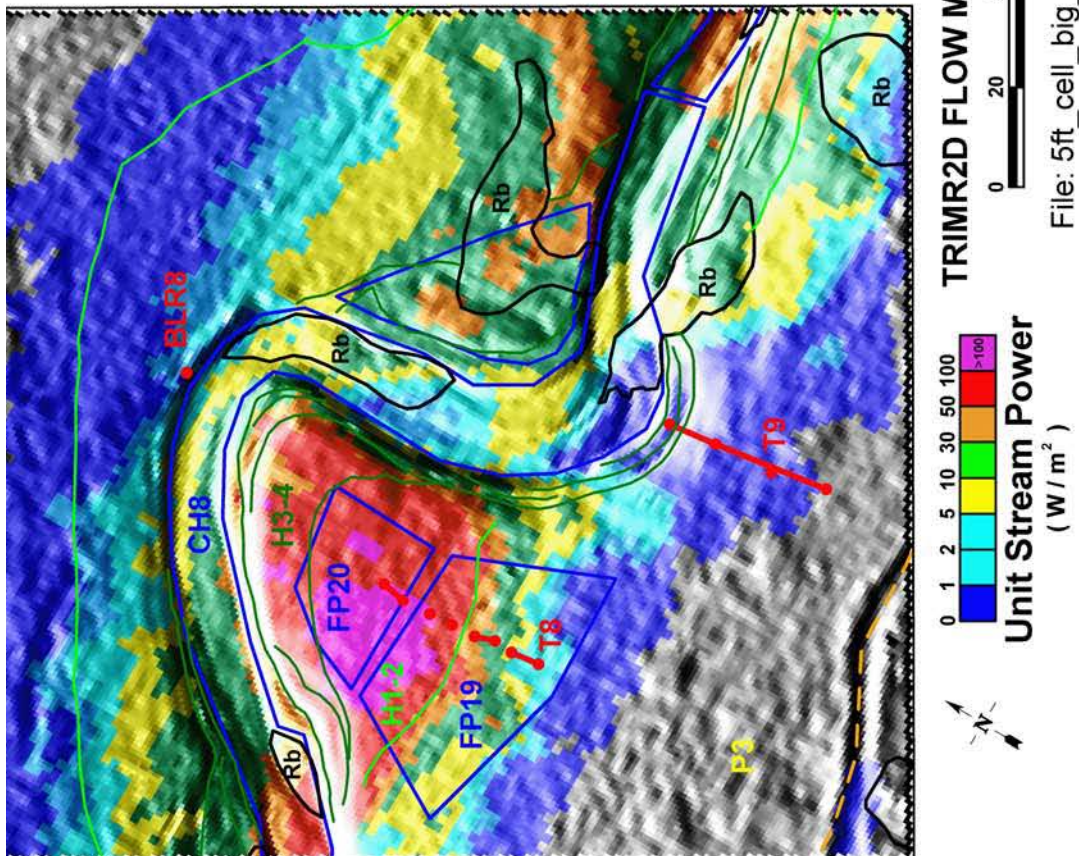
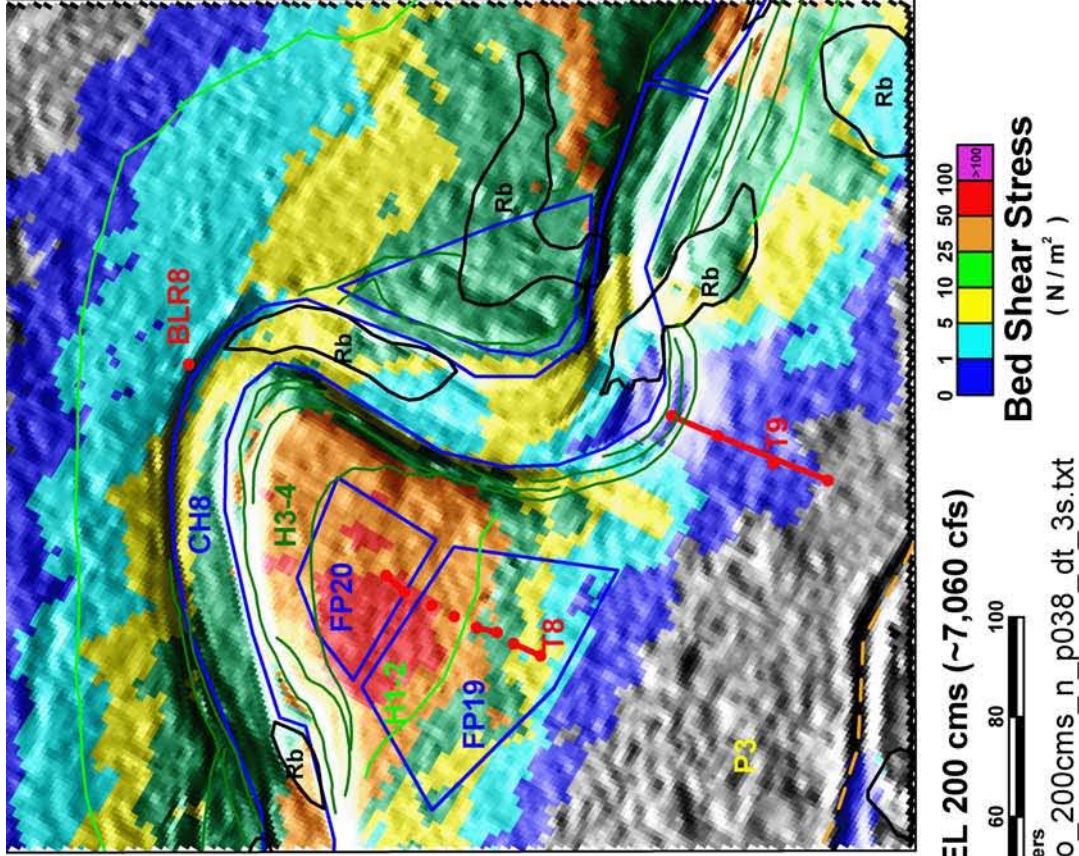
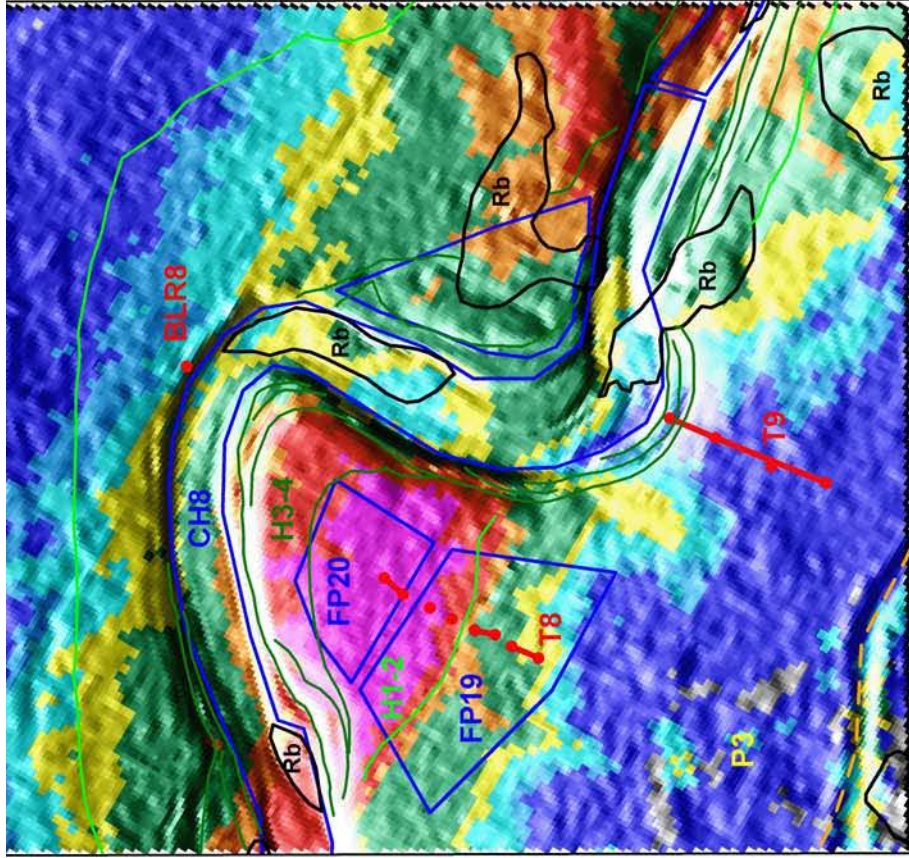
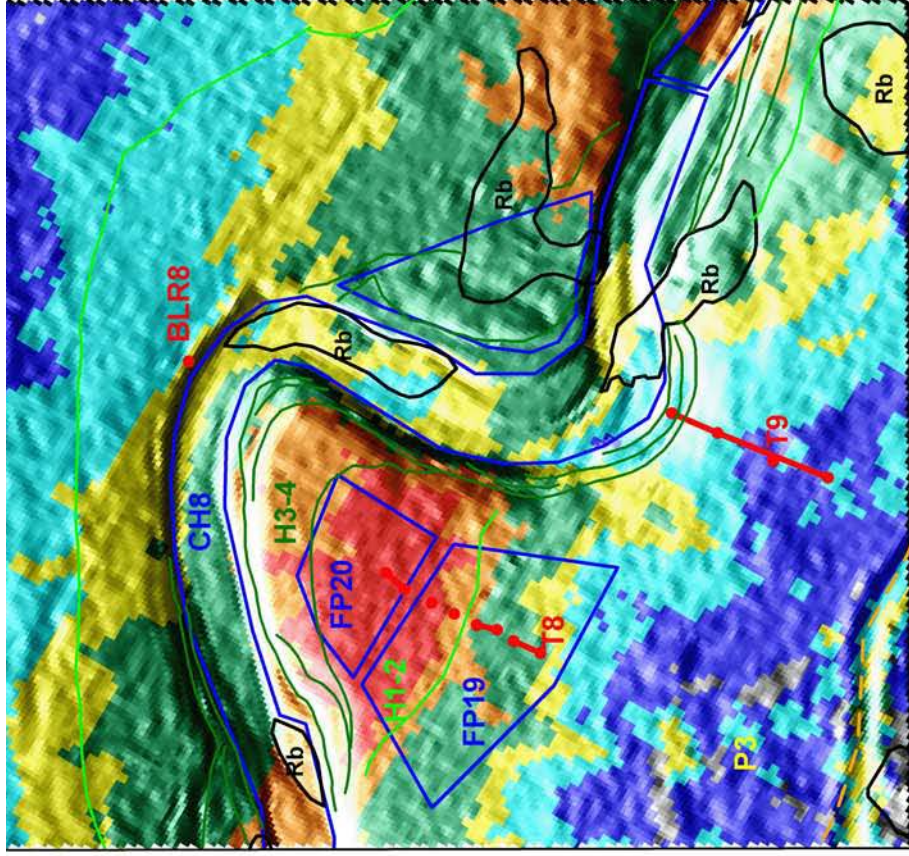


Figure 2-52 5-ft flow model results for 200 m³/s in the BLR8 constriction study area. Base map symbology is from Figure 2-3 and Plate 2.



Unit Stream Power
(W/m^2)



Bed Shear Stress
(N/m^2)

TRIMR2D FLOW MODEL 300 cms (~10,590 cfs)

File: 5ft_cell_big_paleo_300cms_n_p038_dt_3s.txt

Figure 2-54 5-ft flow model results for $300\text{ m}^3/\text{s}$ in the BLR8 constriction study area. Base map symbology is from Figure 2-3 and Plate 2.

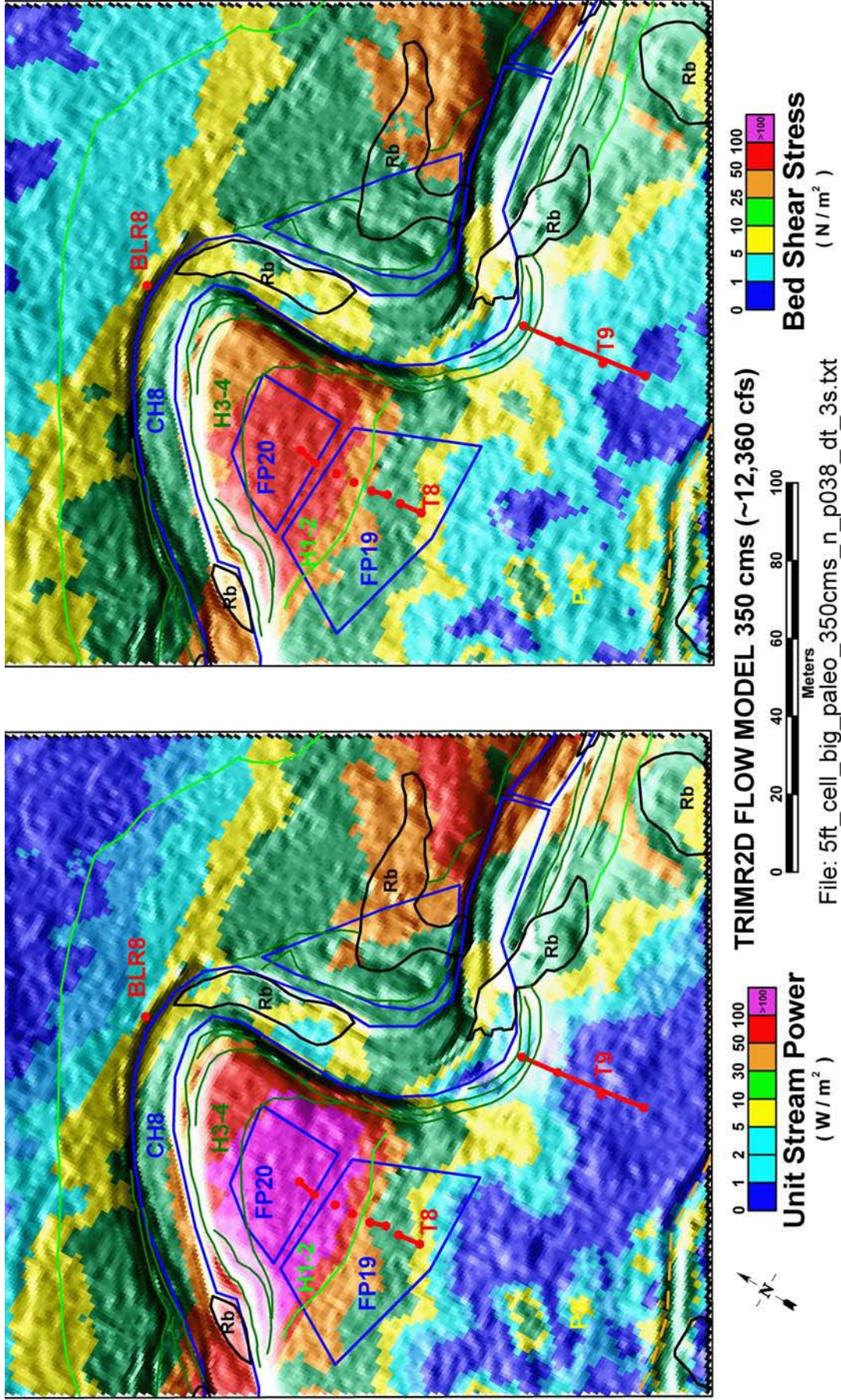


Figure 2-55 5-ft flow model results for 350 m³/s in the BLR8 constriction study area. Base map symbology is from Figure 2-3 and Plate 2.

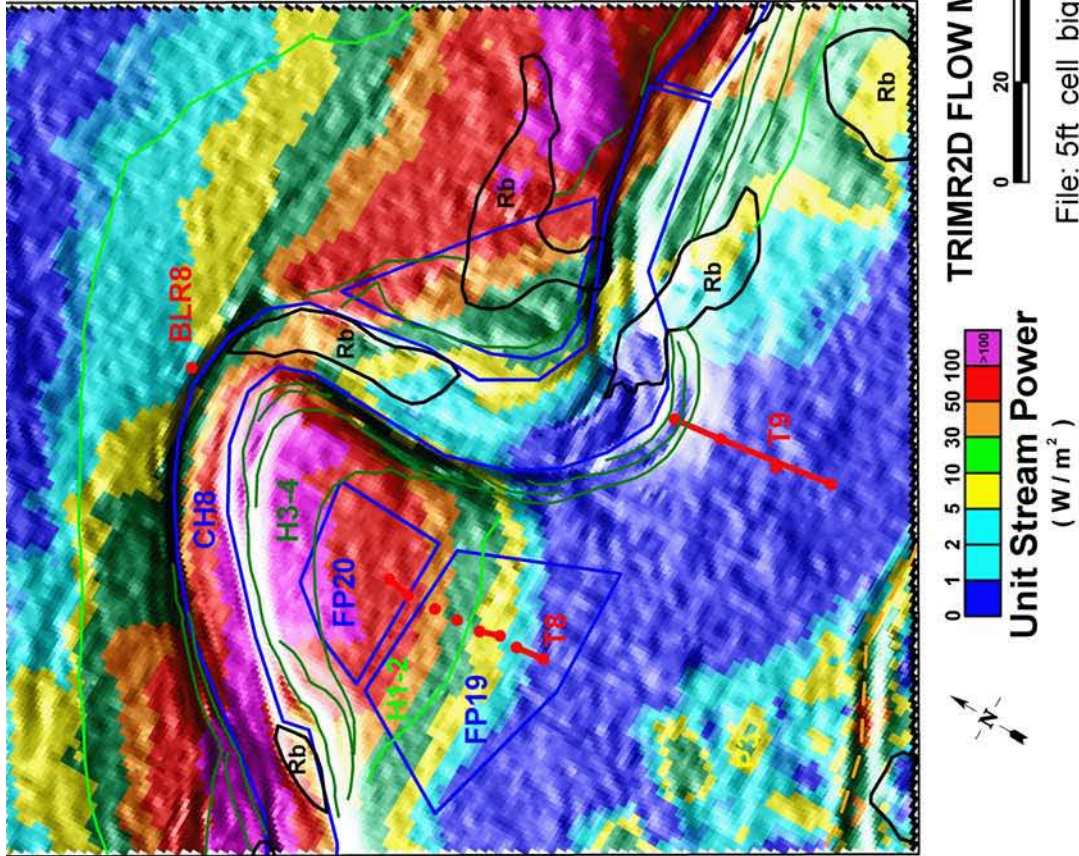
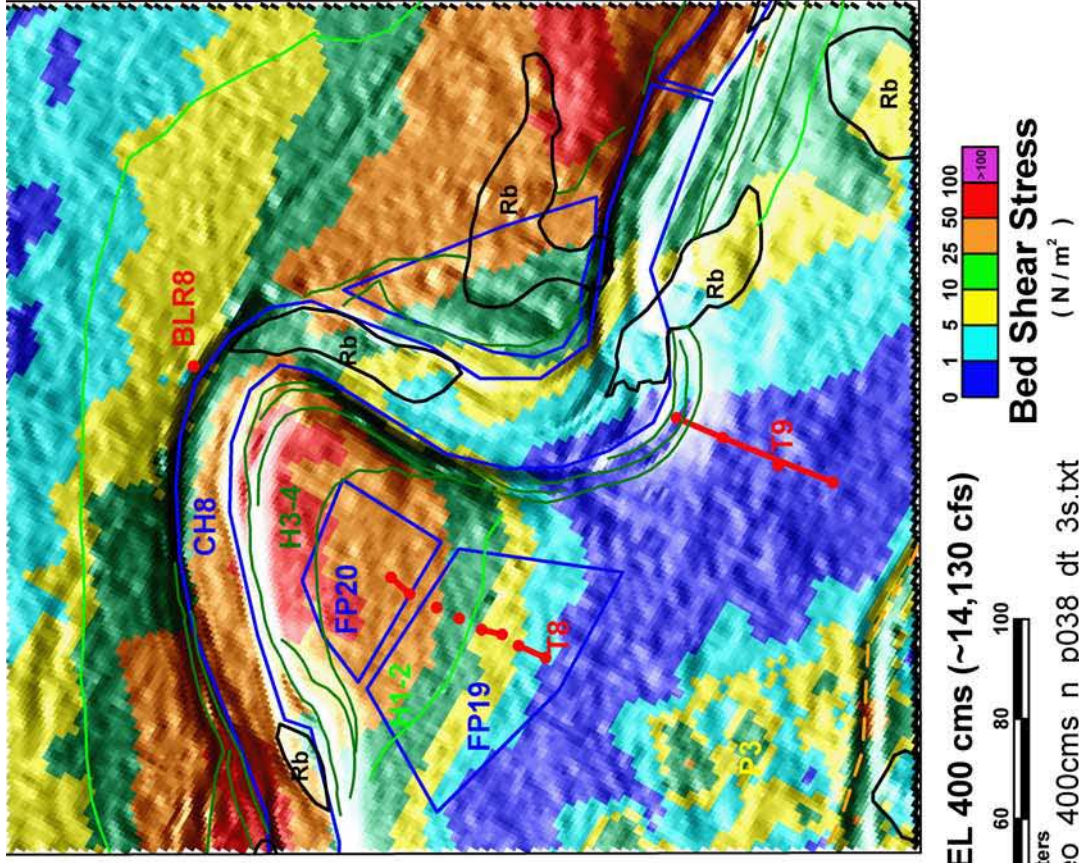


Figure 2-56 5-ft flow model results for 400 m³/s in the BLR8 constriction study area. Base map symbology is from Figure 2-3 and Plate 2.

Tables for Section 2.0

Table 2-1 Discharge and modeling scenarios for the INEEL Diversion Dam study reach

Modeled Discharge ¹ m ³ /s (ft ³ /s)	Topography ²			Potential Significance of Modeled Discharge
	2000 6-ft grid		Reprocessed 1993 5-ft grid	
	n=0.030	n=0.038	n=0.038	
10 (~355)	X	X		Approximate maximum gaged flow downstream of INEEL Diversion (since 1984)
12 (~425)	X	X		
15 (~530)	X	X		
25 (~885)	X	X		Approximate INEEL Diversion Dam release capacity
50 (~1765)	X	X		Range for largest estimated historic floods near INEEL Diversion Dam
70 (~2470)	X	X		
100 (~3530)	X	X		Revised USGS 100-yr flood is 106 m ³ /s (~3740 ft ³ /s) (Hortness and Rousseau, 2002)
130 (~4590)	X	X		
150 (~5295)	X	X		Median value for 10,000 yr paleohydrologic bound (Ostenaar and others, 1999)
175 (~6180)	X	X		Approximate USGS 100-yr flood downstream of INEEL Diversion Dam (Kjelstrom and Berenbrock, 1998)
200 (~7060)	X	X	X	
225 (~7945)	X	X		
250 (~8830)	X	X	X	
300 (~10,590)			X	
350 (~12,360)			X	
400 (~14,130)			X	
Notes:				
¹ Steady-state discharge input at upstream end of reach, downstream of the INEEL Diversion Dam ² All scenarios modeled with TRIMR2D with 5- or 6-ft rectangular grid with input topography as noted.				

Table 2-2 Soils and Radiocarbon Summary

Trench No.	Field Sample No.	Sample Depth (cm)	Material dated	Laboratory number	Radiocarbon age (^{14}C yr B.P.) $\pm 1 \sigma$	Calibrated age range (cal yr B.P.) $\pm 2 \sigma$
T4	T4-20-1AR	20-25	<i>Artemisia</i> charcoal	Beta - 174101	520 \pm 40	630-600; 560-510
	T4-20-2AR	38-51	<i>Artemisia</i> charcoal	Beta - 174102	1070 \pm 40	1060-930
	T4-19-1AR	50-60	<i>Artemisia</i> charcoal	Beta - 174099	1130 \pm 40	1160-950
	T4-19-1CO	50-60	Conifer charcoal	Beta - 174100	1980 \pm 40	2000-1860
	T4-19-3CH	140-155	<i>Chrysothamnus</i> charcoal	Beta - 172812	6330 \pm 40	7320-7200
T5	T5-0-1AR	22-32	<i>Artemisia</i> charcoal	Beta - 174103	780 \pm 40	760-660
	T5-0-2CO	110-130	Conifer charcoal	Beta - 174104	1880 \pm 40	1900-1720
T6	T6-4-1SA	12-25	<i>Salicaceae</i> charcoal	Beta - 174106	630 \pm 40	660-540
	T6-4-1AR	12-25	<i>Artemisia</i> charcoal	Beta - 174105	830 \pm 40	790-680
	T6-6-1YS	95-105	snail shell	Beta - 183387	10390 \pm 50	12800-11940
	T6-4-2MIX	103-121	charcoal fragments	Beta - 172813	3210 \pm 40	3480-3360
	T6-20-2MIX	110-140	charcoal fragments	Beta - 183388	2710 \pm 40	2870-2760
	T6-68-1AR	30-40	<i>Artemisia</i> charcoal	Beta - 174107	620 \pm 40	660-540
T9	T9-32-1PO	35-45	<i>Populus</i> charcoal	Beta - 183391	170 \pm 40	290-250; 230-130; 110-70; 30-0
	T9-32-2CM	105-115	<i>Chrysothamnus</i> charcoal	Beta - 183392	130 \pm 40	290-0
	T9-2-2AR	105-115	<i>Artemisia</i> charcoal	Beta - 183389	2610 \pm 40	2730-2780

Table 2-3 Geologic and Geomorphic Summary for Big Lost River Paleofloods and Paleohydrologic Bounds

Event name	Age or time span (Cal yrs or Cal yr B.P.) ¹	Summary of Evidence
Paleofloods		
"white flood"	>100yr (pre-gaging) but less than 400-600yr	Based on thin deposit in T4. Not recognized in T5 or T6 (slightly higher sites). Possible correlative in T9(?). Age - most likely 100 to 150 years based on absence of soil development
"400-yr" flood	400 to 600 years	Apparently correlative deposits in T4, T5, T6 (also BLR2, BLR7 & BLR8) with similar soils, stratigraphic setting, and radiocarbon ages. Soil has stage I- Bk horizon. Stripping of A and AB/Bw horizons at T8c, partial stripping at T8b; May represent more than one flood.
"older flood"	1000 to 2000 years	Deposits with Stage I to I+ Bk horizon that underlie "400-yr flood" deposits in T4, T5, T6 and T9. Appears to indicate long period of stability with little or no deposition at these sites before deposition of deposits associated with "400-yr" flood. Similar stratigraphy at BLR2 and BLR8. Likely represents multiple floods of similar or smaller maximum discharge. Minimum discharge must inundate FP1-FP4, FP6-8, most of FP7, FP11-13, FP17-18, and FP19-21, which are areas with H1-2 geomorphic surfaces that appear to indicate Holocene flooding.
Paleohydrologic Bounds		
400-yr #1	400-600	Preservation of recognizable stratigraphy at T4 and T6. No stripping of A-horizons from the youngest deposits at T4 and T6. Apparently correlative H1-2 geomorphic surfaces at FP1, FP3-4, FP7, FP11-13, FP17, and FP19-20.
early Holocene (H1 surfaces)	6000 to 8000	Preservation of stratigraphy in T6, T4, and T8a,b,c. Banks at BLR6 and continuity of H1-2 geomorphic surfaces along BLR.
Pleistocene	>10000	Preservation of Pleistocene gravel surfaces throughout the study reach. Actual age of the underlying deposits is older than 12-15 ka (minimum age of deglaciation) and some may be older than 20-25 ka (Last glacial maximum). Length of time span for paleohydrologic bound is limited by post-glacial, warmer climate more similar to present.
Notes: ¹ All age distributions have uniform probability over the indicated time span uncertainty.		

3.0 PALEOFLOODS AND PALEOHYDROLOGIC BOUNDS FOR THE BIG LOST RIVER

3.1 Background to the Use of Paleohydrologic Bounds

The approach taken for this paleohydrologic analysis is similar to that used for the previous paleohydrologic studies at INL (Ostenaar et al., 1999, 2002) as well as several Bureau of Reclamation flood hazard evaluations for dams throughout the western United States (e.g., Ostenaar et al., 1996, 1997; Ostenaar and Levish, 1997). Flood frequency analyses for these studies incorporate paleoflood estimates and paleohydrologic bounds (Levish, 2002; Levish et al., 1994, 1996, 1997; Ostenaar and Levish, 1996) into nonparametric Bayesian analyses that use likelihood functions that incorporate both parameter and data (discharge and geologic age) measurement uncertainties (O'Connell et al., 1996, 1998; O'Connell, 2005).

A paleohydrologic bound is the time interval during which a given discharge has not been exceeded. Paleohydrologic bounds are not actual floods, but instead are limits on paleostage over a measured time interval. These bounds represent stages and discharges that have not been exceeded since a geomorphic surface stabilized. Through hydraulic modeling, discharge for a paleohydrologic bound can be derived from stage, just as a discharge is derived from the paleostage indicators of past floods. Used appropriately, paleohydrologic bounds are powerful constraints in flood frequency analyses, even if the number, timing, and magnitude of individual paleofloods are uncertain (Stedinger and Cohn, 1986).

In this context, the present analysis only assumes that for extreme floods, upstream regulatory structures and diversions do not increase flood magnitudes downstream compared to the unregulated natural flows, except for cases where upstream regulating structures might fail. Flood probabilities for such scenarios should be evaluated separately, and account for the overall failure probability of the structure under all conditions. The impacts of regulation and variations in smaller flows, such as those of historical experience, on frequency estimates of extreme floods are addressed through sensitivity analyses.

3.1.1 Geologic and geomorphic evidence of flooding. There are many different types of geologic and geomorphic information in fluvial systems that provide a direct indication of the

magnitude and frequency of floods (e.g., Baker et al., 1988). Gravel bars and slackwater terraces indicate the minimum stage of past floods. Likewise, evidence for past erosion such as channels on terrace surfaces and truncated soil profiles also indicates the minimum stage of past floods. The age and frequency of the floods that produced these features can be determined by the degree of soil development, the morphology and extent of weathering on surface features, and radiocarbon analysis of organic material within the deposits. For historical or more recent paleofloods, floated debris and subtle erosional scars are a shorter-lived record of the maximum stage.

A complementary indication of the limits of past floods is the recognition of the amount of time during which floods have not modified geomorphic features or deposits. Soil development and the geomorphic evolution of deposits and surfaces are time-dependent processes (e.g., Birkeland, 1999). Thus, the age of stable, non-flood-modified geomorphic surfaces adjacent to streams is an indication of the minimum length of time since last flooding (Costa, 1978). Evidence of modification of these surfaces by floods includes the deposition of sediment resulting in burial of soils, erosion and truncation of soils, erosion of channels on the surfaces, or erosion of the deposits themselves. Estimates of the stage required to modify these surfaces can come from empirical comparisons to data from historical floods or by comparison to hydraulic model results of observed flows. The minimum depth of flow required for the initiation of large-scale erosion or deposition on geomorphic surfaces can also be evaluated formally in terms of shear stress or stream power (e.g., Parker, 1978; Andrews, 1984; Baker and Costa, 1987). This type of approach is expanded upon here based on the criteria discussed below and in **Appendix D**.

3.2 Criteria and Approach for Evaluating Paleohydrologic Information

In evaluating discharge estimates for paleohydrologic bounds, the focus is on developing an estimate of the flood discharge required to modify or erode a geomorphic surface for which stability can be demonstrated for some prior length of time (e.g. Levish, 2002). Evidence of surface stability is primarily shown by the consistency of soil development and stratigraphy that underlie the surface. These geomorphic surfaces are most often terraces, adjacent to the main stream channel. Many geomorphologists have used stream power as a measure of the potential for channel and landscape modification with a focus on channel power or average cross section

power (e.g., Baker and Costa, 1987; Magiligan, 1992). For engineering applications of erosion, channel stability, and sediment transport studies, many empirical and semi-theoretical relationships have been developed for hydraulic parameters such as depth, velocity, shear stress and stream power (e.g., see Carson and Griffiths, 1987 for a summary). However, in neither body of literature are there many examples of sites which might be considered long existing paleohydrologic bounds which have been overtopped by historical floods, and associated model estimates of the flow parameters associated with this overtopping developed. As noted by Jarrett and England (2002), documentation for the relationships between HWM (high water marks) and the estimated stage required to modify a geomorphic surface and thus define a paleohydrologic bound is lacking in the general literature.

Previous paleohydrologic studies of the Big Lost River recognized the value of using stream power or shear stress as quantitative measures of the erosional potential of stream flow across geomorphic surfaces that might be considered as paleohydrologic bounds (Ostenaar et al., 1999, 2002). However, no quantitative criteria for application of these measures to evaluating discharge and associated uncertainty estimates for paleohydrologic bounds were proposed. Ostenaar et al. (1999) noted the presence of "high" stream power and inundation depths typically in the range of 25-90 cm (1-3 ft) as a justification for establishing bounds. Ostenaar et al. (2002) compared modeled channel stream power for a discharge that had significant gravel bedload transport to modeled power on Pleistocene surfaces downstream of a site termed the Saddle. Power in both cases was noted to be in the range of 50 to $>100 \text{ W/m}^2$. Ranges of inundation depths were noted along with observations that shear stress calculations would indicate potential mobility of 2 mm particles for flow depths as shallow as 5-18 cm.

In the present study, we develop a more formal framework for the application of shear stress and stream power to the problem of specification of discharge estimates for paleohydrologic bounds. The difficulties associated with developing conclusions within this framework are similar to those faced in seismic hazard assessment (e.g., SSHAC, 1995), in that uncertainty of the estimates is derived from several sources including limited data, imperfect knowledge and models of salient physical processes, and legitimate differences of scientific opinion.

Three major types of information are used to estimate the discharge range associated with a paleohydrologic bound: 1) stratigraphic and geomorphic data, 2) hydraulic modeling results of depth, stream power, and shear stress for differing input parameters, and 3) a criterion for erosion/modification of geomorphic surfaces based on empirical data compilations of unit stream power and bed shear stress. Results of the geologic/geomorphic investigations were described and compiled in **Section 2.4**, **Plate 2**, and **Appendix B**. The hydraulic modeling approach and results were discussed in **Section 2.5** and portrayed on plots in **Appendix D**. A criterion for erosion/modification of geomorphic surfaces based on stream power and shear stress is developed in **Appendix D** and implemented below.

Geomorphic map units define the spatial extent of areas with similar geologic/geomorphic processes and history. Individual map units are characterized by similarity in relative and absolute age, geomorphic processes and history over broad areas. Differences in age, process, and history between different areas define different geomorphic units. Thus, based on detailed mapping and trenching investigations along the Diversion Dam study reach of the Big Lost River (**Plate 2**, **Appendix B**, and **Section 2.4**), three major geomorphic map groups, H1-2, H3-4, and P2-3, are of primary importance to the issues of specifying paleohydrologic bounds. The similarities and differences within these broad map units are highlighted and defined through "point" investigations with trenches or soil description sites where stratigraphic details are described in detail. These detailed site descriptions provide the basis for areal extrapolation represented by the areal extent of the geomorphic map units. Individual geomorphic map unit areas naturally define the spatial limits of areas within which the variability of hydraulic parameters such as stream power and shear stress can be evaluated when that geomorphic unit is inundated by a modeled flow.

Two-dimensional hydraulic modeling based on relatively small grid cells is used to develop detailed information on the extent and spatial variability of flow for each modeled discharge. From the model results, shear stress and stream power are calculated for each grid cell providing a detailed depiction of the magnitude and spatial variability of these parameters over the inundated areas. This information can then be compared to the spatial extent and characteristics of differing geologic/geomorphic units. Results from the two-dimensional modeling of each discharge that are

used to evaluate paleohydrologic information are 1) depth and spatial extent of inundation over a particular stratigraphic site or geomorphic surface, 2) magnitude and spatial extent of shear stress and/or stream power over a site or geomorphic surface, and 3) magnitude and spatial extent of shear stress and stream power in channel reaches. Evaluation based on depth and extent of inundation primarily considers whether or not a particular site or surface area is inundated by a given flow. For many sites, as a greater percentage of a given site or geomorphic surface is inundated, to progressively greater depths, the probability of surface modification and development of a preservable geologic record increases. Likewise, as the extent and depth of inundation increase, the magnitude and distribution of stream power and shear stress change across the geomorphic surface as well.

The hydraulic conditions associated with flow across a geomorphic surface are varied and non-uniform due to topography, small- and large-scale roughness, turbulence, and mixing. Thus, actual and calculated values of stream power and shear stress vary spatially in magnitude across a given cross section and throughout the area of flow. The results or conclusions drawn from application of any criteria for surface modification is therefore dependent on the location chosen for evaluation. One advantage of the use of high-resolution, two-dimensional hydraulic models is that these models provide outputs that show the spatial variability of flow characteristics. Ideally, the spatial variability shown by hydraulic modeling can be evaluated separately for each geomorphic surface of interest.

The third major type of information used to estimate discharge associated with a paleohydrologic bound are empirical criteria and observational data on the magnitudes of stream power and shear stress that are likely associated with modification or erosion of differing geomorphic surfaces (**Appendix D**). From these data, limiting values for the estimated erosion or modification of differing surfaces can be subjectively estimated for the specific surface conditions and physical properties (e.g., vegetation, soil, and grain size) of each site or geomorphic surface. Because estimates of paleohydrologic bounds will ultimately have a probabilistic description for use in the flood frequency analyses (**Section 4.0**), these criteria are formulated as Probability Density Functions (PDF) that relate the relative probability of surface modification to particular values of shear stress or stream power. In general, the PDF's that describe the probability of surface

modification are triangular distributions based on 3 estimated values. A lower value of shear stress or stream power represents a limit for which there is judged to be a reasonable possibility based on the existing empirical data that significant erosion or surface modification will occur. A central or preferred value represents a large body of data with high confidence. For some PDF's, the central values include a range of equal relative likelihood. An upper value limit defines a boundary beyond which there is virtual certainty of significant erosion or modification based on the available data. For application to the Diversion Dam reach of the Big Lost River, three separate criteria have been developed for stream power and shear stress, respectively (**Figure 3-2** and **Figure 3-3**) and **Appendix D**). Two of the criteria are for application to differing site, soil, and geologic conditions associated the geomorphic surfaces along the Big Lost River (**Figure 3-2**). The third criteria describes the more general conditions under which significant geomorphic modification of portions of the Big Lost River channel might result from various discharge levels (**Figure 3-3**).

Soils and geologic data from the Big Lost River lead to two general categories for erosion and surface modification, termed soil erosion and terrace erosion, based on the contrasting physical and vegetative characteristics of the soils and terrace deposits. Most of the alluvial soils have an upper horizon(s), usually less than 30 cm thick, composed of silt and sand which is generally loose and unconsolidated. These horizons, usually designated as A, AB, and sometimes Bw in soil descriptions (**Section 2.1** and **Appendix B**), lack carbonate cementation, are often bioturbated, and may include in their upper portions some component of recently active eolian sand. Some small grasses and plants have shallow roots in these horizons. In contrast, at most stream terrace sites, below a depth of more than 20-30 cm in most profiles, there is either carbonate cementation or gravel. In deposits that are mostly fine-grained, i.e., silty and sandy, soils with carbonate accumulation are stage I to II. In the gravel deposits maximum clast sizes are generally less than 200 mm, and carbonate stages range from Stage I to III. Larger plants, such as sage, have widely scattered roots that extend into the gravel horizons. Based on the carbonate cementation and generally larger clast size associated with the terrace deposits, larger values of stream power and shear stress are required to initiate erosion relative to the alluvial soils.

The criteria developed for channel stability (**Figure 3-3**) is mainly derived from geomorphic study observations of major channel widening or change following floods (**Appendix D**). This criteria is only applicable to channels where banks are cut in alluvium. Most channel banks along the Big Lost River Diversion Dam study reach are composed of fine-grained alluvium with weakly to moderately developed carbonate soils similar to sections exposed in T4, T5, T6, BLR2, BLR6, BLR7 and BLR8. Gravel, in Holocene fluvial deposits, is not present more than about 1 m above the present channel floor at these exposures. Based on geomorphic mapping (**Plate 2**), only very scattered sections of the channel banks are cut directly in the gravelly Pleistocene alluvium without an inset fine-grained fill terrace. More commonly, scattered basalt outcrops confine one or both channel banks.

3.2.1 Evaluating Spatial Extent and Variability.

The geomorphic maps and the hydraulic modeling results are both two-dimensional datasets that can be overlain and evaluated jointly. This approach allows the spatial extent of geomorphic surfaces and inundation to be evaluated along with the spatial variability of hydraulic modeling results for specific sets of geomorphic surfaces. This type of evaluation could be done in a strict GIS-style, where the full extent of each map unit is evaluated separately, but that approach has not been used here because the mapped geomorphic units include many transitional slopes and areas that are not ideally representative of sites that would be suitable for evaluating paleohydrologic bounds. Specifically, this includes areas such as broad slopes on risers between terraces where some slope erosion and deposition is ongoing, irrespective of the paleoflood and fluvial processes of the Big Lost River. Long-term geomorphic stability cannot generally be demonstrated for these types of transitional areas. For that reason, a more restricted subset of the key geomorphic surfaces were selected for evaluation. Within the Big Lost River Diversion Dam reach, 30 subareas were defined based on geomorphic characteristics (**Figure 3-4**). The boundaries of each subarea were drawn to generally lie within the extent of a single geomorphic map unit along the Big Lost River. Most of the subareas are of sufficient size to include hundreds of computational cells from the hydraulic modeling results and include thousands of square meters of individual geomorphic surfaces. One way of reducing uncertainty associated with paleohydrologic conclusions is to expand the spatial extent of that data throughout a study reach.

The detailed geomorphic and spatial characteristics of the subareas are summarized in **Table 3-1** and **Table 3-2**. Twenty-one subareas, FP1 to FP21, are located on the Holocene and Pleistocene geomorphic surfaces adjacent to the Big Lost River. These subareas range from small areas surrounding the individual trenches, (e.g., FP12 near T4) to subareas which encompass extensive areas of the Pleistocene surfaces flanking the Big Lost River (e.g., FP5 and FP15). Nine subareas, CH1 through CH9, were defined within the channel of the Big Lost River. These channel reaches differ in sinuosity, bed and bank materials, and hydraulic characteristics.

Within each subarea, values for inundation, stream power, and shear stress from each flow simulation are plotted relative to the threshold values for modification defined by empirical data (e.g., end points and peaks on **Figure 3-2** and **Figure 3-3**). From the resulting plots (e.g., **Figure 3-5** and remaining plots in **Appendix D**) a range of discharge values can be defined for each subarea that corresponds to the subjective probability thresholds for modification based on stream power or shear stress. A minimum discharge level for these values is first imposed by the requirement that 90-100 percent of the subarea is inundated by the simulated discharge. This is imposed to assure the uniformity of geomorphic processes within each subarea. Because the subarea boundaries are primarily defined by geomorphic boundaries, and because the age of geomorphic surfaces within each subarea are interpreted to be constrained by similar geologic factors, for flood modification of these surfaces nearly complete inundation is generally a minimum requirement. Inundation extent that is less than 100 percent is allowed for surfaces that include original depositional or erosional relief unrelated to flood modification. This would include transitional areas such as terrace risers that exist between surfaces of differing ages, or constructional relief associated with abandoned bars and channel features. Discharge values that correspond to the erosion/modification thresholds (i.e., PDF of **Figure 3-2** and **Figure 3-3**) are then estimated by choosing a percentage of the subarea that must exceed the threshold value for erosion/modification. The two-dimensional hydraulic modeling demonstrates the spatial variability of hydraulic conditions across individual surfaces. Because the subareas are very large (see **Table 3-1** for sizes), and the scale of geomorphic mapping and observation is also large, geomorphic change that is detectable within the scale of this investigation should result when threshold values are exceeded over much less than 100 per cent of most of the subareas. For the present scale of mapping along the Big Lost River, geomorphic features that are less than about

10 m² (108 ft²), such as outcrops, dunes, mounds, and small channels, are readily observable and detectable. Thus, even for the smallest of the subareas, use of a value of 50 percent area for exceedence of the threshold values of stream power or shear stress corresponds to minimum areas of 35 m² (377 ft²), and for most subareas, it is hundreds or thousands of square meters. The subarea percentages and the discharge ranges derived from analysis of each of the subareas are tabulated in **Table 3-3**.

3.2.1.1 Uncertainty in Discharge Estimates of Modification for each Subarea.

Overall, the uncertainty in the discharge ranges estimated from each subarea is mostly derived from three main sources. The first is the variability in calculated stream power and shear stress that results from changes in the input hydraulic model parameters such as discharge, roughness, or topographic model. This uncertainty is displayed for each subarea by comparison of the curves based on similar discharge, but varied roughness or topographic input, or comparing changes resulting from successive discharge values (e.g. **Figure 3-5** and plots in **Appendix D**). As such, the ranges compiled in **Table 3-3** directly incorporate this uncertainty for range of input parameters used in the simulations.

The second source of uncertainty lies in the PDF's (e.g., **Figure 3-2**) that describe the relative probability of erosion or modification associated with variation in stream power or shear stress. This source of uncertainty is directly linked to the choices and relevance of threshold values from empirical data to associate with surface modification (**Appendix D**). The tabulated empirical data on which these thresholds are based were collected according to a wide variety of scientific and engineering protocols. It is therefore difficult to directly link all of these results directly to the present framework of flow simulation and calculation used in the present study. Further research and data compilation, conducted specifically within the framework of modern two- and three-dimensional flow modeling, is needed to rigorously evaluate whether the present range of values chosen to characterize the erosion/modification thresholds are appropriate, or not. Determining the proper basis for describing and characterizing the spatial variability of flow parameters and erosion over extent varied geomorphic surfaces is a critical component of this uncertainty.

The third source of uncertainty lies in the delineation and choices for the areal extent of a subarea or geomorphic surface which must meet the threshold criteria. This latter factor is somewhat

minimized because stream power and shear stress values develop rapidly over most of the individual subareas with increases in discharge. Thus, the curves on **Figure 3-5** and the additional plots in **Appendix D** are generally very steep, meaning that for most subareas, changing the required percentage that must exceed the threshold does not substantially change the estimate of discharge. Additional small uncertainty is derived directly from the delineation of the subarea boundaries from the geomorphic and geologic data. The extent to which the subareas are reasonable subdivisions or groupings of the geomorphic units can be judged subjectively by comparison of the subareas and geomorphic mapping. As noted above, use of the presently mapped geomorphic boundaries in lieu of the subareas would result in inclusion of larger percentages of transitional topography with increased geologic complexity and variability.

3.2.1.2 Combining Estimates from Multiple Subareas. Sample subareas for stream power and shear stress are located throughout the Diversion Dam study reach (**Figure 3-4**). Hydraulic conditions vary throughout the study reach and although many subareas are located on geomorphic surfaces of similar age where there will be variability within a subarea (**Section 3.2.1**), estimates of unit stream power and bed shear stress are expected to vary between subareas as well. Thus, a consistent approach for combining results from multiple subarea sites is required. For paleofloods, the observed geologic or geomorphic evidence should relate to a pattern of modeling results that is consistent with a single discharge range throughout the study reach. Thus, the estimated discharge for the paleoflood must 1) inundate all sites where correlative flood deposits are observed; and 2) have stream power and shear stress distributions that are consistent with the observed distributions of fine- and coarse-grained deposits of the paleoflood as well as any evidence of erosion that can be associated with the flood. Estimates from multiple sites should be generally consistent if all the sites are associated with a common paleoflood discharge. In contrast, because a paleohydrologic bound represents an exceedence of prior events, and is possibly a hypothetical event that was not associated with deposition of the preserved deposits or geomorphic surfaces, modeled hydraulic conditions may vary greatly between sites of similar age within a reach. Some sites will inevitably be much more strongly limiting than other sites even though they may be of the same general age. This is perhaps most easily illustrated by considering the broad areas of the Pleistocene P2 surfaces that flank the Big Lost River. As the hydraulic modeling results show, these surfaces are slowly and variably inundated over a broad range of

discharge (**Section 2.5** and **Section 3.2.1**). Thus, the estimated discharge required to modify any subsection of the P2 surfaces will vary substantially and for some sites, the criteria for modification (e.g., **Figure 3-2**) may never be met, regardless of discharge. In contrast, some areas of the Pleistocene surfaces may be sites where modification is highly likely at very shallow inundation. These types of sites are more strongly limiting as a basis for evaluating a paleohydrologic bound.

Comparison of possible discharge estimates from several subareas for any group of similar-age surfaces might yield a broad range of discharge values for a paleohydrologic bound, but the final choice of values to describe the bound can be limited to a more narrow range that best describes the uncertainty associated with estimates for a subset of the most strongly limiting sites. Limiting the range based on fewer sites may still be conservative depending on the number and characteristics of the initial group of subareas evaluated. There is no assurance that the subareas chosen include the most strongly limiting site for any age group. On the other hand, initial delineation of the subareas (**Section 3.2.1**) is based on a requirement that the subareas be large enough to include a geologic/geomorphic record or deposit that could be preserved and recognized over geologic time scales.

3.3 Age and Discharge Estimates for Paleofloods

The geologic investigations summarized in **Section 2.4** identified stratigraphic evidence for at least three paleofloods along the Big Lost River that exceeded the stage and discharge of floods in the historic record (**Table 3-5**). Stratigraphic data from trenches and exposures defines the number, relative sizes, and relative ages of these paleofloods. Geologic age-dating methods provide the absolute ages and uncertainty ranges (**Section 2.3** and **Figure 2-8**). Estimates of discharge ranges for the paleofloods are based on the hydraulic modeling results (**Section 2.5**) and the approaches discussed above in **Section 3.2**. The basis for reaching age and discharge conclusions for each of the paleofloods is discussed separately below. Summary data for discharge limits from each subarea are compiled in **Table 3-3**. **Table 3-4** summarizes the applicability of each subarea to evaluation of the individual paleofloods and paleohydrologic bounds.

3.3.1 "White Flood". Stratigraphic evidence for this flood is recognized at a single site, Trench T4 (**Section 2.3.2.1**). A thin, ~ 7 cm, deposit of silty sand caps the sequence of flood deposits in lowest portion of trench T4, stations 19-21, and appears to bury the soil formed on deposits of the underlying "400-yr" flood. Soil descriptions (**Appendix B**) designate this unit as the A1-horizon of the present soil and soil development is weak in comparison to other sites. The deposit is not associated with historic floods because no historic floods would have been large enough to inundate the site (**Section 2.1.1** and **Figure 2-6**). No similar deposit is present or recognized in trenches T5 or T6, both of which are only slightly higher relative to discharge at which they are inundated (e.g. **Figure 2-6**) and it does not appear that soils in deposits of the "400-yr" flood are eroded more recently at these sites (**Section 2.3.2.2** and **Section 2.3.2.3**). A radiocarbon age from the underlying A2 horizon at T4 has a calibrated age range between 630-510 cal yr B.P. (**Table 2-2** and **Appendix B**). Deposits in lowest portions of trench T9 have young radiocarbon ages (**Section 2.3.3.2** and **Table 2-2**), but are also inundated by discharges that might have occurred prior to construction of the INEEL Diversion Dam (**Figure 2-7**). Thus, the age of a paleoflood associated with this deposit is constrained to be prior to the beginning of stream-gaging records (A.D.1903) by the minimum discharge required to reach the site. The deposit is younger than the 630-510 cal yr B.P. age from the underlying soil, and is most likely about 100-150 years based on the relative soil development.

The discharge range for this flood is narrowly constrained by modeling results at the site. A minimum discharge of 70-80 m³/s is required to inundate the deposit (**Figure 2-6**). As discharge increases, unit stream power and bed shear stress increase very rapidly at trench T4 (**Figure 2-31**, **Figure 2-32**, and subarea FP12 in **Table 3-3** and **Appendix D - Figure D3-17**). This constraint indicates that a discharge of more than 100 m³/s would have been very likely to have resulted in erosion of the underlying deposits between stations 20-21 of trench T4. Discharges larger than 100 m³/s (**Figure 2-32**) would also result in inundation of the "400-yr" deposits in the lower elevation portions of trenches T5 and T6. Discharge less than 100 m³/s is consistent with the lack of evidence for very young erosion at the Big Loop subarea FP9 (**Appendix D - Figure D3-14**) and at the BLR8 study area (subarea 20 - **Appendix D - Figure D3-25** and trench T8c - **Section 2.3.3.1**). These constraints lead to limiting the estimated discharge for this paleoflood to a range of 80-100 m³/s (**Table 3-5**).

3.3.2 "400-yr Flood". Stratigraphic evidence for this paleoflood was recognized in the earlier paleoflood study by Ostenaar et al. (1999, 2002) at four sites in the Diversion Dam study reach (**Figure 2-11**). Deposits with similar soils and stratigraphy that are apparently correlative are present in trenches T4, T5 and T6 (**Figure 2-8** and **Section 2.3.2**). These deposits appear to be associated with the prominent geomorphic expression of the H2 surface that can be mapped throughout the study reach (**Plate 2** and **Section 2.2.3**). Soil development in these deposits, and radiocarbon ages from these deposits and from underlying deposits constrain the age to about 600 - 400 cal yr B.P. (**Figure 2-8**).

Because the flood deposits recognized by Ostenaar et al. (1999, 2002) and in the trenches for this study appear to be associated with H2 geomorphic surface, one constraint for the discharge of this paleoflood is that the discharge be large enough to inundate the full extent of this surface throughout the study reach. As shown by the plots in **Appendix D - Electronic Supplement** that cover the entire study reach and the individual study area plots (**Figure 2-12** through **Figure 2-56**) this constraint is met for modeled discharges between 100 to 130 m³/s. The most strongly limiting sites for the lower discharge limit of this flood appear to be the H1-2 surface in the vicinity of trench T6 (**Figure 2-33**) and at the BLR8 study site near trench T8a (**Figure 2-46**). Modeled discharges of only slightly less than 130 m³/s are required at both of these sites to inundate the extent of flood deposits (T6 - **Section 2.3.2.3**) or young erosion (T8a,b - **Section 2.3.3.1**).

An upper limiting discharge for this paleoflood is derived from the observation that in trenches T4, T5, and T6 (**Section 2.3.2**) deposits of the "400-year" paleoflood overlie only slightly eroded soils formed in older flood deposits. At T8a,b (**Section 2.3.3.1**), preservation of Bk horizons in older flood deposits suggests that the primary record of the "400-yr" paleoflood at that site is only limited erosion of upper-most soil horizons. Comparison of unit stream power and bed shear stress values from the subareas that include these sites, and other H1-2 surfaces in the study reach indicates that once discharge exceeds about 175 m³/s, the criteria for terrace erosion is being exceeded at multiple sites throughout the reach (**Table 3-3** and **Figure 3-6**). Thus, if the paleoflood discharge exceeded 175 m³/s, much more extensive erosion should have been associated with these deposits in the trench exposures. Discharge in the range of 130 - 175 m³/s is consistent with the muted expression of earth mounds on the large area of P3 surface northwest of trench T1

(**Plate 2** and subarea FP 6, **Figure 3-4**). In this discharge range, unit stream power and bed shear stress criteria for soil erosion are exceeded over most of this surface (**Appendix D - Figure D3-11** and **Figure 3-6**). In the same discharge range, minor flow is initiated through the braid channel traversed by trench T1, consistent with soils and stratigraphy in the trench and nearby geomorphology (**Section 2.3.1.1**). However, for discharge greater than $175 \text{ m}^3/\text{s}$, unit stream power and bed shear stress increase in this channel (e.g., **Figure 2-15**) implying that significant erosion would be expected.

3.3.3 "Older Flood". Trench and bank exposures along the H1-2 surface all demonstrate that the deposits of the "400-yr" paleoflood overlie eroded soils developed in slightly older, similar flood deposits (Ostenaar et al., 1999, 2002; and **Section 2.3**). The soils in these deposits are generally similar, or slightly more developed than soils developed in the past 400-600 years. This implies a similar length of time over which no flood either eroded or resulted in significant deposition over these deposits. Likewise, the limited extent of the deposits of the "400-yr" flood relative to the H1-2 surface indicate that overall, the surface must be a composite of deposits with similar origins, but differing ages. The significant scatter in radiocarbon ages from site to site, and the variability in soils that underlie the "400-yr" flood deposits appear to support this concept. As shown on **Figure 2-8**, there is much less correlation of the potential time brackets for a single older flood than for the "400-yr" paleoflood and some possibility that multiple floods may have occurred in the time interval since about 3000 cal yr B.P. However, both the stratigraphic and the chronologic resolution to define multiple floods in this time period are lacking in the present exposures. The existing age constraints appear to indicate that a conservative age range for this flood would lie in the range of 2000 to 1000 Cal yr B.P.

The discharge range estimate (**Table 3-5**) for older flood(s) represented within deposits that underlie the H1-2 surface is similar to that for the "400-yr" flood. A minimum discharge must inundate the full extent of the H1-2 surface; an upper limiting discharge must not impose unit stream power and bed shear stress loads that would result in erosion of underlying and adjacent deposits. For these reasons, the same range of discharge, $130 - 175 \text{ m}^3/\text{s}$, is judged to be appropriate for possible "older" paleofloods as for the "400-yr" paleoflood. The spatial extent, and depth of flow, associated with this range of discharge envelopes all of the stratigraphic and

geomorphic evidence of Holocene paleofloods that has been observed along the Diversion Dam study reach (**Section 2.4**).

3.4 Age and Discharge Estimates for Paleohydrologic Bounds

The geologic data show that over different time intervals and areas along the Big Lost River, there is evidence of relative geomorphic stability. Thus, the preservation of paleoflood deposits as the surface units on portions of the H1-2 geomorphic surfaces shows that no floods large enough to modify or remove these deposits have occurred since the time of those paleofloods. As summarized in **Section 2.4**, there is stratigraphic and geologic data along the Big Lost River that allows for defining three paleohydrologic bounds that span differing time intervals over the past 10,000 years (**Table 3-5**). Geomorphic mapping delineates the characteristics and extent of surfaces of similar age that are potentially useful as paleohydrologic bounds (**Section 2.1.2**). Stratigraphic data from trenches and exposures defines the characteristics of the surfaces and the evidence for relative surface stability over time. Geologic age-dating methods provide the absolute ages and uncertainty ranges (**Section 2.3** and **Figure 2-8**). Estimates of discharge ranges for the paleohydrologic bounds are based on the hydraulic modeling results (**Section 2.5**) and the approaches discussed above in **Section 3.2**. The basis for reaching age and discharge conclusions for each of the paleohydrologic bounds is discussed separately below. Summary data for discharge limits from each subarea are compiled in **Table 3-3**. **Table 3-4** summarizes the applicability of each subarea to evaluation of the individual paleofloods and paleohydrologic bounds.

3.4.1 400-yr Flood Bound. In trenches at the Saddle Constriction study area, deposits of a paleoflood with an age of 400- to 600- years are the parent materials of the surface soils (**Section 2.3.2**). Weakly developed soils developed in the flood deposits at these sites indicate that no significant erosion or deposition by other floods or other geomorphic processes have disrupted these surfaces in that time span. Similar relationships, preserved at multiple sites, demonstrate stability of these surfaces since the time of the "400-yr" flood, approximately 400- to 600-years ago (**Section 3.3.2**). Even at trench T4, where the "400-yr" deposits are buried by thin deposit of a younger paleoflood, the soil profile in the underlying deposits is intact, indicating that this site was not significantly eroded by that flood (**Section 3.3.1**), and hence has been stable since

deposition 400-600 years ago. Throughout the reach, the H1-2 surfaces which include these deposits are unmodified by younger erosion (**Section 2.2.3** and **Plate 2**).

The H1-2 surfaces and deposits of the "400-yr" flood are preserved in many differing hydraulic settings throughout the Diversion Dam study reach. Thus, for use as a paleohydrologic bound, some of these sites are much more strongly limiting than others (**Section 3.2.1.2**). In particular, at Trench T4, unit stream power and bed shear stress increase very rapidly with increasing discharge (**Figure 2-31**, **Figure 2-32**, and subarea FP12 in **Table 3-3** and **Appendix D - Figure D3-17**). These data indicate that this site would be likely be subject to significant soil erosion at a discharge exceeding about 100 m³/s, and terrace erosion once discharge exceeded 110-120 m³/s. Modeled values of unit stream power and bed shear stress in this discharge range increase even more rapidly near trench T8c in subarea 20 at the BLR8 study area (**Figure 2-45** and **Figure 2-46**, **Table 3-3** and **Appendix D - Figure D3-25**), where no deposits clearly younger than 400- to 600-years are present (**Section 2.3.3.1**). Unit stream power and bed shear stress values from subarea 17, located on an unmodified H1-2 surface midway between the Saddle Constriction and BLR8 study areas (**Figure 3-4**), also increase rapidly (**Appendix D - Figure D3-22**). Compiled unit stream power and bed shear stress results from subareas throughout the reach show that large areas of the "400-yr" flood deposits would likely be subject to significant soil erosion at relatively low discharges (**Figure 3-6**). In contrast to estimating the discharge for the paleoflood, no requirement to inundate the entire H1-2 surface is imposed. Preservation and demonstration of stability at multiple sites which provide strongest limits on the discharge which might modify these sites is sufficient basis to establish the paleohydrologic bound (**Section 3.2.1.2**). Thus, the discharge limits for the paleohydrologic bound based on the deposits of the "400-year" paleoflood can be somewhat smaller than the discharge estimated for the paleoflood, because even a smaller flood would have a high likelihood of modifying extensive areas of the "400-year" deposits (**Table 3-5**). As discussed above, there are several sites where modification of the "400-year" flood deposits becomes increasingly certain for discharges above 110 m³/s. To characterize the discharge range of the paleohydrologic bound, a modified triangular distribution of relative likelihood is used, with a lower discharge limit of 110 m³/s. A peak is chosen at 130 m³/s, with uniform likelihood extended to 150 m³/s (see **Figure 4-1**).

3.4.2 Early Holocene (H1 surfaces) Bound. The stratigraphic evidence to support this paleohydrologic bound is the preservation of extensive areas of generally fine-grained fluvial sediments with well-developed carbonate soils that underlie the H1-2 surfaces. The most extensive exposures of these sediments and soils are in trench T6, stations 1 to ~30, and in the disconnected sequence of trenches at BLR8 study area, T8a,b,c (**Section 2.3.2.3, Section 2.3.3.1, and Appendix B - Electronic Supplement**). Smaller remnants are present at T4, stations 16 to 20 (**Section 2.3.2.1 and Appendix B - Electronic Supplement**), and at BLR6 (Ostenaar et al., 1999, 2002). These deposits and soils apparently are part of an aggradational fill of latest Pleistocene to early Holocene age (**Section 2.2.3**). Stage II carbonate soil horizons in these deposits are generally 50- to 100 cm thick, indicative of an early Holocene age for stabilization of the surface, and radiocarbon ages from these deposits ranging from about 7200 to 12,800 cal yr B.P support this age (**Section 2.2.3 and Section Table 2-2**). Based on these data, a conservative time interval of 6000 to 8000 years has been chosen for use as a paleohydrologic bound. Most of radiocarbon ages from these sites are older than this range, but the shorter time interval reflects the possible interpretation that aggradation of the sequence continued and the surfaces did not stabilize and begin forming soils until later.

There are fewer sites that constrain discharge estimates for this paleohydrologic bound than for the bound based on the "400-yr" flood (**Table 3-4, compare Figure 3-6 and Figure 3-7**). Discharge constraints based on the exposures at trenches T6 (subarea FP13) and T8a,b (subarea 20) (**Figure 3-7**) indicate that unit stream power and bed shear stress at these sites are high enough and extensive enough to indicate significant terrace erosion at these sites for discharges of $175 \text{ m}^3/\text{s}$ and larger. The H1-2 surface at FP17 (**Figure 3-4**) is similarly impacted. Many sites on Pleistocene P3 surfaces (**Section 2.2.2**) are significantly affected by modeled flows of $175 \text{ m}^3/\text{s}$ and larger as well. Terrace erosion is likely initiated in extensive areas of subareas FP6 and FP8 (**Figure 3-4 and Figure 3-7**), both sites that show geomorphic evidence of the "400-yr" flood (**Section 3.3.2 and Plate 1**). Results also indicate the initiation of soil erosion at sites on the older Pleistocene P2 surfaces (**Section 2.2.2**), such as in subareas FP5 and FP16 (**Figure 3-4 and Figure 3-7**). The geomorphology in these areas indicates that they are beyond the limits of any Holocene floods (**Section 2.4 and Plate 1**). For discharges larger than $250 \text{ m}^3/\text{s}$, judged to be the upper confidence limit for this paleohydrologic bound, significant terrace erosion is indicated for all the

subareas (**Figure 3-7**). At larger discharges, flow also overtops the saddle area (**Section 2.5.1.4**) and impacts significant areas in, and adjacent to, subareas FP14 and FP15.

The paleohydrologic bound based on the early Holocene deposits (**Table 3-5**) potentially includes some conservatism in the time estimates for the bound, 6000 to 8000 years, in that most of the dating results indicate these deposits are likely somewhat older. The discharge range used for this bound, 175 to 250 m³/s, is a range of values beyond any observed evidence for Holocene floods in the Diversion Dam study reach of the Big Lost River.

3.4.3 Pleistocene Bound. The extensive areas of unmodified Pleistocene surfaces that flank the Big Lost River are the stratigraphic and geomorphic basis for this paleohydrologic bound (**Table 3-5**). The Pleistocene P2 surfaces have a braid-channel morphology that is inherited from Pleistocene gravel deposition and unrelated to present flows in the Big Lost River (**Section 2.2.2**). The more limited areas of Pleistocene P3 surfaces generally follow the present river channel and are also underlain by gravels, and likely represent the last episode of Pleistocene deglaciation (**Section 2.2.2**). Trench exposures in T6, T7, T8 and T9 indicate that the last phase of deposition on these surfaces was aggradation of fines in small channels on the P3 surfaces (**Section 2.2.2**, **Section 2.3.2**, and **Section 2.3.3**). Subsequent deposition, shown by the inset deposits that underlie the Holocene surfaces has been dominated by fines. Soils on the Pleistocene surfaces are characterized by an upper loess cap, generally less than 0.5-m-thick in the Diversion Dam study reach and well-developed carbonate morphology (**Section 2.2.2**). The Pleistocene age of both the P2 and P3 surfaces is established regionally by depositional links to regional glaciation, and in a local context by radiocarbons ages of ~10,000 to 12,800 cal yr B.P. obtained from the inset fine-grained deposits (**Section 2.2.2** and **Table 2-2**).

The lower discharge limits for the Pleistocene bound are based on discharges at which significant terrace erosion is indicated on the P3 surfaces, mostly in areas that are slightly modified by the "400-yr" paleoflood (**Figure 3-8**). Within subareas FP6, FP8, and FP19, discharges of 225 m³/s and larger result in unit stream power and bed shear stress values over extensive areas that exceed upper limits for soil erosion and indicate significant potential for terrace erosion. In addition, near this discharge, model results indicate that flow is initiated over multiple locations near the Saddle area (**Section 2.5.1.4**), which produces localized areas with large values of unit stream power and

bed shear stress on the Pleistocene surfaces just downstream. Over broad areas of the Pleistocene surfaces, increasing discharge leads to progressive increases in the extent of significant soil erosion and localized channeling. As discharge approaches 400 m³/s, considered the upper discharge limit for this bound, unit stream power and bed shear stress values reach or exceed the preferred values for terrace erosion over significant portions of all the subareas located on the Pleistocene surfaces. The majority of these exceedences are concentrated braid channels such as those traversed by trenches T1, T2, T3, and T7 where the Pleistocene deposits and soils demonstrate long-term stability of these surfaces and channels (**Section 2.4**).

3.4.3.1 Catastrophic Channel Change. An alternative approach to determine discharge estimates for bounds over long, but non-specific time frames is to estimate the discharge which might result in "catastrophic" channel change (**Appendix D** and **Figure 3-3**). Unlike other estimates, this approach is not specific to the conditions of the Big Lost River, with the caveat that only in reaches where the channel banks are mostly composed of alluvium does this approach apply.

For each of the channel subareas (**Figure 3-4**), a range of values for catastrophic channel change is evaluated based on the subarea results, (**Figure 3-9**; derived from **Appendix D - Figures D3-29 to D3-37**), and the channel profile plots (**Figure 2-9**). A minimum discharge range for bounds has been estimated from the plots based on approximately 10 percent of the channel subarea exceeding the minimum criteria for either unit stream power >200 W/m² or bed shear stress >100 N/m², realizing that some subareas have sections with rock channels and minimum values should be higher in those subreaches (see **Table 3-2** for descriptions of individual channel subareas). A preferred value is taken when there is significant exceedence on the plots (**Appendix D - Figures D3-29 to D3-37**), of the 400 W/m² or 200 N/m², and these exceedences are apparent as well on the channel profile plots (**Figure 2-9**). The existence of large areas of rock outcrops in the channel is a factor that will make this approach non-conservative, but is hard to quantify. Modeling does not extend to large enough discharges to estimate a true upper bound; and this approach is inherently subjective, but we do expect these values to have a degree of consistency with the estimates of paleohydrologic bounds that have durations of thousands of years.

Results from each subarea combined are shown on **Figure 3-9**. A bounding range of discharge that would be associated with catastrophic channel change on this reach of the Big Lost River is judged to be 250 - 450 m³/s based on the compiled results. Within this range five of the subreaches exceed the basis for reaching preferred values. Subarea CH1 is largely discounted because it may include some effects due to flow initiation in the upstream portion of the model, especially for larger flows and because long portions of this subreach include rock channels. Subareas CH4 and CH7 also include significant sections of rock outcrop, but are also representative of the types of sites where empirical data on which this approach is based might have been collected (**Appendix D**). The absence of higher values of unit stream power or bed shear stress in subareas CH3, CH6, and CH8 results from flow stagnation due to downstream channel constrictions (**Section 2.5.1.4**).

Evaluation based on catastrophic channel change is not linked directly to a time period associated with a specific paleohydrologic bound or used subsequently in the flood frequency analyses. For the Big Lost River, these results appear to qualitatively support the range of bounds independently evaluated for periods of 1000's to 10,000 years. Thus, the occurrence of floods with discharges that appear likely to significantly modify the Pleistocene surfaces (**Section 3.4.3**), would also be considered "catastrophic" in a geomorphic sense.

Figures for Section 3.0

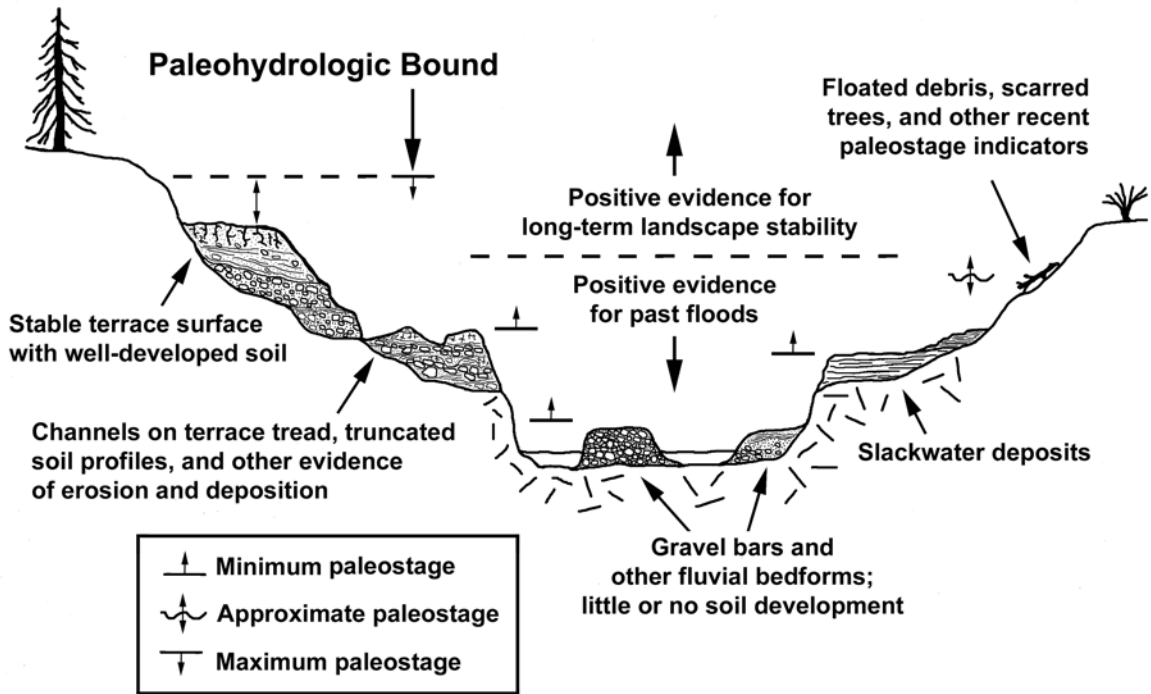


Figure 3-1 Schematic representation of different types of geomorphic and stratigraphic evidence for paleofloods and paleohydrologic bounds.

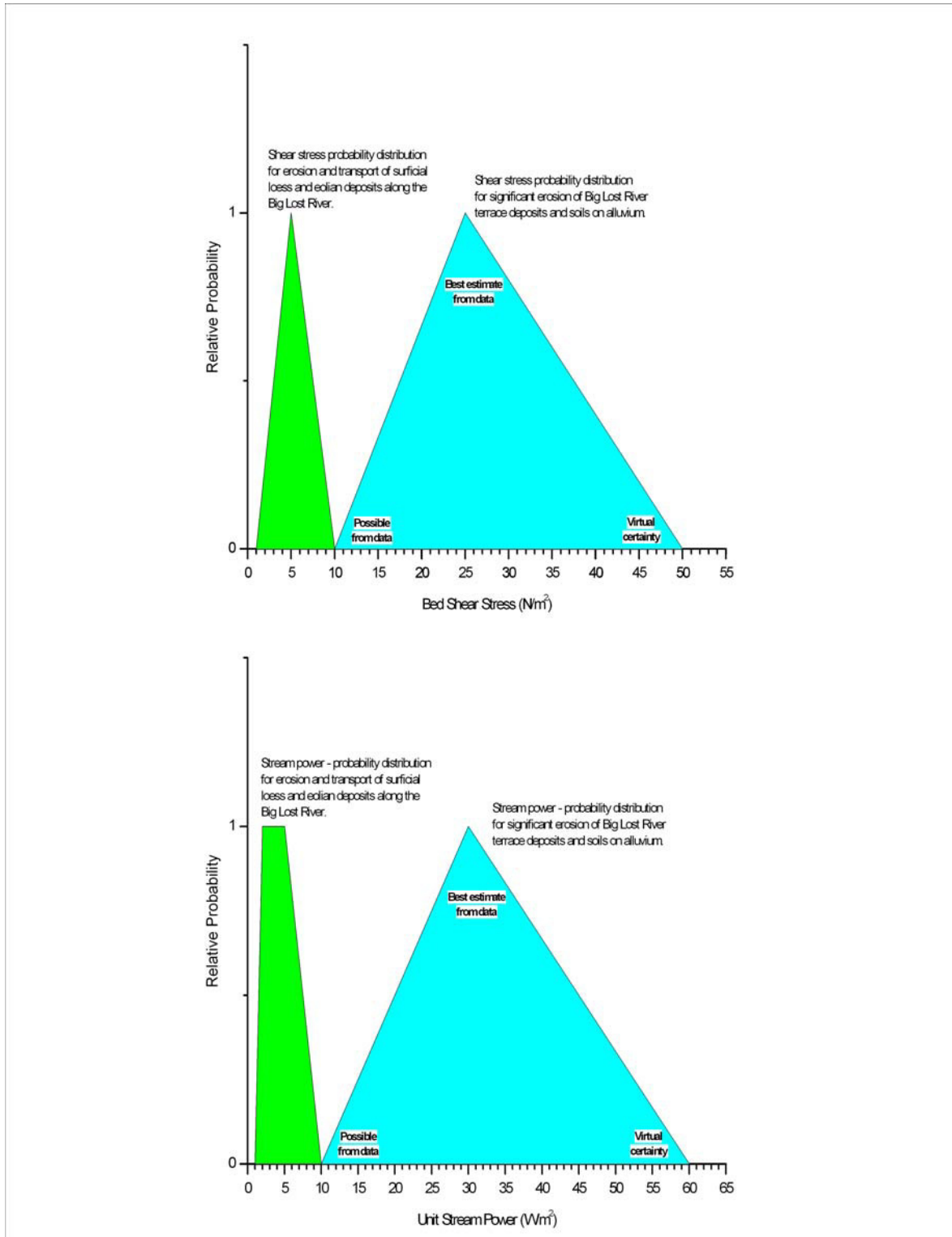


Figure 3-2 Probability density functions for erosion based on shear stress and stream power for Big Lost River applications. See Appendix D for discussion of data used to define these distributions

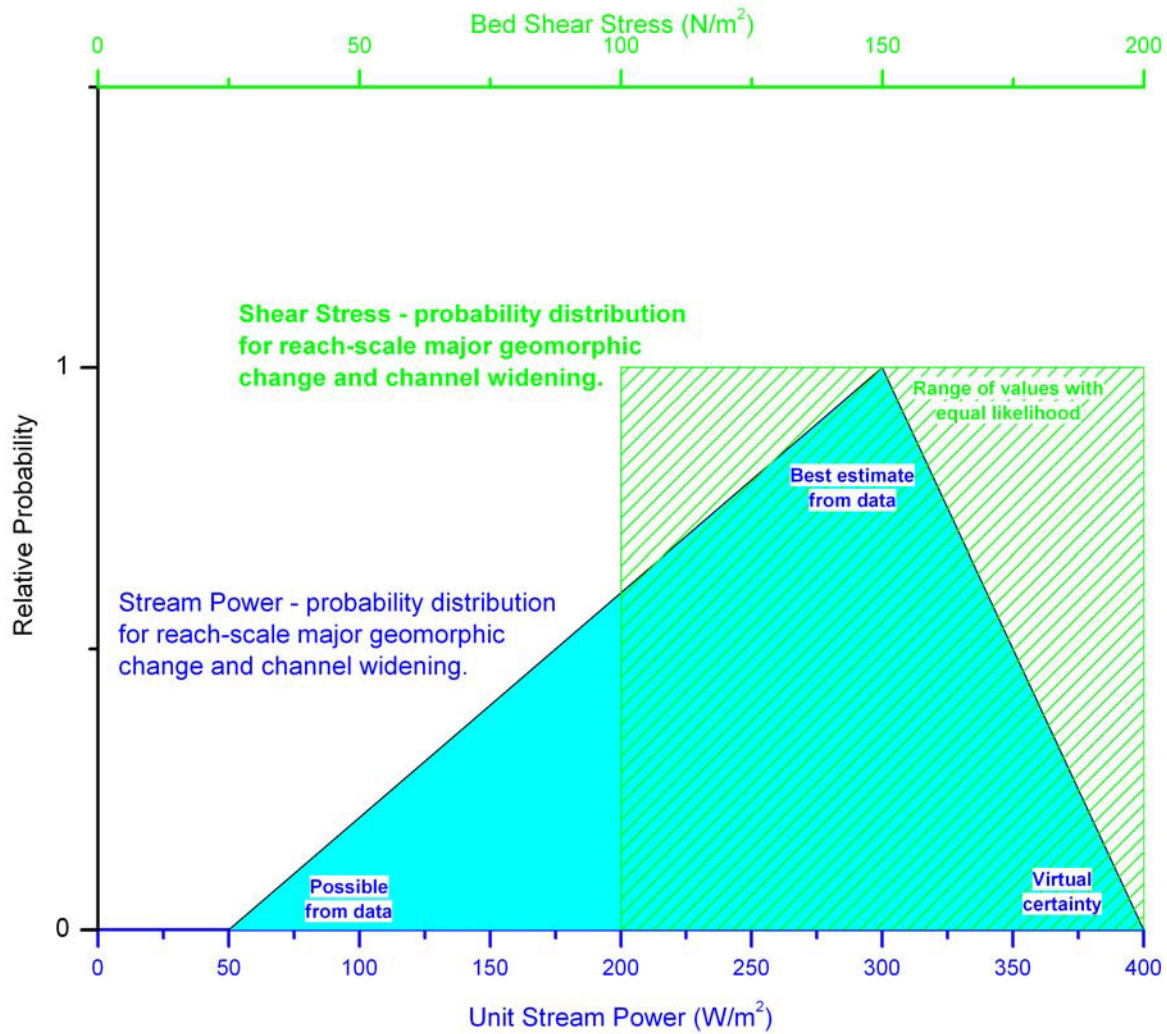


Figure 3-3 Probability distributions for major channel modifications based on channel averaged stream power and shear stress values. See Appendix D for discussion of data used to define these distributions

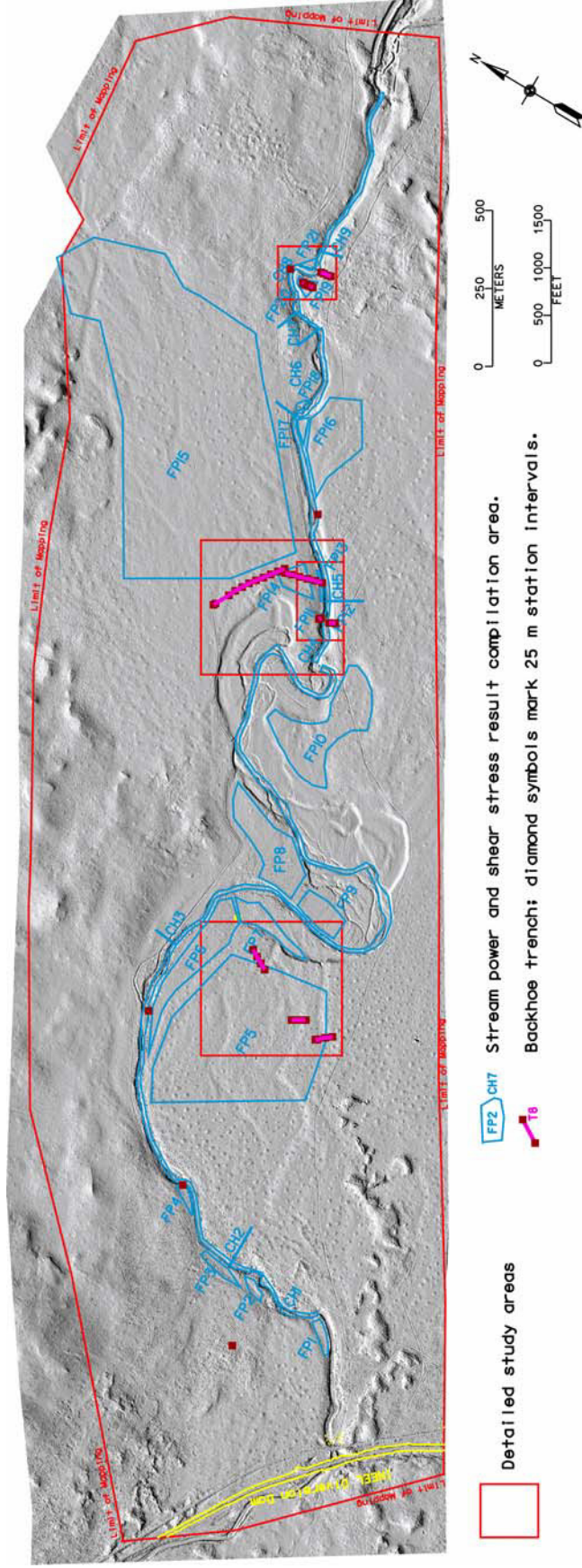


Figure 3-4 Stream power and shear stress sample areas along Big Lost River Diversion Dam study reach. See Table 3-1 and Table 3-2 for summary of characteristics of each subarea.

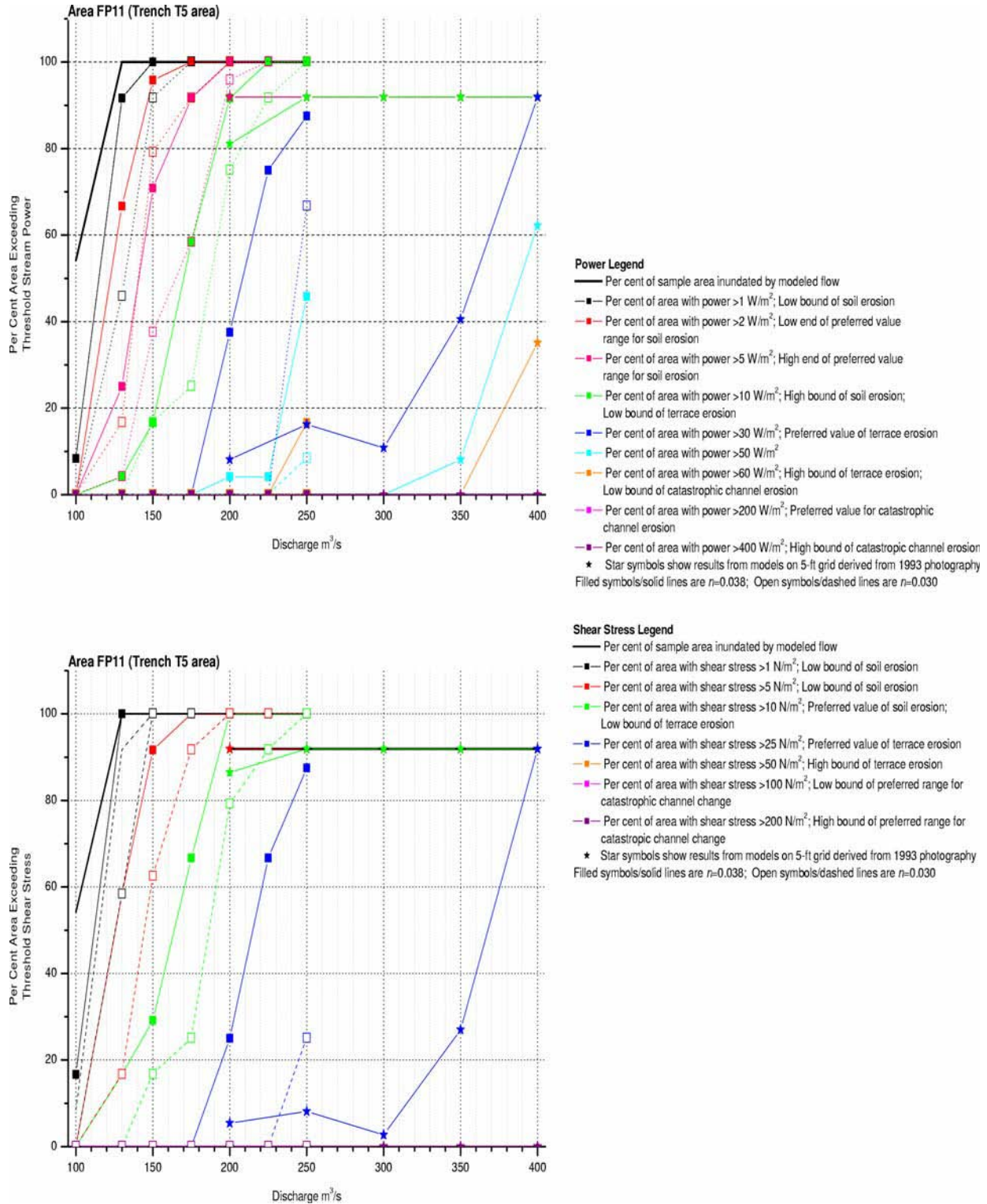


Figure 3-5 Example of stream power and shear stress results for subarea FP11. Colored lines and symbols correspond to key values (listed in legend above) on the PDF of **Figure 3-2**. Each symbol represents the percent area exceeding the threshold values for a single flow simulation. Colored lines between symbols represent change between simulations of different discharge. Lines with colored stars are data from models on 5-ft grid derived from 1993 photography.

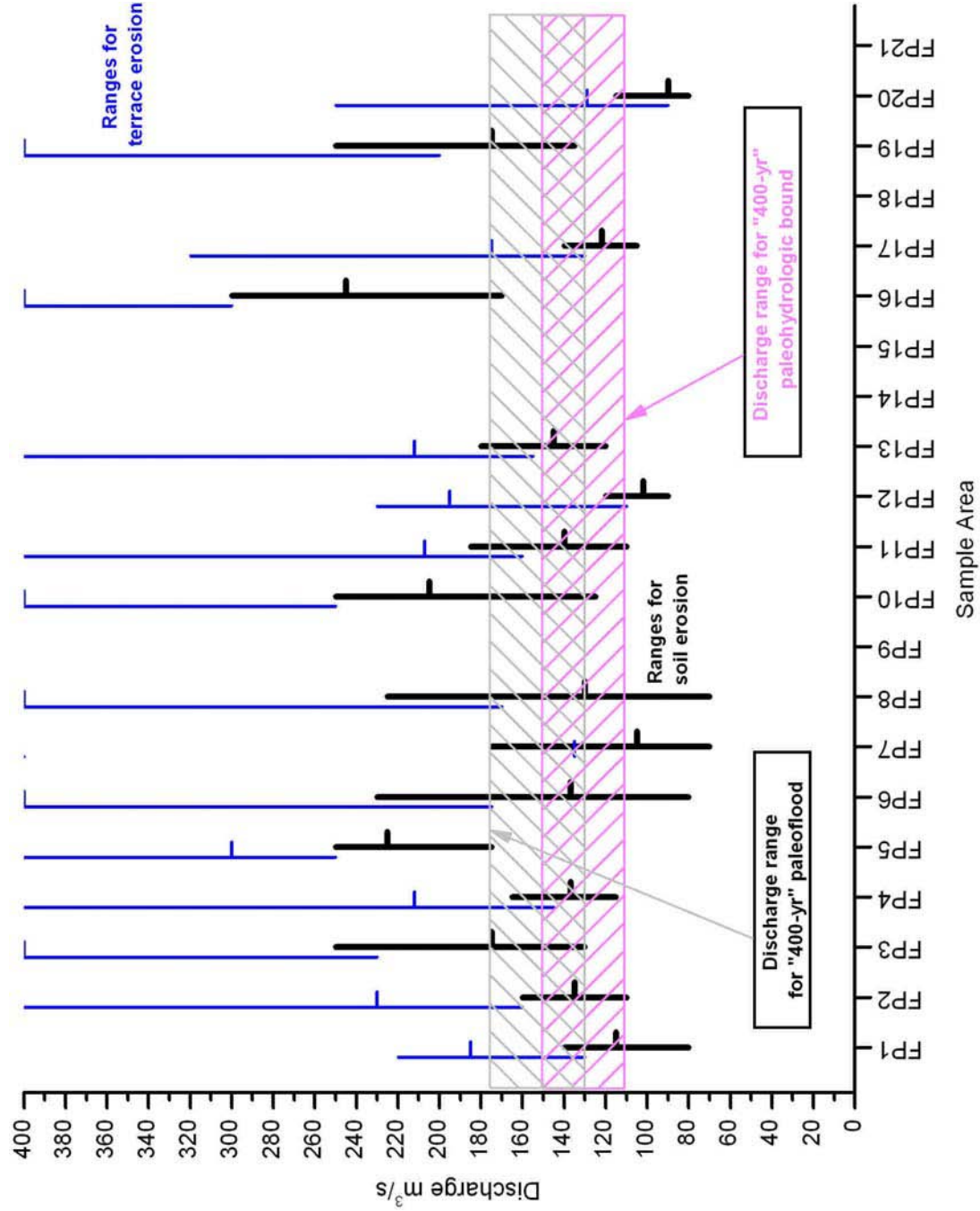


Figure 3-6 Combined discharge limits for late Holocene paleofloods and paleohydrologic bounds. Estimated discharge ranges for soil erosion, black bars and terrace erosion, blue bars are from (Table 3-3). Gray cross-hatching shows discharge range for paleofloods; magenta cross-hatch shows range for paleohydrologic bound (Table 3-5). See (Figure 3-4) for sample area locations, (Table 3-4) for applicability, and (Table 3-1) for sample area descriptions.

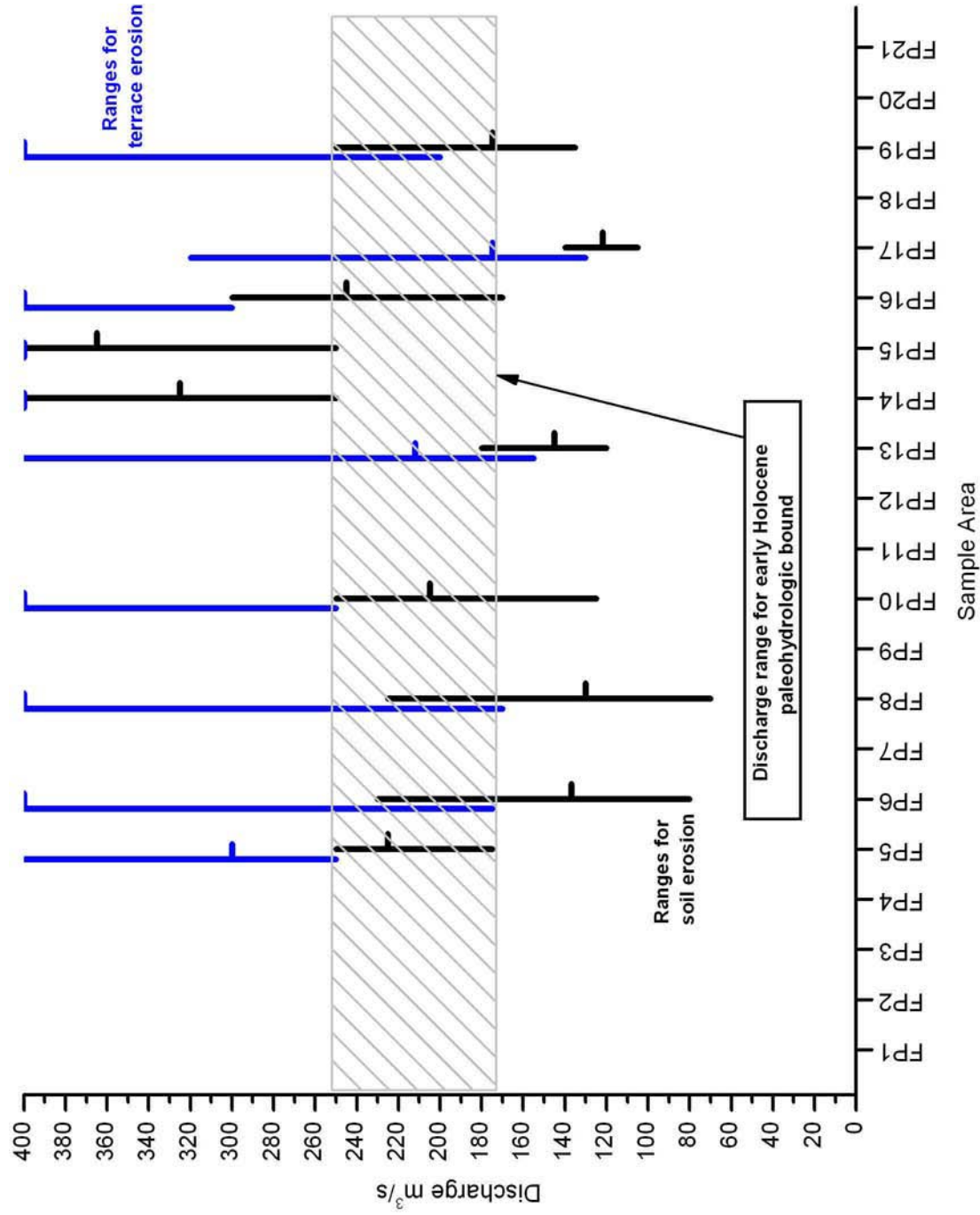


Figure 3-7 Combined discharge limits for early Holocene paleohydrologic bound. Cross hatching shows discharge range for early Holocene (T1) paleohydrologic bound (Table 3-5). See (Figure 3-6) for additional explanation of symbols.

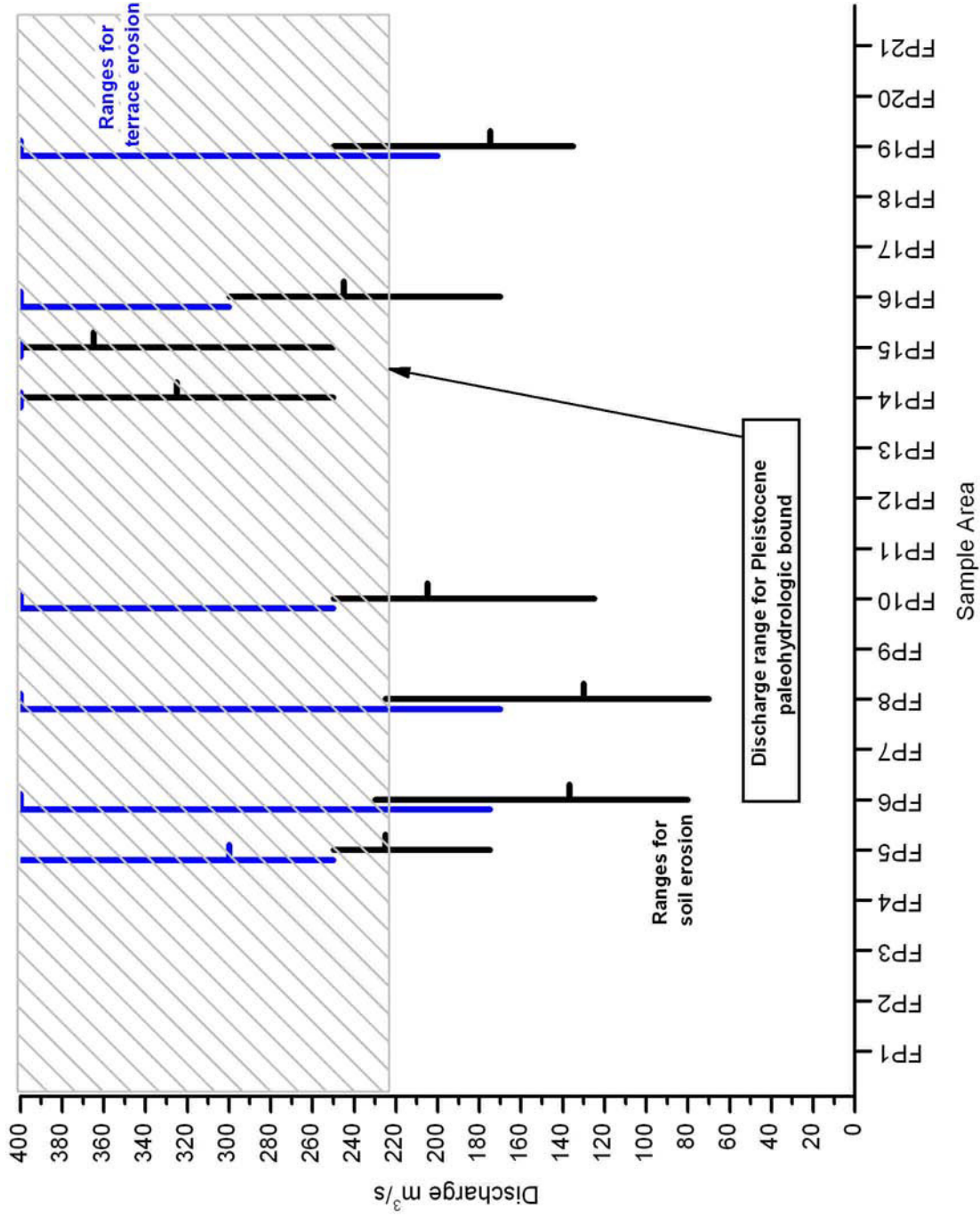


Figure 3-8 Combined discharge limits for Pleistocene paleohydrologic bound. Cross hatching shows discharge range for Pleistocene paleohydrologic bound (Table 3-5). See (Figure 3-6) for additional explanation of symbols.

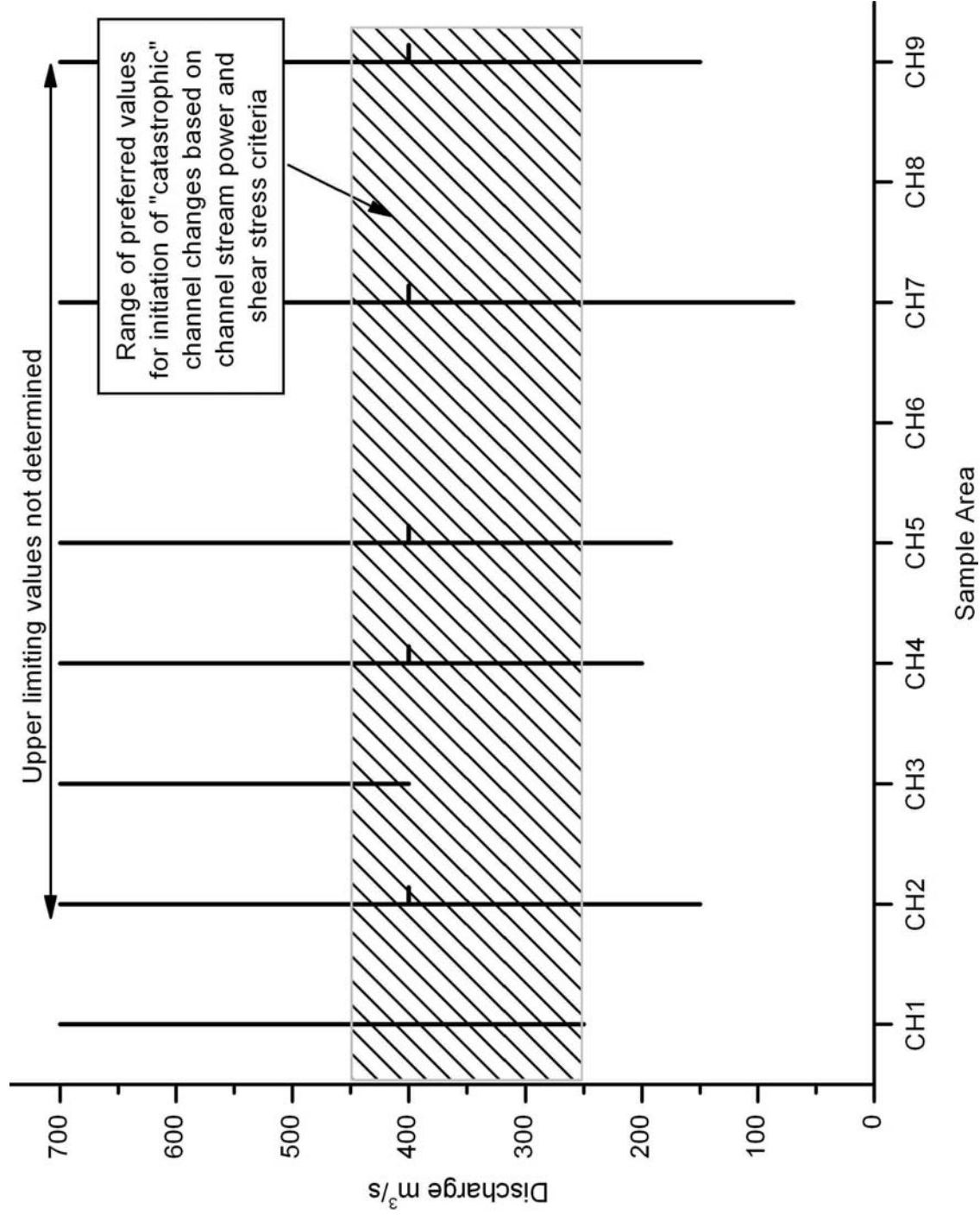


Figure 3-9 Combined discharge limits for catastrophic channel change. Upper limiting values are arbitrarily plotted at 700 m³/s. See **Figure 3-6** for additional explanation of symbols. Sample area descriptions are in **Table 3-2**. Subarea data from **Appendix D, Figure D3-27** through **D3-37**.

Tables for Section 3.0

Table 3-1 Hydraulic modeling sample area characteristics - floodplain subareas

Sub-area	Area and Number of Cells		Geomorphic and Geologic Characteristics					
	Number of 6-ft cells ¹	Area		Map unit and surface morphology	Surficial deposits /soil	Underlying deposits	Trenches or sites	Other
		ft ² (m ²)	acres (hectare)					
FP1	902	32472 (3017)	0.74 (0.30)	H1-2; smooth terrace surface	silt and sand	not exposed	n.a	Beginning of model reach
FP2	595	21420 (1990)	0.49 (0.20)	H3 and Rd; overflow channel; and basalt outcrop	silt and sand in channel; rock outcrop	basalt(?)	n.a.; Juniper Bends site	Probable flow in channel from pre-INEEL Diversion floods
FP3	1068	38448 (3572)	0.88 (0.36)	H1-2 onlap onto Qbd outcrops	silt and sand; minor areas of basalt	Thin(?) veneer of fluvial sediment over basalt	n.a.; Juniper Bends site	
FP4	538	19368 (1799)	0.44 (0.18)	H2; smooth terrace surface	silt and sand	> 1m of fine sediment	BLR7 on d/s edge	
FP5	60286	2170296 (201627)	49.69 (20.11)	P2; subdued braided channels with large earth mounds	silt and sand with local pavement	±0.5 m silt and sand overlying gravel	T1, T2, T3	
FP6	9435	339660 (31555)	7.78 (3.15)	P3/H1-2; smooth terrace; few muted earth mounds	silt and sand	grave(?)	n.a.	BLR2 is on inset terrace at upstream end of FP6 area
FP7	3390	122040 (11338)	2.79 (1.13)	H1-2; mostly smooth surface; minor channels	silt and sand	(?)	n.a.	
FP8	10401	374436 (34786)	8.57 (3.47)	P3/H1; smooth terrace; few muted earth mounds	silt and sand	thin silt and sand grave(?)	n.a.	Historical irrigation ditch on u/s side is not eroded; historical use as field or pasture
FP9	3469	124884 (11602)	2.86 (1.16)	H2/H3; mostly smooth terrace with channels on lower portion	silt and sand	(?)	n.a.	Historical irrigation ditch on u/s side is not eroded; historical use as field or pasture

Notes: ¹ For 5-ft grid models, average number of cells is ~145% of number of 6-ft grid cells.

Table 3-1 Hydraulic modeling sample area characteristics - floodplain subareas

Sub-area	Area and Number of Cells		Geomorphic and Geologic Characteristics					Other
	Number of 6-ft cells ¹	Area ft ² (m ²)	acres (hectare)	Map unit and surface morphology	Surficial deposits /soil	Underlying deposits	Trenches or sites	
FP10	15504	558144 (51853)	12.78 (5.17)	P3/H1; smooth terrace; few muted earth mounds; eroded d/s margin	silt and sand	silt and sand overlying gravel(?)	n.a.	Western portion eroded; earth mounds more prevalent in eastern half; Affected by backwater from saddle constriction
FP11	24	864 (80)	0.02 (0.01)	H1-2; smooth terrace and riser to P2 surface	silt and sand	basalt outcrops in stream bank	T5	
FP12	23	828 (77)	0.02 (0.01)	H1-2; small area between basalt outcrops	silt and sand	basalt outcrops in banks; gravel on higher surface	T4	
FP13	236	8496 (789)	0.19 (0.08)	H1-2; long, narrow, smooth terrace	silt and sand	>1 m fine sediments	T6	
FP14	2095	75420 (7007)	1.73 (0.70)	P3; minor eolian sand; smooth terrace surface	silt and sand	<0.5 m silt and sand overlying gravel	T6	
FP15	152753	5499108 (510884)	125.90 (50.95)	P1-2; subdued braided channels with large earth mounds; minor areas of eolian sand sheets	silt and sand	±0.5 m silt and sand overlying gravel	T7	Several wheel tracks; includes circular area cleared as target for old bombing range

Notes: ¹ For 5-ft grid models, average number of cells is ~145% of number of 6-ft grid cells.

Table 3-1 Hydraulic modeling sample area characteristics - floodplain subareas

Sub-area	Area and Number of Cells		Geomorphic and Geologic Characteristics					
	Number of 6-ft cells ¹	Area ft ² (m ²)	acres (hectare)	Map unit and surface morphology	Surficial deposits /soil	Underlying deposits	Trenches or sites	Other
FP16	10913	392868 (36499)	8.99 (3.64)	P2/P3; braided channels with large earth mounds	silt and sand	±0.5 m silt and sand overlying gravel(?)	n.a.	T6 is on inset terrace near upper end of area
FP17	477	17172 (1595)	0.39 (0.16)	H1-2; smooth terrace	silt and sand	(?)	n.a.	
FP18	199	7164 (666)	0.16 (0.07)	Rb; scoured basalt outcrop	basalt; minor sand and silt	basalt	n.a.	
FP19	427	15372 (1428)	0.35 (0.14)	H1; smooth terrace surface	silt and sand	silt and sand; minor fine gravel	T8b,c	
FP20	178	6408 (595)	0.15 (0.06)	H2; smooth terrace surface	silt and sand	silt and sand; increasing gravel away from channel	T8a,b	BLR8 on similar inset surface across channel
FP21	266	9576 (890)	0.22 (0.09)	Rb; scoured basalt outcrop	basalt; minor silt and sand	basalt	n.a.	

Notes: ¹ For 5-ft grid models, average number of cells is ~145% of number of 6-ft grid cells.

Table 3-2 Hydraulic modeling sample area characteristics - channel subareas

Sub-area	Number of Cells ¹ , Area ² and Length		Geomorphic and Geologic Characteristics		Notes		
	Number of 6-ft cells	Area		Channel form		Bed/bank materials	
		ft ² (m ²)	acres (hectare)				Length ft (m)
CH1	1305	46980 (4365)	1.08 (0.44)	1154 (352)	Mostly straight with small amplitude bends. Single thread; rock controlled.	Common rock outcrops in bed and banks with rock constrictions; long section of fluted and scoured rock bed. Some banks of P2 gravels and fine-grained lateral accretion deposits (H1/H2/H3).	"Juniper Bends area"
CH2	4533	163188 (15161)	3.74 (1.51)	3773 (1150)	Gently curving; one sharp bend at BLR2 (FP4). Single thread.	Scattered rock outcrops in bed throughout length; some rock in banks near and upstream of BLR2 (FP4). Bed mostly sand and fine gravel. Right bank mostly fine-grained lateral accretion deposit (H1-2) against P2 gravel. Left bank mostly H2/H3 fine-grained deposits.	BLR2 and BLR7 bank exposures are in this reach.
CH3	9920	357120 (33178)	8.18 (3.31)	7830 (2387)	Large amplitude s-bends; tighter radius at downstream end. Single thread at upstream end, multi thread in central portion of meanders.	Sand and gravel in bed and banks. Rock outcrops in bed and banks are limited to scattered occurrences at downstream end of sample area just upstream of Saddle constriction. Bank materials are heterogeneous mix of silty/sandy alluvium and gravel of all ages.	"Big Loop"

Notes: ¹ For 5-ft grid models, average number of cells is ~145% of number of 6-ft grid cells.

² Channels are oblique to orientation of rectangular grid in most areas. Sample areas are defined along base of bank for low-flow channel. At most sections, this typically includes 3-5 cells across channel floor, so typical width is about 5-9 m (~18-30 ft).

Table 3-2 Hydraulic modeling sample area characteristics - channel subareas

Sub-area	Number of Cells ¹ , Area ² and Length		Geomorphologic and Geologic Characteristics			Notes	
	Number of 6-ft cells	Area		Channel form	Bed/bank materials		
		ft ² (m ²)	acres (hectare)				Length ft (m)
CH4	877	31572 (2933)	0.72 (0.29)	668 (204)	Straight reach with very gentle s-bend and large rock constrictions. Single thread, rock controlled.	Bed is mostly sand and gravel with scattered rock outcrops. Rock section in bed just upstream. Banks are controlled by rock outcrops. Intervening bank areas are H1/H2 lateral accretion terraces.	"Saddle constriction". Trench sites T4 and T5 (FP11 and FP12) are adjacent to the downstream portion of this reach.
CH5	2444	87984 (8174)	2.01 (0.82)	1965 (599)	Mostly straight reach. Single thread.	Bed is gravel. Right bank mostly P2/P3 gravel with narrow H1/H2 lateral accretion terrace and few rock outcrops. Left bank is wider H1/H2 terrace.	Trench T6 is on left bank in upstream section; BLR6 is on right bank, mid-reach.
CH6	1322	47592 (4421)	1.09 (0.44)	1030 (314)	90° bend at upstream end; mostly straight with gentle left bends. Single thread with rock control.	Rock in bed near upstream portion. Scattered outcrops in bed downstream, otherwise gravel. Scattered rock outcrops along banks; most banks H1/H2/H3 terraces.	
CH7	198	7128 (662)	0.16 (0.07)	260 (79)	Rock constriction. Straight, single thread.	Gravel bed. Banks are rock, with small areas of fine-grained H1/H2 deposits between outcrops.	"Bridge constriction"
CH8	1195	43020 (3997)	0.98 (0.40)	934 (285)	Tight s-bend with rock controls. Single thread.	Mostly gravel bed with many rock outcrops. Large areas of rock control in middle of reach. Rock banks and constriction on middle/downstream portion. Upstream banks are H2/H3 fine-grained deposits.	BLR8 on right bank mid-reach. T8 and T9 trenches on right banks in middle portion of reach.
CH9	1444	51984 (4829)	1.19 (0.48)	1852 (564)	Mostly straight with gentle bends. Single thread with rock control.	Bed is gravel with several rock outcrops. Right bank has narrow H4 fine-grained terrace along most of length with scattered rock outcrops. Left bank is H2/H3/H4 fine-grained terrace with scattered rock outcrops.	

Notes: ¹ For 5-ft grid models, average number of cells is ~145% of number of 6-ft grid cells.

² Channels are oblique to orientation of rectangular grid in most areas. Sample areas are defined along base of bank for low-flow channel. At most sections, this typically includes 3-5 cells across channel floor, so typical width is about 5-9 m (~18-30 ft).

Table 3-3 Summary of limiting discharge values from hydraulic modeling sample areas

Sample Area	Per Cent Area Meeting Erosion Criteria	Discharge (m ³ /s)					
		Soil Erosion			Terrace Erosion		
		Low Bound	Preferred Value	High Bound	Low Bound	Preferred Value	High Bound
FP1	50	80-110	115	130-140	130-140	170-200	220
FP2	50	110	120-150	160	160	220-240	>400(?)
FP3	50	130-140	160-190	230-250	230-250	>400(?)	>400(?)
FP4	50	115	120-145	145-165	145-165	205-220	350-400(?)
FP5	n.a.*	175	225	250	250	300	400
FP6	50	80-100	115-160	175-230	175-230	>400(?)	>400(?)
FP7	50	<70	<90-125	135-175	135-175	>400(?)	>400(?)
FP8	50	<70	95-160	170-225	170-225	>400(?)	>400(?)
FP9	50	<70	<70	80-100	80-100	250	>400(?)
FP10	n.a.*	125-160	160-250	250	250	>400(?)	>400(?)
FP11	50	110	120-160	160-185	160-185	200-215	>400(?)
FP12	50	90	95-110	110-120	110-120	130-160	160-230
FP13	50	115-120	130-160	155-180	155-180	205-220	270->400(?)
FP14	n.a.*	250	300-350	400-450	400-450	>400(?)	>400(?)
FP15	n.a.*	250	330-400	>400(?)	>400(?)	>400(?)	>400(?)
FP16	n.a.*	170-220	220-270	300	300	>400(?)	>400(?)
FP17	50	105-110	115-130	130-140	130-140	165-185	220-320
FP18	50	60	65-70	80	80	100-110	130-190
FP19	50	135-140	150-200	200-250	200-250	>400(?)	>400(?)
FP20	50	80	90	90-115	90-115	120-140	155-250
FP21	50	30	35	40	40	45-60	60-90

Notes:

* n.a. - Flow in these areas is concentrated in paleochannels where initial erosion would preferentially be concentrated in small portions of the sample area.

Table 3-4 Applicability of hydraulic modeling sample areas to paleofloods and paleohydrologic bounds estimates

Sample Area	Event Name					
	Paleofloods			Paleohydrologic Bounds		
	"white flood"	"400-yr" flood	"older flood(s)"	400-yr #1	early Holocene (H1 surfaces)	Pleistocene
FP1		G		G		
FP2		G				
FP3			G	G		
FP4		S	G	G,S		
FP5			G,S		G	G,S
FP6		G,S	G,S	G,S	G	G
FP7		G		G		
FP8		G	G	G	G	G
FP9	G					
FP10		G	G	G	G	G
FP11	S	G,S	G,S	G,S		
FP12	S	G,S	G,S	G,S		
FP13	S	G,S	G,S	G,S	G,S	
FP14						G,S
FP15						G,S
FP16		G	G	G	G,S	G
FP17		G	G	G	G	
FP18	G					
FP19		S	S	G,S	G,S	G,S
FP20		S	S	G,S		
FP21	G					
Notes: S = Stratigraphic evidence; G = Geomorphic evidence						

Table 3-5 Big Lost River Paleofloods and Paleohydrologic Bounds

Event name	Age or time span (Cal yrs or Cal yr B.P.) ¹	Discharge (m ³ /s) and type of distribution	Summary of Evidence
Paleofloods			
"white flood"	>100yr (pre-gaging) but less than 400-600yr	90 (80-100) uniform	Based on thin deposit in T4. Not recognized in T5 or T6 (slightly higher sites). Possible correlative in T9(?). Age - most likely 100 to 150 years based on absence of soil development. Discharge - Upper limit based on rapid increase in power/shear stress at T4 and lack of deposit in T5/T6.
"400-yr" flood	400 to 600 years	150 (130-175) triangular	Apparently correlative deposits in T4, T5, T6 (also BLR2, BLR7 & BLR8) with similar soils, stratigraphic setting, and radiocarbon ages. Soil has stage I- Bk horizon. Stripping of A- and AB/Bw horizons at T8c, partial stripping at T8b; lack of erosion at T8a. May represent more than one flood.
"older flood"	1000 to 2000 years	150 (130-175) triangular	Deposits with Stage I to I+ Bk horizon that underlie "400-yr flood" deposits in T4, T5, T6 and T9. Appears to indicate long period of stability with little or no deposition at these sites before deposition of deposits associated with "400-yr" flood. Similar stratigraphy at BLR2 and BLR8. Likely represents multiple floods of similar or smaller maximum discharge. Minimum discharge must inundate FP1-FP4, FP6-8, most of FP7, FP11-13, FP17-18, and FP19-21, which are areas with H1-2 geomorphic surfaces that appear to indicate Holocene flooding.
Paleohydrologic Bounds			
400-yr #1	400-600	130 (110-150) triangular	Preservation of recognizable stratigraphy at T4 and T6. No stripping of A-horizons from the youngest deposits at T4 and T6. Apparently correlative H1-2 geomorphic surfaces at FP1, FP3-4, FP7, FP11-13, FP17, and FP19-20.
early Holocene (H1 surfaces)	6000 to 8000	225 (175-250) triangular	Preservation of stratigraphy in T6, T4, and T8a,b,c. Banks at BLR6 and continuity of H1-2 geomorphic surfaces along BLR.
Pleistocene	>10000	250 (225-400) triangular	Preservation of Pleistocene gravel surfaces throughout the study reach. Actual age of the underlying deposits is older than 12-15 ka (minimum age of deglaciation) and some may be older than 20-25 ka (Last glacial maximum). Length of time span for paleohydrologic bound is limited by post-glacial, warmer climate more similar to present.
Notes: ¹ All age distributions have uniform probability over the indicated time span uncertainty.			

4.0 REVISED FLOOD FREQUENCY FOR THE BIG LOST RIVER AT THE INEEL DIVERSION DAM

It is necessary to revise flood frequency estimates for two reasons. First, peak discharge values have been slightly modified for several data points, including the paleohydrologic non-exceedence bounds. Second, the distribution of observed peak discharges and paleohydrologic information is sufficiently complex that parametric flood frequency functions are ill-suited to determine statistical quantities, such as credible or “confidence” limits for flood frequency estimates. Consequently, a newly-published nonparametric Bayesian flood frequency estimation approach (O’Connell, 2005) is used to obtain probabilistic minimum-bias estimates of flood frequency.

4.1 Nonparametric Flood Frequency for the Big Lost River at INL

The nonparametric Bayesian Monte Carlo method of O’Connell (2005) is used to estimate flood frequency. This method accommodates complex flood behaviors such as event clustering (repeated instances of similar magnitude floods) and can use varied data, such as gage and historical peak discharges, and paleohydrologic upper and lower bounds on peak discharge, while rigorously accounting for a wide variety of measurement uncertainties. In contrast to nonparametric kernel estimation approaches, the stochastic assumption is used to generate flood frequency models that span the data and provide about twice the number of degrees of freedom of the data. Each generated flood frequency model is scored using likelihoods that account for data measurement uncertainties. A parametric estimation approach ensures high precision because posterior sampling is known. However, parametric approaches can produce substantial biases because the classes of allowed flood frequency models are restricted. These biases are completely undetectable within a parametric paradigm. To minimize these types of biases, the nonparametric approach used here surrenders some precision, but produces greater overall accuracy and assurance; it reveals the annual probabilities where discharge becomes unconstrained by the data, thereby eliminating unsubstantiated extrapolation. Parametric flood frequency estimation introduces strong extrapolation priors that make it difficult, if not impossible, to determine when flood frequency is no longer constrained by the data. These

problems are apparent in the parametric method of O'Connell et al. (2002) used in the previous INL flood-frequency analyses (Ostenaar et al., 1999).

Measurement uncertainty is included using discrete pdf's. Gaussian measurement uncertainties of $2\sigma=25\%$ are used for the gage data (see **Figure 4-1** for an example for the largest gage flood). The smaller (historical) paleoflood is assigned a uniform likelihood for discharges from 80 m³/s (cms) to 105 cms and its corresponding non-exceedence bound is assigned a uniform likelihood for discharges from 80 cms to 110 cms. The non-uniform measurement uncertainties for the rest of the nonexceedence bounds and paleofloods are shown in **Figure 4-1**.

Monte Carlo integration is used with a total of 320,000 randomly-created flood-frequency models to produce posterior estimates of probability density for peak discharge at target annual exceedence probabilities (AEP) and for cumulative probability (which is transformed to AEP for plotting) associated with target peak discharges. The 25 least frequent AEP positions used to randomly generate peak discharge values are shown in **Table 4-1** which reflect about twice the number of degrees of freedom represented by the data for AEP's < 0.1.

Peak discharges were randomly generated at all data points plotted in **Figure 4-2**, with the caveat that the peak discharges for $T < 10$ years were rescaled to a maximum of half their values to avoid having the reordering of small flows influence the distribution of the large flows of interest. The cumulative frequency (*cf*) node positions at $T=30,000$ years and $T=40,000$ years were added to provide an extrapolation limit for the computation. As shown in **Figure 4-2** non-informative peak discharge priors were selected for AEP's < 0.1 by expanding the prior to include discharges much larger than the observed data. These priors adequately represent an ignorance function relative to the magnitude of floods and bounds in the input data. Construction of such a prior is essential for determining the AEP limit where observed data no longer provide any meaningful constraints on flood frequency. The range of peak discharges included in the Bayesian estimation of flood frequency as a function of AEP and return period are shown in **Figure 4-2** by the yellow region. The maximum number of peak discharge resorting operations allowed before rejecting a random flood frequency model was set to seven and represented less than a third of the total number of degrees of freedom.

Monte Carlo nonparametric flood frequency results using 320,000 random models are shown in **Figure 4-2**. Formal Monte Carlo relative errors are 2.7% based on the approach used in O'Connell (2005), but actual convergence appears to be much faster, because flood frequency estimates obtained using 8000, 40,000 and 320,000 random models are virtually the same. Sampling density functions are substantially broader than the nonzero regions of posterior density (**Figure 4-2**). The best-fitting models reproduce all the observed data well (**Figure 4-2**). This result is expected since arbitrary flood frequency shapes can be generated by the nonparametric process. It is instructive to inspect sampling functions, posterior pdf's and *cf*'s for individual return periods that show more detail than can be portrayed in **Figure 4-2**.

The cluster of floods in the 80-90 cms range (**Figure 4-2**) places strong constraints on the $T=100$ year and $T=150$ year discharges, although the $T=150$ -year pdf begins to develop a longer tail at maximum discharges (**Figure 4-3**). The increased uncertainty in estimated discharges for AEP's < 0.01 is apparent in the expanding upper tail in the discharge pdf's for $T=200$ years and $T=350$ years (**Figure 4-4**) which is also clearly apparent in **Figure 4-2**. Since the only definite information available about the occurrence of floods in this region are the historical and paleoflood, a wide range of peak discharge scenarios are consistent with the flood and nonexceedence bound data for $T=150$ years to $T=500$ years, as indicated by the wide region of blue curves in **Figure 4-2** and the expanding upper tails in **Figure 4-3**, **Figure 4-4**, and **Figure 4-5**.

While the discharge mode is dominated by the largest paleoflood for $T=1000$ years and $T=2000$ years (**Figure 4-6**) a relatively large range of discharges are allowed because there is little density information in the form of actual floods (only the historical and paleoflood). Consequently, the higher likelihood discharges vary over a wide range constrained mostly by the nonexceedence bounds and the single paleoflood for AEP's $< 1/1000$ (**Figure 4-2**). This is particularly evident for $T=3500$ years and $T=5000$ years, where discharges from slightly the lower limit of the largest paleoflood discharge up to the upper limits of the early Holocene nonexceedence bound are allowed (**Figure 4-7**). For $T=7500$ years and $T=10,000$ years, the only constraints are that discharge be as large as the largest paleoflood, but smaller than the late Holocene nonexceedence bound (**Figure 4-8**). As T extends beyond 10,000 years, the available data provide diminishing constraints with increasing T (**Figure 4-9**). Once T is about twice the length of record ($T=20,000$

years), constraints on the upper bound for discharge become weak, while the constraint that discharge must be as large as the largest paleoflood remain (**Figure 4-9**). This is evident in the large discharge ranges of high likelihood models for AEP's < 0.0001 (shown as blue lines in **Figure 4-2**).

For discharges > 100 cms credible intervals for AEP can be quite large because there is only positive evidence for the actual occurrence of one such discharge (P in **Figure 4-2**). Consequently, AEP's for discharges > 100 cms are only weakly bounded to the right in **Figure 4-2** and in fact become virtually unbounded to the right (are not required to ever occur) for discharges significantly exceeding the largest observed discharge. This means that the right credible limit for discharges $> \sim 300$ cms becomes a cumulative frequency of one or AEP of zero (**Figure 4-2**, **Figure 4-10**, and **Figure 4-11**). Thus for discharges $> \sim 300$ cms the most meaningful statistic are bounds to the left in **Figure 4-2** which limit the maximum frequencies of occurrence. Central tendency measures like the mean or median lose statistical significance in these situations. However, for all discharges, the nonexceedence discharge bounds place strong limits on the maximum AEP's that can be associated with particular discharges (**Figure 4-2**).

The densities in **Figure 4-10**, **Figure 4-11**, **Figure 4-12**, and **Figure 4-13** look peculiar relative to the cumulative frequencies because all density/cumulative frequencies calculations are performed in cumulative frequency space and then transformed to AEP/T for plotting. This is why it appears that there is more density to the right (small AEP's) than indicated by the cumulative frequency curves or credible limits in **Figure 4-10**, **Figure 4-11**, **Figure 4-12**, and **Figure 4-13**. For example, the AEP density distribution for a discharge of 106 cms appears unbounded to the right, but the cumulative frequency density is well behaved and provides a useful right credible limit (**Figure 4-12**). When the right credible limits are significant (discharges $< \sim 300$ cms), they indicate a 90% probability that the AEP is greater than the right credible limit AEP. The wide ranges of AEP's represented between the 10% and 90% credible limits for discharges < 300 cms (**Figure 4-11**, **Figure 4-12**, and **Figure 4-13**) indicate the large range of recurrence uncertainties that result from the lack of strong density information, i.e., multiple observed discharges or discharge exceedences > 100 cms.

As discussed above for this particular dataset there is more statistical significance to the left credible limits, than the mean or right credible limits for discharges $> \sim 300$ cms. For discharges $> \sim 300$ cms right credible limits may just as easily extend to AEP=0 as the values reported in the nonparametric flood frequency calculations, and the shape of the densities are generally not compatible with a measure of central tendency, such as a mean. Consequently, mean flood frequency estimates for AEP's < 0.0001 are flagged with stars in **Table 4-2**.

Figures for Section 4.0

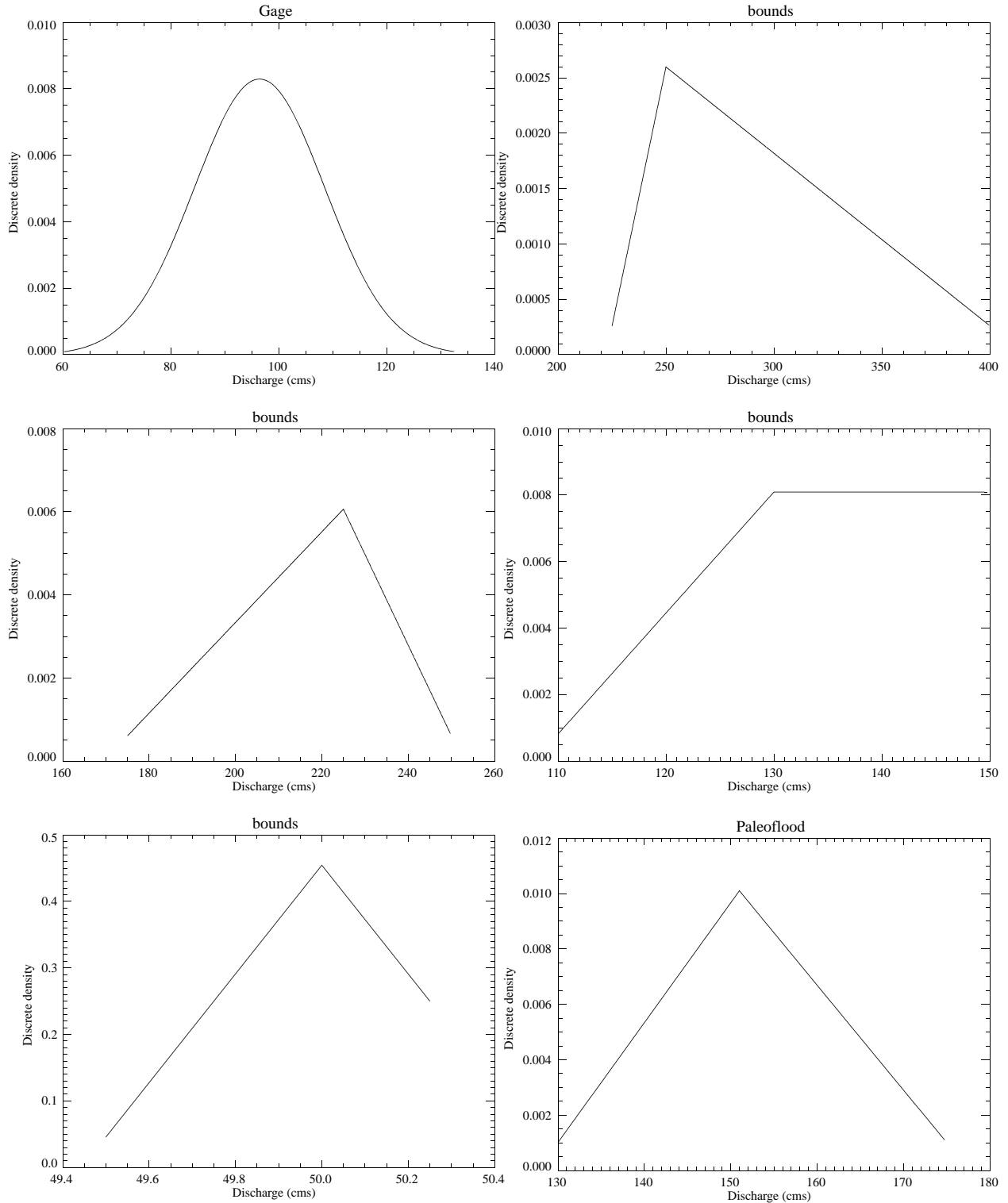


Figure 4-1 Measurement uncertainties for gage, bound, and paleoflood discharges on the Big Lost River at the INEEL Diversion Dam..

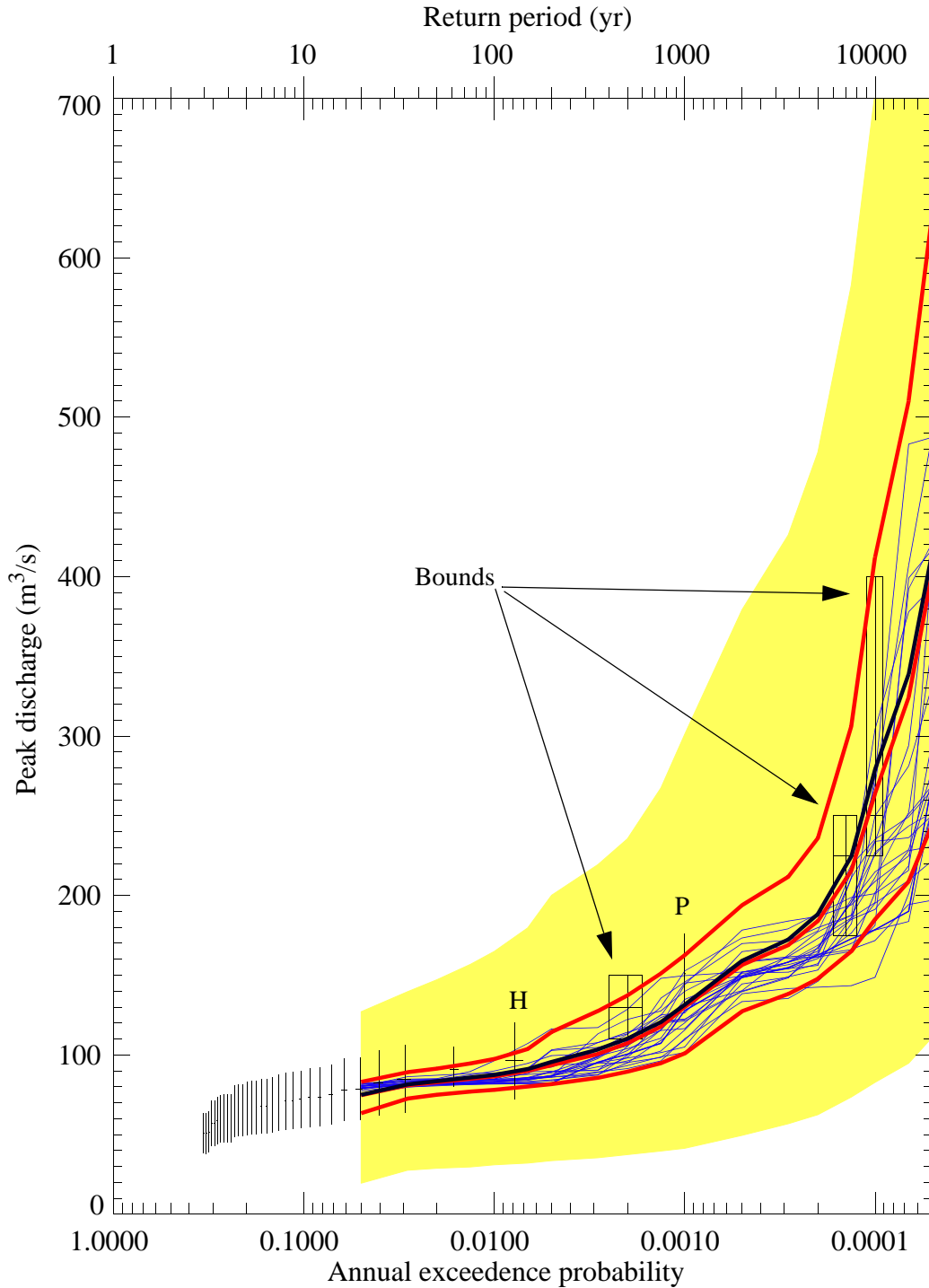


Figure 4-2 Revised flood frequency for Big Lost River at the INEEL Diversion Dam. Gaged flows (vertical black lines, with short horizontal lines indicating preferred discharge and plotting position uncertainty) are from Big Lost River at Howell Ranch (94 years) attenuated to the INEEL Diversion Dam based on methods of Hortness and Rousseau (2002). Geologic data includes two paleofloods (largest discharges labeled H and P) and three paleohydrologic bounds (black boxes - vertical lines indicate discharge range, horizontal lines indicate duration range). Lower and upper red curves are 5% and 95% credible limits (middle red is median, and middle black is mean). Blue curves are models with relative likelihoods > 0.25 of the maximum likelihood. Yellow region indicates the limits of sampling.

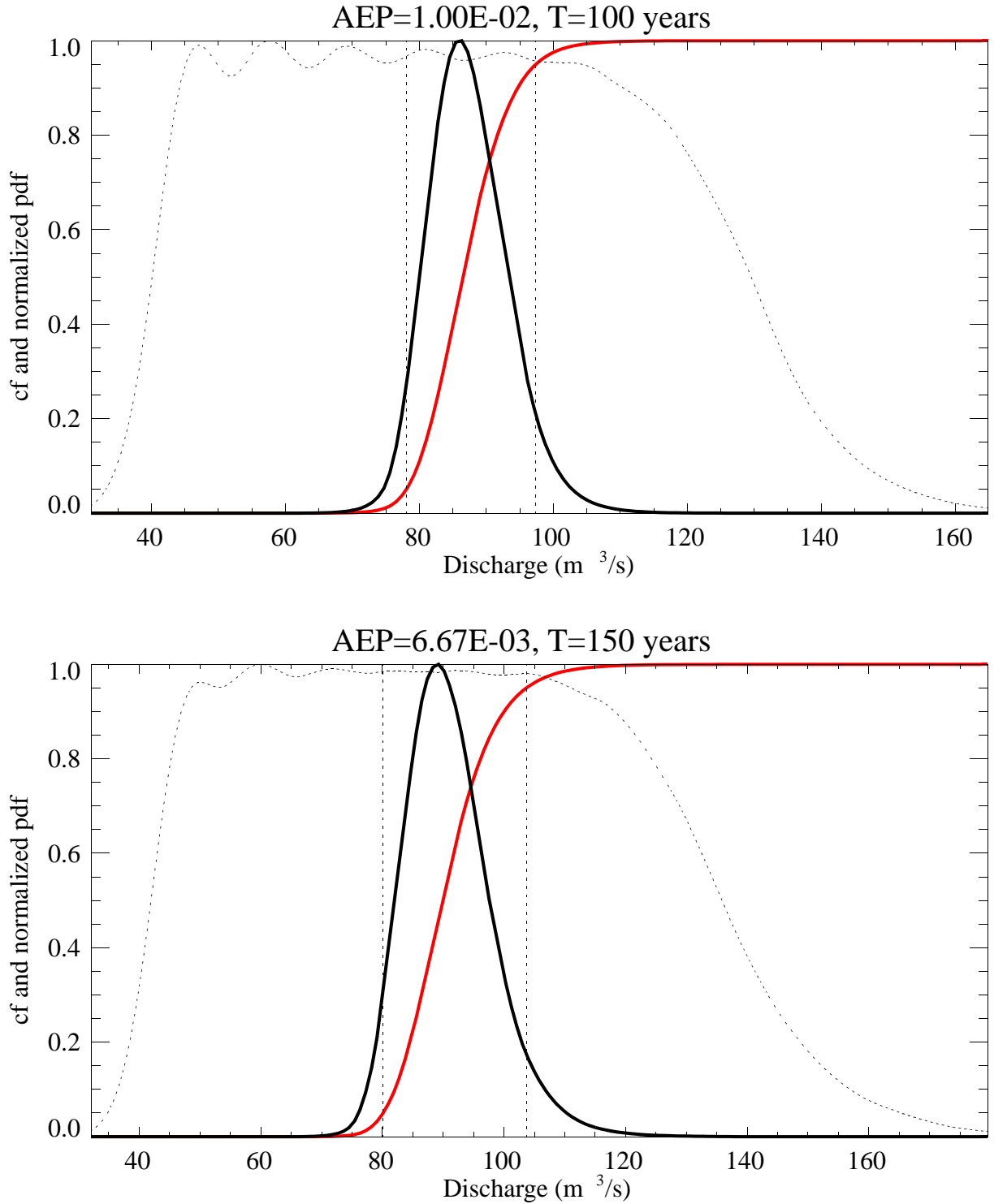


Figure 4-3 Peak discharges distributions for AEP's 0.01 and 0.00667 on the Big Lost River at the INEEL Diversion Dam. Red curves are cumulative probability, dotted curves are sampling density, and black curves are probability density. Vertical dotted lines represent 5% and 95% credible limits.

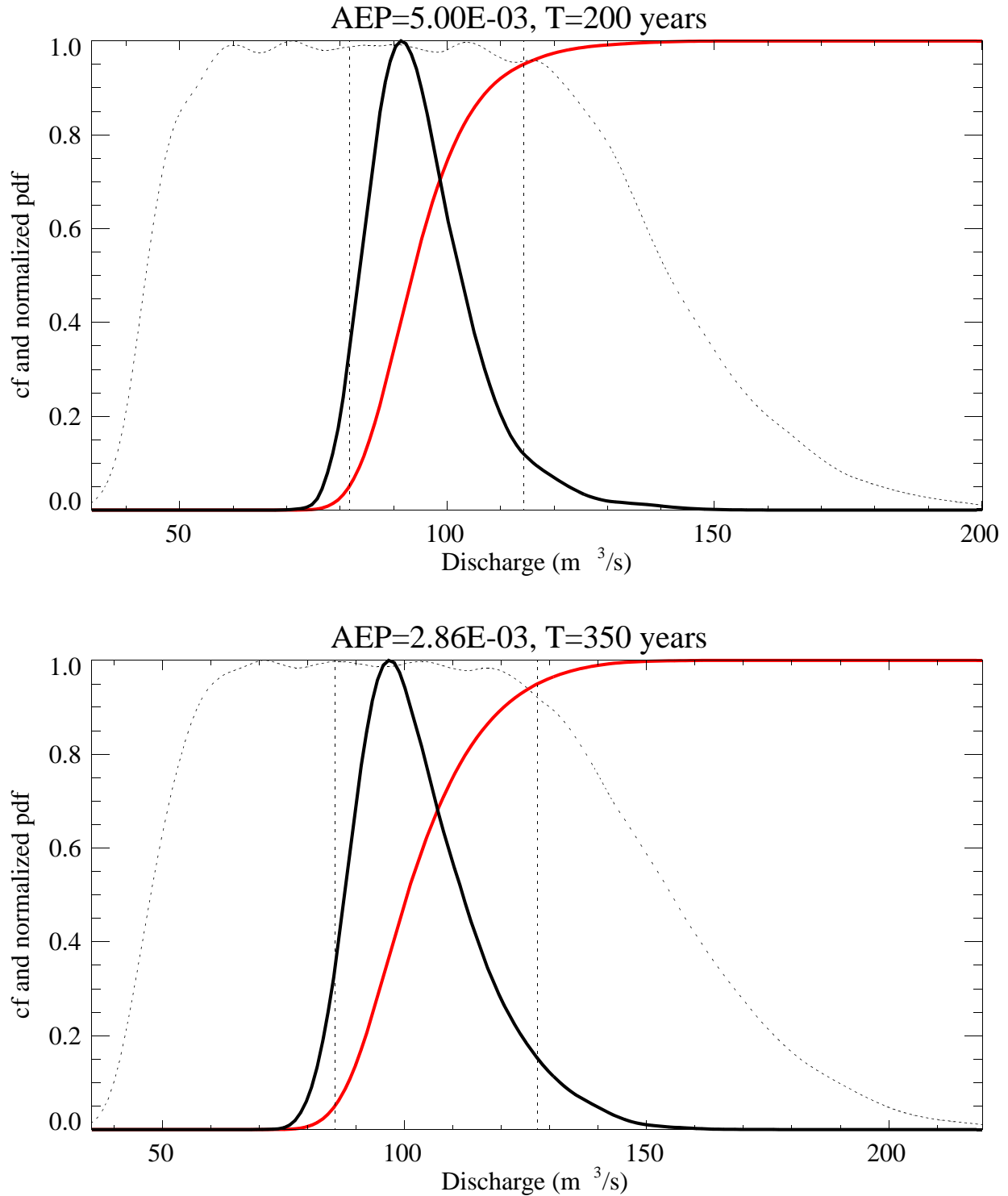


Figure 4-4 Peak discharges distributions for AEP's 0.005 and 0.00286 on the Big Lost River at the INEEL Diversion Dam. Red curves are cumulative probability, dotted curves are sampling density, and black curves are probability density. Vertical dotted lines represent 5% and 95% credible limits.

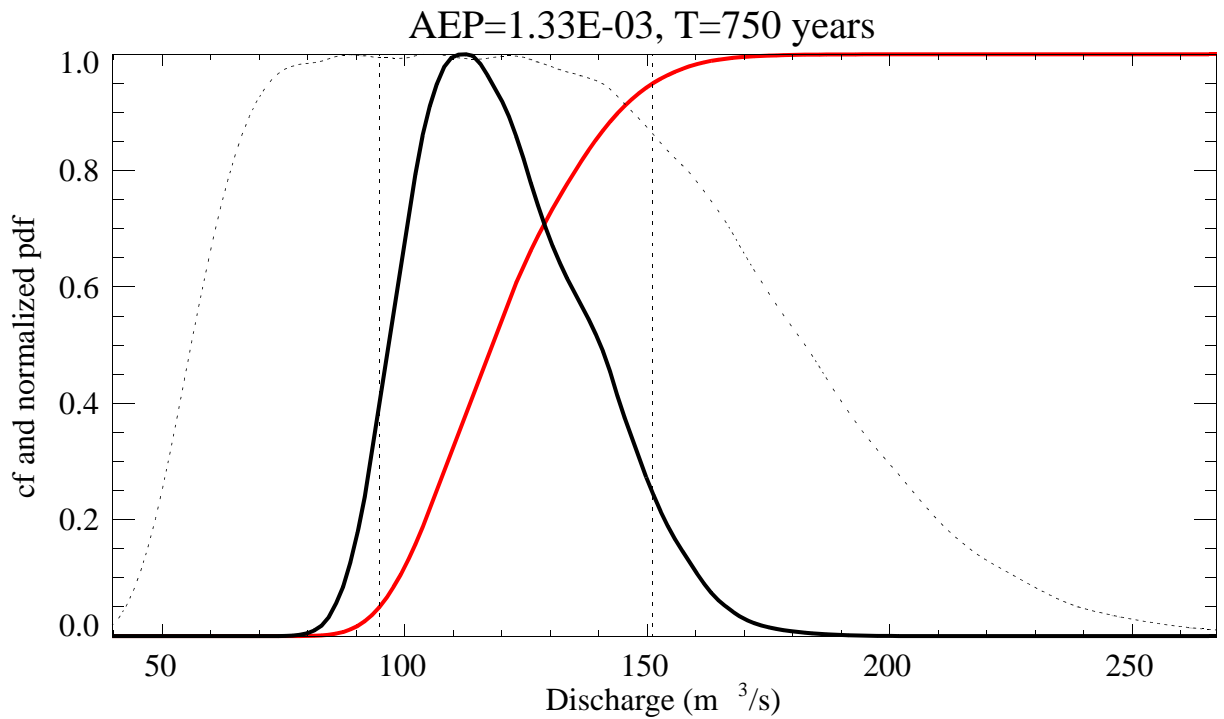
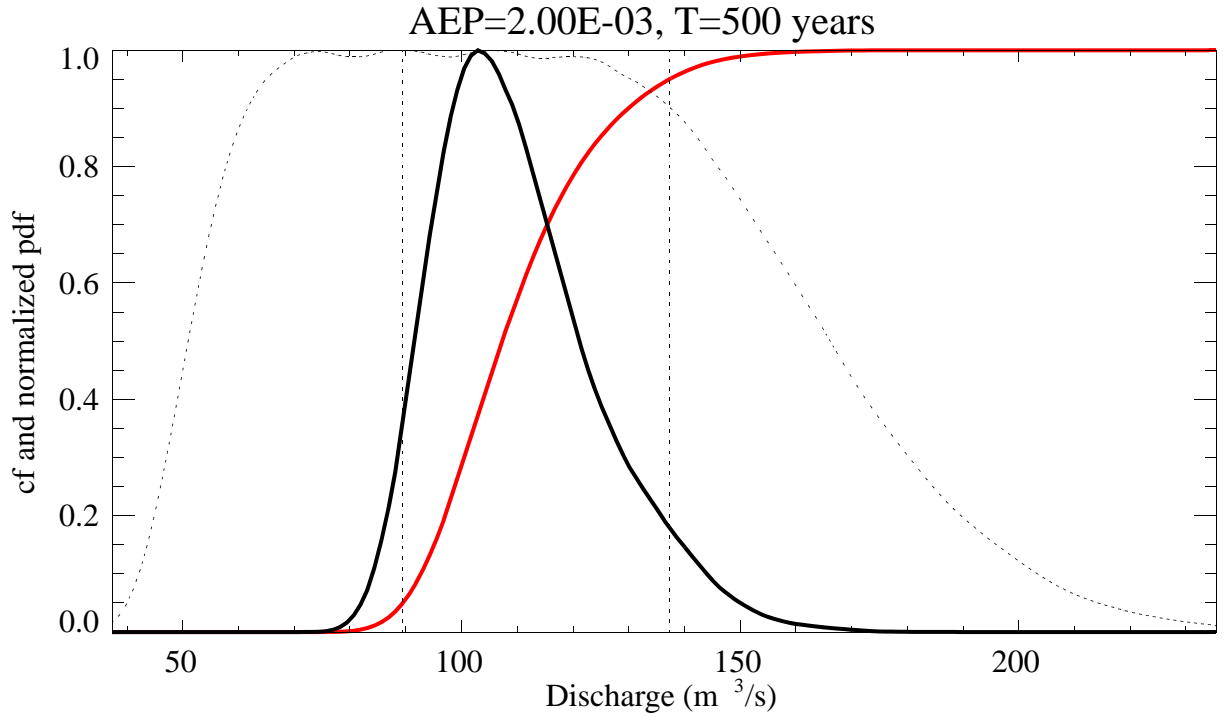


Figure 4-5 Peak discharges distributions for AEP's 0.002 and 0.00133 on the Big Lost River at the INEEL Diversion Dam. Red curves are cumulative probability, dotted curves are sampling density, and black curves are probability density. Vertical dotted lines represent 5% and 95% credible limits.

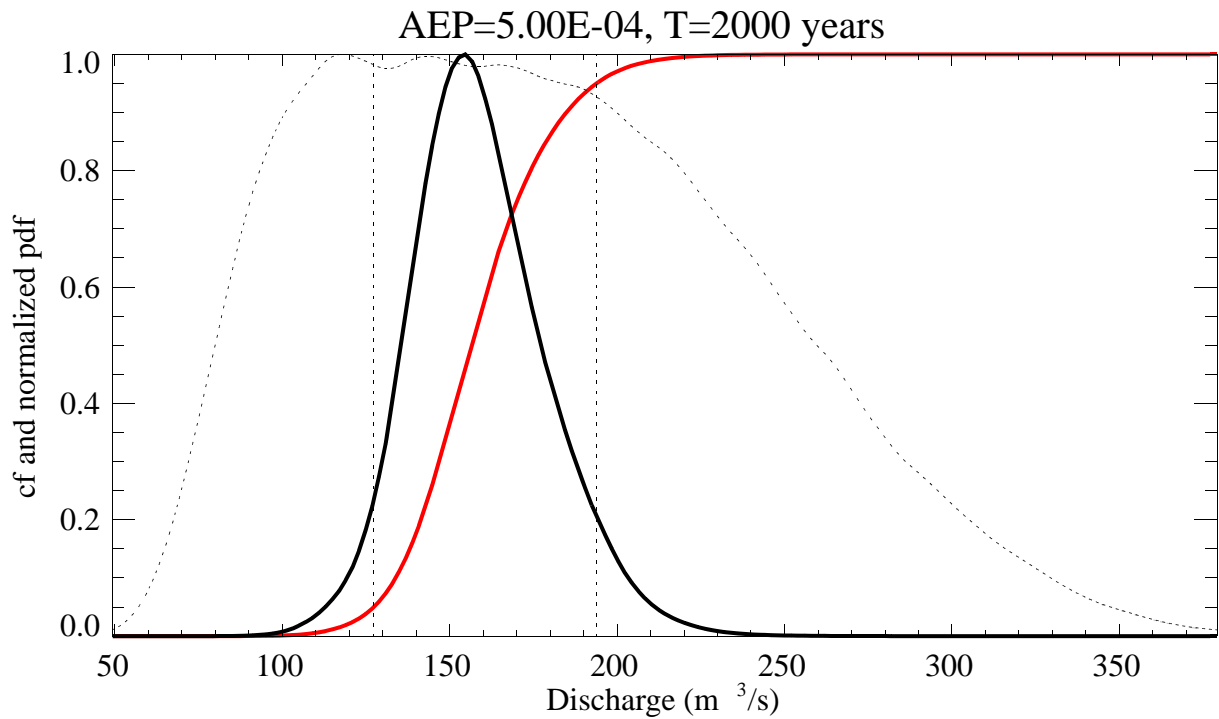
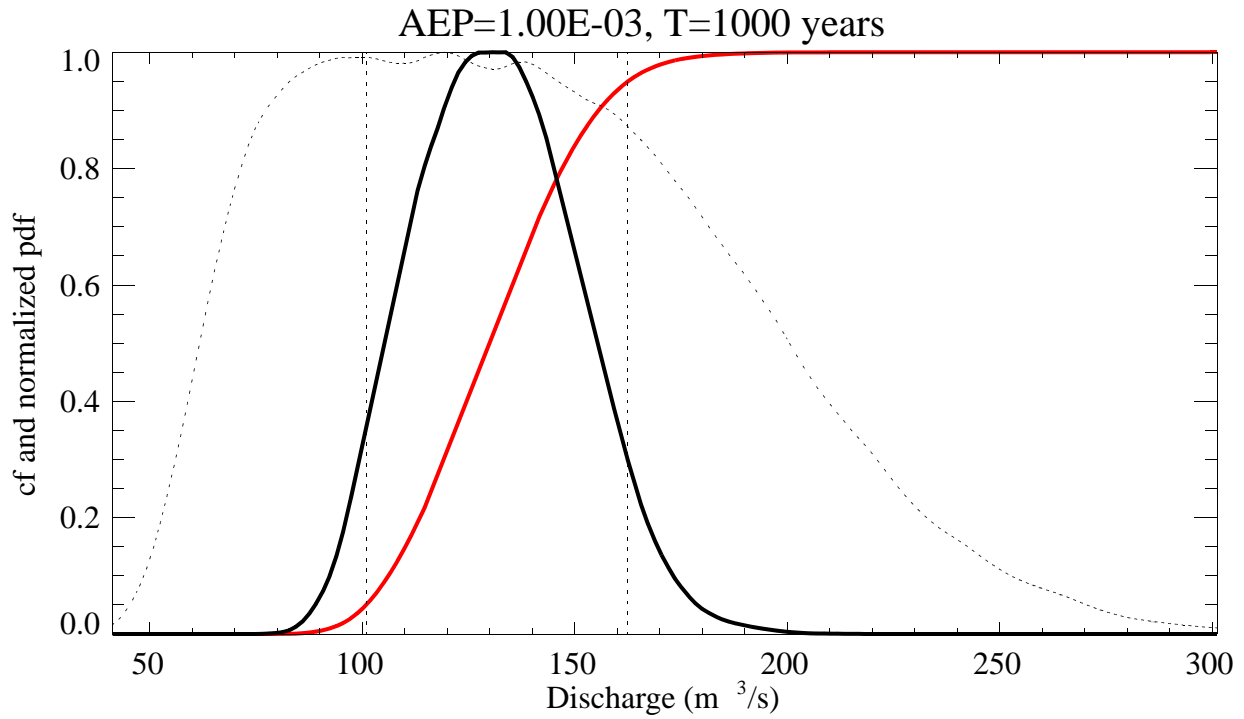


Figure 4-6 Peak discharges distributions for AEP's 0.001 and 0.0005 on the Big Lost River at the INEEL Diversion Dam. Red curves are cumulative probability, dotted curves are sampling density, and black curves are probability density. Vertical dotted lines represent 5% and 95% credible limits.

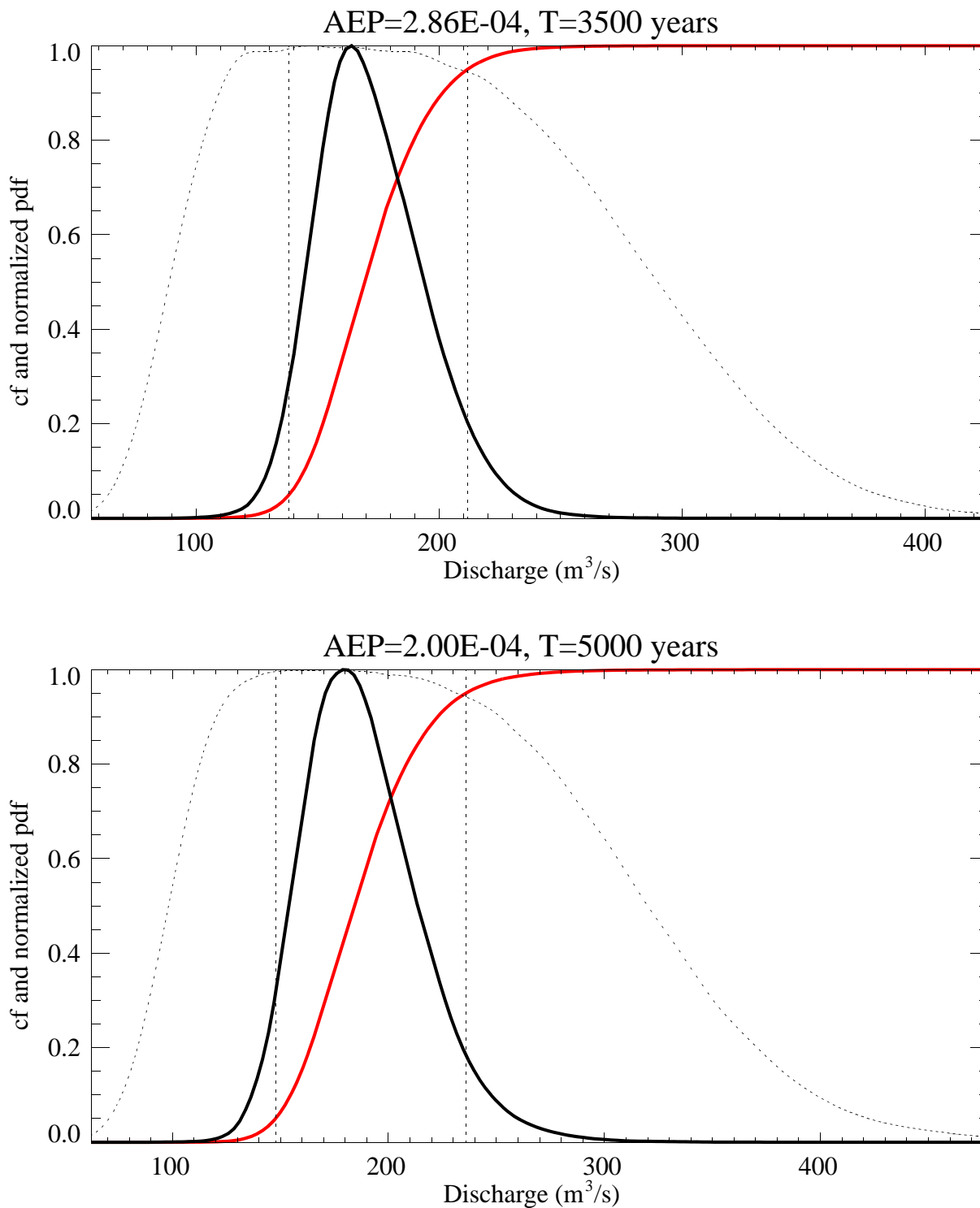


Figure 4-7 Peak discharges distributions for AEP's 0.000286 and 0.00002 on the Big Lost River at the INEEL Diversion Dam. Red curves are cumulative probability, dotted curves are sampling density, and black curves are probability density. Vertical dotted lines represent 5% and 95% credible limits.

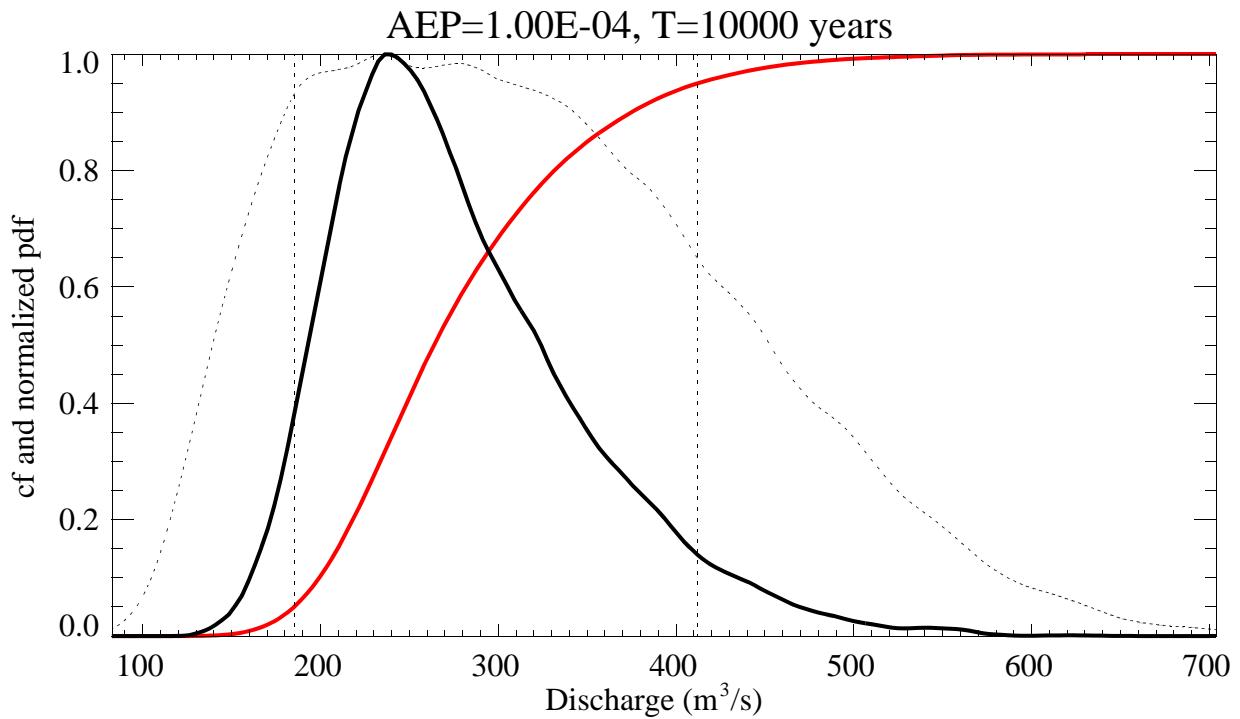
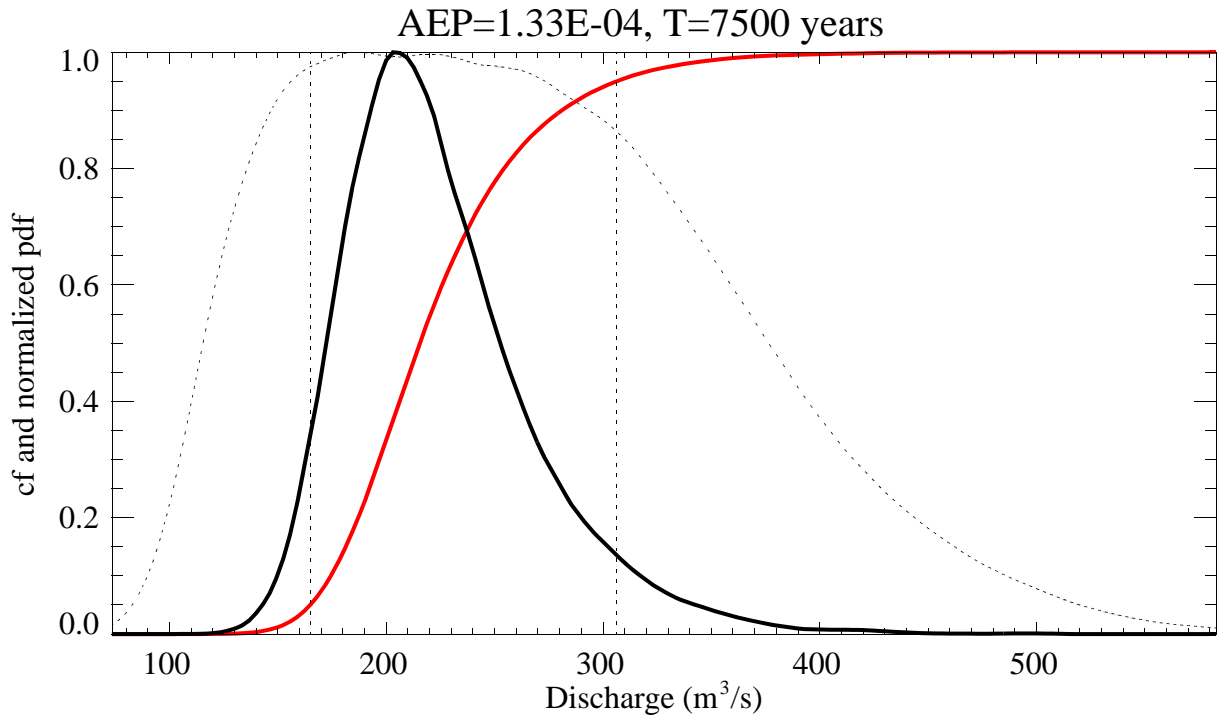


Figure 4-8 Peak discharges distributions for AEP's 0.000133 and 0.00001 on the Big Lost River at the INEEL Diversion Dam. Red curves are cumulative probability, dotted curves are sampling density, and black curves are probability density. Vertical dotted lines represent 5% and 95% credible limits.

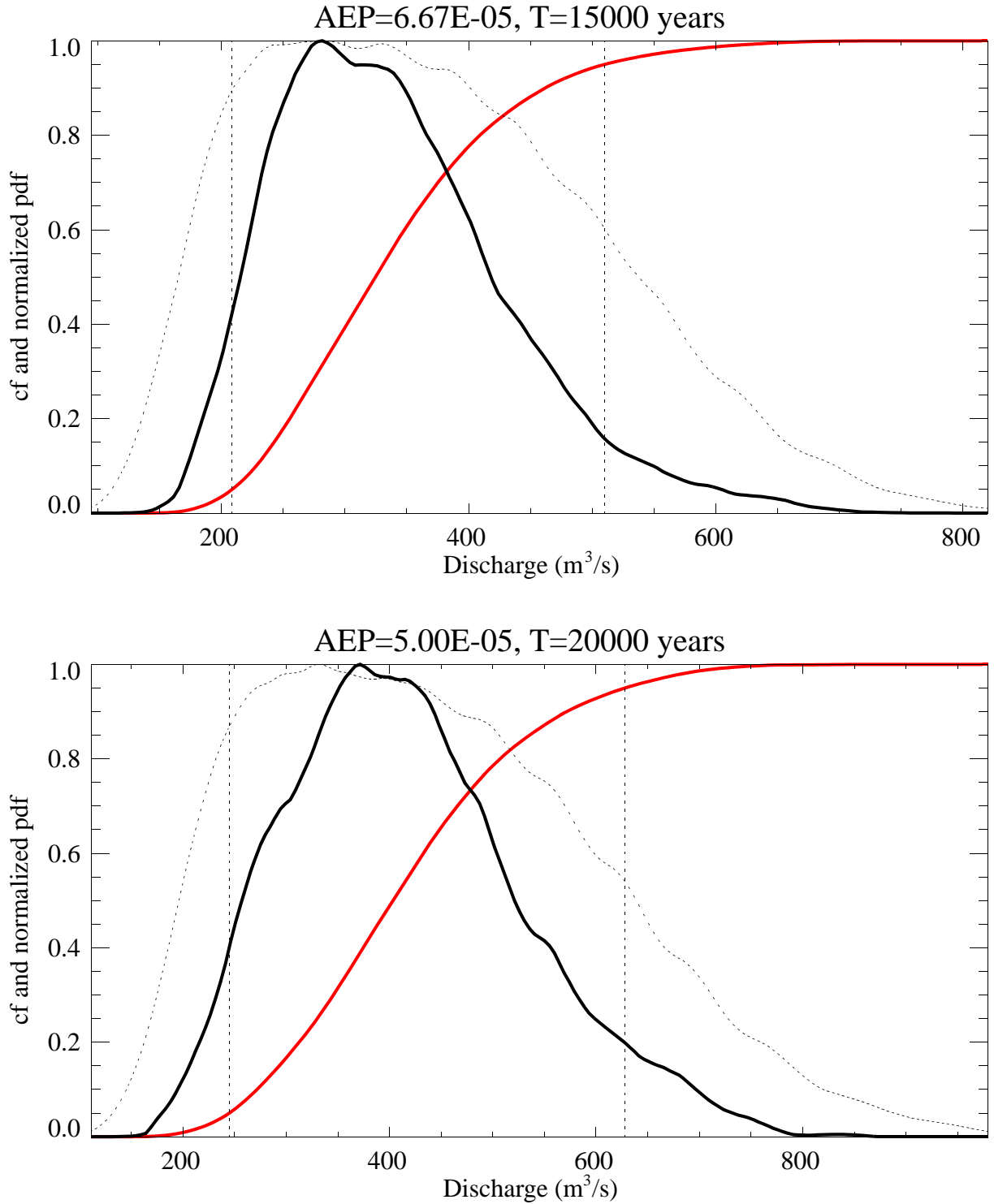


Figure 4-9 Peak discharges distributions for AEP's 0.0000667 and 0.000005 on the Big Lost River at the INEEL Diversion Dam. Red curves are cumulative probability, dotted curves are sampling density, and black curves are probability density. Vertical dotted lines represent 5% and 95% credible limits.

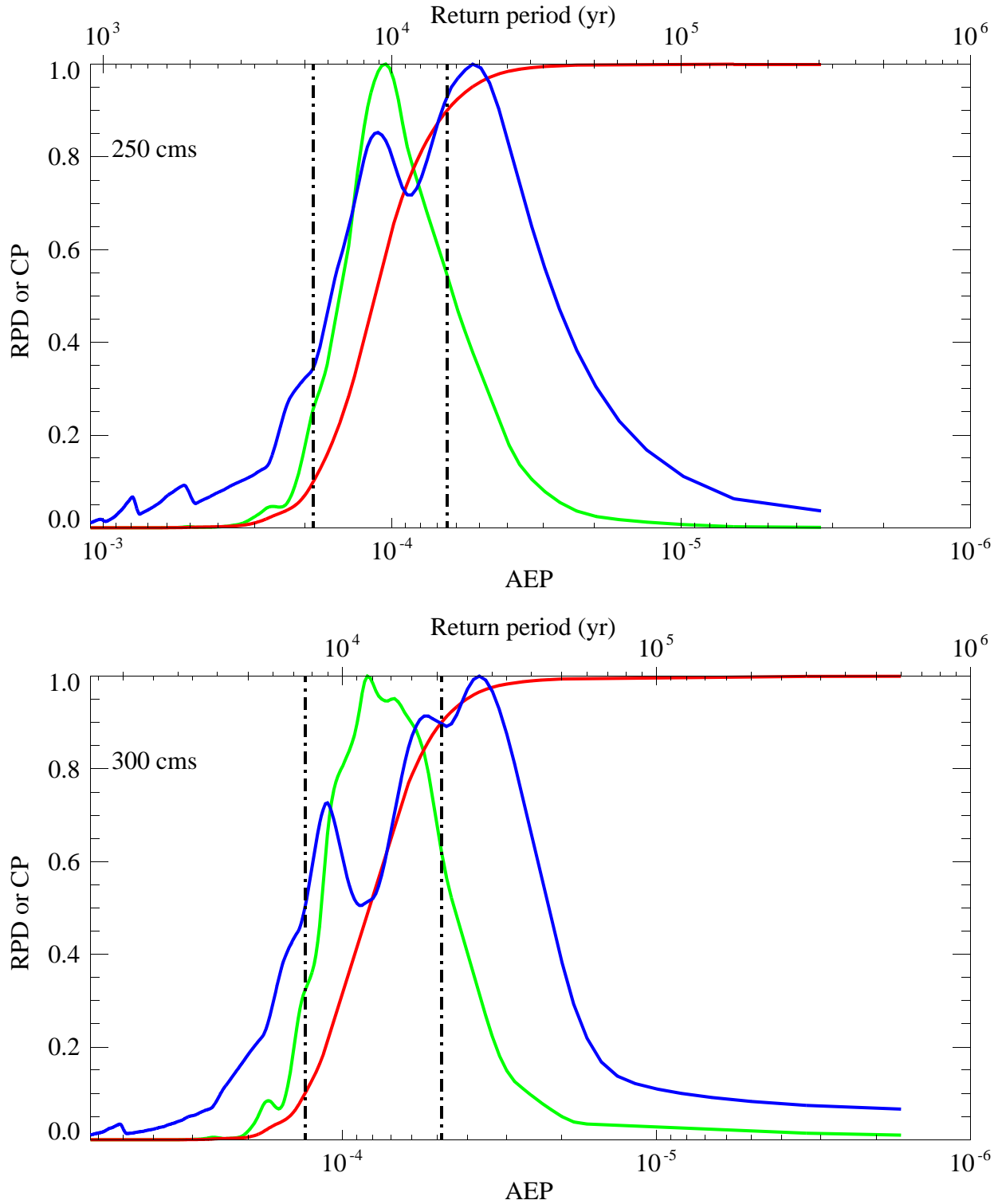


Figure 4-10 AEP distributions for 250 m³/s and 300 m³/s on the Big Lost River at the INEEL Diversion Dam. Red curves are cumulative probability, blue curves are sampling density, and green curves are probability density (from cumulative probability and transformed to AEP). Vertical lines represent 10% and 90% credible limits on AEP, but are not really defined for 300m³/s because nonzero density extends to AEP=0.

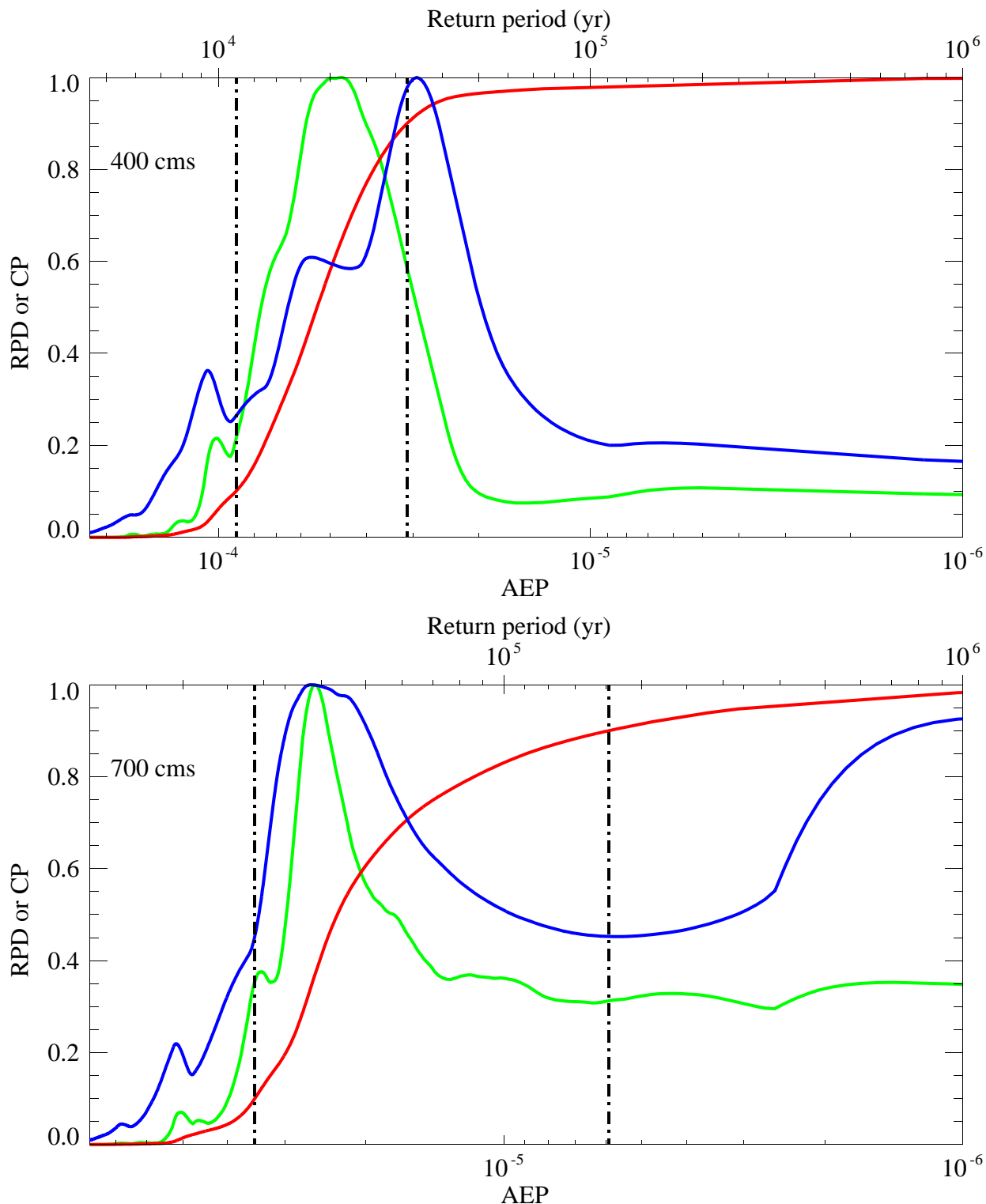


Figure 4-11 AEP distributions for 400 m³/s and 700 m³/s on the Big Lost River at the INEEL Diversion Dam. Red curves are cumulative probability, blue curves are sampling density, and green curves are probability density (from cumulative probability and transformed to AEP). Vertical lines represent 10% and 90% credible limits on AEP, but are not really defined here because nonzero density extends to AEP=0.

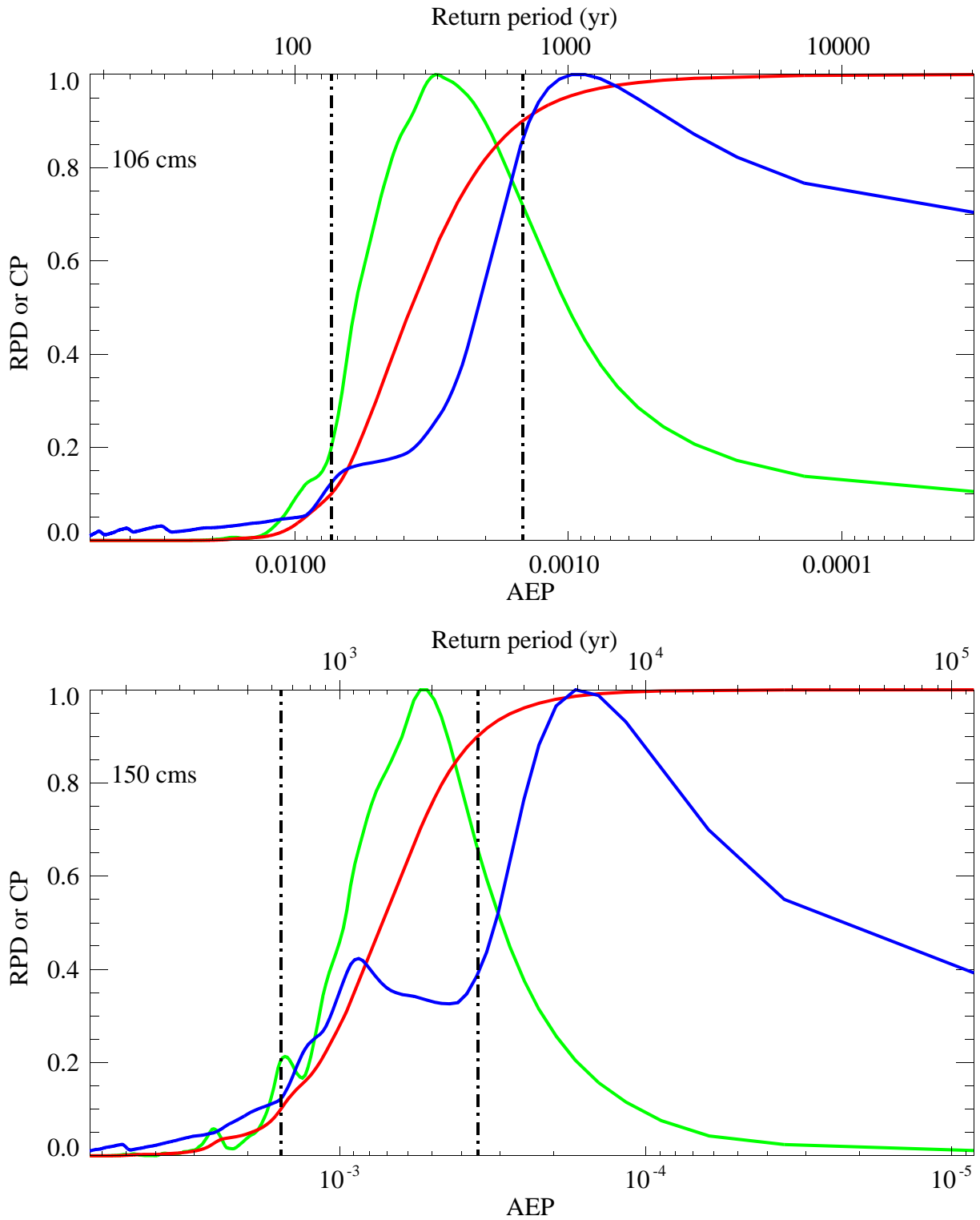


Figure 4-12 AEP distributions for 106 m³/s and 150 m³/s on the Big Lost River at the INEEL Diversion Dam. Red curves are cumulative probability, blue curves are sampling density, and green curves are probability density (from cumulative probability and transformed to AEP). Vertical lines represent 10% and 90% credible limits on AEP.

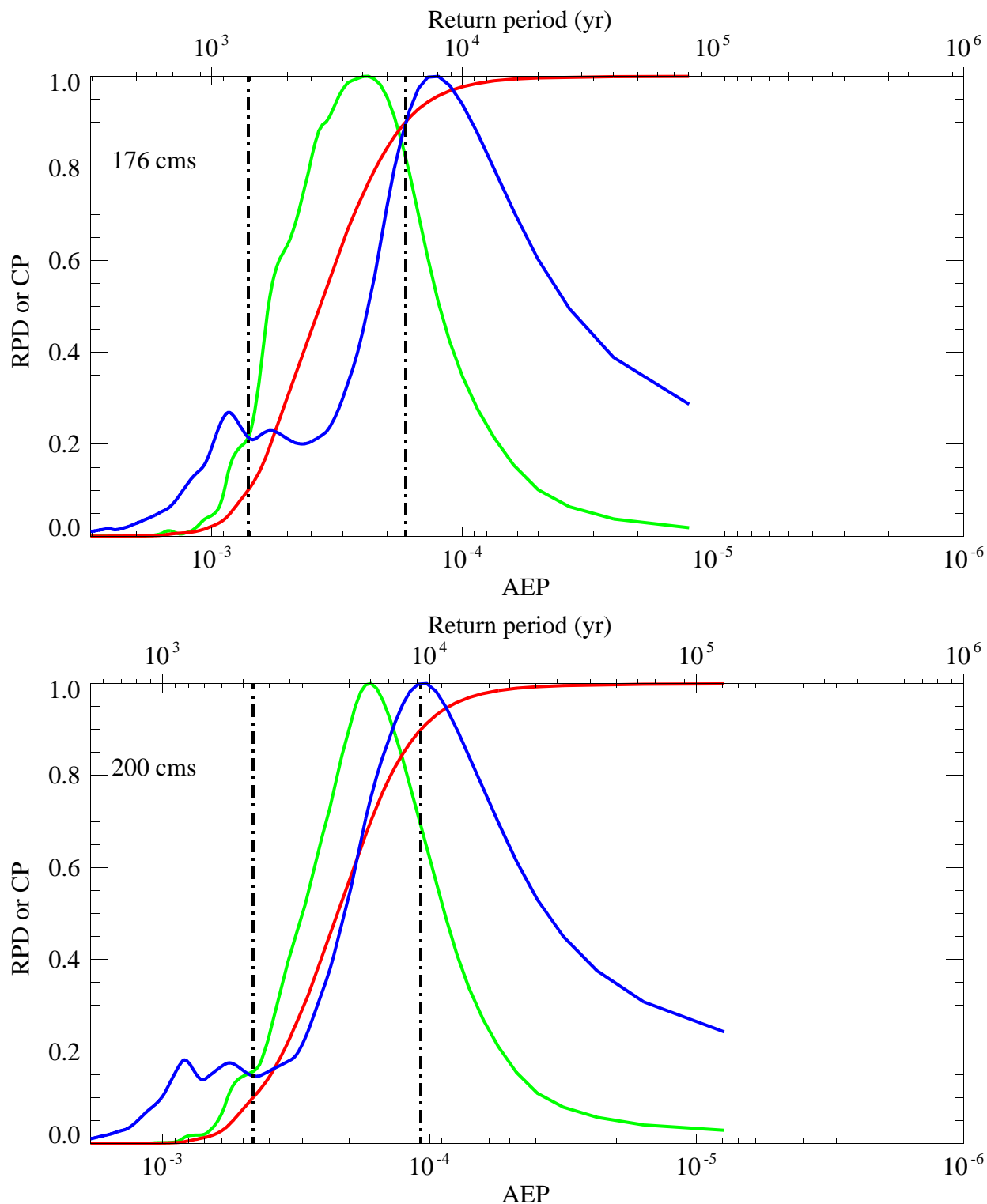


Figure 4-13 AEP distributions for 176 m³/s and 200 m³/s on the Big Lost River at the INEEL Diversion Dam. Red curves are cumulative probability, blue curves are sampling density, and green curves are probability density (from cumulative probability and transformed to AEP). Vertical lines represent 10% and 90% credible limits on AEP

Tables for Section 4.0

Table 4-1 Least frequent peak discharge generation nodes.

<i>C_f</i>	AEP (1/yr)	Return period (yr)
0.885662	0.114338	8.7
0.896279	0.103721	9.6
0.906895	0.093105	10.7
0.917511	0.082489	12.1
0.928128	0.071872	13.9
0.938744	0.061256	16.3
0.949360	0.050640	19.7
0.959976	0.040024	25.0
0.970593	0.029407	34.0
0.983657	0.016343	61.2
0.992182	0.007818	128.
0.995000	0.005000	200
0.997500	0.002500	400
0.998571	0.001429	700
0.999000	0.001000	1000
0.999231	0.000769	1300
0.999500	0.000500	2000
0.999750	0.000250	4000
0.999833	0.000167	6000
0.999875	0.000125	8000
0.999900	0.000100	10000
0.999933	0.000067	15000
0.999950	0.000050	20000
0.999967	0.000033	30000
0.999975	0.000025	40000

Table 4-2 Nonparametric Flood Frequency for the Big Lost River at the Diversion Dam.

AEP (1/yr)	Return period (yr)	5% (m ³ /s)	mean (m ³ /s)	95% (m ³ /s)
5×10^{-2}	20	63	75	83
2.86×10^{-2}	35	73	81	89
2×10^{-2}	50	75	83	91
1.33×10^{-2}	75	77	86	95
10^{-2}	100	78	87	97
6.67×10^{-3}	150	80	91	104
5×10^{-3}	200	82	96	114
2.86×10^{-3}	350	86	103	127
2×10^{-3}	500	89	110	137
1.33×10^{-3}	750	95	121	151
10^{-3}	1000	101	131	163
5×10^{-4}	2000	127	159	194
2.86×10^{-4}	3500	138	172	212
2×10^{-4}	5000	148	188	236
1.33×10^{-4}	7500	165	224	306
10^{-4}	10,000	185	279	412
6.67×10^{-5}	15,000	209	339*	510*
5×10^{-5}	20,000	245	416*	628*
* Values with diminished or little statistical significance.				

5.0 PROBABILISTIC FLOOD STAGE AT INTEC AND TRA

Two-dimensional hydraulic modeling using a broad range of discharges conducted for the reach of the Big Lost River downstream of the INEEL Diversion Dam to approximately the INEEL railroad grade downstream of INTEC and TRA provide one element needed for probabilistic flood stage estimates at these facilities. A conceptual framework for evaluating the model results and flood frequency information was developed in the early stages of this study to guide the evaluations. Uncertainties in probabilistic flood stage estimates are discussed in the context of that framework. Based on this framework, results and uncertainties for stage - probability curves for fifteen specific sites within INTEC and TRA are discussed.

5.1 Topographic Input to Two-Dimensional Models

The 5-ft-spaced reprocessed topographic data from the 1993 aerial photography at INEEL (**Appendix A**) were used to construct the computational meshes for TrimR2D and RiCOM flow modeling of INL inundation. Construction of the TrimR2D grid was relatively straightforward and simply involved subsampling a subset of the rotated topographic data to produce a 10-ft-spacing input file. Details of this process are provided in **Appendix C, Part A, Section 2**. TrimR2D flow results were used to define regions that warranted increased spatial sampling afforded by the finite-element capabilities of RiCOM. The construction of the RiCOM computational mesh was quite involved and is documented in **Appendix C, Part A, Section 2**.

In both grids the minimum elevation in the grid was removed from all points in the grid to maximize numerical precision in quantities involving elevations. Coordinate transformation equations were constructed for both flow grids to convert the local grid coordinates to their original INEEL state-plane coordinates and elevations.

5.2 Two Dimensional Hydraulic Modeling

Discharges were selected for modeling over the full range of flow probabilities to provide representative data from which to construct the stage - probability curves. Specific discharge values were chosen for relevance to historical flood events, system capacities, and flood estimates from previous studies (**Table 5-1**).

The TrimR2D grid consisted of approximately 3.3 million active cells. The RiCOM grid consisted of approximately 7.2 million active elements and nearly 14 million active sides and used a time step 1/5 of the TrimR2D time step. RiCOM calculations were much more computationally demanding than TrimR2D, with RiCOM calculations running at 1/10-1/20 real time, while TrimR2D ran at 1/2 to 1/4 real time. Consequently, TrimR2D was used to perform most of the sensitivity analyses concerning infiltration and culvert scenarios and RiCOM was used to concentrate calculations on the most important subset of flows identified from the TrimR2D flow calculations.

5.2.1 Infiltration Implementation and Scenarios. Infiltration was implemented in TrimR2D and RiCOM as discussed in **Appendix C, Part A, Section 3**. As discussed in **Appendix E**, infiltration estimates from Fiedler (2002) were modified to produce channel loss rates consistent with historical maximum channel discharge losses between the Diversion Dam and Lincoln Avenue of ~15%. The two scenarios in **Table 5-1** represent logical infiltration end-members of no infiltration and full infiltration consistent with the maximum observed historical channel losses between the Diversion Dam and Lincoln Avenue.

5.2.2 Culvert Implementation and Scenarios. As indicated in **Table 5-1**, TrimR2D was used to calculate flows for four scenarios for a full range of discharges. The four scenarios were constructed to determine the relative influence of infiltrations and culverts on estimated inundation. The scenarios represented in **Table 5-1** all assume full Big Lost River conveyance through Lincoln Avenue, the railroad embankment downstream of INTEC, and Highway 20/26. As discussed in detail in **Appendix C, Part A, Section 3**, culvert flow information from Berenbrock and Doyle (2003) was used for all other culverts. Since the RiCOM calculations indicated that topographic grid resolution had a significant impact on estimated inundation in the vicinity of INTEC, RiCOM was also used to estimate the impact of complete blockage of flow by Lincoln Avenue on estimated inundation for the case of full infiltration and full operation of the remaining culverts.

5.2.3 Flow Initialization. The TrimR2D inundation grid was initially wetted with springs distributed along the Big Lost River channel that were activated for several minutes of flow to partially fill the channels. To produce steady-state flows for specific discharges, springs

were activated immediately downstream of the Diversion Dam in the active channel with a total flux equal to the specific discharge. For the TrimR2D flows, 32 springs were used to minimize excess stages in the vicinity of the springs. Because RiCOM used 5-ft elements in the active channel, 886 springs were used to minimize excess stages in the vicinity of the springs. It is important to note, that despite these efforts to minimize excess stages in the vicinity of the input springs, stages near the springs may be up to 1 m higher than would occur if water flowed through the channel at typical velocities of 1-2 m/s. Consequently, inundation of areas immediately south of the channel downstream of the Diversion Dam are overestimated to some degree, particularly for discharges of 300 cms or larger. TrimR2D flows for all discharges started from the same initial low-flow channel wetting conditions so that all discharges in **Table 5-1** could be calculated in parallel. The TrimR2D stages upon completion of the flow simulations (about 40 hours of flow) were used as initial conditions to initialize the RiCOM flow calculations. The outlet flow boundary was located more than 1 km from any regions of interest. Consequently, a simple fixed water surface elevation boundary condition was imposed for simplicity, since the boundary condition had no impact on the interior points of interest in the grids.

5.2.4 Flow Parameters. Time steps were established at 20 s for the TrimR2D 20-ft grid to ensure Courant numbers of larger than 4 for main channel flow velocities for all discharges. A time step of 4 s was used for the RiCOM grid because all significant flow channels used 5-ft elements. This ensured Courant numbers larger than 4 in the main flow channels in the RiCOM flow calculations. Criteria for selection of time step and the impact of time step on computed flows are discussed in detail in **Appendix C, Part A - Section 1** and **Part B - Section 1**. Semi-implicit weights were set to 0.7 for all calculations.

5.2.5 Flow Completion. A total of 15 hydrograph monitoring positions were established throughout inundation grids in both channel and out-of-bank positions. These hydrographs were monitored to determine when the flows had reached steady state. Typically, flow times of about 20-40 hours were required to achieve steady-state conditions throughout the TrimR2D grid, when starting from a modest channel inundation condition. Steady-state flow conditions were obtained in the RiCOM flow calculations in 6-7 hours of flow time, when starting with the TrimR2D inundations at the same discharge. Steady-state conditions were defined as attaining an

essentially static water surface elevation at all the hydrograph monitoring positions (natural high-frequency water surface elevation oscillations, typically of several centimeters, were ignored).

5.2.6 Flow Output. Appendix E - Electronic Supplement presents maps depicting the results of two-dimensional hydraulic modeling conducted to estimate probabilistic flood stage at INTEC and TRA for the discharges listed in **Table 5-1**. These maps show results for both the entire reach downstream of the INEEL Diversion Dam as well as enlarged views in the immediate vicinity of the facilities. For TrimR2D, the output flow quantities included water surface elevations and vector flow velocities interpolated to the water surface elevation positions at cell-centered positions in the staggered grid. Using the known topography, derived quantities such as depth, shear stress, and power were obtained. For RiCOM, the output flow quantities included water surface elevations and vector flow velocities interpolated to the element vertices using the finite-element basis functions. The inverse transformation operators were then applied to produce flow quantities in the INEEL state-plane coordinate system. For most modeled discharges, results are presented for modeled flow depth, unit stream power, and bed shear stress based on the TrimR2D results. RiCOM results are presented mostly as plots showing the difference in water-surface elevation from TrimR2D results for the same input discharge. A full set of RiCOM results (depth, unit stream power, bed shear stress) are presented only for four quantile results of the 100- and 500- yr discharges from the flood frequency analyses. Additional depth difference plots from TrimR2D models depict end member differences for infiltration and culvert scenarios.

5.3 Conceptual Framework for Development of Probabilistic Inundation Maps and Flood Stage Estimates for Facility Sites at INL

Each of the inundation maps for a specific discharge listed in **Table 5-1** could be associated with mean and credible limits on AEP associated with that discharge from **Section 4.0** and **Table 5-2**. However, such AEP's would not represent complete probabilistic inundation maps (PIM) for INL. There are additional probabilities (or weights) that must be assigned to aleatory (random-by-nature) parameters, such as infiltration and culvert conveyance. A conceptual framework for evaluating these uncertainties that was developed in the early stages of this study to guide the investigations is illustrated in **Figure 5-2**. Epistemic uncertainties include factors such as flow model variability and appropriate scenario terrain models used in the simulations. Elicitation and

assignments of weights to all aleatory and epistemic factors are required to produce comprehensive PIM's. Each of the major elements will be briefly described below.

5.3.1 Aleatory Uncertainties.

5.3.1.1 Flood Frequency Analyses. The flood frequency analysis (FFA) can be viewed as the primary input to the PIM process. This is the element by which the annual probability of floods (and hence inundation) are incorporated into the process. Several sources of uncertainty are brought into the PIM process through the FFA, including discharge measurement uncertainties and statistical uncertainties in estimated AEP. The flood frequency results from **Section 4.0** are used to establish probabilistic estimates of mean AEP, and 5% and 95% credible limits on AEP associated with the specific discharges in **Table 5-1**. For instance, a 5% credible limit on AEP roughly represents a 95% probability that the AEP is actually larger than the 5% credible limit AEP (low confidence the AEP will not be exceeded). Conversely, a 95% credible limit on AEP roughly represents a 5% probability that the AEP is actually larger than the 95% credible limit AEP (high confidence the AEP will not be exceeded). As these concepts may not be intuitive, it helps to remember that the conservative limits are represented by the upper hazard curves, which correspond to the 95% credible limit for AEP.

If multiple and complete estimates of flood frequency exist for the site, each of the alternative estimates could be weighted and carried through the PIM process. Because of the wide variation of previous flood frequency estimates for the INL site (**Section 1.0**), it was the original intent of this study to include alternative estimates and propagate this uncertainty through to the estimate of flood stage at the facilities. For example, flood frequency results based on earlier paleoflood studies of the Big Lost River (Ostenaar and others, 1999) would be weighted relative to present study results from **Section 4.0** based on expert opinion. However, because the present study found that the topography used as inputs to earlier paleoflood studies was inadequate (**Appendix A**) making hydraulic model results unreliable, it is now clear that the earlier results must be discounted and effectively given zero weight. As there are no other existing flood frequency analyses for the Big Lost River that can be extended with uncertainties significantly beyond an AEP of 10^{-2} , only the revised analyses described in **Section 4.0** is used. Potential impacts of the differences associated with point estimates for floods of a specific AEP, such as the 100-yr flow

estimate of Hortness and Rousseau (2002) are separately evaluated against the final stage-probability curves later in this section.

5.3.1.2 Hydrograph Shape. The current modeling effort uses a specific hydrograph shape based on an assumption of unregulated long-duration “natural” flow. Here long-duration means sufficient duration to inundate the entire INL inundation grid to the point of steady-state flow. The time required to achieve steady-state flow from initially near-dry conditions (flow confined to the Big Lost River channel) can be as long as about 20 hours. Steady-state flow can be achieved across the entire INL inundation grid in as little as 5-10 hours for modest (~10%) changes in discharge. For the purposes of the PIM, the probabilistic stage estimates correspond to peak flow durations of 20 hours. The effects of regulation and potential dam failure on hydrograph shape would require separate investigations, that would focus on modeling transient flow behavior.

5.3.1.3 Infiltration. The potential variability in inundation due to infiltration is currently evaluated by including two distinct end-member values for this parameter. Interpretation of available data suggests infiltration losses between 0 (no infiltration) and 15% for the study reach of the Big Lost River (**Appendix E**). These two end member values provide information to assess the sensitivity of results to this parameter. The uncertainty in this parameter is composed of the intrinsic spatial variability in infiltration as well as a lack of knowledge regarding methods for estimating the parameter (especially for out-of-bank flows and long durations).

5.3.1.4 Culverts. The probabilistic stage calculations for INL include a simplified representation of the effect of culverts on flow, and hence inundation at the site. Three scenarios are considered. In two scenarios full conveyance of the active Big Lost River channel is allowed through Lincoln Avenue and either, full conveyance, or zero conveyance, occurs through the other culverts. The third scenario involves zero conveyance through the Lincoln Avenue culverts on the active channel of the Big Lost River and full conveyance through the remaining culverts.

5.3.2 Epistemic Uncertainties.

5.3.2.1 Topography and Flow Model Uncertainty. Uncertainties in the modeling of topography will exist in both the FFA results and in the PIM. Currently, these uncertainties are explicitly treated by calculating flow results using two grid resolutions to provide a first-order sensitivity analysis. Potential epistemic uncertainties associated with the two flow models are discussed in **Appendix C, Part B, Section 1**. These tests and output comparisons (difference plots in **Appendix E - Electronic Supplement**) show that negligible differences in water-surface elevation at most sites can be attributed to the choice of flow model. Much larger epistemic uncertainty is associated with the ability to accurately resolve subtle topographic features in the model inputs.

Efforts have been made to ensure that the topographic models will not have systematic biases (**Appendix A**). The observed sensitivity of the flow results to grid resolution suggest that the flow models are likely sensitive to random and transient variations in topography, particularly in regions near the Big Lost River channel and secondary channels associated with old diversions, roadways, ditches, and artificial barriers. These small-scale features play significant roles in determining the path of shallow flow across the broad Pleistocene surfaces near INTEC and TRA.

5.3.3 Scope of Results. Based on the study results, it was deemed unnecessary to attempt to assign weights to the various aleatory and epistemic uncertainty components to produce a comprehensive calculation of PIM. Hence, for this study, the conceptual framework portrayed in **Figure 5-2** has essentially one primary input from which calculated uncertainty is carried forward, that being the revised flood frequency analyses. For the present analyses, the other aleatory components of uncertainty are either beyond the scope of the present study (e.g., hydrograph variability), or can be shown to be not significant based on the modeling results (e.g., effects of infiltration and most culverts). Difference plots of the end member scenarios of infiltration and secondary culvert blockage show that the change in water surface between these scenarios is less than 0.25 ft except for isolated locations along the margin of the inundated area where a small increase in stage overtops a local threshold and leads to inundation of adjacent lower areas (**Appendix E - Electronic Supplement**). Examination of these results shows that in most cases the resulting stage differences are most typically on the order of ~ 0.1 ft.

Stage - AEP curves were constructed for fifteen TRA/INTEC sites of particular interest shown on **Figure 5-1** and listed in **Table 5-3**. Example curves from two INTEC and two TRA sites are shown here as **Figure 5-3** through **Figure 5-6** and a complete set of curves is displayed in **Appendix F**. Curves show mean, 5%, and 95% fractiles based on the associated discharge probabilities derived from the flood frequency analyses in **Section 4.0** and listed in **Table 5-2** and the stage (water-surface elevations) from the TrimR2D and RiCOM hydraulic models. Differences in equivalent fractile curves due to infiltration and culvert scenarios are typically on the order of ~0.1 ft. Differences due to discharge AEP are much larger. For AEP of 0.01 (100-yr) the typical range between the 5% and 95% curves is ~0.3 ft; for AEP of 0.0001 (10,000-yr) the range is typically 0.5- to 1.0 ft. These ranges thus depict the sensitivity of stage to uncertainty in input discharge AEP.

Epistemic uncertainty associated with the input topography for the hydraulic models is not quantified in a statistical sense, but is shown by the differences in stage hazard plots for TrimR2D compared to RiCOM. These effects are often largest for flows less than about 200 cms where the differences the ability of the input grids to resolution subtle features of the input topography leads to areas inundated to higher or lower levels between the flow models (See TrimR2D minus RiCOM difference plots in **Appendix E - Electronic Supplement**). A full appreciation of the impact of these factors on inundation characteristics is best provided by the large-scale inundation maps. On the stage - AEP curves for the fifteen TRA/INTEC sites suggest these effects are mostly less than ~ 0.5 ft (**Appendix F**), but it is the maps (**Appendix E - Electronic Supplement**) that provide the best illustrations of the strong sensitivity of portions of the inundation to topographic resolution and relatively subtle topographic features such as roads and old diversion structures.

5.4 Evaluation of Results

Flow patterns for the modeled flows near and through the facility sites are complex and strongly influenced by small-scale topographic features such as secondary channels, ditches, roads, berms, barriers, buildings and the overall topographic slope across each facility site. Water-surface elevations within the site areas are not always directly linked to the water-surface elevation in the main Big Lost River channel because flow reaches many areas of the site through channel networks that connect to the main Big Lost River as much as several kilometers upstream of the

facilities. In other cases, some areas within each facility are effectively isolated from most flows by local topographic high areas of unknown permanence or integrity. Thus, within each facility, the water-surface elevation shown on the stage-probability plots for a given probability may differ across the facility by as much as 10 ft. **Table 5-4** and **Table 5-5** show the variations in water-surface elevation based on TrimR2D simulations at the fifteen monitoring sites within TRA and INTEC for AEP of 0.01 (100-yr), 0.02 (500-yr), 0.005 (2000-yr), and 0.0001 (10,000).

5.4.1 Flood Stage - Probability at TRA. The situation at TRA illustrates that topographic features located far from TRA have the most profound impacts on potential inundation at TRA. For discharges of 225 cms or larger, flow backwaters behind the constriction upstream of BLR8 (upstream of Hwy 20/26), flows proceed into a channel that extends 1 km north of the Big Lost River, and are entrained on the north side of an old Pioneer diversion canal (that starts 3-4 km upstream of TRA), which delivers the flow directly to the west edge of the TRA (see inundation maps in **Appendix E - Electronic Supplement**). Similarly, inundation hazards for the southern side of the TRA are dominated by flows that escape the primary Big Lost River channel about 3.2 km upstream of Monroe Avenue for discharges of > 100 cms as illustrated in **Figure 5-3** and the inundation maps (**Appendix E - Electronic Supplement**). Other sites in the TRA, like TRA-632 (map ref #7), are influenced by large scale flow features and are almost completely insensitive to topographic resolution, infiltration, or culvert scenarios (**Figure 5-4**). Only topographic resolution (**Figure 5-4a**) has a non-negligible impact on the TRA-632 stage probabilities, but the effect is still small (compare **Figure 5-4a** to **Figure 5-3b** or **Figure 5-5a**).

5.4.2 Flood Stage - Probability at INTEC. Topographic grid resolution also has a profound impact on estimated inundation at several sites at INTEC (**Appendix E - Electronic Supplement; Figure 5-5**) However, full versus blocked conveyance of the Big Lost River at Lincoln Avenue has the strongest impact on estimated inundation at INTEC map ref site #13 (**Figure 5-5**). Similar results are obtained at the INTEC tank farm (map ref #10, **Figure 5-6**) except that RiCOM inundation actually exceeds TrimR2D inundation for discharges larger than 100 cms (**Figure 5-6a**). The contrasts between **Figure 5-5a** and **Figure 5-6a** demonstrate some of the complex dependencies of inundation on topographic grid resolution at INTEC and serve to

emphasize the importance of using the inundation maps (**Appendix E - Electronic Supplement**) to understand the primary factors influencing inundation at INL facilities.

5.5 Inundation Discussion

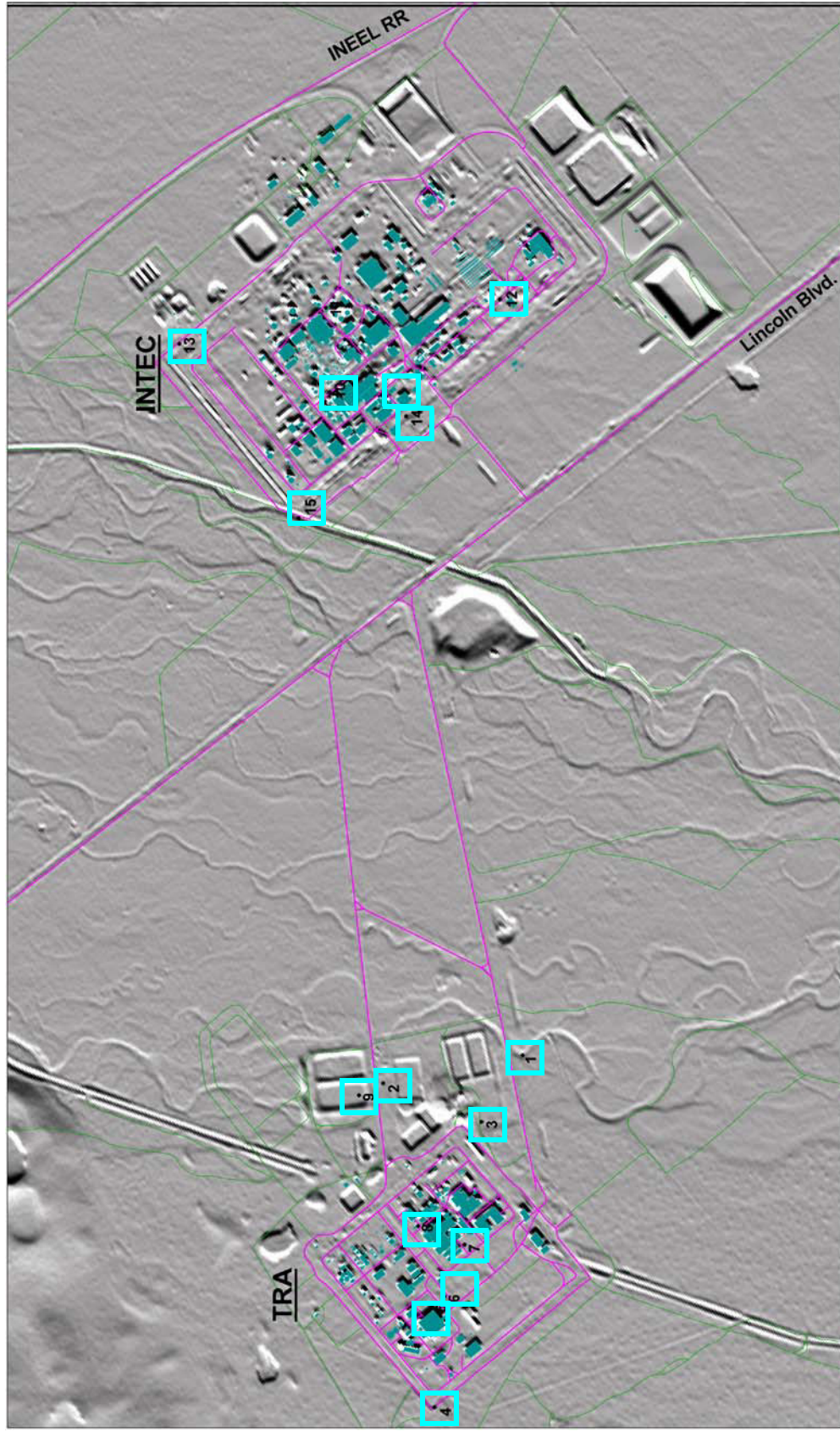
Stage hazard curves are provided in **Appendix F** for fifteen specific sites near TRA or INTEC as listed in **Table 5-3** and shown on **Figure 5-1**. For each site there are four plots of flow simulation results: 1) TrimR2D, 2) RiCOM, 3) TrimR2D - RiCOM comparisons, and 4) RiCOM Lincoln Ave blockage scenarios. Comparisons within and between these four sets of plots isolate or compare specific factors that could influence estimated stages. The TrimR2D simulations are the primary suite of results for final estimate of stage hazard curves and isolate the effects of variations in infiltration and secondary culvert blockage. Generally, the secondary culverts have virtually no impact on inundation at most sites, with only minor impacts on inundation at sites outside TRA along Monroe Avenue. Infiltration has only a modest impact on inundation and generally does not change the hazard curves much. The RiCOM simulations and TrimR2D - RiCOM simulations illustrate the impacts of topographic resolution and persistent topographic features such as roads, old diversions, etc. These factors have the strongest impacts on inundation over the entire site. The RiCOM simulations with blockage of the Big Lost River channel at Lincoln Avenue has the strongest impact on inundation for portions of INTEC, particularly for the simulations of discharges less than about 250 cms.

The inundation maps in **Appendix E - Electronic Supplement** provide an essential tool to understand the stage hazard curves in **Appendix F**. It is clear that small-scale (possibly transient) changes to topography can significantly impact inundation at TRA and INTEC. This is a consequence of the relatively flat terrain in the vicinity of the Big Lost River and these INL facilities. However, the maps also provide a tool to determine small-scale changes to topography that could substantially reduce inundation hazards at TRA and INTEC. For instance, flow along the northern side of the old diversion channel west of TRA could be blocked by rather small-scale topographic modifications about 3.2 km west of TRA near the western end of the old diversion channel. The inundation impacts of topographic modification scenarios could be easily investigated by running new flows with modifications to the detailed topographic RiCOM mesh. Clearly, the performance of the Big Lost River culverts at Lincoln Avenue have a profound

influence on stage hazards for several sites at INTEC, especially for the lower end of the discharges simulated. Similarly, although an explicit culvert blocking scenario was not constructed for the railroad embankment bridge downstream of INTEC, blockage of conveyance through the railroad embankment may also significantly influence stage hazards for portions of INTEC.

The stage hazard curves contained in **Appendix F** have the same limitations for extrapolation to small AEP ($AEP < 0.0001$) as do the flood frequency results presented in **Section 4.0**. Because the flood frequency results are largely unconstrained for small AEP, no meaningful estimate of 95% limits is contained in the revised flood frequency analyses to promulgate into the stage probability estimate. Given the nearly unlimited upper bounds of extrapolation that might be possible for small AEP from the present flood frequency analyses, development of stage hazard curves for smaller AEP would also require additional hydraulic modeling for discharges much larger than 700 cms, which is the largest discharge considered in the present study.

Figures for Section 5.0

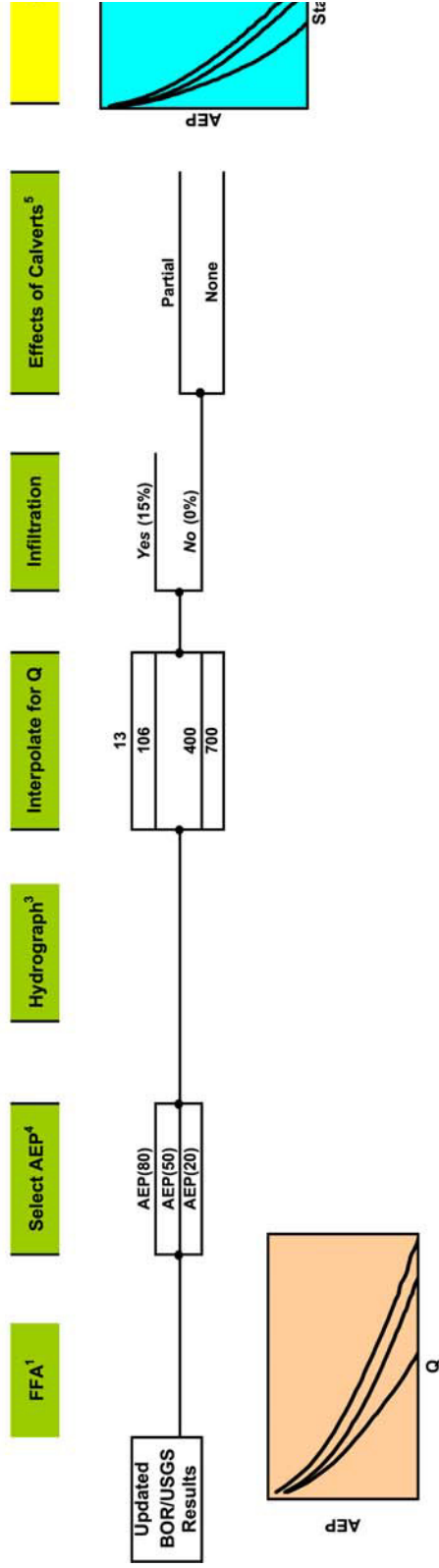


Base map is shaded relief image of 10 ft topographic grid from 1993 photography. Planimetric features are from INEEL Spatial Analyses Laboratory.

3 • Stage-probability estimate site

Figure 5-1 Map of monitoring site locations (numbered black squares within blue boxes) for inundation at TRA and INTEC. Sites 1 through 9 are located within and around TRA; sites 10 through 15 are located within and around INTEC. Numbers by each square are "Map Ref #" listed under "site" in **Table 5-3** and in the headings of each stage-AEP plot.

CONCEPTUAL LOGIC TREE FOR ESTIMATION OF PROBABILISTIC FLOOD STAGE



Alternative FFA Results² (similar to above for alternative FFA results)

- ¹FFA - flood frequency analysis
- ²Could include regulated flow frequency and/or upstream dam failure probability estimates
- ³Hydrographic Shapes are based on assumption of natural, unregulated flow
- ⁴Flow simulations have been run for Q values = 13, 25, 63, 106, 150, 200, 250, 300, 400, 700 hrs
- ⁵For "partial" effect, main stem of river stays open; for "none," all culverts are assumed open

Figure 5-2 Conceptual logic tree for probabilistic INL inundation modeling.

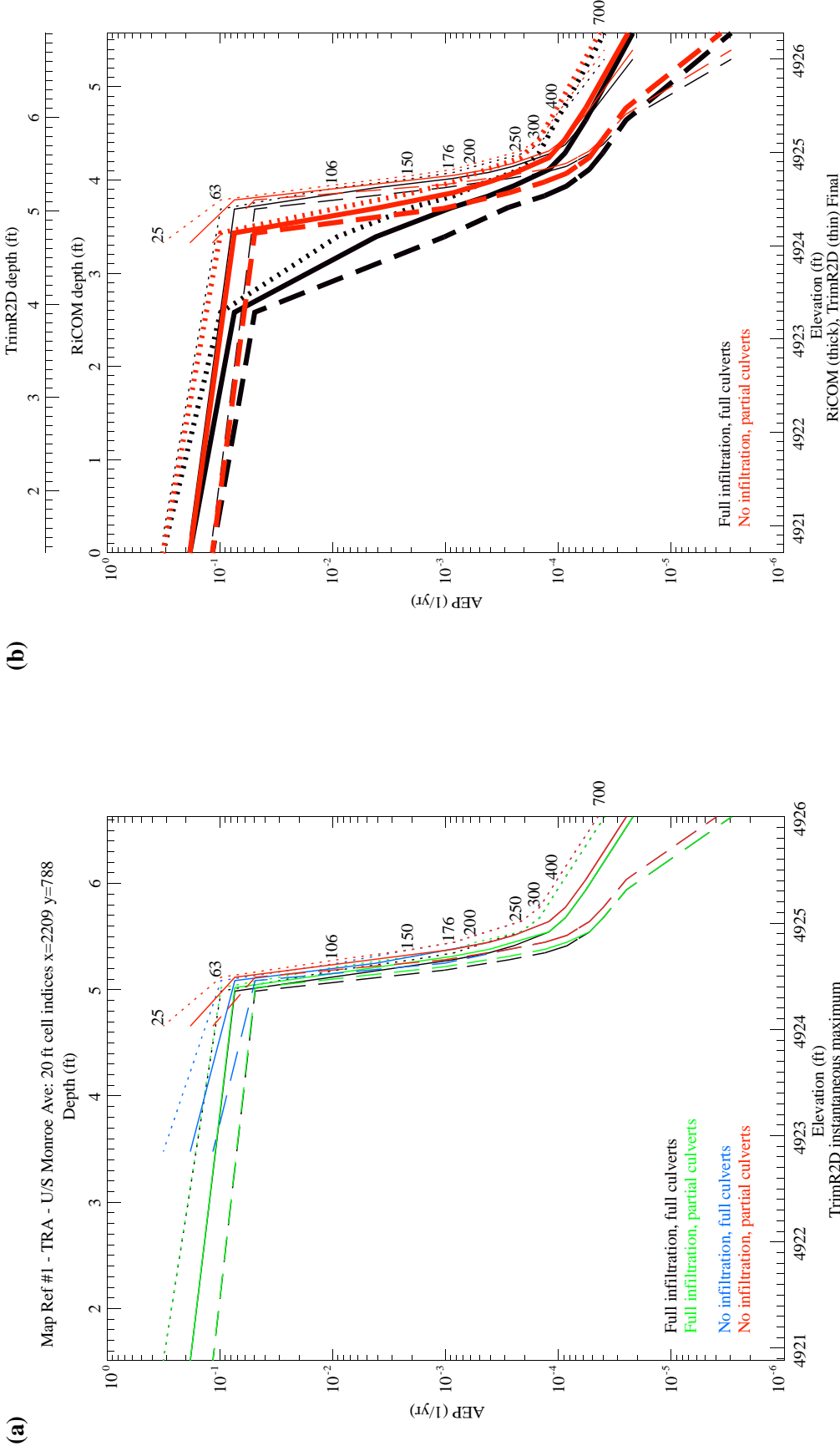
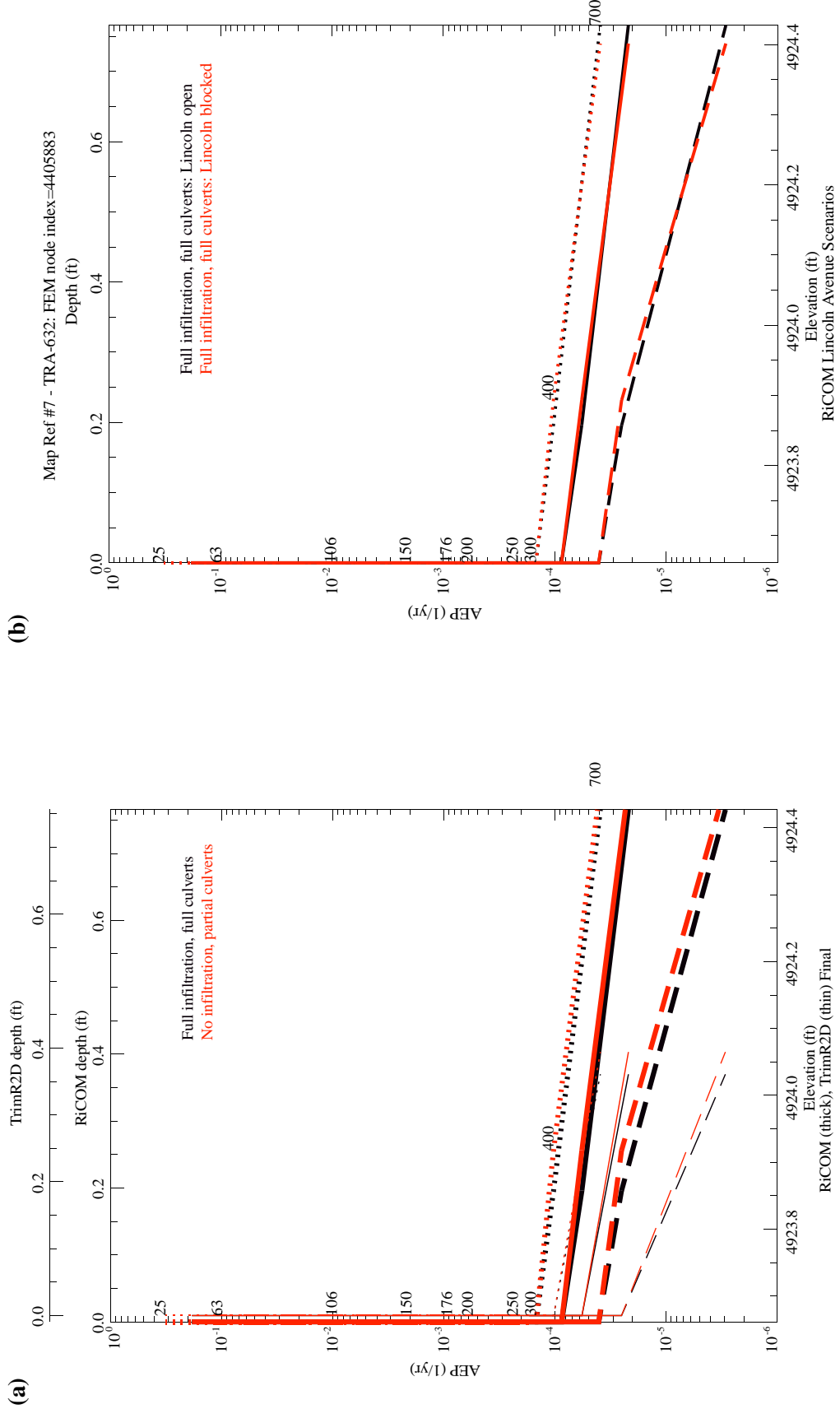
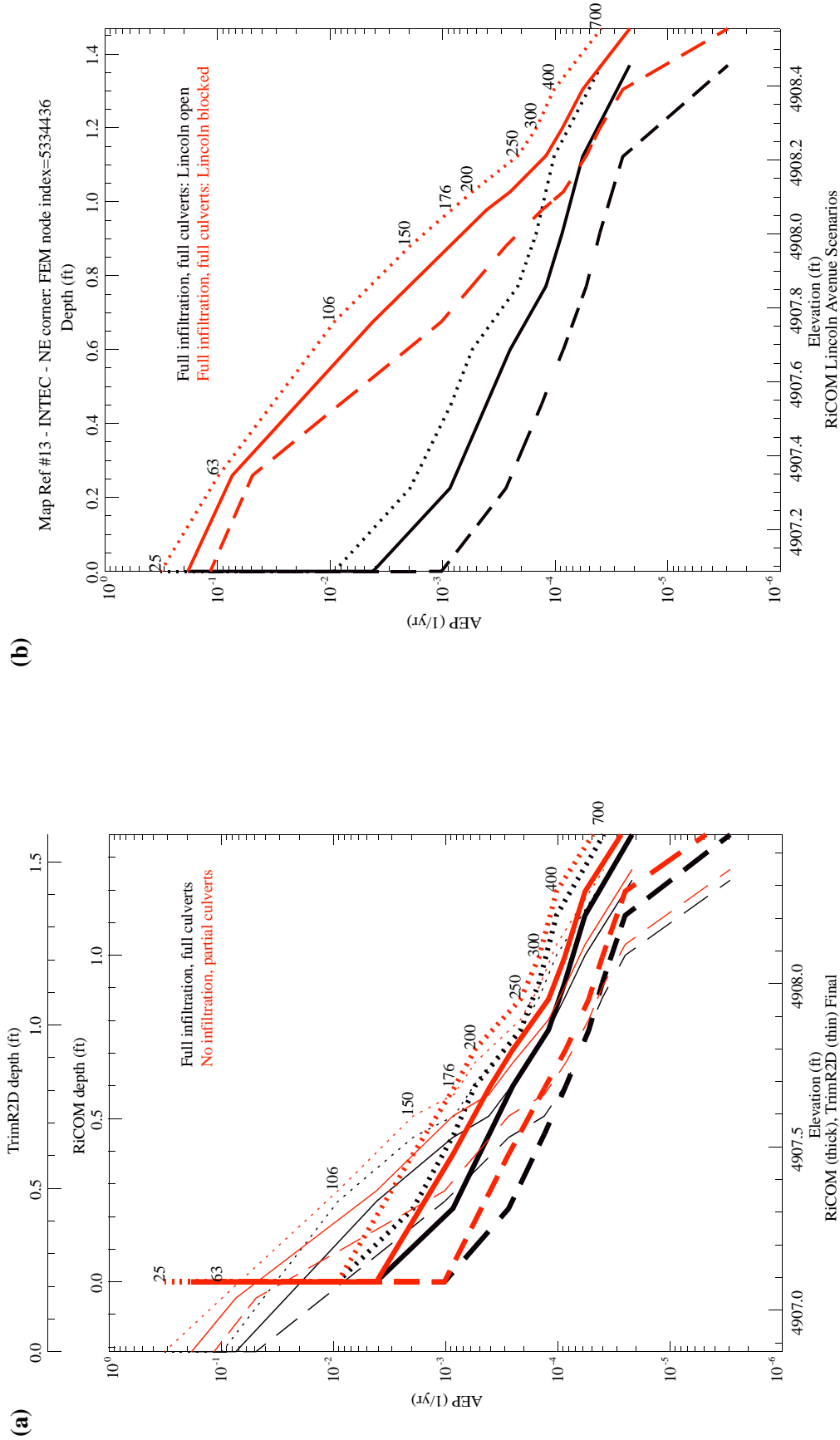


Figure 5-3 Stage hazard curves for site TRA map ref #1. TrimR2D results are shown in (a) and RiCOM results in (b). In the TrimR2D results (a) there are four color-coded infiltration-culvert scenarios (see legend) for fractiles of 5% (dashed curves), mean (solid curves), and 95% (dotted curves). When black or blue curves are not visible the inclusion of culverts outside the Big Lost River main channel had no influence at the site. In (b) comparison of TrimR2D (thin curves) and RiCOM (thick curves) results demonstrate that topographic resolution has the strongest impact on the site inundation. Numbers indicate discharge rates (cms) for specific points along the rightmost 95% curves. See **Figure 5-1** for site location.



Map Ref #7 - TRA-632: FEM node index=4405883

Figure 5-4 Stage hazard curves for TRA-632 map ref #7. (a) comparison of TrimR2D (thin curves) and RiCOM (thick curves) results demonstrate that topographic resolution has a stronger impact on site inundation than infiltration or culverts when the main channel is open. (b) blocking the Big Lost River at Lincoln Avenue (b) has virtually no impact on site inundation. Lines styles indicate fractiles of 5% (dashed curves), mean (solid curves), and 95% (dotted curves). Numbers indicate discharges (cms) for specific points along the rightmost 5% curves. See **Figure 5-1** for site location.



Map Ref #13 - INTEC - NE corner: FEM node index=5334436

Figure 5-5 Stage hazard curves for INTEC map ref #13. (a) comparison of TrimR2D (thin curves) and Ricom (thick curves) results demonstrate that topographic resolution has a stronger impact on site inundation than infiltration or culverts when the main channel is open. (b) blocking the Big Lost River at Lincoln Avenue has the strongest impact on site inundation. Lines styles indicate fractiles of 5% (dashed curves), mean (solid curves), and 95% (dotted curves). Numbers indicate discharges (cms) for specific points along the rightmost 95% curves. See **Figure 5-1** for site location.

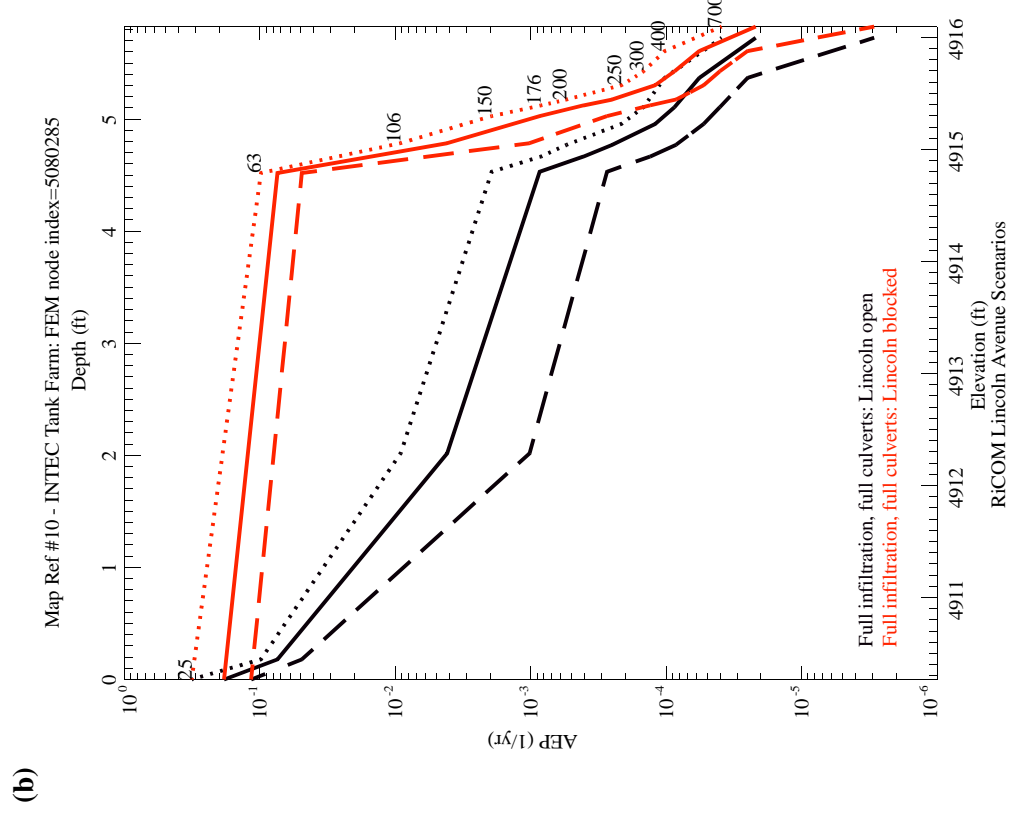
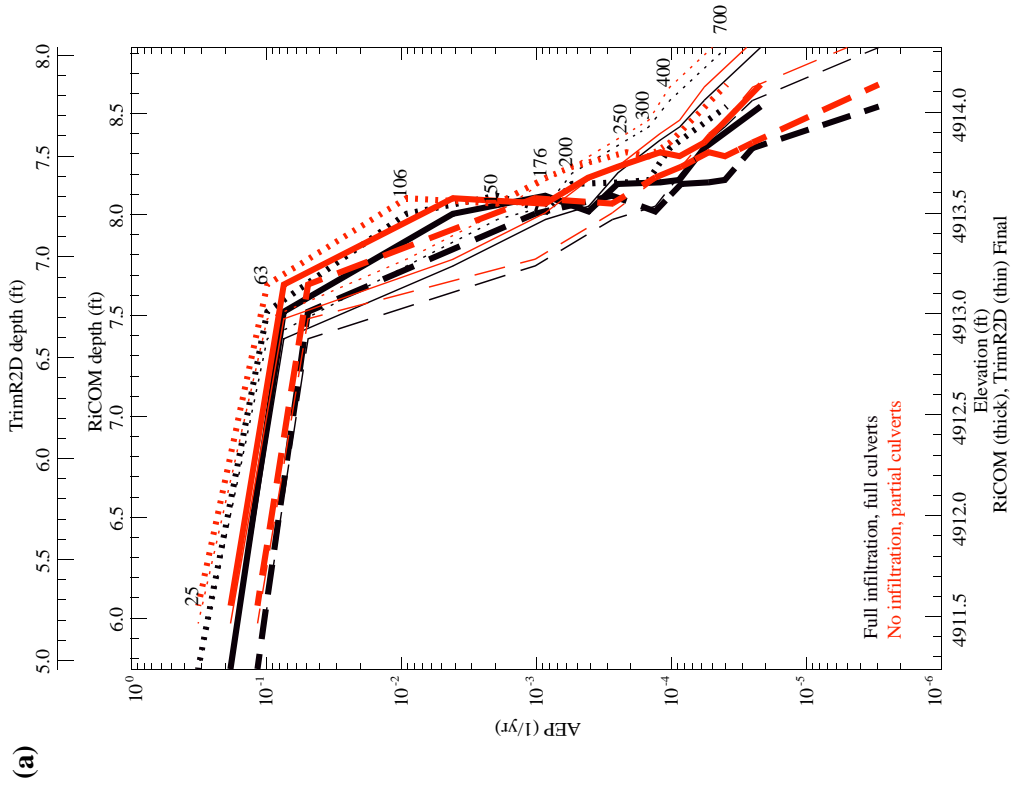


Figure 5-6 Stage hazard curves for the INTEC tank farm map ref #10. (a) comparison of TrimR2D (thin curves) and RiCOM (thick curves) results demonstrate that topographic resolution has a stronger impact on site inundation than infiltration or culverts when the main channel is open. (b) blocking the Big Lost River at Lincoln Avenue has the strongest impact on site inundation. Lines styles indicate fractiles of 5% (dashed curves), mean (solid curves), and 95% (dotted curves). Numbers indicate discharges (cms) for specific points along the rightmost 95% curves. See **Figure 5-1** for site location.

Tables for Section 5.0

Table 5-1 Discharge and modeling scenarios used to construct the stage - probability estimates

Modeled Discharge ¹ m ³ /s (ft ³ /s)	Infiltration ²				Potential Significance of Modeled Discharge
	None		Full		
	Full Culverts	Partial Culverts	Partial Culverts	Full Culverts	
13 (~460)	T	T	T	T	Approximate maximum Big Lost River gaged flow downstream of INEEL Diversion (since 1984)
25 (~885)	T	T,R	T	T,R	Approximate INEEL Diversion Dam release capacity
63 (~2225)	T	T,R	T	T,R	Estimated maximum Big Lost River historic flood (1965) upstream of INEEL Diversion Dam
87		R		R	Revised Big Lost River 100-yr flood (this study)
97		R		R	95% bound on revised Big Lost River 100-yr flood (this study)
106 (~3740)	T	T,R	T	T,R	Revised USGS Big Lost River 100-yr flood (Hortness and Rousseau, 2002)
110		R		R	Revised Big Lost River 500-yr flood (this study)
130		R		R	Data for stage-probability curves
150 (~5295)	T	T,R	T	T,R	Preferred discharge for Big Lost River 10,000-yr paleohydrologic bound (Ostenaa and others, 1999). Preferred discharge for late Holocene Big Lost River paleofloods (this study)
176 (~6215)	T	T,R	T	T,R	USGS 100-yr flood downstream of INEEL Diversion Dam (Kjelstrom and Berenbrock, 1998)
200 (~7060)	T	T,R	T	T,R	Data for stage-probability curves
250 (~8830)	T	T,R	T	T,R	Preferred discharge for Big Lost River 10,000-yr paleohydrologic bound (this study)
300 (~10,595)	T	T,R	T	T,R	Data for stage-probability curves
400 (~14,125)	T	T,R	T	T,R	Data for stage-probability curves
700 (~24,720)	T	T,R	T	T,R	Adopted INEEL interim 100-yr flood; Estimated dam break flow at INTEC for Mackay Dam 100-yr flood failure (Koslow and Van Haaften, 1986)

Notes:

¹ Steady-state discharge input at upstream end of reach near INEEL Diversion Dam

² Entries in table indicate flow model used for each scenario: T - TRIMR2D with 20-ft rectangular grid as input topography; R - RICOM with 5-, 10-, and 20-ft variable grid as input topography. Limits of 5-ft mesh were defined by extent of inundation from TRIMR2D model of 100 m³/s with no infiltration and partial culverts; limits of 10-ft mesh by extent of TRIMR2D 200 m³/s inundation for same scenario.

Table 5-2 Discharge-AEP Results from the FFA.

Discharge	5%	Mean	95%
(cms)	AEP (1/yr,T=yr)	AEP (1/yr,T=yr)	AEP (1/yr,T=yr)
25	1.16×10^{-01} (9)	1.84×10^{-01} (5)	3.19×10^{-01} (3)
63	4.901×10^{-02} (20)	7.41×10^{-02} (14)	9.82×10^{-02} (10)
106	1.02×10^{-03} (977)	4.15×10^{-03} (241)	9.14×10^{-03} (109)
150	2.74×10^{-04} (3651)	8.61×10^{-04} (1162)	1.95×10^{-03} (513)
176	1.32×10^{-04} (7588)	4.10×10^{-04} (2436)	8.42×10^{-04} (1188)
200	8.46×10^{-05} (11,823)	2.51×10^{-04} (3991)	5.44×10^{-04} (1838)
250	5.30×10^{-05} (18,872)	1.21×10^{-04} (8269)	2.15×10^{-04} (4660)
300	4.02×10^{-05} (24,855)*	8.70×10^{-05} (11,499)	1.47×10^{-04} (6784)
400	2.51×10^{-05} (39,851)*	5.71×10^{-05} (17,513)	1.03×10^{-04} (9737)
700	2.92×10^{-06} (342,392)*	2.18×10^{-05} (45,839)*	3.90×10^{-05} (25,653)*
* Values with little or diminished statistical significance (See Section 4.0).			

Table 5-3 Stage - Probability Sites

Site ¹		x-coordinate	y-coordinate	Notes
Map Ref #	Description	20-ft grid	20-ft grid	
TRA Sites				
1	TRA - Monroe Ave	2209	788	upstream side in small channel
2	TRA-715 (evap. pond)	2277	819	sm. channel upstream of old Monroe
3	TRA southeast corner	2222	827	outside fence
4	TRA northwest corner	2212	979	outside fence
5	TRA-670 (ATR)	2225	926	southeast corner
6	TRA-670 (ATR)	2220	921	south side on Cod Street
7	TRA-632	2216	892	
8	TRA-621	2242	888	
9	TRA-715 (evap. pond)	2288	828	inside north pond
INTEC Sites				
10	INTEC Tank Farm	2387	471	NW corner
11	NWCF (Bldg 659)	2399	428	SE corner
12	CPP-749	2311	403	West side
13	INTEC - NE corner	2470	464	outside fence
14	INTEC -nr west gate	2345	474	
15	BLR - NW corner of INTEC	2388	539	in main channel
Notes:				
¹ See Appendix E for plots that show Site No. locations at INTEC and TRA.				

Table 5-4 Probabilistic Stage Estimates for INTEC and TRA Sites (100 and 500 floods).

Map Ref #	Site Description	AEP = 10 ⁻² Return period = 100 yr			AEP = 2 x 10 ⁻³ Return period = 500 yr		
		5%	mean	95%	5%	mean	95%
TRA Sites							
1	TRA - Monroe Ave	4924.49-4924.56	4924.55-4924.60	4924.61-4924.65	4924.58-4924.63	4924.67-4924.70	4924.72-4924.75
2	TRA-715 (evap. pond)	4918.36-4918.56	4918.50-4918.64	4918.63-4918.71	4918.57-4918.67	4918.73-4918.81	4918.81-4918.91
3	TRA southeast corner	dry	dry	dry	dry	dry	dry
4	TRA northwest corner	dry	dry	dry	dry	dry	dry
5	TRA-670 (ATR)	dry	dry	dry	dry	dry	dry
6	TRA-670 (ATR)	dry	dry	dry	dry	dry	dry
7	TRA-632	dry	dry	dry	dry	dry	dry
8	TRA-621	dry	dry	dry	dry	dry	dry
9	TRA-715 (evap. pond)	dry	dry	dry	dry	dry	dry
INTEC Sites							
10	INTEC Tank Farm	4912.57-4913.12	4912.92-4913.29	4913.26-4913.45	4913.09-4913.37	4913.50-4913.65	4913.72-4913.85
11	NWCF (Bldg 659)	dry	dry	dry	dry	dry	dry
12	CPP-749	4916.30-4916.40	4916.42-4916.51	4916.54-4916.60	4916.48-4916.55	4916.63-4916.69	4916.71-4916.78
13	INTEC - NE corner	4907.04-4907.17	4907.18-4907.27	4907.31-4907.35	4907.25-4907.31	4907.42-4907.47	4907.53-4907.59
14	INTEC -nr west gate	4916.30-4916.40	4916.42-4916.51	4916.54-4916.60	4916.48-4916.55	4916.63-4916.69	4916.71-4916.78
15	BLR - NW corner of INTEC	4913.03-4913.10	4913.13-4913.18	4913.22-4913.26	4913.18-4913.22	4913.34-4913.38	4913.46-4913.50

* Values of 0.00-0.00 indicate that site is not inundated by modeled flows for stated AEP.

Table 5-5 Probabilistic Stage Estimates for INTEC and TRA Sites (2000 and 10000 year floods).

Map Ref #	Site Description	AEP = 5×10^{-4} Return period = 2000 yr			AEP = 1×10^{-4} Return period = 10000 yr		
		5%	mean	95%	5%	mean	95%
TRA Sites							
1	TRA - Monroe Ave	4924.68-4924.71	4924.77-4924.80	4924.86-4924.90	4924.83-4924.86	4925.04-4925.09	4925.36-4925.43
2	TRA-715 (evap. pond)	4918.74-4918.82	4918.91-4918.99	4919.06-4919.13	4919.01-4919.07	4919.36-4919.45	4919.89-4919.99
3	TRA southeast corner	dry	dry-4922.21	4922.36-4922.45	4922.20-4922.37	4922.81-4922.96	4923.76-4924.02
4	TRA northwest corner	dry	dry	dry	dry	4923.38-4923.52	4924.14-4924.20
5	TRA-670 (ATR)	dry	dry	dry	dry	dry	dry
6	TRA-670 (ATR)	dry	dry	dry	dry	dry	4923.29-4923.32
7	TRA-632	dry	dry	dry	dry	dry	dry
8	TRA-621	dry	dry	dry	dry	dry	dry
9	TRA-715 (evap. pond)	dry	dry	dry	dry	dry	dry
INTEC Sites							
10	INTEC Tank Farm	4913.54-4913.68	4913.87-4913.98	4914.08-4914.18	4914.01-4914.11	4914.49-4914.57	4914.86-4914.89
11	NWCF (Bldg 659)	dry	dry-4911.35	4911.77-4911.81	4911.22-4911.77	4911.93-4911.96	4912.03-4912.06
12	CPP-749	4916.64-4916.71	4916.79-4916.85	4916.93-4916.96	4916.88-4916.92	4917.15-4917.24	4917.45-4917.48
13	INTEC - NE corner	4907.44-4907.49	4907.58-4907.64	4907.71-4907.77	4907.66-4907.72	4907.91-4907.95	4908.09-4908.13
14	INTEC -nr west gate	4916.64-4916.71	4916.79-4916.85	4916.93-4916.96	4916.88-4916.92	4917.15-4917.22	4917.41-4917.45
15	BLR - NW corner of INTEC	4913.36-4913.40	4913.52-4913.62	4913.71-4913.75	4913.64-4913.71	4913.90-4913.93	4914.07-4914.13

* Values of 0.00-0.00 indicate that site is not inundated by modeled flows for stated AEP.

6.0 REFERENCES

- Andrews, E.D., 1984, Bed-material entrainment and hydraulic geometry of gravel-bed rivers in Colorado: Geological Society of America Bulletin, v. 95, p. 371-378.
- Baker, V.R., and Costa, J.E., 1987, Flood power, in Mayer, L., and Nash, D., eds., Catastrophic Flooding: Boston, MA, Allen & Unwin, p. 1-21.
- Baker, V.R., Kochel, R.C., and Patton, P.C., eds., 1988, Flood geomorphology: New York, John Wiley and Sons, 503 p.
- Berenbrock, C., and Doyle, J.D., 2004, Stage-discharge relations for selected culverts and bridges in the Big Lost River flood plain at the Idaho National Engineering and Environmental Laboratory, Idaho: U.S. Geological Survey Water Resources Investigations Report 04-4066, Idaho Falls, ID, 62 p.
- Berenbrock, C., Rousseau, J.P., Orr, B.R., Twining, B.V., and Whnke, A., in prep., Flood flow and sediment characteristics of bedrock constrictions in the Big Lost River at the Idaho National Engineering and Environmental Laboratory, Idaho [DRAFT]: U.S. Geological Survey Water Resources Investigations Report 03-xxx, Idaho Falls, ID.
- Birkeland, P.W., 1999, Soils and geomorphology: New York, Oxford University Press, 430 p.
- Carson, M. A., and Griffiths, G.A., 1987, Bedload transport in gravel channels: Journal of Hydrology New Zealand, v. 26, no. 1, p. 1-151.
- Cerling, T.E., Poreda, R.J., and Rathburn, S.L., 1994, Cosmogenic ^3He and ^{21}Ne age of the Big Lost River flood, Snake River Plain, Idaho: Geology, v. 22, p. 227-230.
- Connor, M.A., 1998, Final report on the Jackson Lake archeological project, Grand Teton National Park, Wyoming: Report prepared for Bureau of Reclamation, Pacific Northwest Office, Boise, ID, with contributions by K.L. Pierce, S. Lundstrom, and J.M. Good, Technical Report No. 46, Department of the Interior, National Park Service, Midwest Archeological Center, Lincoln, Nebraska, 278 p.
- Cook, J.L., 1987, Quantifying peak discharges for historical floods: Journal of Hydrology, v. 96, p.29-40.
- Costa, J.E., 1978, Holocene stratigraphy in flood frequency analysis: Water Resources Research, v. 14, p. 626-632.
- Fiedler, F.R., 2002, Infiltration rates to support high-resolution hydraulic modeling at Idaho National Engineering and Environmental Laboratory, Department of Civil Engineering, University of Idaho, Moscow, ID, 13 p.
- Forman, S.L., Smith, R.P., Hackett, W.R., Tullis, J.A., and McDaniel, P.A., 1993, Timing of late Quaternary glaciations in the western United States based on the age of loess on the eastern Snake River Plain, Idaho: Quaternary Research, v. 40, p. 30-37.
- Geslin, J.K., Link, P.K., and Fanning, C.M., 2002, High-precision provenance determination using detrital-zircon ages and petrography of Quaternary sands on the eastern Snake River Plain, Idaho: Geology, v. 27, no. 4, p. 295-298.
- Good, J.M., and Pierce, K.L., 1996, Interpreting the landscapes of Grand Teton and Yellowstone National Parks, recent and ongoing geology: Grand Teton Natural History Association, Grand Teton National Park, Moose, Wyoming, 58 p.
- Harding, William M, 2002, Northwind Environmental, Inc. letter report to Dr. Kenneth Reid, State Historic Preservation Office, Boise, ID, dated September 6, 2002, 8 p.

- Hortness, J.E., and Rousseau, J.P., 2003, Estimating the magnitude of the 100-year peak flow in the Big Lost river at the Idaho National Engineering and Environmental Laboratory, Idaho: U.S. Geological Survey Water Resources Investigations Report 02-4299, Idaho Falls, ID, 36 p.
- House, P.K., Pearthree, P.A., and Klawon, J.E., 2002, Historical flood and paleoflood chronology of the lower Verde River, Arizona, *in*: House, P.K., Webb, R.H., Baker, V.R., and Levish, D.R., eds., *Ancient Floods, Modern Hazards: Principles and Applications of Paleoflood Hydrology: Water and Science Application 5*, American Geophysical Union, Washington, D.C., p. 267-293.
- Jarrett, R.D., and England, J.F., Jr., 2002, Reliability of paleostage indicators for paleoflood studies, *in* House, P.K., Webb, R.H., Baker, V.R., and Levish, D.R., eds, *Ancient Floods, Modern Hazards: Principles and Applications of Paleoflood Hydrology: Water Science and Application Volume 5*, American Geophysical Union, Washington, D.C., p. 91-109
- Johnson, D.L., and Johnson, D.N., 2003, Mima and other animal mounds as point-centered biomantles: *Geol. Soc. Amer., Abstracts with Programs v.35;n. 6*, p. 258.
- Kessler, M.A., and Werner, B.T., 2003, Self-organization of sorted patterned ground: *Science*, v. 299, p. 380-383.
- Kjelstrom, L.C., 1991, Idaho, floods and droughts, in Paulson, R.W., Chase, E.B., Roberts, R.S., and Moody, D.W., *National Water Summary 1988-89 – Hydrologic events and floods and droughts: U.S. Geological Survey Water-Supply Paper 2375*, p. 255-262.
- Kjelstrom, L.C., and Berenbock, C., 1996, Estimated 100-year peak flows and flow volumes in the Big Lost River and Birch Creek at the Idaho National Engineering and Environmental Laboratory, Idaho: U.S. Geological Survey Water-Resources Investigations Report 96-4163, 23 p.
- Koslow, K.N., and Van Haaften, D.H., 1986, Flood routing analysis for a failure of Mackay Dam: EG&G Idaho, Inc. report prepared for the U.S. Department of Energy, contract no. DE-AC07-76IDO1570, 33 p.
- Knudsen, K.L., Sowers, J.M., Ostenaar, D.A., and Levish, D.R., 2002, Evaluation of glacial outburst flood hypothesis for the Big Lost River, Idaho, *in*: House, P.K., Webb, R.H., Baker, V.R., and Levish, D.R., eds., *Ancient Floods, Modern Hazards: Principles and Applications of Paleoflood Hydrology: Water and Science Application 5*, American Geophysical Union, Washington, D.C., p. 217-235.
- Kuntz, M.A., Skipp, B., Lamphere, M.A., Scott, W.E., Pierce, K.L., Dalrymple, G.B., Champion, D.E., Embree, G.F., Page, W.R., Morgan, L.A., Smith, R.P., Hackett, W.R., and Rodgers, D.W., 1994, Geologic map of the Idaho National Engineering Laboratory and adjoining area, eastern Idaho, U.S. Geological Survey Miscellaneous Investigation Map I-2330, scale 1:100,000.
- Levish, D.R., 2002, Paleohydrologic bounds - non-exceedence information for flood hazard assessment, *in*: House, P.K., Webb, R.H., Baker, V.R., and Levish, D.R., eds., *Ancient Floods, Modern Hazards: Principles and Applications of Paleoflood Hydrology: Water and Science Application 5*, American Geophysical Union, Washington, D.C., p. 175-190.
- Levish, D.R., Ostenaar, D.A., and O'Connell, D.R.H., 1994, A non-inundation approach to paleoflood hydrology for the event-based assessment of extreme flood hazards, in 1994 Annual Conference Proceedings, Association of State Dam Safety Officials: Lexington, KY, Association of State Dam Safety Officials, p. 69-82.

- Levish, D.R., Ostenaar, D.A., and O'Connell, D.R.H., 1996, Paleohydrologic bounds and the frequency of extreme floods: in Gruntfest, E. (ed.), *Twenty years later what we have learned since the Big Thompson flood*: Boulder, University of Colorado, Natural Hazards Research and Applications Information Center, Special Publication No. 33, p. 171-182.
- Levish, D.R., Ostenaar, D.A., and O'Connell, D.R.H., 1997, Paleoflood hydrology and dam safety: *Waterpower '97, Proceedings of the International Conference on Hydropower*, Atlanta, GA, p. 2205-2214.
- Licciardi, J.M., Clark, P.U., Brook, E.J., Pierce, K.L., Kurz, M.D., Elmore, D., and Sharma, P., 2001, Cosmogenic ^3He and ^{10}Be chronologies of the late Pinedale northern Yellowstone ice cap, *Montana: Geology*, v. 29, p. 1095-1098.
- Licciardi, J.M., Clark, P.U., Brook, E.J., Elmore, D., and Sharma, P., 2004, Variable responses of western U.S. glaciers during the last deglaciation: *Geology*, v. 32, p. 81-84.
- Magilligan, F.J., 1992, Thresholds and the spatial variability of flood power during extreme floods: *Geomorphology*, v. 5, p. 373-390.
- McFadden, L.D., McDonald, E.V., Wells, S.G., Anderson, K., Quade, J., and Forman, S.L., 1998, The vesicular layer and carbonate collars of desert soils and pavements: formation, age and relation to climate change: *Geomorphology*, v. 24, p. 101-145.
- Miall, A.D., 1996, *The Geology of Fluvial Deposits: Sedimentary Facies, Basin Analysis, and Petroleum Geology*: Springer-Verlag, Berlin, Heidelberg, 582 p.
- Miller, A.J. and Cluer, B.L., 1998, Modeling considerations for simulation of flow in bedrock channels: in Tinkler, K.J. and Wohl, E.E., eds., *Rivers over rock: Fluvial processes in bedrock channels*: Washington, DC, American Geophysical Union, Geophysical Monograph 107, p. 61-104.
- NRC (National Research Council), 1995, *Natural climate variability on decade-to-century time scales*: Washington, D.C., National Academy Press, Climate Research Committee, 630 p.
- NRC (National Research Council), 1999, *Improving American River flood frequency analyses*: Washington, D.C., National Academy Press, Committee on American River Flood Frequencies, 120 p.
- O'Connell, D.R.H., 1998, FLDFRQ3 Three-parameter maximum likelihood flood-frequency estimation with optional probability regions using parameter grid integration: User's Guide (Release 1.0), <ftp://ftp.seismo.usbr.gov/pub/outgoing/geomagic/scr/fldfreq3/>, June 2000.
- O'Connell, D.R.H., 2005, Nonparametric Bayesian flood frequency estimation: *Journal of Hydrology*, v. 313, p. 79-96.
- O'Connell, D.R.H., Levish, D.R., and Ostenaar, D.A., 1996, Bayesian flood frequency analysis with paleohydrologic bounds for late Holocene paleofloods, Santa Ynez River, California: in *Twenty years later what we have learned since the Big Thompson flood*: Boulder, University of Colorado, Natural Hazards Research and Applications Information Center, Special Publication No. 33, p. 183-196.
- O'Connell, D.R.H., Levish, D.R., and Ostenaar, D.A., 1998, Risk-based hydrology: Bayesian flood-frequency analyses using paleoflood information and data uncertainties: *Proceedings of the First Federal Interagency Hydrologic Modeling Conference*, April 19 - 23, 1998, Tropicana Hotel, Las Vegas, Nevada, vol. 1, p. 4-101 to 4-108.
- O'Connell, D.R.H., Ostenaar, D.A., Levish, D.R., and Klinger, R.E., 2002, Bayesian flood frequency analysis with paleohydrologic bound data, *Water Resour. Res.* 38 (5), DOI 10.1029/2000WR000028.

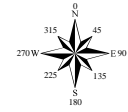
- Ostenaar, D.A., and Levish, D.R., 1996, Event-based assessment of extreme flood hazards for dam safety: in Proceedings, Association of State Dam Safety Officials Western Regional Conference, Association of State Dam Safety Officials, Lexington, KY, p. 41-54.
- Ostenaar, D.A., and Levish, D.R., 1997, Reconnaissance Paleoflood Study for Ochoco Dam, Crooked River Project, Oregon: Denver, CO, Bureau of Reclamation, Seismotectonic Report 96-2, 20 p., 1 folded plate, 2 appendices.
- Ostenaar D.A., Levish, D.R., and O'Connell, D.R.H., 1996, Paleoflood study for Bradbury Dam, Cachuma Project, California: Denver, CO, Bureau of Reclamation, Seismotectonic Report 96-3, 86 p., 1 folded plate, 4 appendices.
- Ostenaar D.A., Levish, D.R., O'Connell, D.R.H., and Cohen E.A., 1997, Paleoflood study for Causey and Pineview Dams, Weber Basin and Ogden River Projects, Utah: Denver, CO, Bureau of Reclamation, Seismotectonic Report 96-6, 69 p., 3 appendices.
- Ostenaar D.A., Levish, D.R., Klinger, R.E., and O'Connell, D.R.H., 1999, Phase 2 Paleohydrologic and Geomorphic Studies for the Assessment of Flood Risk for the Idaho National Engineering and Environmental Laboratory, Idaho: Denver, CO, Bureau of Reclamation, Geophysics, Paleohydrology and Seismotectonics Group, Report 99-7, 112 p., 1 folded plate, 4 appendices.
- Ostenaar, D.A., O'Connell, D.R.H., Walters, R.A., Creed, R.J., 2002, Holocene paleoflood hydrology of the Big Lost River, western Idaho National Engineering and Environmental Laboratory, Idaho *in*: Link, P.K., and Mink, L.L., eds., *Geology, Hydrology, and Environmental Remediation: Idaho National Engineering and Environmental Laboratory, Eastern Snake River Plain, Idaho*: Boulder, CO, Geological Society of America Special Paper 353, p. 91-110.
- Parker, G., 1978, Self-formed straight rivers with equilibrium banks and mobile bed. Part 2. The gravel river: *Journal of Fluid Mechanics*, v. 89, part 1, p. 127-146.
- Peterson, L. and Harding, W., 2002, Mitigation of site 10BT2189 (BLR-8) at the Idaho National Environmental and Engineering Laboratory, Butte County, Idaho: DRAFT, September, 2002, North Wind Environmental, Inc., NW Project 2072.202, Idaho Falls, ID, 51 p.
- Pierce, K.L., 1979, History and dynamics of glaciation in the northern Yellowstone National Park area: U.S. Geological Survey Professional Paper 729-F, 90 p.
- Pierce, K.L., and Good, J.D., 1992, Field guide to the Quaternary geology of Jackson Hole, Wyoming: US Geol. Surv. Open-File Report 92-504, 54 p.
- Pierce, K.L., and Morgan, L.A., 1992, The track of the Yellowstone hot spot: Volcanism, faulting, and uplift, in Link, Paul Karl, Kuntz, M.A., and Platt, Lucian B., eds., *Regional Geology of Eastern Idaho and Western Wyoming*: Geological Society of America Memoir 179, p. 1-53.
- Rathburn, S.L., 1991, Quaternary channel changes and paleoflooding along the Big Lost River, Idaho National Engineering Laboratory: TriHydro Corporation report prepared for EG&G Idaho, Inc., subcontract no. C90-132903, 33 p.
- Richmond, G.M., 1986, Stratigraphy and chronology of glaciations in Yellowstone National Park, *in* Sibrava, V., et al., eds., *Quaternary glaciations in the Northern Hemisphere: Quaternary Science Reviews*, v. 5, p. 83-98.
- Scott, W.E., 1982, Surficial geologic map of the eastern Snake River Plain and adjacent areas, 111° to 115° W., Idaho and Wyoming: U.S. Geological Survey Miscellaneous Investigations Series Map I-1372, scale 1:250,000.

- SSHAC, 1995, Recommendations for probabilistic seismic hazard analysis: Guidance on uncertainty and use of experts: NUREG/CR-6372, 170 p.
- Simpson, D.T., Kolbe, T.E., Ostenaar, D.A., Levish, D.R., and Klinger, R.E., 1999, Lower Big Lost River chronosequence - implications for glacial outburst flooding [abs.]: Geological Society of America, Abstracts with Programs, v. 31, no. 4, p. A-56.
- Stearns, H.T., Crandall, L., and Steward, W.G., 1938, Geology and ground-water resources of the Snake River Plain in southeastern Idaho: U.S. Geological Survey Water-Supply Paper 774, 268 p.
- Stedinger, J.R., and Cohn, T.A., 1986, Flood frequency analysis with historical and paleoflood information: Water Resources Research, v. 22, p. 785-793.
- Sturchio, N.C., Pierce, K.L., Murrell, M.T., and Sorey, M.L., 1994, Uranium-series ages of travertines and timing of the last glaciation in the northern Yellowstone area, Wyoming-Montana: Quaternary Research, v. 41, p. 265-277.
- Thackery, G.D., Lundeen, K.A., and Borgert, J.A., 2004, Latest Pleistocene alpine glacier advances in the Sawtooth Mountains, Idaho, USA: Reflections of midlatitude moisture transport at the close of the last glaciation: Geology, v. 32, no. 3, p. 225-228.
- Tullis, J.A., 1995, Characteristics and origin of earth-mounds on the eastern Snake River Plain, Idaho: Idaho Fall, Lockheed Martin Idaho Technologies, Idaho National Engineering Laboratory, INEL-95/0505, September 1995, 90 p.
- Whitlock, C., 1993, Postglacial vegetation and climate of Grand Teton and southern Yellowstone National Parks: Ecological Monographs, v. 63, p. 173-198.

APPENDIX IV

INTEC 100-YEAR FLOOD PLAIN MAP
(RICOM Flow Model)

Idaho Nuclear Technology and Engineering Center (INTEC)



Legend

- RCRA Treatment, Storage, and Disposal Units
- Buildings and Other Structures
- Roads
- Railroad Tracks
- Fences
- Berms
- Culverts
- Big Lost River
- Ditches
- Ponds
- Storm Water Flow Paths
- 10-ft Index Contours
- 2-ft Contours
- 2-ft Depression Contours
- Lift Station
- Proposed Location of Building CPP-1696

100 Year Flood Plain



NOTES:

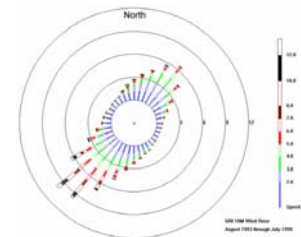
Landuse: INTEC facility boundaries are surrounded by restricted-access federal lands.

Legal Description: INTEC facility boundaries are located in Township 3 North, Range 29 East, Sections 24 and 25; and Range 30 East, Sections 19 and 30.

Base Map: INL Aerial Flyover: Aerial Mapping, October 2002, 2-ft. intervals.

Big Lost River Flood Hazard Study, Idaho National Laboratory, Idaho Report 2005-2, Dean A. Ostenaar and Daniel R. H. O'Connell, United States Bureau of Reclamation, Denver, Colorado (BOR, 2005).

In generating this map for a 100 year flow of 3,072 cubic feet per second it was conservatively assumed that the INL Diversion Dam does not exist and assumes no infiltration. The Federal Energy Regulatory Commission has recently determined that the INL Diversion Dam is adequate for handling flows up to 1 foot of freeboard (Operation Inspection Report For Department of Energy, Federal Energy Regulatory Commission, 2005) or approximately 7,300 cubic feet per second.



Project Number: 14 RCRA-Flumes
 Date: 10/10/2014
 GIS Analyst: Dan Mathews, Linda Tisdale
 Data Source: 2002/05/01
 Description: Contour map showing 100-year flood plain
 File Name: V:\GIS\14_RCRA_Flumes\14_RCRA_Flumes.mxd

APPENDIX IV

SIMULATION OF WATER SURFACE ELEVATIONS FOR A HYPOTHETICAL
100-YEAR PEAK FLOW IN BIRCH CREEK AT THE IDAHO NATIONAL
ENGINEERING AND ENVIRONMENTAL LABORATORY, IDAHO

Simulation of Water-Surface Elevations for a
Hypothetical 100-Year Peak Flow in Birch Creek
at the Idaho National Engineering and
Environmental Laboratory, Idaho

U.S. GEOLOGICAL SURVEY

Water-Resources Investigations Report 97-4083

Prepared in cooperation with the

U.S. Department of Energy



Simulation of Water-Surface Elevations for a Hypothetical 100-Year Peak Flow in Birch Creek at the Idaho National Engineering and Environmental Laboratory, Idaho

By Charles Berenbrock and L.C. Kjelstrom

U.S. GEOLOGICAL SURVEY

Water-Resources Investigations Report 97-4083

Prepared in cooperation with the
U.S. Department of Energy

Boise, Idaho
1997





U.S. DEPARTMENT OF THE INTERIOR
BRUCE BABBITT, Secretary

U.S. GEOLOGICAL SURVEY
Gordon P. Eaton, Director

The use of firm, trade, and brand names in this report is for identification purposes only and does not constitute endorsement by the U.S. Geological Survey.



For additional information write to:

District Chief
U.S. Geological Survey
230 Collins Road
Boise, ID 83702-4520

Copies of this report can be purchased from:

U.S. Geological Survey
Information Services
Box 25286
Federal Center
Denver, CO 80225



CONTENTS

Abstract	1
Introduction	3
Purpose and scope	3
Description of study area.....	3
Previous investigations.....	5
Acknowledgments	6
Geomorphic characteristics of gravel pits and Birch Creek Playa.....	6
Data collection.....	6
Methods of analysis.....	8
Hydrologic analysis.....	8
Hydraulic analysis	8
Simulation of water-surface elevations	9
Cross-sections 1 through 4	9
Cross-section 5	9
Cross-section 6	14
Total flow in channel having lowest streambed elevation.....	14
Cross-sections 18 and 19.....	16
Maximum flow capacities of diversions.....	16
Generalized 100-year flood-prone areas	17
Summary	19
References cited	20

FIGURES

1. Map showing locations of study area, Birch Creek Basin, and part of the Idaho National Engineering and Environmental Laboratory.....	2
2. Map showing locations of Birch Creek, cross sections, diversion channels, gravel pits, and Birch Creek Playa	4
3. Graph showing relations among elevation of land surface, depth below a given elevation, surface area, and volume of Birch Creek Playa	7
4. Graphs showing water- and land-surface elevations, Birch Creek.....	10
5. Map showing peak flow in Birch Creek, maximum capacities of diversions, and volumes of gravel pits 2 and 3	15
6. Map showing generalized flood-prone areas resulting from a 100-year peak flow in Birch Creek.....	18

TABLES

1. Selected geomorphic characteristics of gravel pits 2 and 3 and Birch Creek Playa.....	6
2. Maximum flow capacities of diversions on Birch Creek	16

CONVERSION FACTORS AND VERTICAL DATUM

	Multiply	By	To obtain
acre		0.004047	square kilometer
acre-foot (acre-ft)		.233	cubic meter
cubic foot per second (ft ³ /s)		0.02832	cubic meter per second
cubic foot per second per mile [(ft ³ /s)/mi]		0.0176	cubic meter per second per square kilometer
foot (ft)		0.3048	meter
foot per mile (ft/mi)		0.1894	meter per kilometer
mile (mi)		1.609	kilometer

Sea level: In this report, "sea level" refers to the National Geodetic Vertical Datum of 1929 (NGVD of 1929)—a geodetic datum derived from a general adjustment of the first-order level nets of both the United States and Canada, formerly called Sea Level Datum of 1929.



Simulation of Water-Surface Elevations for a Hypothetical 100-Year Peak Flow in Birch Creek at the Idaho National Engineering and Environmental Laboratory, Idaho

By Charles Berenbrock *and* L.C. Kjelstrom

ABSTRACT

Delineation of areas at the Idaho National Engineering and Environmental Laboratory that would be inundated by a 100-year peak flow in Birch Creek is needed by the U.S. Department of Energy to fulfill flood-plain regulatory requirements. Birch Creek flows southward about 40 miles through an alluvium-filled valley onto the northern part of the Idaho National Engineering and Environmental Laboratory site on the eastern Snake River Plain. The lower 10-mile reach of Birch Creek that ends in Birch Creek Playa near several Idaho National Engineering and Environmental Laboratory facilities is of particular concern. Birch Creek is highly braided, and many anthropogenic features in the study area affect flood hydraulics and flow.

Dikes surround two of the facilities in and around the playa. At the elevation of the top of the dikes, Birch Creek Playa has a volume of 21,600 acre-feet, greater than the volume of 13,000 acre-feet that would be generated by the hypothetical 100-year peak flow. The water-surface elevation resulting from a volume of 13,000 acre-feet is about 2 feet lower than the elevation of the dikes; therefore, no flooding of the facilities would be expected from the hypothetical 100-year peak flow.

Twenty-six channel cross sections were surveyed to develop and apply a hydraulic model to simulate water-surface elevations for a hypothetical 100-year peak flow in Birch Creek. Model sim-

ulation of the 100-year peak flow (700 cubic feet per second) in reaches upstream from State Highway 22 indicated that flow was confined within channels even when all flow was routed to one channel. Where the highway crosses Birch Creek, about 315 cubic feet per second of water was estimated to move downstream—115 cubic feet per second through a culvert and 200 cubic feet per second over the highway. Simulated water-surface elevation at this crossing was 0.8 foot higher than the elevation of the highway. The remaining 385 cubic feet per second flowed southwestward in a trench along the north side of the highway. Flow also was simulated with the culvert removed. Only the maximum flow capacities were determined for diversion channels because they probably would be at full capacity during peak flow.

The exact location of flood boundaries on Birch Creek could not be determined because of the highly braided channel and the many anthropogenic features (such as the trench, highway, and diversion channels) in the study area that affect flood hydraulics and flow. Because flood boundaries could not be located exactly, only a generalized flood-prone map was developed. Upstream from Highway 22, peak flows were confined within the braided channels. At Highway 22 and downstream, flows spread out, probably due to the anthropogenic features. If the anthropogenic features were not present, peak flows probably would be confined within the braided channels of Birch Creek.

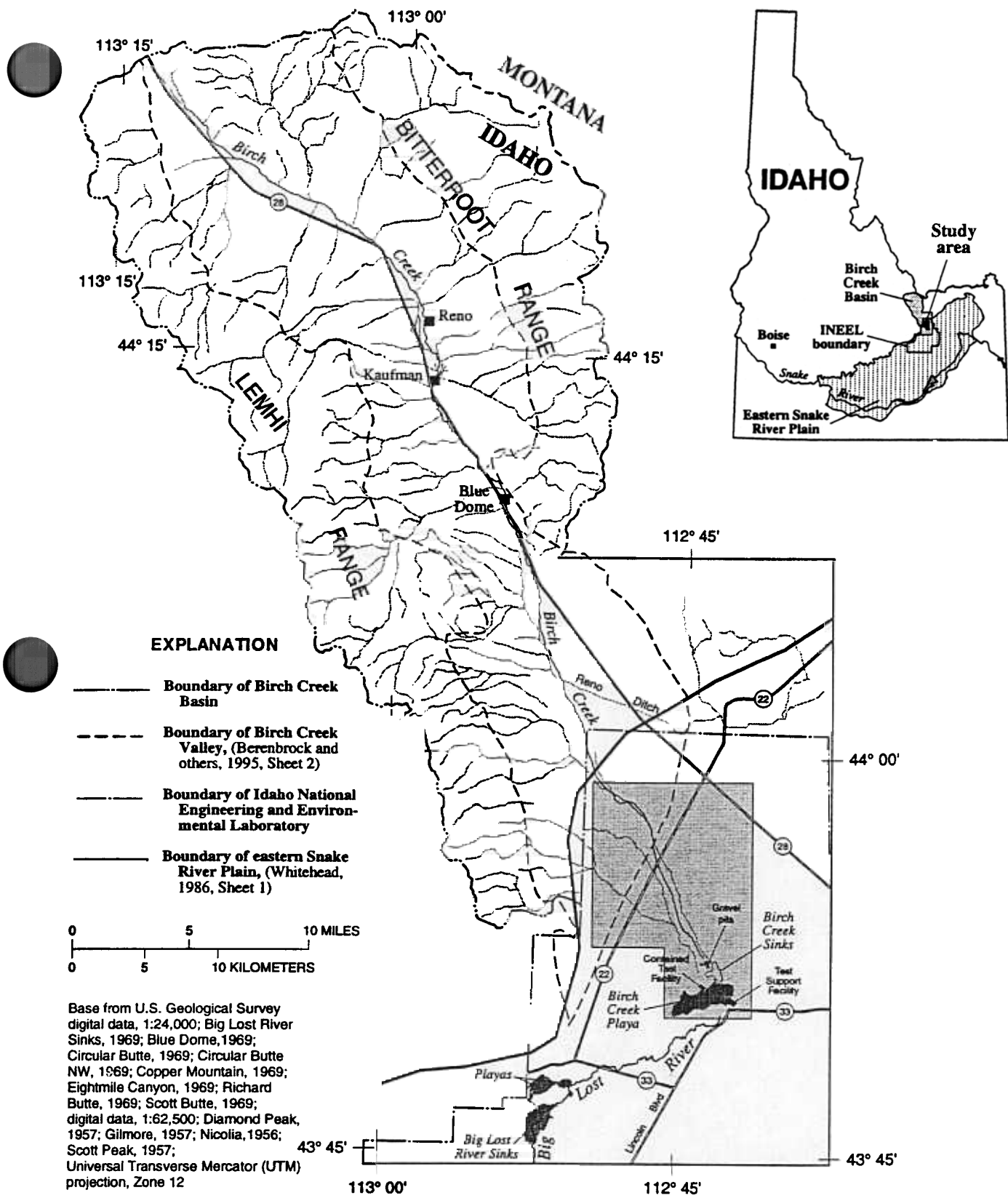


Figure 1. Locations of study area, Birch Creek Basin, and part of the Idaho National Engineering and Environmental Laboratory.

INTRODUCTION

Birch Creek flows southward about 40 mi through an alluvium-filled valley to the eastern Snake River Plain (fig. 1). The Lemhi and Bitterroot Ranges that border the valley are 9,000 to 12,000 ft above sea level. Precipitation in the mountains supplies most water in the valley. Before reaching the eastern Snake River Plain, some flow in Birch Creek is diverted for irrigation and power generation. However, during non-irrigation seasons, this flow is returned to Birch Creek by a canal that runs from the powerplant to a gravel pit just below Highway 22 (fig. 2). In most years, water in Birch Creek infiltrates into the ground or evaporates upon reaching the plain. When water supply is adequate, Birch Creek flows onto the northern part of the Idaho National Engineering and Environmental Laboratory (INEEL) site and terminates in the Birch Creek Playa. At the INEEL, several diversion channels route water to gravel pits to prevent water from reaching INEEL facilities in and around the playa. Because of diversions and infiltration losses, water in Birch Creek rarely reaches Birch Creek Playa. However, in 1969, about 3,500 acre-ft of water accumulated in the playa. Although flow of that magnitude is rare, the extent of possible flooding at the INEEL needs to be determined to fulfill flood-plain regulatory requirements for emergency planning, environmental studies, construction of proposed facilities, and control of flood damage. In 1994, the U.S. Department of Energy (USDOE) at the INEEL entered into a cooperative agreement with the U.S. Geological Survey (USGS) to develop and implement 100-year peak flow studies.

Purpose and Scope

The purpose of this study was to delineate the areal extent of possible flooding at the INEEL resulting from peak flow in Birch Creek having a recurrence interval of 100 years. The Birch Creek flood plain was delineated in three phases. In phase one, Kjelstrom and Berenbrock (1996) estimated 100-year peak flows and flow volumes for the Big Lost River and Birch Creek. In phase two, twenty-six cross sections were surveyed within the boundary of the INEEL. The cross sections provided data needed in phase three to develop a flood-plain model of Birch Creek and to determine flow capacity of diversions. The model simulated a hypothetical 100-year peak flow in Birch Creek and calculated

corresponding water-surface elevations along surveyed cross sections at the INEEL. The simulated water-surface elevations then were used to delineate the areal extent of flooding caused by the hypothetical 100-year peak flow.

This report presents the results of phases two and three and includes a discussion of the effects of State Highway 22, the culvert under State Highway 22, a tributary channel to Birch Creek, and diversion channels on streamflow. Geomorphic characteristics of gravel pits and Birch Creek Playa, ultimate sumps for high flows, also are described.

Description of Study Area

The study area is a 10-mi reach of Birch Creek that ends in Birch Creek Playa at the northern part of the INEEL site (fig. 1). Several INEEL facilities are located in and around Birch Creek Playa. The two main ones are Test Support Facility (TSF) and Contained Test Facility (CTF). In the study area, Birch Creek is an ephemeral stream and is highly braided. South of State Highway 22, it broadens to about 1 mi in width (fig. 2). These stream channels are shallow and water moves rapidly during high flow. Upstream from diversion channel A (fig. 2), Birch Creek crosses southwest-sloping alluvial fans that formed at the base of the Bitterroot Range. Where State Highway 22 crosses Birch Creek, elevation of the streambed is about 75 ft higher than it is 1.5 mi to the southwest. Slope of the streambed 3 to 4 mi upstream from State Highway 22 is about 60 ft/mi, is 56 ft/mi at Highway 22, and is 45 ft/mi at diversion channel A. Downstream from diversion channel A, the streambed slopes gently toward Birch Creek Playa, a dried lake basin, which has the lowest elevation in the study area, 4,763.6 ft. Streambed slope between diversion channel A and cross-section 14 (fig. 2) is about 40 ft/mi; slope between cross-section 14 and gravel pits 2 and 3 is about 30 ft/mi. Between gravel pits 2 and 3 and Birch Creek Playa is an area called Birch Creek Sinks, where streambed slope is about 10 ft/mi. Water entering the sinks usually infiltrates into the ground. Niccum (1973, p. 15–16) noted that water had entered Birch Creek Playa about four times since the 1890's.

Bed material in Birch Creek consists largely of coarse sand, gravel, and cobbles that are mined from the three gravel pits. Gravel pit 1 is composed largely of gravel, whereas gravel pit 3 is composed of coarse sand and some gravel. Gravel and sand are highly transmis-

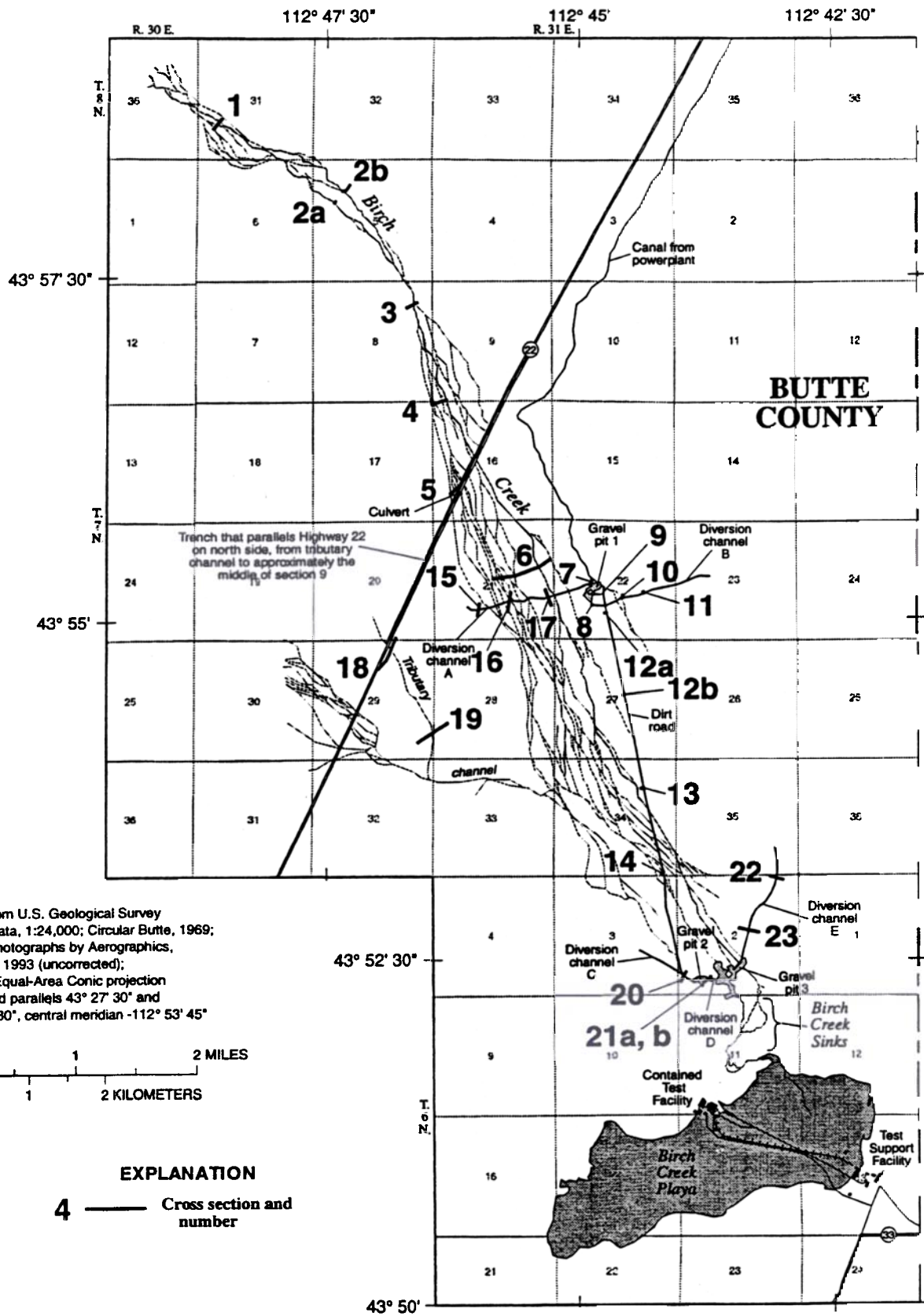


Figure 2. Locations of Birch Creek, cross sections, diversion channels, gravel pits, and Birch Creek Playa.

U sive and permit rapid infiltration of water. Channel infiltration tests on Birch Creek near Blue Dome (fig. 1) have been conducted by the USGS since the 1980's.

Tests indicate that infiltration averages about 4 (ft³/s)/mi; the maximum rate exceeds 10 (ft³/s)/mi when streamflow is about 70 ft³/s. Niccum (1973) noted that flows decreased downstream during the latter part of the 1969 flood, especially south of State Highway 22. Usually, Birch Creek does not flow beyond Birch Creek Sinks; therefore, no infiltration tests have been done in this area. Because materials underlying Birch Creek Sinks are similar to those underlying Big Lost River Sinks (Whitehead, 1986, sheet 1), similar infiltration rates might be expected. Bennett (1990) determined that the largest infiltration losses along the Big Lost River were at Big Lost River Sinks, where the maximum loss was 28 (ft³/s)/mi. Infiltration rates might be lower in Birch Creek Playa, which is underlain by low-permeability silt and clay.

Riparian vegetation in the study area is mainly sagebrush and grass; vegetation growth increases near Birch Creek. Several miles north of Highway 22, cottonwood trees grow along the stream. Sparse grasses grow on Birch Creek Playa.

Many anthropogenic features in the Birch Creek flood plain affect flood hydraulics and flow. State Highway 22 crosses Birch Creek near the middle of the study reach (fig. 2). A single, corrugated-steel-arch culvert, 3.25 ft high, 4.8 ft wide, and 65 ft long, allows water to move under the highway. The top of the culvert is about 2.3 ft below the highway surface, which is at an elevation of 4,999.7 ft. During peak flow, water that does not pass through the culvert or over the highway flows southwestward in a trench that parallels the highway. Water in the trench is intercepted by channels of a tributary to Birch Creek about 1.5 mi to the southwest in sec. 29, T. 7 N., R. 31 E. (fig. 2). There is no culvert or bridge where these channels intersect Highway 22 to permit water movement under the highway.

About 1 mi south of State Highway 22, diversion channel A crosses Birch Creek and its flood plain. The 1-mi-long channel was dug in April 1969, just before the 1969 flood. The channel diverts streamflow eastward to gravel pit 1 (fig. 2). The gravel pit stores floodwater, which then infiltrates into the ground. A channel from the powerplant that receives water from Birch Creek by way of Reno Ditch (fig. 1) enters gravel pit 1 from the north. Maximum flow in this channel is about 7 ft³/s; this channel has water only during the nonirrigation season. The outlet of gravel pit 1, diversion chan-

nel B at the southern end of the pit, diverts water 1 mi to the east. Diverted water spreads out and infiltrates into the ground.

A 3.5-mi-long, southeast-trending dirt road, originating on the east side of gravel pit 1, crosses diversion channel B and ultimately crosses all channels of Birch Creek (fig. 2). During peak flow, embankments cause water to flow down the road, in the direction of CTF, to diversion channel C and gravel pit 2. Overflow from gravel pit 2 moves to gravel pit 3 through diversion channel D. During peak flow, gravel pit 3 also receives water that might be in Birch Creek channels southeast of the dirt road and from diversion channel E. Overflow from gravel pit 3 would move southward into Birch Creek Sinks and, ultimately, into Birch Creek Playa.

Dikes with a top elevation of 4,786.5 ft were constructed around the facilities at TSF and CTF in March 1969. Niccum (1973, p. 13, fig. 3B-3) indicated that, with dikes at an elevation of 4,786.5 ft, storage capacity of Birch Creek Playa would be about 13,000 acre-ft; with dikes at 4,790 ft, storage capacity would be about 28,000 acre-ft. The 1969 flood caused about 3,500 acre-ft of water to accumulate in the playa (Niccum, 1973, p. 12-13). The resulting water-surface elevation of 4,782.2 ft would not have caused flooding at CTF because the floor at CTF is 7.8 ft higher at an elevation of 4,790 ft. However, the floor of the CTF escape tunnel entrance, elevation 4,782.3 ft, probably would have been flooded were the dikes not present.

Previous Investigations

The first reported occurrence of streamflow reaching Birch Creek Playa was in 1894 (Nace and others, U.S. Geological Survey, written commun., 1959). Streamflow also reached the playa several times between 1900 and 1910 and again in 1969 (Niccum, 1973, p. 16). Niccum (1973) also discussed other floods in Birch Creek, flood control structures, and Birch Creek Playa. He estimated the magnitude and frequency of floods in relation to the potential for flooding at the INEEL. Koslow (1984) determined flood-frequency relations at three streamflow-gaging stations, the probable maximum flood based on a probable maximum storm, flooding from local snowmelt, and flooding potential of Birch Creek Playa.

Acknowledgments

Appreciation is extended to Ken Beard, Lockheed Martin Idaho Technologies Company at the INEEL, who obtained horizontal and vertical control data by use of a Global Positioning System (GPS) and converted the data for our use. Appreciation also is extended to Sabrina A. Nicholls and Susan E. Moore, USGS, for their assistance in surveying cross sections.

GEOMORPHIC CHARACTERISTICS OF GRAVEL PITS AND BIRCH CREEK PLAYA

To understand the hydrology of Birch Creek in the study area, it was necessary to define geomorphic characteristics of the gravel pits and Birch Creek Playa. Because the pits and playa seldom contain water, areal and volumetric data were calculated as the difference between hypothetical water-surface elevation at full-pool capacity and land-surface elevation. The maximum water-surface elevation in the gravel pits at full-pool capacity was estimated by determining the elevation of their outlet. Land-surface elevations were obtained from digital elevation models (DEM's).

DEM's are records of land-surface elevation and were digitized by Aerial Mapping, Inc. (Wayne Eskridge, Aerial Mapping, Inc., written commun., 1996) on a 19.7-ft (6-meter) spacing (longitudinally and latitudinally) from 1:10,000-scale aerial photographs. The DEM's were brought into a geographic information system (GIS) to compute surface area and volumetric data.

Selected geomorphic characteristics of gravel pits 2 and 3 and Birch Creek Playa are listed in table 1. Characteristics were not defined for gravel pit 1 because DEM data were not available for that area, no reliable estimates could be obtained from topographic maps, and gravel pit 1 is much smaller than gravel pit 2, so its hydrologic effects were considered insignificant.

The dikes surrounding TSF and CTF are at an elevation of 4,786.5 ft. At that elevation, the surface area of water in the playa is 5,900 acres and the volume is 21,600 acre-ft (fig. 3), greater than the volume of 13,000 acre-ft that would be generated by the 100-year peak flow (Kjelstrom and Berenbrock, 1996). A volume of 13,000 acre-ft results in a water-surface elevation of 4,784.5 ft, which is 2 ft lower than the elevation of the dikes. At an elevation of 4,788 ft, the surface area of water in the playa is 8,140 acres and the volume is 31,800 acre-ft (table 1). An elevation of 4,788 ft was

Table 1. Selected geomorphic characteristics of gravel pits 2 and 3 and Birch Creek Playa

[Locations shown in figure 2]

Characteristic	Gravel pit 2	Gravel pit 3	Birch Creek Playa	
Water-surface elevation at full-pool capacity, in feet	4,797.3	4,788.7	4,780	4,788
Surface area, in acres	3.9	29.7	1,030	8,140
Volume, in acre-feet	20.9	352.4	1,160	31,800
Perimeter, in miles	.5	2.4	16	63
Maximum depth, in feet	12.6	20.0	16.4	24.4
Mean depth, in feet	5.3	11.9	1.1	3.9

chosen because its contour encompassed all the playas (fig. 1). At an elevation of 4,780 ft, the surface area of water in the playa is 1,030 acres and the volume is 1,160 acre-ft (table 1 and fig. 3). Past investigators usually delineated Birch Creek Playa at the 4,780-ft contour. The relations among elevation, surface area, and volume are shown in figure 3.

Elevation values presented in table 1 and figure 3 differ from those of Niccum (1973, p. 13, fig. 3B-3) because his elevations were from topographic maps, whereas elevations used in this study were from DEM data. For example, Niccum (1973, p. 13, fig. 3B-3) estimated that at an elevation of 4,788 ft, Birch Creek Playa contains 18,200 acre-ft of water, about 13,600 acre-ft less than the estimate used in this study. Niccum (1973, p. 13, fig. 3B-3) estimated that at an elevation of 4,780 ft, the playa contains about 1,100 acre-ft of water, similar to the estimate used in this study.

DATA COLLECTION

The computer model used to simulate 100-year peak flow water-surface elevations, described later in this report, required definition of channel and floodplain geometry and roughness coefficients for each of a series of cross sections in the study area. Cross-section geometry was defined by a series of land-surface elevation data measured at variably spaced distances from a reference point along section lines perpendicular to the direction of flow. In June 1995 and May 1996, U.S. Geological Survey personnel surveyed Birch Creek and diversion channels from about 4 mi northwest of State Highway 22 to gravel pits 2 and 3 near Birch Creek Playa (fig. 2). Twenty-six channel cross sections were surveyed: 9 on creeks, 12 on diversion channels, and

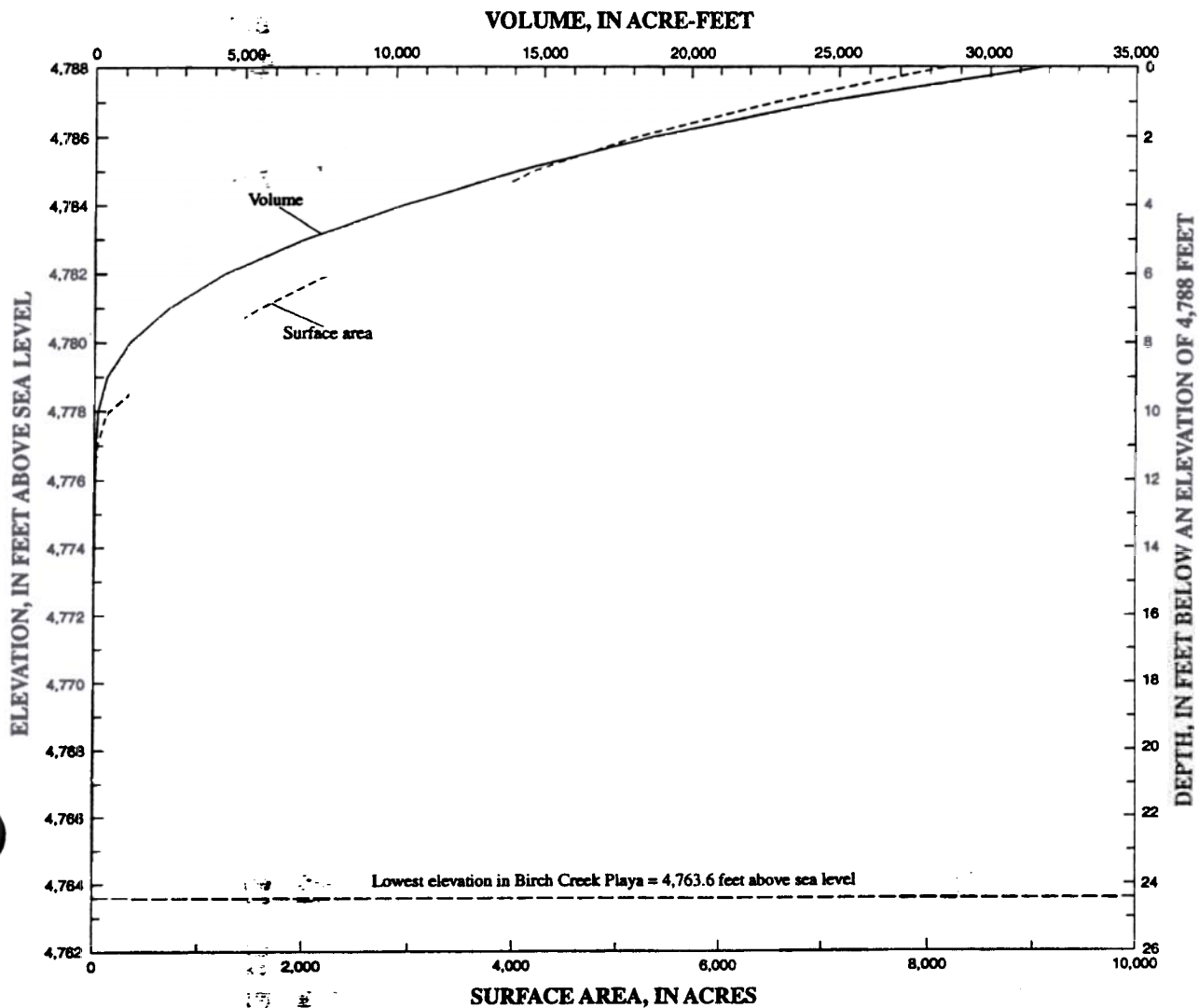


Figure 3. Relations among elevation of land surface, depth below a given elevation, surface area, and volume of Birch Creek Playa.

5 on the dirt road. One culvert near cross-section 5 and the highway near cross-sections 5 and 18 also were surveyed. Each cross section was located to best represent the hydraulic characteristics of that part of the creek, and each diversion channel and road section was surveyed to define its shape.

Channel roughness coefficients (Manning's n) were assigned for each cross section at the time of survey and were based on best engineering judgment. Roughness coefficient represents the resistance to open-channel flow. Factors that affect the roughness coefficient include (1) the type and size of materials that compose the streambed and banks, (2) shape of the channel,

(3) variation in dimensions of adjacent cross sections, (4) riparian and aquatic vegetation, (5) structures, and (6) degree of meandering. Roughness values used in the hydraulic analysis ranged from 0.048 to 0.068 for the main channel, 0.054 to 0.074 for secondary channels and the flood plain, and 0.028 to 0.040 for the highway, diversion channels, and roads.

All cross-section data were based on a common datum. Horizontal control was based on North American Datum of 1927 (NAD 27), State Plane Coordinates, Idaho East Zone, in feet; vertical control was based on the National Geodetic Vertical Datum of 1929 (sea level), in feet. Horizontal and vertical controls for the

surveys were obtained with three Ashtech Z-12 geodetic GPS receivers. Two receivers (base stations) were located within several miles of a cross section over known geographically referenced points. Horizontal and vertical controls were surveyed at a minimum of three sites (hubs) at each cross section using the third GPS receiver. Also, known geographic reference marks were surveyed to ensure accuracy to one-hundredth of a foot in horizontal and vertical directions. Differential corrections were applied to all data collected with the GPS—a process called differential GPS.

METHODS OF ANALYSIS

Regional regression techniques were used to estimate 100-year peak flows in Birch Creek and its diversions (Kjelstrom and Berenbrock, 1996). The 100-year peak flow has a 1-percent chance of being equaled or exceeded in any given year. Although the recurrence interval represents the long-term average period between flows of a specific magnitude, rare peak flows could occur at shorter intervals or even within the same year.

A computer model was used to estimate water-surface elevations for the hypothetical 100-year peak flow in Birch Creek and its diversions. This model incorporated horizontal and vertical data collected along channel cross sections perpendicular to the direction of flow.

Hydrologic Analysis

Kjelstrom and Berenbrock (1996) estimated that the 100-year peak flow of Birch Creek at the INEEL boundary would be about 700 ft³/s. They further estimated that by the time water reached Birch Creek Sinks, the peak would be reduced to about 590 ft³/s because of channel infiltration losses. Channel infiltration losses greater than 10 (ft³/s)/mi have been measured along Birch Creek. However, Niccum (1973, p. 10–12) reported no loss of flow due to infiltration during the early part of the March–April 1969 flooding of Birch Creek. At that time, infiltration was blocked by frozen ground and (or) ice. Niccum (Aerojet Nuclear Company, written commun., 1973) also indicated that similar conditions greatly reduced channel infiltration along the Big Lost River during the floods of 1962 and 1965. Despite these observations, no infiltration losses were

used in the model to provide for the worst case flooding scenario in the study area.

Hydraulic Analysis

Water-surface elevations of Birch Creek and its diversions were computed for the 100-year peak flow using the step-backwater computation model Water-Surface PROfile (WSPRO), developed by the USGS for the Federal Highway Administration (Shearman and others, 1986; Shearman, 1990). WSPRO is a computer program used to analyze one-dimensional, gradually varied, steady flow in open channels with fixed boundaries. The model uses the standard step method (Chow, 1959, p. 265) to determine changes in water-surface elevation from one cross section to the next by balancing total energy head at the sections. The surveyed cross sections and assigned roughness coefficients defined channel and flood-plain hydraulic characteristics used in the model.

To simulate water-surface elevations, starting water-surface elevations at selected cross sections were determined from a slope-conveyance computation of normal depth. Water-surface elevations and roughness coefficients were adjusted from field estimates until the simulated water-surface elevation, velocity, and Froude number ($F = V/\sqrt{gD}$, where F is Froude number; V is mean velocity of flow, in feet per second; g is acceleration of gravity, in feet per second squared; and D is hydraulic depth, in feet) were reasonable because no flow data were available to calibrate the model. Where sections crossed more than one channel, total flow was distributed among all channels (Kjelstrom, 1992, p. 6–8). WSPRO apportions 5 percent of the total flow to each of 20 equal-conveyance tubes. Thus, initial discharge values for each channel were computed from the apportioned discharge for the cross section. Kjelstrom (1992) used this method to apportion flow in channels around islands in the Snake River. He showed that flows apportioned by WSPRO were similar to flows measured with a current meter. Final flows were determined by adjusting roughness coefficient values within reasonable limits. Because changing roughness coefficient changes flow, model calibration for each channel along a cross section required adjustment of values until the simulated water-surface elevation, velocity, and Froude number were reasonable. Where multiple channels were present, simulated water-surface elevation was different for each channel.

A culvert analysis program (Fulford, 1995) was used to compute flow through the culvert under State Highway 22. The program computes flow from upstream and downstream water-surface elevations along with culvert geometry and roughness.

SIMULATION OF WATER-SURFACE ELEVATIONS

Water-surface elevations for 100-year peak flows were simulated with WSPRO. A flow of 700 ft³/s was routed along the entire study reach and used to determine the water-surface elevation at each cross section. Channel infiltration losses were assumed to be zero to provide for the worst case flooding scenario in the study area.

Flows were simulated with and without the culvert under State Highway 22 and with all flow in the channel nearest the right bank. The latter simulation was done because the channel nearest the right bank along cross-sections 2 through 5 had the lowest streambed elevation and also was usually the widest. In that area, Birch Creek crosses southwest-sloping alluvial fans at the base of the Bitterroot Range (fig. 1). Downstream from the fans, the primary channel of Birch Creek is flanked on both sides by secondary channels at higher elevations. Water-surface elevations and flows were determined for primary and secondary channels. Maximum flow capacities were determined for the diversion channels and roads because they probably would be at full capacity during peak flow. The assumption was made that no channels would be breached during the 100-year peak flow.

Cross-Sections 1 Through 4

A peak flow of 700 ft³/s was simulated at cross-sections 1 through 4 (fig. 2) because that reach is not affected by the culvert under State Highway 22, and stream channels have not been altered by construction of roads, dikes, or diversion channels. Simulation results are shown in figure 4 as land- and water-surface elevations and flow rates. For sections with more than one channel, simulated flow was confined within one channel and also was distributed among channels. Resultant water-surface elevations in different channels at a section were equal or near equal; flow differences are shown in figure 4. Peak flows at cross-sections 1

through 4 were confined within stream channels even when all flow was routed through the channel nearest the right bank (fig. 4).

Cross-Section 5

Peak flow in Birch Creek at cross-section 5 (about 225 ft upstream from State Highway 22) is affected by the culvert under the highway and by the deepening and straightening of the main channel. Also, the banks were raised using materials excavated from the main channel. Flows in higher elevation channels along this section are diverted southwestward toward the culvert by a trench on the north side of the highway. Simulation indicated that flow capacity of the trench northeast of the culvert was about 400 ft³/s. Water reaching the culvert can (1) flow through the culvert, (2) continue down the trench on the north side of the highway, or (3) flow over the highway. Simulation indicated that water continued southwestward in the trench that parallels the highway when the water surface at the culvert was greater than 4,997.9 ft—the lowest elevation of the right bank adjacent to the trench. Water flowed over the highway when water-surface elevation exceeded 4,999.7 ft. Flow capacity of the trench southwest of the culvert was about 450 ft³/s.

Simulation indicated that at peak flow (700 ft³/s), water flowed through the culvert, down the trench, and over the highway. At the culvert, the simulated water surface was 5,000.5 ft; 2.6 ft higher than the right bank outlet to the trench and 0.8 ft higher than the highway. Simulation indicated about 115 ft³/s of water (16 percent of the total peak flow) flowed through the culvert, 385 ft³/s (55 percent) flowed down the trench, and 200 ft³/s (29 percent) flowed over the highway (fig. 5). Flow along the highway was confined to the trench. Simulated water-surface elevations are shown in figure 4 and the distribution of flow is shown in figures 4 and 5.

If, during peak flow, the culvert were removed at the start of flooding and the resultant main channel had a trapezoidal shape (similar to channel 5 on cross-section 5, fig. 4) that was 8 ft wide at the bottom and 20 ft wide at the highway surface, model results (fig. 5) indicated that 450 ft³/s of water flowed down Birch Creek, 135 ft³/s more than if the culvert were in place. About 250 ft³/s (36 percent) flowed in the main channel and 200 ft³/s (29 percent) flowed over the highway. The

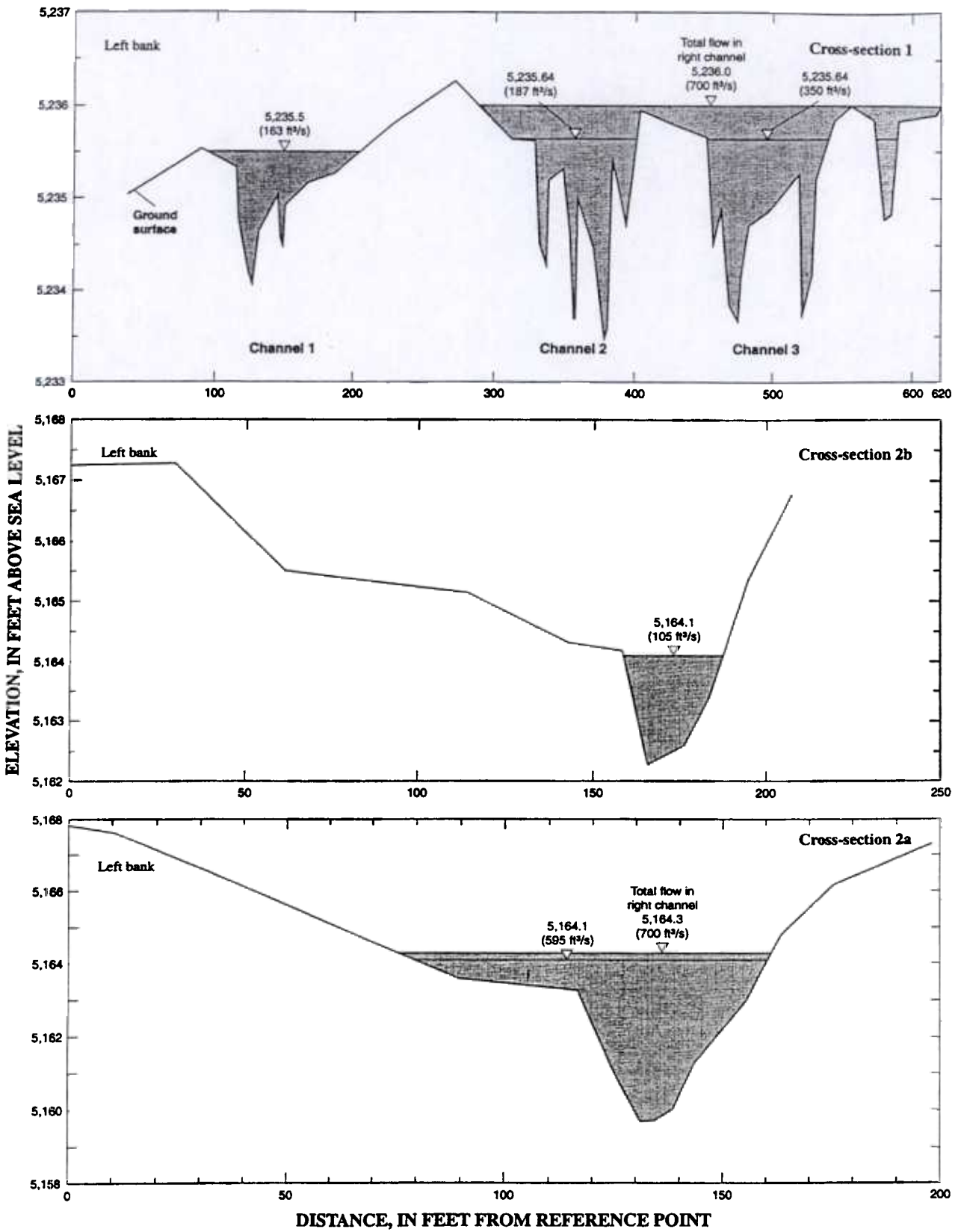


Figure 4. Water- and land-surface elevations, Birch Creek. (Locations shown in figure 2; ft³/s, cubic feet per second)

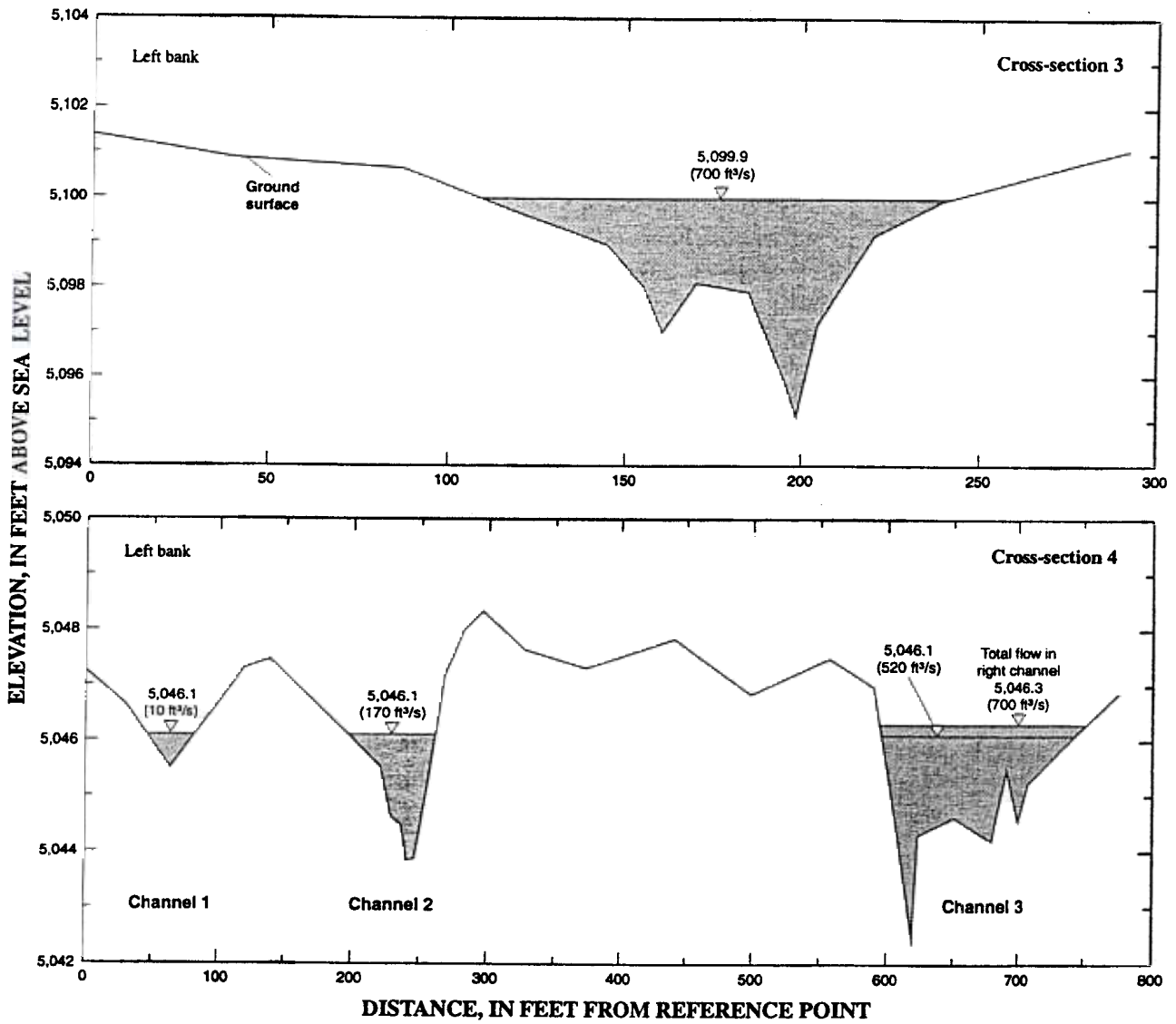


Figure 4. Water- and land-surface elevations, Birch Creek—Continued.

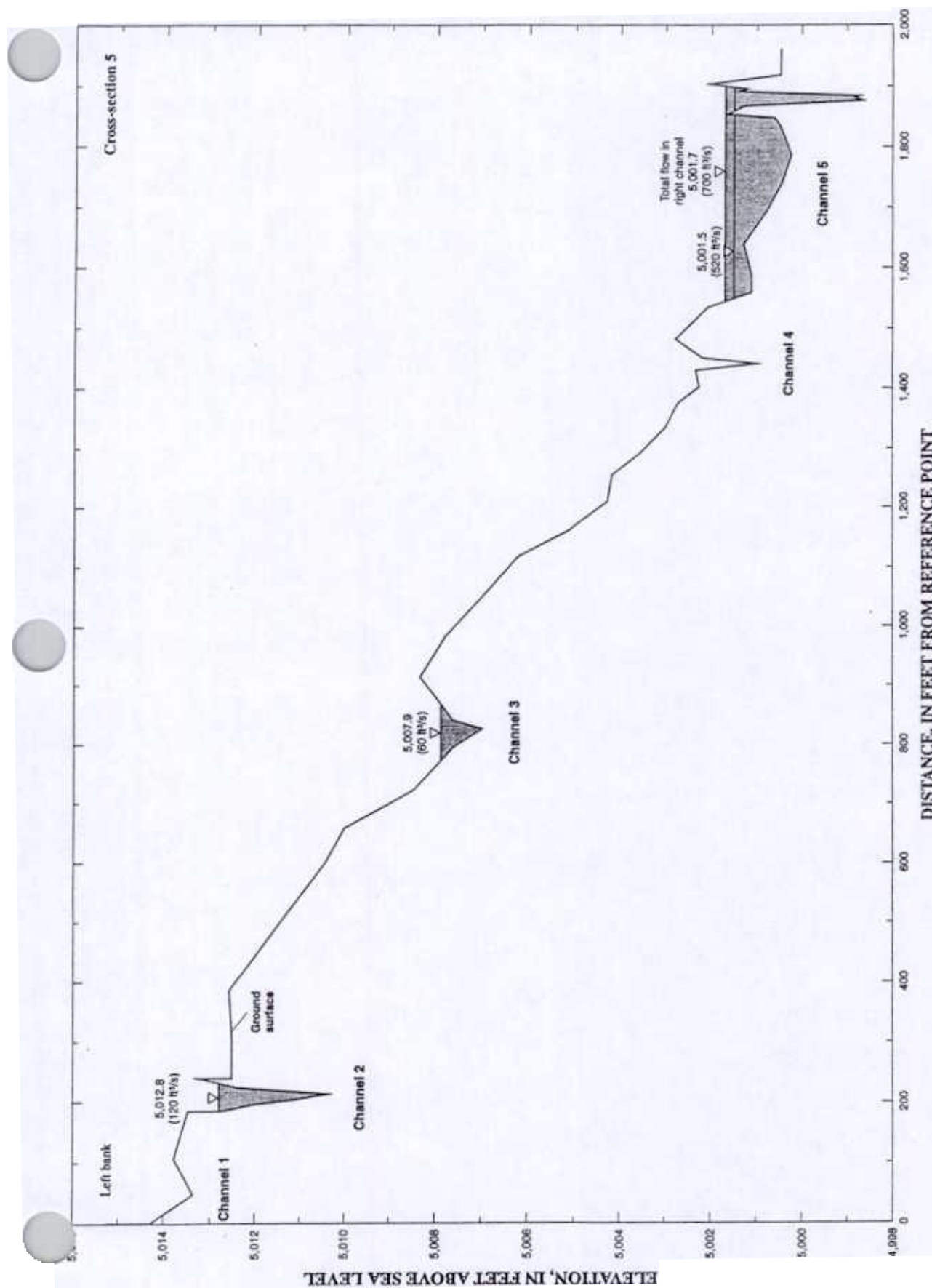


Figure 4. Water- and land-surface elevations, Birch Creek—Continued.

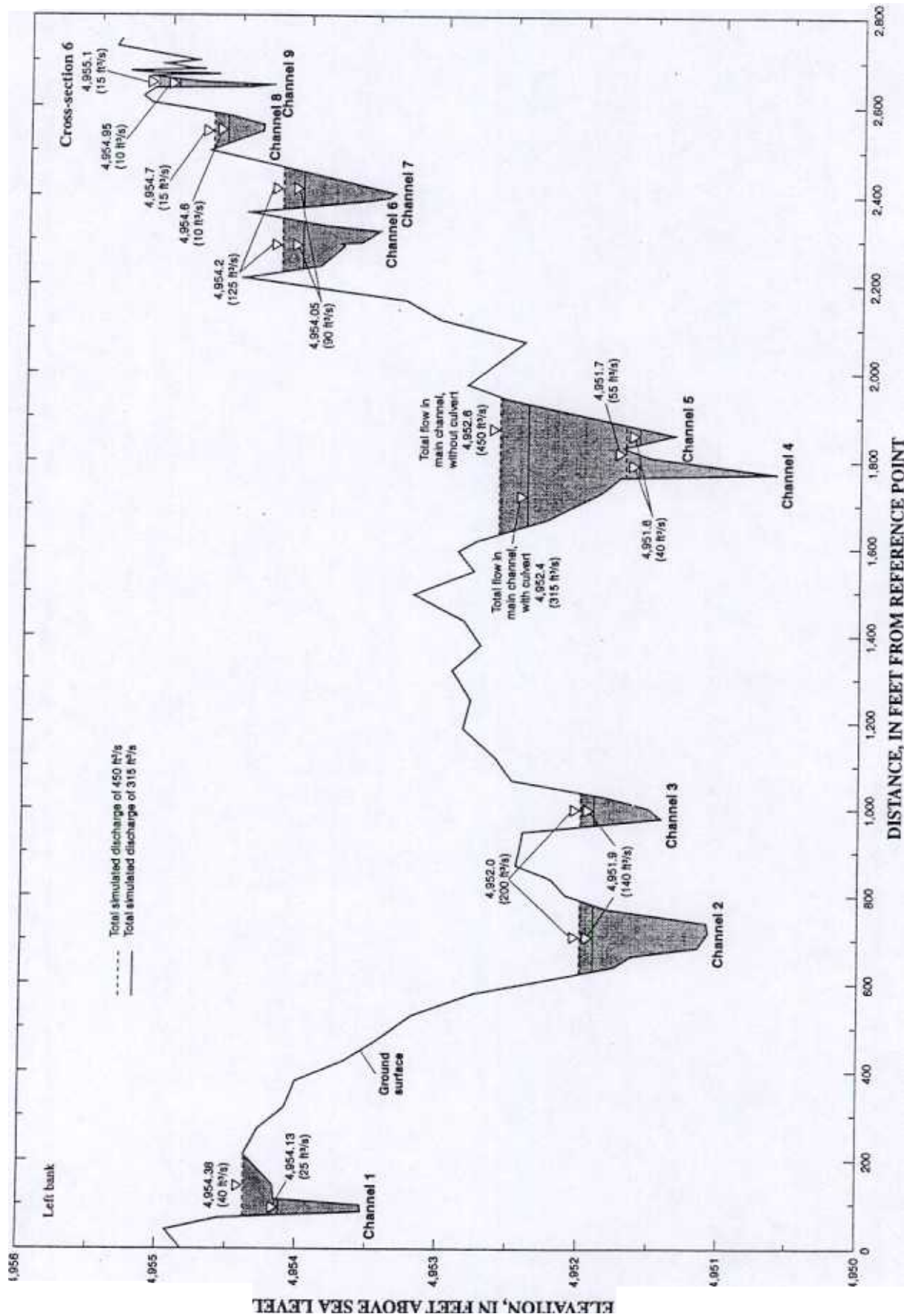


Figure 4. Water- and land-surface elevations, Birch Creek—Continued.

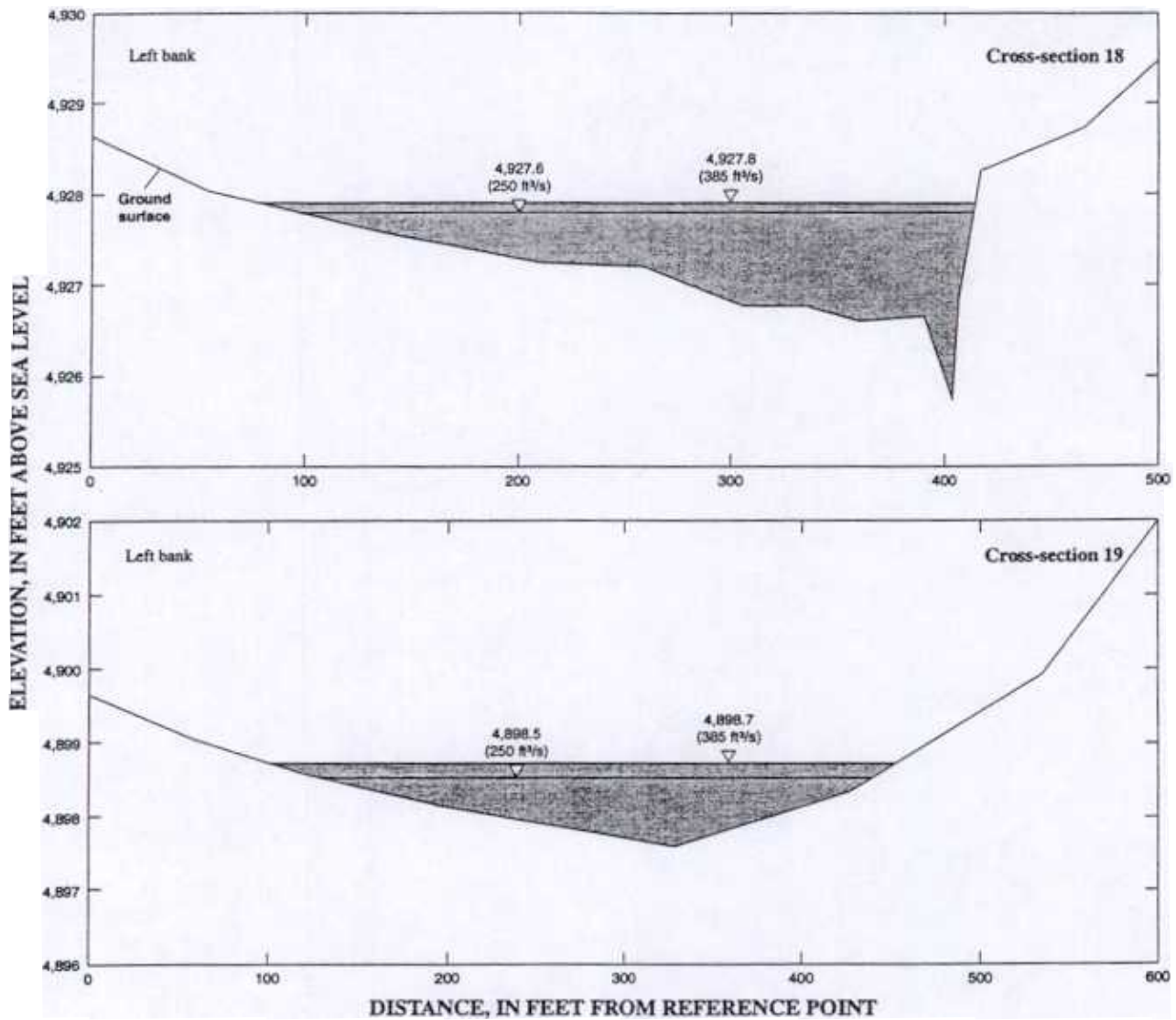


Figure 4. Water- and land-surface elevations, Birch Creek—Continued.

remaining 250 ft³/s (36 percent) flowed southwestward in the trench that parallels State Highway 22.

Cross-Section 6

With the culvert in place, a peak flow of 315 ft³/s (115 ft³/s of water through culvert plus 200 ft³/s over highway) was simulated at cross-section 6 (figs. 4 and 5); with the culvert removed, flow increased to 450 ft³/s and water-surface elevations were at least 0.1 ft higher. The percentage of flow in each channel was about the same.

Total Flow in Channel Having Lowest Streambed Elevation

To study the effects of flooding within one channel, total flow was simulated in the channel with the lowest streambed elevation, which usually was the rightmost channel. Simulation indicated that the channel selected in cross-sections 2, 4, and 5 contained the entire peak flow of 700 ft³/s. At cross-section 1, flow was simulated in both the middle and right channels because the bank separating them was submerged at higher flows. Water-surface elevation was about 0.4 ft

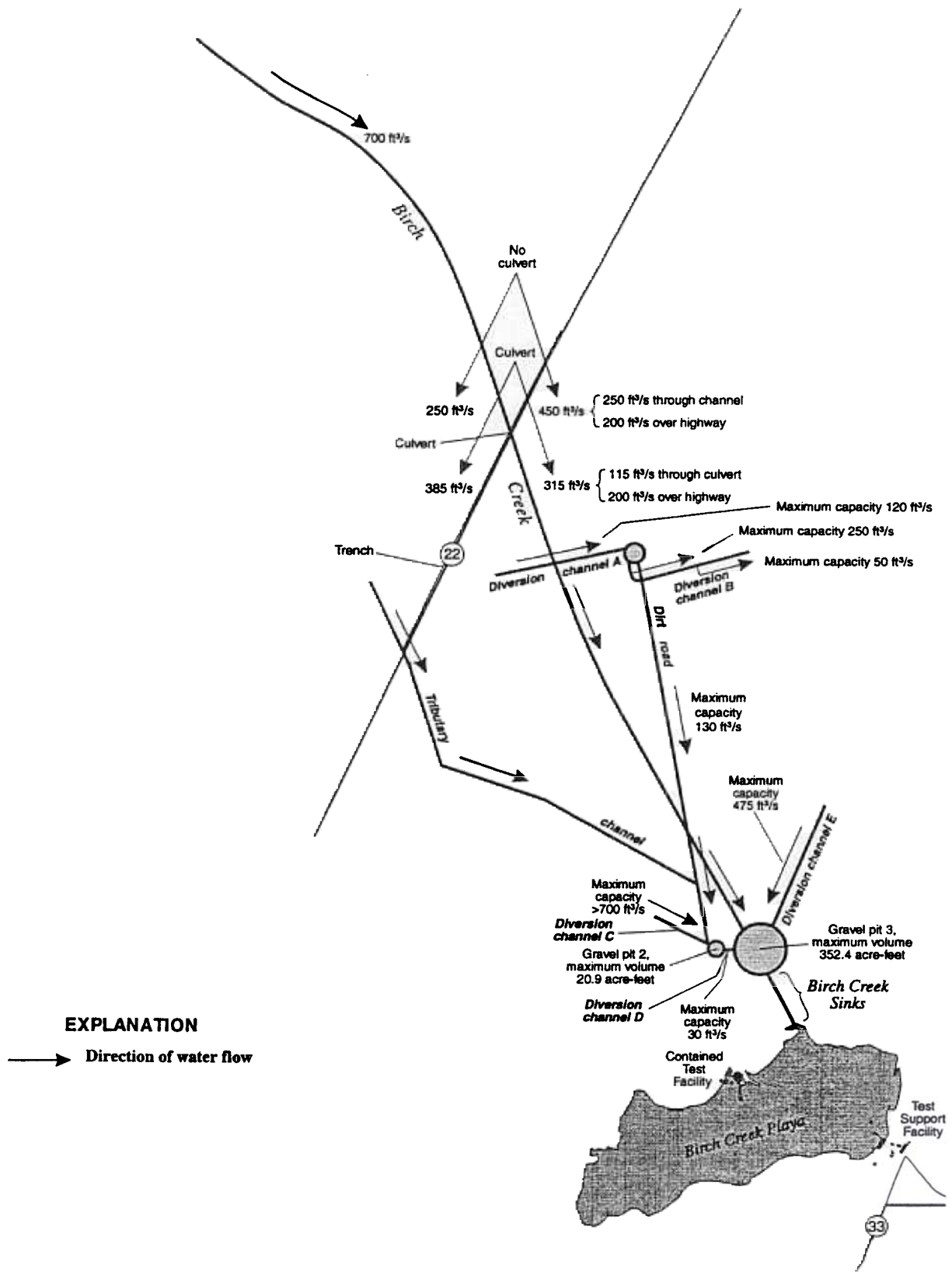


Figure 5. Peak flow in Birch Creek, maximum capacities of diversions, and volumes of gravel pits 2 and 3. (ft³/s, cubic feet per second)

higher than when flow was distributed in all three channels (fig. 4). In cross-sections 2, 4, and 5, the water-surface elevation was about 0.2 ft higher than when the flows were distributed.

At cross-section 6, channels 4 and 5 were combined and used to simulate a peak flow of 315 ft³/s with the culvert and 450 ft³/s without the culvert. Combining several channels was reasonable because the bank separating them was submerged at higher flows. When a flow of 450 ft³/s was simulated, water-surface elevation was about 1 ft higher than when the flows were distributed (fig. 4), channel depth doubled to about 2 ft, and channel width tripled to about 300 ft, compared with distributed flow results. Although large widths and small depths are characteristic of streams and washes in desert areas, flooding in Birch Creek at the magnitude simulated was confined within stream channels.

Cross-Sections 18 and 19

A tributary channel of Birch Creek also received flow because it is downstream and intersects the trench that parallels State Highway 22 in sec. 29, T. 7 N., R. 31 E. (fig. 2). This site is 75 ft lower than where the highway crosses Birch Creek, 1.5 mi to the northeast. There is no culvert or bridge at the site to permit water movement under Highway 22. Flow in the trench was estimated (see section "Cross-Section 5") to be 385 ft³/s with the culvert in place and 250 ft³/s with the culvert removed (fig. 5). At the highway and tributary channel, simulated water-surface elevation at a flow of 385 ft³/s was 4,932.5 ft, 0.9 ft higher than the elevation of the highway; water-surface elevation at a flow of 250 ft³/s was about 0.6 ft higher than elevation of the highway.

Flows in the trench (385 ft³/s and 250 ft³/s) were simulated for the tributary channel at cross-sections 18 and 19. Cross-section 18 is about 200 ft downstream from the highway and cross-section 19 is about 0.8 mi downstream. Simulation results are shown in figure 4. Both simulated flows at these sections were confined within the stream channel (fig. 4).

Maximum Flow Capacities of Diversions

Maximum flows were simulated in diversion channels because they intersect and divert water from Birch Creek. The southeast-trending dirt road (fig. 2) also was modeled as a diversion channel. Diversion

Table 2. Maximum flow capacities of diversions on Birch Creek

[Locations shown in figure 2; >, greater than]

Cross section	Diversion channel	Maximum flow capacity (cubic feet per second)
	A	120
	B	250
	Dirt road	30
	B	250
	B	50
	Dirt road	120
	Dirt road	155
	Dirt road	150
	Dirt road	120
	A	180
	A	350
	A	150
	C	¹ >700
	D	30
	D	30
	E	475
	E	475

¹Water-surface elevation at a flow of 700 cubic feet per second is about 1.2 feet lower than the elevation of the top of the dike.

channel A, about 0.25 mi downstream from cross-section 6, diverts water to gravel pit 1 (fig. 2). Cross-sections 7, 15, 16, and 17 are on diversion channel A. Simulated maximum flow capacities of diversion channel A in cross-sections 7, 15, 16, and 17 were 120, 180, 350, and 150 ft³/s, respectively (table 2). The reason for the large difference in capacity between cross-section 16 and the other cross sections along diversion channel A is that the diversion channel was not constructed to specific engineering plans but was dug rapidly by bulldozers (Koslow, 1984, p. 24), making an irregular-shaped channel. The reduction in flow capacity among sections 16, 17, and 7 caused water to flow over the right embankment, follow the natural slope southeastward, and be intercepted by the dirt road and (or) by diversion channels C, D, E, and (or) gravel pits 2 and 3 (fig. 2). The maximum flow capacity of diversion channel A to gravel pit 1 was 120 ft³/s. When a peak flow of 315 ft³/s passed State Highway 22 (with culvert), 195 ft³/s flowed over diversion channel A because flow into gravel pit 1 was limited by cross-section 7. When peak flow was 450 ft³/s (without culvert), 330 ft³/s flowed over diversion channel A. Estimated flows were based

on the assumption that diversion channels were not roded or breached during peak flow.

Cross-sections 8, 10, and 11 are on diversion channel B, which routes water from gravel pit 1 to the desert in sec. 23, T. 7 N., R. 31 E. (fig. 2). Diversion channel B crosses the dirt road that carries water from the gravel pit southward. Water in diversion channel B will not readily flow down the dirt road because of a 2-ft-high embankment on diversion channel B at the crossing. A maximum flow capacity of 250 ft³/s was simulated at cross-sections 8 and 10, and 50 ft³/s was simulated at section 11 (table 2). Flow capacity decreased between cross-sections 10 and 11 because of a gradual lowering of the right bank, which reduces flow area. The right embankment was about 2 ft high at cross-sections 8 and 10 and 1 ft high at section 11. The reduction in flow capacity between sections 10 and 11 would cause water to flow down the dirt road (fig. 2) and (or) overtop the right embankment and follow the natural slope southeastward.

The southeast-trending dirt road (fig. 2) was considered a diversion channel because it is bounded by embankments and intersects Birch Creek. Embankments along the road are less than 1 ft high. The road at cross-section 9, north of diversion channel B, could carry about 30 ft³/s of water from gravel pit 1. Simulated maximum flow capacities at cross-sections 12a and 14 were 120 ft³/s and, at sections 12b and 13, about 150 ft³/s, at least four times greater than the capacity at section 9 (table 2 and fig. 5). Water overtopping the road embankments would follow the natural slope southeastward and could be intercepted by diversion channels C, D, E, and (or) gravel pits 2 and 3. Water overtopping the dirt road embankments south of sec. 27, T. 7 N., R. 31 E., probably would be intercepted by diversion channel E and directed to gravel pit 3 (fig. 2). Some water could go around diversion channel E and reach Birch Creek Playa.

Simulated maximum flow capacity of diversion channel C where it enters gravel pit 2 (cross-section 20) was much greater than 700 ft³/s (table 2), the 100-year peak flow. The capacity is so large because land surface on the left bank increases very slowly, creating a large flow area. Flow width on the left bank is about 1,000 ft and carries about 68 percent of the flow. At a flow of 700 ft³/s, simulated water-surface elevation was about 1.2 ft lower than the top of the dike, and flow width on the left bank was reduced to about 550 ft.

Cross-sections 21a and 21b are on diversion channel D, which routes water from gravel pit 2 to

gravel pit 3 (fig. 2) and is about 500 ft long. Simulated maximum flow capacities at these sections were 30 ft³/s. Water could flow to the southeast and reach CTF, Birch Creek Playa, and (or) TSF if gravel pit 2 received more than 30 ft³/s when full. If the channel were widened and deepened, greater volumes of water would be diverted to gravel pit 3.

Diversion channel E, trending southwestward, diverts water from the desert north of TSF to the eastern extremity of gravel pit 3 (fig. 2). Cross-sections 22 and 23 are on diversion channel E. A maximum flow capacity of 475 ft³/s was simulated at sections 22 and 23. Water overtopping the right embankment of this diversion channel probably would follow the natural slope southeastward toward Birch Creek Playa and TSF, skirting gravel pit 3.

GENERALIZED 100-YEAR FLOOD-PRONE AREAS

Usually, the extent of flooding is delineated using the simulated water-surface elevation at each surveyed cross section and following the topographic contours between sections. Because Birch Creek is highly braided, and many anthropogenic features in the study area affect flood hydraulics and flow, standard techniques were not used to determine the exact location of flood boundaries. Because flood boundaries could not be located exactly, only a generalized flood-prone map resulting from a 100-year peak flow in Birch Creek was developed (fig. 6). In the reach from cross-sections 1 to 5, peak flows were previously determined to be confined within the braided channels. At State Highway 22 and downstream, anthropogenic features caused peak flows to spread out and encompass large areas. If the anthropogenic features were not present, peak flows probably would be confined within the braided channels to the Birch Creek Playa under similar conditions upstream from Highway 22. The trench along State Highway 22 causes water to flow downstream and into the tributary channel that crosses the highway (1.5 mi southwest of Birch Creek). Diversion channel B probably would cause water to flow into the desert and southeastward toward TSF (fig. 6).

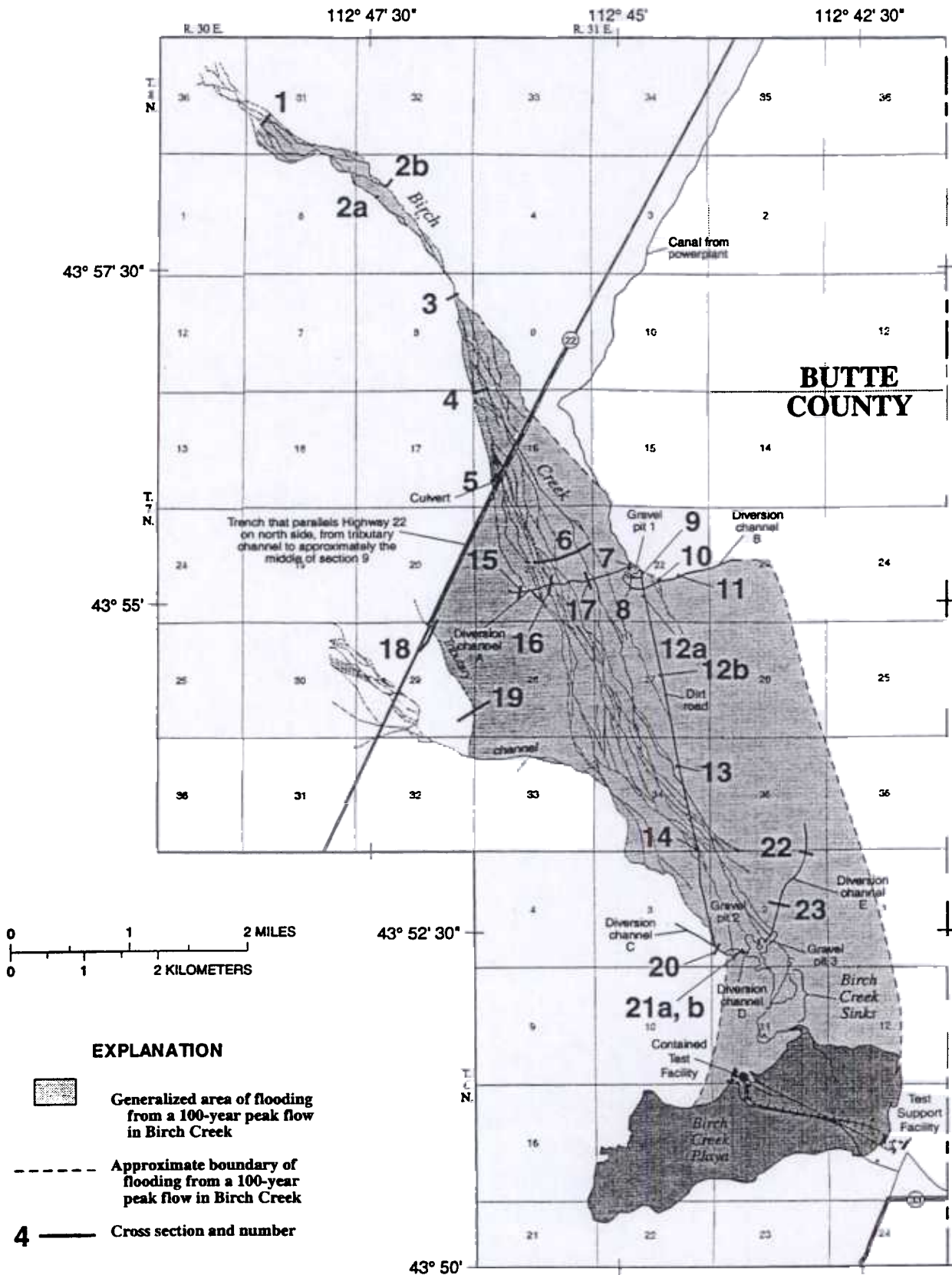


Figure 6. Generalized flood-prone areas resulting from a 100-year peak flow in Birch Creek.

SUMMARY

This report describes results of a study to delineate the extent of possible flooding at the INEEL from a 100-year peak flow in Birch Creek.

Birch Creek flows southward about 40 mi through an alluvium-filled valley to the eastern Snake River Plain. The study area is the lower 10-mi reach of Birch Creek that ends in Birch Creek Playa. Birch Creek is highly braided. Upstream from State Highway 22, it crosses southwest-sloping alluvial fans. Streambed materials are largely coarse sand, gravel, and cobbles that are mined from three gravel pits in the study area. Birch Creek Playa is underlain by silt and clay.

Many anthropogenic features in the study area affect the flood hydraulics of Birch Creek. State Highway 22 crosses Birch Creek and its flood plain and may divert water southwestward in a trench along the highway. About 1 mi south of the highway, diversion channel A crosses the flood plain and routes water to gravel pit 1. An outlet channel from gravel pit 1 routes water eastward to the desert. A 3.5-mi-long, southeast-trending dirt road also was considered a diversion because it crosses Birch Creek and can divert water southward toward CTF. At the southern end of the dirt road, diversion channel C can divert water to gravel pit 2. Diversion channel D conveys water from gravel pit 2 to gravel pit 3, and diversion channel E conveys water southward to gravel pit 3. If gravel pit 3 overflowed, water ultimately would flow to Birch Creek Sinks and Playa.

Geomorphic characteristics of gravel pits 2 and 3 and Birch Creek Playa were defined from DEM data. At full-pool capacity, gravel pit 2 has a water-surface area of 3.9 acres and a volume of 20.9 acre-ft; gravel pit 3 has a water-surface area of 29.7 acres and a volume of 352.4 acre-ft. With dikes at 4,786.5 ft, Birch Creek Playa has a water-surface area of 5,900 acres and a volume of 21,600 acre-ft. The water-surface elevation resulting from the 100-year flow volume (13,000 acre-ft) is about 2 ft lower than the elevation of dikes around TSF and CTF; therefore, no flooding of these facilities would be expected from the hypothetical 100-year peak flow. If water-surface elevation were raised 1.5 ft higher to 4,788 ft, surface area would increase to 8,140 acres and volume would increase to 31,800 acre-ft, more than twice the volume (13,000 acre-ft) that would result from the 100-year peak flow.

Cross-section data were needed to develop and a hydraulic model (WSPRO) to simulate water-

surface elevations for a 100-year peak flow in Birch Creek. Twenty-six channel cross sections were surveyed: 9 on creeks, 12 on diversion channels, and 5 on the dirt road. One culvert near cross-section 5 and the highway near cross-sections 5 and 18 also were surveyed. Roughness values ranged from 0.048 to 0.068 for main creek channels, 0.054 to 0.074 for the flood plain, and 0.028 to 0.040 for the highway, diversion channels, and dirt roads. In the model, water-surface elevation and roughness values were adjusted until the simulated water-surface elevation, velocity, and Froude number were reasonable because no flow data were available to calibrate the model. Where cross sections crossed more than one channel, flow was distributed among all channels. The estimated 100-year peak flow of Birch Creek at the northern boundary of the INEEL (700 ft³/s), was used in the hydraulic model.

Simulation indicated that flow upstream from Highway 22 was confined within channels even when all flow was routed through one channel. Where State Highway 22 crosses Birch Creek, about 315 ft³/s of water flowed downstream from the highway—115 ft³/s through the culvert and 200 ft³/s over the highway. The simulated water-surface elevation at this crossing was 0.8 ft higher than the elevation of the highway. The remainder of the peak flow (385 ft³/s) flowed southwestward in a trench along the north side of the highway. The maximum flow capacity of the trench is about 450 ft³/s. With the culvert removed, about 450 ft³/s of water flowed downstream—250 ft³/s through the breach on the highway and 200 ft³/s over the highway. The remainder of the peak flow flowed southwestward in the trench.

A tributary channel southwest of Birch Creek receives flow because the channel is downstream and intersects the trench that parallels the north side of the highway. At the highway and tributary channel, the streambed elevation is 75 ft lower than that where Birch Creek crosses the highway. Water flows over the highway at this site because there is no culvert or bridge to allow flow under the highway. The simulated water-surface elevation at this crossing was about 0.9 ft higher than the elevation of the highway at a flow of 385 ft³/s and about 0.6 ft higher at a flow of 250 ft³/s. Simulation of tributary flow at cross-sections 18 and 19 indicated that both flows were confined within the channel, although flow widths are large.

Only maximum flow capacities were determined for diversion channels and the dirt road because they probably would be at full capacity during peak flow.

Diversion channel A, 1 mi south of the highway, is perpendicular to Birch Creek and diverts water to gravel pit 1. The maximum capacity of diversion channel A is about 120 ft³/s. If a flow of 450 ft³/s passed State Highway 22, about 330 ft³/s would flow downstream from diversion channel A and some flow could be intercepted by the dirt road, diversion channels C, D, E, and (or) gravel pits 2 and 3. Some water might flow eastward from the outlet of gravel pit 1 through diversion channel B and spread onto the desert. Initially, diversion channel B would carry 250 ft³/s; flow would gradually decrease to 50 ft³/s as the channel area decreased because water would overflow the right embankment. The dirt road acts as a diversion channel because it is bounded by embankments and crosses Birch Creek. Maximum flow of the dirt road is from 120 to 150 ft³/s. Water overtopping the road embankments south of sec. 27, T. 7 N., R. 31 E., probably would be intercepted by diversion channel E and directed to gravel pit 3 before reaching Birch Creek Playa. Diversion channel C at the southern end of the dirt road diverts water to gravel pit 2 and can easily carry the 100-year peak flow of 700 ft³/s. The maximum flow capacity for diversion channel D, between gravel pits 2 and 3, was 30 ft³/s. If gravel pit 2 received more than 30 ft³/s when full, areas to the southeast could be flooded. If the channel were widened and deepened, greater volumes of water would be diverted to gravel pit 3. Diversion channel E diverts water to gravel pit 3 and has a maximum capacity of about 475 ft³/s. Water passing this channel probably would flow toward Birch Creek Playa and TSF, skirting gravel pit 3.

Standard techniques to delineate the 100-year flood boundaries were not used on Birch Creek because it is extensively braided and anthropogenic features in the study area affect flood hydraulics and flow. However, generalized flood-prone areas were mapped. In reaches upstream from State Highway 22, flows were confined within the braided channels. At the highway and downstream, flows spread out and encompassed large areas, probably due to anthropogenic features such as the trench along State Highway 22 and diversion channel B. If the anthropogenic features were not present, peak flow probably would be confined within the braided channels of Birch Creek.

REFERENCES CITED

- Bennett, C.M., 1990, Streamflow losses and ground-water level changes along the Big Lost River at the Idaho National Engineering Laboratory, Idaho: U.S. Geological Survey Water-Resources Investigations Report 90-4067, 49 p.
- Berenbrock, Charles, Bassick, M.D., Rogers, T.L., and Garcia, S.P., 1995, Depth to water, 1991, in the Rathdrum Prairie, Idaho; Spokane River Valley, Washington; Moscow-Lewiston-Grangeville area, Idaho; and selected intermontane valleys, east-central Idaho: U.S. Geological Survey Water-Resources Investigations Report 94-4087, 2 sheets.
- Chow, V.T., 1959, Open-channel hydraulics: New York, McGraw-Hill, 680 p.
- Fulford, J.M., 1995, User's guide to the culvert analysis program: U.S. Geological Survey Open-File Report 95-137, 69 p.
- Kjelstrom, L.C., 1992, Simulation of water-surface elevations for the Snake River in the Deer Flat National Wildlife Refuge, Idaho: U.S. Geological Survey Water-Resources Investigations Report 91-4198, 105 p.
- Kjelstrom, L.C., and Berenbrock, Charles, 1996, Estimated 100-year peak flows and flow volumes in the Big Lost River and Birch Creek at the Idaho National Engineering Laboratory, Idaho: U.S. Geological Survey Water-Resources Investigations Report 96-4163, 23 p.
- Koslow, K.N., 1984, Hydrological characterization of Birch Creek Basin: Idaho Falls, EG&G, Geosciences Section, Earth and Life Sciences Branch, EGG-PBS-6782, 29 p.
- Niccum, M.R., 1973, Discussion of potential flood problems in conjunction with the LOFT program: Idaho Falls, Aerojet Nuclear Company, LTR 10-18, 20 p.
- Shearman, J.O., 1990, User's manual for WSPRO—a computer model for water surface profile computations: U.S. Department of Transportation, 177 p. [available from the National Technical Information Service, U.S. Department of Commerce, Springfield, Va., 22161 as Report No. FHWA-IP-89-027].
- Shearman, J.O., Kirby, W.H., Schneider, V.R., and Flippo, H.N., 1986, Bridge waterways analysis model—research report: U.S. Department of Transportation, 112 p. [available from the National Technical Information Service, U.S. Department of Commerce, Springfield, Va., 22161 as Report No. FHWA/RD-86/108].
- Whitehead, R.L., 1986, Geohydrologic framework of the Snake River Plain, Idaho and eastern Oregon: U.S. Geological Survey Hydrologic Investigations Atlas HA-681, 3 sheets, scale 1:1,000,000.

APPENDIX V

100-YEAR STORM WATER RUNOFF FLOODPLAIN AND 25-YEAR RUNOFF
ANALYSES FOR THE IDAHO NUCLEAR TECHNOLOGY AND ENGINEERING CENTER
AT THE IDAHO NATIONAL ENGINEERING AND ENVIRONMENTAL LABORATORY
(INEEL/EXT-03-01174, REVISION 1, JANUARY 2004)

**NOTE: THIS INFORMATION IS AVAILABLE ELECTRONICALLY ON THE CD
FOUND IN APPENDIX I.**

INEEL/EXT-03-01174

Revision 1
January 2004

**100-Year Storm Water
Runoff Floodplain and
25-Year Runoff
Analyses for the Idaho
Nuclear Technology
and Engineering Center
at the Idaho National
Engineering and
Environmental
Laboratory**

100-Year Storm Water Runoff Floodplain and 25-Year Runoff Analyses for the Idaho Nuclear Technology and Engineering Center at the Idaho National Engineering and Environmental Laboratory

Prepared By:

**Clear Creek Hydrology, Inc.
and
Neil C. Hutten, INEEL**

Published January 2004

**Idaho National Engineering and Environmental Laboratory
Idaho Falls, Idaho 83415**

**Prepared for the
U.S. Department of Energy
Assistant Secretary for Environmental Affairs
Under DOE Idaho Operations Office**

ABSTRACT

This hydrologic study of the Idaho Nuclear Technology and Engineering Center (INTEC) at the Idaho National Engineering and Environmental Laboratory (INEEL) was conducted to identify the 100-year storm water runoff floodplain boundary for the drainage system and surface water channels in the vicinity of the site and to evaluate the capacity of the drainage system during the 25-year storm. The INTEC is subject to permitting under the Resource Conservation and Recovery Act (RCRA), which requires analysis of the 25-year runoff and 100-year floodplain associated with natural and man-made drainages. Storm water drainage diversions, channels, hydraulic control structures and retention areas have been constructed throughout and around the facility to minimize flooding potential and are the subject of these hydrologic and hydraulic analyses and report.

The hydrologic study was conducted to evaluate the largest 25-year and 100-year storm water flood flows through and in the vicinity of this facility. Summer, winter rain on snow, and winter rain on snow with frozen ground conditions were evaluated as a part of this study to identify the maximum flows anticipated for storms with the specified return intervals. Flood flows were generated using hydrologic models of the facility and incorporated into hydraulic models of storm water drainage systems and the Big Lost River. Peak water surface profiles were used to map the 100-year storm water runoff floodplain boundaries to represent conditions at the INTEC as of May 2003, and to evaluate the capacity of the storm water drainage system during the 25-year runoff event.

CONTENTS

ABSTRACT.....	iii
ACRONYMS.....	vii
1. INTRODUCTION.....	1
1.1 General.....	1
1.2 Objective.....	2
1.3 Previous Investigations.....	4
1.4 Acknowledgements.....	5
1.5 Limitations.....	5
2. REGIONAL HYDROLOGY.....	6
2.1 Climatology and Historic Flooding Data Sources.....	6
2.2 Historical Flood Events.....	7
2.3 Summer and Winter Design Storm Conditions.....	8
2.3.1 Design Storm Precipitation.....	8
2.3.2 Snowmelt.....	11
2.3.3 Frozen Ground and Concrete Impermeable Frost.....	11
2.4 Summer and Winter Design Storm Parameters.....	13
3. FIELD INVESTIGATION AND DATA COLLECTION.....	15
3.1 Watershed and Subarea Boundary Verification.....	15
3.2 Hydraulic Structure Inventory.....	15
3.3 Field Surveying and Measurements.....	16
4. HYDROLOGIC MODELING.....	17
4.1 Hydrologic Characteristics and Modeling Parameters.....	17
4.1.1 Watershed and Sub Area Delineation.....	17
4.1.2 Soil Type and Vegetation.....	19
4.1.3 Impervious Surfaces.....	21
4.1.4 Natural and Man-Made Surface and Diversion Channels.....	22
4.1.5 Storm Water Retention Areas.....	22
4.1.6 Big Lost River.....	22

4.2	Hydrologic Modeling and Analysis	23
4.2.1	SCS Curve Numbers and Precipitation Losses	23
4.2.2	Time of Concentration	25
4.2.3	HEC-1 Model Input and Output.....	29
4.2.4	Hydrologic Modeling Approach	29
4.3	Hydrologic Modeling Results	30
4.4	Comparison of Results to Historic Rain/Snow/Frozen Ground Floods	38
5.	HYDRAULIC ANALYSIS	39
5.1	Big Lost River.....	39
5.1.1	Channel Geometry	39
5.1.2	Bridges and Culverts	39
5.1.3	Roughness Coefficients.....	40
5.1.4	Hydraulic Modeling Process and Equations	40
5.1.5	HEC-RAS Model Simulations, Big Lost River.....	40
5.2	INTEC Surface and Subsurface Drainage System Modeling	41
5.2.1	SWMM Program Input Parameters.....	42
5.2.2	Storm Water Runoff Hydrographs	42
5.2.3	SWMM Analysis.....	42
5.2.4	SWMM Modeling Results.	44
5.3	25-year and 100-year Floodplain Mapping.....	45
6.	CONCLUSIONS	46
7.	REFERENCES	47

TABLES

2-1. Precipitation depths (inches) for summer design storms.....	9
2-2. Precipitation depths (inches) for winter design storms.....	10
2-3. Precipitation depths (inches) for winter rain on frozen ground design storms.....	10
4-1. SCS Curve Numbers for sage-grass complexes.	21
4-2. SCS Curve numbers used in hydrologic modeling.....	23
4-3. Sub area flow parameters used in determining time of concentration (t_c) and lag times.....	27
4-4. Time of concentration (t_c) for sub areas.	28
4-5. Peak flow for individual sub areas.	32
4-6. Peak flows for key hydrograph combinations used in hydraulic analyses	33

FIGURES

Figure 1-1. INEEL and INTEC Location.....	2
Figure 1-2. INTEC Plan View	3
Figure 4-1. 25-year summer storm hydrographs for Lincoln Boulevard, Big Lost River	34
Figure 4-2. 25-year summer storm hydrographs for INTEC sub areas.....	34
Figure 4-3. 100-year summer storm hydrographs for Lincoln Boulevard, Big Lost River	35
Figure 4-4. 100-year summer storm hydrographs for INTEC sub areas.....	35
Figure 4-5. 25-year winter storm hydrographs for Lincoln Boulevard, Big Lost River	36
Figure 4-6. 25-year winter storm hydrographs for INTEC sub areas	36
Figure 4-7. 100-year winter storm hydrographs for Lincoln Boulevard, Big Lost River	37
Figure 4-8. 100-year winter storm hydrographs for INTEC sub areas	37

DRAWINGS

Sheet 1. INTEC Facility and Surrounding Area, Watershed and Sub Area Boundaries
Sheet 2. INTEC Facility Detail, 100-Year Floodplain

ACRONYMS

AMC	Antecedent moisture condition
amsl	Above mean sea level
CCH	Clear Creek Hydrology, Inc.
CFA	Central Facilities Area
CFR	Code of Federal Regulations
CFS	Cubic feet per second
CN	Curve Number
DDF	Depth duration frequency
DOE	Department of Energy
EPA	Environmental Protection Agency
F	Fahrenheit
FAA	Federal Aviation Administration
FEMA	Federal Emergency Management Agency
FT	Feet
GPS	Global Positioning System
HEC	Hydrologic Engineering Center
HEC-RAS	Hydrologic Engineering Center's River Analysis System
ID	Idaho
IN	Inches
INEEL	Idaho National Engineering and Environmental Laboratory
INTEC	Idaho Nuclear Technology and Engineering Center
LB	Lincoln Boulevard
MI	Mile
MIN	Minutes
NAD	North American Datum
NGVD	National Geodetic Vertical Datum
NOAA	National Oceanographic and Atmospheric Administration
NRCS	Natural Resource Conservation Service
NWS	National Weather Service
RCRA	Resource Conservation and Recovery Act
RWMC	Radioactive Waste Management Complex
S	Second(s), Slope
SCS	Soil Conservation Service
SWMM	Storm Water Management Model
T	Time
t_c	Time of Concentration
US	United States
USCOE	United States Army Corps of Engineers
USGS	United States Geological Survey

100-Year Storm Water Runoff Floodplain and 25-Year Runoff Analyses for the Idaho Nuclear Technology and Engineering Center at the INEEL

1. INTRODUCTION

1.1 General

The Idaho Nuclear Technology and Engineering Center (INTEC) is located approximately 50 miles west of Idaho Falls in the south-central portion of the Idaho National Engineering and Environmental Laboratory (INEEL) (Figure 1-1). The facility encompasses a total of 420 acres within a perimeter fence and adjoining areas (Figure 1-2).

The INTEC is located at the northeastern end of a large, relatively flat, fan-shaped area dominated by volcanic features including basalt flows. It is located immediately south of the Big Lost River in an arid portion of Idaho where storms are generally infrequent, producing little storm water runoff and flooding potential. Storm water runoff around INTEC generally infiltrates the soils or evaporates before reaching the Big Lost River. The Big Lost River itself generally flows very little near the INTEC due to the lack of precipitation, upgradient water withdrawal for irrigation and the presence of control structures upgradient of the site.

Historically, the INTEC has seen only minor localized flooding and ponding in depression areas inside and around the facility. No significant flooding due to storm water runoff was identified during discussions with INTEC and INEEL personnel, including periods when floods occurred in other locations near INTEC. A storm water drainage network constructed with open surface water channels, culverts, storm water catch basins and subsurface piping serves to manage storm water runoff through the facility, directing it to the northeast edge of the facility where it is discharged into a retention area. Excess water in the retention area overflows towards the Big Lost River during significant runoff events.

Modifications and improvements to the drainage system serving the INTEC facility have been constructed since the mapping and field investigation for this study were completed. Improvements include a new retention basin with additional storage volume for discharge from the facility and other minor drainage modifications and upgrades. The analyses conducted for this study were prepared for conditions existing at the site as of May 2003 and do not include alterations to the drainage system and facilities since that time.

The Big Lost River, immediately north of the INTEC, is controlled by a long barrier dike in the vicinity of the facility to limit flooding potential and flows northeast to its termination in the playas. Big Lost River flows have not entered the INTEC since operations began in the 1950's. This floodplain analysis for the INTEC facility is limited to storm water runoff from the contributing area around the facility. The potential for riverine flooding from the Big Lost River is being studied by others and is beyond the scope of this project and report.

1.2 Objective

The primary objective of this project is to determine the magnitude and extent of the largest 100-year return interval storm and develop a storm water runoff floodplain map for the hypothetical storm as required by state and federal regulations to determine whether INTEC facilities are within the floodplain boundaries and subject to potential flooding. The secondary objective is to ensure that the INTEC storm water drainage system will convey, at a minimum, the 25-year, 24-hour peak storm water runoff flow.

This hydrologic and hydraulic analysis of the INTEC facility was conducted according to the requirements of the Resource Conservation and Recovery Act found in 40 Code of Federal Regulations (CFR) Section 270.14(b)(11)(iii). Additionally, the modeling and mapping prepared for this study were conducted according to the procedures and methods required by the Federal Emergency Management Agency (FEMA).

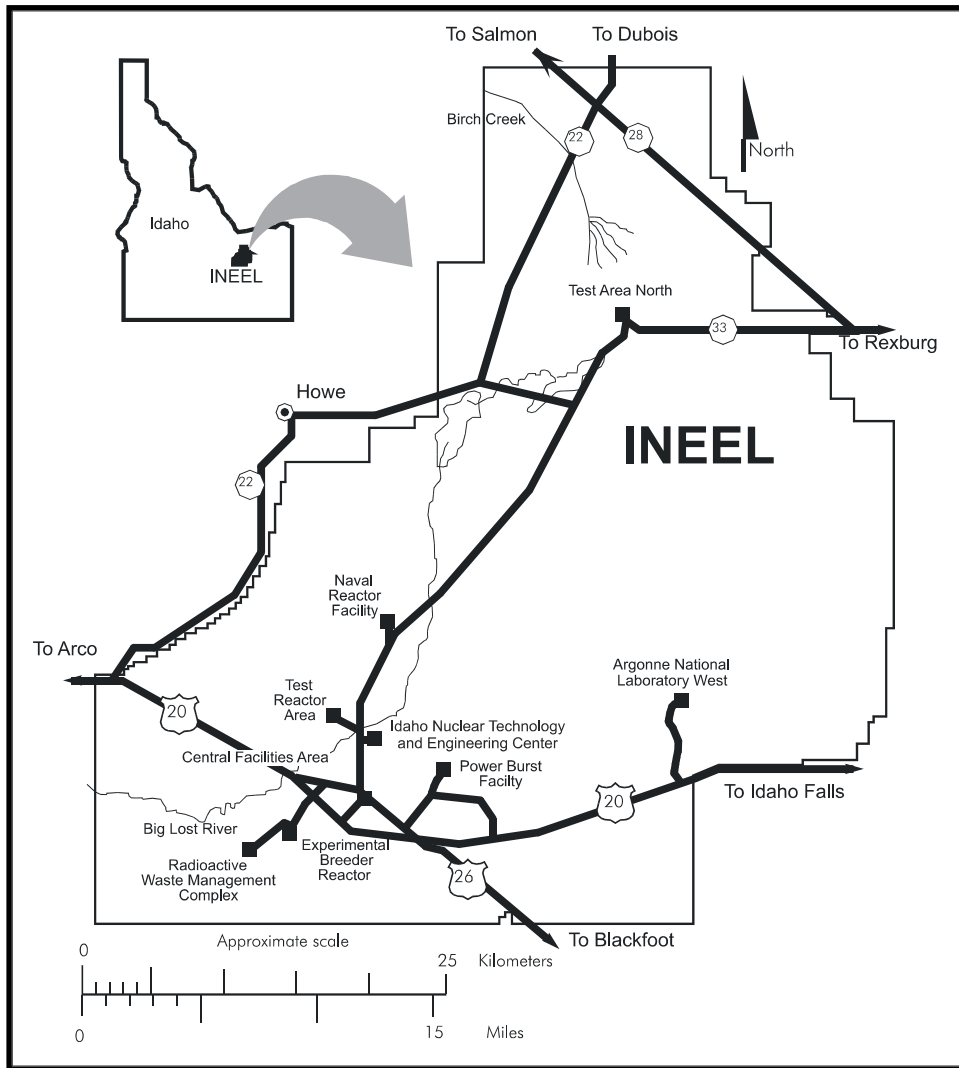


Figure 1-1. INEEL and INTEC location.

Figure 1-2. INTEC plan view.

1.3 Previous Investigations

Previous studies of the area around the INTEC and INEEL have been conducted to evaluate potential flooding events, storm water drainage systems and the Big Lost River. Specific aspects of these studies that are relevant to the current study are discussed in the following paragraphs and in subsequent sections of this report.

Tullis and Koslow (1983) characterized Big Lost River floods with recurrence intervals greater than 25 years by a statistical analysis of short-term historical records and through the study of slack water deposits. The United States Geological Survey (USGS) (Berenbrock and Kjelstrom, 1998) evaluated flood potential on the Big Lost River by utilizing a one-dimensional model to calculate water surface elevations and estimate inundated areas during the 100-year peak flow. Ostenaar, et al., (1999) performed a paleoflood study of the Big Lost River.

Koslow and Van Haaften (1986) utilized the National Weather Service (NWS) DAMBRK model to simulate four different hypothetical Mackay Dam failure scenarios. The magnitude of the combined probability of the 100-year recurrence interval flood with Mackay Dam failure was not specified in this report, but by definition is less than the probability of the 100-year event alone. Likewise, the probability of the hydrologic events discussed in this current report with the simultaneous occurrence of a hypothetical Mackay Dam failure is much less than 0.01. Analyses of the flood magnitude and potential associated with the Mackey Dam and the Big Lost River were considered beyond the scope of this project.

Taylor, et al., (1994) conducted a detailed study of flooding events at the INEEL that occurred in 1962, 1964, 1969 and 1972, resulting from combinations of precipitation, snowmelt and frozen ground. Results of the study concluded that the most significant flooding potential at the INEEL occurs during winter months with rain on snow in the presence of frozen ground. Mitchell, et al., (2002) conducted a detailed hydrologic analysis of the Radioactive Waste Management Complex (RWMC), including a comparison of summer and winter storm events, similar in nature to this current study. Results of the RWMC analysis verified Taylor's findings with the largest 100-year return interval event occurring during the winter rain on snow with frozen ground event and serves as a guideline for the current study of INTEC.

Burgess, J.D. (1991) conducted hydrologic and hydraulic analyses of the storm water drainage system within the INTEC facility perimeter to evaluate adequacy during the 25-year return period event. Results of the investigation included a comparison of the hydraulic capacity of surface channels, storm water piping, culverts and other features with storm water runoff during the 25-year, 24-hour event. It also included recommendations for improvements to the drainage system in order to minimize flooding potential. Results of the Burgess study were used as background information for the 25-year, 24-hour storm event analysis conducted as a part of the current study, however, the Burgess study was conducted prior to additional construction and improvements completed at the INTEC.

The current study was performed to include recent precipitation and temperature data and to address changes in topography and facility drainage structures made after previous investigations were completed. Topographic data used in the current study were collected in an aerial photogrammetry flight by Aerial Services, Inc. of Cedar Falls, Iowa on July 30, 2002.

1.4 Acknowledgements

Appreciation is extended to Mr. Ken Beard of the INEEL and the INTEC facility for his assistance with site surveying and data. Mr. Beard provided extensive surveying of storm water control structures including surface water channels, storm drainage inlets and culverts. He conducted surveying in restricted access areas and provided surveying control point data utilized during the field investigation for this study.

1.5 Limitations

This hydrologic and hydraulic study was conducted for the INTEC facility with base mapping and topography created in 2002, and additional field investigation data collected in May of 2003. Results of this study are presented for conditions at the site as of May, 2003.

Several areas in and around the INTEC facility, the surrounding watershed, and near other facilities were under construction at the time of the field investigation or were modified or improved after the field investigation. Changes in topography, drainage patterns, and facilities completed after May of 2003 are not represented in the analyses and results of this report.

2. REGIONAL HYDROLOGY

Regional hydrology of the southern portion of the INEEL was investigated in the current study for the area around the INTEC facility during the course of this investigation and in a recent study performed for the RWMC (Mitchell, et al., 2002). An investigation and review of available regional hydrology documentation was conducted in order to determine the appropriate design storm conditions and watershed parameters for use in hydrologic and hydraulic modeling of the site. Several sources of information were utilized to determine existing conditions during previous flooding events throughout southeastern Idaho and the surrounding area, which provides a measure of flood and regional hydrologic conditions for the INTEC. This section of the report discusses the sources of information reviewed as a part of the evaluation of regional hydrologic conditions and used to develop design storm parameters and precipitation statistics for the hydrologic modeling.

2.1 Climatology and Historic Flooding Data Sources

Several sources of information relating to climatology and historic flooding were utilized in determining regional hydrologic conditions for the INTEC and the INEEL. Regional hydrologic information is available for southeastern and central Idaho, however, there is limited information relating specifically to stream flows and storm water runoff for the INTEC and INEEL. Data used in this hydrologic study were obtained from the National Weather Service for the area within and surrounding the INEEL. In the absence of site-specific information, data were selected for areas with similar hydrologic regimes outside of the INEEL including southern Idaho, northern Utah, northern Nevada and southwestern Montana. Data sources utilized in this hydrologic investigation include the following:

- United States Geological Survey, Methods for Estimating Magnitude and Frequency of Floods in the Southwestern United States, Open File Report 93-419, 1994.
- National Weather Service, INEEL Winter Flood Events, Idaho Falls 46W Data (1952 – 2000).
- National Weather Service, Idaho Falls FAA, Idaho Falls Airport Gage data (1948 – 1952).
- National Weather Service, Idaho Falls 2ESE Gage Data (1952 – 1960).
- National Weather Service, Idaho Falls 16SE Gage Data (1960 – 1997).
- National Weather Service, Dubois Gage Data (1948 – 1997).
- National Weather Service, Twin Falls Gage Data (1978 – 1997).
- Soil Conservation Service, National Engineering Handbook, 1972.
- United States Army Corps of Engineers, Snow Hydrology Manual, 1998.

In addition to the data sources identified above, several reports and technical memoranda regarding the INTEC facility and other hydrologically similar areas were reviewed to evaluate previous flooding events and hydrologic studies including:

- Eugene L. Peck and E. Arlo Richardson, 1962, *An Analysis of the Causative Factors of the February 1962 Floods in Utah and Eastern Nevada*, National Weather Service, Salt Lake City, Utah.
- United States Army Corps of Engineers, 1975, *Humbolt River and Tributaries, Nevada*, Design Memorandum No. 1, Sacramento District.
- Dr. John H. Humphrey, 1994, *Meteorological Analysis, Flood Control Master Plan*, Washoe County, Nevada.
- CH2MHill, Inc., 1989, *Silver Bow Creek Flood Modeling Study*, Silver Bow County, Montana.
- Burgess, J.D., 1991, *25-year, 24-Hour Storm Analysis for the Idaho Chemical Processing Plant*.
- J. Sagendorf, 1991, *Meteorological Information for RWMC Flood Potential Studies*, National Oceanic Atmospheric Administration, Environmental Research Laboratories, Air Resources Laboratory Field Research Division, Idaho Falls, Idaho.
- J. Sagendorf, 1996, *Precipitation Frequency and Intensity at the Idaho National Engineering Laboratory*, National Oceanic and Atmospheric Administration, Technical Memorandum ERL ARL-215, Air Resources Laboratory, Silver Spring, Maryland.
- Mitchell, T., Mitchell, J. S., Humphrey, J., Kennedy, D., Funderburg, T., 2002, *100-Year Floodplain and 25-Year Runoff Analyses for the Radioactive Waste Management Complex at the Idaho National Engineering and Environmental Laboratory*, Document No. INEEL/EXT-02-00093.

2.2 Historical Flood Events

There have been several significant flood events with documented information in southern Idaho, northern Utah and northern Nevada, dating from the early 1900's through the present. Four events in particular have enough recorded information to estimate conditions experienced during winter rain and snowmelt storms with return periods ranging from 25 to 100 years. The most significant events occurred in February 1962, January 1969, February 1980 and February 1982. Of these events, the 1962 rain-on-snow conditions were estimated to represent a storm with a return period of 50 to 100 years (DOE-ID, 1998). Climatologic and general flooding information was obtained for all of these events and used to evaluate anticipated conditions during a 100-year return period storm. The data provides an approximate measure of the peak flow anticipated for the INTEC facility.

All of the observed events required an unusual set of climatological conditions including a wet fall season, very cold temperatures through December, January, and February, little or no

snow cover, no thawing of the ground, and some accumulation of snow just prior to the flood. This set of conditions results in a shallow snow cover underlain by concrete impermeable frost. The development of concrete impermeable frost and its influence on storm water runoff are discussed further in section 2.3.3 of this report.

Based on historic flooding information (USCOE, 1975, CH2MHill, 1989) and according to limited United States Geological Survey (USGS) stream gage data in the area surrounding INEEL, peak flows of 30 to 60 cubic feet per second per square mile (cfs/mi²) can be expected during a 100-year rain on snow with frozen ground event in watersheds similar in size and nature to that of the INTEC. This regional flood flow information was used as an approximation of the 100-year flood model developed for the INTEC.

In addition to peak flow estimations provided by the USGS documentation, limited information relating to runoff volume was obtained from previous hydrologic studies. Sagendorf (1991) indicates that the 1962 flood event produced a runoff volume of approximately 30 acre-feet in a 3.435 mi² watershed (located at the Radioactive Waste Management Complex). This volume estimate of storm water was used as an indirect correlation to the runoff expected at the INTEC due to the locations of these facilities and their similar hydrologic conditions.

2.3 Summer and Winter Design Storm Conditions

Three separate conditions were considered to evaluate the largest 25-year and 100-year storm water runoff events for the INTEC facility. Design storm data were developed separately for summer cloudburst storms, winter storms, and for winter rain on snow with frozen ground events. Separating the different conditions provides more accurate determination of precipitation depths for various return period storms and better representation of hydrologic conditions during the summer and winter seasons. Design storm parameters for summer and winter conditions are discussed in the following sections.

2.3.1 Design Storm Precipitation

Precipitation depths for summer and winter storms were determined primarily from gage data collected from the City of Idaho Falls and the INEEL. Specific gage sites include the following:

- National Weather Service, INEEL Winter Flood Events, Idaho Falls 46W Data
- National Weather Service, Idaho Falls FAA, Idaho Falls Airport Gage Data

Gage data from these sources are available for approximately 50 years, providing sufficient data to conduct a statistical analysis for precipitation depths. Depth-duration-frequency (DDF) curves were developed for this study from the gage data obtained from the NWS using standard procedures of ranking maximum observed precipitation depths and plotting data on a lognormal probability distribution. Best-fit curves were developed for evaluating precipitation depth-duration-frequency statistics for the INTEC facility. The power curve equation is shown below.

$$D = a * t^b$$

- Where: D = design storm precipitation depth (in)
 a = statistical parameter based on ranked gage data
 b = statistical parameter based on ranked gage data
 t = time (min)

Precipitation depths were determined for storms with durations ranging from 5 minutes to 24 hours and return periods from 2 to 100 years. The precipitation depths developed for design storms used in this hydrologic analysis were prepared independently from studies performed by others, including those prepared by J. Sagendorf (1991 and 1996), Keck (1998) and Dames and Moore (1993). Most significantly, the DDF statistics developed for this hydrologic analysis compare closely with those prepared by J. Sagendorf in 1996. Slight differences can be identified in precipitation depths for each design storm and return frequency due to specific data periods used in developing the statistics, differences in interpretation of best-fit curves and lines, and best engineering judgment.

Summer DDF curves were developed from gage data recorded between the months of May through September. Summer precipitation statistics are shown in Table 2-1.

Table 2-1. Precipitation depths (inches) for summer design storms.

Summer Cloudburst Depth Duration Frequency D=a*t^b										
Recurrence	a	b	5-min	15-min	1-hr	2-hr	3-hr	6-hr	12-hr	24-hr
2-year	0.095	0.305	0.155	0.217	0.331	0.409	0.463	0.572	0.707	0.873
5-year	0.154	0.282	0.242	0.331	0.489	0.594	0.666	0.810	0.985	1.197
10-year	0.199	0.269	0.307	0.412	0.599	0.721	0.804	0.969	1.168	1.408
25-year	0.262	0.257	0.396	0.525	0.750	0.897	0.995	1.189	1.421	1.698
50-year	0.302	0.253	0.454	0.599	0.851	1.014	1.124	1.339	1.596	1.901
100-year	0.359	0.243	0.531	0.693	0.971	1.149	1.268	1.501	1.776	2.102

Winter DDF curves were developed using precipitation gage data recorded during the months from November through March, when wet soil conditions will occur. Winter precipitation depths are shown in Table 2-2.

Table 2-2. Precipitation depths (inches) for winter design storms.

Winter Rainfall Depth Duration Frequency										
$D=a*t^b$										
Recurrence	a	b	5-min	15-min	1-hr	2-hr	3-hr	6-hr	12-hr	24-hr
2-year	0.015	0.506	0.034	0.059	0.119	0.169	0.208	0.295	0.419	0.595
5-year	0.026	0.469	0.055	0.093	0.177	0.246	0.297	0.411	0.569	0.787
10-year	0.035	0.447	0.072	0.117	0.218	0.297	0.357	0.486	0.663	0.903
25-year	0.047	0.427	0.093	0.149	0.270	0.363	0.432	0.580	0.780	1.049
50-year	0.058	0.413	0.113	0.177	0.315	0.419	0.495	0.659	0.878	1.169
100-year	0.071	0.397	0.135	0.208	0.361	0.475	0.558	0.735	0.967	1.274

Winter rain on frozen ground DDF curves were developed using precipitation gage data recorded during the months of January and February, when impermeable conditions will occur. Rain on frozen ground precipitation depths are shown in Table 2-3.

Table 2-3. Precipitation depths (inches) for winter rain on frozen ground design storms.

Winter Rain on Frozen Ground Depth Duration Frequency										
$D=a*t^b$										
Recurrence	a	b	5-min	15-min	1-hr	2-hr	3-hr	6-hr	12-hr	24-hr
2-year	0.011	0.506	0.024	0.042	0.084	0.119	0.147	0.208	0.296	0.420
5-year	0.018	0.469	0.039	0.065	0.125	0.172	0.209	0.289	0.400	0.553
10-year	0.025	0.447	0.051	0.083	0.154	0.210	0.252	0.343	0.467	0.637
25-year	0.033	0.427	0.066	0.106	0.191	0.257	0.305	0.411	0.552	0.742
50-year	0.041	0.413	0.079	0.124	0.221	0.294	0.347	0.462	0.615	0.819
100-year	0.050	0.397	0.094	0.145	0.252	0.332	0.390	0.513	0.675	0.889

The data and procedures used in developing DDF curves for the various seasonal events are standard meteorological methods used by the NWS and National Oceanographic and Atmospheric Administration (NOAA). Differences in the DDF statistics prepared for this study may be identified in precipitation depths associated with the various storm durations and return periods when compared to other DDF curves prepared for INEEL. The differences are the result of the specific seasonal periods used to develop the curves and judgment in best-fit curves for statistical representation of precipitation data.

In preparing the three different sets of DDF curves for this study, data were separated according to seasonal variations when summer, winter and winter frozen ground conditions exist. This separation of the data often results in lower precipitation depths and intensities used for modeling during the winter season as compared to summer and to the year as a whole. Winter storms typically have lower rainfall depth and intensity than other times of the year. Separation of these data from the entire period of record provides a more accurate determination of DDF statistics when evaluating specific seasonal storm events.

2.3.2 Snowmelt

Snowmelt was incorporated into hydrologic models for the INTEC flood study in order to evaluate winter storm events. Data for snow depth and water content were developed from the winter precipitation statistics, and previous rain on snow events observed throughout the region surrounding INEEL. Contributing factors for snowmelt were established from temperature and wind speed gage data according to the following:

- Maximum daily temperature is 46° F and average daily temperature is 42° F
- Wind speed of 20 miles per hour
- Constant snowmelt during the 24-hour storm period
- Little delay for snowmelt contribution to runoff

Using equations presented in the USCOE Snow Hydrology Manual (USCOE, 1998), with a mean temperature of 42° F and wind speed of 20 mph, snowmelt was calculated as 0.06 in/hr. This constant snowmelt was added to the design storm precipitation for use in hydrologic modeling of the winter rain on snow and frozen ground events. The 0.06 in/hr is added to the precipitation depth duration frequency statistics identified earlier, based on the time period (i.e., 12-hour event adds 0.72 inches to the precipitation depth). Snowmelt adds 1.44 inches of water to the rainfall event throughout the duration of the 25-year and 100-year, 24-hour winter events.

2.3.3 Frozen Ground and Concrete Impermeable Frost

Frozen ground and concrete impermeable frost increase runoff volume and associated peak flow during winter storms by limiting the infiltration capacity of the soil, and in the case of concrete impermeable frost, effectively increasing the amount of impervious surface within a watershed. Several climatological factors contribute to developing frozen ground and concrete impermeable frost including, but not limited to, the following:

- Wet fall and early winter season, sufficient to allow accumulation of water in the surface soil layers
- Continuous cold weather
- Little or no snow accumulation to insulate the ground

For the purposes of this study, it is necessary to distinguish between frozen ground and concrete impermeable frost in order to estimate the impervious surface area in the watershed. Frozen ground occurs annually during the winter season as cold temperatures freeze moisture

in surface and vadose zone soils. However, this condition does not preclude infiltration as cracks develop, porosity in the soil-ice structure still exists, and root structures provide additional pathways for water to enter the soil profile. To become a completely impervious frost layer, sufficient moisture must be present to saturate the soil and sustained freezing temperatures must develop frost and ice to eliminate all infiltration capability in the soil profile. This condition is described as concrete impermeable frost.

Previous investigations have been conducted to evaluate the presence and severity of concrete impermeable frost during winter rain on snow and frozen ground events (CH2MHill 1989). During this study, known gage data were used to calibrate hydrologic models of the watershed contributing to Silver Bow Creek during winter storm events in southwest Montana. It was determined through this study that although concrete impermeable frost existed in the watershed, it did not cover the entire surface area, was found to exist only in very narrow elevation ranges throughout the watershed, and that water infiltration occurs in areas where frozen ground (not impermeable frost) exists.

Results of the Silver Bow Creek investigation were used to develop and assign probability to the recurrence of concrete impermeable frost. The probability of concrete impermeable frost is based on rainfall, temperatures, snow and other climatological factors that allow concrete impermeable frost to develop. Statistical analyses of climatological data from the INEEL were used to evaluate the probability of concrete impermeable frost development as a part of this study. The recurrence interval of conditions required to develop impermeable frost is approximately every 5 to 10 years at the INEEL and INTEC based on available gage data from the site and surrounding area.

Additionally, an estimate of the percentage of the ground surface representing concrete impermeable frost was developed from site-specific conditions at INEEL and results of the Silver Bow Creek investigation. Vegetation, exposed surface soils, soil porosity and other factors contribute to the development of concrete impermeable frost. For the watershed surrounding the INTEC, vegetative cover was estimated to be 50% and exposed soils have fairly good water transmission properties (B group). Concrete impermeable frost was estimated to represent 33% of the watershed area during this study, based on the following assumptions:

1. Exposed surface soils represent 50% of the natural watershed area. 67% of exposed surface soils are subject to developing concrete impermeable frost. Total concrete impermeable frost in the natural watershed is then 33%.
2. Concrete impermeable frost will not develop in the remaining 50% of the watershed area due to the presence of vegetative cover and root structure.

Review of previous studies conducted at the INEEL further indicate that although concrete impermeable frost will exist in portions of the watershed, it is overly conservative to assume that the presence of frozen ground eliminates all infiltration. A report prepared in 1994 (Taylor et. al, 1994) states “..the assumption of frozen ground presumes zero infiltration of the surface...zero infiltration appears overly conservative...assumption of zero infiltration was used in order to obtain demonstrably conservative results.” This previous study further supports the assumption that impermeable concrete frost does not exist over the entire watershed area.

Natural watershed areas can have concrete impermeable frost which occupies less than 100% of the natural watershed during winter.

There are no universally accepted methods for establishing recurrence interval or aerial extent of concrete impermeable frost during winter seasons. Generally accepted methods include estimations of impervious surfaces using hydrologic models of watersheds with available stream gage data. In the absence of site-specific data, it is necessary to estimate concrete impermeable frost and resulting impervious surface area from climatological data, known watershed properties, experience with similar sites, and comparison to other studies. Representing 33% of the natural watershed area as concrete impermeable frost provides a reasonable estimate of expected impervious ground conditions during winter storm events for the INEEL based on the hydrologic conditions of the watershed, available surface area for impermeable frost to develop, and experience with similar studies.

2.4 Summer and Winter Design Storm Parameters

Summer and winter design storm parameters were developed for hydrologic modeling of the watershed contributing to the INTEC and surrounding areas. The storm parameters were developed from the statistical analyses of data collected primarily from the INEEL and Idaho Falls gages, with additional supporting information as described in previous sections. The following design storm parameters were used in hydrologic modeling of the various return period and seasonal conditions.

- 25-year and 100-year Summer Thunderstorms (Cloudburst)
 - 25-year and 100-year, 24-hour storm events
 - 1.70 and 2.10 inches of precipitation, respectively, from statistical analyses and data presented in Table 2-1.
 - Embedded peak 5-, 15- and 30-minute, 1-, 2-, 3-, 6-, 12- and 24-hour rainfall intensities.
- 25-year, 24-hour Winter Precipitation (Rain on Snow) with frozen ground
 - 5-year, 24-hour storm event
 - 5-year frozen ground conditions (33% impermeable frost in natural watershed areas)
 - 0.553 inches of direct precipitation
 - 0.06 inches/hour constant snowmelt (1.44 inches total depth for 24 hours)
 - Embedded peak 5-, 15-, and 30-minute, 1-, 2-, 3-, 6-, 12- and 24-hour rainfall intensities.
- 100-year, 24-hour Winter Precipitation (Rain on Snow) with Frozen Ground
 - 20-year, 24-hour storm event
 - 5-year frozen ground conditions
 - 0.72 inches of direct precipitation

- 0.06 inches/hour constant snowmelt (1.44 inches total depth for 24 hours)
- Embedded peak 5-, 15- and 30-minute, 1-, 2-, 3-, 6-, 12- and 24-hour rainfall intensities.

The design storm parameters for the various storms used in this hydrologic study are statistically equivalent to, or greater than, the return frequencies for the 25-year and 100-year events. The return interval for a particular storm event has a probability equal to the inverse of the return interval as shown in the following equation:

$$P = \frac{1}{\text{return period}}$$

Therefore, the probabilities of the 25-year and 100-year events are 0.04 and 0.01, respectively. Additionally, the probability of different events can be multiplied to determine combined probabilities representing statistically equivalent, larger return period events. Using the combined probability approach, a 20-year rainfall was used in conjunction with the 5-year frozen ground (impermeable frost) condition to generate a storm event that is statistically equivalent to the 100-year event according to the following:

$$P_{100} = P_{20} * P_5 = \frac{1}{20} * \frac{1}{5} = \frac{1}{100} = 0.01$$

The combined probability of the 20-year rainfall and 5-year frozen ground represents a 100-year return period probability. For the purposes of this study, the volume of snowmelt was added to the winter design storm events to provide additional runoff. Adding the snowmelt to the design storms increases the return period of the storms, as the presence of snow during the event has additional statistical probability, which should be multiplied in the combined probabilities. However, the probability of snowmelt runoff during the design storms was not included in the return period calculations. This was done to account for possible variations in truly frozen ground, design storm precipitation depths and other hydrologic parameters used to represent the watershed and sub areas. Neglecting the probability of snowmelt in the combined probabilities of the design storm events provides a conservative approach to estimating the peak flood flow anticipated for the INTEC facility and surrounding watershed area.

The probabilities for rainfall and frozen ground occurrence are sufficiently independent to allow their combination in a joint probability distribution. The design storm precipitation is developed from gage data from several different sites around the INTEC and INEEL for periods of record exceeding 50 years in many cases. Further, the probability of the presence of impermeable concrete frost accounts for several environmental factors including precipitation, temperature, snow, wind, and freezing temperature durations and was also developed from gage data for the INEEL and surrounding area. The probabilities for precipitation and the presence of concrete impermeable frost are prepared independently, allowing the use of the combined probability approach.

3. FIELD INVESTIGATION AND DATA COLLECTION

A field investigation of the watershed area in and surrounding the INTEC facility was conducted to verify watershed and sub area boundaries, identify and inventory hydraulic control structures, measure channel cross-sections and gather other hydrologic and hydraulic information for the site. The field investigation was conducted during late April and early May 2003. Details of the specific tasks and data collected during the investigation are included in the following sections.

3.1 Watershed and Sub Area Boundary Verification

A preliminary watershed boundary and sub area map was developed prior to conducting the field investigation. Major and minor drainage boundaries were identified on topographic mapping developed for the site in 2002 and included both natural and manmade features. Natural features included ridges, depressions, drainage swales and others. Manmade features included roads, railroads, berms, channels, pits and others. This preliminary watershed and sub area map was further refined as a result of the field investigation.

Boundaries identified along roads and railroads were reviewed in the field to identify the presence of culverts, hydraulic structures, or other hydrologic features that may serve to alter drainage area boundaries. Where identified, culverts were added to the topographic mapping and sub area boundaries adjusted accordingly. Additionally, drainage ditches and berms were inspected for integrity and function and utilized to identify watershed and sub area boundaries as appropriate. Watershed and sub area boundaries prepared for this study from topographic mapping and investigation are shown on Sheet 1 included with this report.

3.2 Hydraulic Structure Inventory

Previous hydraulic structure investigations and surveys were utilized to generate an inventory for the INTEC facility and surrounding area, including Central Facilities Area, the Guard Training Facilities, and along US Highway 20. A summary of culverts located throughout the watershed area (Kingsford, 2002) was used as a starting point for the inventory and field investigation.

As part of this study, a detailed investigation of the hydraulic structures within the INTEC perimeter was conducted to further the existing database. Hydraulic structures measured in the field included catch basins, pipes, culverts, lift stations and surface drainage channels. Storm water flow paths and connectivity were also confirmed during the investigation for use in subsequent hydraulic modeling.

3.3 Field Surveying and Measurements

Several areas in and around the INTEC facility were surveyed to collect data for use in modeling storm water drainage channels, flow in the Big Lost River and to confirm topographic drainage divides identified during the preliminary watershed and sub area delineation. Surveying was conducted by Mr. Ken Beard of INEEL and CCH, Inc. All surveying was conducted using horizontal and vertical control points established by Mr. Beard, using NGVD29 vertical and NAD27 horizontal Idaho State Plane datums.

Drainage channel geometry was measured using tapes and surveying rods in remote, localized areas to determine properties for use in hydraulic modeling and channel capacity estimates where surface flooding has no potential to impact buildings or areas of concern. Field measured sections were collected for constructed irrigation and diversion channels around the site.

4. HYDROLOGIC MODELING

The HEC-1 computer program was utilized for this hydrologic analysis as it provides flexibility in modeling methods and allows detailed input of watershed parameters, stage-storage-routing information, design storm precipitation, snowmelt and other hydrologic modeling parameters impacting storm water runoff. Specifically, the hydrologic modeling for this study was conducted using ProHEC1 Plus, an enhanced version of the Hydrologic Engineering Center's HEC-1 program (Dodson and Associates, ProHEC1 Plus, 1995). This program generates rainfall/runoff hydrographs for watersheds and sub basins based on several hydrologic parameters including, but not limited to, the following:

- Watershed and sub basin area
- Soil type and vegetative cover
- Impervious surfaces
- Surface features such as exposed bedrock and fractures
- Stream channel flow patterns
- Natural and constructed reservoirs or storm water retention areas
- Storm water runoff controls
- Unique hydrologic features

Details of the hydrologic modeling parameters and processes are included in the following sections.

4.1 Hydrologic Characteristics and Modeling Parameters

Hydrologic characteristics of the watershed are discussed in the following sections and, where applicable, modeling parameters based on conditions observed in the field are discussed.

4.1.1 Watershed and Sub Area Delineation

Topographic mapping and field inspection of hydrologic and hydraulic features were used to delineate the contributing watershed and sub basins of the INTEC and surrounding area. Topographic mapping provided by INEEL (Aerial Services, Inc., 2002) and portions of a USGS quadrangle map were used to identify the outer boundary of the watershed. Sub areas were delineated within the outer watershed boundary based on several factors including the following:

- Major and minor surface water runoff drainage patterns and flow lengths
- Location of culverts, storm water runoff controls, local reservoir areas (storage)
- Key features and junctions in the diversion channels
- General hydrologic regime and field conditions

Aerial Services, Inc. prepared topographic mapping for the INTEC watershed and surrounding area in July 2002. A map of the entire watershed area evaluated during the course of this study is shown on Sheet 1 included with this report.

The watershed area west and south of the immediate vicinity of the INTEC facility was evaluated as a part of this study based on regional topography. During the field investigation, several drainage area divides, both natural and man-made were identified which influence the drainage area characteristics. More detailed discussion of the drainage areas delineated for subsequent hydrologic modeling is included in the following three sections.

The watershed and sub area delineations were completed using 2-foot topographic mapping, field surveying data and a thorough review of the digital elevation models developed during the aerial mapping of the site. The watershed sub areas were carefully delineated to ensure that subsequent hydrologic modeling results would be representative of flow conditions at the site.

4.1.1.1 Areas Contributing Directly to the INTEC

The INTEC has a perimeter road surrounding the facility area, outside of the secure fenced area. This road serves as a major drainage divide around the facility, with only one culvert on the southwest corner of the facility area that allows cross-drainage into the facility. Additionally, the INTEC facility is protected from unauthorized entry by a perimeter ditch constructed to prevent vehicle access to the site. This perimeter ditch functions as a drainage channel for the facility and areas within the perimeter of the INTEC. Due to its proximity to the facility, the perimeter ditch was surveyed and incorporated into hydrologic and hydraulic models to verify its function as a drainage ditch for the facility. The areas contributing directly to the INTEC are identified as INTEC-2 (INTEC perimeter) and INTEC-5 (via culvert flow) on the watershed and sub area map (Sheet 1). The watershed area contributing storm water runoff to the INTEC storm water drainage system is 0.40 square miles.

4.1.1.2 Areas in the Vicinity of the INTEC Perimeter

Several areas around the INTEC facility were included in the watershed mapping and delineation for the site in order to identify any storm water run-on and flooding potential. Additionally, areas in the immediate vicinity of the facility were included in order to evaluate the flow away from the INTEC drainage areas. The areas identified in the vicinity of the facility include sub areas INTEC 1, 3, 4, 6 and 7. The watershed area in the immediate vicinity of the facility included in these sub areas is 1.20 square miles.

4.1.1.3 Area West of Lincoln Boulevard, Central Facilities and Non-Contributing Areas

The INTEC is located at the northeastern edge of a large, fan-shaped regional watershed. The location of hydraulic structures, the lack of culverts or other drainage controls, constructed roads, pits and subtle natural topography breaks serve to limit the watershed contributing directly to the INTEC facility.

Areas west of Lincoln Boulevard were included in the hydrologic modeling for this study in order to evaluate any flooding potential due to flow over Lincoln Boulevard and in the

Big Lost River near the INTEC facility. There are no culverts under Lincoln Boulevard between Central Facilities and the Big Lost River and therefore it serves as a major divide between the INTEC and the watershed extending to the west of the road. Several cross-sections were surveyed along Lincoln Boulevard to confirm the capacity of the drainage ditch and road to convey storm water runoff from west of the road north to the Big Lost River. The watershed area contributing to the west side of Lincoln Boulevard is 10.30 square miles.

The Central Facilities Area was included in this investigation to evaluate potential contributing storm water flow towards the INTEC. There are several constructed pits located to the north of the Central Facilities Area which collect storm water runoff from the CFA sub areas. These pits, in conjunction with a subtle natural drainage divide along the northern end of sub area CFA-1 effectively divert and contain all storm water drainage from the CFA sub areas, eliminating storm water run-on and flooding potential to the INTEC. These areas were included in the hydrologic investigation conducted for INTEC in order to confirm the absence of any contributing flow from CFA. The sub areas included in the CFA are identified as CFA-1, 2, and 3 on Sheet 1 of this report. The watershed area contributing to the constructed pits north of CFA is 1.18 square miles.

Non-contributing areas identified on Sheet 1 include those areas east of the railroad grade, southeast of CFA, and north of the Big Lost River. These areas do not contribute any flow to the INTEC due to either their location hydrologically downgradient of the site, or the presence of drainage barriers, including the railroad grade and the Big Lost River. These areas were not included in the hydrologic investigation and models prepared for this study.

A total watershed area of 13.15 mi² was included in the hydrologic analysis of the site to evaluate any potential effects of storm water runoff and flooding potential outside of the INTEC facility. The watershed area contributing storm water run-on and runoff directly to the INTEC storm water drainage system is limited to 0.40 mi² due to the presence of several storm water diversions and controls.

4.1.2 Soil Type and Vegetation

Native soils in the area of the INTEC are primarily sandy silt loam, with sand fractions ranging in size from very fine to coarse. Soil depths range from very shallow to very deep and are intermixed with basalt flows. Regional data indicates that soils are primarily loess, and are characterized as Hydrologic Soil Group B. This soil group allows moderate infiltration and consists of silts, sands and to a lesser extent, clays.

The vegetation in the watershed surrounding the INTEC is a sage-grass community consisting of sagebrush and primarily wheat grasses. Cover was estimated at approximately 50% during the field investigation conducted at the site. Vegetation within the INTEC facility perimeter, while limited in area, consists of residential lawn grasses (fescue and blue grasses) where present.

The Soil Conservation Service (SCS) National Engineering Handbook provides representative curve numbers (CN) for sage-grass complexes in the Western United States (SCS, 1972). The curve number is used in hydrologic modeling to represent the soil and vegetation conditions within a watershed and accounts for precipitation losses and excesses. According to

the SCS reference, curve numbers may range from 28 to 96 for sage-grass complexes, depending on soil group and vegetative cover. The SCS method categorizes soils into one of four groups, known as Hydrologic Soil Groups A, B, C, or D, based upon their classification (silt, clay, sand, loam, etc.). Low curve numbers indicate Group A and B soils with high percentage of vegetative cover and high numbers indicate Group C and D soils with little or no vegetative cover.

Antecedent moisture conditions (AMC) are used to represent soil and moisture conditions in a watershed prior to the rainfall-runoff event being modeled. AMC II is the standard condition for hydrologic modeling according to the SCS methodology and is the basis for curve numbers presented in the National Engineering Handbook and other references. AMC II curve numbers are adjusted for varying conditions in a watershed, depending on anticipated soil moisture conditions prior to a modeled event. AMC I represents dry conditions typical of summer thunderstorms, with no precipitation prior to the model storm. AMC III represents wet soil conditions during winter and spring seasons, when it is likely that some moisture has been retained in the soils from previous storms and/or snowmelt. Curve numbers taken from the SCS handbook are shown in Table 4-1.

The curve numbers were selected from tables shown in the SCS National Engineering Handbook, Section 4, Hydrology, 1972, page 9.11. Curve numbers were selected to represent natural conditions identified in the field, with further support from SCS documentation and experience with similar sites. Curve numbers were also selected accordingly to represent antecedent moisture conditions anticipated in each storm. AMC III curve numbers were used to represent saturated soils during winter storms. Normal soils during summer events were represented by AMC II, although dry (AMC I) conditions are more likely in the summer.

Curve numbers for sage-grass complexes, Hydrologic Soil Group B and normal AMC (II) range from 28 to 74 for 100% to 0% cover, respectively. These values are shown in Table 4-1.

Based on the vegetative covers with a Hydrologic Soil Group B, a curve number of 52 was selected to represent natural watershed conditions. This CN was used for summer thunderstorm events, although it is more likely that AMC I conditions will be present during summer (dry, which would result in a lower CN). The CN of 52 was adjusted to AMC III conditions (saturated soil condition) for the winter storm events. A CN of 71 was selected to represent the unfrozen portion of soils in the natural watershed during the winter rain on snow and frozen ground events.

Curve numbers were adjusted for areas inside the INTEC facility perimeter based on an assumption that soils in this area are more compacted than natural conditions (allowing lower infiltration rates) due to construction activities, heavy traffic and constructed cover soil areas. A curve number of 80 was selected for modeling the watershed sub areas in the INTEC facility.

Table 4-1. SCS Curve Numbers¹ for sage-grass complexes.

Antecedent Moisture Condition II (Standard)			
Vegetative Cover (%)	Hydrologic Soil Group B	Hydrologic Soil Group C	Hydrologic Soil Group D
0	74	87	96
20	65	78	88
40	56	68	79
60	47	59	70
80	37	49	61
100	28	40	52
Antecedent Moisture Condition I (Summer Condition)			
0	55	73	89
20	45	60	75
40	36	48	62
60	28	39	51
80	20	30	41
100	14	22	32
Antecedent Moisture Condition III (Winter Condition)			
0	88	95	99
20	82	90	95
40	75	84	91
60	67	77	85
80	57	69	78
100	48	60	71
Impermeable Frost	99	99	99

¹Section 4, Hydrology, SCS National Engineering Handbook, 1972.

4.1.3 Impervious Surfaces

There are limited areas of impervious surfaces within the natural watershed around the INTEC. Existing natural impervious surfaces include exposed bedrock outcrops, which, where present, were estimated to cover 5 percent of the surface in sub basins. Man-made impervious surfaces include roads, buildings, parking areas and other impervious surfaces. The impervious surface area created by man-made features was estimated from topographic

mapping and aerial photography of the site. A curve number of 99 was used for all impervious surface portions of the watershed, including areas within INTEC, during all storm events.

A curve number of 99 was also used to represent concrete impermeable ground for winter rain on snow with frozen ground events.

4.1.4 Natural and Man-Made Surface and Diversion Channels

Topography of the watershed at, and immediately around, the INTEC is generally low-lying and flat, with few defined natural drainage channels. In general, incised channels do not form within the natural watershed areas around INTEC due to the low-lying topography, low slope and lack of significant storm water runoff during times when soils are easily eroded (i.e., summer). Where necessary for modeling purposes, natural drainage channels were modeled as very wide-bottom trapezoid-shape channels with low side slopes.

Several man-made diversion and irrigation channels have been constructed in the watershed around INTEC and have been used for storm water runoff and historic irrigation. These channels are generally intact and function to control storm water runoff in the watershed area contributing to the west side of Lincoln Boulevard. The diversion channels were measured in the field in order to provide input data for subsequent hydraulic modeling.

4.1.5 Storm Water Retention Areas

Several storm water retention areas exist within the watershed area contributing to the INTEC, the West Side of Lincoln Boulevard, and CFA-1. The storm water retention areas used for stage-storage-routing in this hydrologic study are subject to flooding during the 25-year and 100-year storm events. Stage-storage-discharge relationships were developed for all storage areas utilized in hydrologic modeling for this study. Stage and storage volume relationships were generated from topographic mapping of the study area and discharge evaluated utilizing open channel flow equations for surface channels and culverts, as appropriate. Water surface elevations identified in the hydrologic models were used to identify inundated areas throughout the watershed. The inundated areas are considered a part of the storm water runoff floodplain delineated on the maps prepared for this study.

4.1.6 Big Lost River

The Big Lost River flows around the northwestern part of the INTEC facility and is bermed along the INTEC side to prevent floodwater from impacting the facility. The Big Lost River has several flow control measures along its length including a water spreading/control area upgradient of the site. Water generated in the watershed above the spreading areas can be effectively controlled by the spreading areas and the flood control gates associated with them.

A detailed analysis of flow in the Big Lost River generated from upgradient watersheds was not included in this study. Other on-going studies are in progress to evaluate flow in the Big Lost River and are not included in the scope of this project. However, in order to evaluate any potential flooding that may result from storm water runoff in the Big Lost River, a portion of the watershed area surrounding the INTEC was assumed to be contributing runoff to the river at the time of the modeled events. Approximately 17 square miles of watershed area were

estimated from topographic mapping as contributing area during the modeled storm events. This area includes the watershed extending upgradient from the INTEC facility to the large spreading areas located on the Big Lost River near the RWMC facility (southwest of INTEC).

Based on results of current and previous studies, a base flow (30 cfs/mi²) for the estimated contributing area was added to hydraulic models of the Big Lost River and used to identify flooding potential (in addition to runoff from the watershed delineated on Sheet-1 for INTEC). The base flow was combined in the Big Lost River with flows contributing to the west side of Lincoln Boulevard in order to identify any flooding potential resulting from insufficient channel or bridge/culvert capacity near the INTEC. Further discussion of the hydraulic modeling of the Big Lost River is included in Section 5.1 of this report.

4.2 Hydrologic Modeling and Analysis

The rainfall-runoff modeling was conducted using ProHEC-1 Plus (Dodson and Associates, 1995), with input parameters based on the design storm statistics and hydrologic conditions of the watershed. The SCS method for storm water loss and excess was used in the hydrologic models to generate storm water runoff hydrographs for selected locations in the watershed area. Specific parameters incorporated into the models created as a part of this study are discussed in the following sections.

4.2.1 SCS Curve Numbers and Precipitation Losses

SCS curve numbers were selected to represent the watershed condition based on soil type, vegetative cover, impervious surfaces and the presence of impermeable frost. For summer conditions, curve numbers were selected from tables presented in the SCS Engineering Handbook as previously described in this report.

Additionally, to represent impermeable conditions during the winter storm events, the sub areas were separated into two portions, designated as A and B in the model. Two-thirds (67%) of the basin was considered as unfrozen ground with AMC III soil conditions. One-third (33%) of the basin was represented as concrete impermeable frost with a curve number of 99 for impervious surface. Hydrographs for the two separate portions of each sub area during winter events were combined to determine peak flow from the whole sub area, prior to combining flows with other sub areas. SCS curve numbers selected for modeling are shown in Table 4-2.

Table 4-2. SCS Curve Numbers used in hydrologic modeling

Sub Area Description	SCS Curve Number Summer Events	SCS Curve Number Winter Events
Natural conditions	52	71
INTEC-2, facility area	80 ⁽¹⁾	94 ⁽¹⁾
Central Facilities Area	62 ⁽¹⁾	80 ⁽¹⁾
Impervious surfaces including frozen ground	99	99

(1) - SCS curve number increased assuming soils have been compacted over time by traffic and construction activities.

The SCS Unit Discharge method was used for modeling rainfall-runoff at the site. The Unit Discharge method requires calculation of a time of concentration and lag time for each watershed sub area, accounts for precipitation losses and excess within the curve number, allows channel routing for hydrographs, includes stage, storage and discharge information and other hydrologic parameters to generate storm water runoff models.

The SCS method accounts for precipitation losses from infiltration and evaporation and precipitation excess contributing to runoff within the curve number. Other methods including Kinematic wave, Muskingum, Muskingum-Cunge account for the losses using initial and constant loss parameters and were tested with variations of the HEC-1 models generated for this study. After evaluation of different methods for determining peak runoff, the SCS method was determined to be the most reasonable for the watershed, rainfall, snowmelt and frozen ground conditions. The Kinematic Wave, Muskingum, and Muskingum-Cunge methods utilize overland flow parameters, shallow concentrated flow conditions and channel flow parameters to determine time of concentration and peak flow within a sub area of the watershed. Input of the sub area parameters into the HEC-1 program generated widely varied results within the different sub areas due to long overland flow lengths anticipated at this site, variations in frozen ground and natural soil conditions, and a variety of other factors affecting the model results.

Precipitation losses are accounted for in the hydrologic models using two different parameters, initial losses and continuous losses. Initial losses are included in the hydrologic models as a depth of precipitation that is abstracted initially before infiltration and runoff begin. The initial loss accounts for depression storage areas on the surface that collect a small amount of precipitation and are generally included in all hydrologic models. The SCS National Engineering Handbook recommends initial losses of approximately 0.5 to 1.5 inches for the types of soils and conditions present in the INTEC and surrounding watersheds. Initial losses were set to 0.6 inches for summer events and 0.1 inches for winter storm events, assuming that the soil will not absorb precipitation during the winter and that depression storage is partially filled before the design storm occurs.

4.2.2 Time of Concentration

The time of concentration is used to assist in the definition of runoff characteristics within the individual sub areas. The time of concentration for a watershed is defined as the travel time of water from the hydraulically most distant point of the watershed to the point of interest (generally the most downstream point). The time of concentration for each sub area was estimated by measuring three components of storm water runoff flow paths including overland flow, shallow concentrated flow, and channel flow, and determining appropriate roughness coefficients and other parameters that influence water flow. Topographic maps and site surveying were used to determine flow distances and slopes, and roughness coefficients were estimated using the aerial photography and observed field conditions. Properties of the individual sub areas used in determining the time of concentrations are shown in Table 4-3. A summary of the travel time associated with the three flow conditions (overland, shallow concentrated, channel flow) and time of concentration for each basin is presented in Table 4-4. The equations used in evaluating total time of concentration are standard equations for the three different flow components and are shown below.

$$t_{overland} = \frac{0.007(nL)^{0.8}}{\sqrt{P_2} S^{0.4}}$$

$$t_{shallow} = \frac{L}{V}, \text{ where } V = 16.1345\sqrt{S}$$

$$t_{channel} = \frac{L}{V}, \text{ where } V = \frac{CR^{0.667} S^{0.5}}{n}$$

Where: n = Manning's roughness coefficient, unitless

L = length of flow, ft

P_2 = 2-year, 24-hour precipitation depth, in

S = slope, ft/ft

R = hydraulic radius, ft

V = velocity, ft/s

C = 1.49 (constant)

These equations can be found in the ProHEC-1 Program Documentation (Dodson and Associates, 1995) and several other hydrologic modeling references. An example of the time of concentration calculations prepared for the watershed sub areas is shown for INTEC-1 in the following equations (parameters taken from Table 4-3).

INTEC-1: Overland Flow: $L = 300$ ft, $n = 0.175$, $P_2 = 0.873$ inches (summer), $S = 0.002$ ft/ft

$$t_{overland} = \frac{0.007 * (0.175 * 300)^{0.8}}{\sqrt{0.873} * 0.002^{0.4}} = 2.14 \text{ min}$$

INTEC-1: Shallow Concentrated Flow: L = 1375, S = 0.0036

$$t_{shallow} = \frac{1375}{16.1345\sqrt{0.0036}} = 1420.35 \text{ sec} = 23.67 \text{ min}$$

INTEC-1: Channel Flow: L = 5450 ft, R = 0.349, S = 0.0018, n = 0.05

$$t_{channel} = \frac{5450}{\frac{1.49 * 0.349^{0.667} * 0.0018^{0.5}}{0.05}} = 8,696.18 \text{ sec} = 144.94 \text{ min}$$

The total time of concentration is the sum of the three component times for each basin (for some basins, with more defined channels contributing to the main channel, two channel flow sections may be used). The total time of concentration for INTEC-1 is shown below.

$$t_c = t_{overland} + t_{shallow} + t_{channel} = 2.14 \text{ min} + 23.67 \text{ min} + 144.94 \text{ min} = 170.75 \text{ min}$$

Table 4-3. Sub area flow parameters used in determining time of concentration (t_c) and lag times.

Kinematic Wave/Muskingum Basin Parameters																	
Collector Channel 1 - Contributor 1				Collector Channel 1 - Contributor 2				Collector Channel 1				Main Channel					
Sub Area Number	Area (sq mi)	Length (ft)	Slope (ft/ft)	Roughness (manning's)	% of Sub Area	Length (ft)	Slope (ft/ft)	Roughness (manning's)	% of Sub Area	Sub Area Number	Length (ft)	Slope (ft/ft)	Roughness (manning's)	Length (ft)	Slope (ft/ft)	Roughness (manning's)	Shape
CFA-1	0.5653	300	0.001	0.175	100					0	CFA-1	1375	0.0036	TRAP	7625	0.0022	TRAP
CFA-2	0.5772	300	0.001	0.175	70	200	0.005	0.175	30	CFA-2	800	0.0075	TRAP	8875	0.0041	TRAP	
CFA-3	0.0324	150	0.005	0.175	100				0	CFA-3	750	0.0110	TRAP	1375	0.0087	TRAP	
INTEC-1	0.3015	300	0.002	0.175	40	200	0.001	0.175	60	INTEC-1	1375	0.0036	TRAP	5450	0.0018	TRAP	
INTEC-2	0.3495	100	0.002	0.1	50	100	0.002	0.1	50	INTEC-2	500	0.0040	TRAP	3000	0.0020	TRAP	
INTEC-3	0.0671	300	0.002	0.175	60	100	0.005	0.08	40	INTEC-3	1000	0.0030	TRAP	1550	0.0030	TRAP	
INTEC-4	0.0651	200	0.002	0.08	50	75	0.001	0.08	50	INTEC-4	600	0.0167	TRAP	800	0.00196	TRAP	
INTEC-5	0.0434	200	0.0043	0.08	65	130	0.005	0.08	35	INTEC-5	800	0.0260	TRAP	590	0.00240	TRAP	
INTEC-6	0.0859	Not included in analysis - sink area															
INTEC-7	0.7663	200	0.001	0.175	50	75	0.001	0.175	50	INTEC-7	400	0.0010	TRAP	7250	0.0022	TRAP	
LB-1	0.2092	50	0.001	0.175	50	100	0.001	0.175	50	LB-1	400	0.0015	TRAP	7200	0.0029	TRAP	
LB-2	0.5135	125	0.002	0.175	50	80	0.001	0.175	50	LB-2	500	0.0015	TRAP	10375	0.0029	TRAP	
LB-3	0.2953	95	0.001	0.175	50	150	0.001	0.175	50	LB-3	560	0.0035	TRAP	9300	0.0030	TRAP	
LB-4	0.1721	50	0.001	0.175	50	150	0.001	0.175	50	LB-4	310	0.0015	TRAP	5375	0.0029	TRAP	
LB-5	0.1494	50	0.001	0.175	50	150	0.001	0.175	50	LB-5	200	0.0035	TRAP	3875	0.0033	TRAP	
LB-6	0.4099	50	0.001	0.175	50	150	0.001	0.175	50	LB-6	250	0.0016	TRAP	9250	0.0031	TRAP	
LB-7	0.4351	50	0.001	0.175	50	125	0.001	0.175	50	LB-7	250	0.0025	TRAP	6000	0.0030	TRAP	
LB-8	0.7509	75	0.001	0.175	50	200	0.001	0.175	50	LB-8	4000	0.0025	TRAP	3250	0.0028	TRAP	
LB-9	0.4458	200	0.045	0.175	60	250	0.025	0.175	40	LB-9	800	0.0085	TRAP	8000	0.0050	TRAP	
LB-10	0.1559	300	0.001	0.175	50	200	0.001	0.175	50	LB-10	400	0.0030	TRAP	3350	0.0020	TRAP	
LB-11	0.2317	75	0.001	0.175	50	185	0.001	0.175	50	LB-11	750	0.0026	TRAP	7000	0.0023	TRAP	
LB-12	0.3234	75	0.001	0.175	50	185	0.001	0.175	50	LB-12	430	0.0030	TRAP	6500	0.0028	TRAP	
LB-13	0.4537	75	0.001	0.175	50	175	0.001	0.175	50	LB-13	300	0.0030	TRAP	8650	0.0027	TRAP	
LB-14	0.4054	100	0.001	0.175	50	200	0.001	0.175	50	LB-14	250	0.0020	TRAP	8500	0.0030	TRAP	
LB-15	0.1885	150	0.001	0.175	50	300	0.001	0.175	50	LB-15	250	0.0020	TRAP	7500	0.0024	TRAP	
LB-16	0.4806	75	0.001	0.175	50	150	0.001	0.175	50	LB-16	400	0.0025	TRAP	10000	0.0034	TRAP	
LB-17	0.4356	75	0.001	0.175	50	150	0.001	0.175	50	LB-17	400	0.0025	TRAP	9500	0.0032	TRAP	
LB-18	0.7317	150	0.001	0.175	70	200	0.005	0.175	30	LB-18	500	0.0040	TRAP	9000	0.0028	TRAP	
LB-19	0.8361	75	0.001	0.175	50	150	0.001	0.175	50	LB-19	1200	0.0065	TRAP	12250	0.0057	TRAP	
LB-20	2.0322	250	0.04	0.175	80	300	0.006	0.175	20	LB-20	1800	0.0189	TRAP	13250	0.0053	TRAP	
LB-21	0.0193	200	0.01	0.175	100	200	0.01	0.175	0	LB-21	375	0.0267	TRAP	1225	0.0114	TRAP	
LB-22	0.0988	300	0.013	0.175	80	200	0.02	0.175	20	LB-22	600	0.0167	TRAP	2250	0.0080	TRAP	
LB-23	0.0197	100	0.01	0.175	100	100	0.01	0.175	0	LB-23	375	0.0133	TRAP	750	0.0146	TRAP	
LB-24	0.3457	125	0.001	0.175	70	150	0.0267	0.175	30	LB-24	1375	0.0065	TRAP	5125	0.0047	TRAP	
LB-25	0.0288	100	0.001	0.08	85	200	0.001	0.175	15	LB-25	450	0.0044	TRAP	3060	0.0013	TRAP	
LB-26	0.1282	100	0.001	0.08	85	200	0.001	0.175	15	LB-26	450	0.0089	TRAP	11000	0.00127	TRAP	

Table 4-4. Time of concentration (t_c) for sub areas.

Sub Area Number	Overland	Shallow		tc (min)	lag time (hours)
	Flow (min)	Concentrated Flow (min)	Channel Flow (min)		
<i>INTEC sub areas</i>					
INTEC-1	2.14	23.67	144.94	170.75	1.71
INTEC-2	0.79	8.17	52.98	61.93	0.62
INTEC-3	2.14	18.86	38.32	59.32	0.59
INTEC-4	0.83	15.17	24.47	40.46	0.40
INTEC-5	0.61	16.21	13.59	30.40	0.30
INTEC-6	Not included in analysis - sink area				
INTEC-7	2.04	13.07	261.61	276.71	2.77
<i>Lincoln Boulevard contributing sub areas</i>					
LB-1	1.17	10.67	226.28	238.13	2.38
LB-2	1.06	13.34	326.07	340.47	3.40
LB-3	1.62	9.78	287.37	298.77	2.99
LB-4	1.62	8.27	168.93	178.82	1.79
LB-5	1.62	3.49	114.17	119.28	1.19
LB-6	1.62	6.46	281.18	289.26	2.89
LB-7	1.40	5.16	185.40	191.97	1.92
LB-8	2.04	82.64	110.01	194.69	1.95
LB-9	0.67	8.96	191.48	201.12	2.01
LB-10	2.82	7.54	168.27	178.64	1.79
LB-11	1.92	15.19	247.03	264.15	2.64
LB-12	1.92	8.11	207.90	217.93	2.18
LB-13	1.83	5.66	288.26	295.75	2.96
LB-14	2.04	5.77	262.65	270.47	2.70
LB-15	2.82	5.77	259.11	267.70	2.68
LB-16	1.62	8.26	290.26	300.14	3.00
LB-17	1.62	8.26	284.23	294.12	2.94
LB-18	1.62	8.17	287.86	297.65	2.98
LB-19	1.62	15.38	228.84	245.84	2.46
LB-20	1.38	13.52	256.70	271.60	2.72
LB-21	0.81	2.37	16.18	19.36	0.19
LB-22	1.01	4.80	35.48	41.29	0.41
LB-23	0.47	3.36	8.75	12.58	0.13
LB-24	1.40	17.62	105.44	124.45	1.24
LB-25	2.04	7.01	95.76	104.81	1.05
LB-26	2.04	4.93	348.27	355.24	3.55
<i>Central Facilities contributing areas</i>					
CFA-1	2.82	23.67	183.43	209.92	2.10
CFA-2	2.82	9.54	156.39	168.75	1.69
CFA-3	0.85	7.39	16.63	24.87	0.25

4.2.3 HEC-1 Model Input and Output

Hydrologic modeling was completed using the HEC-1 computer program with watershed and sub area properties incorporated into the models based on parameters discussed in the previous sections. The models were used to generate peak flows at key locations contributing to the INTEC facility drainage systems, Lincoln Boulevard, the Big Lost River, and the constructed pits in the Central Facilities Area to evaluate the 25-year and 100-year storm water runoff flood profiles.

HEC-1 input is completed using “cards” to represent different sub area parameters, rainfall statistics, reservoir and channel routing parameters, sub area connectivity and hydrograph combinations, and a number of model control and output parameters. The card identifier is the first two characters on the lines contained in the input file, which the HEC-1 program uses to perform the hydrologic modeling process. Limited information is included in text in the HEC-1 input files, identifying sub basins, routing reaches, hydrograph combinations and other significant steps within the models and can, to some degree, be used to follow the general modeling process. Complete descriptions of the “cards” used in the HEC-1 input files can be reviewed in HEC-1 User’s Manuals available from the USCOE website or other HEC-1 resources on the Internet.

The peak flow associated with each sub area within the contributing watershed was evaluated in the HEC-1 program for the modeled events including:

- 25-year, 24-hour summer thunderstorm
- 25-year, 24-hour winter rain on snow with frozen ground
- 100-year, 24-hour summer thunderstorm
- 100-year, 24-hour winter rain on snow with frozen ground

Combined hydrographs defining flow conditions throughout the watershed area were also evaluated in the HEC-1 models. A discussion of the modeling results for the INTEC and the surrounding watershed is included in the following.

4.2.4 Hydrologic Modeling Approach

The entire watershed contributing to the INTEC, Lincoln Boulevard and the Central Facilities Area was modeled to evaluate storm water runoff and determine any flooding potential. For modeling purposes, the HEC-1 models were created to evaluate runoff in the following manner:

1. Determine the 100-year runoff flow from all areas contributing to Lincoln Boulevard, using sequential analysis of the uppermost sub areas and combining flows according to flow path as the runoff approaches the intersection of the Big Lost River and Lincoln Boulevard. Account for stage-storage relationships in depressions storage areas, channel routing in interceptor and irrigation channels and determine the peak runoff entering the Big Lost River just above Lincoln Boulevard. Route flows through the Big Lost River channel and combine with the INTEC runoff below the railroad bridge.

2. Determine the 100-year runoff flow from all areas contributing to the constructed pits in the Central Facilities Area, using sequential analysis of the uppermost sub areas and combining flows according to flow path as the runoff approaches the pits. Allow the constructed pits to serve as the stage-storage area and determine if any flow exits the CFA sub areas and overflows towards the INTEC sub areas. If so, combine CFA flows with INTEC flows accordingly.
3. Determine the 100-year runoff flow from all areas contributing to the INTEC and surrounding area that drains to two culverts located under the railroad grade northeast of the facility area. Account for stage-storage areas and determine peak flow discharging from the facility towards the culverts.
4. Due to the limited area contributing directly to the storm water drainage systems at the INTEC, create a separate HEC-1 model of sub area INTEC-2 using further subdivided areas based on drainage flow paths to evaluate the 25-year runoff and drainage system capacity and the 100-year storm water runoff floodplain for the interior facility area at the INTEC.

A discussion of the results of this modeling approach is included in the following section.

4.3 Hydrologic Modeling Results

The HEC-1 analyses of the different return period storm events indicate that the 25-year and 100-year rain on snow and frozen ground events generate the largest peak flows throughout the watershed sub areas as a whole. These storm events were used to identify the storm water runoff floodplain associated with the Big Lost River, stage-storage areas throughout the watershed, and to evaluate channel capacities outside of the INTEC-2 sub area (main facility).

Inside of the INTEC facility perimeter, the HEC-1 analysis indicates that the 25-year and 100-year summer storm events will generate the highest peak flow from the INTEC-2 (main facility area) sub area. These results are indicative of the amount of impervious surface in the INTEC facility and grounds. Summer events have a higher precipitation intensity, which generally drives peak flow in impervious areas. In order to evaluate the largest flood potential and more accurately identify the 100-year storm water runoff floodplain within the facility area, the summer runoff event was used in the INTEC-2 sub area (resulting from the separate INTEC-2 facility analysis).

A summary of the peak flow within each sub area is provided in Table 4-5 for the summer and winter events for the whole watershed area. A summary of peak flows for several key combinations of sub area hydrographs contributing to the Big Lost River and areas of potential concern is shown in Table 4-6. Representative hydrographs for peak flows are shown in Figure 4-1 (25-year, 24-hour summer storm hydrographs) through Figure 4-8 (100-year, 24-hour winter storm hydrographs). Discussion of specific results of the hydrologic modeling for each individual storm event is provided in the following.

1. The 25-year, 24-hour *winter* rain on snow with frozen ground event generates the highest peak flow in the watershed as a whole for the INTEC and surrounding area, for storms with this return period. The 25-year, 24-hour winter rain-on snow with frozen ground event was used to identify the 25-year storm water runoff floodplain for the Big Lost River and surrounding areas. This event generates 214 cubic feet per second (cfs) at the Lincoln Boulevard Bridge and 270 cfs at the junction downstream of the railroad bridge.
2. The 100-year, 24-hour *winter* rain on snow with frozen ground event generates the highest peak flow in the watershed as a whole for the INTEC and surrounding area, for storms with this return period. The 100-year, 24-hour winter rain-on snow with frozen ground event was used to identify the 100-year storm water runoff floodplain for the Big Lost River and surrounding areas. This event generates 314 cubic feet per second (cfs) at the Lincoln Boulevard Bridge and 393 cfs at the junction downstream of the railroad bridge.
3. The 25-year and 100-year *summer* events generate the highest peak flow for the INTEC-2 (main facility) sub area due to the amount of impervious surface in this basin. The amount of impervious surface within the INTEC-2 boundary was estimated to be 60 %, and when combined with the short time of concentration for this basin, generates approximately 75 cfs during the 25-year summer event, and 106 cfs during the 100-year summer event. The 25-year summer event was used to evaluate the capacity of all storm sewer systems and culverts located within the INTEC perimeter. The 100-year summer event was used to identify the 100-year floodplain in INTEC-2.

Table 4-5. Peak flow (cfs) for individual sub areas.

<i>Intec Area</i>				
Sub Area	25-year Summer	25-year Winter	100-year Summer	100-year Winter
Intec 1	5	12	9	18
Intec 2	75	28	106	46
Intec 3	4	4	7	7
Intec 4	2	3	9	5
Intec 5	5	6	8	11
Intec 6	Sink	Sink	Sink	Sink
Intec 7	9	27	17	39
<i>Lincoln Boulevard contributing sub areas</i>				
Sub Area	25-year Summer	25-year Winter	100-year Summer	100-year Winter
LB-1	3	8	5	11
LB-2	5	17	10	24
LB-3	3	10	6	15
LB-4	3	7	5	10
LB-5	3	6	6	10
LB-6	5	14	9	21
LB-7	6	17	12	25
LB-8	11	29	21	44
LB-9	6	17	12	26
LB-10	2	6	5	9
LB-11	3	8	5	12
LB-12	4	12	8	18
LB-13	5	16	9	23
LB-14	5	14	9	21
LB-15	2	7	4	10
LB-16	5	16	10	24
LB-17	5	15	9	22
LB-18	8	25	15	37
LB-19	10	30	20	45
LB-20	24	71	45	105
LB-21	2	2	3	4
LB-22	4	7	9	12
LB-23	2	2	4	5
LB-24	7	15	14	24
LB-25	2	1	2	2
LB-26	3	5	4	6
<i>Central Facilities contributing areas</i>				
Sub Area	25-year Summer	25-year Winter	100-year Summer	100-year Winter
CFA-1	21	24	33	37
CFA-2	42	33	60	51
CFA-3	2	3	4	5

Hydrographs from individual sub areas were combined in the HEC-1 models according to storm water runoff flow paths as water from one sub area flows into the upper reach of the next downstream sub area or as several sub areas combine at their most downstream point. Combining the sub areas provides a representative model analysis of the entire watershed, allowing evaluation of peak storm water runoff flows at any location within the watershed.

Several locations where hydrographs were combined in the HEC-1 model were selected for hydraulic (HEC-RAS) modeling of the surface water channels to evaluate peak flows where significant flow changes occur. Significant flow changes were identified at channel junctions where combined sub area flows enter the Big Lost River or other key areas. Combined hydrographs and significant changes in peak flow incorporated into subsequent hydraulic models of the surface water drainage system are shown in Table 4-6. The flows identified in Table 4-6 were combined with the estimated base flow (30 cfs/mi², see Section 4.1.6) in the Big Lost River and routed through the channel in hydraulic models created for this study to evaluate any backwater effects and identify any flooding potential from storm water runoff.

Table 4-6. Peak flows for key hydrograph combinations used in hydraulic analyses.

Subarea Hydrograph Combination (CMB)	HEC-1 Combination Label	25-year summer peak flow (cfs)	25-year winter peak flow (cfs)	100-year summer peak flow (cfs)	100-year winter peak flow (cfs)
LB9, LB 8	CMB 1	17	45	33	69
LB 4-LB 9	CMB 4	30	82	58	124
LB 1-LB 9	CMB 7	40	116	77	173
LB 19-LB 24	CMB 11	12	110	36	158
LB 18-LB 24	CMB 12	8	118	15	144
LB 16-LB 24	CMB 13	10	32	19	46
LB 11-LB 24, LB 26	CMB 19	30	91	56	133
All Lincoln Boulevard sub areas	CMB 20	63	214	135	314
All Central Facilities sub areas	CMB 22	63	59	95	90
Intec 1 through Intec 5	CMB 25	76	46	116	74
(CMB 25) Intec 1-5, Intec 7	CMB 26	18	50	37	70
Entire watershed area	CMB 27	80	270	172	393

The hydrologic modeling approach used in this study identified storm water runoff peak flows in the watershed where flooding potential may exist. Flow contributing to the west side of Lincoln Boulevard was included in this study to determine if the road serves as a drainage divide or if overflow may enter the INTEC area. Flow in the CFA sub areas was evaluated to determine any potential overflow from the constructed pits. Peak flows identified in Tables 4-5 and 4-6 were utilized in hydraulic analyses of surface water channels and a comprehensive analysis of the INTEC facility storm water drainage system in order to identify the 100-year floodplain and evaluate capacity of the system during the 25-year, 24-hour runoff.

Figures 4-1 through 4-8 show the storm water runoff hydrographs generated from the HEC-1 program at several key locations for the INTEC and the surrounding watershed during the modeled storm events. Hydrographs for key locations include flows generated west of Lincoln Boulevard, within the INTEC facility perimeter, and in the Big Lost River where all flows combine from the watershed analyzed in this study.

The hydrographs for summer storms show a significant spike in the flow near hour 12 due to the rainfall distribution associated with summer storms. Rainfall intensity increases during a model summer storm near hour 12 causing the peak runoff to occur shortly thereafter. The hydrographs for winter storms show a smaller spike near hour 12, with a more drawn-out flow condition. Rainfall intensity during a winter storm is more consistent throughout the duration of the storm, with a smaller peak intensity near hour 12. Winter storm rainfall distributions create a longer runoff hydrograph, with the peak occurring near hour 12 and sustained flows for the remainder of the storm.

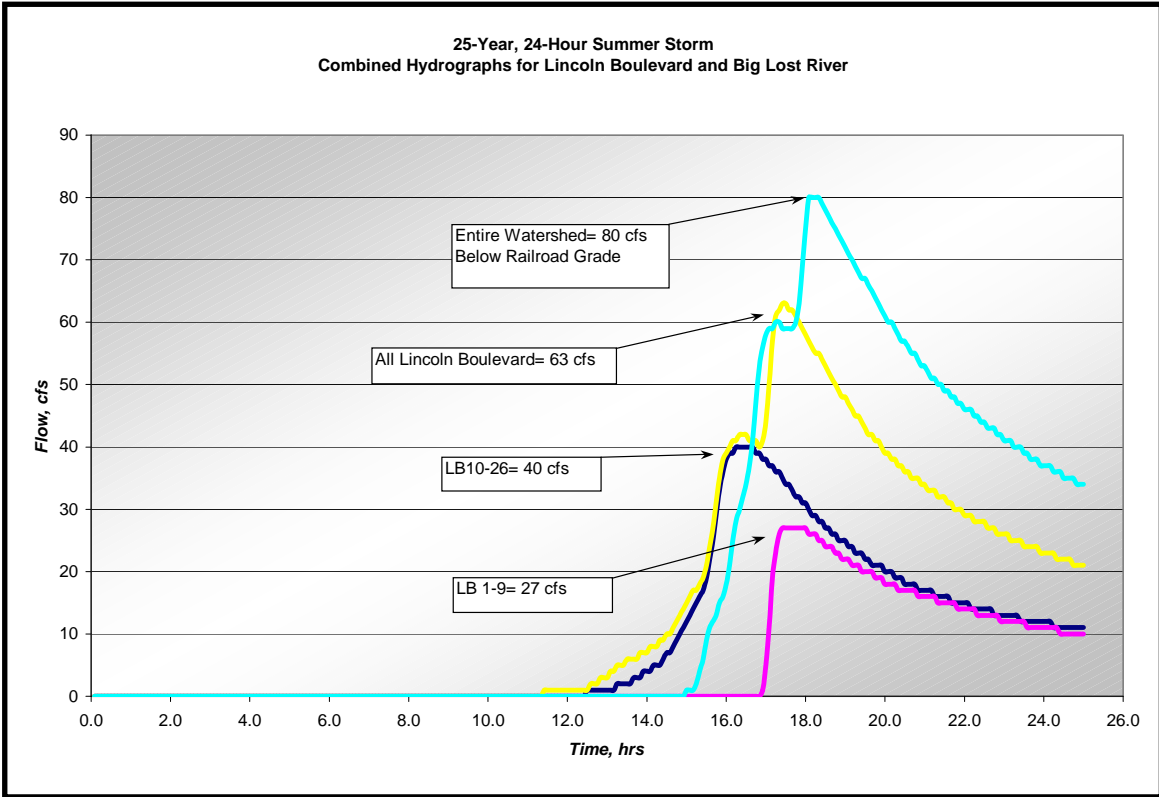


Figure 4-1. 25-year summer storm hydrographs for Lincoln Boulevard, Big Lost River.

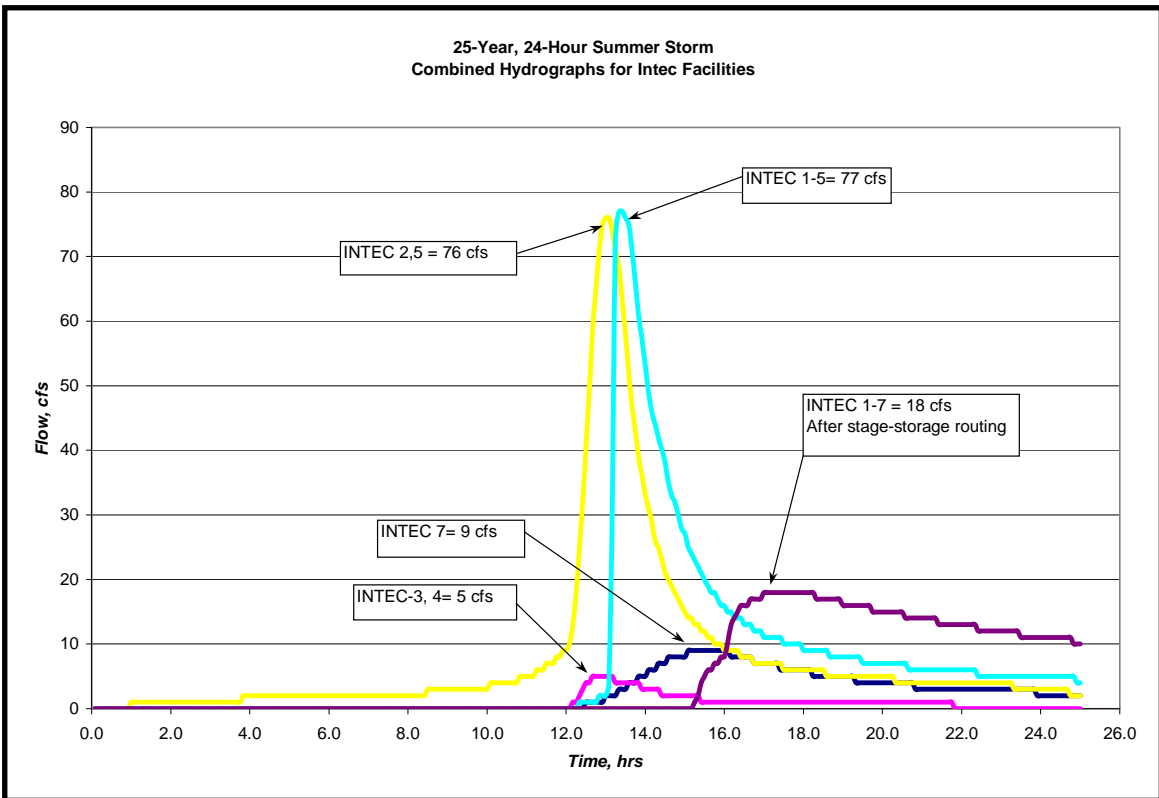


Figure 4-2. 25-year summer storm hydrographs for INTEC sub areas.

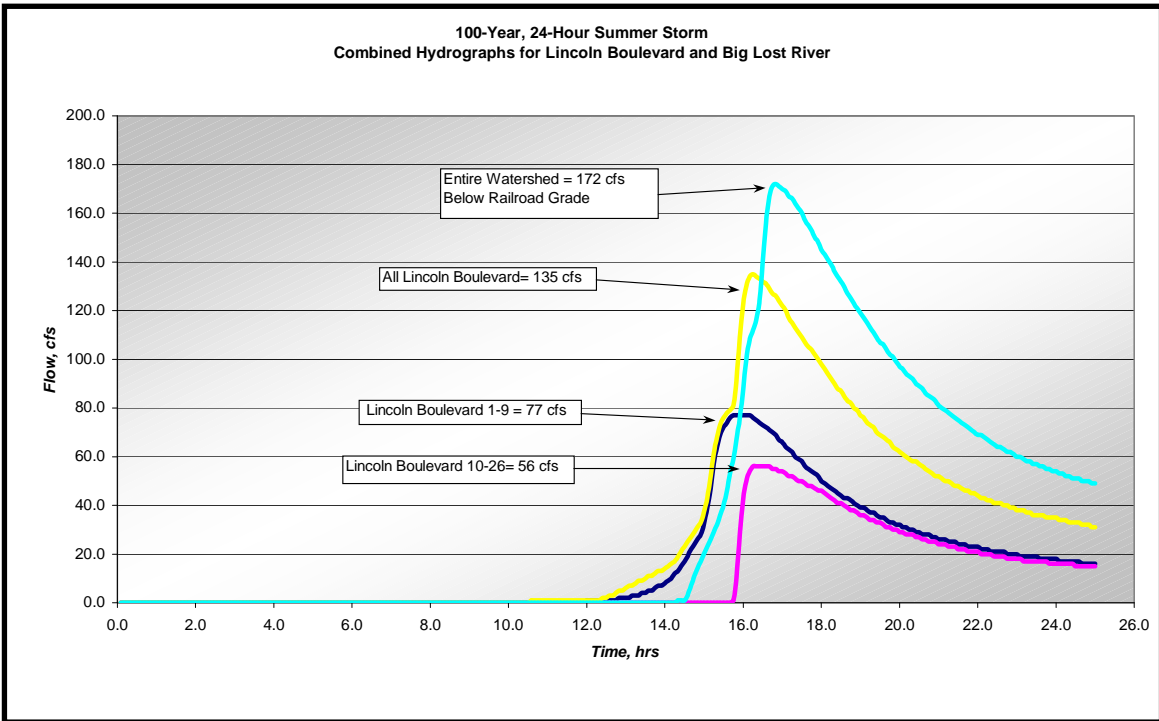


Figure 4-3. 100-year summer storm hydrographs for Lincoln Boulevard, Big Lost River.

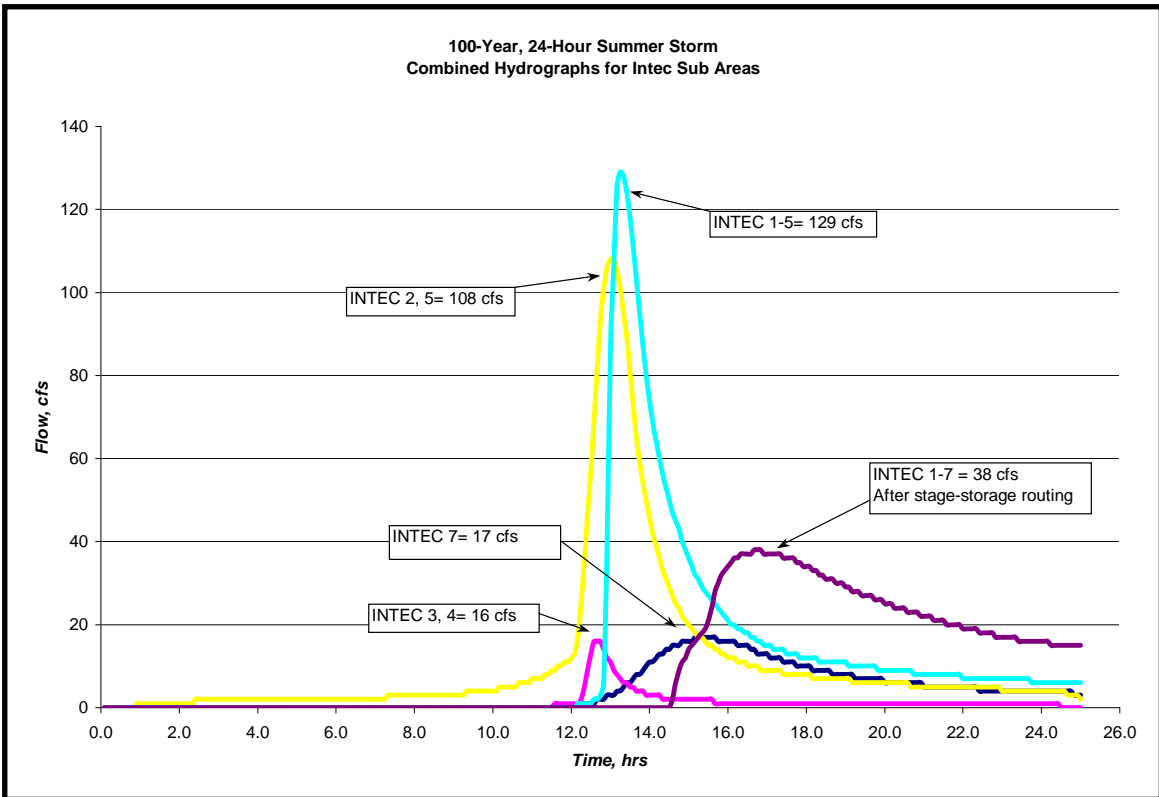


Figure 4-4. 100-year summer storm hydrographs for INTEC sub areas.

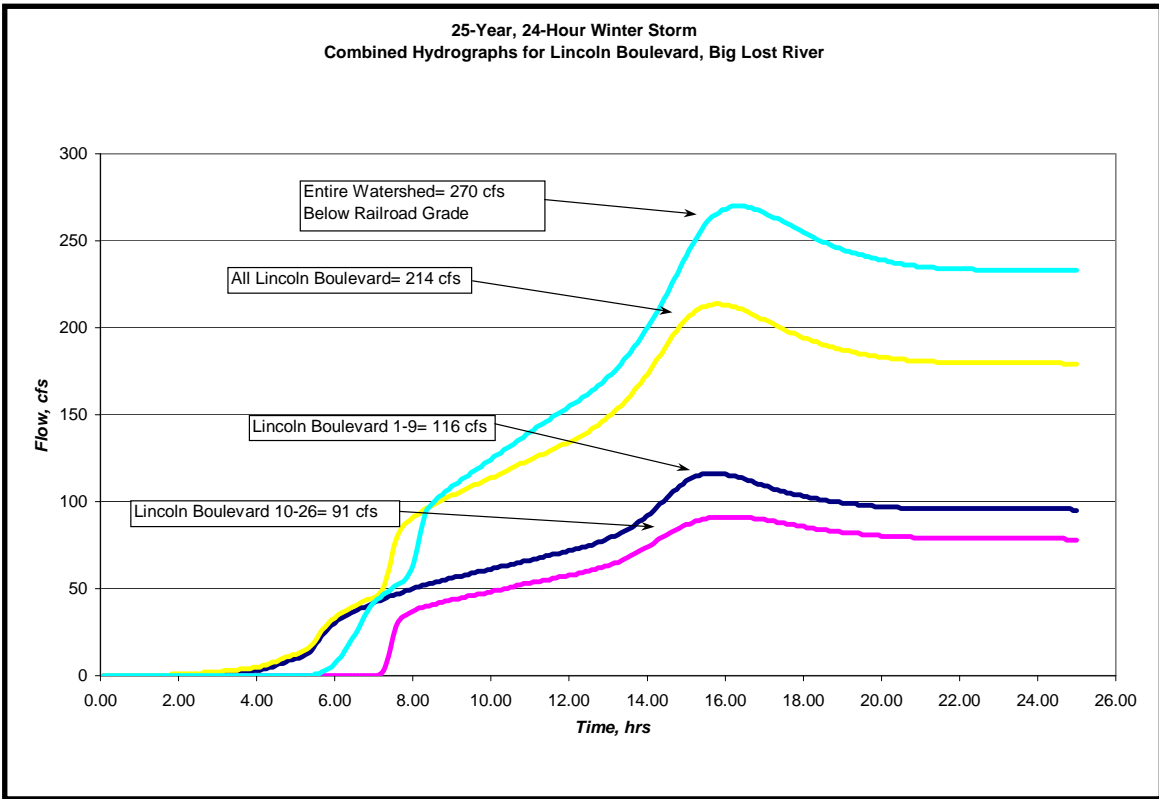


Figure 4-5. 25-year winter storm hydrographs for Lincoln Boulevard, Big Lost River.

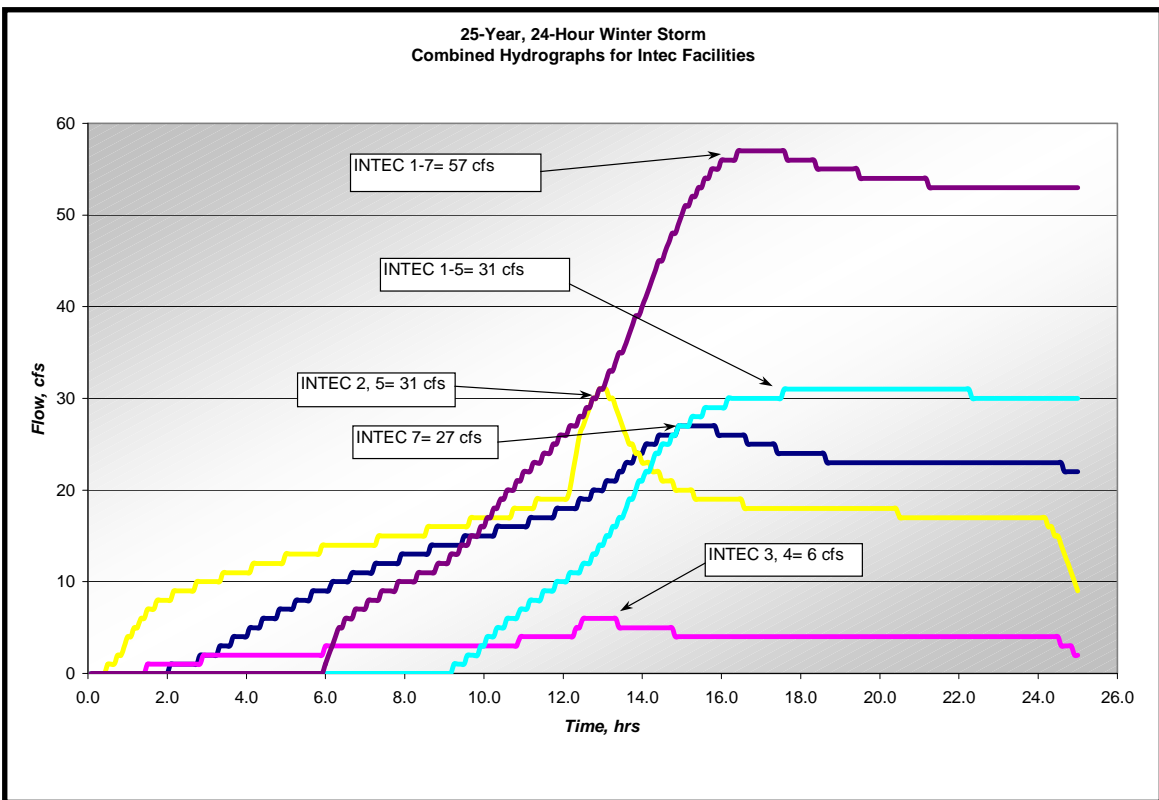


Figure 4-6. 25-year winter storm hydrographs for INTEC sub areas.

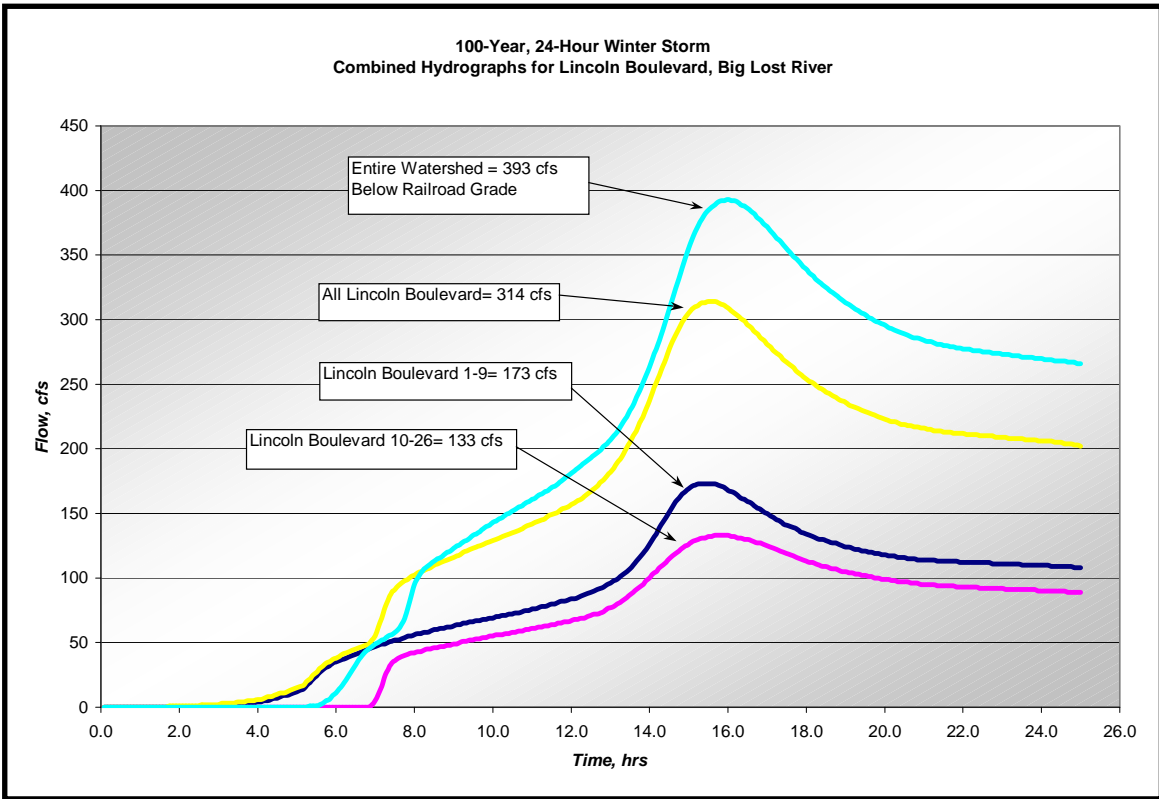


Figure 4-7. 100-year winter storm hydrographs for Lincoln Boulevard, Big Lost River.

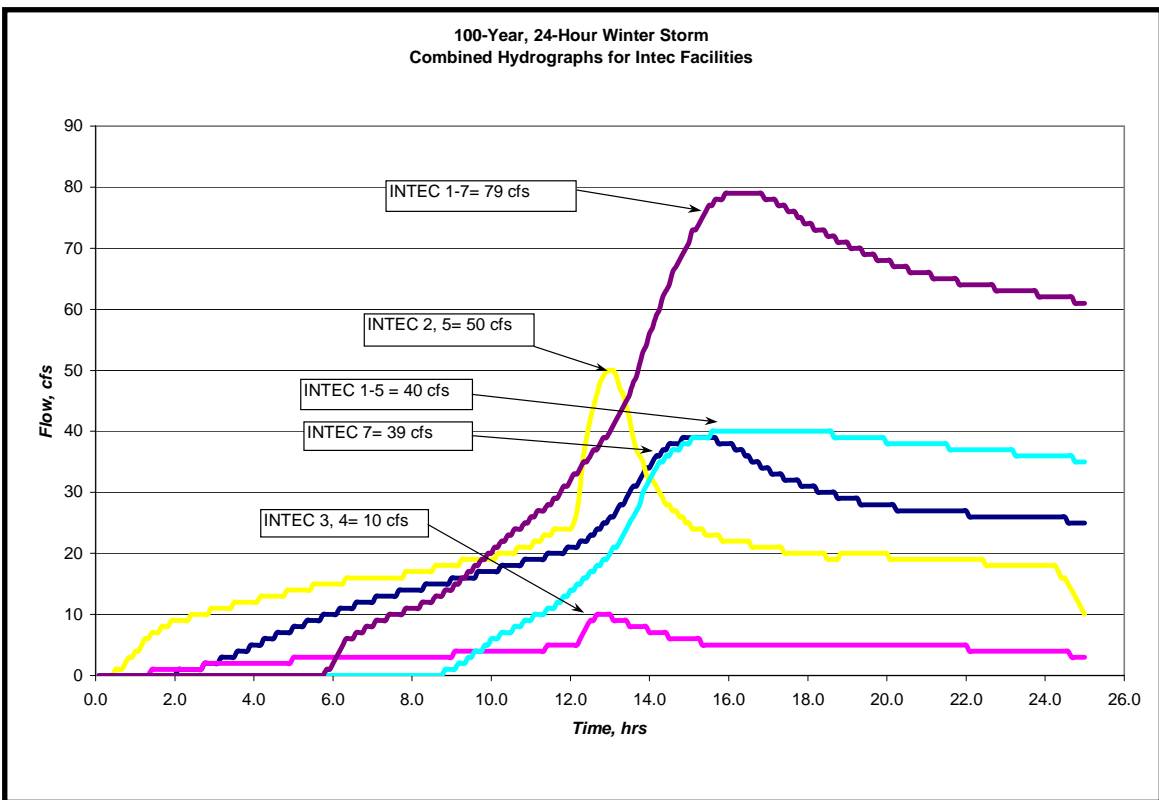


Figure 4-8. 100-year winter storm hydrographs for INTEC sub areas.

4.4 Comparison of Results to Historic Rain/Snow/Frozen Ground Floods

The 100-year peak flow associated with the watershed area contributing to Lincoln Boulevard is estimated to be 314 cfs, according to the HEC-1 analysis for this study. The contributing area to the Lincoln Boulevard is 10.3 square miles, resulting in an average peak flow of 30.5 cfs/mi². The peak flow associated with the entire watershed modeled in this study, including the INTEC facility, is 393 cfs, with a total contributing area of 11.98 square miles, resulting in an average peak flow of 32.8 cfs/mi² (does not include CFA sub areas due to the constructed pits and no outflow). The average peak flows are consistent with flows identified in the historic rain on snow and frozen ground events (~ 30-60 cfs/mi²) documented throughout the region surrounding the INTEC and INEEL. The consistency of the modeling results with documented flood events provides a measure of the reasonableness of watershed parameters, snowmelt and frozen ground parameters, and the overall model setup for the INTEC watershed and surrounding area.

A detailed model calibration was not performed for this hydrologic analysis due to limited availability of documented flood flow conditions throughout the Snake River Plain. There are no sufficient stream gage records throughout the region surrounding the INEEL which are representative of the hydrologic and hydraulic conditions at the INTEC. Typically, with known watershed area, hydrologic parameters, stream channel parameters and climatological, precipitation and stream flow gage data, a model calibration can be conducted, comparing model results to measured data in order to verify modeling results. As an alternative, regional hydrology was used to compare results of this study to historic data, including documented estimations of peak flow expected in upper watershed areas for rain on snow and frozen ground events. Regional hydrologic information compares closely with results of this study indicating that the models are representative of conditions that may occur at the site during the 25-year and 100-year events.

5. HYDRAULIC ANALYSIS

The water surface profiles for the 25-year and 100-year peak flood flows were developed using hydraulic models of the storm water drainage network within the INTEC facility area and the Big Lost River between Lincoln Boulevard and the railroad grade. The 100-year, 24-hour winter rain on snow event was used to identify the storm water runoff floodplain associated with the Big Lost River and key storm water retention areas throughout the watershed area. The 100-year summer event was used to identify the 100-year storm water runoff floodplain limit within the sub areas contributing runoff to the INTEC drainage system. The 25-year summer storm was used to evaluate the capacity of the storm water drainage network in the INTEC facility.

The methodology, assumptions and results of the hydraulic modeling of the surface water channels and storm water drainage systems are discussed in the following sections. Water surface profiles for the Big Lost River and other surface water features outside of the INTEC facility are discussed in Section 5.1. Water surface profiles and the storm water drainage system capacity in the INTEC boundary were developed using hydraulic models of the inlets, pipes, culverts, and surface drainage channels. The methodology, assumptions and results of the hydraulic modeling of the storm drainage systems in the INTEC are discussed in section 5.2.

5.1 Big Lost River

Storm water runoff flow in the Big Lost River was analyzed using the Hydrologic Engineering Center's River Analysis System (USCOE, 2001). Field data collected during the course of this investigation were incorporated into a model of the channel and storm water runoff hydrographs from HEC-1 simulations were input to determine the water surface profile during the different storm events. Additional base flow runoff was included in the HEC-RAS model based on the measured portion of the watershed assumed to be contributing to the Big Lost River upgradient of the study area. Model parameters and assumptions used in generating the water surface profiles are described in the following paragraphs.

5.1.1 Channel Geometry

A portion of the Big Lost River adjacent to the INTEC was surveyed in the field during the course of this investigation using a total station in conjunction with GPS control points. Eleven cross-sections were surveyed in the channel for the purposes of conducting the hydraulic analysis, beginning just upstream of Lincoln Boulevard at the gated culvert entering the channel and continuing downstream past the railroad grade, encompassing the entire area that may influence the INTEC.

5.1.2 Bridges and Culverts

Two hydraulic structures were included in the study reach of the Big Lost River. Three parallel culverts installed at Lincoln Boulevard and a bridge located at the railroad grade crossing were measured, surveyed and incorporated into the hydraulic models of the Big Lost River. Measurements taken at each structure include opening widths, heights and/or diameters as applicable, channel geometry at the faces of the structure, number of culverts, entrance and exit geometry and other parameters that may influence hydraulic capacity.

5.1.3 Roughness Coefficients

Roughness coefficients (Manning's n values) were estimated from field observations of conditions in the channel and overbank areas. The roughness coefficients vary little within the channel and overbank areas, with consistent conditions throughout the study reach. Manning's n values were set at 0.042 and 0.075 for the channel and overbank areas, respectively. These values were taken from the range of values identified in various engineering resource handbooks including the HEC-RAS User's Manual, with specific roughness values selected based on professional engineering judgment and experience with similar channel conditions.

5.1.4 Hydraulic Modeling Process and Equations

The HEC-RAS computer program is used to model water surface profiles in a channel and incorporates channel and overbank geometry, channel length and slope (profile), and roughness coefficients. Channel and flow properties modeled in HEC-RAS are used to evaluate a wide variety of flow conditions including flow depth, velocity, critical depths, and backwater effects from hydraulic structures. The program provides flow property solutions based on three equations; the energy equation, Manning's equation, and where necessary the momentum equation. The primary equation used to relate channel geometry, profile and roughness is Manning's equation:

$$Q = \frac{1.49}{n} A \left(\frac{A}{WP} \right)^{0.667} S^{0.5}$$

Where: Q = discharge, cfs

n = Manning's roughness coefficient

A = flow area, ft²

WP = wetted perimeter, ft

S = channel slope, ft/ft

This equation relates the discharge and channel geometry to evaluate the flow area and wetted perimeter, which, in turn, determines the flow depth and water surface elevation at each cross-section within the model. Using an iterative process of solving the energy equation, Manning's equation and where necessary, the momentum equation, HEC-RAS provides a detailed analysis of the flow conditions in the modeled stream channel.

5.1.5 HEC-RAS Model Simulations, Big Lost River

Peak flows from the 25-year and 100-year hydrographs were taken from the HEC-1 hydrologic simulations and input into the HEC-RAS model of the Big Lost River to identify water surface profiles during the simulated storm events. A total of 3 hydrographs; base flow from upgradient contributing watershed area, flows from the Lincoln Boulevard contributing sub areas, and all contributing flow from the study area, were combined and incorporated into the HEC-RAS model to accurately model channel junctions where flow enters the river.

The HEC-RAS model simulations indicate that the Big Lost River has sufficient capacity to convey all storm water runoff during the design storm events in the vicinity of the INTEC. The barrier dike constructed between Lincoln Boulevard and the railroad grade prevents flood flows in the Big Lost River from impacting the INTEC facility during the 25-year and 100-year events.

One location along the barrier dike was identified where floodwater may flow out of the banks of the river during the 100-year runoff event and is located upstream of Lincoln Boulevard. The dike has a low elevation in this location relative to the remainder of the dike and may be subject to flooding in the overbank area. This location is upgradient of Lincoln Boulevard and, with Lincoln Boulevard serving as an additional flow barrier, does not contribute flooding to the INTEC.

The storm water runoff floodplain for the 100-year event modeled in this study is shown on Sheet 2. The floodplain drawing includes the floodplain associated with storm water flow in the Big Lost River, stage-storage areas inundated during the modeled events, as well as floodplain areas within the INTEC perimeter resulting from the storm water drainage systems. Water surface elevations taken from hydraulic modeling of these areas are included in the floodplain mapping.

It should be noted that the floodplain map was generated using two different storm water runoff events. The Big Lost River storm water runoff floodplain was identified using the 100-year winter rain on snow with frozen ground event and the floodplain within the INTEC facility area was identified using the 100-year summer thunderstorm in order to identify the greatest floodplain extent for the respective areas. Detailed discussion of the flood modeling conducted within the INTEC facility is included in the following section.

5.2 INTEC Surface and Subsurface Drainage System Modeling

The surface drainage channels and subsurface drainage piping system in the INTEC facility area were modeled using the Environmental Protection Agency's Storm Water Management Model (US EPA, SWMM 4.4gu, 1999). This model provides a detailed analysis of storm drainage surface channel and piping networks including pipe and inlet flow conditions, water surface elevations, flow velocities, and design capacities of drainage system components. The program generates detailed flow hydrographs resulting from storm water runoff input into the model, and simultaneously solves for flow conditions in all channels and pipes using the energy equation, Manning's equation and the momentum equation to evaluate the storm drain system as a whole.

The SWM modeling for the INTEC storm drainage system networks was conducted for the 25-year and 100-year summer storm events in order to identify any flooding that may occur and to delineate the 100-year floodplain for the storm water drainage system. Discussion of the SWMM program and modeling parameters used in this analysis are presented in the following sections.

5.2.1 SWMM Program Input Parameters

The SWMM program combines storm water drainage system parameters including open channel, piping and inlet characteristics and configurations and storm water runoff hydrographs to generate a flow model of the drainage network during a design storm event. All connected components of the storm drainage system can be modeled together in order to identify backwater influences and channels and pipes with insufficient capacity.

Input parameters for the SWMM program include the following:

- Pipe diameter, shape, length, upstream/downstream invert elevations and roughness
- Surface channel shapes, lengths and roughness
- Inlet type, surface and invert elevations
- Pipe and inlet connectivity data
- Storm water runoff hydrographs for the duration of the runoff event
- Outfall type and water surface elevation at the outfall during the runoff event (to identify backwater effects on the drainage system where outlet elevations are located near the bottom of surface channels).

The storm water drainage network inlets and culvert locations were surveyed during the field investigation at the INTEC. All necessary data to complete the storm water management model were collected for surface channels, catch basins, lift stations, and culverts in the INTEC area. Field data were incorporated into the SWMM input files and used to determine channel and pipe capacities and peak flow during the modeled runoff events.

5.2.2 Storm Water Runoff Hydrographs

Detailed storm water runoff hydrographs for the INTEC facility were developed from a HEC-1 model prepared specifically for the INTEC-2 sub area identified within the regional watershed area (main facility). The INTEC-2 sub area was further subdivided according to flow paths in the storm water drainage system and used to more accurately evaluate flows in the surface channels, culverts and pipes.

The runoff hydrographs for the INTEC-2 sub area were proportioned to various channels, culverts and inlets throughout the drainage system according to their respective contributing area and surface runoff flow paths. In each major segment of the drainage network, runoff was input into end of line inlets in order to evaluate all pipes and channels in the segment.

5.2.3 SWMM Analysis

The SWMM program analysis provides detailed information regarding peak flows, channel and pipe capacities, flow depths, and, where applicable, pipe surcharge depths in and above the catch basins (inlets). During the modeling process, the SWMM program computes the flow and velocity in each channel and pipe throughout the duration of the storm based on

size, roughness, slope, length and connectivity. The program also computes water surface elevations in the channels and catch basins, including surcharge in inlets and catch basins resulting from insufficient capacity. Water surface profiles and surface elevations computed by the program are used to identify areas where surface flooding may occur. The following is a detailed description of the information input to and output from the SWMM program and used in evaluating any surface flooding resulting from insufficient capacity.

Input information:

- Pipe segment describing upstream and downstream catch basin locations for each pipe or culvert modeled in the program.
- Pipe diameter and roughness (based on material), and pipe length. For modeling purposes, pipes include both subsurface piping and culverts.
- Inlet information including ground elevation and basin invert elevation.
- Surface water channel shape, depths, side slopes, channel slope based on pipe and culvert inlet elevations (as identified in connectivity data) and roughness.
- General connectivity information including upstream and downstream nodes for each surface channel, culvert and storm drain pipe. Outfall data to identify conditions at the downstream limit of the storm water drainage network.
- Storm water runoff hydrographs distributed to the appropriate inlet or node (nodes used to describe upstream and downstream ends of all channels, pipes and culverts).

Output information:

- Channel and pipe capacity (design capacity) and peak flow.
- Ratio of design capacity to peak flow. This ratio may identify channels and pipes where insufficient capacity can cause surface flooding. A ratio less than 1 shows sufficient capacity in the drainage segment for the storm water runoff input into the model. A ratio greater than 1 identifies drainage segments where surcharge is present and additional flow capacity is generated under pressure flow conditions.
- Junction surcharge elevation above ground elevation indicates inlets where surcharge water in the basin has reached the surface and can cause flooding. Values of zero for this output parameter indicate that, although surcharge water may be present in the basin, the water surface elevation does not rise above the ground elevation and cause flooding.

The ratio of design capacity to peak flow is one of the key output parameters utilized from the SWMM program to evaluate the drainage system and flooding potential. When the ratio is less than one, the peak flow is less than the pipe or channel capacity and indicates that the water surface profile and energy grade are contained within the pipe or channel with no backwater effects that can cause flooding. A ratio greater than one indicates that the peak flow

in the pipe or channel is greater than capacity under gravity flow conditions. However, a ratio greater than 1 does not necessarily indicate that the drainage system has insufficient capacity and that flooding will occur because additional flow capacity is generated under pressure flow conditions.

When the peak flow exceeds the design flow of a pipe or channel, water rises above the top of the pipe (surcharge) causing a pressure flow condition allowing greater flow than design capacity. However, in subsurface drainage systems, and in open channels with culverts, the surcharge may not reach the ground surface or top of the open channel and cause surface flooding. Where surcharge is present in the system and the ratio of peak flow to capacity exceeds 1, it is necessary to evaluate the depth of surcharge, site topography and other factors to determine if surface flooding occurs and to what extent.

5.2.4 SWMM Modeling Results

The INTEC storm water drainage system has adequate capacity to convey nearly all storm water runoff during the 25-year event. Insufficient pipe and channel capacity and physical condition deficiencies (improper construction) were identified in the drainage network near buildings T-1 and T-5. This area of the drainage network was constructed at an elevation above the apparent floor elevation of the buildings and during periods of significant runoff may overflow and cause localized flooding. Minor surface flooding at localized areas throughout the remainder of the storm water drainage network is limited to the immediate vicinity of the storm water surface channels and inlets and does not pose a flooding hazard to the surrounding areas.

During the 100-year storm, more extensive flooding will occur in the area around buildings T-1 and T-5, and shallow surface flooding will occur near buildings CPP-651 and CPP-796. This area of the storm water drainage network has insufficient capacity to convey all of the 100-year runoff and will cause localized shallow flooding in the vicinity of these buildings. According to topographic mapping of the site, the limit of the 100-year storm water runoff floodplain will encompass buildings T-1 and T-5. Buildings CPP-651 and CPP-796 are not within the 100-year floodplain boundary.

Surface flooding elevations are identified in the SWM models prepared for the 25-year and 100-year runoff events. The surface flooding elevations were subsequently used to identify floodplain limits for the storm water drainage networks. The storm water runoff floodplain for the 100-year event is shown on Sheet 2.

The SWMM modeling conducted for this study included surface water channels, culverts, catch basins, subsurface piping, lift stations and storm water retention areas. Modeling for storm water drainage network at the INTEC facility assumes that all culverts, pipes, channels and lift stations are maintained in a fully functioning condition. The results for the 25-year and 100-year events indicate that, in general, the storm water drainage network has sufficient capacity to convey runoff away from the facility towards the Big Lost River. With the exceptions described in the previous paragraphs, no surface flooding outside the limits of open surface water drainage channels within the INTEC facility area was identified.

5.3 25-year and 100-year Floodplain Mapping

The 25-year and 100-year storm water runoff floodplains were identified on topographic mapping of the INTEC facility using results of the SWMM and HEC-RAS model analyses. The water surface elevations resulting from the 25-year and 100-year flows were plotted on a base map of the storm water drainage network and the Big Lost River. In locations where the channel capacity was exceeded, surface flooding elevations were identified and delineated on topographic maps to determine the extent of the floodplain. Storm water retention area flood elevations were also identified for the 25-year and 100-year events in order to identify all inundated floodplain areas associated with storm water runoff. The 100-year floodplain boundary for the INTEC storm water drainage network, surface channels and storm water retention areas included in the modeling for this study is shown on Sheet 2.

Additionally, a storm water runoff floodplain for the Big Lost River was delineated to the extent of the water surface elevations identified in the HEC-RAS models created for this study. A short segment of the Big Lost River was modeled as a part of this study to evaluate the function of the barrier dike constructed along the southern bank of the river in the immediate vicinity of the INTEC, and to identify the floodplain limit associated with the 25-year and 100-year storm water runoff events. Using estimates of the base flow in the Big Lost River combined with runoff from the watershed contributing to Lincoln Boulevard, flood flows and water surface elevations in the Big Lost River were compared to the barrier dike profile to identify flooding potential. According to the results of the model analyses, storm water runoff from the watershed west of Lincoln Boulevard will be contained within the limits of the channel and low lying areas to the north of the river. The perimeter dike prevents storm water runoff from entering the area in the immediate vicinity of the INTEC. A detailed study of the 25-year and 100-year riverine floods in the Big Lost River is beyond the scope of this project and is being conducted by others.

6. CONCLUSIONS

Conclusions of this hydrologic and hydraulic study of the 25-year runoff and 100-year storm water runoff floodplain at the INTEC facility are presented in the following.

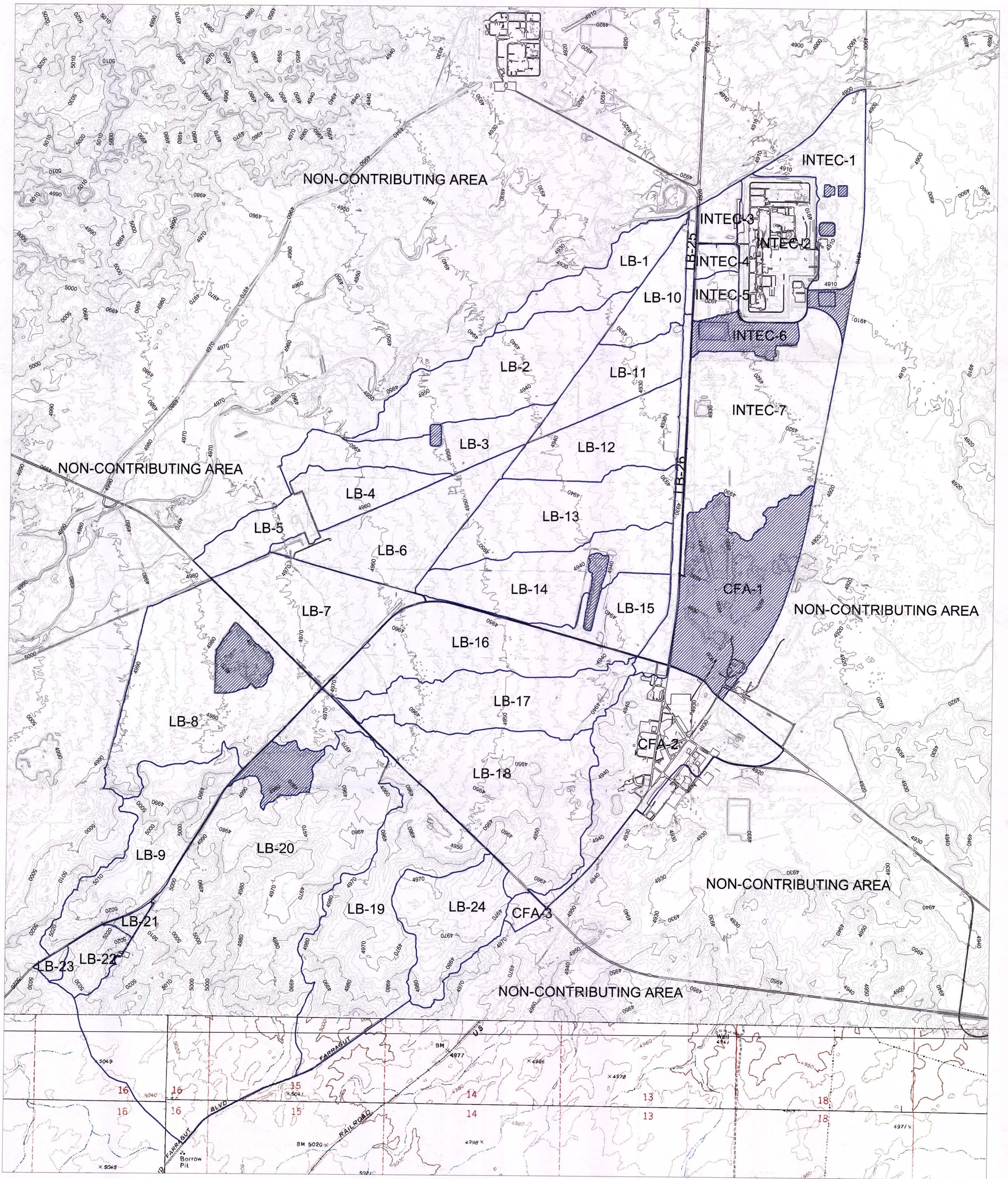
1. One area in the storm water drainage network serving the INTEC facility was identified as hydraulically deficient during the 25-year summer storm event. This surface channel is constructed at an elevation above the surrounding ground and will overflow during the 25-year event, causing localized flooding around Buildings T-1 and T-5.
2. Buildings T-1 and T-5 are located within the floodplain associated with an open surface channel and culverts in their vicinity. This surface channel is constructed at an elevation above the surrounding ground and will overflow during the 100-year event, causing localized flooding in the area. Buildings CPP-651 and CPP-796 are located outside of the limits of the 100-year floodplain according to surface water elevations and topographic mapping in the area.
3. The 25-year and 100-year flood flows throughout the remainder of the INTEC facility area are generally contained within the limits of surface water channels and local storm water retention areas. No other buildings beyond those discussed in items 1 and 2 were identified within the limits of the storm water runoff floodplain boundaries delineated during the course of this study.
4. The limits of the 100-year floodplain associated with flows entering the Big Lost River to the west (upgradient) side of Lincoln Boulevard, including estimated base flow, are contained on the southern side of the channel by the perimeter dike, with the exception of one small area. Immediately west of Lincoln Boulevard, a low elevation in the perimeter dike may allow flood flow to leave the channel. This flow does not have the potential to enter the INTEC facility area as Lincoln Boulevard serves as a drainage divide, with no culverts to allow cross flow.
5. The northern side of the Big Lost River was not thoroughly investigated to identify the full extent of the floodplain to the north of the perimeter dike. Other studies are being conducted to determine the magnitude and extent of the 25-year and 100-year floods associated with the Big Lost River.
6. Storm water retention areas identified throughout the watershed area will collect storm water runoff during the 25-year and 100-year events. These areas will fill to the elevations identified on the floodplain maps and where sufficient storm water accumulation occurs, will overflow into surface water drainage channels. No flooding identified in these areas has the potential to impact the INTEC facility.

7. REFERENCES

- Berenbrock, C., and Kjelstrom, L.C., 1998, *Preliminary Water-Surface Elevations and Boundary of the 100-year Peak Flow in the Big Lost River at the Idaho National Engineering and Environmental Laboratory, Idaho*, United States Geological Survey, Water-Resources Investigations Report 98-4065.
- Burgess, J.D., July 1991, *25-Year, 24-Hours Storm Analysis for the Idaho Chemical Processing Plant*, EG&G Geosciences.
- CH2MHill, Inc., 1989, *Silver Bow Creek Flood Modeling Study*, Butte, Montana.
- Dames and Moore, 1993, *Flood Evaluation Study, Radioactive Waste Management Complex*, Idaho National Engineering Laboratory, Idaho Falls, Idaho.
- DOE-ID, 1998, *Interim Risk Assessment and Contaminant Screening for the Waste Area Group 7 Remedial Investigation (Section 3.1.4, P. 3-6)*, US Department of Energy Idaho Operations Office, DEO/IDD-10569.
- Dodson and Associates, Inc., June 1995, *ProHEC1 Plus Program Documentation*, Houston, Texas.
- Humphrey, J. H., 1994, *Meteorological Analysis, Flood Control Master Plan*, Washoe County, Nevada.
- Kingsford, C.O., 2002, *Culvert Survey Summary*, Document No. INEEL/EXT-01-01179.
- Keck, K. N., 1998, *25-Year, 24-hour Storm Evaluation for the Transuranic Storage Area*, Idaho National Engineering and Environmental Laboratory, INEEL/EXT-98-00472.
- Koslow, K. N., Van Haaften, D. H., 1986, *Flood Routing Analysis for a Failure of a Mackay Dam*, EGG-EP-7-7184, EG&G Idaho, Inc.
- Mitchell, T. S., Mitchell, J. S., Humphrey, J. H., Kennedy, D., Funderburg, T., 2002, *100-year Floodplain and 25-Year Runoff Analyses for the Radioactive Waste Management Complex at the Idaho National Engineering and Environmental Laboratory*, Document No. INEEL/EXT-02-00093.
- National Weather Service, Dubois Gage Data (1948 – 1997).
- National Weather Service, Idaho Falls 16SE Gage Data (1960 – 1997).
- National Weather Service, Idaho Falls 2ESE Gage Data (1952 – 1960).
- National Weather Service, Idaho Falls FAA, Idaho Falls Airport Gage data (1948 – 1952).
- National Weather Service, INEEL Winter Flood Events, Idaho Falls 46W Data (1952 – 2000).
- National Weather Service, Twin Falls Gage Data (1978 – 1997).
- Ostenaar, D. A., Levish, D. R., Klingler, R. E., and O'Connell, D. R., 1999, *Phase II, Paleohydrologic and Geomorphic Studies for the Assessment of Flood Risk for the Idaho National Engineering and Environmental Laboratory, Idaho*, Report 99-7, Geophysics, Paleohydrology, and Seismotectonics Group, Technical Service Center, Bureau of Reclamation, Denver, Colorado.

- Peck, E. L., Richardson, E. A., 1962, *An Analysis of the Causative Factors of the February 1962 Floods in Utah and Eastern Nevada*, National Weather Service, Salt Lake City, Utah.
- Sagendorf, J., 1991, *Meteorological Information for RWMC Flood Potential Studies*, National Oceanic Atmospheric Administration, Environmental Research Laboratories, Air Resources Laboratory Field Research Division, Idaho Falls, Idaho.
- Sagendorf, J., 1996, *Precipitation Frequency and Intensity at the Idaho National Engineering Laboratory*, National Oceanic and Atmospheric Administration, Technical Memorandum ERL ARL-215, Air Resources Laboratory, Silver Spring, Maryland.
- Soil Conservation Service, 1972, *National Engineering Handbook*.
- Taylor, D. D., Hoskinson, R.L., Kingsford, C. O., Ball, L. W., 1994, *Preliminary Siting Activities for New Waste Handling Facilities at the Idaho National Engineering Laboratory*.
- Tullis, J. A., Koslow, K. N., 1983, *Characterization of Big Lost River Floods with Recurrence Intervals Greater than 25 Years*, EG&G Idaho, Inc. Internal Technical Report, RE-PB-83-044.
- United States Army Corps of Engineers, 1975, *Humbolt River and Tributaries, Nevada, Design Memorandum No. 1*, Sacramento District.
- United States Army Corps of Engineers, 1998, *Snow Hydrology Manual*, EM 1110-2-1406.
- United States Army Corps of Engineers, Hydrologic Engineering Center, 2001, *HEC-RAS River Analysis System, Version 3.0.1 User's Manual*.
- United States Environmental Protection Agency, 1999, *Storm Water Management Model, User's Manuals*, Office of Research and Development, Athens, Georgia.
- United States Geological Survey, 1994, *Methods for Estimating Magnitude and Frequency of Floods in the Southwestern United States*, Open File Report 93-419.

DRAWINGS

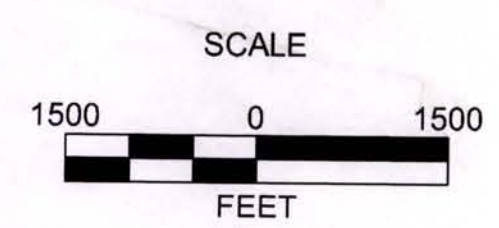


LEGEND:

- MAJOR CONTOUR
- MINOR CONTOUR
- WATERSHED BOUNDARY
- SUB AREA BOUNDARY
- SUB AREA LABEL
- SINK AREA (STORAGE)
- PAVED ROADS
- RAILROAD
- USGS QUAD SECTION NUMBER

NOTES:

1. PLANIMETRIC AND TOPOGRAPHIC DATA DERIVED FROM AERIAL PHOTOGRAMMETRIC IMAGERY COLLECTED BY AERIAL SERVICES, INC., CEDAR FALLS, IOWA, DURING JULY 2002.
2. WATERSHED AND SUB AREA DELINEATIONS ARE BASED ON SEVERAL FACTORS INCLUDING, BUT NOT LIMITED TO; TOPOGRAPHY, STORM WATER FLOW PATHS, HYDRAULIC STRUCTURE LOCATIONS, SIGNIFICANT DRAINAGE AREA DIVIDES AND GENERAL HYDROLOGIC CONDITIONS.
3. THE SOUTHERN LIMITS OF THE WATERSHED AREA WERE IDENTIFIED USING PORTIONS OF A USGS QUADRANGLE (CIRCULAR BUTTE 3, USGS), IMPORTED AND SCALED TO APPROXIMATELY MEET THE TOPOGRAPHY WITHIN THE FLYOVER LIMITS.
4. AREAS WEST OF LINCOLN BOULEVARD (LB##) WERE INCLUDED IN HYDROLOGIC MODELING TO EVALUATE ANY FLOODING POTENTIAL FROM FLOW OVER LINCOLN BOULEVARD OR IN THE BIG LOST RIVER NEAR THE INTEC FACILITY PERIMETER.
5. ALL CENTRAL FACILITIES SUB AREAS (CFA##) FLOW INTO CFA-1 WHICH SERVES A STORM WATER RUNOFF SINK DUE TO THE PRESENCE OF SEVERAL LARGE OPEN PITS.

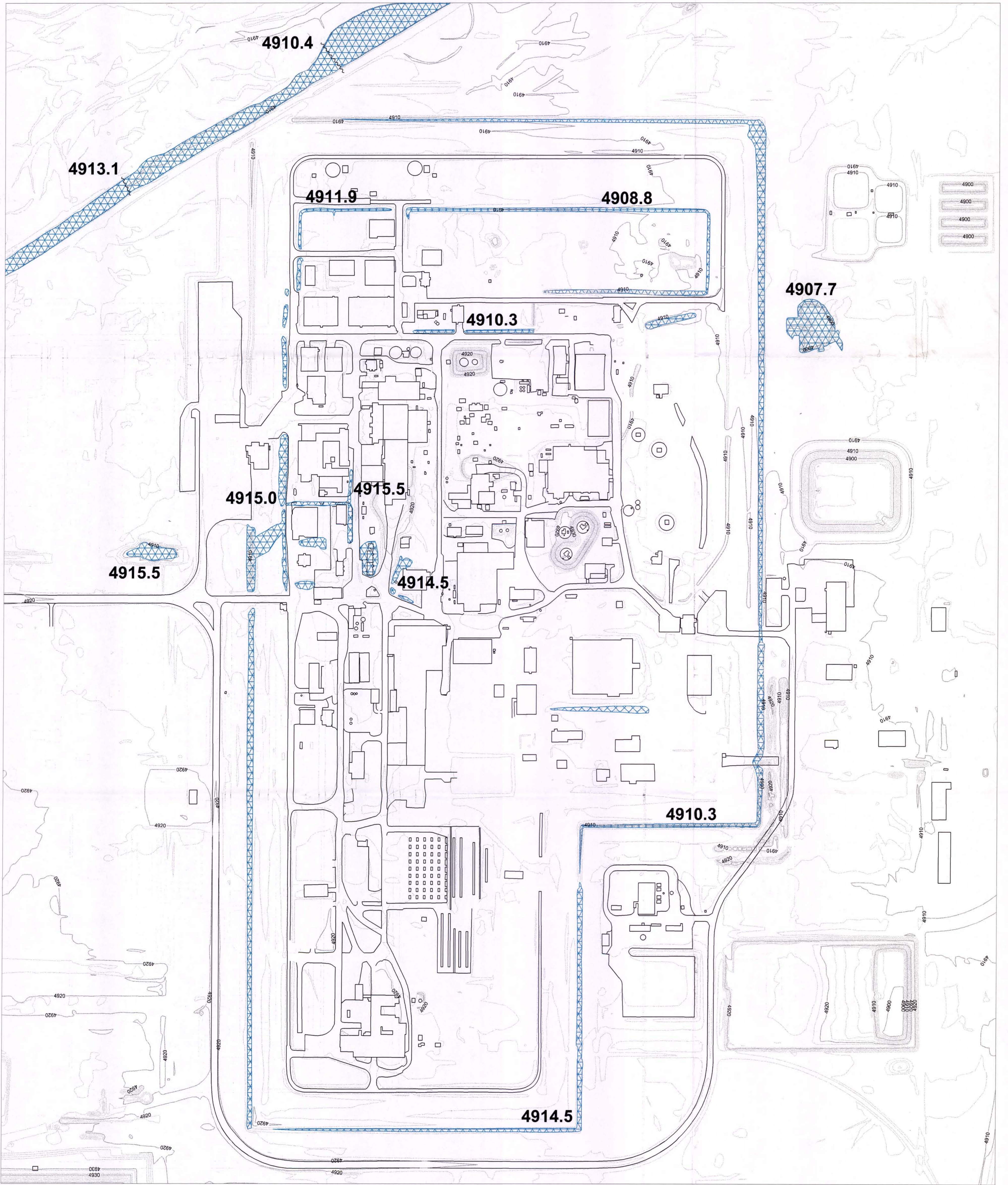


HORIZONTAL DATUM: NAD 27, IDAHO EAST ZONE, STATE PLANE COORDINATES

VERTICAL DATUM: NGVD 29

CONTOUR INTERVAL: 2 FEET

INTEC FLOODPLAIN ANALYSES		Idaho National Engineering and Environmental Laboratory BECHTEL BWXT IDAHO, LLC	
Requester: Neil Hutten		INTEC FACILITY AND SURROUNDING AREA, WATERSHED AND SUB AREA BOUNDARIES	
Drawn: Todd S. Mitchell, PE			
Checked: K. Flynn/J.S. Mitchell			
Subcontract No. 00019200	Size/Scale: C 1-IN = 1,500 FT	Drawing No. SHEET 1	Rev. 0
Date: September, 2003	File: s:\client data\118 INTEC\final drawings\INTEC-1.dwg		

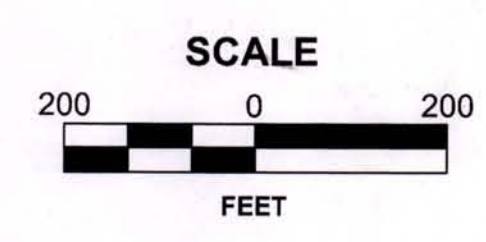


LEGEND:

-  MAJOR CONTOUR
-  MINOR CONTOUR
-  100-YEAR FLOODPLAIN LIMIT
-  BASE FLOOD ELEVATION
-  BUILDING
-  PAVED ROADS

NOTES:

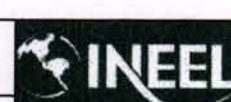
1. FLOODPLAIN AREAS INSIDE OF THE INTEC FACILITY WERE IDENTIFIED USING THE 100-YEAR SUMMER THUNDERSTORM (PEAK RUNOFF FOR FACILITY AREA).
2. BASE FLOOD ELEVATIONS SHOWN IN THE INTEC FACILITY AREA WERE TAKEN FROM DETAILED STORM WATER MANAGEMENT MODELS OF THE DRAINAGE SYSTEM.
3. FLOODPLAIN LIMITS OF THE BIG LOST RIVER ARE SHOWN FOR STORM WATER RUNOFF FROM THE WATERSHED AREAS WEST OF LINCOLN BOULEVARD AND ADDITIONAL WATERSHED AREA (~ 17 SQ. MI.) ASSUMED TO BE CONTRIBUTING TO THE RIVER AT THE TIME OF THE MODELED STORM EVENTS.



HORIZONTAL DATUM: NAD 27, IDAHO EAST ZONE, STATE PLANE COORDINATES

VERTICAL DATUM: NGVD 29

CONTOUR INTERVAL: 2 FEET

INTEC FLOODPLAIN ANALYSES Requester: Neil Hutten Drawn: Todd S. Mitchell, PE Checked: K. Flynn/J.S. Mitchell		 Idaho National Engineering and Environmental Laboratory BECHTEL BWXT IDAHO, LLC	
		INTEC FACILITY DETAIL, 100-YEAR FLOODPLAIN	
Subcontract No. 00019200	Date: July 31, 2003	Size/Scale: C 1-IN = 200 FT	Drawing No. SHEET 2 Rev. 0
		File: s:\client\data\118 INTEC\final drawings\DEQ Sheet 2.dwg	